Scuola Dottorale di Ingegneria
Sezione di Ingegneria Meccanica e Industriale
XXII Ciclo

Thermoacoustic instabilities in Gas Turbine burners: new diagnostic methodology

PhD thesis by
Emanuele Giulietti

Academic year: 2010-2011

Advisor: **Prof. Roberto Camussi**

Coordinator: **Prof. Edoardo Bemporad**

Degree of Doctor of Philosophy

February 2011

In memory of my dear Prof. Giulio Guj

"If I have the gift of prophecy and can fathom all mysteries and all knowledge, and if I have a faith that can move mountains, but have not love, I am nothing. Love never fails.
But where there are prophecies, they will cease; where there are tongues, they will be stilled; where there is knowledge, it will pass away. For we know in part and we prophesy in part, but when completeness comes, what is in part disappears. When I was a child, I talked like a child, I thought like a child, I reasoned like a child. When I became a man, I put the ways of childhood behind me.
For now we see only a reflection as in a mirror; then we shall see face to face. Now I know in part; then I shall know fully, even as I am fully known." (1 Corinthians 13,2.8-12)

"Freely you have received, freely give". (Matthew 10,8)

Index

Index of Attachments

List of symbols

Uppercase Roman

A	flame surface [m^2]
A	absorbance [−]
A_i	generic chemical species [−]
D	mass diffusivity [$m^2\ s^{-1}$]
Da	Damköhler number, $= \frac{\tau_t}{\tau_{ch}}$ [−]
D_i	effective diffusion coefficient of species *i* into the gas mixture [$m^2\ s^{-1}$]
D_{ij}	binary mass diffusivity [$m^2\ s^{-1}$]
D_{ij}^T	thermo-diffusion coefficient [$m^2\ s^{-1}$]
E	energy per unit volume [$J\ m^3$]
E	specific internal energy [$J\ kg^{-1}$]
E	strain rate tensor [s^{-1}]
E_a	activation energy of chemical reactions [$J\ kg^{-1}$]
E_1	period-averaged acoustic energy in the whole combustor [$J = kg\ m^{+2}\ s^{-2}$]
E[x]	statistical expectation of x
F	force per unit volume [$kg\ m^{-2}\ s^{-2}$]
F_1	period-averaged acoustic flux leaving the combustor (acoustic losses) [$W=Js^{-1}= kgm^{+2}s^{-3}$]
$\Im$	*Fourier* transform;
G	specific Gibbs' free energy [$J\ kg^{-1}$]
He	helicity, $= \omega \cdot u$ [$m\ s^{-2}$]
H	specific enthalpy [$J\ kg^{-1}$]
I	identity matrix [-]
I	radiant energy [J]
I	spectral irradiance [$Wm^{-3} = J\ m^{-3}s^{-1}$]
J_i	chemical species diffusive mass flux [$kg\ m^{-2}\ s^{-1}$]
K	specific kinetic energy [$m^2\ s^{-2}$]
K	thermal conductivity coefficient [$J\ m^{-1}\ K^{-1}\ s^{-1}$]
Ka	*Karlovitz* number, $= \frac{\tau_{ch}}{\tau_{st}}$ [−]
L	macroscale length [m]
L	the path length [m]
L_a	acoustic length scale [m]
Le_i	*Lewis* number, $= \frac{\alpha}{D_i} = \frac{Sc}{\Pr}$ [−]
M	*Mach* number, $= \frac{U}{c}$ [−]
N_r	number of chemical reactions

N_s number of chemical species
P power [W]
P(x) probability distribution function
Pr *Prandtl* number, = $\frac{\mu c_p}{K}$ [−]
$\dot{Q}_{loss}$ heat loss [J m^{-3} s^{-1}]
$\dot{Q}_R$ heat source [J m^{-3} s^{-1}]
R universal gas constant, = 8.314 [J $mol^{-1}K^{-1}$]
R_1 averaged source term in criteria for combustion instability [W = J s^{-1}= kg m^{+2} s^{-3}]
R Correlation function;
R_x Auto-correlation function for the stationary random process x(t)
R_{xy} Cross-correlation function between the stationary random processes x(t) and y(t)
Re *Reynolds* number, = $\frac{\rho U l}{\mu} = \frac{U l}{\nu}$ [−]
R_g gas constant [J $kg^{-1}K^{-1}$]
S surface [m^2]
S *Power Spectral Density*
S Swirl number
S_x Auto-spectral density function of the stationary random process x(t)
S_{xy} Cross-spectral densities between the two stationary random processes x(t) and y(t)
Sc_i *Schmidt* number, = $\frac{\nu}{D}$ [−]
St *Strouhal* Number [−]
T temperature [K]
T period [s]
T_{ref} reference temperature, 298.15 [K]
TIT Turbine Inlet Temperature [K]
U specific internal energy [J kg^{-1} = N m kg^{-1} = m^{+2} s^{-2}]
U velocity [m s^{-1}]
V volume [m^3]
V_i diffusion velocity of species i [m s^{-1}]
W_i molecular weight of species i [kg mol^{-1}]
W_{mix} mixture molecular weight [kg mol^{-1}]
W_x equivalent one-sided spectral density function
X_i molar concentration of species i [mol m^{-3}]
X_i volumetric fraction of species i [−]
Y_i mass fraction of species i [−]

Lowercase Roman

a absorptivity (or absorption coefficient) [−]
c local velocity of sound [m s^{-1}]
c_p specific heat at constant pressure [J $kg^{-1}K^{-1}$]

c_v	specific heat at constant volume [J kg^{-1}K^{-1}]
d_i	diffusional driving force [m^{-1}]
e	energy per unit mass [J kg^{-1} = N m kg^{-1} = m^{+2} s^{-2}]
e_s	specific sensible internal energy per unit mass [J kg^{-1}]
e_t	specific total energy per unit mass [J kg^{-1}]
e_1	acoustic energy in reacting flow [kg m^{-1} s^{-2}]
f	body force per unit of mass [m s^{-2}]
f	frequency [Hz]
f_1	local acoustic flux [kg s^{-3}]
h	Plank constant = 6.626 ·10^{-34} [J s]
h	fluid specific enthalpy [J kg^{-1} = m^{+2} s^{-2}]
h_s	specific sensible enthalpy [J kg^{-1} = m^{+2} s^{-2}]
$h^0_{f,k}$	chemical formation enthalphy [J kg^{-1} = m^{+2} s^{-2}]
i	specific chemiluminescence emission [J m^{-3}]
j	imaginary unit ($j = \sqrt{-1}$)
k	a unit vector in the z-direction
k	wavenumber [m^{-1}]
k_B	Boltzmann constant = 1.380 ·10^{-23} [J·K^{-1}]
k	thermal conductivity [W m^{-1} K^{-1}] = [J m^{-1} K^{-1} s^{-1}]
l	generic length scale [m]
m	mass [kg]
m	mean value of a random variable
p	pressure [kg m^{-1} s^{-2}]
p(x)	(first order) probability density function describing the distribution of the random variable x
p(x,y)	second-order probability density function describing the joint distribution of the random variable x and y
q	heat flux [J m^{-2} s^{-1}]
q_D	*Dufour* heat flux [J m^{-2} s^{-1}]
q_F	*Fourier* heat flux [J m^{-2} s^{-1}]
q_{Vi}	diffusional heat flux [J m^{-2} s^{-1}]
r	vector position [m]
r_1	source term [kg m^{-1} s^{-3}]
s	specific entropy [J kg^{-1}K^{-1}]
s_L	laminar flame speed [m s^{-1}]
t	time [s]
u'_{rms}	rms velocity fluctuation [m s^{-1}]
u	velocity vector [m s^{-1}]
u	fluid velocity component in *x* direction [m s^{-1}]
v	fluid velocity component in *y* direction [m s^{-1}]
w	fluid velocity component in *z* direction [m s^{-1}]
x, y, z	frame coordinates

Uppercase Greek

Δ difference between two values
Φ equivalence ratio [−]
Σ surface density [m^{-1}]

Lowercase Greek

α thermal diffusivity, $= \frac{K}{\rho c_p}$ [$m^2 s^{-1}$]
α_λ spectral absorptivity [−]
δ boundary layer thickness [m]
δ_{ij} the *Kronecker* delta (δ_{ij}=0 when $i \neq j$; δ_{ij}=1 when $i=j$)
δ_F flame front thickness [m]
δ_r flame front reaction thickness [m]
ε (or ε_λ) emissivity, or spectral emissivity, or radiant emittance factor in the range 0-1 [−]
γ specific heat ratio ($=c_p/c_v$) [−]
η Kolmogorov dissipative length scale [m]
φ phase angle of the Power Spectral Density [rad]
λ wavelength, $= \frac{c}{f}$ [m]
λ second viscosity coefficient [kg m^{-1} s^{-1}]
λ_T Taylor length scale [m]
μ first viscosity coefficient or dynamic (molecular) viscosity [kg m^{-1} s^{-1}]
μ_B bulk viscosity [kg m^{-1} s^{-1}]
ν kinematic viscosity [m^2 s−1]
ρ fluid density [kg m^{-3}]
ρ_{xy} Correlation coefficient (normalized Covariance) for the random variables x(t) and y(t)
σ standard deviation
σ Stefan-Boltzmann constant = $5.67 \cdot 10^{-8}$ [W m^{-2} K^{-4}]
$\bar{\sigma}$ stress tensor [kg m^{-1} s^{-2}]
τ generic $\Delta\tau$ time separation [s]
τ transmissivity [−]
$\bar{\tau}$ viscous stress tensor [kg m^{-1} s^{-2}]
τ_0 maximum $\Delta\tau$ of the Cross-Correlation function [s]
τ_a acoustic time [s]
τ_c convective time [s]
τ_t turbulent time [s]
τ_{ch} chemical time [s]
ω vorticity [s^{-1}]

ω	$\frac{2\pi}{T} = 2\pi f$; pulsation or angular frequency [rad s^{-1}]
$\dot{\omega}_k$	volumetric rate of production [kg m^{-3} s^{-1}]
$\dot{\omega}_T$	heat release due to combustion per unit volume [W m^{-3} = J m^{-3} s^{-1} = kg m^{-1} s^{-3}]
$\dot{\omega}_i$	reaction rate (production/destruction rate) of species *i* [kg m^{-3} s^{-1}]
$\dot{\omega}_R$	reaction rate [mol m^{-3} s^{-1}]

Subscripts

a	acoustic
b	burnt (gases)
c	convection
f	flame, reacting region
g	mixture gas
p	hot products
R	cold reactants
r	chemical reaction
rad	radicals
ref	reference quantities
rms	root mean square
s	chemical species
S	surrounding space
t	total
u	universal
u	unburnt (gases)
∞	quantities in unperturbed flow
0	reference quantities

Superscripts

*	dimensionless quantity
0	formation quantity
′	fluctuation quantity

Acronyms

ACC	Active Combustion Control
AE	Acoustic Energy
AEE	Acoustic Energy Equation
APE-RF	Acoustic perturbation equations for reacting flows
CAA	Computational Aero-Acoustics

CARS	Coherent Anti-Stokes Raman Scattering
CCA	Computational Combustion Acoustics
CRZ	Central Recirculation Zone formed by swirling flow
DCM	Direct Computational Methods
DFWM	Degenerate Four Wave Mixing
DLE	Dry Low Emissions
DLN	Dry Low NOx (i.e., lean-premixed combustion technologies)
DNS	Direct Numerical Simulation
DOE	U.S. Department of Energy
e.g.	*exempli gratia*
EC	European Commission
ENEA	Italian National Agency for New Technologies, Energy and Sustainable Economic Development
EU	European Union
EVI-GTI	European Virtual Institute – Gas Turbine Instrumentation
FBG	Fiber Bragg Gratings
FDF	Flame Describing Function
FE	Fluctuation Energy
FEE	Fluctuation Energy Equation
FFT	Fast Fourier Transform
FPI	Fabry-Perot Interferometer
HCRV	helical central recirculation vortex,
HFD	High-frequency dynamics
HiTAC	High Temperature Air Combustion
HOV	helical outer vortex,
HP	High Pressure
ICCD	Intensified Charge-Coupled Device camera
IEA	International Energy Agency
i.e.	*id est*
IGCC	Integrated Gasification Combined Cycle
IP	Intermediate Pressure
IR	infrared light (750 –1000000 nm = 0.75 – 1000 μm)
l.h.s.	left-hand side
LBO	lean blow-off
LFD	Low-frequency dynamics
LDV	Laser Doppler Velocimetry
LES	Large Eddy Simulation
LIF	Laser Induced Fluorescence
LII	Laser Induced Incandescence
LMS	Least-Mean-Square Algorithm
MFD	Mid-frequency dynamics
NIR	near infrared light (750 –1400 nm)
OASPL	OverAll Sound Pressure Level, total radiated sound power
OEM	Original Equipment Manufactures
PDA	Phase Doppler anemometry
PIV	Particle Image Velocimetry

PIWG	Propulsion Instrumentation Working Group Consortium
PLIF	Planar Laser Induced Fluorescence
PRI	pseudo-Rayleigh index
PTV	Particle Tracking Velocimetry
PVC	precessing vortex core
r.h.s.	right-hand side
r.m.s.	root mean square
RANS	Reynolds Averaged Navier-Stokes
SOI	Silicon-On-Insulator
SPL	Sound Pressure Level
SRS (or SpRS)	Spontaneous Raman Scattering
Syngas	Synthesis gas: a variable mixture of primarily hydrogen and carbon monoxide.
TBL	Turbulent Boundary Layer
TDLAS	Tunable Diode Laser Absorption Spectroscopy
UHC	unburned hydrocarbon fuel
UV	ultraviolet light (190 – 370 nm)
VIS	visible light (370 – 750 nm)

Abstract

Gas turbine engines for power generation and propulsion applications have traditionally used diffusion-flame combustors because of their reliable performance and reasonable stability characteristics. Unfortunately, this type of combustor usually produces unacceptably high levels of thermal NOx. The increasingly strict regulation for pollutant emissions has recently led engine manufacturers to develop combustors that meet various regulatory requirements. New concepts for combustion technology have been introduced to the Gas Turbine industry, including lean-premixed combustion.
Lean-premixed combustion appears to be the most promising technology for practical systems at the present time. In lean-premixed combustion, the fuel and air are premixed upstream of the combustor to avoid the formation of stoichiometric regions. The combustion zone is operated with excess air to reduce the flame temperature; consequently, thermal NOx is virtually eliminated.
Unsteady flow oscillations, also referred to as combustion instability, however, have emerged as a common problem, and hindered the development of lean-premixed combustors. These oscillations may reach sufficient amplitudes to interfere with engine operation, and in extreme cases, lead to failure of the system due to excessive structural vibration and heat transfer to the chamber. The associated pressure oscillations and possibly enhanced heat transfer can lead to a deterioration in the system performance, and may be sufficiently intense to cause structural damage.
Combustion instability remains a critical issue limiting the development of low-emission, lean-premixed Gas Turbine combustion systems.
Combustion oscillations are not limited to gas turbine engines. They have been observed in the development of virtually all propulsion systems, including liquid rocket engines.
The system usually operates near the lean blowout limit, then a small perturbation in the equivalence ratio may produce a significant variation in heat release, which, if it resonates with the chamber acoustic wave, can result in large excursions of combustion oscillations. The phenomenon may be defined as the unsteady motions in a dynamic system capable of sustaining large oscillations over a broad range of frequencies.
The work is organized in two parts: an extensive bibliographic review of combustion instabilities and the motivation of this work in **part 1**; and the study about a new diagnostic methodology for thermoacoustic instabilities detection and future control in **part 2**. The part 1 is important because of lack of books that describe clearly and exhaustively the complex phenomenology of thermoacoustic instabilities, however the experts of thermoacoustic instabilities can skip directly from it to part 2 where is possible to find the improvements with respect to the state of the art.

The **part 1** is organized into five chapters. The **chapter 1** gives a general background about modern Gas Turbine engine and shows the need of new sensors for measurements systems. The **chapter 2** explains the characteristic of combustion noise, investigates the mechanisms driving combustion instabilities, the causes of instabilities and damping processes, and then provides a comprehensive review of the advances made in thermo-acoustic instabilities. The physics of combustion oscillations, most commonly caused by a coupling between *acoustic waves* and *unsteady heat release*, are discussed, and the concept of using feedback control to interrupt these interactions is introduced. The **chapter 3** provides a survey of recent progress in passive and

active control of combustion instabilities. The objective is to optimize combustor operations, monitor the process and alleviate instabilities and their severe consequences. It contains a review of some facets of combustion and focuses on the sensors that take or could take part to combustion control solutions. The **chapter 4** provides a critical review of analytical and numerical models and criteria for combustion instability. The **chapter 5** shows an application of instability control to real heavy duty Gas Turbine of Vx4.3A Siemens-Ansaldo. It shows the final purpose of the studies about thermo-acoustic instability and one of the industrial fields where the new technique ODC proposed here could be easily applied.

The **part 2** is organized into three chapters. The **chapter 6** explains the conventional optical techniques for concentration of chemical species, velocity measurements and temperatures, and then it gives a theoretical approach for thermal emission of flames. The **chapter 7** proposes a new diagnostic technique named *ODC* (*Optical Diagnostics of Combustion*) developed and patented in ENEA and it shows an experimental approach for radiative emission of flames. Radiant energy spectra have the same dynamics of Turbulence (macroscale, inertial and dissipative ranges; slope= -5/3) and reveal Chemical Kinetics high frequency effects. The chapter also explains why Radiant Energy shows Turbulence dynamics. The **chapter 8** shows the results and gives an experimental proof that real-time information of combustion instabilities and mean velocity component can be performed by analyzing Radiant Energy captured by means of photo-diodes (ODC). It investigates the use of flame Radiant Energy signal: due to its relation with both Turbulence and Chemical Kinetics, it may reveal the state of a flame and the eventual instability precursor events. It shows experimental analysis of turbulent premixed combustion by means of ODC to laboratory and industrial burners. A collection of radiative emissions by several flames is analyzed in this chapter. Such flames have been obtained in a number of burners in a large range thermal power (i.e., 3 kWt-1MWt), either premixed or not, fed with different fuels (i.e., methane, hydrogen, oil) and with different physical states (i.e., gas and liquid fuel), while radiative emission is collected by means of a photo-diode. The purpose of this chapter is to show that the usefulness of measurements of Radiant Energy emission from flames can be enhanced by focusing on a spatially limited region, by means of the *auto-correlation* and *cross-correlation* of signals from two points.
Finally it shows the fulfilment of a test facility for real burner in ENEA Research Center, i.e., *COMET-HP* (*COMbustion Experimental Tests in High Pressure*), 1 MWt premixed CH_4/Air and gives several experimental tests.
Concluding, a new optical instrument based on photo-diodes, called ODC, has been applied for thermoacoustic instability analysis. *ODC* provides information at very low cost and in real time about turbulent and chemical scales.

Lastly five attachments conclude the PhD thesis. The **attachment A** shows Lighthill's theory and acoustic analogy whereby the governing equations of motion of the fluid are coerced into a form reminiscent of the wave equation of "classical" (i.e. linear) acoustics. The **attachment B** provides a brief explanation of random signals, e.g. random vibrations, and spectra analysis, according to which a periodic function can be broken down into its harmonic components. The **attachment C** presents an analytical treatment of acoustic signals. The **attachment D** gives a theoretical approach for thermodynamic equations. Turbulent combustion is a multi-scale problem where complexity lies in the interaction between fluid dynamics and chemistry. This attachment provides a theoretical understanding of some of the scale physics in turbulent reacting flows. The

attachment E provides laws for thermal radiation. At high temperatures thermal radiation is the main mode of heat transfer.

Part 1: BIBLIOGRAPHIC REVIEW

I. Background about modern gas turbine engine

I.1 Introduction

Combustion systems are among the most challenging technologies to study. There are not only high temperatures, but usually very high temperature gradients ranging from the incoming reactants at ambient temperature up to flame temperatures. The fluid flow is typically turbulent and may include swirl. The heat transfer includes conduction, convection and radiation. The radiation is further complicated by the spectral nature of gaseous combustion products. The chemistry is extremely complicated, where the combustion of a relatively simple fuel like methane can involve hundreds of chemical reactions and dozens of species.
The fuel composition can vary widely and may contain multiple components, waste products, and sometimes multiple phases, depending on the process. The length scales in industrial combustion process may vary by orders of magnitude, ranging from millimetres for fuel injection ports up to meters for the combustor itself.
The materials being heated may be solids, liquids or gases and have a wide range of properties.
The field of industrial combustion is very broad and touches, directly or indirectly, nearly all aspects of our lives. The electronic devices we use are generally powered by fossil fuel fired power plants. The cars we drive use internal combustion engines. The planes we fly in use jet fuel powered turbine engines.
As the science of combustion combines heat transfer, thermodynamics, chemical kinetics and multiphase turbulent fluid flow to name a few areas of physics, the study of industrial combustion is interdisciplinary by necessity.
Most of the energy (86%) is produced by the combustion of fossil like petroleum, natural gas and coal. According to *U.S. Department of Energy* (DOE), the demand in the industrial sector is projected to increase by 0.8% per year to the year 2020 [I-1].
Pollution regulations vary by location and continue to get more rigorous. Technology continues to improve as the emission requirements get more stringent.
The *U.S. Department of Energy* sponsored a workshop to develop a roadmap for industrial combustion technology. The resulting report ([I-2], [I-3]) identified the following priority research and development needs:

- Determine advanced methods to maintain a stable flame and achieve low emissions while using different fuels.
- Develop a burner capable of adjusting operating parameters in real time.
- Develop real-time sensors and process controls that are more reliable and robust in harsh environments.
- Develop computational tools that are more accurate in a wide variety of applications through the collection of physical data and model validation.
- Create a pathway to demonstrate and commercialize new technologies and enable information sharing throughout industry about new technologies.
- Develop robust design tools that are more user-friendly and accurate, especially with complex phenomena such as turbulence and create a unified code to allow sharing of information more easily and speed development.

A key aim within Europe and the rest of the world is the cost-effective production and use of energy with reduced emissions at local and global levels. This will be achieved in part by increasing the efficiency of fossil fuel based energy conversion processes, and in part by increasing the utilisation of new and renewable energy sources in the energy system.
The European Commission (EC) has set targets for the development of gas turbines, to achieve in the long term >65% combined cycle efficiencies and >35% simple cycle efficiencies for small scale gas turbines.
To achieve these higher cycle efficiencies, gas turbines are required to operate at higher firing temperatures and higher operating pressures. Firing temperature has an impact on the emission of thermal-NO_x, where NO_x production becomes significant at flame temperatures above around 1800 K. In order to achieve low NO_x emissions, below 25 ppmv (15% O_2, dry), without the use of diluent injection, two elements are required:

- Firstly, a near homogenous air/fuel mixture should be provided prior to combustion (premixing), to ensure locally uniform and low reaction temperatures.
- Secondly, the reaction zone should be operated well away from stoichiometric conditions i.e. fuel lean.

Due to its simplicity, efficiency and reliability, the lean premix combustion approach, known also as *Dry Low Emissions* (DLE), has become the industry standard for achieving the emission targets of modern gas turbines.
However, the lean-premix combustion technique is susceptible to combustion induced *thermoacoustic pressure pulsations*, or oscillations, due the reduced local reaction temperatures.
In the last thirty years noise emission has developed into a topic of increasing importance to society and economy. In fields such as air, road and rail traffic, the control of noise emissions and development of associated noise-reduction technologies is a central requirement for social acceptance and economical competitiveness. The noise emission of combustion systems is a major part of the task of noise reduction. The following aspects motivate research [I-4]:

- Modern combustion chambers in technical combustion systems with low pollution exhausts are 5-8 dB louder compared to their predecessors. In the operational state the noise pressure levels achieved can even be 10-15 dB louder.
- The combustion emissions become a more and more important topic for modern gas turbine engines and for airplanes. The combustion instability and noise issues are one major obstacle for the introduction of green technologies as lean fuel combustion and premixed burners in aero-engines. The direct and indirect contribution of combustion noise to the overall core noise is still under discussion. However, it is clear that the core noise besides the fan tone will become an important noise source in future aero-engine designs.
- The development of layout tools for “quiet” technologies requires calculation methods for predicting of sound power in new technical products.

I.2 General background about world electricity generation by fuels

World's ever increasing energy demand poses great challenges to power generation in the future. In reference scenarios of the *International Energy Agency* (IEA) [I-5] and the *U.S. Department of Energy* (DOE) [I-1], the electricity generation is projected to double in the next 25 years. Although the portion of renewables has to increase dramatically, at least in a mid-term perspective, i.e., until 2050, be covered by fossil fuels ([I-6], [I-7])
In the IEA and DOE reference scenarios, gas turbines, especially in combined cycle power plants, are one of the key technologies with a projected share of 25% of the total power generation in 2030, as shown in Fig. I-1. Coal-fired power plants are expected to deliver 45%. Other studies see gas turbine power plants even at 30-40% in 2030 [I-8].

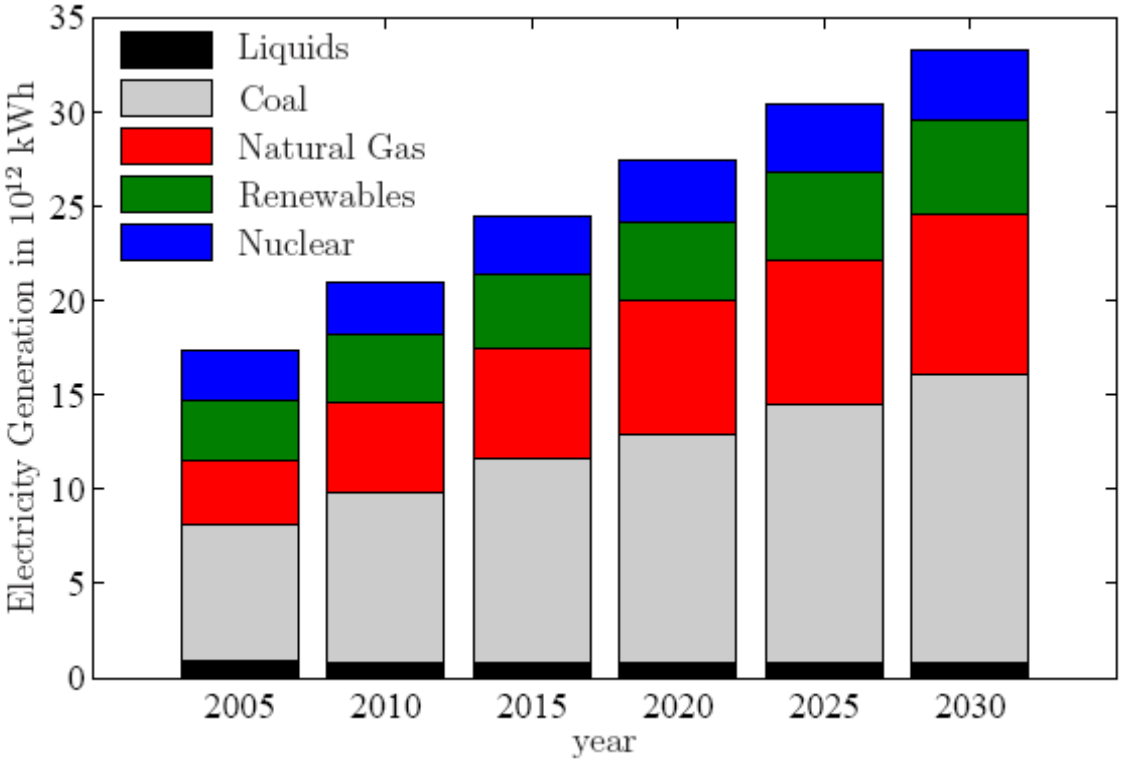

Fig. I-1: Energy mix of world electricity generation by fuels (reproduced from data in reference [I-1] and [I-7]).

Both the IEA and the DOE scenarios are based on the assumption of a continuation of present policies. It is, however, to be expected that emission restrictions will get even more stringent in the future. Gas turbines feature emission characteristics that are by far better than those of coal-fired power plants. This includes CO_2, NOx, and SO_2. Compared to coal-fired plants, gas turbines in combined cycle operation achieve a CO_2 reduction of approximately 50%. This is due to the lower carbon content in natural gas and a higher efficiency, which for combined cycle plants reaches a value of nearly 60% compared to 45% for coal-fired power plants. Therefore, either the

percentage of gas turbines in the energy mix might increase, or parts of the coal-share might be replaced by renewables and the gas turbine portion will be at 25% [I-7].
The *German Federal Ministry of Economics and Technology* [I-8] stated that today gas turbines in single and combined cycle power plants account for more than 50% of the power of new installed plants worldwide.
Besides better emission characteristics and a higher efficiency, gas turbine power plants exhibit several other advantages. These are lower specific investment costs compared to other technologies, flexibility in terms of peak-, part-, and base-load operation, as well as fast installation and amortization times and a smaller footprint [I-7].
Also, the increase of installed power generated by wind power plants, a fast growing industry, is up to now accompanied by an increase of the installed power of fossil power plants, i.e., mainly gas turbines. This is necessary in order to be able to compensate the power outage in case of an unsteadiness of the wind.
The remarks made in this section underline the importance of gas turbines in the energy mix and thus the importance of getting the problem of thermoacoustic instabilities, which are one of the main issues for gas turbine manufacturers, under control.

I.3 Thermodynamic cycle of modern gas turbine engine

Combustor chambers and turbine first stages are well-known as “black” zones because of the lack of good data due to sensor difficulty to survive and maintaining traceable calibration. Accurate temperature measurements in the first stages of the HP (High Pressure) and IP (Intermediate Pressure) turbine are critical for cooling system design and combustor performance assessment, uncertainty of ± 10 K affects the specific fuel consumption of 0.2%. Temperature and pressure ranges at the combustor exit/HP first stator can be as high as **45 bar** pressure for **propulsion gas turbines**, with temperature higher than **2300 K**; at the same location for **energy generation gas turbines** pressure of **20 bar** and **temperature up to 2000 K** are typical.
Then engine performance assessment requires accurate measurements of total pressure, total temperature and gas composition. The hostile environment where the probe is immersed reduces the life of the sensor and induces quick modification of the properties of the materials, therefore changing the calibration and decreasing the accuracy.
In term of gas path measurements for steady stagnation pressure and temperature a good target for the developers is achieving **0.4% of the reading for temperature measurements** and maintaining a **0.05% FS (full scale) for pressure**, where the range of applications will be increased to working temperature above 1500 K assuring reliability, constant calibration and long sensor life (ultimate aim is over 20000 hours).
The *Turbine Inlet Temperature* (TIT) is a critical parameter of Gas Turbine systems influencing both material and coating lifetime of turbines as well as their efficiency. It is well-known that turbine entry temperatures have been steadily increasing over the years in order to increase the thermodynamic cycle efficiency. Over the last 3 decades or so, the turbine entry temperatures have increased by approximately 400°C. Clearly this has put increasing demands on all the materials used for hot section components, including the sensor and sensor packing materials. It should be noted that is not clear whether this trend will continue due to restrictions imposed by EU (*European Union*) regulations on the formation of oxides of nitrogen (NO_x). Hence the

turbine entry temperatures can not continue to be increased indefinitely without contravening the goals set by the EU.

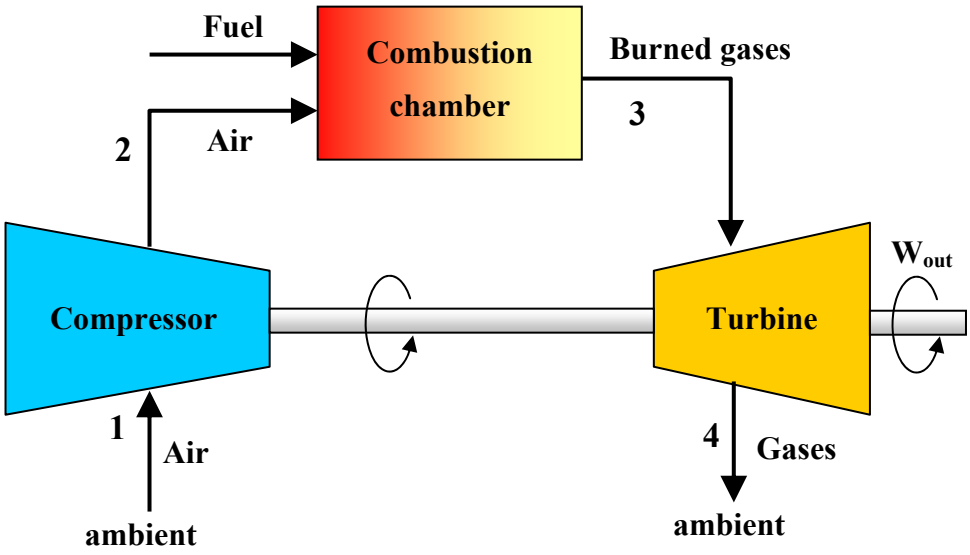

Fig. I-2: Ideal open end Brayton Cycle diagram

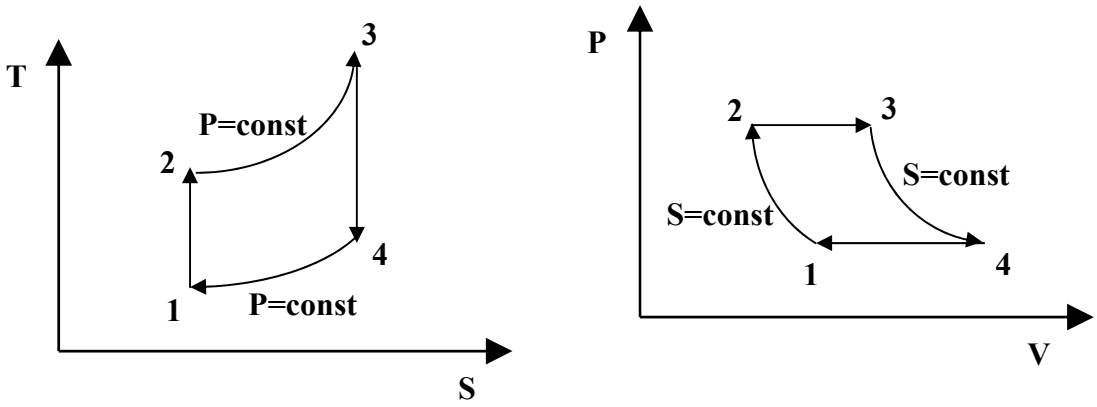

Fig. I-3: Brayton cycle (T/s and P/V diagrams)

Temperatures within the gas turbine engine involve an operating range from ambient at inlet to the fan (compressor, 1), with the maximum at the combustor exit (3) where gas temperature can exceed 2000 °C (see Fig. I-3). Thus the challenge to the sensor developer is the most extreme for components and flow from the compressor discharge (2) and through the high pressure turbine (3).

I.3.1 Fuel and oxidizer: mixing type in combustion burners

Depending upon many factors, certain types of fuels may be preferred for certain geographic locations due to cost and availability considerations. Gaseous fuels, particularly natural gas, are common used in most industrial heating applications in Europe and United States. In Asia and South America, heavy fuel oils are generally preferred although the use of gaseous fuels is on the rise. Fuels also vary depending on the application.
The fuel choice has an important influence on the heat transfer from a flame. In general, solid fuels like coal and liquid fuels like oil produce very luminous flames that contain soot particles that radiate like blackbodies to the heat load. Gaseous fuels like natural gas often produce nonluminous flames because they burn so cleanly and completely without producing soot particles. A fuel like hydrogen is completely nonluminous as there is no carbon available to produce soot.
The predominant oxidizer used in most industrial heating processes is atmospheric air. This can present challenges in some applications where highly accurate control is required due to the daily variations in the barometric pressure and humidity of ambient air. The combustion air is sometimes preheated and sometimes blended with some of the products of combustion, which is usually referred to as flue gas recirculation. For the case of air preheat the adiabatic flame temperature will be increased and result in a subsequent increase of the cycle thermal efficiency. Combustion with ***High Temperature Air Combustion*** (**HiTAC**) has been shown to provide potential for many engineering realities for the twenty-first century.
One common method for classifying burners is according to how the fuel and the oxidizer are mixed:

- In *premixed burners* the fuel and the oxidizer are completely mixed before combustion begins, than the oxidizer is mixed with the fuel before it reaches the flame front. This creates a thin flame front as all of the reactants are readily available. Premixed burners often produce shorter and more intense flames, compared to diffusion flames.
- A *diffusion flame* is a flame in which the oxidizer combines with the fuel by diffusion. As a result, the flame speed is limited by the rate of diffusion. Diffusion flames tend to burn slower and to produce more soot than premixed flames because there may not be sufficient oxidizer for the reaction to go to completion, although there are some exceptions to the rule. The soot typically produced in a diffusion flame becomes incandescent from the heat of the flame and lends the flame its readily identifiable orange-yellow colour. Diffusion flames tend to have a less-localized flame front than premixed flames.

I.4 Theory and experimental observations

It is extremely important to pay attention to the experience gained in the laboratory as well as in full-scale tests of devices. *Theory* is an indispensable aid to making sense of observational results. Conversely, discussion of various *experimental observations* is a natural place to introduce many of the basic ideas contained in the theory. For practical purposes, the theory often serves most successfully when used to analyze, understand, and predict trends of behaviour, thereby also

providing the basis for desirable changes in design. Experimental data are always required to produce quantitative results and their accuracy in turn is limited by uncertainties in the data.
Fluid flow can be studied in a number of ways: complete experimentation, fully theoretical studies (via modelling) or computational fluid dynamics (CFD) which studies the fluid flow, and predicts heat transfer, mass transfer, chemical reactions, and related phenomena by solving governing mathematical equations using a numerical process. There is a key link between measurements provided by sensors and the result of CFD analyses. Engineering data is used for conceptual studies of new designs (Fig. I-4) and in detailed gas turbine engine development.
CFD is relatively low in cost, as using only physical experimental testing to get all essential engineering data for design can be expensive. The CFD simulations are relatively inexpensive, and costs decrease as tools become more powerful. CFD allows the analyst to examine a large number of locations in the region of interest, and yields a comprehensive set of flow parameters for examination.

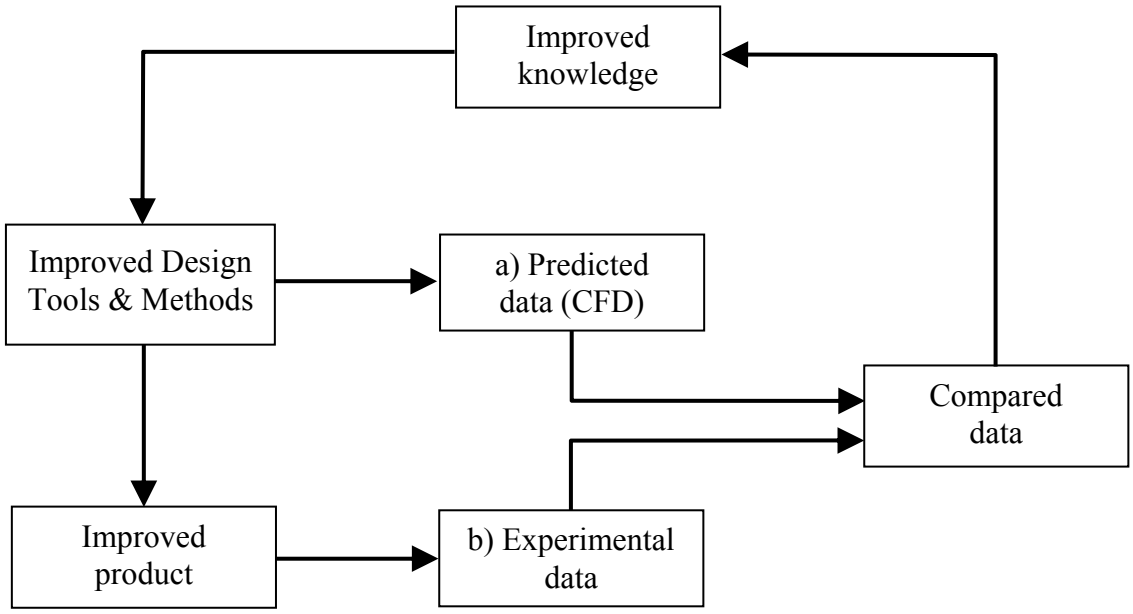

Fig. I-4: Experimental test and design cycle

In terms of a better understanding of turbulent combustion and in terms of providing experimental data for validation of numerical simulations it is crucial, in general, to vary parametrically Reynolds number, equivalence ratio, fuel composition, pressure and swirl intensity.

I.4.1 Testing

There are numerous reasons why tests are conducted in industrial combustion process:

1. Initial new product development is sometimes done at a reduced scale to *minimize costs and risks*. When the product is close to commercialization, large-scale (preferably full-scale) tests are required to validate the technology. End users are not likely to use a new technology until

it has been validated at or near full scale, although they may be willing to do validation testing if the risk is low enough and the reward is large enough.
Testing can be done to determine equipment performance. Performance is a broad term that can encompass many different elements. For burners, some important measurements may include pollution emission (e.g., NO_x, CO), turndown range (minimum and maximum firing rates), fuel variability (e.g., hydrogen content), noise, flame shape (length and cross section), heat flux profile, waste destruction capability for waste fuels, and flame stability (a subjective parameter).

2. Testing may be done to generate data that can be used to *validate computer models*. Nearly all models involve some level of simplification because it is normally prohibitive in terms of time and cost to model the exact physics and because the exact physics are not always known. Experimental validation must be done to show how well models match actual measurements. However, this means the variability in the experimental measurements must be accurately quantified, so the comparisons with modelling results can be fairly judged.
3. Testing is sometimes used to *develop empirical models* that can be used to predict equipment performance. Then, the performance for any size can be extrapolated from the empirical data, without the need to test every possible size.
4. Testing can be used to *validate new experimental techniques*. For example, the optical techniques have been tested against more traditional and well-established techniques such as wire thermocouples and pyrometers.

There are relatively few industrial-scale combustion test facilities outside of equipment manufacturers. A report prepared from a workshop sponsored by the U.S. Department of Energy stases: *"For the most part, the size and type of laboratory test equipment available are inadequate, and the costs are prohibitive"* ([I-2] § p.11)

I.5 Need of new sensor for measurement systems

Applications for gas turbine engines have proliferated after World War II and have been key technology contributors to the expansion of modern aero propulsion in commercial flight, operation of ocean and sea vessels, military aircraft, as well as industrial gas turbine power generation. Over time technical challenges have emerged with higher and expanded expectations for improved performance and still better cycle efficiencies. Improvement in engine efficiency has recently acquired even greater focus because of dwindling fossil fuels and increased global warming.
The need to reduce the consumption of hydrocarbon fossil fuel energies and greenhouse gas emissions are worldwide imperatives that drive the gas turbine industry to continue to improve performance. Greater thermodynamic cycle efficiency cannot occur without engines operating at higher temperatures.
Higher cycle temperatures and pressure brings **new challenges to the instrumentation community** for better measurement methods and development of new approaches and innovation in test technology.
Today new sensors and measurement techniques are needed to provide for high temperature hot section analyses and characterization and that data used to improved CFD and engine modelling tools.

The design, development, and fabrication of new sensors and measurement systems for product characterization to support field service problem evaluations as well as new component and centreline engine qualification and certification are an ongoing focus area.
New sensor and measurement technology can provide one of the greatest opportunities to optimize the engine component efficiencies and allow higher operating temperatures. **Simplicity in application** and **durability** in operation are two important goals for any new sensor or measurement system.

I.5.1 Sensor development requirements

Research activity, aimed at improving the capability of measuring devices in gas turbine, has been recently funded by the European community through a project called **HEATTOP** (*Accurate **H**igh Temperature **E**ngine **A**ero-**T**hermal Measurements for Gas **T**urbine Life **O**ptimisation, **P**erformance and Condition Monitoring*). It was a 9 million euro project within the framework 6 (FP6) program, in the aeronautic and space section. The project has started on 1 August 2006, it lasted for three years and it is due to complete in April 2010. It was a collaborative research project, which aims to develop new, more durable, more accurate instrumentation for high temperature gas turbine applications. This project targets the development and improvement of instrumentation to measure pressure, temperature (gas temperature, surface temperature, blade temperature), flow and tip clearance in gas turbines.
Accurate hot gas path measurements (including combustion diagnostics) are recognized as a major need for the assessment of engine component health and performance. Cost of data acquisition and test affordability are probably the biggest concerns for all gas turbine engine programs and OEM (*Original Equipment Manufactures*) management across the industry landscape.
These facts have been highlighted in a recent study, "The Lab Gap Matrix", carried by *European Virtual Institute – Gas Turbine Instrumentation* (EVI-GTI) [I-9].
The sensor and measurement requirements have been defined by both the European Union *European Virtual Institute – Gas Turbine Instrumentation* (EVI-GTI) organization and the United States *Propulsion Instrumentation Working Group Consortium* (PIWG) [I-10]. A more concerted and cohesive effort is being made to better communicate the needs of the entire EU and US communities to small business suppliers and developers to more effectively address these topics of interest especially high temperature requirements.
The so called *"Lab Gap Matrix"* has been set-up following the inputs of engine OEM's (*Original Equipment Manufactures*), research groups, small business developers and instrumentation vendors to indentify the gaps in the instrumentation capability for measuring in gas turbines and aero-engines.
Besides the interest to validate numerical predictions of engine performance, efficiency, and component life, the availability of high temperature steady and unsteady pressure and temperature data would also enable much progress in the field of condition monitoring and active control technologies. The gas turbine environment is a very challenging place for instrumentation given the extremes of pressure and temperature and the wide operating range required.
Combustion chamber or high pressure turbine sections of gas turbines are probably amongst the most hostile environments to perform measurements. Regarding flow conditions at those

locations, the highest pressure and temperature of the latest aero-engine thermodynamic cycles exceeds **50 bar** and 2000 K, even **up to 2200 K peak temperature**.
Due to limitations of current experimental techniques and of the severe flow conditions, the measurement of pressure and temperature in the hot sections of modern gas turbines still remains a true challenge for test engineers.

I.5.1.1 High temperature pressure sensors for gas turbine applications

Over the last three decades there has been a requirement to measure time-varying pressures in turbomachinery applications which have necessitated measurement bandwidths in the order of 100 kHz.
The requirement to locate pressure transducers in increasingly hostile environments that has led to the development of high temperature pressure transducers. Future developments aimed at increasing the maximum operating temperature of pressure sensors.
High temperature pressure transducers are primarily used in research or development engines and component rig testing for several purposes:

- to validate the design methods and develop the engine/component,
- to gain an understanding of the product performance and behaviour,
- to demonstrate that the product complies with the certification and regulatory requirements.

High temperature pressure transducers are also routinely used in-service for the measurement of combustion instabilities in industrial gas turbine where the use of very lean fuel/air mixtures, which are required to achieve economical operation, can be accompanied by combustion instabilities which must be minimized to avoid structural damage. In the future, high temperature dynamic pressure transducers are likely to be used in production aero gas turbine.
High performance pressure transducers have been around since 1960's. The latest evolution of high temperature leadless transducers, utilizing *Silicon-On-Insulator* (SOI) technology, enabled transducer operability in many harsh environments.
Despite the capability of the latest SOI based technology piezoresistive pressure transducers to withstand temperatures up to 600°C, there are regions of a gas turbine where dynamic gas path pressure are required to be measured which are significantly hotter. A modern high pressure compressor outlet temperature typically exceeds 750°C and the gas temperature in the high pressure turbine can exceed 1400°C. In these ultra high temperature environments the preferred way of measuring these small dynamic pressure reliably is to use either a flush-diaphragm transducer mounted in a water or air cooled jacket, which requires the supply of cool water or air and, although very effective, may be impractical, or the use of a non-resonant *Semi-Infinite Tube* (SIT) system which removes the pressure transducer from the very hot environment by a distance of up to 1 metre [I-11].
Manufacturers are currently researching a range of different materials and glasses in order to extend the maximum operating temperature of the leadless packaging and cables from 700°C to at least 900°C in order to realise the full potential of the silicon carbide based pressure transducer technology.
Measurement of the dynamic pressure within the combustor of a gas turbine engine requires a probe which can provide reliable data at high temperatures. Its calibration must be thermally

stable, or at least must be easily correctable for temperature variations, and it must have a small temperature sensitivity. They are expensive and often difficult to use. The chief problem is that the mechanical and electrical properties of most common transducer materials change rapidly with temperature as combustion temperatures are approached. Special materials must be used just to ensure the mechanical and electrical survivability of the transducer. The extremely limited availability of high-temperature dynamic pressure calibration sources added to the high initial cost and the necessity for post-processing of data make the routine use of this type of transducer unattractive.

I.5.2 Materials for high temperature and gas turbine operation life

In general **operating service above 540 °C is defined as high temperature for gas turbine engines**. More specifically, materials which operate at such temperatures consist principally of various stainless, nickel based super alloys, cobalt based alloys, refractory metals, precious metals, monolithic ceramics, metal matrix composites, and ceramic matrix composites. The applications of these high-temperature materials are found in combustors, turbines, and exhaust systems in aircraft propulsion engines and industrial gas turbine.
In order to perform successfully at high temperatures, a material must have at least two essential characteristics:

1. it must be of high strength at temperature, since increasing temperature tends to reduce integrity,
2. it must have resistance to its environment, since time dependent creep, chemical activity, oxidation, and corrosion increase significantly with temperature.

New turbine component materials necessitate new sensors and measurement systems that can also operate at very high temperatures.
Sensor and measurement systems must be robust, reliable, and the expectation is that the sensors can be reused and reapplied to other following test articles. Ultimately the hope is that the sensors would have infinite life and durability.
The durability of a sensor or measurement device may be directly tied to performance or more importantly identify issues regarding equipment safety. **Land power generation turbines can operate 24 hours a day and in one year complete 8760 hours of operation.** Every hour of downtime for any gas turbine engine whether power generation or aero propulsion is an hour of lost revenue as well as the cost of maintenance and overhaul.

I.5.2.1 Sapphire crystal for combustion applications

The core of the technology is the sensor head which can be fabricated from sapphire (e.g. ODC; [I-12]). Sapphire is a single crystal aluminium oxide which is the hardest form of the oxide crystals, is chemically inert and is an electrical insular.
Sapphire has been selected largely for its high temperature performance but in addition for its chemical durability and thermal properties which are well matched to suitable packaging materials.
Summering, the sapphire is:

- well known engineering industrial material;

- available in multiple form and widely available (many high temperature applications, e.g. sapphire light-guides and high temperature windows);
- excellent chemicals, mechanical and high temperature proprieties;
- inert to chemical attack.

The proprieties of a number of optical and packaging materials can be seen in the Tab. I-1:

Material	***Melting point*** [°C]
Sapphire	2053
Alumina	2037
Silicon Carbide	1825
Silicon	1415 (with plastic deformation > 600°C)
Hastelloy	1340-1390

Tab. I-1: Optical sensor and packaging materials.

Measurements of the heat release fluctuations can be carried out using an optical system consisting of a sapphire fibre sensing the CH intensity emissions (wavelength = 430 nm, $\Delta\lambda$ = 10 nm) from the flame front ([I-13], [I-14]). The light beam can be sent through a convex lens to a filter and through another convex lens to a photodiode.

I.6 Combustion species emissions

In the last three decades, environmental restrictions have been implemented to reduce emissions from power generation and propulsive devices. A primary focus has been to reduce the **nitrogen oxides** (**NO_x**) emissions. "NO_x" refers to the sum of **NO** (**nitric oxide**) and **NO_2** (**nitrogen dioxide**), which have long been identified as harmful atmospheric pollutants, contributing to acid rain production, photochemical smog and ozone depletion.
Burning of fossil fuels in power generation, transportation and industrial burners has been shown to be a major source of NO_x in the world. NO_x is primarily produced during combustion by the oxidation of atmospheric nitrogen in the high temperature regions (above 1850 K) of the post-flame gases where there is enough energy to overcome the high activation energy of the formation reactions of NO_x.
Stoichiometric burning creates the highest combustion temperatures, and since NO_x emissions increase exponentially with temperature, diffusion combustors produce high levels of NO_x (without water injection). Therefore, the engine manufacturers were compelled by emission regulations to make design changes.
Gas turbine engine exhaust gas emissions include **CO_2** and **H_2O** as well as **CO**, **NO_x**, **unburned hydrocarbon fuel (UHC)** and **smoke**. Gas samples are usually extracted from many points in the exhaust plume at the nozzle exit by a probe rake system, transported through many feet of heated tubing, and assessed by gas analyzers. Profiles of engine performance in terms of combustion

efficiency and fuel/air ratio indicate there are zones of incomplete combustion. Bulk averages of the multi-point samples are used to define the pollution emission indexes.

I.7 Turbulent combustion in a gas turbine combustor

The combustion process in a practical gas turbine combustor is always **turbulent**. There are several reasons why this is desirable:

- First, since turbulence encourages mixing of the fuel and air with each other and with the hot products of combustion, a turbulent flame is more compact. This permits the engine itself to be smaller and lighter. Next, the turbulent wake downstream of a swirler or behind a flame holder anchors the flame in a well-defined location.
- The enhanced mixing of the hot products of combustion with dilution air introduced downstream of the primary combustion zone leads to a shorter secondary zone and a more uniform temperature field entering the turbine.
- Turbulence-enhanced mixing ensures more complete combustion, thereby improving efficiency and reducing some harmful emissions.

Unfortunately, turbulent flames are inherently noisy.

I.7.1 Flame dynamics of lean premixed swirl injectors

Lean-premixed combustion technologies have been adopted by virtually every industrial gas turbine manufacturer as a *Dry Low* NO_x (DLN) method to meet emissions regulations which are being implemented in the US and in many regions worldwide. But to meet more stringent ultra-low emissions standards being proposed, the DLN combustors have to operate at conditions near the lean limit of their stability envelopes where noise, instability, fl ame blowoff, and flashback can seriously affect engine performance.
Fuel injection and mixing are critical to achieving efficient and clean combustion in modern gas-turbine engines, whether they are powered by gaseous or liquid fuels:

- For *gaseous fuels*, the major concern is to obtain an optimal level of mixing between air, fuel, and combustion products in the combustion zone.
- When *liquid fuels* are employed, they must be atomized into small droplets and then distributed in an airstream before entering the combustion zone.

Swirl is a key element in all gas-turbine engines and is used to create a region of high entrainment and mixing for the fuel-air mixture. Swirl also provides an *efficient mechanism to stabilize the flame* in a compact region without requiring a physical flame holder.
Most gas-turbine injectors employ swirl configurations that produce central toroidal recirculation zones to provide the dominant flame-stabilization mechanism. Flows in this region are generally associated with *high shear rates* and *strong turbulence intensities* resulting from vortex breakdown.
The inlet to the combustor typically contains a complex swirl-vane structure that induces a swirl to the hot air from the compressor. The airflow may be split into multiple streams and each stream swirled independently in either the counterdirection or the codirection. Fuel (liquid or gas)

is injected before, through or after these swirl vanes, and fuel-air mixing occurs in a highly turbulent, swirling flow.
Most technical combustion systems use turbulent premixed or non-premixed swirl flames with high volumetric reaction densities. To realize good ignition stability, especially, when using high air equivalence ratio to prevent thermal NO_x-emissions, the flow field is swirl stabilized. The swirl flow forms a *central toroidal inner recirculation zone* (CRZ) and causes a *longer residence time of reactive species* and enables the formation of short flames of high reaction densities with the benefits of *high ignition stability due to the recirculation of hot gases* ([I-15], [I-16]) and the achievable *low-pollution combustion*. Another advantage of premixed swirl-stabilized flames is the option to *reduce pollutant emissions of modern combustion systems* materialized in industrial, traffic, power plant and aircraft applications compared to diffusive flames by cost-efficient design solutions.
Basic research investigation of swirl flames is given by [I-17] and [I-18]. Swirl flows and flames tend to generate *periodic flow instabilities*, which lead to an *increasing noise emission* and *problem of flame stability*.
Combustion instabilities in swirl flames have been investigated intensively in the recent years ([I-4] § 2, [I-19], [I-20], [I-21], [I-22], [I-23], [I-24], [I-25], [I-26], [I-27], [I-28], [I-29], [I-30]) and they reveal the importance of coherent structures in the forward flow surrounding the inner recirculation zone. The existence and the influence of coherent structures on the noise emission of the flame and thus of the combustion system requires more physical knowledge to minimize combustion noise in modern industrial and aircraft applications already during the design process. Another disadvantage of swirl flames are their *high noise levels* caused by high reaction densities and amplified by the use of premixed flames in industrial furnaces.

I.7.1.1 Swirl number

In a typical swirl injector, the flow is deflected by an array of vanes positioned either *axially* or *radially* ([I-31], [I-32]), as illustrated in Fig. I-5. Both single and multiple swirlers have been employed to provide the desired fuel/air distribution for efficient combustion.

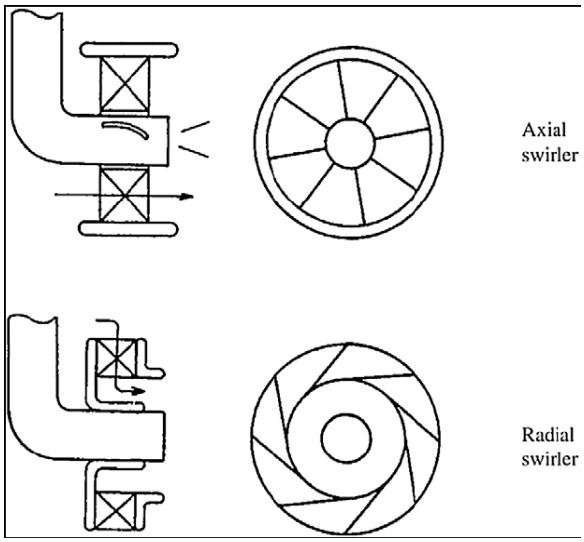

Fig. I-5: Schematics of axial and radial swirlers ([I-31], [I-32]).

The radial swirler performed better than the axial swirler, however, in emissions performance, despite an increased premixing length.
If the swirl strength is strong enough, as characterized by a nondimensional *swirl number S*, an internal recirculation zone could be established that recirculates hot product gases from downstream and serves as a reservoir of heat and chemical radicals to enhance flame stabilization. The existence and shape of this recirculation zone strongly influences flame stability.
Swirling flows have been widely used in industrial burners in order to increase fuel-air mixing and to improve flame stabilization. It has been shown that swirl can increase mixture homogeneity and shorten the characteristic time for NO_x formation and result in *lower NO_x emissions*. In fact, swirl increase can help the *reduction of temperature gradient* during the development of combustion reactions, also improving reactants pre-heating and leaning the mixture with respect to feeding conditions, positively influencing NO_x emissions at the exhaust, which resulted quite independent (almost in the lean regime) from the equivalence ratio fed to the burner.
In general, the extent of swirl is typically defined by the *swirl number* (*S*). Two different swirl numbers:

1) The ***formal definition*** of *S* is based on the ratio of angular to axial linear flow momentum [I-17]:

$$S = \frac{G_{ang}}{R_b G_x} = \frac{\int_0^\infty \rho U W r^2 dr}{R_b \int_0^\infty \rho \left(U^2 - \frac{1}{2} W^2 \right) r \; dr} \qquad \text{(I-1)}$$

where R_b is the burner radius (nozzle exit radius), r is the radial position, G_{ang} (=G_φ) is the angular momentum in the swirled section and G_x is the axial flux of axial momentum, then the linear momentum flux through the unswirled center core and the swirled annulus. These terms can be calculated by integrating the mean axial, U, and the mean swirl, W, velocity components across the burner exit.
Another formal definition of *swirl number* is ([I-33], [I-34]):

$$S = \frac{\int_0^{R_b} \left[U W + < uw > \right] r^2 dr}{R_b \int_0^{R_b} \left[U^2 - \frac{1}{2} W^2 + < uu > - \frac{\left(< vv > + < ww > \right)}{2} \right] r \; dr} \qquad \text{(I-2)}$$

where the Reynolds stresses involved were the normal stress in the axial direction <*uu*>, the normal stress in the radial direction <*vv*>, the normal stress in the tangential direction <*ww*>, and the shear stress in the tangential direction <*uw*>. The <·> is the averaging operator.
It is worth noting that the definition (I-2) of the *swirl number* is one choice out of a variety of swirl numbers in use ([I-35], [I-36]).
A second possible definition is given, for example, by neglecting the influence of turbulence in equation (I-2) [I-37]:

$$S = \frac{\int_0^{R_b} U W r^2 dr}{R_b \int_0^{R_b} \left(U^2 - \frac{1}{2} W^2 \right) r \; dr} \tag{I-3}$$

and a third possibility is given by ([I-35], [I-38]):

$$S = \frac{\int_0^{R_b} U W r^2 dr}{R_b \int_0^{R_b} U^2 r \; dr} \tag{I-4}$$

For a typical single-element injector (Fig. I-5) with a flat vane swirler the swirl number S can be defined as the ratio of the axial flux of the angular momentum to the product of the inlet radius and axial flux of axial momentum [I-32]:

$$S = \frac{\int_{Rcb}^{Rid} \bar{u} \; \bar{w} r^2 dr}{\int_{Rcb}^{Rid} R_{id} \bar{u}^2 r \; dr} \tag{I-5}$$

where R_{cb} is the radius of the centerbody, R_{id} is the radius of the inlet duct, u is the axial velocity and w is the azimuthal velocity.
Other parameters – such as inlet swirl-vane geometry, Reynolds number, confinement geometry, and inlet velocity (both mean and fluctuation) profiles – can all affect swirl effects.

2) The formal definition of swirl number is not convenient because velocity data are not usually available. For engineering applications, a swirl number definition based on the *geometry* of the device is more amenable. With the assumption that the distribution of the axial flow remains flat, and U and W at the burner exit are kinematically related to the blade angle as $\tan\varphi = U/W$, the axial flux of angular momentum in the annular section is then written as follows:

$$G_{ang} = 2\pi\rho \int_{R_c}^{R_b} U_a \left(U_a \tan\varphi \right) r^2 dr = 2\pi\rho U_a^2 \tan\varphi \left(\frac{R_b^3 - R_c^3}{3} \right)$$

Here, U_a is a mean axial velocity supplied through the swirl annulus, R_c is the central core radius, and φ is the swirler (guide) van angle. By assuming flat axial velocity distribution, the linear momentum flux from the two regions of the burner is then calculated as follows:

$$G_x = 2\pi\rho \int_{R_c}^{R_b} U_a^2 \, r \, dr + 2\pi\rho \int_0^{R_c} U_c^2 r \, dr = \pi \left[\rho U_a^2 \left(R_b^2 - R_c^2 \right) + \rho U_c^2 R_c^2 \right]$$

where U_c is a mean axial velocity through the center core. Then, the equation of the geometric swirl number (I-1) for the vane swirl burner can be written:

$$S = \frac{G_{ang}}{R_b G_x} = \frac{\frac{2}{3}\tan\varphi\left(1-R^3\right)}{\left(1-R^2+\frac{U_c^2}{U_a^2}R^2\right)} = \frac{2}{3}\frac{1-R^3}{1-R^2+\left[m^2\left(\frac{1}{R^2}-1\right)^2\right]R^2}\tan\varphi \qquad \text{(I-6)}$$

Here, R is the ratio of centerbody to burner radii $R = R_c/R_b$. It is simplified further when U_c/U_a is expressed in terms of m the mass flux ratio (flow-split) $m = \dot{m}_c/\dot{m}_a$ through the centerbody ($\dot{m}_c$) and annular ($\dot{m}_a$). The mass flux ratio is the same as the ratio of the effective areas of the center core and the swirl annulus and can be determined simply by the use of standard flow pressure drop procedure. Obviously, it is a more convenient form for engineering designs.
If we assume that the axial and azimuthal velocities are uniform and that the vanes are thin, the ***geometrical swirl number*** can be written as [I-15]:

$$S = \frac{2}{3}\left[\frac{1-\left(R_{cb}/R_{id}\right)^3}{1-\left(R_{cb}/R_{id}\right)^2}\right]\tan\varphi \qquad \text{(I-7)}$$

I.7.1.2 Unsteady cold flow evolution in swirl coaxial injector

The analysis of dynamics of coherent structures in swirl injector turns out to be very difficult, and the results may depend on the flow considered. Thus, the modifications of these coherent structures (the underlying mechanisms of mixing enhancement) by swirl is not well understood at present.
Investigations of swirl effects by experiments and numerical simulations are very challenging. Experimental studies may provide insight into the spatial changes of mean flow and turbulence characteristics. However, information about characteristic length and time scales of turbulent motions and insight into the temporal dynamics of coherent structures are difficult to obtain in this way. Numerical simulations can provide insight into the mechanism of swirling turbulent jets.
Swirl coaxial injectors are commonly used in modern gas turbine engines to achieve efficient and clean combustion. In addition to its primary functions of preparing a combustible mixture and stabilizing the flame, the injector acts as a sensitive element that may generate and modulate flow oscillations in the chamber through the following two mechanisms. First, the internal flow evolution in an injector is intrinsically unsteady and involves a wide variety of structures with different time and length scales. These structures, when convected downstream, can easily interact with the flowfield near the injector exit and modify the local flame-zone chemistry. Second, the injector flow may interact resonantly with the acoustic waves in the combustor.
The flow evolution inside a combustor chamber with swirl injector exhibits several distinct features, as follows. First, the flowfield is essentially irrotational after passing through the radial-entry swirl vanes. Strong vorticity then develops in the *boundary layers* near the walls, and in the

regions downstream of the guide vanes and the centerbody, due to the large velocity difference in the shear layers.
Second, when the flow travels downstream of the centerbody, the strong swirling motion and its associated centrifugal force produces large radial pressure gradients, which then induce a low-pressure core around the centerline. As the flow expands and the azimuthal velocity decays with the axial distance, the pressure is recovered. A positive pressure gradient is consequently generated in the axial direction and leads to the formation of a *central recirculating zone* (CRZ) *flow*, a phenomenon commonly referred to as *vortex breakdown* or *vortex burst*. The formation of the recirculation flow zone, a form of *vortex breakdown*, acts as an aerodynamic blockage or the threedimensional bluff body which serves to stabilize flames. The resultant flow detachment from the rim of the centerbody gives rise to a vorticity layer, which subsequently rolls, tilts, stretches, and breaks up into small eddies. These small vorticity bulbs interact and merge with the surrounding flow structures while being convected downstream. The entire process is highly unsteady and involves a wide range of length and time scales.
Third, because of the opposition of the swirler vane angles, two counter-rotating flows with different velocities in the streamwise and azimuthal directions merge at the trailing edges of the guide vanes. Vortices are generated in the shearlayer regions and shed downstream sequentially due to the *Kelvin–Helmholtz instabilities*[1]. In comparison with the vortex-breakdown-induced central recirculating flow, the flow structures associated with the periodic vortex shedding in the outer region are small and well organized. The shearlayer instability, along with the helical and centrifugal instabilities, induces large asymmetric structures on the transverse plane.
Finally, the aforementioned flow structures in various parts of the injector and their underlying mechanisms interact and compete with each other. When the swirl number changes, the dominant instability mode may switch correspondingly.

I.7.1.3 Precessing Vortex Core and Central Recirculation Zones in lean premixed swirl injectors

Three main spiral vortex structures controlling the flow field near the burner mouth were identified [I-39]:

1. *precessing vortex core* (PVC),
2. *helical central recirculation vortex* (HCRV),
3. *helical outer vortex* (HOV)

The jet breakdown zone is the conjunction of a pair of co-rotating co-winding spiral vortices (PVC and HCRV). The outer vortex (HOV) is responsible for controlling fluid entrainment in the outer shear layer of the jet. The HOV sign is opposite to the sign of the internal vortices (PVC and HCRV). All the structures are left handed spirals (sense of winding opposite to basic flow rotation) but with drastically different pitches: the PVC has a large pitch and axis aligned along the axial coordinate; the HCRV and HOV are tightly coiled helices with a small pitch and axis

[1] The *Kelvin-Helmholtz* instability, after Lord Kelvin and Hermann von Helmholtz, can occur when velocity shear is present within a continuous fluid, or when there is sufficient velocity difference across the interface between two fluids.
The theory is used to predict the onset of instability and transition to turbulent flow in fluids of different densities or moving at various speeds. Any time there is a non-zero curvature, the flow of one fluid around another will lead to a slight centrifugal force which in turn leads to a change in pressure thereby amplifying the ripple.

aligned azimuthally (orthogonally to the PVC axis). The PVC is the primary and most powerful structure (the PVC core includes primary vorticity generated by the swirler); the HCRV and HOV are considered here as secondary vortical structures. Interaction between the PVC and HCRV leads to their eventual merging and disintegration. In the near field region (z<0.5d), the instantaneous central reverse flow area is intrinsically asymmetrical, following the PVC locus shifted away from the burner geometrical centre. At greater distances (after PVC dissipation) the flow becomes nearly axisymmetric.

The onset of different recirculation regions, connected to swirl strength, can strictly influence the main combustion features. In fact, while the toroidal *central recirculation zone* (CRZ) is important for reactants mixing and flame stabilisation, the *corner recirculating zone* (close to the combustion chamber walls) induces entrainment of a large amount of hot burned gases into the outflowing reactant mixture.

One of the most important flow characteristics of a swirl injector is *vortex breakdown*, a phenomenon that manifests itself as an abrupt change in the core of a slender vortex, and usually develops downstream into a recirculating bubble or a spiral pattern. The flow region of vortex breakdown provides the dominant flame stabilization mechanism, and is characterized by the existence of internal stagnation points and reversed flows.

Although various forms of vortex breakdown have been identified (e.g., bubble and spiral type breakdown) [I-41], they all share as a common and predominant feature an abrupt deceleration of the flow near the axis leading to the formation of a stagnation point, as if a solid obstacle had been introduced into the flow ([I-40], [I-41]).

When increasing the swirl, a strong coupling develops between axial and tangential velocity components. A *vortex breakdown* is a change in structure of a vortex initiated by a variation in the characteristic ratio of tangential to axial velocity components [I-41].

Many combustion systems and lean-premixed gas turbine combustors use swirl-induced recirculation for flame stabilization and mixture formation. Swirl-induced *central recirculation zones* (CRZ) are a result of the *vortex breakdown* phenomenon which occurs in high swirling flows and can impact on combustor dynamics through the appearance of a *precessing vortex core* (PVC), where the whole CRZ rotates around the combustor axis (Fig. I-6 and Fig. I-7). Since the PVC is an unsteady periodic phenomenon, unwanted combustion induced oscillation may result and may affect lean stability limits and combustion dynamics. The ability of CFD methods to predict swirl-induced phenomena is under investigation and it seems that only the Large Eddy simulation (LES) approach is capable of capturing the 3D time-dependent flow structures that have been observed experimentally.

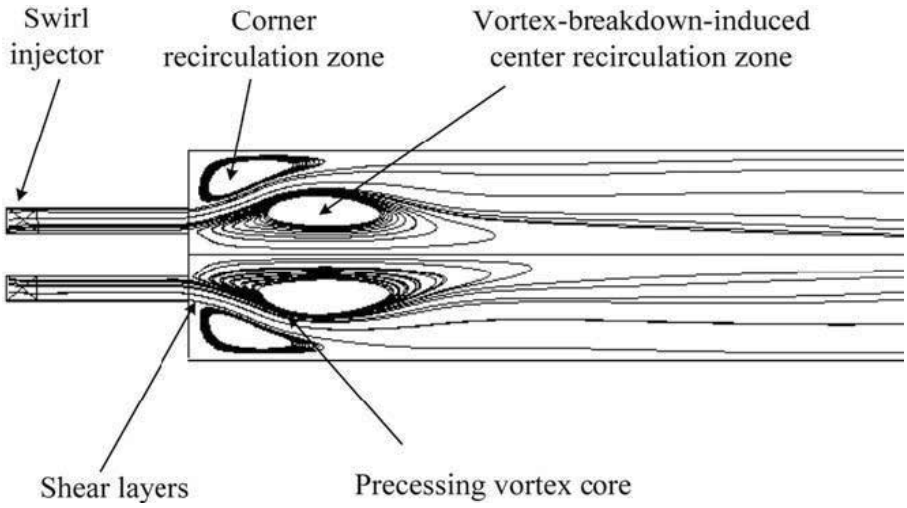

Fig. I-6: Flow structures of a typical gas turbine combustor with a coaxial injector. [I-32]

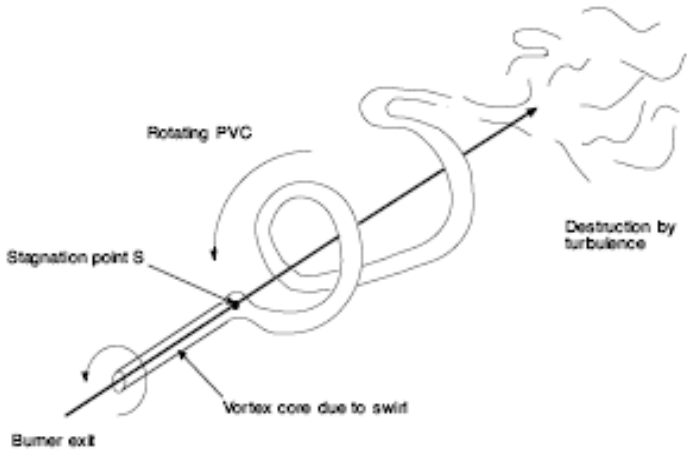

Fig. I-7: Schematic representation of a generic PVC.

When a PVC appears it is linked and possibly coupled with the CRZ. Typically, it is of helical form and is wrapped around a distorted asymmetrical CRZ. This flow combination also excites secondary flows especially radial axial eddies, and recent LES work indicates that these eddies, shed from the edge of an inlet shear flow can propagate downstream and help to initiate thermoacoustic instability.

Under isothermal conditions the frequency of the PVC can be characterised for a range of different swirl flow systems by a Strouhal (*St*) and Swirl number (*S*). There is evidence that a central fuel injector or bluff body of significant size can allow the formation of the PVC to much lower levels of swirl than previously thought especially when the central fuel jet is of low velocity [I-30].

Under combustion conditions the behaviour is more complex, the PVC occurrence and amplitude are also strong functions of mode of fuel entry, equivalence ratio (Φ) and level of confinement.

Axial fuel entry, except at exceptionally weak mixture ratios, often suppresses the vortex core precession. A strong double PVC structure is also found under certain circumstances [I-30].
Values of Strouhal number are very much a function of Swirl number, less so of equivalence ratio, also being complicated by the occurrence of double PVC for certain swirl number ranges.
Premixed or partially premixed combustion can produce large PVC, similar in structure to that found isothermally: this is attributed to the radial location of the flame front at the swirl burner exit.
Although PVCs and vortex shedding have been investigated in various publications of non-reacting swirling flows, not much is known about the impact of these flow instabilities on combustion ([I-30], [I-42]).
Systematic studies of precessing vortices in combustor systems began with the work of Syred and Beer [I-43] and have continued up to the present time ([I-30], [I-44], [I-45], [I-46]). It has been established that this instability may be coupled with acoustic or combustion instability modes.
Rotating modes are instabilities which are commonly observed in swirling flows. A paper of Selle et al. [I-47] shows that, in complex geometry swirled combustors, such modes can appear for both cold and reacting conditions but that they have different sources: while the cold flow rotating mode is essentially hydrodynamic and corresponds to the well-known PVC (*Precessing Vortex Core*) observed in many swirled unconfined flows, *the rotating structure observed for the reacting case inside the combustion chamber is not hydrodynamically but acoustically controlled*, then their nature is very different: for the cold flow, the rotating mode is an hydrodynamic mode, but it becomes acoustically controlled when combustion is activated. The two *transverse acoustic modes* (i.e. tangential azimuthal and/or radial) of the combustion chamber couple and create a rotating motion of the flame which leads to a self-sustained turning mode which has the features of a classical PVC but a very different source (acoustics and not hydrodynamics).
For low swirl numbers coherent structures are relatively weak, while with higher swirl numbers their intensity increases substantially. For applications, coherent structures play an important role as they influence mixing of heat and species to a large extent and hence the entire reaction process in swirl burners.

I.8 Active combustion control

Future aircraft engines must provide ultra-low emissions and high efficiency at low cost while maintaining the reliability and operability of present day engines. The demands for increased performance and decreased emissions have resulted in advanced combustor designs that are critically dependent on efficient fuel/air mixing and lean operation. In order to meet these goals advanced combustor designs will be required. Active Combustion Control which consists of feedback-based control of the fuel injection, the fuel-air mixing process, and the staging of fuel sources, can provide an approach to achieving acceptable combustor dynamic behaviour while minimizing emissions, and thus can provide flexibility during the combustor design process. The three main areas of interest in active combustion control are [I-48] (see Tab. I-2):

1) combustion instability control,
2) emission minimizing control,
3) burner pattern factor control.

The long-term intent is to combine the objectives of each individual Active Combustion Control technology into a single intelligent fuel/air management system to provide low emissions

throughout the engine operating envelope. These areas are described below and the parameters of interest for feedback control are introduced [I-48].

Main areas of interest in active combustion control	Example of parameters of interest for feedback control: sensing specifications
1) Combustion instability control	• ~ ±1 psi (= 6890 Pa = 0.07bar) dynamic pressure measurements • active control of high frequency combustion instability, ~ 700 Hz bandwidth • ±5% accuracy • +2800 ºF (=1537°C), +400 psi (=27.5 bar) combustor environment
2) Emissions minimizing control	• Array of emissions species (CO, CO_2, NO) measurements at the HPT stator vanes • ~2500 º F (=1371°C) environment • ±5% accuracy • < 5 Hz bandwidth - or - • Dynamic pressure measurements
3) Burner pattern factor control	• Circumferential array of temperature measurements mounted at HPT stator vanes • ~2500 º F (=1371°C) environment • ± 2 % accuracy • < 1 Hz bandwidth

Tab. I-2: Example of parameters of interest for feedback control in Active Combustion Control [I-48].

I.8.1 Combustion instability control

As the requirements for reducing emissions become more stringent, the combustor designs move towards a "lean" burning solution where the fuel/air mixture contains more air to allow for complete combustion of the fuel while forming less pollutants. However, such combustor designs are more susceptible to instability due to thermo-acoustic driven pressure oscillations. Active control of such oscillations can allow for more efficient, lower emissions combustor designs. Then, in recent years, there has been considerable research into combustion instability suppression.
Effective suppression of the high frequency combustion instabilities (e.g., which result from the relatively short aero-engine combustor geometries) is a critical enabling technology for lean-burning low emission combustors and requires several key issues to be addressed:

1. First, a **combustion instability controllers**, that are ***sensors*** **and** ***algorithms*** **able to detect and interpret the instability** need to be developed.

2. Second, an ***actuator*,** that is a device that can introduce controlled perturbations into the combustor to affect change on the instability is needed.
3. And lastly, suitable ***control algorithms*** are needed to drive the actuators to obtain suppression of the instability. Usually control methods use pressure sensors and they are based on an adaptive, phase-shifting approach. They sense the combustion pressure, calculate the average power in the pressure oscillations, and adapt the phase of the valve-commanded fuel flow variations in order to reduce the power in the pressure oscillations.

In recent years, there has been considerable activity addressing Active Combustion Control (ACC). Government, academia, and industry research efforts, through analysis and the use of laboratory combustors, have shown the considerable potential for active control.
Developing practical and affordable sensor technology capable of measuring parameters in this extremely harsh environment will be a major challenge.

I.8.2 Emission minimizing control

Due to non-uniformities in the fuel/air mixing and in the combustion process, there typically exist **hot streaks in the combustor exit plane entering the turbine**. These hot streaks limit the operating temperature at the turbine inlet and thus constrain performance and efficiency. In addition, these hot streaks can be zones of increased formation of nitrogen oxides (NO_x). Elimination of the hot streaks can provide greater turbine life, can effectively increase the maximum combustor operating temperature and thus increase engine efficiency and performance, and can also contribute to emissions reduction.
Finally, the **combustor flame temperature** is largely a function of the combustion zone fuel-air mixture ratio (Φ). In order to minimize the formation of carbon monoxide (CO) and unburned hydrocarbons (UHC), it is desirable to maintain a mixture ratio near stoichiometric. Unfortunately, mixture ratios near stoichiometric give high flame temperatures that lead to increased NO_x formation. In order to simultaneously minimize production of carbon monoxide (CO), unburned hydrocarbons (UHC), and oxides of nitrogen (NO_x), tight control over the fuel-air ratio is required throughout the operating range of the combustor. The challenges for this technology are the development of simplified emission production models that can be used for control design, development of suitable approaches to actively control the fuel/air mixture ratio, and the development of the necessary feedback control sensors for operation within the engine environment. It is desirable to have emission species sensors for direct feedback control purposes. A secondary traditional option is to use pressure sensors through which the level of emission production can be inferred.

I.8.3 Burner pattern factor control

Burner pattern factor is an indicator of the difference between the maximum and average temperature at the turbine inlet. Reducing the burner pattern factor can eliminate some of the hot streaks at the turbine inlet which will increase the life of turbine blades.
Reducing the burner pattern factor may also result in more uniform fuel burning and reduced emissions. Burner pattern factor control seeks to develop an active engine fuel distribution system capable of producing a more uniform combustor exit temperature. Burner pattern factor control

frequently employs a temperature feedback approach: based upon temperature feedback from circumferentially arranged temperature sensors at the combustor exit plane, the control system issues commands to fuel flow valves circumferentially arranged inside the combustor so as to achieve as uniform a temperature distribution at the exit plane as possible. Some of the past temperature feedback sensing options considered for burner pattern factor control included an array of thin film thermocouples attached to the high pressure turbine stator vanes, and acoustic tomography. Developing sensors which can survive in this harsh environment, and which are readily accessible for maintenance purposes are key design issues.

I.9 Future

Industrial combustion is expected to continue to play a prominent role in the future. It is directly related to the vast majority of energy consumption in the world and indirectly related to many of the products people use on a daily basis. The increasing attention on the environment means that industrial combustion pollution emission are expected to continue to reduce over time. Energy efficiency is also expected to be of interest as well.
A wide range of testing configurations will continue to be used to simulate realistic operating conditions. It is expected that field testing in particular, with all of its limitations, will continue to be an important component of a combustion technology development program, especially since most end users will be unwilling to use a technology that has not been verified on a large scale, preferably in an operating plant.
The use of *optical instrumentation* is expected to increase in the future because it has some important advantages compared to physical probes. The main barrier to using many of the optical techniques has been adapting them for use in an industrial environment. More experience continues to be gained using these sophisticated techniques in the harsh environments often present in industry.
While computer modelling continues to grow in popularity, current models can not replicate the complete physics of an industrial combustion system because of computer hardware limitations and because not all of the physics are completely known. In nearly all models, simplifications need to be made to get results in a reasonable amount of time. In addition, those models still need experimental data for validation.

References

[I-1] U.S. Department of Energy (DOE), Energy Information Administration, "International Annual Energy Outlook 2008"; report DOE/EAI-0384, Washington, DC, released June 26, 2009, www.eia.doe.gov/oiaf/ieo/index.html

[I-2] Energetics Incorporated, "Industrial Combustion Technology Roadmap: A Technology Roadmap by and for the Industrial Combustion Community", October 2002 (accessed July 29, 2009).

[I-3] Baukal C.E. Jr., "Industrial Combustion Testing", CRC Press, Taylor & Francis Group, 2011.

[I-4] Schwarz A., J. Janicka, "Combustion Noise", Springer edition, Berlin, Heidelberg, 2009.

[I-5] International Energy Agency (IEA), 2006, "World Energy Outlook 2006"; http://www.worldenergyoutlook.org/2006.asp

[I-6] Grassl H., Kokott J., Kulessa M., Luther J., Nuscheler F., Sauerborn R., Schellnhuber H.-J., Schubert R., and Schulze E.-D., "World in Transition: Towards Sustainable Energy Systems", Earthscan London and Sterling, VA, 2004; http://www.wbgu.de/wbgu_jg2003 engl.html

[I-7] Bothien M.R., "Impedance Tuning: A Method for Active Control of the Acoustic Boundary Conditions of Combustion Test Rigs", PhD Thesis, Berlin, October 2008.

[I-8] German Federal Ministry of Economics and Technology, "COORETEC Lighthouse Concept – The path to fossil-fired power plants for the future", Research Report, No. 566, 2008; http://www.bmwi.de/English/Navigation/Service/publications,did=259508.html

[I-9] European Virtual Institute – Gas Turbine Instrumentation (EVI-GTI) website: http://www.evi-gti.com/ , Lab Gap Matrix, Research Themes and HEATTOP, excel file.

[I-10] United States Propulsion Instrumentation Working Group Consortium (PIWG) website: http://www.piwg.org/sensor/ , Sensor specifications.

[I-11] Kurtz A.D., Chivers J.W.H., Ned A.A., Goodman S., Beheim G., "Advanced high-temperature instrumentation for gas turbine applications", VKI Lecture Series 2009-06, High temperature pressure sensors for gas turbine applications, Von Karman Institute for Fluid Dynamics, May 11-14 2009.

[I-12] Giacomazzi E., Troiani G., Giulietti E., Bruschi R., "Effect of Turbulence on Flame Radiative Emission", Experiments in Fluids, Springer Berlin/Heidelberg, vol.44, Issue 4, pp.557-564, April 2008.

[I-13] Fichera A., Pagano A., "Monitoring combustion unstable dynamics by means of control charts", Applied Energy, Vol. 86, pp.1574–1581, 2009.

[I-14] Cammarata L., Fichera A., Pagano A., "Neural prediction of combustion instability", Applied Energy, Vol.72, pp.513–28, 2002.

[I-15] Beer J.M., Chigier N.A., "Combustion aerodynamics", Applied Science Publisher, London, 1972; Robert E. Krieger Publishing Company, Malabar, FL, p. 112, 1983.

[I-16] Leuckel W., Fricker N., "The characteristics of swirl-stabilized natural gas flames. Part I: Different flame types and their relation to flow and mixing patterns", Journal of the Institute of Fuel, Vol.49, pp.103-112, June 1976.

[I-17] Gupta A.K., Lilley D.G., Syred N., "Swirl Flows", Abacus Press, Kent (U.K.), 1984.

[I-18] Keck O., Meier W., Stricker W., Aigner M., "Establishment of a confined swirling natural gas/air flame as standard flame: Temperature and species distribution from laser Raman measurements", Combustion Science Technology, Vol.174, Issue 8, pp.117-151, 2002.

[I-19] Büchner H., Lohrmann M., "Coherent Flow Structures in Turbulent Swirl Flames as Drivers for Combustion Instabilities", Proceeding of International Colloquium on Combustion and Noise Control, Cranfield University, Cranfield, 2003.

[I-20] Kühlsheimer C., Büchner H., "Combustion Dynamics of Turbulent Swirling Flows", Combustion and Flame, Vol. 131 Issue 1-2, pp.70-84, 2002.

[I-21] Schadow K., Gutmark E., Parr T.P., Parr D.M., Wilson K.J., Crump J.E., "Large-scale coherent structures as drivers of combustion instability", Combustion Science Technology, Vol. 64, pp.167-186, 1989.

[I-22] Straub D.L. and Richards G.A., "Effect of axial swirl vane location on combustion dynamics", American Society of Mechanical Engineers, ASME Paper 99-GT-109, 1999.

[I-23] Straub D.L. and Richards G.A., "Effect of fuel nozzle configuration on premixed combustion dynamics", American Society of Mechanical Engineers, ASME Paper 98-GT-492, 1998.

[I-24] Hermsmeyer H., Prade B., Gruschka U., Schmitz U., Hoffmann S., Krebs W., "V64.3A Gas Turbine Natural Gas Burner Development", American Society of Mechanical Engineers, Proceedings of ASME TURBO EXPO 2002, ASME Paper GT-2002-30106, Amsterdam, The Netherlands, June 3-6, 2002.

[I-25] Lawn C.J., "Thermo-acoustic frequency selection by swirled premixed flames", 28th International Symposium on Combustion, vol.28, pp.823-830, The Combustion Institute, Edinburgh, Scotland, 2000.

[I-26] Lawn C.J., "The thermo-acoustic response of a premixed swirl burner", Professional Engineering Publishing, vol. 214, Issue 4, pp.333-354, 2000.

[I-27] Lawn C.J., Evesque S., and Polifke W., "A Model for the Thermo-Acoustic response of a premixed swirl burner. Part I: Acoustic Aspects", Combustion Science and Technology, vol.76, Issue 8, pp.1331-1358, August 2004.

[I-28] Lawn C.J., and Polifke W., "A Model for the Thermo-Acoustic response of a premixed swirl burner. Part II: The Flame Response", Combustion Science and Technology, vol.76, Issue 8, pp.1359-1390, August 2004.

[I-29] Hosseini S.M.R., Gardner C. and Lawn C.J., "Saturation in the thermoacoustic response of a premixed swirl stabilised burner to forced excitation", Third European Combustion Meeting (ECM 2007), Crete, Greece, published on CD, 11-13 April 2007.

[I-30] Syred N., "A review of oscillation mechanisms and the role of the precessing vortex core (PVC) in swirl combustion systems", Progress in Energy and Combustion Science, Vol. 32, pp.93–161, 2006.

[I-31] Winterfeld G., Eickhoff H.E., Depooter K., "Fuel injectors", Chapter 3, in "Design of modern gas turbine combustors", San Diego, CA, Academic Press, pp. 229–341, 1990.

[I-32] Huang Y., Yang V., "Dynamics and stability of lean-premixed swirl-stabilized combustion", Progress in Energy and Combustion Science, Vol. 35, Issue 4, pp. 293-364, 2009.

[I-33] Shiri A., George W.K., Naughton J.W., "Experimental Study of the Far Field of Incompressible Swirling Jets" ,AIAA Journal, Vol. 46, Issue 8, pp. 2002–2009, 2008.

[I-34] Zemtsop C.P., Stöllinger M.K., Heinz S., Stanescu D., "Large-Eddy Simulation of Swirling Turbulent Jet Flows in Absence of Vortex Breakdown", AIAA Journal, Vol. 47, Issue 12, pp.3011-3021, December 2009.

[I-35] Stein C.F., "Toward a Vortex Breakdown Condition for Swirling Annular Jets", Journal of Fluids Engineering, Vol. 121, Issue 1, pp. 102–105, 1999.

[I-36] Toh I.K., Honnery D., Soria J., "Axial plus tangential entry swirling jet", Experiments in Fluid, Vol. 48, pp.309-325, 2010.

[I-37] Komori S., Ueda H., "Turbulent Flow Structure in the Near Field of a Swirling Round Free Jet", Physics of Fluids, Vol. 28, Issue 7, pp. 2075–2082, 1985.

[I-38] Schneider C., Dreizler A., Janicka J., "Fluid Dynamical Analysis of Atmospheric Reacting and Isothermal Swirling Flows", Flow, Turbulence and Combustion, Vol. 74, Issue 1, pp. 103–127, 2005.

[I-39] Cala C.E., Fernandes E.C., Heitor M.V., Shtork S.I., "LDA analysis of PVC-central recirculation zone interaction in a model vortex burner", 12th International Symposium on Applications of Laser Techniques to Fluid Mechanics, Lisbon, Portugal, July 12-15, 2004.

[I-40] Billant P., Chomaz J.-M., Huerre P., "Experimental study of vortex breakdown in swirling jets", Journal of Fluid Mechanics, vol. 376, pp. 183-219, 1998.

[I-41] Lucca-Negro O., O'Doherty T., "Vortex breakdown: a review", Progress in Energy and Combustion Science Vol.27, pp.431-481, 2001.

[I-42] Cozzi F., Capelli F., Mirelli F., Coghe A., "Flow Instabilities in a Swirl Burner", XXXIII Event of the Italian Section of the Combustion Institute, Second S4FE, Processes And Technologies For A Sustainable Energy, Ischia, June 27-30, 2010.

[I-43] Syred N., Beer J.M., "The damping of precessing vortex cores by combustion in swirl generators", Astronautica Acta, Vol.17, pp.783–801, 1972.

[I-44] Anacleto P.M., Fernandes E.C., Heitor M.V., Shtork S.I., "Swirl flow structure and flame characteristics in a model lean premixed combustor", Combustion Science and Technology, Vol.175, Issue 8, pp.1369–1388, 2003.

[I-45] Al-Abdeli Y.M., Masri A.R., "Precession and recirculation in turbulent swirling isothermal jets", Combustion Science and Technology, Vol. 176, pp.645–665, 2004.

[I-46] Syred N., Wong C., Rodriquez-Martinez V., Dawson J., Kelso R., "Characterisation of the occurrence of the precessing vortex core in partially premixed and non-premixed swirling flow", Proceedings of the 12th international symposium on applications of laser techniques to fluid mechanics, Lisbon, 2004.

[I-47] Selle L., Benoit L., Poinsot T., Nicoud F. and Krebs W., "Joint use of Compressible Large-Eddy Simulation and Helmholtz solvers for the analysis of rotating modes in an industrial swirled burner", http://www.cerfacs.fr , 2005.

[I-48] Simon D.L., Garg S., Hunter G.W., Guo T-H., Semega K.J., "Sensor needs for control and health management of intelligent aircraft engines", in Proceeding of the ASME Turbo Expo, ASME GT2004-54324, June 2004.

II. Thermo-acoustic instabilities: fundamental processes and mechanisms

II.1 Introduction

Flow oscillations always exist in a practical combustion device, even under stable operating conditions. Combustion with small amplitude pressure fluctuations (e.g., **less than about 5% of the mean chamber pressure** for certain combustors) is defined as **stable combustion**. Combustion with large-amplitude periodic pressure oscillations is termed unstable (oscillatory) combustion, and is referred to as **"combustion instability"** ([I-32], [II-1]).
Turbulent combustion involves many individual, physical processes of high complexity, e.g. chemical kinetics, differential molecular diffusion, radiative heat transfer, phase transition, flame/acoustics interactions, and of course the turbulent flow itself, which is indeed also an unsolved issue. The nonlinear coupling between all these phenomena completely determines the behaviour of practical systems. Due to this complex coupling truly predictive numerical models are not available at present for realistic installations, although they are of course necessary to improve existing devices and develop new configurations.
Two categories of combustion oscillations exist: *forced oscillations* and *self-sustained oscillations*.

- *Forced* (or *resonant*) *oscillations* occur as a response of the burner/combustion chamber system to an external driver that generates a harmonic signal in resonance with one of the acoustic modes of the system.
- On the contrary, *self-sustained oscillations* do not need an external source and may arise from infinitesimally small initial perturbations of the heat release at the flame front. Under stable operation these perturbations result in a white combustion noise, whereas the spectra of the pressure signals produced by combustion instabilities feature single frequencies that can be easily identified because of their significant amplitudes and correspond to the unstable acoustic modes.

The term *"combustion instability"* indicate a particular case of *thermo-acoustic instability* and it means generally an oscillation of the pressure in a combustion chamber, having a fairly well-defined frequency which may be as low as 10-20 Hz or as high as several tens of kilohertz.
Combustion instabilities are characterized by large-amplitude oscillations of one or more natural acoustic modes of the combustor. Such instabilities have been encountered during the development and operation of *propulsion* (e.g. rockets and ramjets), *power generation* (e.g. industrial land-based gas turbine combustor), *boiler* and *heating systems*, and *industrial furnaces*.
In general, the occurrence of thermo-acoustic instabilities is problematic because they produce *large-amplitude pressure and velocity oscillations*, flame *blow-off* or *flashback*, *excessive noise*, severe *vibrations that interfere with control-system operation*, *limit operational flexibility*, *enhanced heat transfer* and *thermal stresses* to combustor walls, oscillatory mechanical loads that result in *low- or high-cycle fatigue* of system components, and finally they can even result in *structural damage* and may result in *premature component wear* that could lead to costly shutdown or catastrophic component and/or mission failure.
Then, combustion noise and stability have received sustained attention in both the academic and industrial communities, particularly over the last fifty years. During this time, the literature on

this issue has grown enormously, and now spans numerous applications, including *industrial land-based gas turbine combustors* ([II-2], [II-3], [II-4], [II-5], [II-6], [II-7], [II-8], [II-9], [II-10], [II-11]), *rocket engines* and *aeroengines* ([II-12], [II-13], [II-14], [II-15], [II-16], [II-17], [II-18], [II-19], [II-20], [II-21]). Both solid and liquid fuelled *propulsion systems* for *rocket engines* can be prone to instability, and this effect has been extensively studied for a long time (e.g., [II-20], [II-21], [II-22], [II-23], [II-24], [II-25], [II-26]).
In land-based gas turbines, the system pressure ranges up to 3.5 MPa and pressure fluctuations of the order of 1% of the mean pressure were observed, which could reach up to 0.1 MPa [I-7]. In solid propellant and liquid-fuelled rocket engines, where the mean pressure level is considerably higher, i.e., up to 40MPa, pressure fluctuations can easily reach up to 10% of the mean pressure.
The previous effects, that thermoacoustic instabilities might have, can be here divided in three categories:

1) Impact on the quality of the combustion process by **increasing NOx and CO emissions**, causing **flashback**, or leading to **extinction**.
2) **Reduction of component lifetime** and, in the worst case, **total system failure**. This can be due to structural vibrations causing wear and tear that result in low- or high-cycle fatigue as well as increased heat transfer to the combustor walls causing increased thermal stresses.
3) **Increased noise emissions** and impact on health.

Generally, all three of them involve a deterioration of system performance, as they cause thrust oscillations and limited operating regimes that may prohibit the operation at the design point.

II.2 Acoustic-vortex-flame interactions in Gas Turbines

During combustion instabilities three physical mechanisms interact in a highly nonlinear and unsteady manner. These three mechanisms are *vortex motion* (i.e. fluid-dynamic *vorticity*), *unsteady combustion heat release* (i.e. *flame*, or *entropy waves*) and *acoustic fluctuations*.
Earlier studies in 1958 [II-27] characterized these three mechanisms as *vorticity*, *entropy waves* and *acoustic*, although only the acoustic field behaves as a wave, whereas both vorticity and entropy "waves" are convected at the local flow velocity. In combustion systems, *entropy fluctuations* can be attributed to unsteady flame propagation.
How is it possible that apparently coherent, nearly classical acoustic waves exist in chambers containing highly turbulent non-uniform flow? [II-27]:

- Any *small amplitude* (linear) disturbance may be synthesized of three modes of propagation:
    1. *Vortical* or *shear waves* characterized by nonuniform vorticity.
    2. *Entropy waves* or *"spots"*, small regions having temperatures slightly different from the ambient temperature of the flow. They are generated by the *unsteady heat release*.
    3. *Acoustic waves*.

  Entropy waves are compressional waves (i.e., fluctuations in pressure and density) in which the internal energy and velocity remains constant.
  Sounds waves (e.g. fast/slow waves), like entropy waves, are fluid dynamic compressional waves that propagate a fluctuation in pressure and density. Unlike entropy waves, the internal energy of *sound waves* varies while entropy remains constant.

- In the *linear approximation*, if the flow is uniform, the three types of waves propagate independently, but may be coupled at boundaries (e.g. nozzles) or in combustion zones.

II.2.1 Characteristics of acoustic, vortical and entropy disturbances

Several characteristics of acoustic, vortical and entropy disturbances can be noted:

a) *Entropy* and *vortical waves* having small amplitude propagate (are "convected") in a uniform field with the mean flow speed (the bulk velocity, u_0), but *acoustic waves* propagate with their own speeds of sound (c). Consequently, in low-Mach number flows, these disturbances have substantially different length scales. *Acoustic* properties vary over an acoustic length scale, given by $\lambda_a = c / f$, whereas *entropy* and *vorticity* modes vary over a *convective length scale* (λ_c), given by $\lambda_c = u_0 / f$. Thus, the entropy and vortical mode wavelength is shorter than the acoustic wavelength by a factor equal to the mean-flow-Mach number $\lambda_c / \lambda_a = u_0 / c = Ma$. This can have important implications on acoustic-flame interactions.
   In the *linear limit*, only acoustic waves carry disturbances of pressure. All three types of waves possess velocity fluctuations and the three modes can become coupled. As a result, each of the waves may then carry pressure, temperature and velocity fluctuations.
b) *Entropy* and *vorticity* disturbances propagate with the mean flow and diffuse from regions of high to low concentration. In contrast, *acoustic* disturbances, being true waves, reflect off boundaries, are refracted at property changes, and diffract around obstacles. In general, the reflection of acoustic waves from multidimensional flame fronts results in a complex, multidimensional acoustic field in the vicinity of the flame.
c) In a homogeneous, uniform flow, these three disturbance modes propagate independently in the *linear approximation*.

II.2.2 Length and time scales

Acoustic-vortex-flame interaction occurs in many devices, such as liquid-propellant and solid-propellant, ramjet engines and dump combustors.
The interaction between acoustic waves, vortex motion and unsteady flame motion involves a wide range of time and length scales, and this range depends not only on the actual sources (e.g. compressibility, shear layer separation and roll-up, or heat release) but also the geometry.
If these modes are to interact, there has to be some overlap between their respective time and length scales. Therefore, it is instructive to make some order-of-magnitude estimates of these time and length scales for a typical gas turbine combustor (see Fig. II-1):

1. **Fluid-dynamic length scales**
From geometric data, the characteristic length scale of the combustor in gas turbine is the *integral scale* ($l \cong D$) that is in the range 0.01-0.1 m. The integral scale represents the characteristic energy-containing eddies that play a major role in energy and scale transport in shear flows.
For the preceding length scales, the turbulent Reynolds number, $\mathrm{Re}_l = \frac{u'l}{\nu}$, where u' is the turbulence intensity, is estimated to be in the 10^2-10^4 range. On using inertial range scaling, $\frac{l}{\eta} \approx \mathrm{Re}_l^{3/4}$, the Kolmogorov scale η can be estimated to be in the range 10^{-4}-10^{-5} m. Thus, fluid dynamic length scales that are characteristic of vortex motion range from 10^{-5}-10^{-1} m.
Shear flow is the source of vorticity generation and convection. The flow from the inlet duct forms a complex three-dimensional swirling shear flow in the combustor and contains large-scale coherent structures that undergo growth and eventual breakdown into fine-scale three-dimensional turbulence further downstream.

2. **Reacting flows length scales: entropy scales**
For reacting flows, additional length scales have to be considered. For example, in two-phase systems, droplets are in the 10^{-4}-10^{-6} m range, whereas molecular mixing and combustion occur in the 10^{-8}-10^{-9} m range. This is just an estimate, since mixing and flame regions vary over a wide range.
Combustion-related unsteady heat release is the source of *"entropy"* mode, which is typically characterized by fluctuations in temperature. Combustion occurs in a compact region because the flame is stabilized in a region upstream of a recirculation bubble that is created by the swirl in the incoming flow.

3. **Acoustic length scales**
Acoustic timescales can also be estimated on the basis of the range of frequencies known to be excited in gas turbine engines. Typical frequencies are in the range of 100-10000 Hz, and under standard conditions the typical acoustic length scales of interest (λ_a) are in the 10^{-2}-10^{0} m range.
Compressibility (i.e., density variation resulting in pressure fluctuations) is the source of acoustic wave motion. Because of the many ducts and passages in a gas turbine, there are many possible acoustic modes in the combustor. The entire region from the compressor exit to the turbine entrance boundary can play a role in acoustic wave motion. Because of the geometric nature of the combustor and the swirling flame structure, radial and circumferential acoustic modes can also exist.

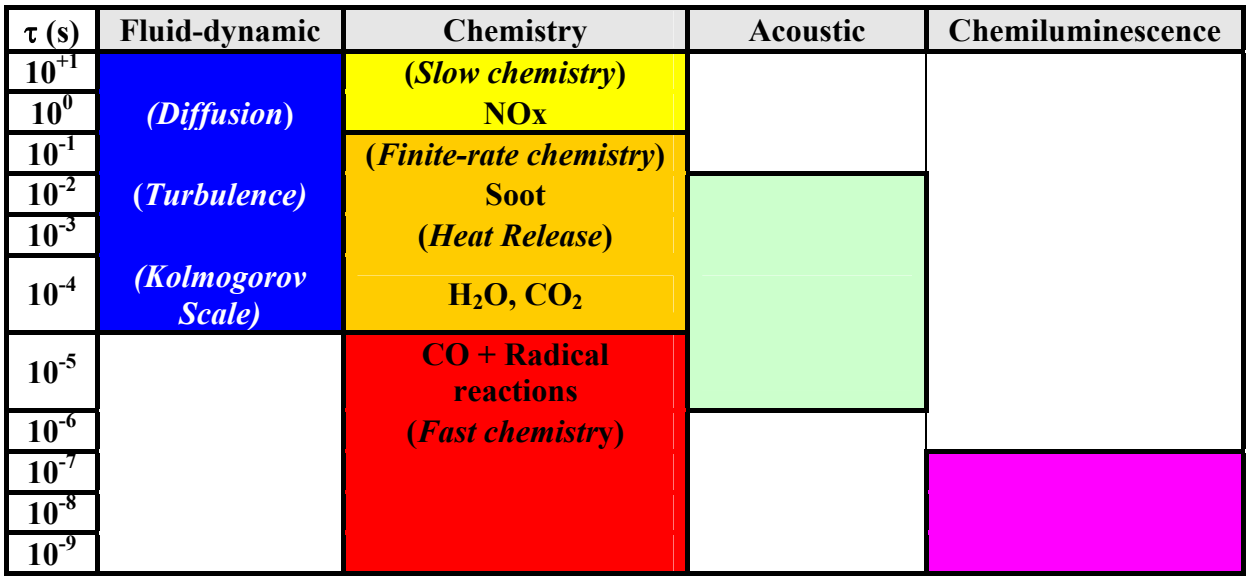

Fig. II-1: Table of multi-scale interaction phenomena in combustion instability field.

These estimates suggest that although a significant disparity exists between the characteristic length scales in which vortex motion, acoustic fluctuations, and heat release each dominate, there are also some regions of overlap.

The preceding argument is a rather simplistic view, since in reality, eddies of all scales coexist and interact in a highly nonlinear manner in a turbulent flow. For example, the flame-response timescale, $\tau_f = \delta_f / S_L$, where δ_f and S_L are the laminar flame thickness and speed, respectively, for a premixed system, is in the range of 10^{-3}-10^{-2} s, which is of the same order as acoustic timescales for frequencies in the 100-1000 Hz range. Thus, it is possible for an acoustic field to couple with heat release even in the absence of a turbulent cascade of length scales.

This wide range of scales offers a serious challenge to both experimentalist and modellers. Experimental diagnostic tools and simulation models both have to be refined well enough to capture this wide range of scales accurately. That is easier said than done.

Studies often find that a Strouhal number, defined as $St = \frac{\omega L_f}{u_0} = \frac{2\pi L_f}{\lambda_c}$, is a key parameter that affects the flame response to perturbations. Note that *St* is proportional to the ratio of the *flame length* (L_f) and *convective wavelength* ($\lambda_c = u_0 / f$). A flame whose length is much less than an acoustic or convective wavelength is referred to as acoustically or convectively compact.

II.3 Combustion instabilities in the new generation of gas turbine

II.3.1 Decreasing in pollutant emission

Modern gas turbine combustion chamber have little in common with the combustion system used for the world's *first industrial gas turbine* to go into commercial operation, at Neuchatel in Switzerland, built in 1939 by Alstom. The thermal combustion intensity has increased from 10 MW/m^3 up to levels of more than 200 MW/m^3. At the same time, the requirement to meet ever increasing environmental standards has brought emission levels down from more than 500 *ppm* NO_x to below 25 *ppm*. This dramatic increase in combustion efficiency and decrease in pollutant emission has essentially become possible through the development of lean-premixed combustion technology.
Until fairly recently, combustion instabilities in *land-based gas turbines* had received much less attention than in other systems (e.g. propulsion systems made of rockets, thrust augmenters and ramjet engines). The situation changed with increased emphasis on reducing air pollution during the past twelve years, in particular of the major pollutant oxides of nitrogen, NO (more generally NO_x).
A strategy for reducing emission of NO_x, is **to lower the average temperature at which primary combustion occurs and takes place**, in accordance with the *Zel'dovich mechanism* for producing Thermal NO_x [II-28], then the generation of NO_x by the thermal mechanism is reduced. However, at lower temperatures, the rate of production of another pollutant, carbon monoxide (CO), is increased. At high temperatures, the equilibrium of CO_2 and CO is shifted as CO_2 dissociates to form more CO. Thus in practice, the production, or rather the equilibrium concentration of carbon monoxide, is minimum in a range of temperature not too high, not too low.
Lower combustion temperature may be achieved by operating under lean conditions, when the flame stabilization processes tend to be unstable. Unfortunately, at lower temperatures achieved by operation at lower local values of fuel/air ratio, **the processes stabilizing the flame are less stable and tend to encourage the excitation of oscillations**. Fluctuations of the flame cause fluctuations of energy release, which in turn may produce fluctuations of pressure, exciting acoustical motions in the chamber. As a result, during the past ten-twelve years combustion instabilities have become a serious problem in the development of stationary power generation systems based on combustion, mainly of hydrocarbon fuels.
Burners submitted to instabilities near stoichiometric conditions usually have a best compromise between high efficiency and high NO_x emission rate but the Sound Pressure Level (SPL) in conditions of incipient extinction can reach high critical values. Lean premixed combustion is especially prone to combustion instabilities ([II-29], [II-30]), and this is leading to long and expensive development. At low combustion temperatures, realized in lean flames, the *emission of* NO_x decreases, but the flames tend to be *unstable near the lean limit* (LBO, lean blow-off), and their coupling with combustor acoustics may result in *combustion instability*.

II.3.2 Damaging of combustors

Thermo-acoustic combustion dynamics are objectionable for at least two primary reason:

1) Under some circumstances, the activity within the combustor generates **an externally audible tone at intolerable levels**.
2) More frequently, the pressure oscillation can also drive **resonant vibrations in mechanical components, resulting in significant hardware damage** (e.g., using a multidisciplinary approach combining computational fluid dynamics CFD and finite element FE [II-31], [II-32], [II-33]).

In the last years, interest for interaction between acoustics and premixed flames did grow a lot because sometimes this interaction generates a thermo-acoustic instability phenomenon that may damage combustors proportionally to the power of the system. This is a major problem and an active research topic in modern gas turbine industry.
In the context of *gas turbines*, burning at lean operating conditions is attractive from the point of view of reduced NO_x formation; on the other hand, in *propulsion devices*, such as *ramjet engines*, burning under near stoichiometric conditions is desirable since this leads to enhanced heat release and therefore high performance. Amplitudes of pressure fluctuations can reach more then 120 dB in *atmospheric flames*, and several MPa (up to 40 Mpa) in *rocket engines*. If thermo-acoustic instability occurs, the ***frequency spectrum*** of the resulting pressure and velocity oscillations typically exhibit one or several distinct peaks, with frequencies often (but not necessarily) close to the acoustic eigenfrequencies of the enclosure (or the complete combustion system) without unsteady heat release.
The *rms level of pressure fluctuations* is clearly affected by the distribution of heat release inside the combustor. In general, the pressure oscillation amplitude scales linearly with the combustor pressure. Thus, **the potential for structural damage is much higher at high engine pressure ratios** ([II-34] § 4).
For combustion systems **working under pressure**, such as gas turbines, the sound pressure generated will reach very high levels. Owing to the large surfaces of such systems, high mechanical loads on the combustion chamber as well as on upstream and downstream components will arise. Also the *thermal load* on the chamber walls will rise considerably. Depending on sound pressure amplitudes, components will fail sooner or later; thus, this kind of oscillation must be avoided by all means if those combustion systems are to be operated safely.
"Hot tones" ($50 < f < 1000$ Hz) are also detrimental to combustion hardware if allowed to run at excessive amplitudes for extended periods, however it seems that they are less destructive than ***"cold tones"*** ($f < 50$ Hz) or ***"screech"*** ($f > 1000$ Hz). It is difficult to say exactly which parts are being affected by either *hot* or *cold tones* without knowledge of material characteristics, natural frequencies, etc. Most combustion hardware that exhibits distress caused by combustion dynamics or pulsations associated with instabilities fails in low-cycle fatigue because of either thermal or mechanical stress, and then the crack propagates in high-cycle fatigue caused by a combination of acoustic, mechanical, or thermal contributions. **Crack initiation is usually at an area of high-stress concentration** caused by material, geometry, welds, or even cooling holes.
"Screech tones" can damage hardware very rapidly. For this reason it is difficult to try to tune out of such situations. One of the reasons that screech is so unique is that the part can fail in high-cycle fatigue simply because of cycles to failure. The most destructive manifestations of screech usually occur when a particular part goes into resonance, driven by the acoustic pulsations.

Indications of liner crack growth can be found in *changes in emissions*. Low NO_x depends on good mixing and distribution of fuel and air, both of which can be affected by liner damage, resulting in significant variations in NO_x emissions ([II-34] § 8).
Combustion instabilities have been responsible for damaging a variety of hardware, including *fuel nozzles, combustor cans* and *transition pieces*. Gas turbine users have found that components such as combustor liners, transition pieces, and fuel nozzles need routine examination for part cracking or excessive wearing because of induced vibration. At a minimum, this requires downtime for inspections and part repair, thereby reducing machine availability. Every hour of downtime for any gas turbine engine whether power generation or aero propulsion is an hour of lost revenue as well as the cost of maintenance and overhaul. At the worst, a cracked piece may be liberated into the hot gas path, potentially requiring replacement of expensive turbine components.

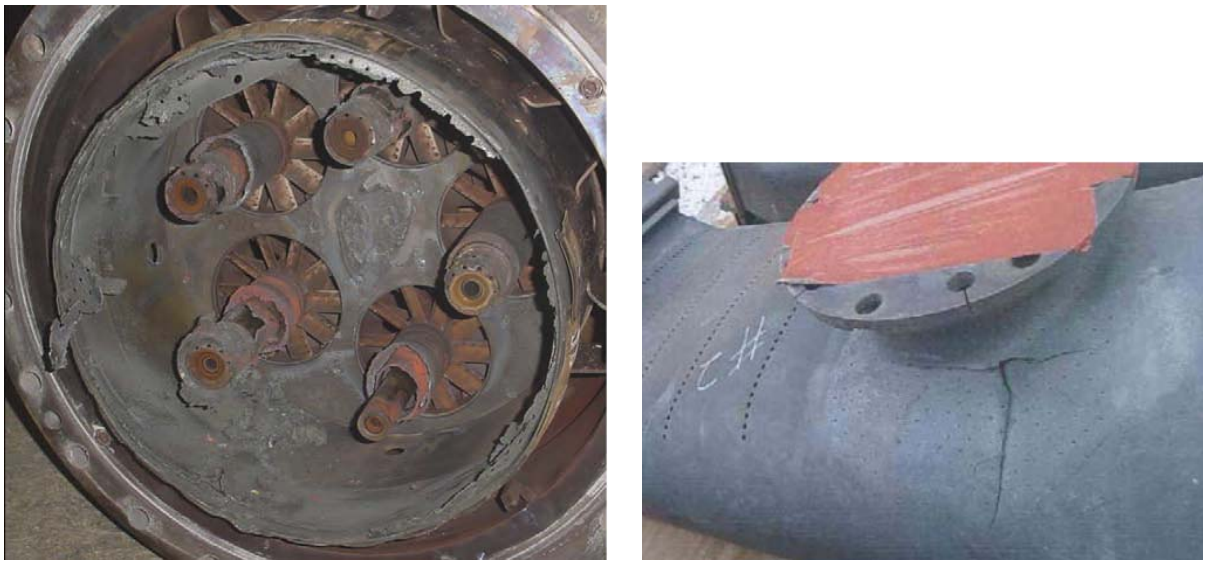

(a) (b)

Fig. II-2: Burner assembly (a) [I-32] and combustor liner (b) damaged by combustion instability.

Combustion failure can be extremely costly, not only because of the cost of replacement hardware, but also in terms of loss in electricity generation. Unplanned shutdowns incur additional financial penalties in a dynamic energy-trading market because the shortfall in generation must be brought in from other generators. It is, therefore, beneficial to continuously monitor the health of the gas turbine and its combustion system to obtain the earliest possible indication of deterioration or failure. Early detection of abnormal operation enables commercially appropriate action to be planned, whether this involves a machine inspection or the reoptimization of the combustion system.
Then, over the last decade, substantial efforts have been expended in the industrial, government, and academic communities to understand the issues associated with combustion instabilities in low-emissions gas turbine.
On-line combustion-dynamics monitoring offers significant commercial advantages to power generators by providing a tool with which greater gas-turbine reliability and availability can be achieved. Although the cost of installing monitoring equipment may be high, the potential

savings resulting from the increased flexibility of operation and the avoidance of catastrophic failure far outweigh the cost. As a result, combustion monitoring has become a valuable component of the integrated health-screening activity.

II.3.3 Local and overall phenomena in thermo-acoustic instability: chemiluminescence emission

II.3.3.1 Local phenomena

Unsteady combustion is an efficient *acoustic source* ([II-35], [II-36]), and combustors tend to be highly resonant systems. Therefore, when unsteady heat release generates acoustic waves, these reflect from the boundaries of the combustor to produce flow unsteadiness near the flame. This may cause more unsteady *heat release* ($\dot{\omega}_T^1$), e.g. through *local changes in the fuel-air ratio* [II-30] or through *hydrodynamic instabilities* ([II-37], [II-38]).
Combustion processes are sensitive to fluctuations of *pressure* ($p' \equiv p_1$), *density* ($\rho' \equiv \rho_1$), and *temperature* ($T' \equiv T_1$) of the environment. A fluctuation of burning produces local changes in the properties of the flow. Those fluctuations propagate in the medium and join with the global unsteady field in the chamber. Under favourable conditions, the field develops to a state observable as a combustion instability.
Thermo-acoustic instability establishes when the acoustics of the system generates a feedback mechanism between pressure fluctuations (p_1) and heat release ($\dot{\omega}_T^1$) ([II-39],[II-40]). Acoustic waves could lead to fluctuations in the heat release of the flame, which could amplify the acoustic wave and lead to an increase in the acoustic energy in the system, provided the *Rayleigh's criterion* is satisfied. The acoustic signal generated in the combustion chamber modulates fuel feeding and sometimes, pressure waves lead to fluctuating fuel flow near the fuel injector, thereby introducing local equivalence ratio variations (Φ') and as a result heat release variations ($\dot{\omega}_T^1$).

II.3.3.2 Overall phenomena

Unlike other flow instabilities, thermo-acoustic instabilities are *not a local phenomenon* in the sense that stability proprieties are not determined solely by the dynamics of the heat source and the flow field in its immediate surrounding. Instead, acoustic waves travel back and forth across the extent of the system, and as a consequence acoustic boundary conditions far away from the heat source may strongly influence stability properties. In premixed flames, *convective transport of fuel inhomogeneities* from the fuel injector to the flame, or of *entropy inhomogeneities* ("hot spots") from the flame to the exhaust, are other non-local phenomena which influence system stability.
Oscillations in heat release generate *vorticity*, *entropy* and *acoustic perturbations*. An acoustic oscillation incident on a flame generates entropy and vorticity disturbances. Also, the unsteady wrinkling and subsequent curvature of the flame front induced by the acoustic perturbations causes additional generation of unsteady vorticity.

II.3.3.2.1 Global heat-release rate

The amount of heat released by a three-dimensional lean flame per unit time is ([II-41], [II-42]):

$$Q(t) = \int dm_f \, \Delta h_f = \int \left(Y_f \, dm\right) \Delta h_f = \int Y_f \left(\rho_f S_f \, dA_f\right) \Delta h_f = \int_{Af} \rho_f \, S_f \, Y_f \, \Delta\omega_R \, dA_f \qquad \text{(II-1)}$$

where the integration is performed along the instantaneous flame front, considered here as a discontinuity of the reacting flow of zero thickness, separating cold reactants from hot products.
The integral is performed over the flame surface (A_f), m_f and m are the instantaneous values of the mass fluxes of fuel and mixture (unburnt gas) entering the reaction zone, S_f is the flame speed (laminar burning velocity averaged across the flame front), Y_f ($=m_f/m$) is the mass fraction of fuel in the premixed gases entering the flame, Δh_f is the chemical enthalpy of the fuel, and $\Delta\omega_R$ ($=\Delta h_f$) is the heat release per unit mass of reactant fuel (specific enthalpy of combustion).
This equation shows the four fundamentally different ways of generating heat-release disturbances in a premixed flame: fluctuations in density of the reactants (ρ_f) and flame speed (S_f), mass fraction of fuel (Y_f), heat of reaction ($\Delta\omega_R$), or flame area (A_f). They can be classified based on either their modification of the local internal structure of the flame (such as the local burning rate) or its global geometry (such as its area):

a) Fluctuations in the *mass flow rate of reactive mixtures* into the flame, corresponding to $\rho_f S_f$, is the most basic mechanism of heat-release oscillation. These density fluctuations could be caused by both acoustic and entropy fluctuations. The flame's burning rate S_f is sensitive to the perturbations in pressure, temperature, strain rate, or mixture composition that accompany the acoustic wave. These pressure and temperature fluctuations are usually generated by acoustic perturbations, whereas the strain-rate fluctuations are associated with acoustic or vortical velocity fluctuations.
b) *Flame-area fluctuations* (A_f) are associated with disturbances in the flame's position and orientation that, in turn, are generated by fluctuations in either the local burning rate of flow velocity.
c) *Fluctuations in heating value* ($\Delta\omega_R$) are driven by variations in reactive mixture composition.

In gas turbine combustion the density perturbations arising from acoustic pressure are typically much smaller than the other terms and are often neglected. On the other hand, factors such as unsteady aerodynamics may produce a significant modulation in flame area and may not be neglected. Likewise, changes in the flow of either fuel and/or air will change the fuel mass fraction (Y_f) and the flame speed (S_f).
In short, numerous mechanism can generate perturbations in the heat release at the flame. In most practical applications, it is difficult to separate and control these mechanisms to achieve stable combustion.
Splitting each variable into a mean, stationary component ($\overline{(\ldots)}$), supposed to be spatially uniform upstream of the flame front, and a fluctuating component (index 1), which is also assumed to be uniform in the reaction region, Equation (II-1) can be rearranged as:

$$Q(t) = \overline{Q} + Q_1(t) = \overline{Q} + [(Q_1)_\rho + (Q_1)_{Sf} + (Q_1)_Y + (Q_1)_\xi] + Q'' \qquad \text{(II-2)}$$

where the mean *global heat-release rate* (flux) of a premixed flame is the product of the reactants consumed by the flame (m_f) and the heat of reaction (H_f is the chemical enthalpy of the fuel), then it is given by

$$\overline{Q} = m_f H_f = m Y_f \, \Delta h_f = \left(\overline{\rho}_f \, \overline{S}_f \, \overline{A}_f\right)\overline{Y}_f \, \Delta h_f \tag{II-3}$$

while, for its normalized fluctuating components, we have:

$$\left(\frac{Q_1}{\overline{Q}}\right)_\rho = \frac{1}{\overline{A}_f}\int_{\overline{A}_f} \frac{(\rho_f)_1}{\overline{\rho_f}} d\overline{A}_f \tag{II-4}$$

$$\left(\frac{Q_1}{\overline{Q}}\right)_{Sf} = \frac{1}{\overline{A}_f}\int_{\overline{A}_f} \frac{(S_f)_1}{\overline{S_f}} d\overline{A}_f \tag{II-5}$$

$$\left(\frac{Q_1}{\overline{Q}}\right)_Y = \frac{1}{\overline{A}_f}\int_{\overline{A}_f} \frac{(Y_f)_1}{\overline{Y_f}} d\overline{A}_f \tag{II-6}$$

$$\left(\frac{Q_1}{\overline{Q}}\right)_\xi = \frac{(A_f)_1}{\overline{A}_f} \tag{II-7}$$

Equations (II-4)-(II-7) indicate that fluctuations in the rate of heat release can be caused by fluctuations in density (ρ_f), mixture fraction (Y_f), flame speed (S_f) and flame surface area (A_f, and ξ is the flame displacement normal to the mean flame), plus the combined fluctuations in two or more of these variables, represented by Q''. Since we are interested in investigating the linear acoustic regime, where the amplitude of the acoustic waves is small compared to the mean flow quantities, the term Q'' becomes negligibly small compared to the first-order fluctuations Q_1, and can therefore be dropped from Equation (II-2).
Fluctuations in density, on the other hand, are usually of higher order than those of the other fluid dynamics variables, and can thus be neglected [II-41]. Thus:

$$\left(\frac{Q_1}{\overline{Q}}\right) \cong \left(\frac{Q_1}{\overline{Q}}\right)_{Sf} + \left(\frac{Q_1}{\overline{Q}}\right)_Y + \left(\frac{Q_1}{\overline{Q}}\right)_\xi \tag{II-8}$$

Whenever a combustion system is operated in fully premixed mode, with fuel and oxidizer already well premixed upstream of the combustion chamber, equivalence ratio fluctuations, and therefore turbulent burning rate fluctuations, are suppressed, and only flame surface area fluctuations will be responsible for the unsteadiness in the heat release rate.

II.3.3.2.2 Overall chemiluminescence emission of flames

Najm et al. [II-43] have shown that PLIF measurements of many flame species do not correlate quantitatively with heat release rates in hydrocarbon flames. Samaniego et al. ([II-44], [II-45]) have shown that for the lean flames considered in their study, chemiluminescent emission from CO_2* may be used to determine quantitatively *heat release rates*. Samaniego et al. have derived a quantitative relationship between CO_2* *emission intensity* and the r*ate of heat release* for the lean hydrocarbon flames. This relationship is based on detailed kinetic simulations which yield, in the case of a purely strained (i.e., in the absence of curvature) flame:

$$\frac{Q}{Q_0} = \left(\frac{I}{I_0}\right)^n \tag{II-9}$$

where Q and I are quantities integrated across the flame zone, and represent the *rate of heat release per unit flame surface area*, and the CO_2* *emission intensity per unit flame surface area*, respectively; the subscript 0 refers to unstrained flame quantities, and the exponent n (<1) depends on the combustible mixture.
In a 2D image (e.g. in a PLIF image) the integrated emission intensity, I, could be computed as a function of the curvilinear coordinate along the flame front, A_f:

$$I = I_{chem\_overall} = \int_{Af} I_{ch}(x,y)\,dA_f \approx \int_{Af} [i_{rad}\,\gamma^*_{rad}(T_f)\,Y_{rad}(t)]\,dA_f \tag{II-10}$$

where $I_{ch}(x,y)$ is the two dimensional chemiluminescence intensity distribution of energy radiant emission. Local chemiluminescence emission (I_{ch}) for individual radicals (subscript *rad*) is proportional to the product $i_{rad}\,\gamma^*_{rad}Y_{rad}$, where *i* is the specific chemiluminescence emission, *Y* is the mass fraction and γ* its excited fraction.
Another important observation is that the *overall chemiluminescence intensity* is a function of both the fuel flow rate, that is, the *overall heat-release rate* ($\omega_{T\,overall}$), and the *equivalence ratio* (Φ): this observation has important implications regarding the use of the overall chemiluminescence emission as a measure of the overall rate of heat release during unstable combustion. It is the flame *temperature* (T_f), and not the *equivalence ratio* per se, that affects the intensity of the chemiluminescence emission, in fact the overall chemiluminescence can be increased by increasing either the equivalence ratio or the *inlet temperature* ([II-34] § 16, [II-45]).
The *local rate of heat release* ($\omega_{T\,local}$), that is the rate of heat release per unit flame area, and the *local chemiluminescence emission* (I_{ch_local}) are affected by unsteady strain and flame curvature and they increase exponentially with temperature, leading to a power-law relationship between the local chemiluminescence emission and the local rate of heat release, that is,

$$I_{ch\_local} \propto (\omega_{T\,local})^{\alpha(T)} \tag{II-11}$$

where the exponent α is a positive number and depends on the *flame temperature* and the effects of unsteady strain and flame curvature ([II-34] § 16, [II-45]).
By systematic measurements of OH chemiluminescence [II-46], flame chemiluminescence intensity has frequently been reported to depend linearly on the *mass flux* (mass flow rate $m=\rho S_L A$; that is when the equivalence ratio Φ and the pressure P in the combustion chamber are constant) and exponentially on the *fuel mass fraction of the mixture* entering the flame (Y_f) ([II-46], [II-47]). Therefore, the recorded chemiluminescence intensity (e.g., about OH chemiluminescence intensity at 305.4 nm in [II-46], [II-48]) is assumed to have the following dependency of mass flux and fuel mass fraction:

$$I_{ch\_local} = k\, m Y_f^{\alpha} \qquad \text{(II-12)}$$

or

$$I_{ch\_local} = k\, m \Phi^{\beta 1} P^{\beta 2} \qquad \text{(II-13)}$$

where k, α, β_1 (>1) and β_2 (<0) are constants for the optical signal.
The experimental results ([II-46], [II-48]) indicate that for these conditions OH chemiluminescence monotonically increases for increasing equivalence ratios and decreasing pressures. OH chemiluminescence appears to exhibit significant dynamic range, particularly with equivalence ratio. That is, **small changes in equivalence ratio have an exponential effect on light emission**.
It is assumed that the Mach number is sufficiently small ([II-49], [II-50]).
The power dependence of equivalence ratio and pressure on OH chemiluminescence can be found with a correlation of the form:

$$\log(I_{ch\_local}) = A_0 + A_1 \log(\Phi) + A_2 \log(P) + A_3 \log(m) \qquad \text{(II-14)}$$

where A_0 is arbitrary and A_3 has been shown to be unity.
To determinate the relationship between the *overall chemiluminescence emission* ($I_{ch\_overall}$) and the *overall of heat release* ($\omega_{T\,overall}$), one must integrate the local values over the *flame front area* (A_f), that is:

$$I_{ch\_overall} = \int_{Af} I_{ch\_local}\, dA_f \qquad \text{and} \qquad \omega_{T\,overall} = \int_{Af} \omega_{T\,local}\, dA_f$$

If the flame temperature (T), that is, the equivalence ratio (Φ), unburned gas temperature, dilution, and radiation losses, is constant and the effects of strain and flame curvature are negligible or constant, then I_{ch_local}, $\omega_{T\,local}$, and α are constant over the flame. These constant values result in the proportionality of the *overall chemiluminescence emission* and the *overall rate of heat release*, that is,

$$I_{ch\_overall} = C(T)\, \dot{\omega}_{T\,overall} \qquad \text{(II-15)}$$

where the constant C depends on the *flame temperature* (i.e. equivalence ratio, unburned gas temperature, dilution and radiation losses) and the effects of strain and curvature.
If the equivalence ratio is constant (Φ=const.), it is possible to assume that the relation between *overall chemiluminescence emission* and *overall rate of heat release* is linear [II-51]. It is usually

considered that the dependence with respect to curvature, strain and unsteadiness is less important and that the corresponding variations are small. It is then possible to use a scaling factor β and obtain an estimate of the volumetric heat release rate in Wm^{-3}. This is admittedly an approximation but it provides an order of magnitude which can be quite useful. For example the values obtained in this way can be compared with those deduced from calculations thus serving as a guide to modeling CFD.
For a axisymmetric geometry, one may then write:

$$\dot{\omega}_{T\,local}(r,x,t) = \beta\ I_{ch\_local}(r,x,t) \tag{II-16}$$

where $\dot{\omega}_{T\,local}$ is the local heat release rate, expressed Wm^{-3}.
The scaling factor β can be determined by integrating the previous expression over the flame volume:

$$\dot{\omega}_{T\,overall} = \int \dot{\omega}_{T\,local}(r,x,t)\,2\pi\, r\, dr\, dx = \beta \int I_{ch\_local}(r,x,t)\,2\pi\, r\, dr\, dx = \beta\ I_{ch\_overall} \tag{II-17}$$

where $\dot{\omega}_{T\,overall}$ is the overall heat release rate, expressed W.
Assuming complete combustion, the *overall rate of heat release* in the flame is given by $\dot{\omega}_{T\,overall} = \dot{m}_f \Delta h_f$, where $\dot{m}_f$ is the fuel mass flow rate and Δh_f is the heat released by conversion of a unit mass of fuel. The *scaling factor* β, expressed in Wm^{-3}, is then equal to:

$$\beta = \frac{\dot{\omega}_{T\,overall}}{I_{ch\_overall}} = \frac{\dot{m}_f \Delta h_f}{\int_0^R \int_0^X I_{ch\_local}(r,x,t)\,2\pi\, r\, dr\, dx} \tag{II-18}$$

This factor β can be used to generate distributions of volumetric heat release rate.
The relationship between the *overall chemiluminescence emission* and the *overall rate of heat release* is more complicated if the equivalence ratio (Φ) and/or the effects of strain and curvature vary over the flame surface. For example, a more complicated relationship would occur in a partially premixed turbulent flame in which the equivalence ratio is not constant over the flame surface. In this case, the exponent α, in the equation relating the *local chemiluminescence emission* to the *local rate of heat release*, varies with location on the flame surface, which in turn affects the relationship between the *overall chemiluminescence emission* and the *overall rate of heat release*.
The other factor affecting the *overall chemiluminescence emission* and the *overall rate of heat release* is the *area of the flame* (A_f). Any factors causing the flame area to change, for example, flame-vortex interaction, will result in a change in the overall chemiluminescence emission and the overall rate of heat release. If the effects of stretch and/or curvature change over the flame surface as the flame area changes, as might be expected during flame-vortex interaction, then the relationship between the overall chemiluminescence emission and overall rate of heat release is likely to change as the flame area changes.
If we consider only small perturbation of the flow conditions, thus it justifies a linearization of equations:

$$\frac{Q_1}{\overline{Q}} = \frac{m_1}{\overline{m}} + \frac{Y_1}{\overline{Y}} \tag{II-19}$$

$$\frac{I_{ch\_1}}{\overline{I_{ch}}} = \frac{m_1}{\overline{m}} + \alpha \frac{Y_1}{\overline{Y}} \tag{II-20}$$

These relations show that in case of α=1 or Y_1=0 the chemiluminescence (I_{ch}) is proportional to the heat release (Q). However, as pointed out in [II-42], [II-49], [II-50], typically $\alpha \neq 1$ so, **the *chemiluminescence intensity* is not proportional to the *heat release* if equivalence ratio fluctuations are present**.

II.3.3.2.3 Flame Describing Function

It is possible to define a *Flame Describing Function* (FDF):

$$FDF(\omega, u') = \frac{\dot{\omega}'_{T\,overall} / \overline{\dot{\omega}_{T\,overall}}}{u'/\overline{u}} \tag{II-21}$$

where u' is the rms axial velocity [m/s], $\overline{u}$ is the mean axial velocity [m/s], and $\dot{\omega}'_{T\,overall}$ is the rms overall heat release rate [W]. A transfer function depending on frequency (f is the frequency of incident perturbations; $\omega=2\pi f$ is the angular frequency [rads^{-1}]) and amplitude of incident perturbations coming from a loudspeaker. The FDF can be determined for a range of frequencies and for different levels of incoming velocity perturbations.

It has been shown recently ([II-51], [II-52]), that the *Flame Describing Function* gives access to nonlinear features of combustion dynamics.
The *overall rate of heat release* $\dot{\omega}_{T\,overall}$ is generally estimated by recording the global emission signals of excited radicals like CH* or OH* using a photomultiplier detecting the total light radiated by the flame. The axial velocity u disturbance can be measured with a LDV system. One can then write this flame describing function as a function in terms of the OH* chemiluminescence signal by PLIF technique [II-52]:

$$FDF(\omega, u') = \frac{\dot{\omega}'_{T\,overall} / \overline{\dot{\omega}_{T\,overall}}}{u'/\overline{u}} \cong \frac{I'_{OH*} / \overline{I_{OH*}}}{u'/\overline{u}} \tag{II-22}$$

This FDF can be expressed as a complex number in terms of a gain G and a phase difference φ which depend on the frequency and the incoming perturbation level. The classical Flame Transfer Function (FTF) then corresponds to the Flame Describing Function (FDF) obtained for a fixed perturbation level:

$$FDF(\omega,u') = G(\omega,u')\,e^{i\varphi(\omega,u')} \qquad \text{(II-23)}$$

The gain *G* reflects the level of response while the phase φ defines the *time delay* between velocity and emission signals. It is possible to write φ=ωτ where ω=2π*f* and determine the delay which is in this case associated to a convective time, which corresponds to the time required by a disturbance to be convected to the flame and reach the flame edge. This can be seen by calculating this delay for the flame geometry under investigation: the *time delay* is $\tau_d \cong L/U_b$, where L is a characteristic length of the flame under unsteady operation and U_b is the injector bulk velocity.

II.3.4 Combustion noise

II.3.4.1 Introduction of noise and sound: Sound Pressure Level and frequency

Noise is commonly referred to as unwanted sound. Noise is a common by-product of our mechanized civilization and is an insidious danger in industrial environments Noise pollution is usually a local problem and so is not viewed on the same scale of importance as the more notorious industrial emission like NO_x, CO and particulates. Nonetheless, it is an environmental pollutant of significant impact.
Considering the impact on people, noise is most often a source of annoyance, but it can also have much more detrimental effects, such as causing actual physical injury. The sense of hearing is a fragile and vital function of human body. It is similar to vision, more so than the other senses, because permanent and complete damage can be sustained quite commonly in an industrial environment. So it follows that noise pollution has been recognized as a safety concern for a long time, and has been appropriately regulated.
Pressure level defines the loudness of sound, while frequency defines the pitch or tone of the sound. Pressure level is the amplitude of the compression, or rarefaction, of the pressure wave. The common unit of pressure level in Decibel, abbreviated to “dB”.
Frequency is the number of pressure waves that passes by an arbitrary point of reference in a given unit of time. The frequency *f*, the speed of sound *c* and the wavelength λ are related as follows: $c = \lambda f$
The typical range of human hearing extends from 20 Hz to 20 kHz. It is important to note that the ear is not equally sensitive over the entire range from 20 Hz to 20 kHz. There is a curve which is a map of the threshold of hearing in humans. Any *Sound Pressure Level* (SPL) at a frequency that falls below the curve will be inaudible to humans. Humans are most sensitive to sounds in the so called midfrequencies from 1 kHz to about 5 kHz. This is generally the region in which most of our everyday hearing activities take place.
Sound meters have the capability to measure with equal sensitivity over the entire audible range. However, since humans do not hear with equal sensitivity at all frequencies, the sound meter measurement needs to be modified to quantify what really affects us. This can be done using a correction curve. The most common correction is the A-scale correction curve, which resembles

an idealized inverse of the threshold of hearing curve. The others, less used correction scales are named, as may be expected B, C, and D.
It is not unusual for a person to encounter SPLs of 100 to 110 dB at sporting event, in a stadium full of cheering fans, and yet not be perturbed by it. Tab. II-1 gives some typical noise levels for various scenarios.

Thresholds of hearing	0 dBA
Rustle of leaves, desert	10 dBA
Broadcasting studio	20 dBA
quite room, whisper quiet library	30 dBA
Big city street at night	40 dBA
Busy street through closed windows	50 dBA
Busy street through open windows, normal conversation (at 1 m, 3-5'),	60 dBA
City street with very busy traffic,	70-80 dBA
Noisiest spot at Niagara Falls	85 dBA
Camion, motorcycle, underground train	90 dBA
Level at which sustained exposure may result in hearing loss	90-95 dBA
Pneumatic drill (at 1 m), noisy motorcycle	100 dBA
Threshold of pain	120 dBA
Jet engine (at 50 m)	130 dBA
Even short term exposure can cause ***permanent damage*** *- Loudest recommended exposure with hearing protection*	140 dBA
Rocket (at 50 m), aircraft at take off	200 dBA

Tab. II-1: Sounds levels of various sources.

II.3.4.2 Mechanisms of industrial combustion equipment noise

There are four major mechanisms of noise production in industrial combustion equipment. They can be categorized as predominantly low frequency or high frequency sources. They are [I-3]:

1. *Low frequency noise* sources:

a) Combustion roar and **instability flame**

- *Combustion roar* is low frequency sound and so can travel a great distance without being substantially attenuated by the atmosphere. High levels of turbulence increase the combustion roar. The signature of low frequency combustion roar noise typically consists of broadband spectrum with a single peak.
- The periodic lifting and reattachment of an *unstable flame* from the burner drives the low frequency rumbling noise mechanism.

b) Fan noise

The noise emitted from industrial fans typically consists of two noise components: broadband and discrete tones. Vortex shedding of the moving blades and the interaction of the turbulence with the solid construction parts of the fan creates the broadband noise. This broadband noise is of the dipole type, meaning that the noise is directional. On the other hand, the discrete tones are created by the periodic interactions of the rotating blades and nearby upstream and downstream surfaces. Discrete tonal noise is usually the loudest at the frequency at which a blade passes a given point. The tonal frequency is easily calculated by multiplying the number of blades times the impeller rotation speed in revolutions per second.

2. *High frequency noise* sources:

a) Gas jet noise

Gas jet noise is very common in the combustion industry and in many instances it can be the dominant noise source within a combustion system. The noise that is created when a high-speed gas jet exits into an ambient gas usually consists of two principal components: *gas jet mixing noise* and *shock-associated noise*.

- The source of ***gas jet mixing noise*** begins near the nozzle exit and extends several nozzle diameters downstream. Near the nozzle exit the scale of the turbulent eddies is small and predominantly responsible for the high frequency component of the mixing noise. The lower frequencies are generated farther downstream of the nozzle exit where the large-scale orderly pattern of the gas jet exists.
  Gas jet mixing noise consists of a broadband frequency spectrum. The frequency at which the spectrum peaks depends on several factors (e.g., diameter of nozzles, Mach number of the gas jet, the angle of the observer). The gas jet mixing noise of combustion burners typically peaks somewhere between 2 kHz and 16 kHz.
- When a burner operates above a certain fuel pressure a marked change occurs in the structure of the gas jet. Above a certain pressure, called the critical pressure, the gas jet develops a structure of ***shock waves*** downstream of the nozzle. These shock cells consist of compression and expansion waves that repeatedly compress and expand the gas as it moves downstream. These shock cells are responsible for creating two additional components of gas jet noise: ***screech tones*** and broadband ***shock-associated noise***.
  - ***Screech tones*** are distinct narrowband frequency sound that can be described as a ***"whistle"*** or ***"screech"***. The literature reports that these tones are emitted from fourth and fifth shock cell downstream of the nozzle exit [II-53].
    The sound waves from these shock cells propagate upstream where they interact with the shear layer at the nozzle exit. This interaction then creates oscillating instability waves within the gas jet. When these instability waves propagate downstream they interfere with the fourth and fifth shock cell causing them so emit the *screech tones*.
    Screech tone noise is not highly directional, unlike gas jet mixing noise. The peak frequency associated with screech tones depends on the nozzle diameter, fully

expanded jet Mach number and velocity, and the angle of the observer relative to the jet centreline velocity vector.

- ***Broadband shock-associated noise*** occurs when the turbulent eddies within the gas jet pass through shock waves. The shock waves appear to suddenly distort the turbulent eddies that creates a noise that can range over several octave bands. The broadband shock-associated peak frequency noise typically occurs at a higher frequency than the *screech tone* peak frequency.

b) Valve and piping noise

When a gas flowing steadily in a pipe encounters a valve, a change in the flow pattern and pressure will occur that can create turbulence and shock waves downstream of the valve. Typically, when valves are partially closed, creating a reduction in flow area, the small flow passage behaves much like an orifice and produces jet noise.

Turbulence and shock waves create mixing noise and shock-associated noise. This noise can radiate downstream through the pipe and exhaust into the environment at an outlet and/or radiate through the pipe wall not only into the space near the valve itself.

Usually butterfly valves and ball valves are noisier than globe valves. Butterfly valves and ball valves typically have a smaller vena contracta than a globe valve operating at the same pressure drop that results in higher levels of mixing and shock-associated noise. A general guideline when the pressure ratio across a valve is less than approximately three, the mixing noise and shock-associated noise are within about the same order of magnitude. Although, with pressure ratios greater than three, shock noise usually dominates over the mixing noise [II-54].

Usually a typical SPL spectrum emitted from a burner can have two major peak frequencies: the low frequency contribution is from the *combustion roar* while the high frequency noise contribution is from the *fuel gas jets* (*jet mixing noise* and *screech noise*). Usually an intermediate peak is a result of *valve and piping noise*. Notice that the *gas jet mixing noise* is a broadband frequency spectrum while the *screech noise* occurs over a fairly narrow bandwidth.

It is obvious that the SPL increase substantially when the operation is accompanied by instability, since combustion instability noise has high efficiency of conversion of chemical energy to noise. When several burners are installed in a furnace, however, the noise level from the burner may be higher than for a single burner due to the noise contribution from surrounding N burners:

$$L_{p\,total} = 10\log 10 \sum_{i=1}^{N} 10\exp\left(L_{p\,i}/10\right)$$

where L_p is the sound pressure level.

II.3.4.3 Acoustic noise emissions in the combustor

Some evidence has suggested that *entropy noise* is perhaps the major source of external noise in aero-engine combustion and is generated in the outlet nozzles of combustors [II-55]. Low-frequency entropy noise, which is predicted in theory and numerical simulations, has been detected in a generic aero propulsion engine combustion chamber. It has been shown that entropy noise dominates even in the case of thermo-acoustic resonances. In addition to this, a different noise generating mechanism was discovered that is presumably of even higher relevance to jet engines: there is strong evidence of broad band entropy noise at higher frequencies of 1 to 3 kHz. This unexpected effect can be explained by the interaction of small scale entropy perturbations or hot spots with the strong pressure gradient in the outlet nozzle. The *direct combustion noise* of the flame zone seems to be minor importance for the noise emission to the ambient [II-55].

II.3.4.3.1 Noise propagation from the combustion chamber

In its simplest form, a combustor is a forced acoustic resonator. The combustor cavity is bounded by the fuel injector at the front and the turbine stator at the back.
The total noise emitted by a combustion chamber is classified according to source mechanism ([I-4] § 5, [II-56]) and it consists of *direct* and *indirect combustion noise*. Only the ***direct combustion noise*** is directly related to the combustion process. ***Indirect combustion noise***, also called ***entropy noise***, is related to the acceleration of gas temperature nonuniformities which result from the unsteady combustion processes.
Two main mechanisms have been identified regarding noise propagation from the combustion chamber to the far field (see Fig. II-3):

- ***direct combustion noise***: acoustic perturbations generated by the unsteady heat release from the turbulent flame [II-57] propagate either upstream or downstream through the turbomachinery stages and can reach the far field after it has been drastically distorted by the mean flow and also diffracted and reflected by the solid walls within the diffuser, the distributer and the turbine and compressor blades;
- ***indirect combustion noise***: entropy fluctuations generated within the combustion chambers (e.g. by hot spots, imperfect mixing, etc.) are propagated downstream (towards the nozzle) and interact with accelerating mean flow.

In all cases the sources of combustion noise (*direct* and *indirect*) are related to the flame dynamics (i.e. *turbulent shear layer*) and to *unsteady rates of heat release*, that is the dominant source of noise. The analysis of combustion noise is then intimately tied to an understanding of dynamics of perturbed flames.
The wave of combustion noise can be (Fig. II-3):

- ***Entropy waves*** are linked to *indirect noise* and they are compressional waves (i.e., fluctuations in pressure and density) in which the internal energy and velocity remains constant.
- ***Sounds waves*** (***acoustic waves***; e.g. fast/slow waves), that are linked to *direct noise*, like entropy waves, are fluid dynamic compressional waves that propagate a fluctuation in

pressure and density. Unlike entropy waves, the internal energy of sound waves varies while entropy remains constant.

The *indirect* and *direct sources* of combustion noise are shown in the sketch of Fig. II-4: during the interaction between direct and indirect noise, part of the energy contained in the *entropy mode* is transferred into the *acoustic mode* and the subsequent acoustic waves are transmitted to the far field through the turbine stages in a similar way as for the direct combustion noise.

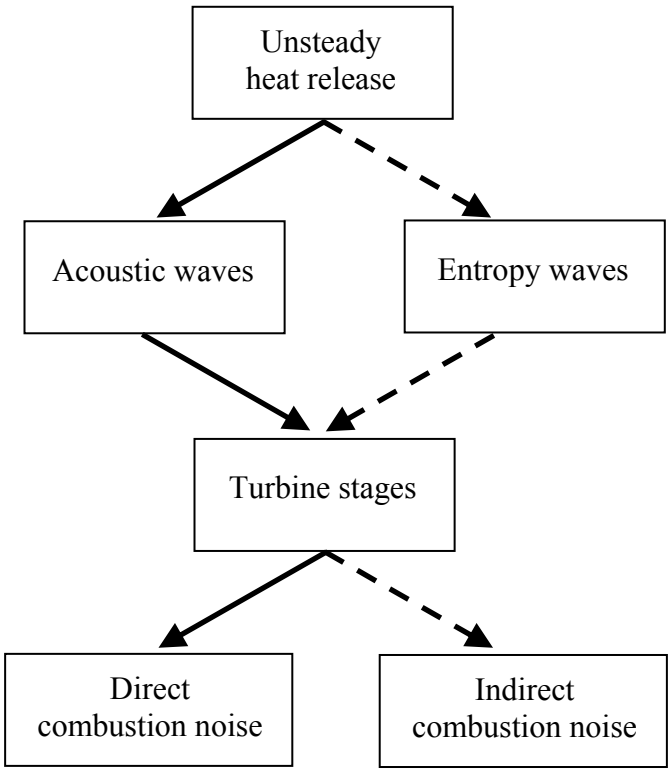

Fig. II-3: The two main mechanisms for noise generation from confined flames: direct (——) and indirect (- - -) noise.

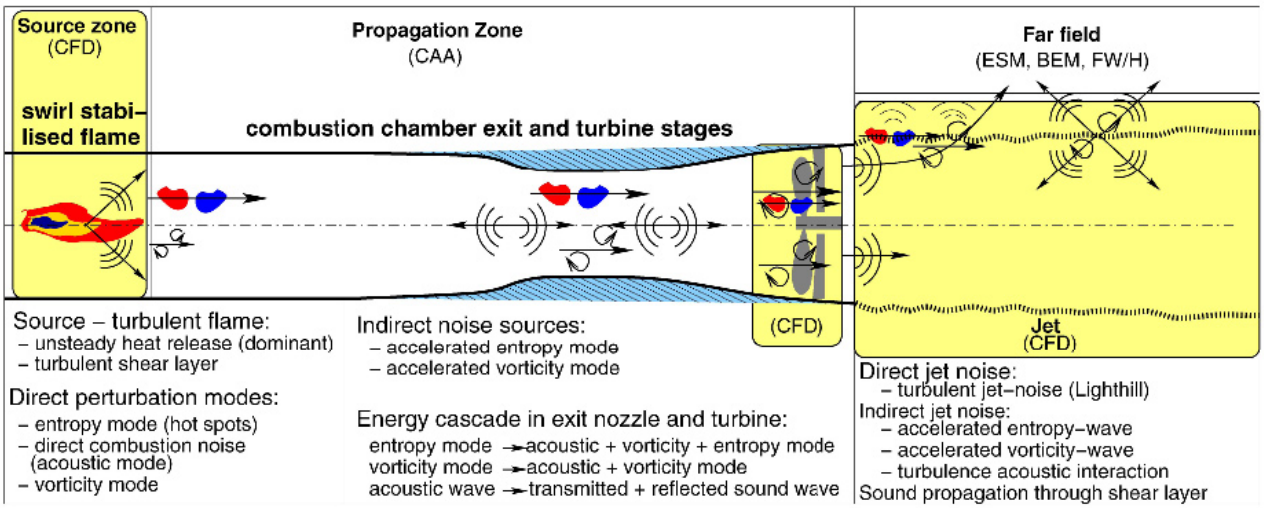

Fig. II-4: *Direct* and *indirect noise* sources in a combustion system, which are correlated due to their common origin from the initial entropy perturbation. ([I-4] § 8).

The combination of *direct* and *indirect combustion noise* in a gas turbine engine makes up an important part of what is generally called ***"core noise"***, that is a broadband entropy or vortex noise generation in the frequency range between 1 and 3 kHz. It is not generally possible to estimate the relative importance of *direct* and *indirect noise* contributions to the overall sound radiation from a combustor, and it is similarly difficult to estimate the relative impact of entropy modes on the system stability.

With respect to combustion oscillations Polifke et al [II-58] presented analytically the possibly constructive or destructive interference of *direct combustion noise* and *indirect noise*. But following Sattelmayer [II-59] the indirect combustion noise has no noticeable destabilizing effect on the stability of a simplified combustor model due to the high dispersion rate of the convecting entropy waves. In a mathematical approach Ali and Hunter [II-60] formulate on the other hand a possible resonant interaction between *sound waves* and quasi spatially fixed *entropy waves*.

Just recently the investigations on a combustor test rig provided manifestations on a very dominant contribution of *entropy noise* on the total emitted sound power of the system ([I-4] § 5). While theoretically well known, a decomposition of *direct* and *indirect noise* in measurements of real combustion systems proves difficult to obtain, as has for instance been described by Bake et al [II-55]. The difficulty is probably related to the coherence of vortical and acoustic perturbations with the initial entropy mode and acoustic field which is generated directly by the combustion process, such that any spectral decomposition leads to correlations between all signals.

II.3.4.3.2 Direct combustion noise

Direct combustion noise is produced by the combustion process itself and it is related to the creation of local hot spots in the combustor. *Direct combustion noise* results when a volume of mixture expands at constant pressure as it is rapidly heated by combustion. This local expansion causes the cooler surrounding gas to be pushed back; that is, the expanding gas does work on its surroundings. This work in turn produces waves in the surrounding gas which propagate into the far field as sound. Such sources are called acoustic *monopoles*.
Then *direct combustion noise* is due to *periodic combustion oscillations* (e.g. ***turbulent shear layer***) or *stochastic fluctuations of the heat release*. It results from the *unsteady processes of volumetric expansion* in the reactive region ([II-61], [II-62], [II-63], [II-64]). The main source of direct noise results from the rate of *change of heat release rate* (***fluctuation of the heat release***) associated with the chemical conversion of the reactants ([II-35], [II-65], [II-66], [II-67], [II-68], [II-69]).
Direct combustion noise can be divided in two different types:

A) ***"Combustion roar"*** is a turbulent combustion noise with a *broadband noise* in the spectrum ([II-5], [II-6], [II-7], [II-67], [II-70], [II-71], [II-72]). Under normal operating conditions the noise sources are incoherent and radiate a *broadband of frequencies*. It is a source term which is independent of the acoustic pressure field (the flame as autonomous source of sound).
Combustion roar, which shows a broad spectrum, is caused by the (autonomous) noise generation by a flame due to the turbulent fluctuations in the flame, possibly in combination with acoustic resonance. Combustion roar is further interesting from an academic point of view since the noise from a flame can be thought of as a *'fingerprint' of the turbulence in the flame*; *noise measurements can be used to qualify flames*.
The study of combustion roar has become important with the increasing interest in *environmental noise pollution*. Especially the noise generation by jet engines from aircrafts has received a lot of attention. From that research it appeared to be very hard to make the flame more silent.

B) ***"Combustion driven oscillations"*** that combustion instabilities with *narrowband noise* in the spectrum ([II-3], [II-72], [II-73]): they are characterized by a *discrete frequency* and a *feedback* cycle to maintain the oscillation. It is a source term that is a function of the acoustic pressure field, then the flame acts as amplifier of sound. Under *unstable operation* a feedback is established between the sound sources and pressure perturbations propagating in the system. To be able to study the occurrence of combustion driven oscillations it is necessary to take the acoustic system of the complete combustion installation into account.
Then *combustion driven oscillations* involve a feedback cycle that converts chemical energy into oscillatory energy. *Combustion driven oscillations* always involve one (or more) specific frequencies. The pressure amplitude at this frequency can be very high (in certain cases up to 50% of the mean pressure in the combustion chamber). These large pressure amplitudes may cause serious damage to the combustion installation.
Noise radiation becomes more coherent as it is tuned on one of the resonance frequencies of the system ([II-26], [II-34], [II-47], [II-74], [II-75]). This usually involves a cyclic

perturbation of the flow inducing a periodic motion of the flame and associated fluctuations in *heat release rate*. The heat flux to the combustor walls are intensified, structural vibration is induced and this may lead in extreme cases to failure (e.g. *Rayleigh criterion*).
In the period of the first rocket launches (about 1950-1970) a lot of research was performed on the very severe combustion driven oscillations which were observed in rocket engines.
At about 1970 there was a renewed interest for combustion driven oscillations. One of the reasons was the switch over of many combustion installations from oil to natural gas. Under certain circumstances these installations with gas burners showed instabilities where the same installation with oil burners had been stable. One of the remedies in power plants was to redistribute the burners in the boiler 'wall', by this redistribution the coupling between the acoustics and combustion was changed.
Since about 1990 the interest in the occurrence of combustion instabilities is growing, especially in gas turbine combustion research. Due to stricter environmental legislation with respect to the emission of pollutants, especially NO_x, it has become necessary to use lean premixed combustion. It appears that this type of combustion is accompanied in many cases with instability problems.
Many modern gas turbines (of all manufacturers) have a limited window of parameters in which they can operate stably. This window of stable operation is determined by trial and error during operation in the field. It is not (yet) possible to predict under which circumstances an installation will be stable or unstable. From history it can be found that for (almost) all new types of burners there have been problems with combustion driven oscillations.

In an unsteady flame the *fluctuating density* acts as a volume source of sound (the volume of the flame fluctuates with the reciprocal of the density). The main cause for the fluctuating density are ***fluctuations in the heat release***. The distinction between ***combustion roar*** and ***combustion driven oscillations*** is based on the origin for these *heat release fluctuations*. In *combustion roar* the density fluctuations are caused by autonomous (e.g. turbulent) fluctuations in the heat release. In the case of *combustion driven oscillations* the heat release of the flame depends on the acoustic phenomena in the combustion chamber, due to a feedback loop between acoustics and combustion.
Then the *direct combustion noise* source depends more directly on the combustion process and is controlled by the unsteady heat release taking place in the combustion region. This process is also influenced by interactions with the *boundaries*, which partially reflect sound waves generated by combustion.
In addition, some other direct combustion noise phenomena are possible, such as the interaction with ***vortex shedding*** and the combustion amplification of periodic flow phenomena (***Strouhal-type combustion noise***).
This is a useful classification system because it helps the researcher focus his efforts on a given aspect of combustion noise generation. Two or more of *these combustion noise mechanisms can and generally do coexist* in a given situation, thus making it difficult to isolate one from the other experimentally.

II.3.4.3.3 Indirect combustion noise (entropy noise)

Indirect combustion noise, or *entropy noise* as it is sometimes called ([I-4] § 5, [II-47], [II-55], [II-57], [II-76], [II-77], [II-78], [II-79]), occurs when the hot products of combustion (i.e. the hot spots) pass through the steep pressure gradients encountered in the turbine and exhaust nozzle. It is generated mainly by *temperature non-uniformities*, which are convected out of the combustion chamber and then accelerated ([II-66], [II-76], [II-80]) for example downstream the gas-turbine combustion chambers in the first turbine stage.
Only a small fraction of the perturbation energy is *directly* radiating as noise (direct noise) from the flame front. The rest is carried silently by the hydrodynamic modes of perturbation through the combustion chamber. Such hydrodynamic modes (i.e. velocity components, vorticity) of perturbation are *non-isentropic perturbations* of the fluid state and vortices according to the definition of Chu and Kovasznay ([I-4] § 8, [II-27]). In contrast to the isentropic linear acoustic perturbation of direct noise, they move with the flow speed as a pattern of *"frozen turbulence"*.
In a homogeneous moving fluid the interaction of the hydrodynamic perturbations with each other and with sound waves is of second order according to Chu and Kovasznay [II-27]. However, the interaction becomes first order, once the gradients of the average flow field reach the order of the average field quantities.[2] Thus, such large flow gradients lead to a relevant energy transfer between *acoustic* (i.e. pressure, transmitted and reflected sound wave of direct combustion noise), *vorticity* (i.e. velocity components) and *entropy mode* (i.e. temperature and composition fluctuations) waves.
The sound of *entropy noise* is therefore generated during the passage of a "silent" fluid inhomogeneity, such as an entropy spot (i.e. hot spots), that past an obstacle in the flow. It is produced by the acceleration of a fluid particle with an entropy different from the main flow.
Indirect combustion noise results when relatively ***large-scale temperature nonuniformities*** (T') generated by turbulent combustion are convected through pressure gradients in the turbine. This produces an *entropy fluctuation* (S') in conformity with the first and second laws of the thermodynamics. Since the density of an ideal gas depends on any two independent thermodynamic properties, say entropy and pressure, a *density fluctuation* (ρ') occurs whenever an entropy nonuniformity is convected through the pressure drop associated with a stage of the turbine. Then, *entropy noise* is the large amplitude pressure wave that can be generated by the interaction of ***density oscillations*** with the ***pressure gradient***.
This large amplitude pressure perturbation propagates in the downstream direction (towards the nozzle) and constitutes a source of *indirect noise*.
Indirect noise is produced when ***temperature fluctuations*** due to the combustion process traverse an inhomogeneous region characterized by mean flow gradients. Then *it is generated by the coupling between a* ***convective entropy mode*** *and the* ***mean flow velocity*** *or* ***pressure gradients***.
Using *pressure*, *vorticity* and *entropy* the basic flow equations decouple for homogeneous mean flow and small perturbations into three wave equations: it is named ***"Entropy waves"***.
In a non-constant mean flow like in an accelerating nozzle flow the flow equations are coupled and entropy waves are source terms in the acoustical wave equation: it is named ***"Entropy noise"***.

[2] The speed of sound has to be considered as reference for the velocity to define a large gradient ([I-4] § 8).

In the case of a combustion system the non-isentropic modes of perturbation which show up as *hot* and *cold spots* (e.g. imperfect mixing, etc.), which are referred to as entropy modes are thought to carry particularly large amounts of energy. The flow gradient in the contracting outlet nozzle then allows a leakage of energy from the hydrodynamic modes into the acoustic and other hydrodynamic perturbation modes. Sound waves, which travel at the speed of sound, and secondary vortices are generated ([II-27], [II-76], [II-81]). The process repeats itself in each turbine stage with the remaining hydrodynamic perturbation and an additional contribution of the secondary vortices to the indirect noise generation as described by Richter and Thiele [II-82]. The secondary vortices are generated by the interaction of non-isentropic perturbations with the rotor and stator blade flow field. Accordingly, additional indirect noise is radiated from the outlet nozzle of the combustion chamber and each turbine stage. This indirect noise generation is sometimes also addressed by the terms *entropy noise* or *excess noise* or even as acoustical *"bremsstrahlung"* by Ffowcs Williams and Howe [II-81].
Usually the source on *indirect combustion noise* is a *dipole source*.
Since the nozzle guide vanes of the first turbine stage in high performance propulsion systems are choked under almost every relevant operating condition of aero-engines, hot spots passing through the nozzle are connected with mass flow variations (*monopole sound source*) and also with momentum flux variations (*dipole sound source*). Gas temperature nonuniformities may cause also broadband noise in all turbine stages, since the related density fluctuations cause pressure fluctuations during the acceleration through each turbine stage.
Entropy noise receives increased interest by the aero-engine industry because it may have a major contribution to the total noise emission of combustion systems. Direct Numerical Simulations (DNS) of turbulent combustion flows [II-83] resolved the sound generated by accelerated entropy waves as the main contribution to the total noise radiation. Just recently the results of a numerical study [II-84] have been published, which predict the relevance of *indirect combustion noise* compared to direct combustion noise to be a factor *10 larger at aero-engines*. Then, the *indirect noise* produced in the combustion chamber exit nozzle of a modern aero-engine is **one order of magnitude larger than the *direct noise* of the turbulent flame** [II-84]. Thus, the phenomenon can be considered essential to the understanding of turbo-machinery core noise for current and future aero-engine designs.
With the noise reducing improvements achieved for other aero-engine components, e.g. low noise fan design and jet noise reduction by high bypass ratios, the noise concern in aero-engine developments also includes the combustion noise issue. Especially at helicopter engines, which emit almost no jet noise, the **entropy noise seems to be of high importance**.
The *indirect combustion noise* source is of importance in high performance propulsion systems because the combustor operates at elevated pressures and burnt gases are exhausted through turbine bladerows or directly through a nozzle. The coupling between hot spots generated by combustion and mean flow gradients then gives rise to pressure perturbations. The amplitude level of the radiated pressure depends in this case on the combustion mode and on the type and intensity of temperature fluctuations reaching the combustor exhaust section and convected into the mean flow velocity gradient.
Effects of entropy waves on the combustor stability were studied by many authors with diverse conclusions ([I-4] § 5, [II-85]). It is generally admitted that **convection of *entropy fluctuations*** (e.g. *Chu's criterion*, [II-86], [II-87]) **may be significant in the development of instabilities** if the flame region is not too far from the nozzle exit, but this will depend on the dispersion and dissipation of these waves as they travel through the system.

The generation mechanisms and parameter dependencies of entropy noise are still not completely explained. A clear and distinct experimental proof of the existence of entropy noise was not carried out up to now and a comprehensive parameter study on entropy noise for validation purpose of numerical and analytical models is still missing.

II.3.5 Experimental diagnostics of combustion instability

Instrumentation for Combustion-Dynamics Monitoring systems takes a variety of configurations that varies between the *Original Equipment Manufacturers* (OEM), engine class, and user. In general, qualitative accuracy of pressure pulsations combustion-dynamics monitoring data is not as important as, say, temperature or static-pressure measurements. The reason for this is that original equipment manufacturers do not know a priori what an unacceptable level of pressure amplitude at a given frequency is based on part-life or failure analyses. Rather, in general, such information is determined, empirically often by the users.
To minimize development costs and time, it is critical to possess the ability to evaluate the dynamic behaviour of a combustor design during the component-development phase, thereby mitigating the need for design changes during expensive full-scale engine testing late in the development cycle. Solutions can be evaluated and developed proactively and more quickly through analyses and laboratory-scale experiments, enabling a faster transition of technology into production engines.
It should be obvious that the complete and accurate description of a thermo-acoustic instability can be a daunting task, since the system under consideration may involve a variety of fluid-dynamic and physico-chemical phenomena, covering a wide range of space and time scales.
Combustion noise is characterized by three information and then by three results:

1. the **spectral analysis** and the **peak frequency** of the radiated sound;
2. the **directional distribution** (or **directivity**);
3. the **overall radiated sound power** (or the **thermo-acoustic efficiency**).

II.3.5.1 Spectral analysis

Combustor dynamics are commonly analyzed in the frequency domain by applying a *Fast Fourier Transform* (FFT) to the time-domain pressure signal of each combustor (see Attachments B and C). Although the FFT is rigorously defined, important field issues associated with how the FFT has been set up arise when comparing amplitudes from engine and when trying to compare the different *Original Equipment Manufacturers* (OEMs).
Spectral data are recorded and stored by a data-acquisition system. It is not practical to save continuous frequency and amplitude data of the entire spectrum for every combustor. A common practice is to save the peak amplitude observed within each spectral bin (called ***"peak hold"***) over some interval, commonly 1 minute. These data are then compared with frequency-dependent alarm-threshold levels, which warn of harmful or abnormal conditions. Note that these alarm thresholds are determined empirically. All that is really known from this type of data is that large amplitudes are damaging and low amplitudes are less damaging.
The **sound spectrum** of a turbulent flame is rich in information about turbulence scales, burner geometry, convective velocities, flame speed, and so forth. This has led to the development of a

school of combustion diagnostics which exploits details of the spectral shape out to frequencies of several thousand hertz.

II.3.5.2 Directivity effects

While combustion noise is essentially radiated isotropically, experiments on open turbulent flames indicate that there are some *directivity effects*. Smith and Kilham in 1963 [II-62] found that the preferred directions of acoustic propagation for the flames tested lie between 40° and 80° from the burner axis. These authors attribute the measured directivity to convection of sound sources by the flow. Price et al. in 1969 [II-88] also confirms the quasi-isotropic character of noise radiation when the acoustic wavelength greatly exceeds the typical dimensions of the flame ($\lambda_a >> L$) with a preferred direction at 80° for long turbulent non premixed jet flames when the flame length L is no longer small compared to λ_a ($L<\lambda_a$).
Some directivity can be due to propagation of sound through flow field inhomogeneities and specifically temperature gradients [II-69].

II.3.5.3 The thermo-acoustic efficiency

The key parameter for determining the overall radiated sound power is the ***thermo-acoustic efficiency***, defined as the fraction of the combustion heat release which is radiated away as acoustic energy in the far field.
It has been observed that *the overall radiated acoustic power associated with gas turbine combustion noise is of the order of only a few parts per million of the total thermal power. Only a small part of the total power produced in a combustor is involved in combustion instabilities*, then it suggests that *the existence and severity of these instabilities may be sensitive to apparently minor changes in the system* (e.g., $\dot{\omega}_T^1$ or p_1). That assertion is confirmed by experience.
The thermo-acoustic efficiency of an open turbulent flame generally changes when the same flame is placed within an enclosure. There are two reasons for this change:

- The enclosure modifies the steady flow through the flame, thereby producing fundamental changes in the combustion process.
- In certain particular situations, coupling may exist between the acoustic response of the combustion system and the heat release process. The presence of an enclosure can cause pressure waves created in the flame zone to be returned to the flame zone with a *time delay* that depends on the length and average sound speed in the combustor. Energy is added to the pressure wave at any frequency for which the instantaneous peak in *acoustic pressure* (p) in the flame zone coincides with the instantaneous peak in *heat release* ($\dot{\omega}_T$). When this critical situation holds, the wave grows in amplitude.

II.4 Flame/acoustic interactions

Coupling mechanisms between acoustic waves and flames have become central issues in the development of many combustion systems because of both environmental issue (noise) and the destructive interactions that acoustics can generate in combustors.
Flame/acoustics coupling can operate in different way:

a) ***flames produce noise*** ([II-35],[II-36],[II-56]) and environment issues make the reduction of noise an important topic;
b) ***flames can be influenced by noise*** and acoustic waves leading to a *resonant interaction*.

a) The first manifestation of such instabilities have been known for a long time (Rayleigh [II-39]; Putnam [II-3], [II-4], [II-5], [II-6], [II-7]; Williams [II-89]) in many practical systems. In the 1802 Higgins ([II-90], [II-91]) discovered ***"singing flames"*** when a jet of ignited gas was inserted into the tube open at both ends. The frequency of singing coincided with the natural frequency of the tube. Sound was produced only at certain ranges of system parameters.
The simplest demonstration of combustion instabilities, and thus one of the most studied systems, is the *Rijke tube*. This phenomenon was discovered by De Rijke in the 1859 [II-92] and it was analyzed by Rayleigh in the 1877 [II-93]. In a Rijke tube, a heat source, usually a flame, is placed in a tube open at both ends: if the flame is placed in the lower quarter of the tube, the pressure and velocity are in phase making the Rayleigh index positive, and the oscillation grows to a *self-excited limit cycle*. It is assumed that the heat release rate varies approximately with the velocity. A Rijke tube is a convenient system for studying thermo-acoustic instabilities both experimentally and theoretically. An excellent review of Rijke tube work was performed by Raun [II-94] and by Bisio and Rubatto [II-95].
When the heat release is due to a flame, much energy can be injected into the oscillation modes and the effects of the resonant interaction and combustion instabilities can be spectacular: in addition to inducing oscillations of all flow parameters (*pressure*, *velocities*, *temperature*, etc), such phenomena increase the amplitude of *flame movements* and the *levels of heat transfer to walls*; in some extreme cases, they can destroy part of the burner and induce a loss of control of the system. At the same time, burners submitted to instabilities usually have a *higher efficiency*: pulse combustors which are designed to oscillate have high burning rates ([II-96], [II-97]).
However, most combustors are not designed for such regimes and combustion instabilities are usually undesired and harmful phenomena.

b) The sensitivity of flames to music at a musical party was noted by Le Conte in 1858 [II-98] and described like the ***"dancing flames"*** in the following quotation: *"Soon after the music commenced, I observed that the flame exhibited pulsations exactly synchronous with the audible beats. This phenomenon was very striking to everyone in the room, and especially so when the strong notes of the violoncello came in … A deaf man might have seen the harmony…"*.
Even when flames are not submitted to strong combustion instabilities, acoustic wave interact with turbulent combustion in a number of situations and can modify flames as significantly as turbulence does. Moreover, *acoustic wavelengths* in most combustion chambers are of the

order of 10 cm to 3 m and acoustic perturbations have a spatial coherence which can amplify their effects over the full combustion chamber (while turbulent length scales are much smaller). Then *the effect of acoustics on turbulent combustion can be both significant and very different from the action of turbulence*, suggesting that a proper description of turbulent combustion chambers must incorporate effects of acoustic wave.
Numerically the importance of acoustic waves also emphasizes the need for sophisticated boundary conditions: using boundary conditions which can handle correctly the transmission and the reflection of acoustic waves on boundaries become a critical issue in many reacting flows.
Studies of combustion instabilities and noise are numerous ([II-35], [II-36], [II-56], [II-73], [II-99], [II-100], [II-101], [II-102], [II-103]) and started long ago by Rayleigh [II-39].

II.4.1 Coupling mechanisms between acoustic waves and flames

Coupling mechanisms between acoustic waves and flames have become central issues in the development of many combustion systems because of environmental issue (noise) and due to the structural damage that such an interaction may produce in combustors (thermo-acoustic instabilities). The effect of acoustics on turbulent combustion can be significant and very different from the action of turbulence itself, suggesting that a proper description of turbulent combustion chambers must incorporate effects of acoustic waves. Understanding these interaction is also important for combustion diagnostic and control.
Currently little is known about the mechanisms by which the flame responds to acoustic waves. The complexity of such an interaction is higher for turbulent flames than for laminar flames, due to the larger variety of fluid-dynamic and thermo-chemical scales involved both in space and time. Efforts in understanding this interaction have been mainly done by means of *numerical approaches* ([II-104], [II-105], [II-106] § 8.3.7), while less has been done *experimentally* ([II-37], [II-47], [II-107], [II-108], [II-109], [II-110], [II-111], [II-112]).
Attention is usually focused on three themes ([II-113], [II-114]): effect of external acoustic oscillations on nonreactive flowfields (no flame present), response of flames to harmonic oscillations, and flame-vortex interaction. Studies are commonly performed on injection systems equipped with a bluff-body that favours flame stabilization by means of the associated recirculation zone: hence, bluff-body devices are good models of burners used in industrial applications.
It was observed that forced acoustic oscillations favour vortex roll-up in separated shear layers of nonreactive flowfields at frequency commensurate with the excitation frequency, and also produce velocity fluctuations at other frequencies due to nonlinearity ([II-113], [II-115], [II-116]). In experiments with weakly turbulent flames, it was also observed that no periodic disturbances of the flame front appear in the absence of acoustic forcing, although it does exhibit occasional corrugations ([II-115], [II-117]), but the flame front is periodically distorted, especially close to the injection, as acoustic forcing is introduced, due to the roll-up of the separated shear layer into coherent structures [II-115]. Besides these observations, it must be reminded that even if a flame is distorted by shear layer instabilities, at the same time it tends to dampen these fluctuations (via the increased molecular viscosity and local dilatation due to heat release) smoothing out the produced wrinkles during its front propagation ([II-113], [II-114],

[II-118], [II-119]). Furthermore, the presence of a flame front causes acoustic wave reflection and changes the phase of velocity perturbation ([II-120], [II-121], [II-122], [II-123]).
As a matter of fact, the nature of a flame can be strongly altered depending on the amplitude of the acoustically generated vorticity perturbation, as shown by fundamental studies of vortex-flame interaction ([II-113], [II-124], [II-125], [II-126]). An important phenomenon affecting this interaction is the baroclinic effect that couples pressure and density gradients. Its torque action becomes stronger with increasing the amplitude of the perturbation [II-114]. However, even though in case of strong flame distorsion the baroclinic term can produce vorticity of opposite sign along a corrugated flame sheet [II-126], its global effect has been proved to be secondary with respect to shear layer generated vorticity [II-114].

II.5 Causes of instabilities and damping processes

Turbulence in the flow and the flame causes an unsteady variation of the flame shape and the local reaction rates, thus, causing a broadband noise level, commonly referred to as *combustion noise*.
Turbulence, inherent in the inlet air and fuel mass flows, causes a fluctuating heat release and thus a fluctuation of density and pressure, i.e., a generation of sound. These pressure disturbances propagate as acoustic waves through the combustion chamber, are reflected at the boundaries, and travel back to the burner. Here, they modulate the inlet mass flows and the thermoacoustic feedback cycle is closed. If the phase relationship is as such that it promotes constructive interference, disturbances, which were initially infinitely small, might grow until the process is saturated by *non-linear effects*. At a first glance, this thermoacoustic feedback cycle is rather easy to understand. However, the physical mechanisms involved, are manifold and very complex.
Although known for more than 200 years (in fact, Higgins was the first to document the *"singing flame"* around 1802) and having an industrial relevance for nearly 80 years, thermoacoustic instabilities still pose what is probably the largest problem in *ultra low-NO_x gas turbines*. A great many of researchers from industry and academia were and are devoted to this problem and a vast amount on excellent publications on the individual driving mechanisms exists. Although probably all major mechanisms leading to thermoacoustic instabilities are identified, up to know, not all of these mechanisms, above all their non-linear saturation effects as well as the importance of each of them, are fully understood.
Furthermore, the complex interactions between these mechanisms often do not allow to decouple them and usually more than one is responsible for an instability to occur.
The prevalence of instabilities in combustion systems can be primarily attributed to two fundamental causes:

a) **combustion chambers are almost entirely closed** and the internal processes tending to attenuate unsteady motions are weak;
b) the energy required to drive unsteady motions represents an exceedingly **small fraction of the heat released by combustion**.

These underlying issues are present in any combustion chamber, but are especially consequential for systems such as gas turbine engines, in which energy intensity is quite high.

II.5.1 Feedback loop responsible for combustion instabilities

Combustion instabilities are excited by feedback between the combustion process and acoustic oscillations that depends on the system characteristics and operating conditions. The generic feedback loop responsible for combustion instabilities consists of the following sequence of events:

1. *Fluctuations in the velocity* and/or *thermodynamic-state variables* induces a *fluctuation in the heat-release rate*.
2. *The heat-release fluctuation* excites *acoustic oscillations*.
3. The *acoustic oscillations* generate the velocity and thermodynamic-state variable fluctuations that are described in step 1, thus closing the feedback loop.

Depending on the relative magnitudes of the energy added and removed from the acoustic oscillations, the amplitude of oscillations may decrease, remain constant, or grow during each cycle of this loop.

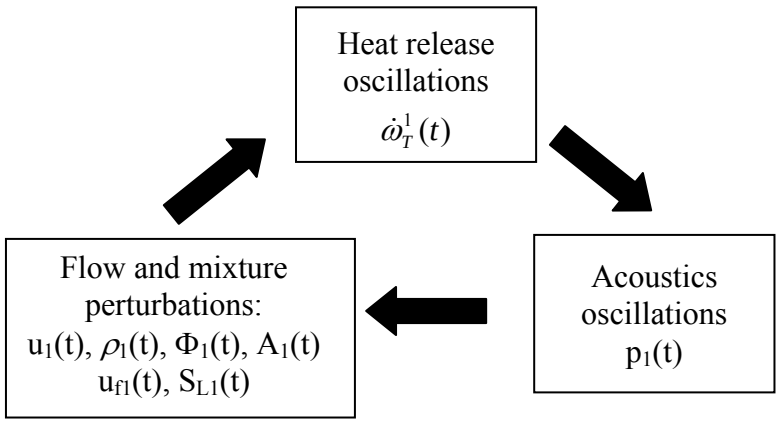

Fig. II-5: Scheme of the feedback processes responsible for combustion instabilities.

II.5.2 Mechanisms of driving combustion instabilities

In all cases the sources of combustion noise (direct and indirect) are related to the flame dynamics and to unsteady rates of heat release. The analysis of combustion noise is then intimately tied to an understanding of dynamics of perturbated flames. The relationship with the heat release oscillations has been explored in a set of recent studies. On the experimental side much has been learnt from detailed experiments.
In combustion noise research for flows at low Mach numbers the effect of *unsteady heat release* was considered the most dominant source contribution and therefore, the investigations mainly pursued analyzing the acoustic output of that mechanism ([II-68], [II-127], [II-128], [II-129]): heat release from chemical reactions is the major energy source driving unsteady flow oscillations in combustion systems. The dominant contribution of the *unsteady heat release* to the acoustic pressure field led in the research field of flame diagnostics to the idea of formulating an inverse problem in which the unsteady heat release distribution is determined by measuring the acoustic pressure field in open [II-130] and in confined ([II-131], [II-132]) systems.
The flame's fluctuating heat release was inferred from chemiluminescence measurements. It was shown that the inferred *heat release spectra* had peaks at the same frequencies as the *pressure* and *velocity spectra*, although the spectral content is greater at lower frequencies, suggesting that **the flame acts in a similar way to a low-pass filter**, as reported in several studies ([II-133], [II-134], [II-135], [II-136], [II-137]).
It is often difficult to sort out cause-and-effect relationships from measurements made on an unstable system. A large number of potential coupling mechanisms could be at work in any one system. Modelling and detailed experimentation are often required to acquire this information.
Several mechanisms capable of driving combustion instabilities in gas turbines have been identified ([I-32]; [II-34] § 1, 4 and 9):

A) Heat release as a pressure source

Because self-excited oscillations are typically caused by a coupling between the heat-release rate of the flame and the acoustics, eliminating the heat-release fluctuations ($\dot{\omega}_T^1$) also eliminates the acoustic oscillations (p_1).

1) **Flame interactions**
By using well-controlled experiments, it is shown that *rapid changes of the flame surface* (A_1) generate an intense radiation of sound. In practical situations, there are many possible mechanisms that may produce or destroy flame surface at a fast rate, such as *flame-wall interactions* and *collisions between adjacent flames* or *between neighbouring flow structures* like vortices or reactant jets. These processes may feed energy into a resonant mode if they are properly phased with respect to the pressure. Fast changes in *flame-surface area* (A) constitute an important driving process of combustion instabilities. Three distinct mechanisms are usually involved (e.g., [II-47], [II-107], [II-138]):

   a) ***Flame-vortex interaction: vortex shedding and flame roll-up by vortex structures***
   In the first mechanism, *the flame is rapidly changing because of vortex roll up*.

The vorticity fluctuations (Ω_1) directly causes a volumetric expansion (and then A_1), leading to the heat-release fluctuations ($\dot{\omega}_T^1$) and then to a pressure pulse (p_1, pressure wave radiations). This can be represented globally by the following expression:

$$\text{Flow perturbation } u_1 \rightarrow \Omega_1 \rightarrow \text{flame roll-up} \rightarrow A_1 \rightarrow \dot{\omega}_T^1 \rightarrow p_1$$

Large-scale, coherent vortical structures caused by flow separation from flame holders and rapid expansions, as well as vortex break-down in swirling flows, are often present in gas-turbine combustors.
The mere observation of vortex shedding at the instability frequency under *limit-cycle* conditions does not necessarily imply that it is also responsible for initiating the instability. Vortex shedding can be forced at the frequency of an external excitation when the forcing occurs at sufficiently large amplitude, even if this frequency does not coincide with the natural shedding frequency.
These oscillations are often detected as a *very-low-frequency* mode, with $f < 30$ Hz.
Then, *flame-vortex interaction* ([I-21], [II-37], [II-113], [II-115], [II-139]) refers to the interaction between the flame front and vortices that are periodically shed at the entrance to the combustor. As the vortex passes through the flame front, the flame is stretched by the vortex. Depending on the rate at which the flame is stretched and the local equivalence ratio (Φ_1), this interaction can either increase the flame area (A_1) and hence the rate of heat release ($\dot{\omega}_T^1$), or it can lead to local extinction and as a result decrease the rate of heat release.

b) *Flame-flame interaction and mutual annihilation of flame area*

In the second mechanism, the rapid consumption of reactants trapped between two adjacent flames may produce a heat-release pulse ($\dot{\omega}_T^1$) and the subsequent emission of pressure waves (p_1). If this interaction is properly phased with respect to an acoustic eigenmode, it may drive the unstable motion.
This can be represented globally by the following expression:

$$\text{Flow perturbation } u_1 \rightarrow \text{Flame wrinkling} \rightarrow \text{flame front annihilation } A_1 \rightarrow \dot{\omega}_T^1 \rightarrow p_1$$

c) *Flame-wall boundary interaction*

In the third mechanism, *the vortex interacts with a wall* or another structure, which induces a sudden ignition of fresh material or thermal losses. Interactions of flames with solid walls constitute a source of heat-release fluctuations. The interaction of a perturbed flame with a wall can induce rapid changes of flame-surface area (A_1) and heat-release fluctuations of large amplitude ($\dot{\omega}_T^1$), and these fluctuations can generate an intense sound field (i.e., p_1, pressure wave radiations):

$$\text{Flow perturbation } u_1 \rightarrow \text{Flame wrinkling} \rightarrow \text{wall} \rightarrow A_1 \rightarrow \dot{\omega}_T^1 \rightarrow p_1$$

Previous data have concerned unconfined flame configurations driven by velocity perturbations. These cases are less dependent on the geometry because sound generation is not modified by reflection from boundaries. It is also easier to examine unconfined flames with optical techniques. However, in many applications, combustion takes place from the combustor inlet or exhaust sections. The presence of boundaries has two main effects:

- boundaries modify the reflection response of the system;
- boundaries modify the flame dynamics by changing the geometry of the flow in the system.

The first item is easily treated by considering the eigenmodes of the system and expanding the pressure field on a basis formed by these modes. The second item is less well documented but is clearly important. The presence of boundaries not only modifies the structure of the mean flow but also influences the flame dynamics.

2) **Equivalence ratio oscillations** (i.e., **fuel/air ratio oscillations**). This type of interaction ([I-32], [II-59], [II-140], [II-141], [II-142], [II-143], [II-144], [II-145]) is often identified with *midrange frequencies*, with f=50-1000 Hz.

3) **Fuel feed line-acoustic coupling** (i.e., **fuel flow rate oscillations**)
Feed-system coupling [II-30] refers to a modulation of the fuel flow rate caused by pressure fluctuations in the combustor and fuel-delivery system. This modulation results in a fluctuating fuel concentration that is convected to the flame front and produces a fluctuating rate of heat release. If the fuel fluctuation arrives at the flame front in-phase with the pressure fluctuation, the resulting heat-release fluctuation amplifies the oscillations, whereas, if the fuel fluctuation arrives at the flame front out-of-phase with the pressure fluctuation, the resulting heat-release fluctuation damps the oscillations.

4) **Oscillatory atomization, vaporization and mixing**
Interactions of acoustic field with the fuel spray produce periodic variations of the fuel-spray shape, droplet sizes, evaporation rates, and mixing rates of the fuel vapour with surrounding gases.
Spray-flow interactions ([I-32], [II-26]) refer to several phenomena that act to drive unstable combustion, including oscillations in droplet atomization and droplet vaporization and spray-vortex interaction. Any of these phenomena can cause modulation of the fuel concentration and/or fuel distribution and thereby produce fluctuations in the rate of heat release.
Fuel/air mixing is a possible mechanism of flow instabilities and then leading to oscillations of thermo-acoustic instabilities ([I-32], [II-59], [II-140], [II-146]).
The fluctuations of the mixing can be attributed to flow instabilities, e.g. *Kelvin-Helmholtz instabilities* [II-147], *vortex shedding* and PVCs (i.e., *precessing vortex core*) ([I-30], [II-148]) which may feed combustion oscillations.

Two mechanisms are known to be particularly significant in ***premixed systems***: these are ***vortex shedding*** and ***fuel/air ratio oscillations.***

- The *vortex shedding mechanism*, as its name suggests, is due to large scale, coherent vortical structures. These structures are the result of flow separation from flameholders and rapid expansions, as well as vortex breakdown in swirling flows. They are convected by the flow to the flame where they distort the flame front and thereby cause the rate of heat release to oscillate.
- In the second mechanism, acoustic oscillations in the premixer section cause *fluctuations in the fuel and/or air supply rates*, thus producing a reactive mixture whose *equivalence ratio varies periodically in time*. The resulting mixture fluctuation is convected to the flame where it produces heat release oscillations that drive the instability. The coupling of the premixer acoustics with the fuel system is affected by the pressure drop across the fuel injector.

Vortex shedding and *fuel/air ratio oscillations* become important when the resulting heat release perturbation is in phase with the pressure fluctuation. This can be expressed by the following relationship:

$$\tau_{conv} + \tau_{chem} = kT \qquad \text{(II-24)}$$

where τ_{conv} refers to the time required for either the equivalence ratio perturbation or the vortex to convect from its point of formation to the "center of mass" of the flame, τ_{chem} refers to the chemical delay time, T refers to the acoustic period, and k is an integer constant whose value depends upon the combustion chamber acoustics ([II-145], [II-149], [II-150]).
Variations in fuel composition impact the phase relationship expressed by Eq. (II-24) by affecting both the convective and chemical times. The effect of fuel composition on the chemical time (τ_{chem}) is clear. The effect on the convective time (τ_{conv}) can be better understood from the following equation which expresses the convective time as the sum of the *convective time in the premixer* (τ_{pm}) and the *convective time in the combustor* (τ_{comb}):

$$\tau_{conv} = \tau_{pm} + \tau_{comb} = \frac{L_{pm}}{u_{pm}} + \frac{L_f}{\alpha\, u_{comb}} \qquad \text{(II-25)}$$

where L_{pm} refers to the distance from the point of origin of the disturbance to the entrance to the combustor, u_{pm} refers to the mean convective velocity in the premixer, L_f refers to the distance the perturbation travels from the combustor entrance to the center of mass of the flame, and u_{comb} refers to the mean convective velocity in the combustor, which can be expressed as a fraction α of the velocity in the premixer.
The effect of variations in fuel composition on the convective time is primarily the result of the effect of flame speed on the location of the flame center of mass. For example, *increasing the percentage of hydrogen in a syngas* fuel will increase the flame speed and therefore change the location of the flame center of mass.
As the flame speed increases, as a result of increasing the equivalence ratio, the distance to the flame center of mass decreases, which corresponds to a shorter convection time in the combustor: such a change can cause a stable combustor to go unstable or an unstable combustor to go stable.

B) Heat-release fluctuations driven by pressure waves

1) **Flame response to upstream modulation: oscillatory flame area variation**
This path may be investigated by moduling an initially stable flame by acoustic waves, in fact the forcing technique is used to study the presence of a coupling mechanism.
Interactions of acoustic velocity oscillations with the flame cause periodic variation of the *flame area* and, thus, a periodic heat-addition process that drives the acoustic field. This type of interaction is often identified with *high-frequencies*, with f >1000 Hz.
This interaction can be represented schematically by

Acoustic wave motion p_1 → Flow modulation u_1 → Flame surface wrinkling A_1 → $\dot{\omega}_T^1$

2) **Flame response to composition inhomogeneities**
Experiments and theoretical analysis indicate that certain types of instabilities in lean premixed combustors may be driven by perturbations in the fuel-air ratio (Φ_1).
This situation can be illustrated by assuming that pressure oscillations (p_1) in the combustor interact with the fuel-supply line (injection perturbation) and change the fuel flow rate (u_{f1}).
The interaction may also take place with the air supply, which will also affect the equivalence ratio (Φ_1). This type of interactions will produce a heat-release perturbation ($\dot{\omega}_T^1$), which, if properly phased with the pressure, may feed energy in the resonant acoustic mode involved in the process. This interaction can be represented schematically by

Acoustic wave motion p_1 → injection perturbation → u_{f1} → Φ_1 → convection → $\dot{\omega}_T^1$

3) **Flame response to unsteady strain-rate**
An unsteady strain-rate field can be induced by the resonant acoustic motion acting on the flow. Flow modulation may result from the field of variable strain-rate (ε_1), which can be induced by the unsteady motion (u_1) in the combustor (e.g. by premixed velocity). The variable strain-rate can produce or diminish the flame-surface area (A_1), and modify the local rate of reaction per unit surface ($\dot{\omega}_T^1$). If the fluctuations are suitably phased, they will feed energy back into the acoustic motion. This interaction can be represented schematically by

Acoustic wave motion p_1 → Flow modulation u_1 → Strain-rate ε_1 → Flame surface wrinkling A_1 → $\dot{\omega}_T^1$

The Fig. II-6 shows a simplified scheme of key instability mechanisms believed to be present in most practical lean premixed systems.
The fuel-air ratio disturbance is convected through the premixer into the combustion zone, leading to an oscillation in heat release. It is important noting that because of the low Mach

number of the flow in the passage of the flow velocity (typically, Ma~ 0.05), small pressure fluctuations (p_1) can result in significant fuel-air ratio oscillations. This can be seen by noting that

$$\frac{u_1}{U} = \frac{1}{\gamma Ma} \frac{p_1}{P}$$

If the heat release ($\dot{\omega}_T^1$) associated with the fuel-air ratio oscillations (Φ_1) is in phase with the original pressure waves (p_1), the oscillating heat release will augment the original pressure waves in the combustion chamber.
A finite convective ***time delay*** between the generation of a pressure wave and the associated fuel-air ratio exists. Once a perturbation in airflow (or fuel flow) occurs at the point of fuel injection, a finite time (of the order of milliseconds) is needed for this disturbance to be convected to the zone of heat release ([II-34] § 4). This travel time is also the time during which the mixing of the fuel and air takes place.

II.5.2.1 Energy transfer mechanisms

The energy exchange mechanisms in a turbulent reacting flow are summarized in the schematic diagram shown in Fig. II-7 ([I-32], [II-151]). The oscillatory motions can acquire energy through several different pathways. They may extract energy from the mean flowfield and chemical reactions, exchange energy with background turbulent motion, or be dissipated into thermal energy through viscous damping. When there are no chemical reactions, the primary energy provider for periodic motions is the mean flowfield and/or boundary effects. With combustion, heat release from chemical reactions is the major source for driving periodic motions. The transfer of energy from chemical reactions to the periodic flowfield only takes place when *heat release* is in phase with *pressure oscillation*.
The above analysis suggests that the dominant physical processes or mechanisms responsible for driving unsteady flow oscillations in a combustion system arise from either *heat release* or *gas dynamic fluctuations*, or both. The latter include acoustic motions in the chamber, evolution of large-scale coherent structures, and other flow phenomena. Heat release is largely related to local equivalence ratio and mass flow rate, together with instantaneous pressure and temperature. In a gaseous premixed flame, heat release fluctuations may result from flame surface variations, equivalence ratio fluctuations, mass flow rate oscillations, and vortex shedding processes due to hydrodynamic instabilities. In systems using liquid fuel, atomization and droplet vaporization are additional sources of periodic exothermicity of the combustion process. Many of these mechanisms capable of driving combustion instabilities in gas turbines have been identified and summarized by Zinn and Lieuwen ([II-34] § 1) and Ducruix et al. [II-152].

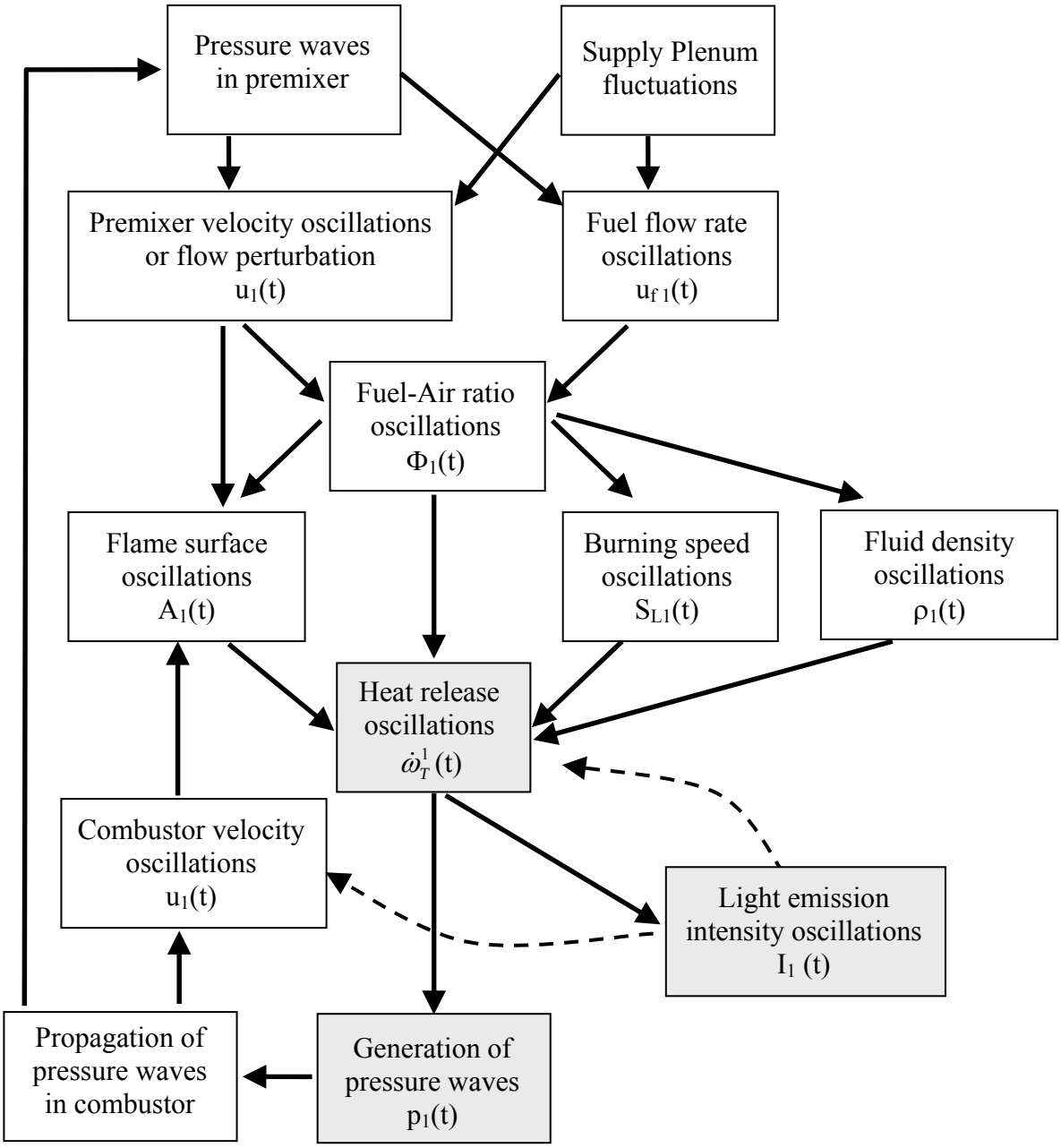

Fig. II-6: Driving mechanisms for combustion instability (modified by [II-34] § 4).

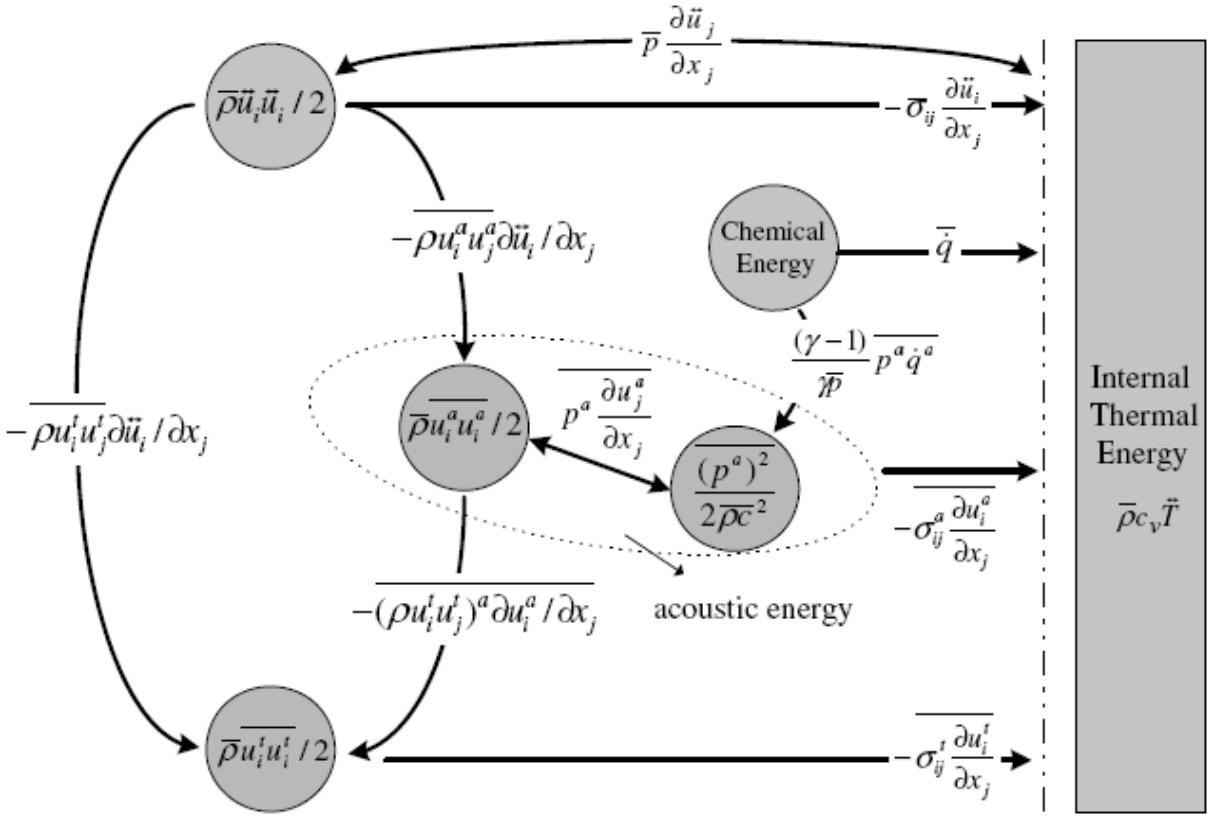

Fig. II-7: Diagram of energy exchange among mean, periodic, and stochastic motion in turbulent reacting flows ([I-32], [II-151]). Each flow variables $\Im$ cane be expressed as the sum of density-weighted long-time-averaged ($\overline{\tilde{\Im}}$), periodic (coherent, $\Im^a$) and turbulent (stochastic, $\Im^t$) quantities.

II.5.3 Frequency ranges in combustion instabilities

Combustion instability in a specific gas turbine engine can generally be classified by the oscillation frequencies and grouped into the following categories: *low-frequency*, *intermediatefrequency*, and *high-frequency instabilities*, but there is no universally accepted criterion with well-defined frequency boundaries currently available to define these three types of instabilities.
Three frequency ranges can be defined to describe combustion instabilities:

1) ***Low-frequency dynamics*** (LFD) occur at frequency ***f<50 Hz***. These dynamics are frequently referred to as ***"roar"***, ***"rumble"***, ***"breathing" modes***, ***"bulk" modes*** (i.e., ***"Helmholtz" modes***[3]). Because of the low frequency of these type of instabilities, this phenomenon is sometimes called ***"humming"***. In the industry, these types of oscillations

[3] It is a bulk pressure fluctuation that takes place inside the burner and occurs at relatively low frequency and the pressure is essentially uniform throughout the volume. The unsteady velocity is close to zero, but the pressure rises and falls.

are referred to as ***"cold tones"*** because their amplitude increase as the flame temperature decreases. They are often observed at very lean conditions near *blowout*. Low-frequency dynamics is one of the easiest modes to identify, and it is very audible and may sound like a freight train is running through the plant.

2) ***Mid-frequency dynamics*** (MFD) occur at frequencies in the range ***50<f<1000 Hz***. In general, the *first natural mode* in industrial gas-turbine combustor is between 50 and 300 Hz, depending on the geometry and firing temperature. In industry, these oscillations are often referred to as ***"hot tones"*** because their amplitude often increases with firing temperature and engine power output.
   This *intermediate-frequency* are usually associated with the *coupling between the fuel–air ratio and acoustic oscillations*. This type on instabilities usually correspond to the ***longitudinal acoustic modes*** of the combustor ([I-32], [II-34] § 5).
   Research efforts in the area of thermoacoustics address the feedback cycles of this kind of instability.
   Both *"hot tones"* and *"cold tones"* are rarely present at the same time. The amplitude allowable for *cold tones* is typically less than for *hot tones*.

3) ***High-frequency dynamics*** (HFD) occur at frequencies ***f> 1000 Hz***. These types of oscillations are called ***"screech"***, and they are occasionally observed in industrial gas turbine. In general high-frequency dynamics refers to three-dimensional acoustic modes: they are caused by interactions between acoustic disturbances and flame evolution. To date, research efforts have not revealed the feedback cycles exciting this type of combustion instability.
   Although not very common, high-frequency dynamics is particularly destructive to engine hardware, in fact parts have been observed to fail in as little as a few minutes during these types of oscillations.
   The origin of high-frequency dynamics should be found in the reacting ***shear layer***.
   High-frequency dynamics are usually related to ***transverse*** (i.e., tangential) ***acoustic modes*** ([I-32], [II-34] § 5).

Note that the three frequency ranges defined here are used for convenience in describing various dynamics that may be observed, but they should not be interpreted as rigid boundaries of physical behaviour.
The mechanisms that drive *low-*, *mid-* and *high-frequencies dynamics* are different, although all involve coupling between the heat release of the combustion process and the acoustic-pressure field.
Note that different frequencies respond to changes in operating conditions differently. Whereas one intermediate-frequency dynamics mode may be damped by an increase in the fuel-gas fraction in one of the fuel stages, another mode's amplitude may increase because of the same action. Changes in combustor design also have similar tradeoffs for optimizing the dynamic response of the combustion system.
The acoustic waves have long wavelengths compared with the dimensions of the combustion system and they expand over several gas-turbine components, including the compressor, burner plenum and turbine. Therefore, all these components play a pivotal role in combustion-dynamics analysis.

The acoustic geometry of the combustor determines the shape of the acoustic modes, which are also influenced by the acoustic-boundary conditions at the combustor exit. The distribution of the pressure on the surface of the combustion chamber is important information for the optimum arrangement of resonators on the combustor shell. Furthermore, mode shapes of acoustic pressure are needed to analyse structural vibrations and to determine the life of the combustor shell.
The thermoacoustic instability induced inside the combustor also generates dynamic-pressure oscillations in the plenum, upstream of the burners.

II.5.4 Acoustic motion in combustor chamber: resonant frequencies

The most problematic type of instability involves the coupling between acoustic motion and transient combustion response. A major reason for the prevalence of acoustically coupled instabilities in gas turbine combustors and many other propulsion systems is the relatively closed acoustic environment within which combustion occurs, and the relatively large amount of energy available from chemical reactions to drive the acoustic field. In addition, acoustic waves can propagate throughout the entire chamber and affect the flame dynamics, thereby providing a pathway for energy feedback between the flow motion and combustion process. Thus a prerequisite of any instability research is the identification of *acoustic modes in the combustion chamber*.
With the expression of a flow variable as the sum of a mean and a fluctuating part, one can derive a wave equation from the linearized conservation equations of mass, momentum and energy as follows, neglecting all source terms,

$$\nabla^2 p' - \frac{1}{\bar{c}^2}\frac{\partial^2 p'}{\partial t^2} = 0 \qquad \text{(II-26)}$$

where $\bar{c}$ is the mean sound speed in the chamber. If we consider a cylindrical combustion chamber with a closed boundary, by using the method of separation of variables, a general solution to equation (II-26) can be written as:

$$p' = \sum_{l,m,n} A_{lmn} J_m(k_{rmn} r)\cos(m\theta + \gamma_{lmn})\cos(k_{zl} z) e^{j\omega_{lmn} t} \qquad \text{(II-27)}$$

where l,m and n are integers; J_m is the Bessel function of the first kind of order m; $k_{zl} L = l\pi$ where L is combustion chamber length; $k_{rmn} R = j'_{mn}$ where j'_{mn} is the nth extremum of the mth Bessel function of the first kind; and finally R is the chamber radius. The permitted radian frequencies are determined from:

$$\omega_{lmn} = \bar{c}\left(k_{rmn}^2 + k_{zl}^2\right)^{1/2} \qquad \text{(II-28)}$$

The term in equation (II-28) with $m=n=0$, $l\neq0$ describe **longitudinal modes**; those with $l=m=0$, $n\neq0$ correspond to **radial transverse modes**; and those with $l=n=0$, $m\neq0$ represent **tangential** (or **azimuthal**) **transverse modes**.
In general, combustion instabilities occur at frequencies associated with natural acoustic modes of the combustor. These include, for example, *bulk* (i.e. *Helmholtz-type* oscillations), *axial* (i.e. *longitudinal*), and *transverse* (i.e. tangential azimuthal and radial) modes (Fig. II-8).
There are two basic types of wave motion for mechanical waves:

1) **longitudinal waves** (Fig. II-8a)
   In a longitudinal wave the particle displacement is parallel to the direction of wave propagation, and the particles do not move down the tube with the wave; they simply oscillate back and forth about their individual equilibrium positions. The wave is seen as the motion of the compressed region (ie, it is a pressure wave), which moves from left to right.
2) **transverse waves** (Fig. II-8b,c,d)
   In a transverse wave the particle displacement is perpendicular to the direction of wave propagation, and the particles do not move along with the wave; they simply oscillate up and down about their individual equilibrium positions as the wave passes by.

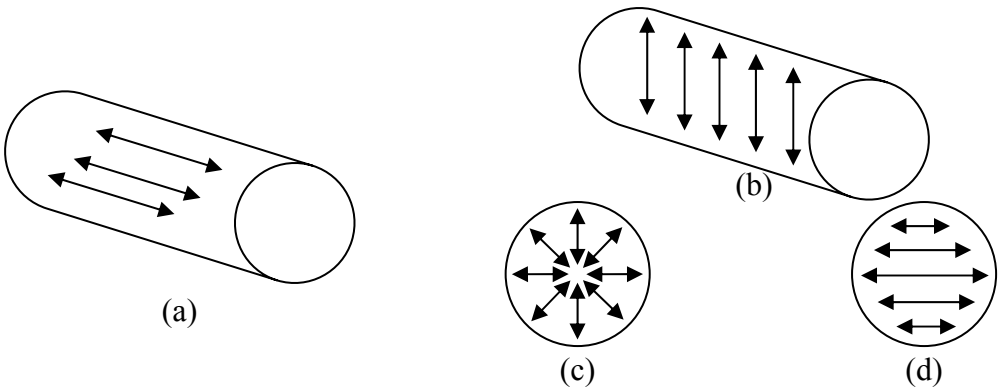

Fig. II-8: Examples of *longitudinal* (a) and *transverse* acoustic modes (b) [*transverse radial mode* in (c), *transverse azimuthal mode* in (d)] that are excited in cylindrical combustors ([II-34] § 1).

The estimated frequencies of oscillations obtained from the above classical acoustics analysis commonly lie within 10–15% or less of the frequencies observed in experiments for combustion instabilities [II-13]. A combustion chamber contains a non-uniform flow of chemically reacting species. The flow is normally turbulent and may include regions of separation. Yet estimates of the frequencies of oscillations computed with acoustic formulas for the natural modes of a closed chamber containing a uniform gas at rest commonly lie within 10-15% or less of the frequencies observed for combustion instabilities, if the speed of sound is correctly chosen. It is precisely the departure, however, from classical acoustics that defines the class of problems we call combustion instabilities. According to Culick [II-13], there are three main reasons that *the classical view of acoustics is a good first approximation to wave propagation in the combustion chamber*. First, the Mach number of the mean flow is usually so low that convective and refractive effects are small. Second, if the exhaust nozzle is choked, the incident waves are efficiently reflected, and the exit plane can be regarded as a rigid surface, acoustically. Third, in the limit of small-amplitude disturbances, the unsteady motion in the compressible flow can be decomposed into three independent modes of propagation: *acoustic*, *vortical* and *entropy waves*. Even in the highly turbulent non-uniform flow usually present in a combustion chamber, acoustic

waves behave according to their own simple classical laws. The role of the classical linear acoustic analysis should not, however, be exaggerated. It cannot decide which modes of acoustic oscillations will be excited, nor is it able to predict the amplitude of the excited modes.
The most obvious evidence that combustion instabilities are related to classical acoustic resonances is the common observation that frequencies measured in tests agree fairly well with those computed with classical formulas. Generally, the frequency *f* of a wave equals its speed of propagation, *c*, divided by the wavelength, λ:

$$f = n\frac{c}{\lambda}$$

where *n*=1,2,3,… is the number of *n*-th harmonic.
On dimensional grounds, or by recalling classical results, we know that the wavelength of a resonance or normal mode of a chamber is proportional to a length, the unobstructed distance characterizing the particular mode in question. Thus the wavelengths of the organ-pipe modes are proportional to the length, *L*, of the pipe, those of modes of motion in transverse planes of a circular cylindrical chamber are proportional to the diameter, *D*, and so forth, hence (in the case of first harmonic, i.e. *n*=1):

1) **Longitudinal mode**

$$f_{LR} \approx \frac{\bar{c}}{L}$$ ***longitudinal resonant frequency***

2) **Transverse modes**

a) $$f_{TRR} \approx \frac{\bar{c}}{(D/2)}$$ ***transverse radial resonant frequency***

b) $$f_{TAR} \approx \frac{\bar{c}}{2\pi(D/2)}$$ ***transverse tangential*** (*or* ***azimuthal) resonant frequency***

There are two basic implications of the previous formulas, with suitable multiplying constants, seem to predict observed frequencies fairly well: evidently the geometry is a dominant influence on the spatial structure of the instabilities; and we can reasonably define some sort of average speed of sound in the chamber, based on an approximation to the temperature distribution. In practise, estimates use the classical formula $\bar{c} = \sqrt{\gamma R_{gas}\bar{T}}$ with $\bar{T}$ the average flame temperature inside the combustion chamber for chemical system in question, and with the properties γ and R_{gas} calculated according to the composition of the mixture in the chamber. If large differences of temperature exist in the chamber, as in a flow containing flame fronts, nonuniformities in the speed of sound must be accounted for to obtain close estimates of the frequencies.
Whatever the system, most combustion instabilities involve excitation of the acoustic modes, of which there are an infinitive number for any chamber. The values of the frequencies are functions primarily of the geometry and of the speed of sound, the simplest examples being

the *longitudinal* and *transverse modes* of a circular cylinder. Which modes are unstable depends on the balance of energy supplied by the exciting mechanisms and extracted by the dissipating processes. In general the losses and gains of energy are strongly dependent on frequency.

3) **Bulk mode** (or **"Helmholtz" mode**)

Our global view, then, is that a combustion instability is an oscillatory motion of the gases in the chamber, which can in first approximation be synthesized of one or more modes related to classical acoustic modes. The mode having *lowest frequency* is a **"bulk" mode** (or **"Helmholtz" mode**) in which *the pressure is nearly uniform in space but fluctuating in time*. Because the pressure gradient is everywhere small, the velocity fluctuations are nearly zero. This mode corresponds to the vibration of *Helmholtz resonator* (i.e. cavity resonator, then volume; see Fig. II-9) obtained, for example, by blowing over the open end of a bottle. The cause in a combustion chamber may be the burning process itself, or it mat be associated with oscillations in the supply of reactants, caused in turn by the variations of pressure in the chamber.
Helmholtz resonators were first described in the literature by Hermann Ludwing Ferdinand von Helmholtz in 1860. Helmholtz described the first mathematical theory for cavity resonators (volume) having a circular opening, and presented a mathematical formula for calculating their resonance frequencies. The formula was based on the volume of the cavity (V) and the radius of the opening (or neck, r), and is given by

$$f_{HR} = \frac{c}{2\pi}\sqrt{\frac{2r}{V}}$$

where c is the speed of sound.
Later, Rayleigh [II-93] presented a simplified theory of Helmholtz resonators. He stated that in practice, the length of the opening (or neck) is not merely constrained to the thickness of the cavity wall. He suggested that the fluid particles in close proximity to the opening take part in the induced motion of the fluid oscillating inside the neck. Therefore, an additional length should be added to the actual length of the neck (or cavity wall thickness) in order to include the mass loading of the fluid at the two ends of the neck. The additional length is more commonly referred to as an end-correction in many acoustic text books ([II-153], [II-154], [II-155]). Rayleigh [II-93] made clear that two *end-correction factors*, one for each end, must be added to the physical length of the neck. These two end-correction factors are (Fig. II-9): (1) *interior end-correction factor* (δ_i), which corresponds to the neck-cavity interface, and (2) *exterior end-correction factor* (δ_e), which corresponds to the opening face of the neck in communication with the environment.
Rayleigh [II-93] derived the expression for the exterior end-correction factor of the neck using the model of a circular piston radiating from an infinite baffle, and assuming a constant velocity profile of the fluid over the neck cross-sectional area. The expression for the exterior end-correction factor was also used as a basis to calculate the interior end-correction factor of the neck. Rayleigh [II-93] also developed the formula for calculating the resonance frequencies of Helmholtz resonators which, in addition to the volume of the cavity and cross-

sectional area of the opening, also includes the effective length of the neck, l_{eff}. The formula, which is more commonly referred to as the classical formula ([II-153], [II-154], [II-155]), is based on the assumption that all the fluid particles in the neck oscillate at same velocity and phase, and also applies when a short tube of the same external diameter as the opening is placed in the opening, and is given by

$$f_{HR} = \frac{\bar{c}}{2\pi}\sqrt{\frac{\pi r^2}{l_{eff}\,V}} = \frac{\bar{c}}{2\pi}\sqrt{\frac{S_{neck}}{l_{eff}\,V}} \qquad \textbf{\textit{Helmholtz resonant frequency}}$$

where, l_{eff} is the cavity wall thickness (or length of the tube, L, if applicable) plus the two end-correction factors: $l_{eff} \cong$ (neck length + exterior end correction + interior end correction)
In 1953, Ingard ([II-156], [II-157], [II-158]) presented a series of work on resonators covering a wide range of topics. Pertinent to the interior end-correction factor of the neck, which was assumed to be equal to the exterior end-correction as proposed by Rayleigh [II-93], Ingard [II-157] found that the application of Rayleigh's formula for calculating the interior end-correction is only valid for the cases where the dimensions of the neck are very small compared to the dimensions of the cavity, and that the formula can lead to significant errors when this condition is not satisfied. He derived different mathematical equations for the interior (neck-cavity interface) end-correction factor with respect to different geometries, modelling the neck as a piston oscillating into an expanded pipe of infinite length.

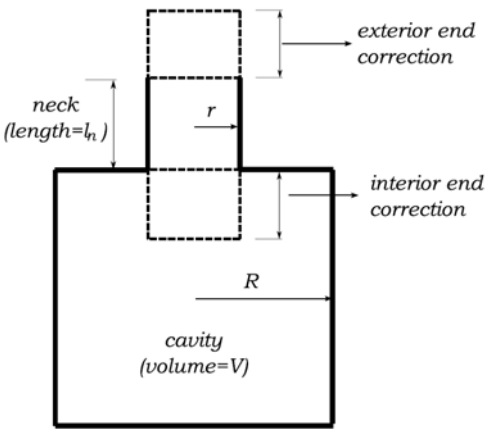

Fig. II-9: A Helmholtz resonator [II-159].

Two global aspects of minor importance in most classical acoustics are fundamental to understanding combustion instabilities: *transient characteristics* and *nonlinear behaviour*. Both are associated with the property that with respect to combustion instabilities, a combustion chamber appears to an observer to be a self-excited system: the oscillations appear without the action of externally imposed forces. Combustion processes are the sources of energy which ultimately appear as the thermal and mechanical energy of the fluid motions. If the processes tending to dissipate the energy of a fluctuation in the flow are weaker than those adding energy, then the disturbance is unstable.

II.5.5 Damping processes

Energy can be dissipated/removed from an unstable mode via the following three processes:

a) **Transfer of acoustic energy to vortical or entropy disturbances through viscous and heat-transfer processes, respectively.**
   This mechanism can be further subdivided into two submechanics:
   - **Boundary-layer losses,** that occur when acoustic motions are present in the vicinity of surfaces on which viscosity and thermal-dissipation effects dominate.
   - **Flow separation losses** at sharp edges or during rapid flow expansions also dump acoustic waves by converting acoustic energy into vorticity.

b) **Convection and/or radiation of acoustic energy out of the system.**
   Acoustic energy inside a duct can leave the system by propagation and/or convection by the mean fluid motion out of the system. In general, this damping mechanism scales with frequency as (fD/c), where f, D and c are frequency, pipe diameter and sound speed, respectively.

c) **Transfer of energy between acoustic modes, out of natural acoustic frequencies to other frequencies.**
   Oscillations in an unstable combustor, in general, are composed of one or more nearly pure tones at specific frequencies. This composition occurs because combustors are generally lightly damped acoustic resonators that respond to external disturbances over very-narrow-frequency ranges. Consequently, mechanisms that do not directly dissipate acoustic energy but transfer energy from the excited modes to other modes that oscillate at frequencies that are either not amplified in the combustor or at which the energy is more readily dissipated, effectively constitute "dissipation" mechanisms for a given natural acoustic mode.

II.5.6 State of art

From a practical point of view, three basic instability characteristics must be predicted and understood (they are listed in increasing order of predictive difficulty):

1. ***Frequency* of oscillations.**
   Prediction of instability frequencies is a relatively mature area. Although good success has been obtained in predicted *acoustic mode shapes* and *frequencies*, the *amplitude* of the oscillations are not easy to predict.
2. ***Conditions* under which the oscillations occur.**
   Predicting the conditions under which instabilities occur is considerably more difficult than predicting acoustic mode shape and frequencies, because it requires knowledge and modelling of the interactions of the flow and mixture disturbances with flames and damping processes.
3. **The *final limit-cycle* amplitude of the oscillations.**
   The prediction of the limit-cycle amplitude of the instability and the conditions under which large-amplitude disturbances destabilize a linearly stable system (triggering) require solution of non linear models of the combustor processes.

II.6 Critical review of causes and effects of instabilities

This chapter proposes a review of the state of knowledge in the field of combustion noise, in particular for Gas Turbine.
The transfer of energy from chemical reactions to the periodic flowfield only takes place when heat release oscillations are in phase with pressure oscillations. The major driving mechanisms of combustion instabilities in lean-premixed gas turbine engines are *hydrodynamic instabilities*, *flame surface variations*, *equivalence ratio fluctuations*, and *oscillatory fuel atomization and vaporization*.

II.6.1 Pressure oscillations and radiative emission of flame: early combustion noise theory and comparison with experiments

One of the earliest combustion noise theory was that of S.L. Bragg ([II-61], [II-160]) in the 1963. Bragg's theory is based on the *direct combustion noise* source model in which the flame zone is assumed to consist of a region of uncorrelated flamelets, created by turbulent mixing, which produce monopole-type sound upon burning. Then in the theory established by Bragg (1963), it was postulated that a turbulent flame behaves as a net monopole radiator. This theory appeals to purely physical reasoning to deduce that *the sound power radiated from a turbulent flame should vary as the fuel reactivity and as the square of the mixture flow velocity*. Bragg predicted a *thermo-acoustic efficiency*[4] of about 10^{-6} with a peak frequency around 500 Hz for a typical hydrocarbon fuel.
Thomas and Williams ([II-63], [II-160]) measured in 1966 the sound power radiated from burning soap bubbles filled with combustible mixtures. The measured and predicted thermo-acoustic efficiency were shown to vary with flame speed over a range of about two orders of magnitude centered about a value of 10^{-5}.
The principle of the Thomas and Williams' experiment [II-63] was to fill soap bubbles with a reactive mixture and record the pressure field radiated by the burning of each isolated bubble. It was found that the pressure signal could be described as the sound generated by a monopole source of strength $\frac{d\Delta V}{dt}$, where ΔV represented the volume increase due to thermal expansion of the gases crossing the reactive front. In this early model, the farfield pressure signal p' was expressed in terms of the volume acceleration induced by unsteady combustion:

$$p'(\bar{r},t) = \frac{\rho_\infty}{4\pi r}\frac{d^2\Delta V}{dt^2} \qquad \text{(II-29)}$$

where ρ_∞ is the farfield air density at the measurement location $\bar{r}$ and r designates the distance between the compact flame and the observation point. According to eq. (II-29) combustion noise results from the flow expansion determined by the heat release rate. It was argued that *since this source is isotropic there is no preferential direction of radiation*.

[4] The thermo-acoustic efficiency is defined as the fraction of the chemical heat release in the combustion process which appears as acoustic energy in the far field of the burner.

In an extension of Thomas and Williams' work, Hurle at al. [II-64] in the 1968 postulate, on the basis of simple *monopole source theory*, that the sound pressure radiated from an open turbulent premixed flame should vary as the time rate of change of light emission by certain free radicals in the reaction zone. A key element in the development is their demonstration that *the intensity of emission by these free radicals increases directly as the flow rate of combustible mixture* for both laminar and turbulent flames. They interpreted their experimental confirmation of this idea for ethylene-air flame as supporting both the monopole source nature of combustion noise and the flamelet, or wrinkled flame, model of turbulent flames. This result is significant because it establishes *a direct relationship between the radiated sound pressure and the combustion heat release fluctuation*.
Starting from eq. (II-29) and assuming that a turbulent flame is acoustically equivalent to a distribution of *monopole sources* of sound with different strengths and frequencies distributed throughout the reaction zone [II-62], it was possible to express the farfield sound pressure *p'* radiated by the turbulent reacting flow as a function of the *volumetric rate of consumption of reactants q* by the flame ([II-64], [II-88]):

$$p'(\bar{r},t) = \frac{\rho_\infty}{4\pi r}\left(\frac{\rho_u}{\rho_b} - 1\right)\left[\frac{dq}{dt}\right]_{t-\tau} \qquad \text{(II-30)}$$

In this expression, $\frac{\rho_u}{\rho_b} = \frac{V_b}{V_u}$ designates the volumetric expansion ratio of burnt to unburnt gases, and τ is the time required for acoustic propagation from the combustion region to the measurement point *r*. In eq. (II-30), it was assumed that acoustic wavelengths λ_a are large compared to any of the characteristic scales of the flow ($\lambda_a >> L$) and that the measurement point *r* is far from the source region ($r << \lambda_a$).
The previous expression provides the sound pressure in the farfield for a compact source region, but it can be used indifferently for premixed or nonpremixed flames [II-88].
In the *premixed* case and for *lean conditions* the *volumetric rate of reactants consumption q* can be estimated from the ***light emission intensity*** *I* of excited radicals like C_2* or CH* ([II-64], [II-161]) and OH* [II-162] in the reaction zone. This yields an elegant optical method to measure the *volumetric rate of reactants consumption* [II-47]:

$$q = k\,I \qquad \text{(II-31)}$$

The coefficient *k* depends on the fuel, the free radical observed, the combustion regime, the flame shape and type and the experimental setup. This relation can be used to study combustion noise from a homogeneous reactive mixture submitted to flow perturbations. Concerning inhomogeneous mixtures (*diffusive flame*), the relation between the radiated *pressure* and the flame *chemiluminescence* is not as straightforward as in the premixed case and one can not deduce the rate of reaction from emission from excited free radicals.
Combining eq. (II-30) and eq. (II-31), *the radiated farfield sound pressure field can be linked to the light emitted from the turbulent combustion region*:

$$p'(\bar{r},t) = \frac{\rho_\infty}{4\pi r}\left(\frac{\rho_u}{\rho_b} - 1\right) k \left[\frac{dI}{dt}\right]_{t-\tau} \tag{II-32}$$

Efforts to clarify and improve Bragg's theory (1963) were undertaken by Strahle in the early seventies ([II-67], [II-68], [II-69]). Using the balance equations of fluid dynamics and Lighthill's analogy for aerodynamic sound ([II-163], see attachment A), it is possible to derive an expression for the sound radiated from a region undergoing turbulent combustion. This can be used to link farfield acoustic *pressure fluctuations* (p') to *density fluctuations* (ρ') inside the combustion region [II-67]:

$$p'(\bar{r},t) = c_0^2 \rho'(\bar{r},t) = -\frac{1}{4\pi r}\frac{\partial^2}{\partial t^2}\int_V \rho'_T\left(\overline{r_0}, t - \frac{\left|\bar{r} - \overline{r_0}\right|}{c_0}\right) dV(\overline{r_0}) \tag{II-33}$$

where ρ'_T are density fluctuations dominated by turbulent fluctuations and not by the acoustic field.
Then according to Strahle (1971) [II-67], *combustion noise is generated by the violent density changes inside the combustion region*.
These initial developments led to the more complete combustion noise theory [II-35].
This brief review indicates that *sound radiation from flames results from the unsteadiness of the combustion process. Intense levels of noise are produced by interactions involving rapid changes of the rate of chemical conversion*. When the flame zone is compact with respect to the acoustic wavelength the time delays between the different sources of sound can be neglected and noise radiation is essentially isotropic. Some directivity can be due to propagation of sound through flow field inhomogeneities and specifically temperature gradients [II-69].

II.6.2 Vortex shedding due to hydrodynamic instability

In gas turbine and many other types of combustors, strong shear layers are often formed downstream of fuel injectors and flame holders. Such transitional shear layers are usually characterized by large-scale coherent structures or vortices ([I-32], [II-22]).
Fresh mixture is entrained by vortical structures, and ignition takes place after a certain characteristic time. Delayed periodic combustion in shed vortices causes periodic acoustic oscillations. The fluctuating velocity of the acoustic field interacts with shear layers and closes the loop.
The shear layer is usually characterized by several instability frequencies associated with different sizes of vortices. When acoustic waves interact with the shear layer, the stabilization of the vortex size depends on the match between acoustic and shear layer instability frequencies. The vortices are smallest when the acoustic frequency equals the initial vortex shedding frequency (most amplified mode). The vortices attain their largest size when the acoustic frequency is near the preferred-mode frequency (jet-column mode). In nonreacting flow tests, the acoustic emission of vortices is low. There is no obvious feedback between the flow and acoustic pressure in the chamber. In reacting flows, however, the periodic heat release from the

combustion inside the vortices provides the missing link for the necessary feedback loop. Thus, the evolution of coherent flow structures leads to periodic heat release, which, when in phase with the pressure oscillation, can drive the instabilities as stated by the Rayleigh criterion. Recent overviews on shear-flow-instability driven combustion oscillations can be found in [II-164].

II.6.3 Change of flame surface area in premixed flames

For a gas-fueled premixed flame, the heat release per unit volume can be expressed as [I-32]:

$$\dot{\omega}_T^1 = q\,\rho\,S_L A$$

where S_L is the flame speed, A the flame surface area per unit volume, ρ the density of unburnt gas, and q the heat of reaction per unit mass. Assuming that all properties except the flame surface area are constant, ***the fluctuation of the heat release rate is proportional to the variation in the flame surface area***:

$$\dot{\omega}_T^1 \sim \mathrm{A}_1$$

Considering the case of premixed flames, it was noted by Thomas and Williams in 1966 [II-63], and later by Abugov and Obrezkov in 1978 [II-165] and Clavin and Siggia in 1991 [II-166], that *sound radiation can be related to the rate of change of the flame surface area* (A) by assuming that the burning velocity is constant.
The *radiated acoustic power for a premixed flame* has the following expression [II-47]:

$$W_a = \frac{\rho_\infty}{4\pi c_\infty}\left(\frac{1}{\rho_b}-\frac{1}{\rho_u}\right)^2 (\rho_u S_L)^2 \overline{\left(\frac{dA}{dt}\right)^2} \qquad \text{(II-34)}$$

where S_L is the laminar burning velocity and A(t) is the flame surface area.
It is very difficult to test this expression in the general case of a turbulent flame because the instantaneous surface area is not directly accessible experimentally. It is easier to use periodically perturbed laminar flame configurations to determine the instantaneous flame surface area and express the pressure signal to the rate of change of surface area. For a mixture of fresh reactants at a constant equivalence ratio, the pressure field is directly linked to the instantaneous flame surface area. Assuming a constant laminar burning velocity (S_L), one may extract the pressure signal from a direct measurement of the wrinkled flame surface area:

$$p'(\bar{r},t) = \frac{\rho_\infty}{4\pi r}\left(\frac{\rho_u}{\rho_b}-1\right) S_L \left[\frac{dA}{dt}\right]_{t-\tau} \qquad \text{(II-35)}$$

Alternatively, this can be accomplished by measuring light emission from free radicals in the flame, deducing from this measurement the heat release rate and determining the resulting pressure field from expression (II-32). However the laminar burning velocity (S_L) is not constant

but depends on the local strain rate and curvature. It is shown theoretically that these effects act in combination in the form of flame stretch ([II-167], [II-168], [II-169], [II-170]) and that this may induce some additional radiation of sound.
According to Candel and Poinsot [II-107] the rate of change of the local flame surface area (A, and thus the heat release rate fluctuations, $\dot{q}'$) changes like the square of the flame surface area when this surface is being destroyed, while this rate of change of the flame surface area only increases linearly when flame area is being produced:

$$\frac{d\Sigma}{dt} = \varepsilon\Sigma - \beta\Sigma^2 \qquad \text{(II-36)}$$

where Σ is the flame surface area per unit volume. The conclusion of this analysis was that *physical processes leading to flame surface reduction (destruction) should be the main mechanism leading to direct combustion noise production*.
Among all mechanisms limiting the flame surface area, three types were studied in details by Candel and Poinsot ([II-47], [II-107]) using controlled experiments in simple flow configurations for premixed flames:

1. the first case involves ***flame-vortex interactions***, then ***partial extinction of the flame*** *due to large scale vortex structures convected in the outer shear layer* formed between a premixed jet and the ambient atmosphere.
2. the second concerns extinction by ***thermal losses of a flame impinging on a cold boundary***: thermal losses during unsteady flame-wall interactions may constitute an intense source of combustion noise, for example during extinctions of large coherent structures entrained by the flow and impacting on solid boundaries ([II-138], [II-171]), then ***flame-wall interactions***;
3. the third involves ***mutual annihilation of neighbouring flame elements***, a mechanism which is suspected to limit the amount of flame surface area in turbulent combustors;

The main objective was to prove that the noise radiated by these types of flame interactions (five different flame geometries), although diverse in nature, can mainly be attributed to the same mechanism of *flame surface area destruction*.
In the cases explored by Candel and Poinsot ([II-47], [II-107]), the flames were modulated by an external perturbation to allow phase average conditional analysis of the flame motion and the radiated sound field. The perturbations were produced by a *loudspeaker* driven by an amplifier, fed by a signal synthesizer. When coupled with a resonant acoustic mode of the burner, the pressure fluctuations were strong and robust enough to generate self sustained combustion oscillations ([II-108], [II-109], [II-110]).
The rapid rates of change of flame surface area constitute a strong source of combustion noise, a mechanism which could be the source of much of the noise radiated by turbulent flames. Events corresponding to large and fast rates of variation of the flame surface area were also identified as the main contribution to the overall radiated noise.
Flame-wall interactions, *mutual annihilations* of flame elements and to some extent *flame-vortex interactions* correspond to mechanisms limiting the flame surface area. It was shown here that these processes may induce large negative rates of change of the heat release rate $\left(\frac{d\dot{q}}{dt}\right)$. Values of this quantity are larger during phases of flame surface destruction than during phases of flame

surface production, implying that *flame surface dissipation is the dominant mechanism of combustion noise production* in combustors operating in a continuous mode (gas turbine combustors, industrial boilers, furnaces...). This is so because extinction or dissipation of flames are usually faster than flame surface generation.
However, it is important to note that there exist also other mechanisms leading to noise production during *flame stretch*, *collective effects* and *flame surface creation*. In automotive engines for example, where combustion noise mainly originates from the violent ignition of the reactants introduced in the cylinder, the fast rate of production of flame surface area is the dominant mechanism.
The flame interactions were studied by Candel and Poinsot ([II-47], [II-107]) in configurations open to *atmospheric condition*: *sound is only radiated from the flame towards the farfield or eventually interacts with the upstream burner*. Such interactions may also drive instabilities under resonant conditions with the upstream manifold as shown in the studies [II-47], [II-108], [II-109], [II-110], [II-172].

II.6.4 Equivalence ratio fluctuation

The influence of equivalence ratio oscillations on combustion instability has been widely recognized. Equivalence ratio oscillation is one of the major sources of heat release fluctuations, especially at lean conditions. One explanation for the susceptibility of lean premixed combustion to instabilities can be given in terms of the relationship between equivalence ratio and chemical reaction time.
The gradient of chemical reaction time with respect to equivalence ratio, $\partial\tau_{chem}/\partial\phi$, increases significantly as the flame gets leaner ([I-32], [II-173]). Since the chemical reaction time is inversely proportional to the reaction rate, a small variation in ϕ can create large fluctuations in the reaction rate at lean conditions, as compared to the stoichiometric condition. Consequently, pressure oscillations tend to grow strongly in amplitude when the fluctuations in the chemical heat release are coupled with the acoustics of the combustion system.
Acoustic waves, originating from the combustion chamber, travel upstream and modulate the fuel and air mass flows in the injectors, which in turn produce a local equivalence ratio oscillation. The resultant disturbance is convected downstream into the combustion zone, leading to pulsating heat release. A feedback loop between heat release and acoustic waves thus forms and drives oscillatory combustion.

II.6.5 Non-premixed flames and pilot flame

The sound field from non-premixed and partially premixed flames is less well characterized than that radiated by premixed flames. It is however the subject of some recent experiments (e.g. [I-4], [II-72], [II-174], [II-175]) and of many numerical calculations (e.g. [II-57], [II-72], [II-176], [II-177], [II-178]).
Applying a premixed pilot flame, the non-premixed flames are always more quiet than the comparable premixed flame, which can be explained by lower reaction density of the non-premixed flames ([I-4] § 2). In a diffusion flame, the local reaction rate is controlled by the local mixing processes instead of the overall fuel-air ratio. Thus, momentary perturbations in the fuel or air supply cannot produce an appreciable change in the reaction rate.
Theoretical analysis of nonpremixed flames is more difficult because the rate of heat release is less easily modelled in this case, and this quantity also can not be extracted from direct measurements of free radical emission.

II.6.6 Nearfield effects

A good observation point of combustion noise is in the *nearfield*, when the distance *r* between the source region and the detector is no longer large compared to the characteristic size *L* of the flame. Sound radiation in this region is less well documented but it is important in practical applications because the flame dimension can be quite large. Smith and Kilham in 1963 [II-62] found that for a distance r < 30d, where *d* is the burner diameter, the acoustic intensity ceases to vary like the inverse of the distance square $1/r^2$. *Sound in this region is influenced by the closest noise sources*. These nearfield effects are of primary importance for noise production in a *confined environment*. Results obtained in the farfield region can be extrapolated to some extent to the nearfield. This can be used to analyse combustion instabilities coupled by noise generation in the flame and emission.
An example is given by Noiray et al. in 2006 [II-172] where synchronized nearfield effects lead to a coherent amplification of the sound output from a distribution of identical flames.

II.6.7 Confinement effects on combustion noise

Considering that *flames open to atmospheric conditions constitute relatively weak noise sources compared to enclosed flames* [II-70], one may except that these flame interactions also largely contribute to broad band noise production in a confined environment.
Most of the work on combustion noise has concerned radiation from *unconfined flames*. This case is less dependent on the geometry because sound generation is not modified by reflection from boundaries. It is also easier to examine unconfined flames with optical diagnostics. However, in many applications combustion takes place in *confined environments* and sound is radiated from the combustor inlet or exhaust sections. Confinement also induces interactions between the radiated wave fields and their sources. There are two general types of interactions:

a) The first corresponds to ***weak coupling*** manifested by *enhancement of sound radiation by system resonances*. This is characterized by the presence of ***discrete peaks*** in the radiated sound spectrum. A typical core noise spectrum measured in the far field of an engine has the general form of an open flame spectrum, but with a superimposed series of relatively sharp peaks corresponding to the resonant frequencies of the engine [II-70]. Combustion under these conditions remains globally stable and interactions between waves and combustion noise sources are relatively weak. Pressures waves generated by the flame and reflected back towards the combustion region from the boundaries are also scattered by the flame [II-179] and the *turbulent combustion region is only weakly modified by acoustic perturbations*.
b) The second type leads to ***strong coupling*** in which acoustic energy fed into one of the burner eigenmodes is sufficient to destabilize the reactive flow. The flow inside the chamber evolves into *a self-sustained oscillations accompanied by strong noise production inside the system* [II-75] and ***a modification of the radiated farfield spectrum***. In these strongly coupled regimes, acoustic fluctuations and large coherent eddies of the reactive flow are synchronized around the resonant frequency. Strongly coupled operation differs from weakly coupled cases in that *pressures waves generated by the flame carry enough acoustic energy to modify the flow and affect the combustion process*.
The origin of the coupling mechanism is always associated with combustion noise radiated back towards the burner and triggering the instability ([II-47], [II-109], [II-110], [II-172]).

The analysis of confinement effects is conveniently carried out by expanding the pressure field on a basis of eigenmodes ([II-26], [II-47]).
The presence of boundaries not only changes the structure of the mean flow but also influences the flame dynamics. This was demonstrated in a set of recent experiments in which the lateral confinement is varied systematically [II-180]. The influence of confinement on the flame motion was examined by measuring the response for different diameters of the duct bounding the flame. It was found that when the confinement ratio is low, the time delay between the velocity signal at the burner outlet and heat release perturbations remains essentially constant indicating that the flame is weakly affected by the presence of the wall. As the confinement ratio was increased, the time delay and the gain of the flame *transfer function* are altered. The interaction with the wall change the dynamics of the flame tip and the flame wrinkling geometry in the vicinity of the boundary.
Whilst thermoacoustic instability has been studied extensively in premixed combustors over the last few decades, most studies have concentrated on combustors with acoustically open exits. The effect of a *choked exit nozzle* of a combustion chamber has received less attention [II-133]. Choked exit nozzles allow to have controlled boundary conditions for numerical simulations. This is an important omission, given that some of those studies that have been carried out suggest that a choked exit nozzle can have a strong effect on the system stability ([II-181], [II-182], [II-183], [II-184], and that most in service combustors feature a choked, or nearly choked, nozzle downstream of the combustion chamber.
Such behaviour with a choked exit can perhaps be explained by Marble and Candel's [II-76] theoretical work, which showed that a choked nozzle produces upstream travelling pressure fluctuations in response to incident acoustic pressure and convected entropy fluctuations. MacQuisten and Dowling [II-182] reported a strong low-frequency instability in their combustor

when the exit was choked, and speculated that this was the cause. Hield and Brear [II-183] also observed a similar low-frequency instability, and showed experimentally that the conversion of incident entropy disturbances to upstream travelling sound can be significant.
Zhu et al. [II-16] performed numerical simulations of a combustion chamber with a spray atomiser, and compared open and choked downstream boundary conditions. They showed that a choked nozzle downstream of the combustor leads to limit cycles that are not present with the open exit, and demonstrated the link between the convection of the entropy fluctuations generated by the flame and the cycle frequency. Although they did not give an explicit formula for the frequency, they stated that: *"the period of oscillation is approximately twice the convection time through the combustor"*.

II.6.8 Hysteresis

The existence of hysteresis in the dynamical behaviour of combustions is both an interesting phenomenon to investigate and a characteristic that has potentially important practical consequences [II-20]. It seems that the first evidence for hysteresis in combustors was found by Russian researchers concerned with instabilities in liquid rockets ([II-21], [II-185], [II-186], [II-187]). In that case, Natanzon and his co-workers proposed bifurcation of steady states of combustion, and the associated hysteresis, as a possible explanation for the random occurrences of combustion instabilities. The Russian workers were in a special situation affording them the opportunity to make such observations. The large Russian boosters were designed to use many (as many as thirty-three) liquid rocket engines in a single stage. Hence large numbers of nominally identical engines were manufactured and tested for operational use. Sufficient data were obtained that statistical analysis of the behaviour could be carried out. A basis therefore existed for identifying random behaviour.
Recent experimental works ([II-188], [II-189], [II-190], [II-191]) have shown how active control can be used to extend the range of steady operation into the hysteretic region.

II.6.9 Combustion roar and Strouhal-type combustion noise in real burners

Putnam A.A., whose work is characterized by an interest in "real" rather than laboratory-scale burners, has made several significant contributions to the understanding of noise production by large industrial combustion systems. Putnam's first contribution in the open literature in this field was evidently in 1968 [II-4] when he reported the results of noise measurements on a burner (the so-called "octopus" burner) consisting of eight fuel nozzles (used with natural gas diffusion-flame) directed from the corners of a cube toward the center. He found acoustic activity in two frequency ranges: a high-frequency range (~10^4 Hz) which he interpreted as representing simple amplification of the jet noise, and a low frequency range (100-500 Hz) representing direct combustion noise. The *thermo-acoustic efficiency* of this burner varied with firing rate (fuel flow rate), nozzle diameter and spacing, and degree of convergence of the nozzles toward a common center over a range from about 10^{-8} to about 10^{-7}, which is comparable to values obtained by other investigators. Although he does not give an expression, Putnam claims a satisfactory correlation of these data based on an assumption of *monopole*-type sources.

Putnam returns to the problem of *"combustion roar"* in turbulent diffusion flames in a 1970 paper with Giammar [II-5]. *"Combustion roar"* is the generic term, generally attributed to Putnam [II-6], for *noise generation by turbulent flames in the absence of combustion-driven oscillations*.
Two specific areas of combustion noise are discussed in references [II-7] and [II-71]:

1. ***Combustion roar***, in the absence of acoustic distortion effects, shows a *broad spectrum* and it is characterized by a smooth noise spectrum related to the reacting chemistry of the flame and the turbulence level of the combustion region. Putnam states that the mechanism for *combustion roar* in the turbulent flame is *"the movement of the flame front …, as the volume of the gas increases on passing through (the) flame front"*, but that the specific details which would permit prediction of combustion roar are still unknown.
2. ***Combustion-driven oscillations*** are characterized by a *discrete frequency* and a *feedback* cycle to maintain the oscillation. ***Pulse combustion*** is the name of positive application of combustion-driven oscillations.

In addition, some other direct combustion noise phenomena are possible, such as the interaction with ***vortex shedding*** and the combustion amplification of periodic flow phenomena (***Strouhal-type combustion noise***).
This is a useful classification system because it helps the researcher focus his efforts on a given aspect of combustion noise generation. Putnam points out that two or more of *these combustion noise mechanisms can and generally do coexist* in a given situation, thus making it difficult to isolate one from the other experimentally. This is particularly true of *combustion roar* and *Strouhal-type combustion noise*, the latter correlating with characteristic length and velocity scales of the burner. Both lead to a rather smooth noise spectrum with a single broad peak in the same (low) frequency range, and are thus hard to separate. This probably partly explains why some investigators ([II-62], [II-192], [II-193], [II-194], [II-195]) favour a *Strouhal number correlation for the peak frequency of combustion noise*, while others ([II-5], [II-128], [II-196], [II-197]) insist that the peak frequency depends chiefly on the *fuel reactivity*.
It was given an experimental demonstration that the peak frequency of acoustic emission from premixed flames scales with the *Strouhal number* [II-195]. This not only lends some insight on the frequency scaling of the spectrum, but also gives us an insight on the major parameters affecting the OASPL. This has led to a simplified scaling expression for the OASPL of combustion noise.
The critical review of the literature by Giammar and Putnam [II-5] was presented aimed at clarifying the question of whether the noise reported by earlier investigators is independently produced combustion noise or merely frequency selective amplification of turbulence already present in the cold jet. They left largely unanswered the question of whether combustion noise is independently produced or merely the amplification of pre-existing turbulence in the fuel jet. They pointed out, as will others, that the noise spectra of all hydrocarbon-fuel burners peak in the 300 to 600 Hz frequency range, suggesting that the peak frequency may be chemically controlled. They also reported results from their own experimental study of two industrial natural gas diffusion-flame burners: a coaxial impinging jet burner and the so-called "octopus" [II-4]. Results indicate that jet noise (high frequency range) is amplified on the order of 20 dB when the impinging fuel jets are ignited. For the combustion noise from the impinging coaxial jet burner, the *Strouhal number* based on the spacing between the fuel nozzles and the peak frequency is constant at about 0.24.

In 1976 Putnam [II-6] provides more data from a wide variety of gas fired industrial burners which tend to lend further support to the hypothesis that *combustion roar is the result of a turbulence driven monopole-type source mechanism*. He reports that for seven practical burners of widely differing design (including four nozzle mix burners and three premix burners) whose rated firing rates range from 400,000 Btu/h (≈ 117 kW) to 750,000 Btu/h (≈ 220 kW), the thermo-acoustic efficiency varies as the 1.8 to 2.0 power of firing rate. This is in excellent agreement with simple theory based on the hypothesis that ***the sources are acoustic monopoles*** created by the turbulent mixing of unburned mixture with the hot products of combustion, which predicts an exponent of 2.0. He explains the deviation from this law, which occurs when the burners are operated above their rated firing rates, in terms of *"super-turbulence"*, defined as combustion induced turbulence related to incipient blow-off.
Noting that the thrust of a burner should also vary as the square of the firing rate, Putnam postulates that the *thermo-acoustic efficiency should be related to thrust*. He finds that in general the ratio of thermo-acoustic efficiency to the thrust per unit area (made nondimensional by the ambient pressure) for a given burner is independent of firing rate but varies widely from burner to burner. This observation tends to verify the intuitively pleasing idea that the thermo-acoustic efficiency must be intimately related to other burner performance parameters.
In 1973 Roberts and Leventhall [II-198] offer compelling evidence that *the predominant noise generating mechanism in open turbulent premixed flames is the turbulent velocity fluctuation at the flame front* rather than the entrainment and subsequent combustion of individual turbulent eddies, or "cells", of mixture as they penetrate into the combustion zone.

II.6.10 Nonlinear mechanisms and limit cycle in combustion instabilities

The term thermoacoustic *instability* is somehow misleading, because it is normally used to describe the state of a combustion system that, due to a constructive feedback-interference of heat release and acoustics, exhibits high amplitude oscillations of both, whose amplitudes actually are determined by a stable *limit-cycle*.
In case of destructive interference or losses across the system boundaries that exceed the net gain of acoustic energy, the system is in a stable fixed point. *Small fluctuations* around this stable stationary state can be described by a *linear system*. Consider now the case for which a system parameter, for example, power or equivalence ratio, is changed as such that a positive thermoacoustic feedback is established and the net gain is larger than the losses. Through this, the fixed point is not stable anymore and infinitely small perturbations cause the system to become linearly unstable. Therefore, it is shifted from its initially stable equilibrium state with low-amplitude oscillations to one with a *stable limit-cycle* exhibiting high amplitude coherent oscillations. Literally, the combustion system is only linearly unstable during the onset of the instability, which causes an exponential growth of the pressure and heat release oscillations. From a mathematical point of view, an *unstable linear system* would grow infinitely in time. However, in all practical cases, the amplitude will somehow be saturated by *non-linear effects*, which, at a certain amplitude, balance the production terms. This is a stable limit-cycle exhibiting high amplitude oscillations.
Nonlinear features are abundant in a combustion process. The most dominant of these is a *limit cycle* behaviour that is exhibited by almost all the variables in the process, including pressure, velocity, and heat release. The typical dynamic response of any of these variables consists of a

divergent set of oscillations that transition to a sustained periodic signal, which is almost sinusoidal in nature. Several speculations have been made regarding mechanisms responsible for such a behaviour. *Nonlinearities in the heat-release dynamics* have been noted in several works ([II-134], [II-190], [II-199], [II-200], [II-201], [II-202]), whereas *nonlinearities in acoustics are claimed to be responsible for these limit cycles* in [II-22], [II-203], [II-204].
The presence of limit cycles suggests the obvious presence of bifurcations. A key parameter that appears to induce these bifurcations is the mean equivalence ratio (Φ). Two distinct ranges of Φ appear to be of interest, depending on the application:

1. in *ramjet engines* and *afterburners*, instability appears to result close to *stoichiometry*, which is then followed by a *Hopf bifurcation*.
2. in gas turbine *engines* with *strict emission requirements*, as one attempts to burn lean, a *"blow-out" limit* is reached that once again is accompanied by these bifurcations.

In many of these cases, more than one limit cycle is encountered [II-190], suggesting the presence of both sub- and supercritical bifurcations.
In [II-189], keeping other parameters constant as Φ is increased steadily and then decreased, the behaviour at the same value changes from instability to stability, and a drastic change in the flame structure is observed at some of these instances. In [II-189] and [II-205], it is shown that once such a mechanism is present, appropriate use of it can be made in designing *active control strategies* to reduce the amplitude of oscillations.
The *nonlinear behaviour of flames* is often evoked in combustion instability analysis, its experimental consequences are well documented in a variety of laminar or turbulent flame configurations but the standard interpretation is usually based on *linear stability theory* in which one calculates the growth rate of infinitesimally small perturbations: it is important to recognize that *Rayleigh* and *Chu criteria* (see paragraph III.7) are all linear and strictly valid only during the linear growth phase [II-86].
In most cases however, experiments are carried out on systems executing a *limit cycle* at a finite amplitude level. There is clearly a gap between theoretical results and experimental data despite the fairly large number of analytical studies which try to fill this gap and propose nonlinear descriptions of combustion dynamics (e.g. [II-202], [II-204], [II-206], [II-207]).
Among the various theoretical methods, one may distinguish two general classes:

1. The first which relies on a *Galerkin projection on the modes of the system* has been extensively used to investigate nonlinear acoustics as the mechanism responsible for amplitude saturation (e.g. [II-204], [II-206]).
2. In the second class one finds a large set of models which infer that combustion is the central nonlinearity and constitutes the key element governing the system dynamics and setting limit cycle parameters (e.g. [II-52], [II-134], [II-208], [II-209]).

The Fig. II-10 shows a typical time evolution of pressure oscillations in a combustor where an instability is triggered a t=0. It is possible to recognize three different zones:

a) First, *linear oscillations* appear. If $R_1 > F_1$ (e.g., see Extended Rayleigh's Criterion) their amplitude grows exponentially, however amplitudes do not grow indefinitely.
b) Quite often an *overshoot period* where $R_1 < F_1$ is observed during which the amplitude of pulsation is larger than the following limit cycle amplitude.
c) If the combustor does not explode or blow-off at the end of the linear zone and the exponential growth, a *limit-cycle* is reached (as is most often the case in experiments) in which non-linear effects are essential. The amplitude of this period regime is constant,

therefore $R_1 = F_1$. This can be due to an increase of the acoustic losses (increased F_1) or to a phase change between unsteady pressure and heat release (decreased R_1).

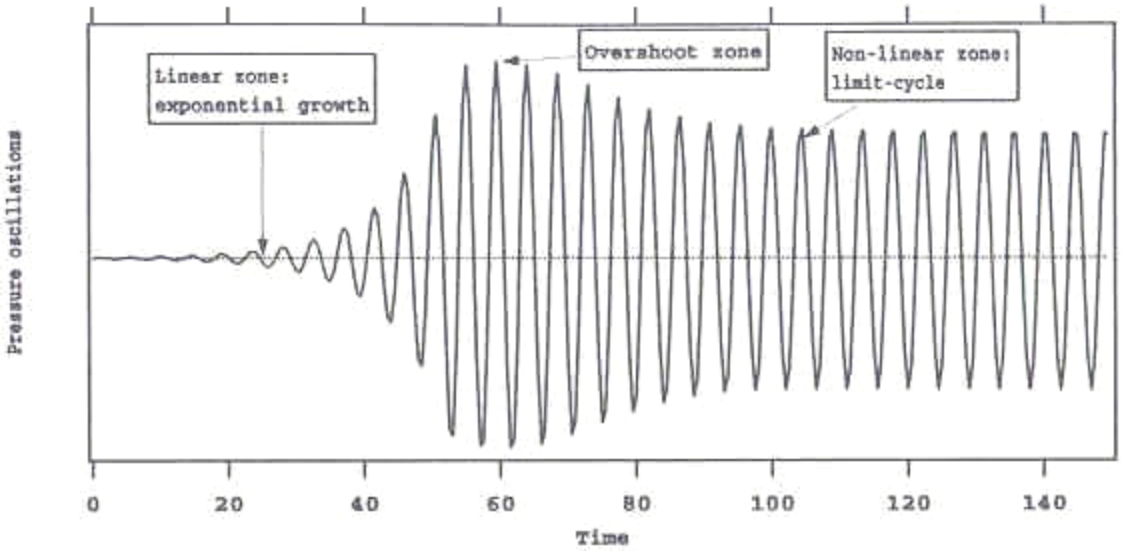

Fig. II-10: Growth of a combustion instability to stable limit cycle.

A system (or a system state) may be called *stable* against a perturbation, if some time after the perturbation is imposed, the initial system state is re-established. It follows quite naturally from this definition that in order to investigate the stability properties of a system, one must determinate the response of the system to perturbations.
Often it is fairly easy to compute the response to perturbations with infinitesimally small amplitudes. In this case the governing equations may be simplified by neglecting the so-called *non-linear terms*, i.e. terms which are higher order in perturbation amplitudes. A system is accordingly called *linearly stable*, if it returns to its initial state after a slight perturbation. Note that it is not specified what kind of perturbation is imposed, except that the amplitude be small in some sense.
In linearly unstable systems a dominant or most unstable mode, i.e. a distant pattern of vibration with a particular frequency *f*, develops in the very early stages of the instability.
Significant *growth of amplitudes* is associated with linear instability, correspondingly the departure from exponential growth is due to non-linear terms, i.e. those terms of higher order in oscillation amplitudes, which were neglected in the linearized analysis. Exponential growth of the form $A_0 e^{\alpha t}$, where A_0 is the amplitude of the initial small disturbance, is characteristic of the initial stage (linear behaviour) of an instability in a self-excited system [II-20].
During the *non-linear phase of evolution of instability*, the frequency spectrum typically shows more than one peak, often a dominant peak at the frequency *f* and lower-amplitude, but still rather distinct peaks at integer multiples $n \cdot f$ of fundamental frequency (*harmonics*).
The scenario of *linear instability* → *growth of dominant mode* → *non-linear saturation* → *limit cycle* is a well established paradigm in instability theory ([II-210], [II-211]).

Many combustion systems, while not exhibiting a strong thermo-acoustic instability, show significant fluctuation levels (of pressure, velocity, heat release rate) over a band of frequencies (often in the vicinities of combustor *eigenfrequencies*). Such a state should perhaps not be described as the *limit cycle* of an instability, but rather as *resonant amplification* of combustion noise by the combustion chamber.
For practical applications, it is desirable to know how the amplitude of the *limit cycle* depends on the parameters characterizing the system. That information may serve as the basis for changing the characteristics to reduce the amplitude, the goal in practice being zero.

II.6.11 Acoustic modal analysis of a full-scale annular combustor in propulsion engine

Combustion instabilities in combustion chambers for propulsion systems were discovered in the late 1930s as anomalies in firings of solid and liquid rockets [II-20]. During World War II, experience gradually suggested that certain problems encountered in development and actual use of solid rockets were especially associated with pressure oscillations having relatively high frequencies ranging from a few hundred to several thousand Hertz. Associated problems were *structural vibrations*; *greatly increased surface heat transfer rates*; sometimes *impaired performance*; and, in extreme cases, *failure of the combustion system* and *destruction of vehicles*.
By the 1950s, forms of combustion instabilities had been identified in all types of rockets, gas turbines, thrust augmenters and ramjets. Although the problem had been encountered in ramjet engines in the 1950s, it became a matter of greater concern in the late 1970s and 1980s. The problem continues to the present time and will always be found in combustion systems, particularly those intended to provide high performance. Eliminating instabilities therefore becomes an important task in a development program.
Mainly three characteristics of a system influence its dynamical behaviour:

1. the physical state in which reactants are introduced (solid, liquid, gas);
2. the geometry of the system;
3. the specific mechanism causing the instabilities to occur.

Instabilities have significantly hindered the development of various liquid-fueled rockets. Notable were the instabilities encountered during the development of the F-1 engine that powered Saturn rockets (1965), which were used in the first manned mission to the moon (July 16, 1969). The F-1 encountered instabilities with amplitudes up to 100% of the mean combustor pressure (i.e., more than 2000 psi=138 bar) with frequencies in the 200-500 Hz range. These instabilities caused significant damage to the combustor, and their elimination required a costly trial and error, development program that included ~ 2000 full-scale tests (of a total of 3200). One of the solutions developed involved welding a system of baffles to the injector face. These baffles prevented the excitation of the transverse acoustic oscillations that could be driven by the combustion process near the injector face.
Combustion instabilities have also been encountered in numerous solid-propellant rockets, including the Space Shuttle solid-propellant rocket boosters.
Combustion instabilities in ramjet-powered missiles have also been problematic because they cause thrust oscillations and shock-system oscillations in the inlet diffuser, which lead to a reduced stability margin of the inlet flow [II-20].

In the early 1980s, some illuminating experimental combustion noise measurements were conducted by Karchmer [II-15], and Krejsa and Karchmer [II-212]. Resonances in a combustor (e.g. combustor of propulsion engine, [II-15]; [II-19]) and tailpipe ([II-19], [II-212]) can play an important role in determining the amplitudes and frequencies of peaks observed in far field combustion noise measurements.
In Schuster et al. [II-19] an array of internal and external sensors was used to collect data to support the investigation of combustor noise source generation, modulation, and radiation. The primary objectives of the test were to conduct modal measurements (circumferential) of the acoustic field inside the combustor, to conduct modal measurements (longitudinal) of the acoustic field inside the tailpipe, to measure radiated exhaust noise with a farfield microphone array, and to apply multiple microphone techniques for discrimination of the combustor and jet noise sources. Analysis of the test data yielded a number of interesting results concerning the relationship between the *internal* and *far field* spectra, confirming and extending the previous test results of Karchmer and Krejsa ([II-15], [II-212]).
Simultaneous internal and external noise measurements were conducted on a Honeywell RE220 APU. The measurements enabled a number of features of combustion noise to be investigated. Modal decomposition of the internal combustion noise spectra shows that the spectral peaks correlate with the *cut on frequencies* of annular duct modes. Comparisons of internal and external peaks show that *the far field noise appears to be dominated by tailpipe resonances*.

- Substantial peaks are evident in the spectra of *combustor internal measurements*. The peaks shift to higher frequencies as the operating temperature increases. This behaviour is suggestive of combustor resonances, where the resonant frequencies are proportional to the sound speed, assuming that the geometric length scale is constant. The peaks of internal combustor spectra were seen to be essentially invariant to the tailpipe length: the peaks are not dominant in the far field and they appear largely unaffected by tailpipe length.
- In *tailpipe measurements* it appears that most of the far field spectral peaks correlate strongly with the tailpipe spectral peaks. Most of the spectral peaks in the tailpipe data appeared to shift to higher frequencies as the tailpipe temperature increases, and appear to shift to lower frequencies as the tailpipe length increases. The wave resonances in the tailpipe govern most of the peaks observed in the far field.

Combustion noise in the *far field* measurements was generally considered to peak at 60 degrees relative to the jet axis.
An impressive overview on unsteady motions in combustion chambers for propulsion systems was written by Culick in 2006 [II-20] and by Dranovsky in 2007 [II-21].
Almost all solid rockets exhibit instabilities, at least during development, and occasionally motors are approved even with low levels of oscillations. Actual failure of a motor itself is rare in operations, but vibrations of the supporting structure and of the payload must always be considered. To accept the presence of weak instabilities in an operational system one must have sufficient understanding and confidence that the amplitudes will not unexpectedly grow to unacceptable levels.

References

[II-1] Sutton G.P., Biblarz O., "Rocket propulsion elements", 7th ed., John Wiley and Sons, 2000.

[II-2] Dowling A. and Stow S., "Acoustic analysis of gas turbine combustors", AIAA Journal of Propulsion and Power, vol. 5, No.19, pp.751-764, 2003.

[II-3] Putnam A.A., "Combustion driven oscillations in industry, fuel and energy science series", New York: American Elsevier, 1971.

[II-4] Putnam A.A., "Noise Measurement of Turbulent Natural-Gas Diffusion Flames of 120,000- to 750,000-Btu/h Output", Journal of the Acoustical Society of America, vol. 43, Issue 4, pp.890-891, 1968.

[II-5] Giammar R.D. and Putnam A.A., "Combustion Roar of Turbulent Diffusion Flames", ASME Transactions, Series A, Journal of Engineering for Power, vol. 92, Issue 2, pp.157-165, April 1970.

[II-6] Putnam A.A., "Combustion Roar of Seven Industrial Gas Burners", Journal of the Institute of Fuel, pp.135-138, September 1976.

[II-7] Putnam A.A., "Combustion Noise in Industrial Burners", Noise Control Engineering, vol.7, pp.24-34, July-August 1976.

[II-8] Lee J.G., Hong B.S., Kim E.S., Yang V., and Santavicca D.A., "Optimization of Active Control Systems for Suppressing Combustion Instability", Proceedings of NATO-RTO Symposium on Gas Turbine Engine Combustion, Emissions and Alternative Fuels, RTO-MP-14, pp. 41/1-41/12, Lisbon, Portugal, October 1998.

[II-9] Yang V. and Schadow K.C., "AGARD Workshop on Active Combustion Control for Propulsion Systems", Proceedings of NATO-RTO Symposium on Gas Turbine Engine Combustion, Emissions and Alternative Fuels, RTO-MP-14, pp.36/1-36/20, October 1998.

[II-10] Seume J., Vortmeyer N., Krause W., Hermann J., Hantschk C., Zangl P., "Application of active combustion instability control to a heavy duty gas turbine", ASME, Journal of Engineering for Gas Turbines and Power, vol.120, Issue 4, pp.721-726, 1998.

[II-11] Mongia H.C., Held T.J., Hsiao G.C., Pandalai R.P., "Challenges and progress in controlling dynamics in gas turbine combustors", AIAA Journal of Propulsion and Power, vol.19, Issue 5, pp.822-829 , 2003.

[II-12] Flandro G.A., "Energy balance analysis of nonlinear combustion instability", AIAA Journal of Propulsion and Power, vol. 3, Issue 1, pp.210-221, 1985.

[II-13] Culick F.E.C., "Dynamics of combustion systems: fundamentals, acoustics and control", Active control of engine dynamics, pp.89-206, NATO, Von Karman Institute for Fluid Dynamics, Lecture Series, May 14–18, 2001.

[II-14] Crocco L. and Cheng S.I., "Theory of Combustion Instability in Liquid Propellant Rocket Motors", London, Butterworths Scientific Pubblications, 1956.

[II-15] Karchmer A.M., "Acoustic Modal Analysis of a Full Scale Annular Combustor", NASA-TM-83334, NASA Center: Glenn Research Center, April 1983, (also 8th AIAA Aeroacoustics Conference, AIAA-83-0760, p. 17, Atlanta, GA, 11-13 April 1983).

[II-16] Zhu M., Dowling A.P., Bray K.N.C., "Self-excited oscillations in combustors with spray atomizers", ASME, Journal of Engineering for Gas Turbines and Power, vol.123, Issue 4, pp.779-786, October 2001.

[II-17] Giuliani F., Gajan P., Diers O., Ledoux M., "Influence of pulsed entries on a spray generated by an airblast injection device: an experimental analysis on combustion instability processes in aeroengines", Proceedings of the Combustion Institute, vol.29, pp.91-98, 2003.

[II-18] DeLaat J.C and Chang C.T., "Active control of high frequency combustion instability in aircraft Gas-Turbine engines", NASA Technical Report, NASA TM-2003-212611, ISABE-2003-1054, September 2003.

[II-19] Schuster B. and Mendoza J., "Auxiliary Power Unit Combustion Noise Measurements", 11th CEAS-ASC Workshop on "Experimental and Numerical Analysis and Prediction of Combustion Noise", Lisbon, Portugal, 27/28 September 2007.

[II-20] Culick, F.E.C., "Unsteady motions in combustion chambers for propulsion systems", AGARDograph, NATO/RTO-AG-AVT-039, December 2006.

[II-21] Dranovsky M., Yang V., Culick F.E.C., Talley D.G., "Combustion Instabilities in Liquid Rocket Engines: Testing and Development Practices in Russia", Progress in Astronautics and Aeronautics Series, 221, Published by AIAA, Hardback, 2007.

[II-22] Culick F.E.C., "Combustion instabilities in liquid-fuelled propulsion systems – an Overview", AGARD Conference on Combustion Instabilities in Liquid-fuelled Propulsion Systems, AGARD Conference Proceedings, paper 1, the 72nd(B) Propulsion and Energetics Panel Specialists, Meeting AGARD-CP-450, pp. 1-1 – 1-73, 1988.

[II-23] Margolin A., "Early investigations of solid-propellant combustion instability in Russia", Journal of Propulsion and Power, vol.15, Issue 6, pp.922-925, 1999.

[II-24] Vuillot F., "Vortex-Shedding phenomena in Solid Rocket Motors", Journal of Propulsion and Power, Vol. 11, Issue 4, pp. 626-639, 1995.

[II-25] Apte S. and Yang V., "Unsteady flow evolution and combustion dynamics of homogeneous solid propellant in a Rocket Motor", Combustion and Flame, Vol. 131, Issue 1-2, pp. 110-146, 2002.

[II-26] Culick F.E.C. and Yang V., "Liquid Rocket Engine Combustion Instability", AIAA Progress in Astronautics and Aeronautics, edited by V. Yang and W.E. Anderson, vol. 169, Chapter 1: "Overview of combustion instabilities in liquid-propellant rocket engines", Washington, DC, pp.3-37, 1995.

[II-27] Chu B.-T. and Kovasznay L.S.G., "Non-linear Interactions in a Viscous Heat-Conducting Compressible Gas", Journal of Fluid Mechanics, vol. 3, Issue 5, pp.494-512, 1958.

[II-28] Zel'dovich Ya.B., Barenblatt G.I., Librovich V.B. and Mikhviladze G.M., "The Mathematical Theory of Combustion and Explosions", translated from the Russian by D.H. McNeill, Consultants Bureau (Plenum Press), New York, 1985.

[II-29] Correa S.M., "Power Generation and Aeropropulsion Gas Turbines: from Combustion Science to Combustion Technology", 27th Symposium (International) on Combustion, Pittsburgh: The Combustion Institute, Boulder, CO, vol.2, pp. 1793-1807, 1998.

[II-30] Richards G.A. and Janus M.C., "Characterization of Oscillation During Premix Gas Turbine Combustion", ASME, Journal of Engineering for Gas Turbines and Power, vol.120, Issue 2, pp.294-302, 1998.

[II-31] Breard C., Sayma A.I., Vahdati M., Imregun M., "Aeroelasticity analysis of an industrial gas turbine combustor using a simplified combustion model", Journal of Fluids and Structures, Vol. 16, Issue 8, pp. 1111–1126, 2002.

[II-32] Tinga T., van Kampen J.F., de Jager B., Kok J.B.W., "Gas Turbine Combustor Liner Life Assessment Using a Combined Fluid/Structural Approach", Journal of Engineering for Gas Turbines and Power, ASME, Vol. 129, pp. 69-79, January, 2007.

[II-33] Pozarlik A., Kok J.B.W., "Numerical prediction of interaction between combustion, acoustic and vibration in gas turbine", Acoustics'08 Paris, pp. 2749-2754, June 29-July 4, 2008.

[II-34] Lieuwen T.C. and Yang V., "Combustion Instabilities in Gas Turbine Engines: Operational Experience, Fundamental Mechanisms, and Modelling", AIAA-book, Progress in Astronautics and Aeronautics Series,Volume 210, 2005.

[II-35] Dowling A. and Ffowcs Williams J.E., "Sound and sources of sound", Ellis Horwood, Chichester, UK, 1983.

[II-36] Candel S., Durox D., Schuller T., "Flame interactions as a source of noise and combustion instabilities", 10th AIAA/CEAS Aeroacoustics Conference, AIAA-2004-2928, Manchester, Reston, VA, Great Britain, May 10-12, 2004.

[II-37] Poinsot T., Trouvè A., Veynante D., Candel S. and Esposito E., "Vortex driven acoustically coupled combustion instabilities", Journal of Fluid Mechanics, vol.177, pp.265-292, 1987.

[II-38] Renard P.H., Thevenin D., Rolon J.C., Candel S., "Dynamics of flame/vortex interactions", Progress in Energy and Combustion Science, vol.26, Issue 3, pp.225-282, 2000.

[II-39] Rayleigh Lord J.W.S., "The explanation of certain acoustic phenomena", Royal Institution Proceedings, Nature, London, vol.8, pp.536-542, 1878.

[II-40] Poinsot T. and Veynante D., "Theoretical and Numerical Combustion", Second edition, Edwards, USA, Philadelphia, 2005.

[II-41] Borghesi G., Biagioli F., Schuermans B., "Dynamic response of turbulent swirling flames to acoustic perturbations", Combustion Theory and Modelling, Vol. 13, Issue 3, pp.487–512, 2009.

[II-42] Schuermans B., Guethe F., Pennel D., Guyot D., Paschereit C.O., "Themoacoustic modelling of gas turbine using transfer functions measured at full engine pressure", ASME Turbo Expo 2009, Power Land, Sea and Air, GT2009-59605, Orlando, Florida, USA, June 8-12, 2009.

[II-43] Najm H.N., Paul P.H., Mueller C.J., Wycoff P.S., "On the Adequacy of Certain Experimental Observables as Measurements of Flame Burning Rate", Combustion and Flame, Vol. 113, pp.312–332, 1998.

[II-44] Samaniego J.M., Mantel T., "Fundamental Mechanisms in Premixed Turbulent Flame Propagation via Flame–Vortex Interactions Part I: Experiment", Combustion and Flame, Vol.118, pp.537–556, 1999.

[II-45] Samaniego J.M., Egolfopoulos F.N., Bowman C.T., "CO2* Chemiluminescence in premixed flames", Combustion Science and Technology, Vol. 109, Issue 1, pp. 183-203, 1995.

[II-46] Higgins, B., McQuay, M., Lacas, F., Rolon, J., Darabiha, N., and Candel, S., "Systematic measurements of OH chemiluminescence for fuel-lean high-pressure, premixed, laminar flames". FUEL, Vol. 80, pp. 67-74, 2001.

[II-47] Candel S., Durox D., Ducruix S., Birbaud A.-L., Noiray N., Schuller T.; "Flame dynamics and combustion noise: progress and challenges", 11th CEAS-ASC Workshop on "Experimental and Numerical Analysis and Prediction of Combustion Noise", Lisbon, Portugal, 27/28 September 2007.

[II-48] Higgins B., McQuay M.Q., Lacas F., Candel S., "An experimental study of the effect of pressure and strain rate on CH chemiluminescence of premixed fuel-lean methane/air flames", Fuel, Vol.80, Issue 11, pp.1583–91, 2001.

[II-49] Schuermans B., Guethe F., Mohr W., "Optical transfer function measurements for technically premixed flames". ASME GT2008-51500, Proceeding of ASME Turbo Expo 2008, Berlin, June 9-13, 2008.

[II-50] Guyot D., Moeck J.P., Paschereit C.O., Schuermans B., "Optical Transfer Function Measurement for a Premixed Swirl-Stabilized Flame at Atmospheric Conditions", 47th AIAA Aerospace Sciences Meeting, AIAA 2009-1236, Orlando, Florida, 5-8 January 2009.

[II-51] Palies P., Durox D., Schuller T., Candel S., "The combined dynamics of swirler and turbulent premixed swirling flames", Combustion and Flame, Vol.157, pp.1698–1717, 2010.

[II-52] Noiray N., Durox D., Schuller T., Candel S., "A unified framework for nonlinear combustion instability analysis based on the flame describing function", Journal of Fluid Mechanics, vol. 615, pp. 139-167, 2008.

[II-53] Shen H., Tam C.K.W., "Numerical Simulation of the Generation of Axisymmetric Mode Jet Screech Tones", AIAA Aerospace Sciences Meeting and Exhibit, AIAA Journal, Vol. 36, Issue 10, pp. 1801-1807 , October 1998.

[II-54] Beranek L.L., "Noise and Vibration Control", New York, McGraw Hill Book Company, 1971.

[II-55] Bake F.M.U., Michel U., Roehle Ingo, "Investigation of Entropy Noise in Aero Engine Combustors", Journal of Engineering Gas Turbine Power, Vol. 129, Issue 2, pp. 370-376, April 2007.

[II-56] Strahle, W. C. "Combustion Noise", Progress in Energy and Combustion Science, vol. 4, Issue 3, pp.157-176, 1978.

[II-57] Ihme M., Pitsch H., Bodony D.J., "Radiation of noise in turbulent non-premixed flames", Proceeding of the Combustion Institute, 2008.

[II-58] Polifke W., Paschereit C.O., Döbbeling K., "Constructive and destructive interference of acoustic and entropy waves in a premixed combustor with a choked exit", International Journal of Acoustics and Vibration, vol.6, Issue 3, pp.135-146, 2001.

[II-59] Sattelmayer T., "Influence of the combustor aerodynamics on combustion instabilities from equivalence ratio fluctuations", ASME Turbo Expo 2000, ASME, Munich, Germany, 2000-GT-0082, 2000; Journal of Engineering for Gas Turbines and Power, Vol. 125, Issue 1, pp. 11–19, 2003.

[II-60] Ali G., Hunter J.K., "The resonant interaction of sound waves with a large amplitude entropy wave", SIAM Journal on Mathematical Analysis , Vol. 61, Issue 1, pp.131–148, 2000.

[II-61] Bragg S. L., "Combustion Noise", Journal of the Institute of Fuel, vol. 36, pp.12-16. January 1963.

[II-62] Smith T.J.B. and Kilham J.K., "Noise Generation by Open Turbulent Flames", Journal of the Acoustical Society of America, vol. 35, Issue 5, pp.715-724, May 1963.

[II-63] Thomas A. and Williams G.T., "Flame Noise: Sound Emission from Spark-Ignited Bubbles of Combustible Gas", Proceeding of the Royal Society of London, series A, vol. 294, Issue 1439, pp.449-466, 18 October 1966.

[II-64] Hurle I.R., Price R.B., Sugden T.M. and Thomas A., "Sound Emission from Open Turbulent Premixed Flames", Proceeding of the Royal Society of London, series A, vol. 303, Issue 1475, pp.409-427, 19 March 1968.

[II-65] Dowling A., "Thermoacoustics and Instabilities" - in Crighton et al.: Modern methods in analytical acoustics. Springer-Verlag, 1992.

[II-66] Dowling A., "Acoustics of unstable flows" - in Theoretical and Applied Mechanics. T. Tatsumi, E. Watanabe, and T. Kambe eds., Amsterdam, 1996.

[II-67] Strahle W.C., "On combustion generated noise", Journal of Fluid Mechanics, vol. 49, part 2, pp.399-414, 29 September 1971.

[II-68] Strahle W.C., "Some results in combustion generated noise", Journal of Sound and Vibration, vol.23, pp.113–125, 1972.

[II-69] Strahle, W.C., "Refraction, convection, and diffusion flame effects in combustion generated noise", Fourteenth Symposium (International) on Combustion, The Combustion Institute, Pittsburgh, pp.527–535, 1973.

[II-70] Mahan J. and Karchmer A., "Aeroacoustics of Flight Vehicles: Theory and Practice, Volume 1: Noise Sources", vol. 1. NASA. Langley Research Center, Chapter 9: Combustion and core noise, pp. 483-517, August 1991.

[II-71] Putnam A.A. and Faulkner L., "Overview of Combustion Noise", Journal of Energy, 0146-0412, vol.7, Issue 6, pp.458-469, 1983.

[II-72] Klein S., "On the acoustics of turbulent non-premixed flames", PhD thesis, University of Twente, 2000.

[II-73] Mugridge B. D., "Combustion driven oscillations", Journal of Sound Vibration, vol.70, pp. 437-452, 1980.

[II-74] Candel S., "Combustion instabilities coupled by pressure waves and their active control", 24th Symposium (International) on Combustion, The Combustion Institute, Pittsburgh, pp.1277-1296, 1992.

[II-75] Candel S., "Combustion dynamics and control: progress and challenges", Proceedings of the Combustion Institute, vol.29, pp.1-28, 2002.

[II-76] Marble F. and Candel S.; "Acoustic disturbance from gas non-uniformities convected through a nozzle", Journal of Sound and Vibration, 1977, Vol. 55, Issue 2, pp.225–243, 22 November, 1977.

[II-77] Leyko M., Nicoud F., Moreaud S., Poinsot T., "Numerical and analytical investigation of the indirect combustion noise in a nozzle", Comptes Rendus Mecanique, Vol. 337, pp.415-425, 2009.

[II-78] Bake F., Michel U., Röhle I., Richter C., Thiele F., Liu M., Noll B., "Indirect combustion noise generation in gas turbines", 11th AIAA/CEAS Aeroacoustics Conference, AIAA 2005-2830, 2005.

[II-79] Bake F., Kings N., Röhle I., "Fundamental mechanism of entropy noise in aero-engines: Experimental investigation", J. Eng. Gas Turbines Power, Vol. 130, Issue 1, pp.6, 2008.

[II-80] Morfey C., "Amplification of aerodynamic noise by convected flow inhomogeneities", Journal of Sound and Vibration, Vol. 31, Issue 4, pp.391–397, 1973.

[II-81] Ffowcs Williams J.E., Howe M., "The generation of sound by density inhomogenities in low Mach number nozzle flows", Journal of Fluid Mechanics, Vol.70, Issue 3, pp.605–622, 1975.

[II-82] Richter C., Thiele F., "Computation of indirect combustion noise by a CAA method", Proceedings of the 14th International Congress on Sound and Vibration, ICSV14, Cairns, Australia, 2007.

[II-83] Tanahashi M., Tsukinari S., Saitoh T., Miyauchi T., Choi G., Ikame M., Kishi T., Harumi K., Hiraoka K., "On the sound generation and its controls in turbulent combustion field", 3rd Symposium on Smart Control of Turbulence, March 3-5, 2002.

[II-84] Leyko M., Nicoud F., Poinsot T., "Comparison of indirect and direct combustion noise in aircraft engines", 11th CEAS-ASCWorkshop & 2nd Scientific Workshop of X3-Noise: Experimental and Numerical Analysis and Prediction of Combustion Noise, Instituto Superior Tecnico, Lisbon, Portugal, 27-28 September, 2007.

[II-85] Eckstein J. and Sattelmayer T., "Low-order modelling of low-frequency of combustion instabilities in aeroengines", Journal of Propulsion and Power, vol.22, Issue 2, pp.425-432, 2006.

[II-86] Poinsot T. and Veynante D., "Theoretical and Numerical Combustion", Second edition, Edwards, USA, 2005.

[II-87] Chu B.T., "On the energy transfer to small disturbances in fluid flow (Part I)", Acta Mechanica, pp.215-234, 1965.

[II-88] Price R., Hurle I.R., Sugden T.M., "Optical studies of the generation of noise in turbulent flames", 12th Symposium (International) on Combustion, The Combustion Institute, Pittsburgh, pp.1093-1102, 1969.

[II-89] Williams F. A., "Combustion Theory", Benjamin Cummings, Menlo Park, CA, 1985.

[II-90] Higgins B., Journal of Natural Philosophy and Chemical Arts, vol.1, p.129, 1802.

[II-91] Jones A.T., "Singing Flames", Journal of the Acoustical Society of America, vol. 16, Issue 4, pp.254-266, 1945.

[II-92] Rijke P.L., "Notiz über eine neie art, die luft in einer an beiden enden offenen Röhre in schwingungen zu versetzen", Annalen der Physik, vol.107, pp.339-343, 1859.

[II-93] Rayleigh Lord J.W.S., "The theory of sound" (Two Volumes), Macmillan, London, 1877-1878 (2nd ed. 1894); reprinted by Dover Publications reprint, New York, 1945.

[II-94] Raun R.L., Beckstead M.W., Finlinson J.C., and Brooks K. P., "A review of Rijke tubes, Rijke burners and related devices", Progress in Energy and Combustion Science, vol. 19, pp.313-364, 1993.

[II-95] Bisio G. and Rubatto G., "Sondhauss and Rijke oscillations – thermodynamic analysis, possible applications and analogies", Energy, vol.24, Issue 2, pp.117-131, 1999.

[II-96] Dec J.E. and Keller J.O. "Pulse combustor tail-pipe heat-transfer dependence on frequency, amplitude, and mean flow rate", Combustion and Flame, vol. 77, pp. 359-374, 1989.

[II-97] Dec J.E. and Keller J.O. "Time-resolved gas temperatures in the oscillating turbulent flow of a pulse combustor tall pipe", Combustion and Flame, vol. 80, pp. 358-370, 1990.

[II-98] Le Conte J., Philosophical Magazine HP, 235, 1858.

[II-99] Crocco L., "Aspects of combustion instability in liquid propellant rocket motors", Part I, Journal of the American Rocket Society, vol. 21, pp.163-178, 1951.

[II-100] Barrère M. and Williams F. A., "Comparison of combustion instabilities found in various types of combustion chambers", Proceeding of the Combustion Institute, vol.12, pp.169-181, 1968.

[II-101] Harrje D.J. and Reardon F.H., "Liquid propellant rocket instability", NASA, Report SP-194, Washington DC, pp. 467-468, July 1972.

[II-102] Crighton D. G., Dowling A., Ffowcs Williams J.E., Heckl M., Leppington F., "Modern methods in analytical acoustics", Springer Verlag, New York, 1992.

[II-103] Candel S., Huynh C. and Poinsot T., "Some modeling methods of combustion instabilities", "Unsteady combustion", NATO ASI Series, Proceedings of the NATO Advanced Study Institute, Kluwer Academic Publishers, Dordrecht, part I, Issue 5, pp.83-112, Praia da Granja, Portugal, September 6-17, 1996.

[II-104] Lieuwen T., "Analysis of acoustic wave interactions with turbulent premixed flames", Proceedings of the Combustion Institute, vol. 29, Issue 2, pp.1827-1824, 2002.

[II-105] Nicoud F. and Poinsot T., "Thermoacoustic instabilities: Should the Rayleigh criterion be extended to include entropy changes?", Combustion and Flames, vol.142, pp.153–159, 2005.

[II-106] Poinsot T. and Veynante D., "Theoretical and Numerical Combustion", Edwards, USA, Philadelphia, 2005.

[II-107] Candel S. and Poinsot T., "Flame stretch and the balance equation for flame surface area", Combustion Science and Technology, vol.70, pp.1-15, 1990.

[II-108] Durox D., Schuller T., Candel S., "Self-sustained oscillations of a premixed impinging jet flame on a plate", Proceedings of the Combustion Institute, vol.29, Issue 1, pp.69-75, 2002.

[II-109] Schuller T., Durox D., Candel S., "Self-induced combustion oscillations of laminar premixed flames stabilized on annular burners", Combustion and Flame, vol.135, pp.525-537, December 2003.

[II-110] Durox D., Schuller T., Candel S., "Combustion dynamics of inverted conical flames", Proceedings of the Combustion Institute, vol.30, Issue 2, pp.1717-1724, January 2005.

[II-111] Smith D. and Zukoshi E., "Combustion instability sustained by un steady vortex combustion", 21th Joint Propulsion Conference, AIAA, Monterey, AIAA paper 85-1248, 1985.

[II-112] Candel S., Durox D., Ducruix S., Birbaud A.L., Noiray N., Schuller T., "Flame dynamics and combustion noise: progress and challenges", International Journal of Aeroacoustics, Vol.8, Issue 1, pp.1–56, 2009.

[II-113] Shanbhogue S. and Lieuwen T., "Studies on the vorticity field of harmonically excited bluff body flames", 46th AIAA Aerospace Sciences Meeting and Exhibit, Reno, Nevada, AIAA paper 2008-122, 2008.

[II-114] Shanbhogue S., Plaks D., Lieuwen T., "The K-H instability of reacting, acoustically excited bluff-body shear layers", 43rd AIAA/ASME/SAE/ASEE Joint Propulsion Conference and Exhibit, Cincinnati, Ohio, AIAA paper 2007-5680, 2007.

[II-115] Shanbhogue S., Plaks D., Lieuwen T., "Interaction of bluff body flames with the shear layer under harmonic excitation", 21st ICDERS (International Colloquium on the Dynamics of Explosions and Reactive Systems), Poitiers, France, 2007.

[II-116] Sheridian J., Soria J., Jie W., Welsch M., "The Kelvin-Helmholtz instability of the separated shear layer from a circular cylinder", Proceeding of IUTAM (International Union of Theoretical and Applied Mechanism), Symposium, in: Bluff-BodyWakes, Dynamics and Instabilities (eds. Eckelmann H., Graham J.M.R., Huerre P., and Monkewitz P.A.), Goettingen, Germany, pp.115-117, 1992.

[II-117] Mehta P. and Soteriou M., "Combustion heat release effects on the dynamics of bluff body stabilized premixed reacting flows", 41st Aerospace Sciences Meeting and Exhibit, Reno, Nevada, AIAA paper 2003-0835, 2003.

[II-118] Blackshear P., "Growth of disturbances in a flame generated shear region", Technical Report NACA Technical Note 1360, NASA Glenn Research Center, 1958.

[II-119] Yu K., Trouve A., Candel S., "Combustion enhancement of a premixed flame by acoustic forcing with emphasis on role of large-scale vortical structures", 29th AIAA Aerospace Sciences Meeting, Reno, Nevada, AIAA paper 1991-367, 1991.

[II-120] Hermanson J., Dimotakis P., "Effects of heat release in a turbulent reacting shear layer", Journal of Fluid Mechanics, vol. 199, pp. 333–375, 1989.

[II-121] McMurtry P., Riley J., Metcalfe R., "Effects of heat release on the large-scale structure in turbulent mixing layers", Journal of Fluid Mechanics, vol.199, pp.297-332, 1989.

[II-122] Soteriou M., Ghoneim A., "Effects of the free-stream density ratio on free and forced spatially developing shear layers", Physics of Fluids, vol.7, issue 8, pp.2036-2051, 1995.

[II-123] Erikson R., Soteriou M., Mehta P., "The influence of temperature ratio on the dynamics of bluff body stabilized flames", 44th AIAA Aerospace Sciences Meeting and Exhibit, Reno, Nevada, AIAA paper 2006-753, 2006.

[II-124] Wu M.S. and Driscoll J., "A numerical simulation of a vortex convected through a laminar premixed flame", Combustion and Flame, vol 91, issue 3-4, pp.310–322, 1992.

[II-125] Sinibaldi J., Mueller C., Tulkki A., Driscoll J., "Suppression of flame wrinkling by buoyancy: The baroclinic stabilization mechanism", AIAA Journal vol. 36, issue 8, pp.1432–1438, 1998.

[II-126] Louch D. and Bray K. "Vorticity in unsteady premixed flames: vortex pair-premixed flame interactions under imposed body forces", Combustion and Flame, vol. 125, issue 4, pp.1279-1309, 2001.

[II-127] Klein S.A., Kok J.B.W. "Sound generation of turbulent non-premixed flames", Combustion Science and Technology, Vol. 149, pp.267–295, 1999.

[II-128] Hassan H.A., "Scaling of Combustion-Generated Noise", Journal of Fluid Mechanics, vol.66, Issue 3, pp.445-453, 1974.

[II-129] Chiu H.H., Summerfield M., "Theory of combustion noise", Acta Astronautica, Vol. 1, Issue 7-8, pp.967–984, 1974.

[II-130] Ramachandra M.K., Straehle W.C., "Acoustic Signature from Flames as a Combustion Diagnostic Tool", AIAA Journal, Vol.21, Issue 8, pp.1107–1114, 1983.

[II-131] Subrahmanyam P.B., Sujith R.I., Ramakrishna M., "Determination of unsteady heat release distribution from acoustic pressure measurements: A reformulation of the inverse problem", The Journal of the Acoustical Society of America, Vol. 114, Issue 2, pp.686–696, 2003.

[II-132] Lieuwen T.C., Neumeier Y., Zinn B.T., "Determination of unsteady heat release distribution in unstable combustor from acoustic pressure measurements", Journal of the Acoustical Society of America, Vol.15, Issue 4, pp.613–616, 1999.

[II-133] Hield P.A., Brear M.J., Jin S.H., "Thermoacoustic limit cycles in a premixed laboratory combustor with open and choked exits", Combustion and Flame, Vol.156, pp.1683–1697, 2009.

[II-134] Dowling A., "Nonlinear self-excited oscillations of a ducted flame", Journal of Fluid Mechanics, vol. 346, pp.271-290, 1997.

[II-135] Bloxsidge G., Dowling A., Langhorne P.J., "Reheat buzz: an acoustically coupled combustion instability. Part 2. Theory", Journal of Fluid Mechanics, Vol. 193, pp. 445-473, 1988.

[II-136] Fleifil M., Annaswamy A.M., Ghoneim Z.A., Ghoniem A.F., "Response of a Laminar Premixed Flame to Flow Oscillations: A Kinematic Model and Thermoacoustic Instability Results", Combustion and Flame, vol. 106, pp. 487-510, 1996.

[II-137] Chaparro A., Landry E., Cetegen B.M, "Transfer function characteristics of bluff-body stabilized, conical V-shaped premixed turbulent propane-air flames", Combustion and Flame, Vol. 145, Issue 1-2, pp.290-299, 2006.

[II-138] Smith D.A. and Zukoshi E.E., "Combustion instability sustained by unsteady vortex combustion", 21th Joint Propulsion Conference, AIAA paper 85-1248, Monterey, 1985.

[II-139] Culick F.E.C. and Magiawala K., "Excitation of acoustic modes in a chamber by vortex shedding", Journal of Sound and Vibration, vol.64, pp.455-457, 1979.

[II-140] Lieuwen T. and Zinn B.T., "The role equivalence ratio oscillations in driving combustion instabilities in low NOx gas turbines", Proceeding of the Combustion Institute, Vol. 27, The Combustion Institute, Pittsburgh, PA, pp.1809-1816, 1998.

[II-141] Lee J.G., Kim K., Santavicca D.A., "Measurement of equivalence ratio fluctuation and its effect in heat release during unstable combustion", Proceeding of the Combustion Institute, Vol. 28, The Combustion Institute, Pittsburgh, PA, pp. 415-421, 2000.

[II-142] Lee J.G., Kim K., Santavicca D.A., "A study of the role of equivalence ratio fluctuation during unstable combustion in a lean premixed combustor", AIAA Paper 2002-4015, July 2002.

[II-143] Hardalupas Y. and Orain M., "Local measurements of the time-dependent heat release rate and equivalence ratio using chemiluminescent emission from a flame", Combustion and Flame, vol.139, Issue 3, pp.188-207, November 2004.

[II-144] Lee J.G., Gonzalez E., Santavicca D., "On the applicability of chemiluminescence to the estimation of unsteady heat-release during unstable combustion in lean premixed combustor", 41st AIAA/ASME/SAE/ASEE Joint Propulsion Conference and Exhibit, AIAA, AIAA paper 2005-3575, Tucson, Arizona, 2005.

[II-145] Lieuwen T., McDonell V., Petersen E., Santavicca D., "Fuel Flexibility Influences on Premixed Combustor Blowout, Flashback, Autoignition, and Stability", ASME, Journal of Engineering for Gas Turbines and Power, Vol. 130, pp. 011506-1 011506-10, January 2008.

[II-146] Richards G.A., Straub D.L., Robey E.H., "Control of combustion dynamics using fuel system impedance", American Society of Mechanical Engineers, ASME Paper GT-2003-38521, 2003.

[II-147] Coats C.M., "Coherent structures in combustion", Progress in Energy and Combustion Science, Vol. 22, Issue 5, pp 427-509, 1996.

[II-148] Escudier M., "Confined Vortices in Flow Machinery", Annual Review of Fluid Mechanics, Vol. 19, pp. 27-52, January 1987.

[II-149] Lieuwen T., Torres H., Zinn B. and Johnson C., "A mechanism of combustion instability in lean premixed gas turbine combustors", Journal of Engineering for Gas Turbines and Power, vol.123, Issue 1, pp.182-189, 2001.

[II-150] Gonzalez-Juez E., Lee J., Santavicca D., "A study of combustion instabilities driven by flame-vortex interactions", 41st AIAA/ASME/SAE/ASEE Joint Propulsion Conference and Exhibit, AIAA paper 2005-4330, Tucson, Arizona, 2005.

[II-151] Huang Y.,Wang S.,Yang V., "Asystematic analysis of combustiondynamics in a lean-premixed swirl-stabilized combustor", AIAA Journal, Vol.44, Issue 4, pp.724–40, 2006.

[II-152] Ducruix S., Schuller T., Durox D., Candel S., "Combustion dynamics and instabilities: elementary coupling and driving mechanisms", Journal of Propulsion and Power, vol.19, Issue 5, pp.722–34, 2003.

[II-153] Beranek L.L., Ver L., "Noise and Vibration Control Engineering", John Wiley & Sons, 1992.

[II-154] Bies D.A., Hansen C.H., "Engineering Noise Control", Spon Press, Third edition, 2003.

[II-155] Pierce A.D., "Acoustics", The Acoustical Society of America, 1989.

[II-156] Ingard U., Lyon R.H., "The impedence of a resistance loaded Helmholtz resonator", ournal of the Acoustical Society of America, Vol. 25, Issue 5, September 1953.

[II-157] Ingard U., "On the theory and design of acoustic resonators", Journal of the Acoustical Society of America, Vol. 25, Issue 6, pp.1037-1061, 1953.

[II-158] Ingard U., "The near field of a Helmholtz resonator exposed to a plane wave", Journal of the Acoustical Society of America, Vol. 25, Issue 6, November 1953.

[II-159] Singh S., "Tonal noise attenuation in ducts by optimising adaptive Helmholtz resonators", PhD Thesis in Engineering Science, School of Mechanical Engineering, University of Adelaide, Australia, 2006.

[II-160] Mahan J.R., "A Critical Review of Noise Production Models for Turbulent, Gas-Fueled Burners", NASA Contractor Report 3803, NASA, June 1984.

[II-161] Shivashankara B.N., Strahle W.C., Handley J.C., "Evaluation of combustion noise scaling laws by an optical technique", AIAA Journal, vol.13, pp.623–627, 1975.

[II-162] Katsuki M., Mizutani Y., Chikami M.T.K., "Sound emission from a turbulent flame", 21th Symposium (International) on Combustion, The Combustion Institute, Pittsburgh, pp.1543-1550, 1986.

[II-163] Lighthill M. J., "On sound generated aerodynamically. I. General theory", Proceeding of the Royal Society of London, series A, vol. 211, pp.564-587, London, 1952.

[II-164] Ghoniem A.F., Annaswamy A., Wee D., Yi T., Park S., "Shear flow-driven combustion instabilities: evidence, simulation, and modelling", Proceedings of the Combustion Institute, Vol.29, pp.53–60, 2002.

[II-165] Abugov D. and Obrezkov O., "Acoustic noise in turbulent flames", Combustion, Explosions and Shock Waves, vol.14, Issue 5, pp. 606–612, 1978.

[II-166] Clavin P. and Siggia E., "Turbulent premixed flames and sound generation", Combustion Science and Technology, vol. 78, Issue 1-3, pp.147-155, 1991.

[II-167] Markstein G., "Non Steady Flame Propagation", Pergamon Press, Elmsford, Macmillan, NY, 1964.

[II-168] Pelc'e P. and Clavin P., "Influence of hydrodynamics and diffusion upon the stability limits of laminar premixed flames", Journal of Fluid Mechanics, vol.124, pp.219–237, 1982.

[II-169] Matalon M. and Matkowsky B., "Flames in fluids: their interaction and stability", Combustion Science and Technology, vol.34, pp.295–316, 1983.

[II-170] Sivashinsky G.I. and Margolis S.B., "Some new solutions of the flame front equation", Numerical Simulation of Combustion Phenomena, pp.131-136, 1985.

[II-171] Kendrick D.W., Zsak T., Zukoski E., "An experimental and numerical investigation of premixed combustion in a vortex in a laboratory dump combustor", "Unsteady combustion", NATO ASI Series, Proceedings of the NATO Advanced Study Institute, Kluwer Academic Publishers, Dordrecht, part I, Issue 3, pp.33-69, Praia da Granja, Portugal, September 6-17, 1996.

[II-172] Noiray N., Durox D., Schuller T., Candel S., "Self-induced instabilities of premixed flames in a multiple injection configuration", Combustion and Flame, vol.145, Issue 3, pp.435–446, May 2006.

[II-173] Zukoski F.E., "Afterburners", Chapter 21. in: Oates G., editor. "The aerothermodynamics of aircraft gas turbine engines", Air Force Aero Propulsion Laboratory, AFAPL-TR-78-52, 1978.

[II-174] Singh K., Zhang C., Gore J., Mongeau L., Frankel S.H., "An experimental study of partially premixed flame sound", Proceedings of the Combustion Institute, vol.30, Issue 2, pp.1707-1715, January 2005.

[II-175] Hardalupas Y., Selbach A., "Imposed oscillations and non-premixed flames", Progress in Energy and Combustion Science, Vol. 28, pp. 75-104, 2002.

[II-176] Ihme M., Bodony D.J., Pitsch H., "Towards the prediction of combustion-generated noise in non-premixed turbulent flames using large-eddy simulation", Center for Turbulence Research, Annual Research Briefs, pp. 311-323, 2005.

[II-177] Ihme M., Bodony D.J., Pitsch H., "Prediction of combustion-generated noise in non-premixed turbulent jet flames using large-eddy simulation", AIAA Paper 2006-2614, 2006.

[II-178] Ihme M., Pitsch H., Kaltenbacher M., "Prediction of combustion-generated noise in non-premixed turbulent flames using large-eddy simulation", 5th US Combustion Meeting, paper B38, March 25-28, 2007.

[II-179] Lieuwen T. and Cho J.H., "Coherent acoustic wave amplification/damping by wrinkled flames", Journal of Sound and Vibration, vol.279, Issues 3-5, pp.669-686, January 2005.

[II-180] Birbaud A.L., Durox D., Ducruix S., Candel S., "Dynamics of confined premixed flames submitted to upstream acoustic modulations", Proceedings of the Combustion Institute, vol.31, Issue 1, pp.1257-1265, 2007.

[II-181] Dowling A.P., "The calculation of thermoacoustic oscillations", Journal of Sound and Vibration, Vol. 180, Issue 4, pp. 557–581, 1995.

[II-182] MacQuisten M.A., Dowling A.P., "Low-frequency combustion oscillations in a model afterburner", Combustion and Flame, Vol. 94, Issue 3, pp. 253-264, August 1993.

[II-183] Hield P.A., Brear M.J., "Comparison of open and choked premixed combustor exits during thermoacoustic limit cycle", AIAA Journal, vol. 46, Issue 2, pp. 517-526, 2008.

[II-184] Heitor M.V., Taylor A.M.K.P., Whitelaw J.H., "Influence of confinement on combustion instabilities of premixed flames stabilized on axisymmetric baffles", Combustion and Flame, Vol.57, pp. 109–121, 1984.

[II-185] Natanzon M.S., "Unsteady Combustion in Liquid Rocket Engines", 1999; Electronic translation from the Russian edition (1984) with a revised Chapter 8 on Bifurcations; translation editor Culick F.E.C.

[II-186] Natanzon M.S. and Menshikova O.M., "Bifurcation of steady combustion regimes and their influence on the onset of high-frequency oscillations in combustion chambers", Physics of Combustion and Explosion, vol. 23, Issue 4, pp.10-18, 1992.

[II-187] Natanzon M.S., Lapina Z.S., Merkerlov I.V., "Combustion Stability in a Combustion Chamber", Doklady, AN USSR, Series Power Engineering and Transport, Issue 4, pp. 137-146, 1985.

[II-188] Knoop E., Culick F.E.C., Zukoski E.E., "Extension of the stability of motions in a combustion chamber by nonlinear Active Control based on hysteresis", Combustion Science and Technology, vol. 123, pp.363-376, 1996.

[II-189] Isella G., Seywert C., Culick F.E.C., Zukoski E.E., "A further note on Active Control of Combustion Instabilities based on hysteresis", Combustion Science and Technology, vol. 126, pp.381-388, 1997.

[II-190] Lieuwen T. and Zinn B.T., "Experimental investigation of limit cycle oscillations in an unstable gas turbine combustor", AIAA Paper 2000-0707, 38th AIAA Aerospace Sciences Meeting, Reno, NV, January 2000.

[II-191] Richards G.A., Janus M., and Robey E.H., "Control of Flame Oscillations with Equivalence Ratio Modulations", AIAA Journal of Propulsion and Power, vol. 15, Issue 2, pp. 232-240, 1999.

[II-192] Kotake S. and K. Hatta, "On the Noise of Diffusion Flames", Japan Society of Mechanical Engineers Journal, vol. 8, Issue 30, pp.211-219, 1965.

[II-193] Knott P.R., "Noise Generated by Turbulent Non-Premixed Flames", AIAA Paper 71-732, 1971.

[II-194] Kumar R.N., "Further Experimental Results on the Structure and Acoustics of Turbulent Jet Flames", AIAA Paper 75-523, AIAA Second Aeroacoustics Conference, Hampton, VA, March 24-26, 1975.

[II-195] Rajaram R., Gray J., Lieuwen T., "Premixed combustion noise scaling: total power and spectra", 12th AIAA/CEAS Aeroacoustics Conference (27th AIAA Aeroacoustics Conference), AIAA paper 2006-2612, Cambridge, Massachusetts, 8-10 May 2006.

[II-196] Shivashankara B.N., Strahle W.C., Handley J.C., "Combustion Noise Radiation by Open Turbulent Flames", AIAA Paper 73-1025, AIAA Aeroacoustics Conference, Seattle, WA, 15-17 October, 1973.

[II-197] Strahle W.C., "A Review of Combustion Generated Noise", AIAA Paper 73-1023, AIAA Aeroacoustics Conference, Seattle, WA, 15-17 October, 1973.

[II-198] Roberts J.P. and H.G. Leventhall, "Noise Sources in Turbulent Premixed Flames", Applied Acoustics, vol. 6, pp.301-308, 1973.

[II-199] Peracchio A.A. and Proscia W., "Nonlinear heat release/acoustic model for thermoacoustic instability in lean premixed combustors", ASME Gas Turbine and Aerospace Congress, Stockholm, Sweden, 1998.

[II-200] Fleifil M., Annaswamy A.M., Ghoniem A.F., "A physically based nonlinear model of combustion instability and active control", Proceedings of the Conference on Control Applications, Trieste, Italy, August 1998.

[II-201] Rumsey J., Fleifil M., Annaswamy A.M., Hathout J.P., Ghoniem A.F., "Low-order nonlinear models of thermoacoustic instabilities and linear model-based control" Proceedings of the Conference on Control Applications, Trieste, Italy, August 1998.

[II-202] Lieuwen T., "Experimental Investigation of limit-cycle oscillations in an unstable gas turbine combustor", AIAA Journal of Propulsion and Power, vol.18, Issue 1, pp.61-67, 2002.

[II-203] Yang V. and Culick F.E.C., "Nonlinear analysis of pressure oscillations in ramjet engines", 24th Aerospace Sciences Meeting, AIAA Paper 86-0001, Reno, NV, 6-9 January, 1986.

[II-204] Culick F.E.C., "Some recent results for nonlinear acoustics in combustion-chambers", AIAA Journal, vol. 32, Issue 1, pp.146-169, January 1994.

[II-205] Prasanth R., Annaswamy A.M., Hathout J.P., Ghoniem A.F., "When do open-loop strategies for combustion control work?", AIAA Journal of Propulsion and Power, vol. 18, Issue 3, pp.658-668, 2002.

[II-206] Zinn B. T. and Lores M. E., "Application of Galerkin method in solution of nonlinear axial combustion instability problems in liquid rockets", Combustion Science and Technology, vol.4, Issue 6, p.269, 1972.

[II-207] Poinsot T., Yip B., Veynante D., Trouve A., Samaniengo J.M., Candel S., "Active control - an investigation method for combustion instabilities", Journal de physique III, vol. 2, Issue 7, pp.1331-1357, July 1992.

[II-208] Dowling A.P., "A kinematic model of ducted flame", Journal of Fluid Mechanics, vol.394, pp.51-72, 1999.

[II-209] Noiray N., Durox D., Schuller T., Candel S., "A method for estimating the noise level of unstable combustion based on the flame describing function", 11th CEAS-ASC Workshop on "Experimental and Numerical Analysis and Prediction of Combustion Noise", Lisbon, Portugal, 27/28 September 2007.

[II-210] Dowling A.P., "The calculation of thermoacoustic oscillation", Journal of Sound and Vibration, vol.180, pp.557-581, 1995.

[II-211] Keller J., "Thermoacoustic oscillations in combustion chambers of gas turbine", AIAA Journal, vol.33, Issue 12, pp.2280-2287, 1995.

[II-212] Krejsa E.A. and Karchmer A.M., "Acoustical modal analysis of the pressure field in the tailpipe of a turbofan engine", NASA-TM-83387, NASA Center: Glenn Research Center, May 1983.

III. Control strategies: passive and active control

We generally wish to eliminate instabilities in combustion systems. Traditionally that has meant designing systems so that small disturbances are stable, or adding some form of energy dissipation to compensate the energy gained from the combustion processes, that is, ***passive control***. However, in the past few years interest has grown in the possibility of ***active control*** of instabilities.
Various acoustic-control strategies are applied to deal with the unacceptable levels of dynamics. The conventional approach to this problem is mostly based on empirical correlations and design experience. However, the application of these strategies is a largely empirical process with little assurance of success.
Methods for controlling combustion dynamics in practical gas-turbine combustors fall into two categories: *passive* and *active control*.

1. *Passive control* solutions act either on the combustor (by changing resonant frequency or adding damping) or on the unsteady heat release (by changing the response of the flame to acoustic pressure fluctuations).
2. *Active control* solutions use feedback control to attenuate the instabilities and have typically employed unsteady-pressure sensors and high-speed fuel flow rate actuation.

Both types of control require an understanding of the root-case physics behind the thermoacoustic-coupling process. Whereas passive-solution techniques are somewhat mature, active-instability-control techniques are still immature.

III.1 Passive control

A suitably design and well-located *pressure-wave attenuator* clearly can significantly reduce the strength of feedback coupling for most if not all feedback mechanisms that can lead to combustion instabilities. Despite the great care taken to remove fuel-air ratio oscillations from the premixers, industry manufacturers included several pressure-wave attenuators as part of the combustor structure.

III.1.1 Methods to improve combustion stability

Passive control approaches are typically a part of the hardware design or operating envelope, so they include ([II-34] § 17):

1) Modifying the dynamic response of the feed system

Unsteady aerodynamics can produce a variation in heat-release caused by changes in flame area or vortex shedding/merging. These flame dynamics can occur without any perturbations in fuel-air ratio. Making passive adjustments to the feed-system dynamics, it is possible to produce stability at selected conditions by controlling the arrival of fuel-air perturbations ([II-142], [II-146]).

a) ***Design changes to the fuel-air mixing device*** have been shown to have significant impact on combustion-dynamics behaviour ([I-22],[III-1]). Care is taken usually to immerse *resonators within the combustor case plenum* upstream of the burners. This position ensure that the air temperature within the resonators is unaffected by ambient conditions around the engine. Furthermore, all resonators are directly connected to the flame tube, that is, they are located as close as possible to the combustion zone itself. A significant number of frequencies are covered by means of several resonating cavities, all naturally integrated within the combustor architecture.
Main design modifications affect the *burner design* and hence the flame response. The location of heat release is mainly aerodynamically determined by the size of recirculation zones. Then, other examples of design changes are the changing *burner exit*, *burner diameter*, *swirl number*, then recirculation zone and flame front position.
The motivation for burner-design modifications is that the flame response plays an important role as the thermoacoustic source and the burner is the part that can be replaced most easily in an existing design.

b) ***Aerodynamic device***
One of the mechanisms that can lead to combustor pressure oscillations is an upstream-velocity fluctuation convected from the plenum, through the premixer, and then the combustion zone. Potential sources of plenum-velocity fluctuations are the turbulent-flow structure surrounding the combustor. Large-scale eddies convected to the premixers can cause significant velocity fluctuations, which disturb the combustion process.
These device are located upstream of the premixers. Some of the configurations tested included a number of reticulated materials, such as *perforated plates*, *honeycomb* and *metal foams*, all of which are tested for various thickness, porosity and pressure-loss characteristics. Note that the pressure loss introduced by the aerodynamic damping device is typically very low, less than 0.2%.
The premixers and, hence, the flame experience a reduced level of velocity fluctuation, resulting in a quieter combustion process.

2) Changing the average convective time-lag and increasing the time-lag distribution by introducing multiple time-lags

The perturbations are transported downstream to the flame with a convection *time lag* τ. The time τ is an average representation of the time from fuel injection to the time of combustion. It depends on the flame location and the flame shape. In practical systems, neither flame location nor flame shape is easily measured experimentally or predicted ([I-22], [I-23], [I-24], [II-30], [II-149], [III-1]). Additional time lags may characterize the combustion process (e.g., the time need to burn the reactants) and could be included in an overall time lag.
An example of changing the average convective lag is obtained by a modular premixer design that allows *the position of fuel injection to be changed from three position*, or simultaneously from two of the three positions ([I-23], [II-30]).

Usually a single (i.e. average) value for the convective time lag is used. In practice, however, a distribution of time lags will be produced by various mechanism (i.e., turbulent diffusion, flame location, flame shape, etc.). This time-lag distribution can also be changed by the design of the supply system (i.e., *multiple fuel-injection locations*, *adjusting flow splits* and *multiple injectors with different fuel-injection locations*) ([I-23], [I-32], [II-34] § 4, [II-211], [III-2], [III-3], [III-4]).
Both fuel-injection points produce richer and leaner packets of fuel-air mixture in response to variations in the premix airflow. However, only one of these packets can produce heat-release rate perturbations that are in phase with the pressure perturbations; the other packet may be arranged to produce perturbations that are out of phase with the acoustic pressure. The out-phase perturbations add a considerable amount of damping to the systems.
An interesting practical application of the multiple time-lag concept has been demonstrated by Berenbrink and Hoffmann [III-3]. These authors recognized that the time lags can be *adjusted on the individual fuel injectors* so that the combined combustion response is more stable. This approach has an advantage compared with placing multiple fuel ports in a single injector, because it is easier to optimize the mixing from a single fuel port.
In addition, a slightly different approach using *asymmetric burners* [III-3] has also produced comparable stabilization. The asymmetric burner concept simply placed different fuel injectors at different angles relative to the combustor flow axis. The resulting asymmetry in the flame shape prevents uniform coupling to the acoustics and also has the effect of shifting the flame position on different oriented injectors. The net effect is again a distribution of time lags among the different injectors.

3) Changing the flame location: flame-geometry and flame anchoring effects

Another consideration that has an impact on the time-lag distribution is the *geometry of the flame*. This effect can be understood by noting that the arrival of fuel-air perturbations is distributed over the surface of what is typically a conical-flame geometry. The conical geometry means that the delivery of a fuel perturbation will produce a combustion response that is distributed over the surface of the flame and subsequently over a range of time-lags.
Flame anchoring, which establishes the instantaneous location of the flame, is another important consideration for reducing the flame dynamics.
The addition of a *pilot flame* is a common approach to reducing flame dynamics and for the stabilization of flame, but the stabilizing mechanism is often uncertain. Different authors ([I-4] § 2, [III-5], [III-6]) attribute *pilot-enhanced stability* to an improvement in flame anchoring, but there are additional reasons why pilot flames may improve stability. The pilot flame is typically operated as a diffusion flame or partially premixed, and it may have a lower dynamic response than a purely premixed flame. In a diffusion flame, the local reaction rate is controlled by the local mixing processes instead of the overall fuel-air ratio. Thus, momentary perturbations in the fuel or air supply cannot produce an appreciable change in the reaction rate. Control by local mixing processes reduces the likelihood of oscillations in diffusion flames and may explain why diffusion pilots can be used to silence oscillations. Although more work is needed to understand the stabilizing effect of pilot flames, diffusion-pilot flames are undesirable, because they contribute significantly to NO_x emissions.

An original instability control technique acting on thermo-acoustic combustion instabilities appearing in an experimental lean premixed burner is the control by *local swirling injection of a high heating value fuel*, like hydrogen [III-7]: it consists in a local injection of a more energetic fuel in an unstable lean premixed hydrocarbon/air flame. Several diagnostic techniques have been used to characterize the burner behaviour and to evaluate the effects of hydrogen injection on both combustion instabilities and pollutant emissions. It was shown that *hydrogen injection* induces a significant decrease of the amplitude of pressure oscillations while the heat release oscillations remain at the same level. It had been shown that the hydrogen injection has no negative effects on NO emission but induces a strong increase of CO emission.

III.1.2 Acoustic dampers

Although *acoustic dampers* are commonly used to stabilize rocket and afterburner applications, less emphasis has been given to the use of acoustic dampers in gas-turbine applications. In stationary engines, the disparity of damper use may be related to the relatively low frequencies encountered in most *turbine applications (hundred of Hertz)* vs those typically encountered in *rocket engines (kilohertz range)*. The lower frequencies require physically larger dampers, which complicates engine packaging, and may be a potential drawback. Nevertheless, dampers should not be overlooked in a strategy to stabilize combustion.
The simplest damper of all is a ***hole***, releasing acoustic energy from the combustion chamber that would otherwise return to the feedback loop. The efficacy of this method is well known to practicing combustion engineers. Putnam ([II-3], [II-34] § 17) noted the following advice for practitioners faced with stubborn oscillation problems in industrial burners: *"To solve an oscillating combustion problem, drill a hole. If that doesn't work, drill two holes"*. Although this anecdote is a humorous, it represents genuine experience that reducing the acoustic gain can stabilize oscillating systems. Conversely, eliminating holes can lead to combustion instabilities. Modern premixed combustors are designed specifically to avoid dilution holes, removing a source of acoustic damping. The avoidance of holes is yet another reason why premixed combustors tend to have problems with dynamics. Earlier diffusion flame combustors used numerous dilution holes around the perimeter of the liner, providing a source of acoustic damping that is absent in premixed combustors.
Although drilling holes may be an acceptable control strategy in industrial burners, it is not an option for gas-turbine combustors in which flow splits must be accurately controlled to meet performance targets. Alternatively, closed resonators could be used to absorb acoustic energy. Because the resonators are closed, they do not compromise the designed flow splits.
Then, other typical passive controls are ***Helmhotz resonators*** ([II-159], [III-8], [III-9], [III-10], [III-11]) or ***quarter-wave tubes*** [III-12], and serve as damping devices in the oscillating system. The incident and reflected acoustic waves in the diffuser cavity are significantly altered to the extent that certain discrete oscillations are attenuated and therefore become less destructive to the combustor. When pressure oscillations occur, flow enters and exits the resonator mouth. The energy dissipated at the entrance-exit provides damping to the system. The greatest losses are generated by tuning the resonator so that the natural frequency (e.g., $f_0=f_{Helmholtz}$) is close to the frequency that is to be damped in the combustor.

These devices have demonstrated successful suppression of acoustics in gas-turbine combustors. A disadvantage of these devices is that they only operate over a limited frequency range, thus requiring empirical selection on the number and configuration of the devices. The development of a pressure-wave attenuator requires some knowledge about the acoustic mode being excited. The frequency of the mode affects the sizing of the attenuator (larger dimensions give lower frequencies), whereas the mode shape determines the optimal location of the attenuator.
Selecting the position and number of resonators is an important consideration. It does little good to place the resonator at an acoustic node. Resonators added at these node positions will not provide damping, because there is no acoustic pressure to drive the oscillator. Attempts to position resonators at the pressure antinodes may be frustrated by a repositioning of the node to the new resonator location.
It is sometimes overlooked that dampers themselves participate in the overall acoustic response of the combustion chamber. When dampers with sufficient mouth area represent a considerable portion of the combustor volume, their presence can lead to a change in the natural frequency of the entire combustion system, and they may actually destabilize an otherwise stable system [III-10].
The devices are installed additionally and inevitably to suppress undesirable acoustic oscillations if they should be. And thus, negative effects of engine-performance degradation and complexity in engine manufacture accompany the installation of these devices.
Although the origin of the phenomenon remains unclear, *high-frequency dynamics* can be well damped by resonators.

III.1.2.1 Helmholtz resonators

With Helmholtz resonators (e.g., Fig. II-9 and Fig. III-1), a cavity is acoustically connected to the inside of the combustion chamber by an orifice. The eigenfrequency of a typical *Helmholtz resonator* configuration is given by:

$$f_{Helmholtz} = \frac{c}{2\pi}\sqrt{\frac{S_{neck}}{V\left(L+\Delta L\right)}}$$

where

$S_{neck} = \pi \frac{D_{tube}^2}{4}$ is the area of the orifice of the Helmholtz resonator

$\Delta L = 0.85\ D_{tube} = 1.7\ R_{tube}$

The eigenfrequency is determined by the ratio of the area (S_{neck}) of the orifice of the resonator tube and resonator volume V times the length of the resonator tube L. ΔL expresses the elongation of the resonator tube to take into account radiation effects. ΔL is computed approximately as 0.85 diameter of tube D_{tube} (=1.7 radius of tube R_{tube}). The speed of sound is denoted by c.
It has been shown that appreciable attenuation can be achieved if the volume of the resonator (V) is approximately 7% of the combustion volume [III-10]. The area of the orifice of the Helmholtz resonator (S_{neck}) is usually chosen about 10% of the combustor cross section.
To increase the damping performance of *high-frequency resonators*, the acoustic-absorption area of the resonators has to be high.

Placing of the resonators is critical to their overall performance. The resonators should be placed near pressure antinodes, which can be measured or predicted by using three-dimensional CFD techniques. A good starting point is to place the resonators at the axial location of maximum heat release because the flame is the source of the acoustic energy, However, in some cases, this may not be possible because of geometrical constraints.
Helmholtz resonators may also be used for suppressing *intermediate-frequency* dynamics.

Fig. III-1: Helmholtz resonators mounted in the Siemens annular combustor rig ([I-32], [II-34] § 5).

III.1.2.2 Quarter-wave tubes

In the quarter-wave design, the natural frequency can only be established by the length:

$$f_{Quarter-wave\,tube} = \frac{1}{4}\frac{c}{L}$$

Others works ([III-13], [III-14], [III-15]) suggest that the optimal length of the resonator be a half wavelength of the first longitudinal overtone mode traveling in the resonator with the acoustic frequency intended for damping in a combustion chamber of a liquid rocket engine. A ***half-wave resonator*** was suggested for maximum damping through linear acoustic analysis.

III.2 Active control

Active control offers the potential to readjust the combustion dynamics to accommodate problems like changing ambient conditions, fuel composition, or engine wear. Although active control concepts have significant potential and may become a preferred stabilization strategy in the future, at the present time most engine developers are using passive methods to stabilize combustion.
There are two active control methods:

1) ***Active combustion control*** (**ACC**) or ***automatic tuning systems*** use low-bandwidth control (<30 Hz, e.g. industrial fuel-control valves) to make adjustments to the mean operating conditions (airflow, fuel flow, and fuel distribution).
2) ***Active instability control*** (**AIC**) systems achieve stability by perturbating the combustion process at or near the frequency of the combustion instability (normally 100-200 Hz).

Both the *low-bandwidth* and *high-bandwidth* control approaches require reliable real-time measurement of the combustion-process oscillations. Dynamic *pressure transducers* or *accelerometers* are typically used in industrial applications.
Active combustion control (ACC), which provides feedback-based control of the fuel injection, the fuel-air mixing process, and the staging of fuel sources can provide an alternative approach to achieving acceptable combustor dynamic behaviour, and thus can provide flexibility during the combustor design process.
The basic idea to suppress combustion oscillations by an active feedback loop was published in a theoretical paper on rocket engines by Tsien as early as 1952 [III-16]. However, it took until the eighties to convert this idea into a practical device. Various authors described successful tests based on laboratory scaled burners with a thermal power of between 1 kW and 250 kW ([III-17], [III-18], [III-19]). For all these publications, attenuation of combustion oscillations is achieved by anti-sound signals generated via loudspeakers. In addition to this method, other types of intervention and control strategies were researched for various combustion systems; however, all tests were performed at lab scales ([I-32], [III-20], [III-21], [III-22], [III-23], [III-24], [III-25], [III-26], [III-27], [III-28]). The first industrial-size application of Active Instability Control (AIC) was realised by Seume et al. ([II-10], [III-29]) in 1997 in the test facility of Siemens on the V84.3A based on a land-based gas turbine delivering 160 MW of electrical power. For this full-scale industrial gas turbine, active control was achieved by means of anti-cyclical fuel injection, with direct drive valves serving as actuators. This technique was then also extended to the largest type of this family of gas turbines, the **V94.3A** with an electric power output of 267 MW ([II-34] § 19, [III-30], [III-31], [III-32]). For the largest version of gas turbine type Vx4.3A, that is V94.3A, the eigenmode is excited at a frequency of approximating 170 Hz [III-32].
Although significant suppression of combustion dynamics has been demonstrated in several subscale laboratory combustors, several barriers to implementation in full-scale gas-turbine combustors still exist. First, the geometry of an annular combustor is far more complex than that of a simple “can”-type laboratory combustor. The control algorithms for controlling the complex acoustic mode structures in an annular combustor still need to be developed and proven. Also, the reliability and durability of the *sensors*, *control systems* and *actuators* need to be comparable to those of the gas turbine itself to avoid causing unscheduled maintenance events.
The active-control system consisted of three parts (Fig. III-2): a *sensor*, a *control algorithm* and an *actuator*.

Note that important differences exist between behaviour observed in small laboratory combustion-control experiments and full-scale industrial combustors. Laboratory combustors typically have no liner and thus have lower damping than industrial combustors. At the same time, laboratory combustors may have lower turbulence levels than larger, more complex devices.

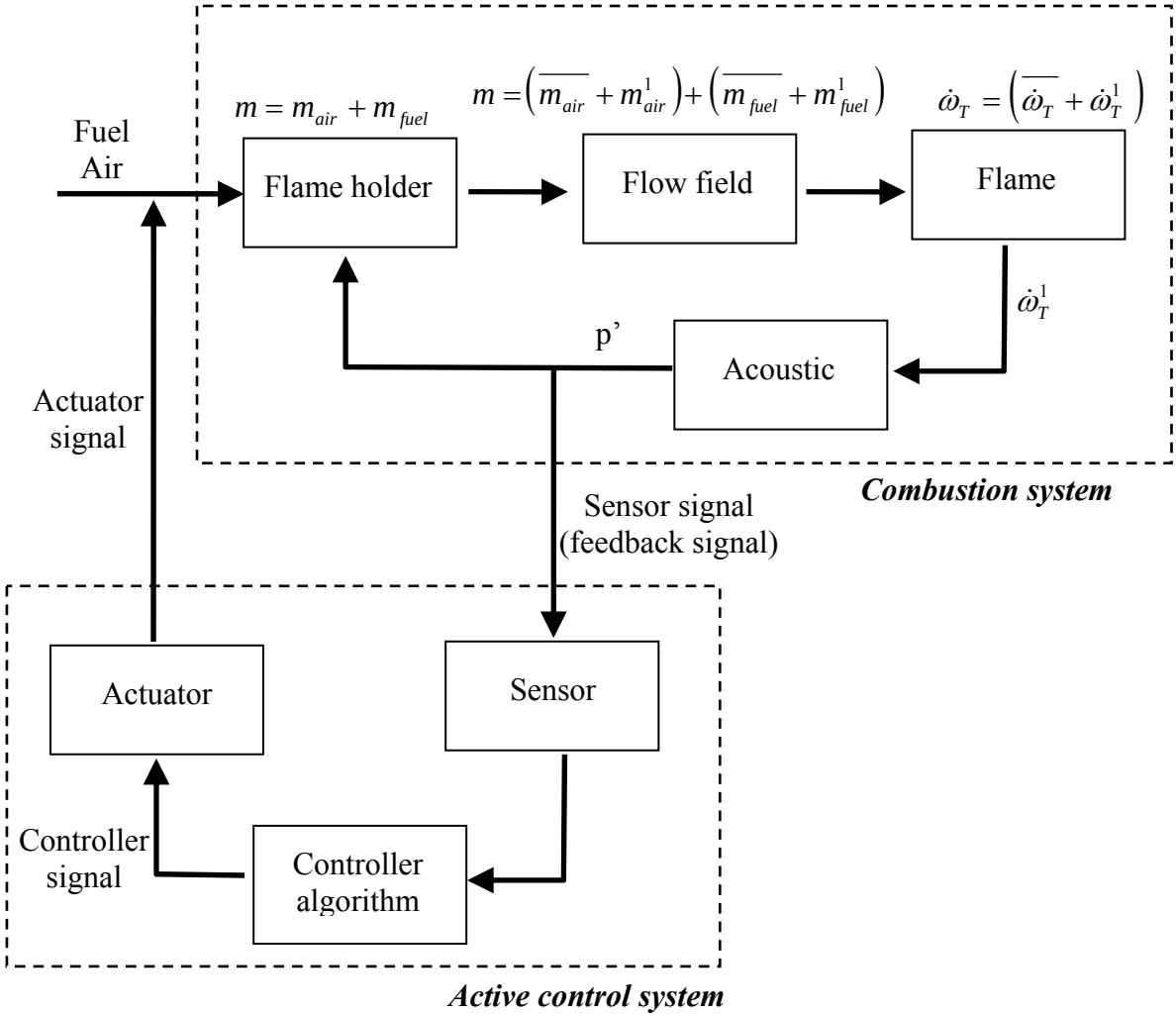

Fig. III-2: Scheme of the feedback processes in an Active Control system.

According to the mechanism generating self-excited combustion oscillations there are two basic possibilities for active control of combustion instabilities via actuators: by *influencing the combustion system acoustics* or by *controlling the flame itself*.

a) For actively *intervening via acoustical means*, sound pressure fluctuations within the combustion chamber are damped by means of an anti-sound signal. Owing to the direct coupling between sound pressure fluctuation and related oscillations of the heat release rate within the flame, the combustion zone itself will likewise be smoothed out.
   For combustion systems operating under pressure or characterised by high volume flow rates, the acoustic power that can be generated by *loudspeakers* is insufficient to appropriately

damp any self-excited sound field. Moreover, there will be problems with installing this type of actuator. For instance, loudspeakers have to be built in as flush as possible with the chamber walls in order to guarantee good sound emission. In view of the high wall temperatures characterising combustion systems, doing so is normally impractical. Installing acoustic actuators within the air/fuel supply system likewise creates practical problems if mass flows are pre-heated or flammable.

b) By contrast, when actively *controlling via the flame*, fluctuations of the heat release rate are attenuated by anti-cyclically injecting air and/or fuel mass flows.
   Compared to acoustics, influencing the flows introduced into combustion systems offers a better control potential. Fuel supplies are normally particularly suitable because, in industrial combustion systems, volume flow rates of fuel are often substantially lower than those of air. This is particularly true for gaseous fuels supplied under high pressure, for highly caloric gaseous fuels, or when burning liquid fuels.
   In general **no more than 3-4% of additional fuel** will be required to control combustion oscillations ([II-34] § 19, [III-21], [III-25], [III-32])

Active controls take multiple forms, the most common being *modulation of the fuel flow* with a frequency and phase relationship designed to destructively interact with the combustion-dynamic oscillation. This modulation can take the form of the main fuel flow ([III-33], [III-34]), or a smaller secondary fuel-injection site [III-35], possibly intended to act more directly on regions in which the *Rayleigh index* is largest.
An good overview on active control system in combustion chambers was written by Dowling in 2005 [III-26] and by Huang in [I-32].

III.2.1 Sensors and diagnostic techniques for the monitoring and control of practical flames

The development of *diagnostic methods* suitable for the monitoring of practical flames is an important objective, which is receiving a growing attention and significant research efforts. This is motivated by the need to achieve a more precise description of the process and, ultimately, implement efficient and reliable control and optimisation methods as a key step towards the development of more efficient, flexible, reliable and clean combustion systems. Many and interesting attempts have been proposed, involving widely different approaches in terms of the instrumentation utilized and the concepts proposed to convert sensorial information into various meaningful parameters [III-36].
Basically, every parameter that is part of the oscillation at issue can be used as input signal for an active feedback control. In practice, however, only those will be used that can be measured easily by suitable sensors, i.e. mainly sound pressure and heat release rate of the flame. Sound pressure can be measured very easily, e.g. by *microphones* or *piezo pressure transducers*, while *photomultipliers* or *photodiodes* are particularly useful to measure the unsteady heat release rate of the flame. In order to obtain a resolution sufficient for the time scales of the oscillations, the emissions of short-lived intermediate reaction products are measured, such as the formation of free *OH radicals*.
Active Instability Control (AIC) sensors have to be positioned in spots where the parameter to be measured correlates sufficiently with combustion oscillations and is reasonably proportional. *Optical sensors* to measure heat release rates for the AIC must cover no less than that area of the

combustion zone where fluctuations of the reaction rate occur, the entire combustion zone being preferable. If only a small portion of the combustion zone is covered, any displacement of this zone may blind the sensor to prevailing oscillations. A further problem with optical sensors is fouling, e.g. by soot.
Sensors must provide measurement of a dynamic quantity related to the combustion oscillations. Although this is a relatively straightforward task for an unstable system, it is more difficult for low-amplitude controlled oscillations.
The possibilities for permanent optimization of combustion equipment are currently very limited. The monitoring and control of most practical burners is based, apart from the mandatory flame management system, on the *analysis of flue gases*. This suffices to achieve the desired excess air or to check the levels of undesirable emissions (e.g., CO, NO_x, particulates).
Conventional instruments are customarily used to measure global variables such as input flow rates and flue gas composition (e.g., O_2, CO, NO_x, SO_2), but they afford a very limited description of the process taking place inside the combustion chamber. A precise diagnostic would require much richer information on the properties of the flame, as the core of the combustion process. This is even more evident in multi-burner combustors, where the behaviour of individual flames can be very different from that estimated from global values.
However, the information provided by the *gas analysers* constitutes a highly incomplete description of the combustion process and is clearly insufficient to act on the burner settings in an effective and safe way.
The development of flame monitoring techniques suitable for practical applications appears as an important prerequisite for the design of ambitious supervision and control strategies of combustion equipment. Numerous and interesting attempts in this respect have been reported, especially during the last decade.

III.2.1.1 Pressure Measurements

The information contained in acoustic flame signals is intimately related with the very nature of the combustion process and, therefore, may offer interesting possibilities for flame monitoring.
The most basic measurement to detect and characterize unstable combustion is obtained by the dynamic pressure in the combustor: *microphones* and *pressure transducers* (e.g. fast-response transducers piezoelectric) are the most commonly used sensors. They have the advantage that because acoustic waves propagate throughout the entire combustion system, they do not need to be placed close to the high temperatures of the heat-release zone. They have large bandwidth and are reasonably robust. Their location within the combustor is important; attention must be paid to the likely mode shapes to avoid placement near a pressure node and ideally to maximize the signal-to-noise ratio.
To accurately measure combustor pressure fluctuations, the pressure transducer should be mounted flush with the inner wall of the combustor chamber. In some combustors the design of the combustion chamber does not allow for this or there might be concerns about exposing the transducer to the high temperatures of combustion.
In general, the instrumentation configuration is driven by the temperature limitations of the transducers. Because of the lack of suitable high-temperature pressure instrumentation, the sensor is always physically placed away from the flame. This necessarily introduces some *transfer function* between the actual pressure in the combustion chamber and that measured at the

transducer. Depending on the stand-off tube configuration and sensor location, amplitude roll off or attenuation can become significant.
In such cases it is necessary to isolate the transducer from the combustion chamber by using a recess mount with a small-diameter passageway between the transducer and the combustion chamber. When the pressure transducer is mounted in this manner, it is important to account for the acoustic characteristics of the passageway, because they can alter the amplitude and phase of the measured pressure signal [II-101]. Another consideration when making pressure measurements is that the interaction between the flame and the pressure wave results in a three-dimensional acoustic field in the vicinity of the flame. Under some circumstances, the pressure at the wall of the combustor, where it is often measured, can differ in amplitude and phase by as much as 20% from the pressure at the flame ([II-34] § 16).
In addition to measuring pressure fluctuations in the combustor, it is useful to simultaneously measure pressure fluctuations in the nozzle and the fuel line, because they can also used as a guide when attempting to modify the nozzle or fuel-system geometry to alter the relative phase of the equivalence ratio and heat-release fluctuations to suppress the instability.
Examples of microphones and pressure transducers used as sensors in full-scale demonstrations were experiments of Seume et al. ([II-10], [II-34] § 19, [III-29]) and Moran et al. [III-37].
In enclosed flames, the noise spectrum is not only determined by the flame emission sound but it can be *strongly influenced also by the acoustic characteristics of the combustion chamber* [II-3]; therefore, the acoustic signal is the result of the particular flame-enclosure combination and may not be an intrinsic characteristic of the flame. This is relevant for flame monitoring applications, as the acoustic signature of a burner may change when it is installed in different combustion chambers.
When the pressure signal exceeds a defined threshold, a safety procedure may be started to bring the system to stable operation (e.g., by increasing equivalence ratio).
A robust control procedure was demonstrated in commercial gas turbines in [III-38] based on the permanent monitoring of dynamic pressures during modifications of operating conditions to minimize NOx emissions. Even though the control actions favouring pollutant reduction may have a deleterious effect on flame stability, this strategy allowed achieving the minimum NOx levels compatible with a safe operation. A similar idea, although at laboratory scale, was evaluated in ([III-39],[III-40]), where burner settings were automatically modified in searches for optimal operation. The setpoint issued by a NOx-minimization algorithm was altered when the standard deviation of pressure exceeded a defined threshold.

III.2.1.2 Flame Spectroscopy and Chemiluminescence Measurements

Several phenomena make flames to spontaneously emit electromagnetic radiation [III-41]:

- Solid bodies (e.g., soot, ash or char particles) produce the so-called black-body spectrum, which is continuous and exhibits a peak at wavelengths decreasing with the temperature.
- Gas molecules at high temperatures display rotation-emission bands. Radiation due to H_2O and CO_2 accounts for most of the radiative heat transfer in particle-free flames.
- Some chemical reactions generate excited species, a part of which reach their equilibrium ground state through the *emission of light* (*chemiluminescence*).

The spectral range varies for the different effects. Chemiluminescence occurs in the UV and VIS ranges whereas, at typical flame temperatures, thermal radiation by solid bodies and gases is found in VIS-IR and IR, respectively. By amount of energy emitted, black-body radiation is the main effect (in particle-laden flows) and chemiluminescence the weakest. Therefore, the visible colour of a flame is dominated by the emission of particles (if present), and due to chemiluminescence in particle-free flames.

The naturally occurring flame chemiluminescence has proven extremely useful in characterizing unstable combustion. *Chemiluminescence* is the *radiative emission from electronically excited species formed by chemical reactions*. The intensity of the chemiluminescence emission is directly related to the concentration of the electronically excited species, which is determined by the competition between the chemical reactions that produce the excited species and collisional quenching reactions. The intensity of the chemiluminescence emission from lean premixed hydrocarbon flames has been shown to be an indicator of the rate of heat release; hence this technique has been widely used for measuring both local and overall rates of heat release in lean premixed combustors under both stable and unstable operating conditions. The strongest chemiluminescence emission from lean hydrocarbon flames comes from CH*, OH*, or CO_2* radicals (the asterisk indicates an excited species), whereas in rich hydrocarbon flames strong chemiluminescence emission also comes from C_2* ([II-42], [III-42])

The chemiluminescence emission from **CH*** (**387 nm**; **431.5 nm**) and **OH*** (**282.9 nm**; **307-309 nm**) occur at distinctly different and relatively narrow-wavelength intervals, whereas the **CO_2*** chemiluminescence lies over a broad-wavelength interval (continuous spectrum **350-600 nm**, in particular it has a peak around **450 nm**). The measured CO_2* chemiluminescence signal strength can be significantly increased over that of OH* and CH* chemiluminescence by using a very broad filter, for example $\Delta\lambda$=100-200 nm. The chemiluminescence emission from **C_2*** radicals have a peak around **515 nm**.

Measurements of the chemiluminescence emission from lean premixed flames have been used in numerous studies to indicate the location of the *reaction zone* and to infer *local* and *overall heat-release rates* ([II-143], [III-43], [III-44], [III-45], [III-46]).

Intensities of chemiluminescence from OH* and CH* and background intensity from CO_2* are good indicators of *heat release rate*, whereas that from C_2* is not ([II-143], [III-47]).

Nori and Seitzman ([III-48], [III-49]) note, however, that due to the influence of equivalence ratio and pressure on OH^* and CH^* emission, their associated signals may not be fully reliable as heat release markers. Numerical results of Najm et al. [II-43] suggest that chemiluminescence due to OH^*, C_2^* and CH^* may fail as local markers of heat release in high curvature regions of flames; other studies, however, point out to the need for additional work and experimental evidences in

order to verify that conclusion [II-143]. Fahrat at al. [III-50] also suggest that OH^* and CH^* may not be reliable indicators of unsteady heat release at some locations in a flame disturbed by standing waves (namely, in rarefaction zones). For the case of internal combustion engines, Kim et al. [III-51] found a good correlation between chemiluminescence in the range 350–390 nm and heat release rate in cool flames.
All chemiluminescence contributions (OH^*, CH^*, C_2^* and CO_2^* continuum) increase with ***equivalence ratio*** in lean flames ([II-46], [II-48], [II-143], [III-36], [III-52]): OH^* and CH^* intensities normalised with fuel mass flow rate have been reported to vary with $\mathbf{\Phi}^{5.23}$ [II-46] and $\mathbf{\Phi}^{2.72}$ [II-48], respectively.
Some authors suggest that a 'universal' relationship might exist between selected *chemiluminescence ratios* (e.g. OH^*/CH^*) and Φ. The analysis of the published results reveals, however, different qualitative and quantitative patterns and more research would be needed to establish a sufficiently general law. A part of the differences might be explained by the particular method applied in the various studies ([III-36], [III-49]).
The on-line detection of equivalence ratio opens interesting possibilities to develop operating-point control schemes able to regulate and maintain flame stoichiometry at the desired setpoint. This has been demonstrated in [III-53], where a calibrated optical sensor guided the closed-loop controller. This work reports a notably good performance of the control system, which was able to respond in a few seconds to changes in f setpoint and to maintain the burner within a narrow band about the desired state.
Pressure also has a strong influence on the shape of the emission spectra. The effect of pressure on absolute intensities due to OH^* and CH^* per unit of fuel mass flow rate has been quantified by Higgins et al. as $\boldsymbol{p}^{-0.86}$ [II-46] and $\boldsymbol{p}^{-0.22}$ [II-48], respectively.
Chemiluminescence sensing requires collecting light at specific wavelength bands. The most common option are single detectors (*photomultipliers* or, less commonly, *photodiodes*) fitted with *bandpass filters* at selected central wavelengths and with bandwidths usually of the order of a few nm. Arrangements with several sensors enable the simultaneous detection of different light bands from the same region of the flame. Spectrometers or monochromators can also be applied to analyze the full emission spectrum or to select any particular wavelength for subsequent processing ([II-143], [III-48], [III-49], [III-53], [III-54], [III-55], [III-56]).
Such sensors are independent of mode shape, but may be susceptible to changes in flame location as the stability of the system changes. They also require *optical access* to the system; although *optical fibres* provide a means of achieving this, they have a limited field of view and tend to give noisy light-intensity readings. Examples of chemiluminescence used as a sensor signal range from the earliest experimental demonstration of active control on a *Rijke tube* to much larger-scale demonstrations.

A) Laser Absorption Spectroscopy (TDLAS)

Interesting developments in sensing include the use of *diode lasers* ([III-57]; ***Tunable Diode Laser Absorption Spectroscopy***, **TDLAS**), which are based on *line-of-sight absorption spectroscopy*.
Absorption spectroscopy is based on the Lambert–Beer law as follows:

$$\left(\frac{I}{I_0}\right)_\nu = \exp\left(-\kappa(\nu)L\right)$$

where I_0 is the intensity of incident radiation, I is the intensity of transmitted radiation, $\kappa(\nu)$ is absorption coefficient, L is the length of homogeneous absorbing media in which laser passes and $\kappa(\nu)L$ is defined as *absorbance*.

Tunable semiconductor diode lasers emit light and fast semiconductor detectors monitor the incident and transmitted intensities. They have recently been used to sense *temperature* in combustion control experiments, and are presently being extended to directly measure *fuel concentrations*. A detailed review of the state of the art in sensors is included in Docquier & Candel [III-58].

Absorption spectroscopy is a well-known technique for the measurement of gas composition, based on the attenuation of a light beam across a gas sample at specific wavelengths, which are characteristic of the different chemical species (absorption spectrum). Extractive sampling has several limitations such as slow time response as well as practical problems associated with the use of probes (condensation, corrosion, pluggage), which make the continuous, real-time measurement in harsh combustion ambient very difficult.

Laser spectroscopy TDLAS can be adapted for the measurement of species concentration, *temperature*, *velocity* and *pressure* [III-36]. Typical species that can be measured by using TDLAS are oxygen, carbon monoxide, water vapour, selected hydrocarbons species.

Temperature measurements can be obtained by probing two different transition lines and calculating the ratio of the integrated absorbance of each transition. TDLAS can be also adapted to extract a flow velocity from a Doppler shift applied to a laser beam and pressure measurements from the collision broadening of the line shape.

An important advantage of TDLAS with respect to conventional gas and temperature sensors (e.g., extractive sampling or thermocouples) is its much faster response, with temporal resolutions ranging from a few Hz to several kHz. Therefore, diode-laser based sensors are suitable for the study of flame dynamics and combustion instabilities or unsteady pulsed combustors as well as for the development of fast-response controllers (the performance of a laboratory combustor was optimized within 100 ms in [III-59]).

The most obvious consideration is that the chemiluminescence-emission measurement is a *line-of-sight measurement*, that is, one measures the total emission integrated along the line of sight. This effect can be significantly reduced by using an optical arrangement with a very short depth of field; however, this reduction is at the expense of significantly reduced signal strength. The major limitation of this technique is the fact that it is a line-of-sight measurement, that is, the measured attenuation is the result of the integrated absorption over the entire beam path and, therefore, is a *measure of the average flowfield properties along the beam path*.

B) Flame imaging

Visualization methods have been historically an invaluable diagnostic tool in fluid mechanics and combustion, since information on the spatial distribution of the relevant variables (even just as qualitative patterns) can be most helpful to describe, or even understand, important features of a flow or a flame. A wide range of laser-based imaging techniques are nowadays available for combustion research (see, for example, [III-60], [III-61], [III-62]]).

Chemiluminescence emission can be recordered by using an ***Intensified Charge-Coupled Device* (ICCD) camera** to obtain an image of the flame structure during unstable combustion that represents the spatial distribution of the flame's heat release.
It is obvious that chemiluminescence-emission measurement can be used to monitor fluctuations in the flame's overall heat release and fluctuations in the flame's structure during unstable combustion. Simultaneous measurements of overall heat-release and pressure fluctuations provide information related to the overall system gain and damping, according *Rayleigh criterion*.
In the current state-of-art, the recording of radiation naturally emitted by the flame appears to be the most feasible method; in particular, it avoids the need for seeding or external illumination (e.g., LIF) and is amenable to low-cost, rugged CCD cameras. The use of vision-based methods for the monitoring of practical flames has been explored in a number of works, whose results confirm its suitability for industrial applications.
The hardware needed to record self-illuminated flame images includes, basically, CCD cameras and frame-grabbers. If narrowband radiation has to be recorded, bandpass filters must be installed and, due to the dramatic drop in the intensity of the optical signal, intensified CCD sensors may be required. Most of the difficulties with the hardware are associated with installation in the combustion chamber and protection of instruments from high temperatures and fouling. The image must be collected through the chamber wall, which usually is relatively thick and hot. The usual solution consists of inserting through a wall opening fibre optics or endoscopes, protected with cooling jackets and air purges ([III-36], [III-63]).

III.2.1.3 Acoustical-optical technique in high-pressure case

At *high-pressure* the correct measurement of the flame chemiluminescence is more challenging than at *atmospheric conditions*. This is due to constrains regarding optical access to the flame, an *overlapping of the wavelengths bands of flame luminescence and the combustor walls' heat radiation*, and the generally lower probability of the formation of the chemical species associated to the flame chemiluminescence under high pressures. Therefore, the error of the acoustical-optical technique is expected to be larger than under atmospheric conditions.
Although the technology for sensing combustion instabilities may be fairly mature (e.g., *high-response pressure transducers* or *optical chemiluminescence measurements*), the implementation of these sensors in a control system can be critical to the system's performance.
Sensors must be placed at the proper locations relative to the acoustic mode shape to properly identify phase information and to maximize the signal-to-noise ratio. Filtering, signal processing and averaging may also be necessary, depending on the nature of the sensed signal.

III.2.2 Controller

A *controller* (or *control algorithm*) is the relationship between the measured signal by sensors and the signal used to drive the actuator.
To achieve closed-loop suppression of the combustion instability, a controller must sense the combustion pressure oscillations and actuate the fuel at a frequency and phase that interferes with

the instability. In addition, to avoid damage to the combustor, it is desirable that the controller be able to *isolate and mitigate the instability while it is still small*, that is still on the same order as the combustor noise.
A full review about active control algorithms is possible to find in [I-32].
In industrial applications, a self-adapting control strategy and/or control parameter compensation depending on operating points are indispensable. Thus, in the past, a great variety of control strategies such as model-based controllers, self-adapting controllers based on LMS (Least-Mean-Square Algorithm) algorithms or self-tuning controllers were researched [III-64].
The aim is to design the controller such that the unsteady heat release and acoustic waves interact differently, leading to decaying, rather than growing, oscillations.
The controller must be based on system measurements, although the consequences of instability may be so severe that obtaining these is not straightforward in certain operating regimes.
In order to see the source of instability, ***pseudo-Rayleigh index*** (**PRI**) could be calculated, assuming that chemiluminescence intensity is proportional to heat-release rate of the flame:

$$\boxed{R_I = \frac{1}{\tau}\int_{\tau} p_1(t)\, I_1(t,x,y)\, dt} \qquad \text{(III-1)}$$

where τ denotes the time period in one cycle.

III.2.3 Actuators

The first actuators applied to combustion control were *loudspeakers* ([III-17], [III-22], [III-65]). Although these have a good high-frequency response, they are not sufficiently robust for use in industrial systems and their power requirements become prohibitive at larger scales.
In most systems, the fuel flow rate has been controlled via some sort of *fast-response valve*. This valve must be fast enough to modulate fuel flow a the required frequency and, potentially, over a range of frequencies. This bandwidth requirement will set specifications for the valve's bandwidth and natural frequency bandwidth.
An efficient means of actuation exploits the chemical energy released in combustion by modulating the fuel supply. For ideal actuation, a *fuel valve* should have a linear response (to allow linear control theory to be used), large bandwidth, sufficiently large control authority to affect the limit cycle oscillation, a small amplitude response that does not exhibit hysteresis, a fast response time, and good robustness and durability.
Obtaining a satisfactory fuel valve is one of the main challenges facing reliable implementation of feedback control on practical combustion systems.
Techniques using modulation of some sort of fuel flow as an actuation technique have used existing fuel-system components or have added secondary fuel injectors. Three critical factors are limiting the control of lean, premixed combustor design:

1. The obvious actuation technology barrier is represented by the *ability to modulate large fuel flows at the high frequencies* at which combustion instabilities occur (normally hundreds of Hertz in gas turbine).

2. A second, less obvious barrier that relates to actuation, is the physics of the actuation process. For an actuator to be effective, it must have *the ability to interfere with the coupling process* between the acoustic pressure field and the combustion heat-release rate. An actuator that modulates fuel flow may not have significant authority (effectiveness) if the fuel is not injected in a manner that allows it to interfere with the coupling process.
3. Another consideration that affects the authority of actuation systems is the *time delay* between the actuator moves and when the effect of that actuation is observed at the flame front.

III.2.4 Advantages of active control

Compared with passive measures, AIC systems have many advantages:

a) While the damping effect of passive measures frequently remains restricted to narrow frequency or operating ranges of the combustion system concerned, the AIC is distinguished by its *high degree of flexibility and its wide range of operation.*
b) For damping low-frequency oscillations numerous passive measures such as *Helmholtz resonators* or *sound absorbers* require a great deal of space and thus cause much unwanted design complications, while the AIC system needs *little space* and can be installed in a comparatively simple manner.
c) Another AIC advantage is that – thanks to its degree of development reached by now – it takes significantly *less time to install* and requires fewer tests. Accordingly, novel combustion systems can be commissioned faster and take less time to market. By comparison, developing suitable passive measures is still mostly a trial-and-error process and takes much experimenting, that means time and money.
d) It is possible with an activated AIC to operate the gas turbine at *lower levels of pilot gas mass flows* than without the system, and the pilot flames are very important for influencing NO_x emissions of gas turbines.
e) Engines equipped with AIC are generally protected against the sudden development of combustion instabilities caused by *changes in environmental conditions* such as ambient temperature or fuel composition.

Persistent problems of combustion instabilities have motivated serious interest in possible application of feedback control to combustion systems. The idea is quite simple; successful practical implementation is another matter and truly successful implementations remain to be found.

Feedback controls nowadays play a large part in changing the performance there have been considerable advances in the performance of gas turbines, notably emissions and fuel consumption, for which feedback control has been a crucial matter.

References

[III-1] Steele R.C., Cowell L.H., Cannon S.M., Smith C.E., "Passive control of combustion instability in lean premixed combustors", Journal of Engineering for Gas Turbines and Power, Vol. 122, Issue 3, pp. 412-419, 2000.

[III-2] Lovett J.A., Uznanski K.T., "Prediction of Combustion Dynamics in a staged premixed combustor", American Society of Mechanical Engineers, paper GT-2002-30646, 2002

[III-3] Berenbrink P. and Hoffmann S., "Suppression of dynamics combustion instabilities by passive and active means", American Society of Mechanical Engineers (ASME), Paper 2000-GT-0079, May 8-11, 2000.

[III-4] Scarinci T., Halpin J.L., "Passive control of combustion instability in a low emissions aero-derivative gas turbine", ASME Paper 2004-GT-53767, 2004.

[III-5] Kendrick D.W., Anderson T.J., Sowa W.A., Snyder T.S., "Acoustic sensitivities of leam-premixed fuel injectors in a single nozzle rig", Journal of Engineering for Gas Turbines and Power, Vol. 121, Isuue 3, pp.429-436, 1999.

[III-6] Pascheriet C.O., Flohr P., Knopfel H., Geng W., Steinbach C., Stuber P., Bengtsson K., Gutmark E., "Combustion control by extended EV burner fuel lance", American Society of Mechanical Engineers, ASME Paper GT-2002-30462, 2002.

[III-7] Barbosa S., Garcia M.L.C., Ducruix S., Labegorre B., Lacas F., "Control of combustion instabilities by local injection of hydrogen", Proceedings of the Combustion Institute, Vol. 31, pp. 3207–3214, 2007.

[III-8] Schlein B.C., Anderson D.A., Beukenberg M.M.K.D., Leiner H.L., Traptau W., "Development history and field experiences of the First F T8 Gas Turbine with Dry Low NOx Combustion System", American Society of Mechanical Engineers, ASME Paper 99-GT-241, 1999.

[III-9] Bellucci V., Rohr P., Paschereit C.O., Magni F., "On the use of Helmholtz resonators for damping acoustic pulsations in industrial gas turbines", American Society of Mechanical Engineers, ASME, Journal of Engineering for Gas Turbines and Power, Vol. 126, Issue 2, pp.271–75, 2004.

[III-10] Gysling D.L., Copeland G.S., McCormick D.C., Proscia W.M., "Combustion system damping augmentation with Helmholtz resonators", American Society of Mechanical Engineers, ASME, Journal of Engineering for Gas Turbines and Power, Vol. 122, Issue 2, pp.269–74, April 2000.

[III-11] Zhaoa D., Morgans A.S., "Tuned passive control of combustion instabilities using multiple Helmholtz resonators", Journal of Sound and Vibration, Vol.320, pp.744–757, 2009.

[III-12] Joshi N., Epstein M., Durlak S., Marakovits S., Sabla P., "Development of a fuel air premixer for aero-derivative dry low emissions combustors", American Society of Mechanical Engineers, ASME Paper 94-GT-253, The Hague, New York, 1994.

[III-13] Sohn C.H., Park I.-S., Kim S.-K., Kim H.J., "Acoustic tuning of gas–liquid scheme injectors for acoustic damping in a combustion chamber of a liquid rocket engine", Journal of Sound and Vibration, Vol.304, pp.793–810, 2007.

[III-14] Sohn C.H., Park I.-S., "Effects of inlet blockage of gas–liquid scheme injector on acoustic tuning for acoustic damping in a combustion chamber", Journal of Mechanical Science and Technology, Vol.22, pp. 330–337, 2008.

[III-15] Park I.-S., Sohn C.H., "Nonlinear acoustic damping induced by a half-wave resonator in an acoustic chamber", Aerospace Science and Technology, Vol.14, pp.442–450, 2010.

[III-16] Tsien H.S., "Servo-stabilisation of combustion in rocket motors", Am. Rocket Soc. J., Vol. 22, pp.256-263, 1952.

[III-17] Lang W., Poinsot T., Candel S., "Active Control of Combustion Instability", Combustion and Flame, Vol. 70, Issue 3, pp. 281-289, 1987.

[III-18] Gulati, A., Mani, R., "Active Control of Unsteady Combustion-Induced Oscillations", Journal of Propulsion and Power, Vol. 8, No. 5, pp. 1109-1115, 1992.

[III-19] Poinsot T., Veynante D., Bourienne F., Candel S., Esposito E., "Initiation and Suppression of Combustion Instabilities by Active Control", 22nd Symposium (International) on Combustion, Seattle, pp. 1363-1370, 1988.

[III-20] Bloxsidge G., Dowling A., Hooper N., Langhorne P.J., "Active control of reheat buzz", AIAA Journal, Vol. 26 , Issue 7, pp. 783-790, 1988.

[III-21] Langhorne P.J., "Reheat Buzz an acoustically coupled combustion instability", Journal of Fluid Mechanics, vol.193, pp. 417-443, 1988.

[III-22] Poinsot T., Candel S., Esposito E., Lang W., Bourienne F., "Suppression of combustion instabilities by active control," Journal of Propulsion and Power, Vol. 5, pp. 14-20, 1989.

[III-23] Wilson K.J.; Gutmark E.; Schadwo K.C., "Flame-Kernel Pulse Actuator for Active Combustion Control", ASME 1992, Active Control of Noise and Vibration, DSC-Vol. 38, pp. 75-81, 1992.

[III-24] Yu K.H., Parr T.P., Wilson K.J. Schadow K.C., Gutmark E.J., "Active Control of Liquid-Fueled Combustion Using Periodic Vortex-Droplet Interaction", Twenty-sixth Symposium (International) on Combustion, Vol. 2, pp. 2843-2850, 1996.

[III-25] Yu K., Wilson K.J., Schadow K.C., "Scale-Up Experiments on Liquid-Fueled Active Combustion Control", AIAA 98-3211, 1998.

[III-26] Dowling A.P. and Morgans A.S., "Feedback control of combustion", Annual Review of Fluid Mechanics, Vol.37, pp.151–82, 2005.

[III-27] Hermann J., Gleis S., Vortmeyer D., "Active Instability Control (AIC) of Spray Combustors by Modulation of the Liquid Fuel Flow Rate", Combustion Science and Technology, Vol. 118, pp.1-25, 1996.

[III-28] Hantschk C., Hermann J., Vortmeyer D., "Active Instability Control with Direct Drive Servo Valves in Liquid-Fuelled Combustion Systems", 26 Int. Symposium on Combustion, Naples, 1996.

[III-29] Seume J. R., Vortmeyer N., Krause W., Hermann J., Hantschk C.-C., Zangl P., Gleis S., Vortmeyer D., Orthmann A., "Application of active combustion instability control to a heavy duty gas turbine", Journal of Engineering for Gas Turbines and Power, ASME paper No. 97-AA-119, 1997.

[III-30] Hoffman S., Weber G., Judith H., Herrmann J., Orthmann A., "Application of Active Combustion Instability Control to Siemens Heavy Duty Gas Turbine", Symposium of the AVT Panel on Gas Turbine Engine Combustion, Emissions and Alternative Fuels, RTO-Meeting Proceedings 14, AGARD, NATO Research & Technology Organization, pp. 40-1 – 40-13, Lisbon 12-16 October 1998.

[III-31] Hermann J., Orthmann A., Hoffmann S., "Application of Active instability control to a heavy duty gas turbine", 14th International Symposium on Air Breathing Engines (ISABE), paper 99-7185, Florence, Italy, 5-10 September, 1999.

[III-32] Hermann J., Orthmann A., "Combustion Dynamics: Application of Active Instability Control to Heavy Duty Gas Turbines", RTO AVT Course on "Active Control of Engine Dynamics", RTO-EN-020, Brussels, Belgium, 14-18 May 2001.

[III-33] Johnson C.E., Neumeier Y., Lubarsky E., Lee J.Y., Neumaier M., Zinn B.T., "Suppression of combustion instabilities using a fast adaptive control algorithm", AIAA Paper 2000-16365, 2000.

[III-34] Paschereit C.O. Gutmark E., Weisenstein W., "Structure and control of thermoacoustic instabilities in a Gas-Turbine Combustor", Combustion Science and Technology, Vol. 138, pp. 213-232, 1998.

[III-35] Magill J., Bachmann M., McManus K., "Combustion dynamics and control in Liquid-Fuelled Direct Injection Systems", AIAA paper 2000-1022, 2000.

[III-36] Ballester J., Garcìa-Armingol T., "Diagnostic techniques for the monitoring and control of practical flames", Progress in Energy and Combustion Science, Vol.36, pp. 375–411, 2010.

[III-37] Moran A.J., Steele D., Dowling A.P., "Active control and its applications", presented at "Proceeding RTO AVT Symposium, Active Control Tech., Enhanced Performance Operational Capabilities Military Aircraft, Land Vehicles Sea Vehicles", Braunschweig, Germany. Neuilly-Sur-Seine, France: RTO, NATO, 2000.

[III-38] Kokanovic S., Guidati G., Torchalla S., Schuermans B., "Active control system for reduction of NOx and pulsation levels in gas turbines", Proceedings of GT2006-ASME Turbo Expo 2006: Power for Land, Sea and Air, GT2006-90895, Barcelona, 2006.

[III-39] Sanz A., Ballester J., Hernandez R., "Advanced monitoring and control of burners using flame sensors", 7th European Conference on Industrial Furnaces and Boilers, Porto, 2006.

[III-40] Ballester J., Sanz A., Hernandez R, Smolarz A., "Diagnostic and control of lean premixed combustion with alternative fuels", 13th International Congress on Sound and Vibration, Vienna, Austria, 2006.

[III-41] Gaydon A.G., "The Spectroscopy of Flames", Wiley, New York, 1957; London: Chapman and Hall, 2nd edition 1974.

[III-42] Clark T., "Studies of OH, CO, CH and C2 radiation from laminar and turbulent propane-air and ethylene-air flames", Technical report, NACA Technical Note 4266, 1958.

[III-43] Ikeda Y., Kojima J., Nakajima T., Akamatsu F., Katsuki M., "Measurement of the local flame front structure of turbulent premixed flames by chemiluminescence", Proceeding of the Combustion Institute, Pittsburg, PA, Vol. 28, Issue 1, pp.343–350, 2000.

[III-44] Kojima J., Ikeda Y., Nakajima T., "Spatially resolved measurement of OH*, CH*, and C2* chemiluminescence in the reaction zone of laminar methane/gase premixed flames", Proceeding of the Combustion Institute, Pittsburg, PA, Vol. 28, pp.1757–1769.

[III-45] Kojima J., Ikeda Y., Nakajima T. "Measurement of the local flame front structure of turbulent premixed flames by local chemiluminescence", Proceedings of the AIAA/ASME/SAE/ASEE, JPCE Conference, Reston, VA, Vol.36: pp. 3394–3405, 2000.

[III-46] Beduneau J.-L., Ikeda Y., "Application of laser ignition on laminar flame front investigation", Experiments in Fluids, Vol. 36, pp. 108–113, 2004.

[III-47] Gillet B., Hardalupas Y., Kavounides C., Taylor AMKP, "Infrared absorption for measurement of hydrocarbon concentration in fuel/air mixtures (MAST-BLIQUID)", Applied Thermal Engineering, Vol.24, Issue 11–12, pp.1633–53, 2004.

[III-48] Nori V.N., Seitzman J.M., "Chemiluminescence measurements and modeling in Syngas, methane and Jet-A fueled combustors", 45th AIAA Aerospace Sciences Meeting and Exhibit, Paper No. AIAA 2007-0466, 2007.

[III-49] Nori V.N., Seitzman J.M.. "CH* chemiluminescence modeling for combustion diagnostics", Proceedings of the Combustion Institute, Vol.32, Issue 1, pp.895–903, 2009.

[III-50] Fahrat S.A., Ng W.B., Zhang Y., "Chemiluminescent emission measurement of a diffusion flame jet in a loudspeaker induced standing wave", Fuel, Vol.84, pp.1760–1767, 2005.

[III-51] Kim B., Kaneko M., Ikeda Y., Nakajima T., "Detailed spectral analysis of the process of HCCI combustion" Proceedings of the Combustion Institute, Vol.29, Issue 1, pp.671–677, 2002.

[III-52] Docquier N., Belhalfaoui S., Lacas F., Darabiha N., Rolon C., "Experimental and numerical study of chemiluminescence in methane/air high pressure flames for active control applications", Proceedings of the Combustion Institute, Vol. 28, pp.1765–1774, 2000.

[III-53] Docquier N., Lacas F., Candel S., "Closed-loop equivalence ratio control of premixed combustors using spectrally resolved chemiluminescence measurements", Proceedings of the Combustion Institute, Vol.29, Issue 1, pp.139–45, 2002.

[III-54] Cheng T.S., Wu C.Y., Li Y.H., Chao Y.C., "Chemiluminescence measurements of local equivalence ratio in a partially premixed flame", Combustion Science and Technology, Vol.178, pp.1821–41, 2006.

[III-55] Muruganandam T.M., Kim B.H., Olsen R., Patel M., Roming B., Seitzman J.M., "Chemiluminescence based sensors for turbine engines", 39th AIIA/ASME/SAE/ASEE Joint Propulsion Conference and Exhibit, Paper No. AIAA-2003-4490, 2003.

[III-56] Muruganandam T.M., Kim B.H., Morrell M.R., Nori V.N., Patel M., Roming B.W., et al., "Optical equivalence ratio sensors for gas turbine combustors", Proceedings of the Combustion Institute, Vol.30, Issue 1, pp.1601–9, 2005.

[III-57] Zhou X., Liu X., Jeffries J.B. and Hanson R.K., "Diode Laser Sensors for Combustion Control," paper AIAA 2003-1010 at 41st Aerospace Sciences Meeting, Reno, NV, Jan. 2003.

[III-58] Docquier N, Candel S., "Combustion control and sensors: a review", Progress in Energy and Combustion Science, Vol.28, Issue 2, pp.107–50, 2002.

[III-59] Furlong E.R., Baer D.S., Hanson R.K., "Real-time adaptive combustion control using diode-laser absorption sensors", Proceedings of the Combustion Institute, Vol.27, pp.103–11, 1998.

[III-60] Eckbreth A.C., "Laser Diagnostics for Combustion Temperature and Species", 2nd edition Combustion Science and Technology Book Series, Gordon and Breach Publishers, 1996.

[III-61] Kohse-Hoinghaus K., Jeffries J.B., "Applied combustion diagnostics", New York: Taylor & Francis, 2002.

[III-62] Kohse-Hoinghaus K., Barlow R.S., Alden M., Wolfrum J., "Combustion at the focus: laser diagnostics and control", Proceedings of the Combustion Institute, Vol.30, pp.89–123, 2005.

[III-63] Huang Y., Yan Y., Riley G., "Vision-based measurement of temperature distribution in a 500 kW model furnace using the two-colour method. Measurement", Vol.28, pp.175–83, 2000.

[III-64] Dowling P. A., "Active Control of Instabilities in Gas Turbines", NATO/RTO Active Control Symposium, Braunschweig, Germany, May 8-12, 2000.

[III-65] Dines P.J., "Active control of flame noise", PhD thesis, Univ. Cambridge, 1983.

IV. Thermo-acoustic instabilities: analytical and numerical models

IV.1 Introduction

There are three main strategies to simulate turbulent reacting flows in general: the *Reynolds-averaged Navier-Stokes* formulation (RANS), where all turbulent scales are modelled; *Large Eddy Simulations* (LES), in which small scales are modelled while large scales are solved exactly; and as a last alternative, *Direct Numerical Simulations* (DNS), where all physical scales are resolved on the grid.
Despite the fact that progress in computer technology now sometimes allow Direct Simulations (DNS) of turbulent flames relying on complete reaction schemes and realistic, multicomponent transport models, the associated computational cost in terms of computing time and required memory remain tremendous. Though limited to some simple configurations, corresponding single processor computing times are expressed at best in months, usually in years. For more realistic configurations (complex three-dimensional geometry), or when systematic studies are required (long physical times, several simulations), such computations remain completely impossible at present.
RANS require simplified turbulent combustion models and thus cannot be used for an a priori analysis of the coupling process (e.g. flame/acoustics or turbulence/chemistry interactions). LES need a subgrid model to describe all physical processes taking place below grid resolution. Both, though highly interesting in particular for solving large scale problems with a complex geometry, are thus associated with many unsolved issues and challenges.
Although analytical techniques have improved markedly during the past few years, the difficulty in representing the combustion-pressure wave interaction will likely remain a barrier to full predictive capability. Thus, it is likely that a combined approach, including both experimental and high-fidelity unsteady CFD modelling, will be required to develop models of the full annular combustor response that will have utility in defining design direction.
Much of the current effort in the field of combustion noise focuses on *numerical* estimation techniques using modern computational tools. The approaches of the *computational combustion acoustics* (CCA) are very similar to those of the *computational aeroacoustics* (CAA) ([II-112], [IV-1]). However, the numerical simulation of combustion noise is more complex since turbulence, acoustics and chemical reaction coincide. The state of the art of *computational combustion acoustics* (CCA) is less advanced than in *computational aeroacoustics* (CAA) but it is possible to foresee that computational combustion acoustics will progressively evolve into a well established scientific field.
Like in CAA *direct computational methods* (DCM) are considered as the more accurate technique for CCA. DCM solve the complete, fully coupled compressible Navier-Stokes equations and resolve the unsteady reactive flow and the acoustic field at the same time. However, due to the application of Direct Numerical Simulations (DNS) or Large Eddy Simulations (LES) the prediction of combustion noise is expensive. Thus, DNS/LES methods especially for industrial users are very costly. However, the strongly varying length- and time scales of turbulence, acoustics and chemistry as well as the need of high order discretization schemes to avoid dissipation and dispersion of acoustic waves initiated the development of

hybrid CFD/CAA-approaches, which split the combustion noise simulation into a simulation of the turbulent reactive flow and a subsequent simulation of the acoustic processes in the time domain.
Combining LES (including chemical reactions) with CAA methods for propagating sound into the far field is a promising technique for the investigations of combustion noise for small Mach numbers, but the influence of the acoustics on the reacting flow is not considered because sometimes the CAA techniques are used as a post-processing method for the LES results.
As already explained, the understanding of turbulent combustion relies on many, strongly coupled and highly complex physical phenomena. Some of the major challenges are:

- *Numerical complexity*: the spatial and temporal dynamics are inherently coupled, with a wide range of relevant scales for the turbulence and chemical reactions, which must be adequately resolved or modelled.
- *Chemical complexity*: complete chemical schemes often involve a large number of species and elementary reactions (for instance hundreds of species and thousands of reactions).
- *Transport complexity*: differential diffusion at molecular scale as well as turbulent transport of heat and species control mixing and heat transfer.
- *Multi-physics complexity*: practical flow configurations often involve multiphase flows (such as in spray combustion, for soot emission, ...), thermal radiation, complex thermodynamics, acoustics, turbulence/chemistry interactions.
- *Post-processing complexity*: numerical simulations lead nowadays to huge quantities of raw data, from which useful information must be extracted and analyzed as efficiently as possible.

It is apparent that only a transient CFD approach is potentially able to take into account all the chemical and physical aspects involved in the coupling between flame heat release and acoustic modes. However, this approach can be extremely expensive in terms of computational effort when:

- grids are made of a high number of cells (up to millions of cells);
- computational demanding physical models are used;
- very small time steps are required to capture the propagation of pressure waves or the oscillations of high frequency acoustic modes;
- a large number of time steps is required to observe the onset of self-sustained unstable oscillations.

IV.2 Hybrid approaches for the investigation of combustion noise

Hybrid approaches for the investigation of combustion noise, in which the turbulent reactive flow in the source region and the acoustic far field are computed separately, are widely used and well accepted in aero-acoustics. Especially at low Mach number flows, the fluid dynamic and acoustic length scales are separated by more than an order of magnitude. Generally, hybrid aeroacoustic methods are based on the scale separation. Due to the large difference in hydrodynamic and acoustic length scales, the problem of interest, e.g., jet noise predictions, is divided into two sub-problems in non-reacting flows. Turbulent reacting flows, however, possess an additional range of scales, i.e., the chemical time and length scales. Therefore, a hybrid aeroacoustic approach in

terms of combustion noise is to be divided into three sub-levels, namely the chemical, hydrodynamic, and the acoustic range of length and time scales. This allows the application of specialized techniques for each domain, namely the source region using computational fluid dynamics (CFD) and the acoustic propagation region all the way into the far field using computational aero-acoustics (CAA). Especially for turbulent combustion systems with moderate velocities the low Mach number approximation is applicable and yields satisfying results.
Using LES, one can extract acoustic sources from the instationary flow field and investigate the propagation of sound through the flame, in terms of the temporarily and strongly changing fluid properties inside a turbulent flame. The combustion noise could investigated using an LES/CAA hybrid approach, combining the reactive LES with a wave propagation method.
The LES/CAA hybrid approach is based on the observation, that for a turbulent flame the global and the local Mach number within the flame are usually very small, i.e. $Ma \leq 0.1 \ll 1$. This is due to two effects. First, the flow speed of the fuel at the nozzle exit is usually rather small, since the flame is supposed to burn stably at the nozzle. Second, the high temperature in the flame region increases the speed of sound by roughly a factor of three. This allows the flow field to be treated independently of the acoustic propagation, as long as there is no feedback of the acoustic to the flame, which is the case for open configurations.
Using a reactive LES with a low Mach number approximation to compute a turbulent flame enables the temporally resolved extraction of all required properties for the propagation of acoustic waves - speed of sound, density, flow velocities and the acoustic sources. Using the classical wave equation in terms of pressure disturbance p, the acoustic field around the flame can be described by an appropriate simulation technique. The evaluation of the components of the *Lighthill tensor* showed that turbulent reacting flows (the source term related to the density) dominate the tensor by approximately two orders of magnitude.
The utilization of CFD such as the LES method is preferable since the turbulent spectrum does not have to be modeled completely. In the stationary RANS approach for the CFD part the turbulent spectrum and therefore the noise producing structures have to be modeled completely, thus limiting the general applicability of the hybrid approach, compared to LES. Finally, a direct approach such as DNS of the flow field is beyond any admissible computational costs for technically relevant systems.
Investigating the potential of *Large Eddy Simulation* for the prediction of different configurations with premixed, partially premixed and non-premixed flames is currently an important aspect in the scientific community ([I-4] § 3, [II-57], [II-77], [II-176], [II-177], [II-178], [IV-2]).

IV.3 Brief critical review of analytical models

IV.3.1 One-dimensional analytical model in industrial gas turbine

Mahan and his students began their study of combustion generated noise in 1977. This work was initially motivated by the problem of fatigue damage to components in large industrial gas turbines due to combustion-driven pressure oscillations. Later, emphasis shifted to reducing the environmental impact of aircraft jet engine combustion noise. Under contract to General Electric, Mahan developed a *one-dimensional analytical model* [IV-3] for combustion noise generation and propagation in long ducted combustion systems typical of those in industrial gas turbines. The model, which is based on the linearized one-dimensional conservation equations for an ideal

gas, include steady flow effects, such as axial gradients in temperature, velocity and pressure, which occur as a result of combustion heat release and heat loss to the walls. The acoustic source activity is modelled as an unsteady heat release term in the linearized energy equation which is assumed proportional to the local steady heat release.
In 1979 Mahan and Kasper [IV-4] report the results of a study, based on this model, of the influence of the steady combustion heat release distribution on the acoustic response of ducted burners. In this study the source field is suppressed and only the influence of flow and the associated axial gradients on the propagation of acoustic waves through the combustor is investigated. It is shown that the dynamic response of the combustor, as characterized by its local driving point impedance, is sensitive to the axial distribution of steady combustion heat release as well as the total burner power.
In a direct application of the *one-dimensional non-homogeneous wave equation* developed earlier by Mahan [IV-3] and modified by Mahan and Kasper [IV-4], Mahan et al. [IV-5] and Mahan and Jones [IV-6] they were able to recover the variation with frequency of the thermo-acoustic efficiency for a ducted turbulent hydrogen-flame burner from the measured farfield sound spectrum. The only assumption required, other than that the wave propagation model used is valid, is that *combustion noise is a direct consequence of unsteady heat release*. The range of thermo-acoustic efficiency obtained, 10^{-4}-10^{-5}, is consistent with values obtained by previous investigators for hydrocarbon fuels if the predicted increase in thermo-acoustic efficiency with reactivity of the hydrogen fuel is taken into account. Also, the thermo-acoustic efficiency is shown to decrease monotonically with frequency between 150 Hz and 1500 Hz. *The thermo-acoustic efficiency decreases with the increasing of frequency* since the wavelength of the acoustic waves in the reaction zone become shorter than the flame length.

IV.3.2 Numerical models of interaction phenomena in combustion noise: amplifiers and resonators

Analytical studies of combustion noise generally focus on situations where the flow dynamics can be considered to be independent of the radiated sound. It is implicitly assumed that *the flow dynamics is decoupled from the induced wave motion* and the sound emission from unstable flames is generally not considered when dealing with combustion noise. It is however not always possible to obtain a complete decoupling between the flow and its acoustic radiation because practical systems are confined and the boundaries reflect sound towards the reactive region.
Currently little is known about the mechanisms by which the flame responds to the acoustic feedback and understanding these mechanisms is an area of active investigation.
The combustion process can be subdivided into subdynamics: acoustics, convective phenomena, molecular transport processes, chemical kinetics, flame kinematics, heat transfer and feedline dynamics of the reactants.
Heat release fluctuations ($\dot{\omega}_T^1$) can be produced by local air-fuel ratio fluctuations (Φ_1). These can in turn be driven by fuel or air line delivery fluctuations, as well as change in atomization and mixing patterns ([II-30], [II-191], [II-149], [IV-7]). Heat release fluctuations can be also made from the effect of large scale vortex shedding affecting flame shape (A_1), mixing and entrainment ([II-30], [IV-8]). These mechanisms are often present simultaneously in practical devices, and the identification of the separate factors is not easily done.

Efforts in understanding these interactions have been made mainly in developing numerical models of the interaction ([II-40] §8.3.7, [II-104], [IV-9]), while experimental investigation appears less developed ([II-37], [II-138]).
Since *the sound field associated with subsonic cold flows represents only a minute fraction of the energy in the flow* (in fact the *thermo-acoustic efficiency* is very low, 10^{-8}-10^{-7} according [II-4], 10^{-6} according [II-61], 10^{-5} according [II-63] or 10^{-5}-10^{-4} according [IV-3]) the accuracy of numerical simulations must be very high to capture the sound production. To understand the various strategies used to study acoustical combustion instabilities with LES numerical models, the difference between amplifiers and resonators must be recalled ([II-37], [II-40], [IV-10]). There are two main paths to use LES to predict unstable combustion in a burner:

- ***Forced response*** (***amplifiers***): if the feedback loop leading to instabilities is inhibited and the flow becomes *stable*. The amplifiers are convectively unstable flow and any perturbation induced locally in the flow at time $t=t_0$ propagates downstream and is eventually washed away at later time.

- ***Self-excited modes*** (***resonators***): if the feedback loop (especially acoustic waves) can not be inhibited and the flow is dominated by its own *instability mode*. The resonators are absolutely unstable and a perturbation at time $t=t_0$ propagates in all directions and is not dissipated.

Combustors submitted to combustion instabilities are obviously *resonators* because of the strong feedback created by acoustic waves and can be studied as such using LES [II-40]. However, in certain cases, resonators may be transformed into *amplifiers* if part of the feedback loop is suppressed.
Successful computations of both *forced modes* [IV-11] and *self-excited modes* ([IV-12], [IV-13]) may be found in the literature indicating that both strategies may be valid.

IV.3.3 Noise prediction method and combustion noise scaling laws

Turbulent premixed combustion processes are inherently unsteady and, thus, a source of acoustic radiation. The objective of this paragraph is to examine the basic scaling of the flame's acoustic emission spectra and establish its dependence upon geometric and flow variables. The flame's acoustic spectrum has a nearly universal shape that can be characterized by four parameters: the *total acoustic power* (OASPL), the *frequency of peak emissions* (f_{peak}), and the *power law scaling of the spectra* in the low ($f<f_{peak}$) and high ($f>f_{peak}$) frequency regime [II-195].

IV.3.3.1 Overall sound pressure level (OASPL)

Strahle [II-67] proposes a version of the *flamelet model* which permits the introduction of two time scales, one due to convection and one due to diffusion. This leads to an expression for the thermo-acoustic efficiency estimate having two adjustable exponents whose values depend on the relative dominance of the two rate processes. Strahle demonstrates that the experimental trends from the literature for open premixed flames can be predicted by this theory if appropriate values of the two adjustable exponents are chosen.
A new version of Strahle's theory [IV-14] predicts that the *sound power radiated* (in watts) from a can-type combustor which is perfectly impedance matched to the surroundings should be given by

$$P_{eq} = a_1 p^{a_2} V_{ref}^{a_3} T_i^{a_4} F^{a_5} N_f^{a_6} A_{exit}^{a_7} \left(\frac{A_{exit}^{1/2}}{l} \right)^{a_8} \qquad \text{(IV-1)}$$

where p is the combustor mean pressure, V_{ref} is the mean flow velocity, T_i is the combustor inlet temperature, F is the fuel-air ratio, N_f is the number of fuel nozzles, A_{exit} is the cross-sectional area at the combustor exit.
In general, *the accuracy of a noise prediction method decreases as it becomes more universal*: while it is relatively easy to develop an accurate noise prediction method for parametric variations within a given engine design, it is significantly more difficult to develop a method of comparable accuracy which is valid for a range of engine designs.
According to the core noise prediction method used at General Electric Co. [IV-15], the *overall sound pressure level* (OASPL) is given by:

$$OASPL = 10\log\left(\frac{\dot{m} c_0^2}{P_{ref}} \right) + 10\log\left[\left(\frac{T_{out} - T_{in}}{T_{in}} \right)^2 \left(\frac{p_{t,in}}{p_0} \right)^2 \left(\frac{\Delta T_{des}}{T_0} \right)^{-4} \right] - 60.5 \qquad \text{(IV-2)}$$

where $\dot{m}$ is the combustor mass flow rate, T_{in} is the combustor inlet temperature, T_{out} is the combustor outlet temperature, ΔT_{des} is the design point temperature drop across the turbine, $p_{t,in}$ is the combustor inlet total pressure and P_{ref} is the reference power (10^{-12} W). The subscript *0* refers to standard sea level conditions.
Because the General Electric prediction method is based entirely on engine data, it necessarily contains several empirical constants. Its main advantage is that it involves relatively few parameters while achieving remarkable universality.
Scaling laws can be derived from basic expressions for the pressure in the farfield in a manner which parallels that used by Lighthill in his classical analysis of jet noise. The *radiated power* is obtained for example by integrating the acoustic intensity over a large sphere. Among the many possibilities explored in the literature are Clavin and Siggia [II-166], Rajaram et al. ([IV-16], [II-195]) and Candel et al. [II-47].

IV.3.3.2 Acoustic power spectral density (PSD)

The power spectral density of radiated sound may be determined by taking the *Fourier transform* of the *correlation function*. It is difficult to give a general expression for this quantity but it is possible to continue the calculation in some special cases. Experiments indicate that *power spectral densities of sound exhibit a range where the spectrum decays according to a power law but the exponent value changes from case to case*.
A typical combustion noise spectrum is shown in Fig. IV-1.

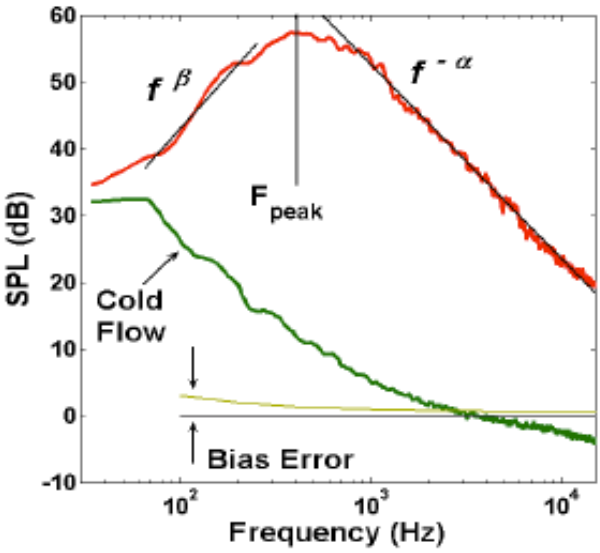

Fig. IV-1: Typical combustion noise spectrum [II-195]: dependence of low frequency decay exponent (β) and dependence of high frequency decay exponent (α) of upstream turbulence.

a) Low Frequency Spectral Characteristics

In the low frequency range one may assume that the power spectral density of the unsteady heat release rate only weakly depends on frequency and the sound spectrum then follows a f^{+2} law (i.e., with β=2 in). This seems to be well confirmed by experiments of Rajaram et al. [II-195].
One can see that the sound power should scale as f^{2}, as long as the flame is acoustically compact and the coherence volume of the heat release fluctuations does not change with frequency. While clearly this caveat could not apply at high frequencies, it seems reasonable at lower ones.

b) High Frequency Spectral Characteristics

By restricting their analysis to premixed turbulent flames in the wrinkled flame regime, Clavin and Siggia [II-166], were able to show that the rate of change of flame surface area

followed a power law with respect to frequency and that **the power spectral density of sound radiated by the flame featured a $f^{-5/2}$ dependence with respect to frequency**.
Abugov and Obrezkov [II-165] found that the spectrum exhibits a power law dependence with an exponent of α = 5/2 over the 2 kHz to 10 kHz frequency range. Power law behaviour with a similar exponent, although in a range of values above and below 5/2, was also measured by Belliard [IV-17], Rajaram and Lieuwen [IV-18] and Wäsle et. al [IV-19]. Clavin and Siggia [II-166] and Clavin [IV-20] provided insight into these decay exponents with their theoretical analysis of combustion noise. Using Kolmogorov scaling arguments and, in particular, assuming a $k^{-5/3}$ inertial subrange spatial velocity spectrum, they arrive at an acoustic power spectrum in the corresponding frequency range with an α = 5/2 dependence. Huff's analysis [IV-21] predicted an α=2 dependence.
The decay exponent, α, is quantified in range values between approximately 2.2–3.6 [II-195], and it is in reasonable agreement to Clavin and Siggia's predicted value of 2.5 [II-166].
Falling outside of the regime of validity of the Clavin and Siggia theory does not change the fact that the spectrum has a power law, and therefore self-similar character, it only changes the value of the decay exponent.
Clearly, these basic power law characteristics of the acoustic spectra are far more general than those that the Clavin and Siggia theory is restricted to. These observations point to the need for further theoretical work on these high frequency acoustic characteristics.

The heat release rate fluctuations in the Power Spectral Density equation of radiated sound is usually used [II-47], then the modelling of *heat release rate fluctuations* ($\dot{\omega}_T^1$) constitutes a central issue in the combustion noise analysis. In general these fluctuations are not easy to measure experimentally. *In the premixed case one may link* $\dot{\omega}_T^1$ *to the light emission intensity of radicals* like CH*, C_2 or OH but the measurement is usually carried out over a line of sight and the fluctuation is integrated over a path through the flame. This method is not directly applicable in the nonpremixed or partially premixed cases.
One possible alternative explored by Boineau ([II-47], [IV-22]) consists in relating $\dot{\omega}_T^1$ to the temperature fluctuations in the flow (T'). This is accomplished by making use of a linearized version of the energy equation:

$$\rho c_p \frac{\partial T'}{\partial t} = \dot{\omega}_T^1 \qquad \text{(IV-3)}$$

This expression is obtained by neglecting diffusion fluxes and by suppressing the rate of change of the pressure perturbation ∂p'/∂t. This last approximation is not easy to justify but allows a direct estimate of heat release fluctuations in terms of temperature fluctuations. It is convenient to introduce the relative fluctuation of temperature θ' = T'/ T. An expression for the *radiated sound power spectrum* [II-47]:

$$S(\omega) = \frac{1}{8\pi^2} \frac{\rho_0 \omega^4}{c_0} \int R_{\theta'\theta'}(\bar{r}_0^{'}, \xi_0, \tau)\, e^{i\omega\tau}\, d\tau\, d\bar{r}_0^{'}\, d\xi_0 \qquad \text{(IV-4)}$$

where $R_{\theta'\theta'}(\bar{r}_0^{'}, \xi_0, \tau)$ designates the relative temperature fluctuation space time correlation function, $\bar{r}_0^{'} = r_0^{'}$ and $\bar{r}_0^{''} - \bar{r}_0^{'} = \xi_0$.

IV.4 Lighthill's aeroacoustic theory and combustion noise theories

Combustion noise is created by the conversion of some of the thermal energy available in the fuel gas to acoustic power.
Several competing combustion noise theories have emerged in recent years. Many of these theories provide reasonable estimates of observable trends in combustion and core noise behaviour. The differences between the most successful of these theories are frequently only superficial, in fact the underlying and mathematics are often essentially the same.
The most rigorously complete direct combustion noise theories are those that have been inspired by Lighthill's aeroacoustic theory ([II-163], see attachment A) of the 1952. While Lighthill's theory explains *jet noise* in terms of *acoustic quadrupoles produced by turbulent mixing in a shear layer*, many of the more promising direct combustion noise theories, while attributing combustion noise to equivalent acoustic monopole activity, draw heavily on Lighthill's formalism.
Unfortunately, a quantitative prediction of combustion noise from first principles is not yet possible because the equations describing turbulent flow, which are central to Lighthill's analogy, can not yet be solved. At best, combustion noise theories inspired by Lighthill's theory can be used to predict noise trends only when simplifying assumptions are made about the turbulence structure and its relationship to the unsteady heat release.
Not all theoretical developments which successfully predict observed combustion noise trends have been inspired by Lighthill's theory. An alternative approach involves postulating a physical model for the dependence of the *unsteady volumetric combustion heat release distribution* (R_1 in the *Rayleigh* and *Chu's criterion*) on the local flow and thermodynamic variables, but this is done on the basis of either physical arguments.
This combustion heat release term is introduced into the *appropriate energy equation* which, together with the continuity and momentum equations and an equation of state, describes the resulting unsteady flow in the combustor.
Two continuations are possible after the unsteady volumetric heat release term has been defined and the governing equations have been established:

a) In the first, *the equations are linearized* by assuming small perturbations of the flow variables (added to the mean flow), cast in the form of a wave equation and then solved, usually numerically.
b) Alternatively, *the equations are sometimes simplified* by rejecting certain terms on the basis of order-of-magnitude arguments. In this case it is often possible to obtain a closed-form analytical expression for the acoustic pressure in terms of the source term and other physical variables.

Regardless of the theoretical approach used to predict combustion noise, the results obtained ultimately depend on the assumed form of the unsteady volumetric heat release term (R_1 in the *Rayleigh* and *Chu's criterion*).

IV.5 Acoustics equation for non-reacting and reacting flows

All problems of unsteady motion in combustion systems can be divided into the two classes: *linearized* and *nonlinear*. From the earliest discoveries of their transient behaviour until the late 1950s, "combustion instabilities" implied small amplitude unsteady (and unwanted) motions growing out of a condition of linear instability. Even with the expanding awareness that the nonlinear properties must be understood as well, linear behaviour always remained an essential part of understanding all aspects of combustion instabilities, including the consequences of nonlinear processes.

Among the earliest interpretations of combustion instabilities there was the idea of unstable disturbances having *small amplitude*. That idea lies behind the characterization of small oscillations and is commonly assumed to explain the initial stage, and hence the origin, of an oscillation in a combustion chamber.

It is linear behaviour, especially linear stability, that is most easily understood and therefore has dominated discussions of combustion instabilities, particularly for solid propellant rockets. For example, the conclusion that a disturbance is unstable if the gain of energy exceeds the loss of energy in a short time interval, is founded in the first instance on linear ideas, although properly interpreted it is true generally. Because in a combustor there are many species and processes, the situation is extremely complicated. Moreover, unlike the case for linear motions, there are almost no generalizations available for nonlinear behaviour to serve as the basis for classifying the results of either experiments or of theory.

While there is a broad spectrum of nonlinear problems that arise in combustion systems, two kinds of behaviour have most recently received much of the attention: unsteady flows in *solid propellant rockets*; and the motions in *gas turbine combustors*, that are particularly common in systems intended for power generation.

Little attention has been paid to understanding nonlinear behaviour in works on control of combustion instabilities. One justification for that deficiency has been the view that if control of the oscillations works properly, it should stop the growth of the motion before its amplitude reaches a large value. There are several reasons why that reasoning is flawed [II-20]:

1. if the growth rates are unusually large, the control system may not have a sufficiently large bandwidth to be effective;
2. because combustion systems are intrinsically nonlinear, design of a control system based only on linear behaviour may produce a control system far from optimal;
3. linear control demands actuation at the frequency of the oscillation to be controlled, while nonlinear control of particular types may be effective at frequencies lower than that of the oscillation being controlled;
4. observed nonlinear behaviour contains much information about properties of the system in question and the interests of understanding should not be ignored.

Limitations of an interpretation based entirely on linear behaviour may therefore become especially evident in attempts to control an unstable motion. Existing examples of controlling combustion instabilities have almost totally ignored issues of *nonlinear* behaviour, although such behaviour is evident in all experimental work [II-20]. In no demonstration, either laboratory or full-scale, the amplitudes of the oscillations have been predicted or interpreted either before or after control has been exercised. Hence nothing has been learned about why the initially unstable

motions reach the amplitudes they did, or why the control system affected them in the observed way. In fact, few attempts exist to determine quantitatively the stability of motions.
Consequently the subject of controlling the dynamics of combustion systems has largely been a matter at best of exercising the principles of control with little attention paid to the characteristics of the systems ("plants") being controlled. It seems that following this strategy is likely not the most fruitful way of achieving meaningful progress. Especially, this is not a sound approach to developing the basis for designing control systems. The current practice in this field is often that feedback control is designed and applied in *ad hoc* fashion for systems already built and exhibiting instabilities.

IV.5.1 Acoustics for non-reacting flows

A simple framework to introduce acoustic theory is linear acoustics in non-reacting flows. Acoustic perturbations are small amplitude changes of thermodynamic variables and velocity. These perturbations are present in all gases and appear in all codes using a compressible formulation. Equations of acoustics are derived from the main conservation equations: mass, momentum and energy.
We can analyse the classical elements of acoustics in a simplified case, according the following hypothesis:

- H0 – no combustion
- H1 – zero volume forces (f_k=0)
- H2 – zero volume heat sources ($\dot{Q} = 0$)
- H3 – negligible viscous forces, then non viscous stresses are retained in the volume ($\tau_{ij} = 0$).
- H4 – linear acoustics: acoustic variables are indexed "1" and supposed to be small compared to reference quantities indexed "0": $p_1 << p_0$, $\rho_1 << \rho_0$, $u_1 << c_0$ (the reference speed in acoustic is not the mean flow speed u_0 but the sound speed c_0).
- H5 – isentropic variations: under the previous assumptions (no heat release, no viscous terms), the flow remains isentropic if it is homogeneous and isentropic at the initial time t=0. Then the energy equation may be replaced by the isentropic relation:

$$s_0 = c_v \ln\left(\frac{p}{\rho^\gamma}\right) \qquad \text{or} \qquad p = \rho^\gamma e^{\frac{s_0}{c_v}}$$

- H6 – low-speed mean flow: $\bar{u}_0 = 0$

Under these assumptions, the equations of mass, momentum and energy are (Attachment D):

$$\frac{\partial \rho}{\partial t} + \nabla \cdot \rho \bar{u} = 0 \qquad \frac{D\rho}{Dt} + \rho \nabla \cdot \bar{u} = 0 \tag{IV-5}$$

$$\rho \frac{\partial \bar{u}}{\partial t} + \rho \bar{u} \nabla \bar{u} = -\nabla p \qquad \rho \frac{D\bar{u}}{Dt} = -\nabla p \tag{IV-6}$$

$$p = \rho^\gamma e^{\frac{s_0}{c_v}} \tag{IV-7}$$

Considering the simple case of small-amplitude fluctuations (index 1) superimposed to a zero Mach number mean flow (index 0), then assuming small acoustic perturbations of the flow variables (p_1, ρ_1, $\bar{u}_1$) added to the mean flow (p_0, ρ_0, $\bar{u}_0$)

$$p_1 << p_0 \qquad \rho_1 << \rho_0 \qquad \bar{u}_1^2 << c_0^2$$

it is possible to write:

$$p = p_0 + p_1 \qquad \rho = \rho_0 + \rho_1 \qquad \bar{u} = \bar{u}_1$$

Note that the zero Mach number assumption for the mean flow (M=0, u_0=0) implies $\nabla p_0 = 0$, using equation (IV-6).
Substituting p and $\bar{u}$ into the conservation equations of mass (IV-5) and momentum (IV-6), and conserving only first order terms, then making a linearization, gives:

$$\frac{\partial \rho_1}{\partial t} + \rho_0 \nabla \cdot \bar{u}_1 = 0 \tag{IV-8}$$

$$\rho_0 \frac{\partial \bar{u}_1}{\partial t} + \bar{\nabla} p_1 = 0 \tag{IV-9}$$

Linearizing the energy equation (IV-7) replaced by the isentropic relation:

$$p_1 = c_0^2 \rho_1 \tag{IV-10}$$

then $\dfrac{\partial \rho_1}{\partial t} = \dfrac{1}{c_0^2} \dfrac{\partial p_1}{\partial t}$

where $c_0^2 = \left(\dfrac{\partial p}{\partial \rho} \right)_{s=s_0}$

and for a perfect gas, the sound speed is obtained using the isentropic relation:

$$c_0^2 = \sqrt{\gamma \frac{p_0}{\rho_0}} = \sqrt{\gamma \frac{R}{W} T_0} = \sqrt{\gamma R_g T_0}$$

Density variations (ρ_1) may be eliminated into the equation (IV-8), therefore two variables (e.g. p_1 and $\bar{u}_1$) are sufficient to describe acoustic waves:

$$\frac{1}{c_0^2} \frac{\partial p_1}{\partial t} + \rho_0 \nabla \cdot \bar{u}_1 = 0 \tag{IV-11}$$

$$\rho_0 \frac{\partial \bar{u}_1}{\partial t} + \nabla p_1 = 0 \qquad \text{(IV-12)}$$

Taking the time derivative $\left(\frac{\partial}{\partial t}\right)$ of the conservation of mass (IV-11) and the divergence ($\nabla \cdot$) of the conservation of momentum (IV-12), by adding these equations the well-known wave equation is obtained:

$$\boxed{\nabla^2 p_1 - \frac{1}{c_0^2}\frac{\partial^2 p_1}{\partial t^2} = 0} \qquad \text{(IV-13)}$$

IV.5.2 Acoustics for reacting flows

For a reacting flow, the derivation of a acoustic wave equation is a more complex task. A convenient way to derive this equation is to work with the logarithm of pressure.
Assuming zero volume forces (f_k=0) and zero volume heat sources ($\dot{Q} = 0$), the mass and momentum conservation like for non-reacting flows are:

$$\frac{D\rho}{Dt} + \rho \nabla \cdot \bar{u} = 0 \qquad \text{(IV-14)}$$

$$\rho \frac{D\bar{u}}{Dt} = -\nabla p + \nabla \cdot \tau \qquad \text{(IV-15)}$$

where we used the total derivatives of a function f as $\frac{Df}{Dt} = \frac{\partial f}{\partial t} + \bar{u} \cdot \nabla f$.
The energy equation for a not adiabatic flow is

$$\rho c_p \frac{DT}{Dt} = \dot{\omega}_T^{/} + \frac{Dp}{Dt} + \tau : \nabla \bar{u} - \left(\rho \sum_{k=1}^{N} c_{p,k} Y_k \bar{V}_k \right) \cdot \nabla T \qquad \text{(IV-16)}$$

where V_k is the diffusion velocity vector of species k.
Dividing the energy equation (IV-16) by $\rho c_p T$:

$$\frac{1}{T}\frac{DT}{Dt} = \frac{1}{\rho c_p T}\left[\dot{\omega}_T^{/} + \frac{Dp}{Dt} + \tau : \nabla \bar{u} - \left(\rho \sum_{k=1}^{N} c_{p,k} Y_k \bar{V}_k \right) \cdot \nabla T \right] + \frac{1}{\rho c_p T}\frac{Dp}{Dt}$$

Using the equation of state $p = \rho R_g T$, remembering that $\gamma = \frac{c_p}{c_v}$ and $R_g = c_p - c_v$, using the mass conservation (IV-14) give:

$$\frac{1}{T}\frac{DT}{Dt}-\frac{1}{\rho c_p T}\frac{Dp}{Dt}=\frac{D(\ln T)}{Dt}-\frac{r}{p c_p}\frac{Dp}{Dt}=\frac{D(\ln p)}{Dt}-\frac{D(\ln \rho)}{Dt}-\frac{D(\ln r)}{Dt}-\frac{r}{c_p}\frac{D(\ln p)}{Dt}=$$
$$=\frac{1}{\gamma}\frac{D\ln(p)}{Dt}+\nabla\cdot\bar{u}$$

This is a convenient method to obtain an equation for *ln*(p):

$$\boxed{\frac{1}{\gamma}\frac{D\ln(p)}{Dt}+\nabla\cdot\bar{u}=\frac{1}{\rho c_p T}\left[\dot{\omega}_T^{/}+\tau:\nabla\bar{u}-\left(\rho\sum_{k=1}^{N}c_{p,k}Y_k\bar{V}_k\right)\cdot\nabla T\right]+\frac{1}{R_g}\frac{Dr}{Dt}} \qquad \text{(IV-17)}$$

Note that the momentum equation (IV-15) may be written as a function of ln(p):

$$\frac{D\bar{u}}{Dt}+\frac{c_0^2}{\gamma}\nabla\ln(p)=\frac{1}{\rho}\nabla\cdot\tau$$

IV.5.3 A wave equation in low Mach-number reacting flows

Since many applications within the combustion community can be considered low Mach number problems, numerous articles deal with combustion simulations using a low Mach number approximation, where detailed chemical reactions can be used at reasonable computational costs. However, the disadvantage of this low Mach number
approximation from an acoustic point of view is that no sound propagation can be directly computed in the flow analysis. In other words, the possible impact of the acoustic field on the flow and the combustion problem, respectively, is neglected.
The pressure equation can be approximated linearizing it, then the pressure is written $p = p_0 + p_1$ with $\frac{p_1}{p_0} << 1$ so that it is possible to use the following approximation: $\ln(p) \cong \frac{p_1}{p_0}$.
One additional assumption may be introduced to derive a simple wave equation in reacting flows:

- H7 – identical molecular weights (w_i) for all species, and then identical R_g.

Using it and the hypothesis H6 of low-speed mean flow ($\bar{u}_0 = 0$) that are not very restrictive, brings many simplifications:

- $\dot{\omega}_T^{/}$ can be replaced by $\dot{\omega}_T$ since all molecular weights are equal
- γ is constant and the mean pressure p_0 is also constant so that $\gamma p_0 = \rho_0 c_0^2$ is constant (which does not mean that ρ_0 and c_0 are constant).

An order of magnitude analysis ([II-86], [IV-23]) leads to the simplified equations:

Non-reacting flows	$c_0^2\nabla^2 p_1 - \frac{\partial^2 p_1}{\partial t^2} = -\gamma p_0 \nabla\bar{u}:\nabla\bar{u}$	(IV-18)

Reacting flows	$\nabla\cdot\left(c_0^2\nabla p_1\right)-\frac{\partial^2 p_1}{\partial t^2}=-\gamma\, p_0\nabla\bar{u}:\nabla\bar{u}\ -(\gamma-1)\frac{\partial\dot{\omega}_T}{\partial t}$	(IV-19)

For the non-reacting case, the $\nabla\bar{u}:\nabla\bar{u}$ term is retained and is responsible for turbulent flow noise. The main complexity brought by combustion is the variable sound speed c_0 which must be kept in the $\nabla\cdot$ operator and the additional source term found on the right-hand side terms for the pressure equation with combustion.

IV.6 The acoustic energy balance in reacting flows

Coupling mechanisms between acoustic waves and flames have become central issues in the development of many modern combustion systems. For a reactive flow, the derivation of a wave equation is a very complex task.
Standing pressure waves are produced in any confined chamber, the amplitudes of which are functions of the geometry, boundary conditions, and the medium. Often, these pressure variations serve as a host oscillator in a combustion system.

IV.6.1 Acoustic energy density and flux

The notion of acoustic energy is useful to describe combustion instabilities. Its simplest derivation is given here for non-reacting flows. The acoustic energy measures the total level of acoustic fluctuations in a given domain and corresponds to the linearized form of the mechanical energy [IV-24] but a simpler derivation is presented here.
Starting from the conservation equations of mass (IV-11) and momentum (IV-12), obtained by eliminating the density variations ($\rho_1 << \rho_0$), multiplying the first equation by $\frac{p_1}{\rho_0}$ and the second one by $\bar{u}_1$ and adding them gives:

$$\frac{\partial}{\partial t}\left(\frac{1}{2}\rho_0\bar{u}_1^2+\frac{1}{2}\frac{p_1^2}{\rho_0 c_0^2}\right)+\nabla\cdot\left(p_1\bar{u}_1\right)=0 \qquad \text{(IV-20)}$$

The **classic acoustic energy** (**AE**) in a reacting flow may be defined by

$$\boxed{e_1=\frac{1}{2}\rho_0\bar{u}_1^2+\frac{1}{2}\frac{p_1^2}{\rho_0 c_0^2}} \qquad \text{(IV-21)}$$

where index 0 refers to mean values and index 1 to perturbations.
The *local acoustic flux* may be defined by

$$f_1 = p_1 \bar{u}_1 \tag{IV-22}$$

Then we can write the equation (IV-20) in this way

$$\boxed{\frac{\partial e_1}{\partial t} + \nabla \cdot f_1 = 0} \tag{IV-23}$$

This equation shows that the acoustic energy e_1 varies only because of the local acoustic flux f_1. This local energy may be integrated over a domain V (e.g. the computational domain in a CFD case) bounded by a surface A to yield:

$$\frac{\mathrm{d}}{\mathrm{dt}} \int_{\mathrm{V}} \mathrm{e}_1 \mathrm{dV} + \int_{\mathrm{A}} \mathrm{f}_1 \cdot \bar{\mathrm{n}} \mathrm{dA} = 0 \tag{IV-24}$$

where $\int_{\mathrm{V}} \mathrm{e}_1 \mathrm{dV}$ is the total acoustic energy present in the domain and $\bar{\mathrm{n}}$ is the normal to the surface A. This equation shows that the changes in the total energy are only due to fluxes crossing the boundaries.

IV.6.2 Extended of the acoustic energy equation

The classic acoustic energy equation (AEE) is obtained by linearizing a global energy equation directly deduced from the Navier-Stokes equation.

Using the relation between energy (e) and enthalpy (h): $\mathrm{h} = \mathrm{e} + \frac{\mathrm{p}}{\rho}$

and the total mass conservation equation, $\frac{D\rho}{Dt} + \rho \frac{\partial u_i}{\partial x_i} = 0$, yields:

$$\rho \frac{De_S}{Dt} = \rho \frac{Dh_S}{Dt} - \frac{Dp}{Dt} - p \frac{\partial u_i}{\partial x_i} \tag{IV-25}$$

The conservation equation for the sensible enthalpy h_s is:

$$\rho \frac{Dh_s}{Dt} = \dot{\omega}_T + \frac{Dp}{Dt} + \frac{\partial}{\partial x_i}\left(\lambda \frac{\partial T}{\partial x_i}\right) - \frac{\partial}{\partial x_i}\left(\rho \sum_{k=1}^{Ns} h_{s,k} Y_k V_{k,i}\right) + \tau_{ij} \frac{\partial u_i}{\partial x_j} + \dot{Q} + \rho \sum_{k=1}^{Ns} Y_k f_{k,i} V_{k,i} \tag{IV-26}$$

where $\dot{\omega}_T$ is the *heat release per unit volume* due to combustion:

$$\dot{\omega}_T = -\sum_{k=1}^{N_S} \Delta h_{f,k}^0 \dot{\omega}_k$$

where $h_{f,k}^0$ is the chemical formation enthalpies.

The equation for the sensible energy e_s may be deduced from equations (IV-25) and (IV-26) and remembering that $\tau_{ij} = \sigma_{ij} + p\delta_{ij}$:

$$\rho \frac{De_s}{Dt} = \dot{\omega}_T + \frac{\partial}{\partial x_i}\left(\lambda \frac{\partial T}{\partial x_i}\right) - \frac{\partial}{\partial x_i}\left(\rho \sum_{k=1}^{Ns} h_{s,k} Y_k V_{k,i}\right) + \sigma_{ij}\frac{\partial u_i}{\partial x_j} + \dot{Q} + \rho \sum_{k=1}^{Ns} Y_k f_{k,i} V_{k,i} \qquad \text{(IV-27)}$$

where the total derivative of e_s is $\frac{De_s}{Dt} = \frac{\partial e_s}{\partial t} + \bar{u}\cdot\nabla e_s = \frac{\partial e_s}{\partial t} + \frac{\partial}{\partial x_i}(u_i e_s)$.

If all heat capacities c_v are equal (an assumption which is not often true in flames but is often used) and independent of temperature (c_v=constant) it is possible to write, using the state equation:

$$\rho e_s = \rho\left(\int_{T_0}^{T} c_v dT - \frac{RT_0}{W}\right) = \rho\left(c_v T - c_v T_0 - \frac{RT_0}{W}\right) = \frac{p}{\gamma - 1} - \rho c_p T_0 \qquad \text{(IV-28)}$$

Using the expressions of total derivate of e_s and equation (IV-28), yields:

$$\rho \frac{De_s}{Dt} = \frac{\partial \rho e_s}{\partial t} + \frac{\partial}{\partial x_i}(u_i \rho e_s) = \left(\frac{1}{\gamma - 1}\frac{\partial p}{\partial t} - c_p T_0 \frac{\partial \rho}{\partial t}\right) + \frac{\partial}{\partial x_i}\left(\frac{u_i p}{\gamma - 1} - u_i \rho c_p T_0\right) \qquad \text{(IV-29)}$$

It is possible to assume that the mixture heat capacity c_p is constant: this approximation is slightly inconsistent but it is used in Kuo [IV-25] to derive the equations.
Using the continuity equation yields:

$$\begin{aligned} \rho \frac{De_s}{Dt} &= \frac{1}{\gamma - 1}\frac{\partial p}{\partial t} - c_p T_0 \frac{\partial \rho}{\partial t} + \left[\frac{1}{\gamma - 1} u_i \frac{\partial p}{\partial x_i} + \frac{1}{\gamma - 1} p \frac{\partial u_i}{\partial x_i} - c_p T_0 \frac{\partial (u_i \rho)}{\partial x_i}\right] = \\ &= \frac{1}{\gamma - 1}\frac{Dp}{Dt} + \frac{1}{\gamma - 1} p \frac{\partial u_i}{\partial x_i} \end{aligned} \qquad \text{(IV-30)}$$

Then the equation (IV-27) turns into an equation for pressure p replacing ρe_s with the expression (IV-30). Replacing $\sigma_{ij} = \tau_{ij} - p\delta_{ij}$ and if all species have the same sensible enthalpy $\sum_{k=1}^{Ns} h_{s,k} Y_k V_{k,i} = h_s \sum_{k=1}^{Ns} Y_k V_{k,i} = 0$, yields:

$$\frac{1}{\gamma - 1}\frac{Dp}{Dt} = -\frac{\gamma}{\gamma - 1} p \frac{\partial u_i}{\partial t} + \dot{\omega}_T + \frac{\partial}{\partial x_i}\left(\lambda \frac{\partial T}{\partial x_i}\right) + \tau_{ij}\frac{\partial u_i}{\partial x_j} + \dot{Q} + \rho \sum_{k=1}^{Ns} Y_k f_{k,i} V_{k,i} \qquad \text{(IV-31)}$$

Considering zero volume heat sources ($\dot{Q} = 0$), zero volume forces ($f_k = 0$), negligible viscous forces that is no viscous stresses are retained in the volume ($\tau_{ij} = 0$), but conserving the thermal diffusion ($\lambda \neq 0$) and multiplying the equation (IV-31) by $(\gamma - 1)$, the pressure equation can be written as:

$$\frac{Dp}{Dt} = -\gamma p \nabla \cdot \bar{u} + (\gamma - 1)\left[\dot{\omega}_T + \nabla \cdot (\lambda \bar{\nabla} T)\right] \tag{IV-32}$$

where we can write $\gamma = \frac{\rho_0 c_0^2}{p_0} = \frac{c_0^2}{R_g T_0}$.

The momentum equation (IV-9) can be written as:

$$\rho \frac{\partial \bar{u}}{\partial t} + \bar{\nabla} p = 0$$

and taking the dot product of it with $\bar{u}$ leads to an equation for $\bar{u}^2$:

$$\rho \frac{D\left(\frac{\bar{u}^2}{2}\right)}{Dt} + \bar{\nabla} \cdot (p\bar{u}) = p \nabla \cdot \bar{u} \tag{IV-33}$$

The equation (IV-32) can be used to express the product of pressure p with divergence of velocity $(\nabla \cdot \bar{u})$ and using this expression to eliminate the divergence of velocity in equation (IV-33) leads to a ***non-linear*** **form of acoustic energy equation**:

$$\rho \frac{D\left(\frac{\bar{u}^2}{2}\right)}{Dt} + \frac{1}{\rho c_0^2} \frac{D\left(\frac{p^2}{2}\right)}{Dt} + \bar{\nabla} \cdot (p\bar{u}) = \frac{(\gamma - 1)}{\gamma}\left[\dot{\omega}_T + \nabla \cdot (\lambda \bar{\nabla} T)\right] \tag{IV-34}$$

The equation (IV-34) is exact (no linearization). It is possible to consider the simple case of small acoustic perturbation variables (index 1) added to the mean flow variable (index 0) to a zero Mach number mean flow, then it is possible to write:

$$\bar{u} = \bar{u}_1 \qquad p = p_0 + p_1 \qquad \dot{\omega}_T = \dot{\omega}_T^0 + \dot{\omega}_T^1 \qquad T = T_0 + T_1$$

For simplicity the temporal fluctuations of the thermal diffusivity (α), dynamic viscosity (μ) and heat capacities (c_p, c_v and γ) can be neglected.
Note that the zero Mach number assumption for the mean flow (u_0=0, M=0) implies $\nabla p_0 = 0$, using momentum equation (IV-6), and $\dot{\omega}_T^0 + \nabla \cdot (\lambda \bar{\nabla} T_0) = 0$ using equation (IV-32).
The assumption for zero mean flow (u_0=0) implies the approximation that $\frac{D}{Dt} \approx \frac{\partial}{\partial t}$ for any fluctuating quantity.
The mean pressure p_0 being constant over space and the mean velocity being u_0=0, the following expression holds for the flux term of equation (IV-34):

$$\overline{\nabla}\cdot\left(p\,\overline{u}\right)=p_0\overline{\nabla}\cdot\overline{u}_1+\overline{\nabla}\cdot\left(p_1\overline{u}_1\right)$$

Making a linearization of equation (IV-34) around the mean state (index 0) gives ([II-86], [IV-26]):

$$\boxed{\frac{\partial e_1}{\partial t}+\overline{\nabla}\cdot\left(p_1\overline{u}_1\right)=\frac{(\gamma-1)}{\gamma\,p_0}\,p_1\,\left[\dot{\omega}_T^1+\nabla\cdot\left(\lambda\,\overline{\nabla}\,T_1\right)\right]} \qquad \text{(IV-35)}$$

which is simply the extension of the **classic acoustic energy equation (AEE)** (IV-23) including the *source term* r_1:

$$\boxed{\frac{\partial e_1}{\partial t}+\nabla\cdot f_1=r_1} \qquad \text{(IV-36)}$$

where e_1 is the *acoustic energy in a reacting flow* (IV-21) and f_1 is the *local acoustic flux* (IV-22). All terms are time dependent.
If we consider the case with the viscous forces ($\mu\neq 0$) and the viscous stresses ($\tau_{ij}\neq 0$) in the volume the complete classic acoustic equation is:

$$\frac{\partial e_1}{\partial t}+\overline{\nabla}\cdot\left(p_1\overline{u}_1\right)=\frac{(\gamma-1)}{\gamma\,p_0}\,p_1\,\left[\dot{\omega}_T^1+\nabla\cdot\left(\lambda\,\overline{\nabla}\,T_1\right)\right]+\overline{u}_1\cdot\left(\overline{\nabla}\cdot\overline{\tau}_1\right) \qquad \text{(IV-37)}$$

Making a linearization of equation (IV-32), yields:

$$\frac{Dp_1}{Dt}=-\gamma\,p\nabla\cdot\overline{u}_1+(\gamma-1)\left[\dot{\omega}_T^1+\nabla\cdot\left(\lambda\,\overline{\nabla}\,T_1\right)\right] \qquad \text{(IV-38)}$$

with $\mathrm{p}=\mathrm{p}_0+\mathrm{p}_1$, it is clear that $p^2=p_0^2+2p_0p_1+p_1^2$ and then $\frac{D\left(\frac{p^2}{2}\right)}{Dt}=p_0\frac{Dp_1}{Dt}+\frac{D\left(\frac{p_1^2}{2}\right)}{Dt}$, can be obtained easily (remembering that u_0=0, $\nabla p_0=0$):

$$\frac{Dp_1}{Dt}=\frac{1}{p_0}\frac{D\left(\frac{p^2}{2}\right)}{Dt}-\frac{1}{p_0}\frac{D\left(\frac{p_1^2}{2}\right)}{Dt}=\frac{1}{p_0}\frac{D\left(\frac{p^2}{2}\right)}{Dt}-\frac{1}{p_0}\frac{\partial\left(\frac{p_1^2}{2}\right)}{\partial t}$$

The equation (IV-38) become:

$$\frac{D\left(\frac{p^2}{2}\right)}{Dt}\cong\frac{\partial\left(\frac{p_1^2}{2}\right)}{\partial t}-\gamma\,p\,p_0\nabla\cdot\overline{u}_1+p_0\,(\gamma-1)\left[\dot{\omega}_T^1+\nabla\cdot\left(\lambda\,\overline{\nabla}\,T_1\right)\right] \qquad \text{(IV-39)}$$

IV.7 Criteria for combustion instability

Two forms of energy are defined: the first is the classic acoustic energy (AE), and the second is the fluctuation energy (FE). Both equations are rederived in a compact manner starting from full nonlinear forms. It is shown that the classic Rayleigh criterion naturally appears as the source term of the AE equation, while the FE form leads to a different criterion stating that temperature and heat release must be in phase for the instability to be fed by the flame/acoustics coupling. The FE form also integrates the fluctuations of three variables (pressure, velocity, entropy), while the AE form uses only pressure and velocity perturbations. It is shown that only the FE form should be used in flames, in contradiction to many current studies performed for combustion instabilities.

IV.7.1 Classical Rayleigh's criterion

The acoustic energy equation (IV-35) for classical Rayleigh's criterion, that does not include the heat diffusion effects, then $\nabla \cdot \left(\lambda \overline{\nabla} T_1\right) = 0$, yields:

$$\frac{\partial e_1}{\partial t} + \overline{\nabla} \cdot \left(p_1 \overline{u}_1\right) = \frac{\left(\gamma - 1\right)}{\gamma\, p_0} p_1 \dot{\omega}_T^1 \qquad \text{(IV-40)}$$

where the *source term* r_1 is:

$$r_1 = \frac{\left(\gamma - 1\right)}{\gamma\, p_0} p_1 \dot{\omega}_T^1 \qquad \text{(IV-41)}$$

In this case the source term r_1 is a correlation between unsteady pressure p_1 and unsteady heat release $\dot{\omega}_T^1$. It is due to combustion and can act as a source or a dissipative term for the acoustic energy.
The local acoustic energy equation (IV-36) may be integrated over a domain V (e.g. the computational domain in a CFD case) bounded by a surface A. If it is integrated over the whole volume V of the combustor:

$$\frac{d}{dt}\int_V e_1 dV + \int_A f_1 \cdot \overline{n} dA = \int_V r_1 dV \qquad \text{(IV-42)}$$

To provide meaningful information on the growth of the instability, this last equation must also be averaged over time. Integrating equation (IV-42) over a period of oscillation $\tau = \frac{2\pi}{\omega}$ and dividing by τ:

$$\frac{dE_1}{dt} + F_1 = R_1 \qquad \text{(IV-43)}$$

where:

- E_1 measures the period-averaged *acoustic energy* in the whole combustor

$$E_1 = \int_V E dV \qquad \text{with} \qquad E = \frac{1}{\tau}\int_0^\tau e_1 dt$$

- F_1 is the period-averaged *acoustic flux leaving the combustor*, that are *acoustic losses*

$$F_1 = \int_A F \cdot \bar{n}\, dA \qquad \text{with} \qquad F = \frac{1}{\tau}\int_0^\tau f_1 dt$$

Loss of acoustic energy – through viscous dissipation, through transfer of acoustic energy to hydrodynamic or evanescent modes, or through radiation losses at the system boundary – tends to stabilize a thermo-acoustic system.

- R_1 is the average *source term*

$$R_1 = \int_V R dV \qquad \text{with} \qquad R = \frac{1}{\tau}\int_0^\tau r_1 dt = \frac{(\gamma - 1)}{\tau \gamma p_0}\int_0^\tau p_1 \dot{\omega}_T^1 dt$$

It describes the exchange of energy between the combustion and the acoustic waves. Considering conservation equations, Culick [IV-27] derived a similar expression for the energy addition to the acoustic mode.

Energy	**Flux**	**Source**	**Characteristic**	
			(according space)	(according time)
e_1	f_1	r_1	local	instantaneous
E	F	R	local	period-averaged
E_1	F_1	R_1	volume (or surface) averaged	period-averaged

Flame/acoustic coupling is now represented in R_1 from the space-averaged integral (over V) of the period-averaged value of unsteady pressure multiplied by unsteady heat release.
Lord Rayleigh [II-39] proposed a qualitative criterion for combustion instability (R_1 must be positive to increase the acoustic energy of the oscillation) and he formulated the following explanation for the production of tones in a *Rijke tube*:

> *"If heat be periodically communicated to, and abstracted from, a mass of air vibrating (for example) in a cylinder bounded by a piston, the effect produced will depend upon the phase of the vibration at which the transfer of heat takes place. If the heat is given to the air at the moment of greatest condensation, or be taken from it at the moment of greatest rarefaction, the vibration is encouraged. On the other hand, if heat be given at the moment of greatest rarefaction, or abstracted at the moment of greatest condensation, the vibration is discouraged".*

That paragraph has become probably the most widely cited explanation for the presence of combustion instabilities generally. For easy reference, the explanation has long been referred to as ***"Rayleigh's Criterion"***.
Putnam [II-3] has made the most extensive use of Rayleigh's Criterion in practical situations. His book and papers give many examples of applying the Criterion as an aid to making changes of design to avoid oscillations generated by heat release, particularly in power generation and heating systems. In the past fifteen years many groups have been making direct observations on laboratory systems to check the validity of the implications of Rayleigh's Criterion. The key step is based on the assumption that *radiation by certain intermediate radical species in hydrocarbon reactions* (CH* and OH* are the most common identifiers) *can be interpreted as a measure of the rate of chemical reactions taking place and hence of the rate at which energy is released*. Simultaneous measurements are made of the spatial distribution of radiation in a system, and of the pressure oscillations. The results then allow at least a qualitative assessment of the extent to which the oscillations are being driven by the energy released in the combustion field, or whether other mechanisms may be active and important. It is an important method with many useful applications.
R_1 is positive when r_1 is positive, i.e. if the pressure oscillations (p_1) are in phase with the unsteady heat release ($\dot{\omega}_T^1$), r_1 acts as a *source term* for acoustic energy and the instability is locally amplified.

$$\boxed{R_1 = \frac{(\gamma-1)}{\tau\gamma\, p_0}\int_V\int_0^\tau p_1\dot{\omega}_T^1\, dt\, dV > 0}$$

On the other hand, if unsteady heat release is maximum when pressure is minimum, the instability decreases ($R_1<0$).
It is often used in experimental or numerical studies to quantify the energy transfer from the combustion process to the acoustic field.
Equivalently one may say that the absolute value of the phase difference between the *pressure* (p_1) and *heat release signals* ($\dot{\omega}_T^1$) should be less than $\pi/2$ or that:

$$\left|\arg.\left(\frac{\dot{\omega}_T^1}{p_1}\right)\right| < \frac{\pi}{2} \qquad \Rightarrow \qquad -\frac{\pi}{2} < \arg.\left(\frac{\dot{\omega}_T^1}{p_1}\right) < \frac{\pi}{2}$$

Then, the sign of this integral depends on the phase difference between the heat-release and pressure oscillations and is positive (negative) when this phase difference is smaller (larger) than 90 deg.
The heat-addition process locally adds energy to the acoustic field when the magnitude of the phase between the pressure and heat-release oscillations, $\theta_{p\omega_T} = \arg.\left(\frac{\dot{\omega}_T^1}{p_1}\right)$, is less than 90 deg (i.e, $0 < \left|\theta_{p\omega_T}\right| < 90$). Conversely, when these oscillations are out of phase deg (i.e, $90 < \left|\theta_{p\omega_T}\right| < 180$), the heat-addition oscillations damp the acoustic field.

To evaluate the *Rayleigh criterion*, the phase shift between *pressure* and *heat release fluctuations* can be used. Phase shifts occur because every heat release fluctuation produces the corresponding pressure fluctuation only after a certain delay or "time lag" (and vice-versa).
Time lags in combustion systems consist of various component τ_i, e.g. acoustic and convective time lags, as well as time lags attributable to the process of mixing and reacting.
Although this qualitative criterion for combustion instability seems a rather natural statement, many experiments do not actually support this result in a straightforward manner. The index r_1 changes with time and with location: some regions of a given combustor usually excite the oscillation by burning in phase with pressure ($r_1>0$) while other regions damp ($r_1<0$) the instability by burning out of phase with pressure ([II-37], [IV-28]).
The first obvious observation is that the acoustic energy growth rate depends on the Rayleigh term ($p_1\dot{\omega}_T^1$) but also on the *acoustic fluxes* (*acoustic losses*) $\overline{\nabla}\cdot\left(p_1\overline{u}_1\right)$ so that the ***Rayleigh's criterion*** **is only a necessary condition (but not sufficient condition) for instability to occur**.

IV.7.2 Extended Rayleigh's criterion

A criterion more complex and that includes more acoustic effects than classical Rayleigh's criterion is:

$$g = \frac{R_1 - F_1}{2E_1} > 0$$

then $R_1 > F_1$, i.e.

$$\boxed{\frac{(\gamma-1)}{\gamma\, p_0}\int_V\int_0^\tau p_1\dot{\omega}_T^1\, dt\, dV > \int_A\int_0^T p_1\overline{u}_1\, dt\, dA} \qquad \text{(IV-44)}$$

The combustor will oscillate and the total acoustic energy will grow if $R_1 > F_1$, or in other words if the *source term* (R_1) due to combustion is larger than the *acoustic losses* (F_1) on the combustor inlet and outlet surface A.
The practical implication of equation (IV-44) is that the classic Rayleigh's criterion should not be used alone but should also include *acoustic losses* (F_1). This task is difficult in experiments because it requires the evaluation of acoustic fluxes $\overline{\nabla}\cdot\left(p_1\overline{u}_1\right)$ on the boundaries of the burner, but it can be done in LES simulation.
Then, **the *Rayleigh's criterion is "necessary, but not sufficient for instability to occur"* because loss mechanism are not taken into account**.

IV.7.3 Classical and extended Chu's criterion

Stability considerations based on a balance between generation and loss of acoustic energy may appear to be an almost self-evident generation of Rayleigh's criterion. However, quantitative methods for stability analysis based on this idea have been proposed only recently (Ibrahim et al. [IV-29], [IV-30]; Nicoud and Poinsot [IV-26]; Giauque et al. [IV-31], [IV-32]).

IV.7.3.1 Expression for a stabilizing factor by means the instantaneous density of acoustic energy

Ibrahim et al. ([IV-29], [IV-30]) base their analysis on an expression for *the instantaneous density of acoustic energy* [IV-33],

$$e = \left[\frac{\rho}{2} \left(\frac{p'}{\rho c} \right)^2 + u'_i \, u'_i \right] \tag{IV-45}$$

The first term is the potential acoustic energy, the second term (with summation over repeated indices implied) is the kinetic acoustic energy.
The conservation of acoustic energy is then formulated as a transport equation for energy density e,

$$\frac{\partial e}{\partial t} + \frac{\partial}{\partial x_i}\left(p' u'_i\right) + \frac{\partial}{\partial x_i}\left(e\, u_i\right) = \Phi \tag{IV-46}$$

where

$$\Phi = \frac{\gamma - 1}{\gamma} p' q' - \frac{\partial u'_i}{\partial x_j} \tau'_{ij} \tag{IV-47}$$

The second and third term on the left-hand side of equation (IV-46) represent the flux of acoustic energy, with convection by the mean flow $\bar{u}$ retained. Φ is the source term and it comprises thermo-acoustic and viscous contributions, where the former is obviously related to the Rayleigh integral.
Introducing an average over the oscillation period T, integrating over the domain considered and employing the divergence theorem, the energy balance can be written as follows

$$\frac{\partial}{\partial t}\int_V \left(\frac{1}{T}\int_0^T e \; dt \right) dV = -\int_A \left(\frac{1}{T}\int_0^T p' u'_i \; dt \right) dA_i - \int_A \left(\frac{1}{T}\int_0^T e\, u_i \; dt \right) dA_i + \int_V \left(\frac{1}{T}\int_0^T \Phi \; dt \right) dV \tag{IV-48}$$

From the balance equation (IV-48), an *amplification coefficient* α is then defined,

$$\alpha \equiv \frac{-\int_A \left(\frac{1}{T}\int_0^T p'u'_i \; dt\right) dA_i - \int_A \left(\frac{1}{T}\int_0^T e u_i \; dt\right) dA_i + \int_V \left(\frac{1}{T}\int_0^T \Phi \; dt\right) dV}{2\int_V \left(\frac{1}{T}\int_0^T e \; dt\right) dV} \tag{IV-49}$$

The first term in the numerator represents boundary work, the second term represents advection of acoustic energy across the boundary by the mean flow, the third term is the net production (the thermo-acoustic source vs. the viscous sink). Some of these contributions to the overall amplification increase the acoustic energy and are denoted α_{amp}, while the magnitude of contributions that represent a loss of energy are denoted α_{damp}, such that for the overall amplification coefficient $\alpha = \sum \alpha_{amp} - \sum \alpha_{damp}$. Separation of destabilizing and damping effects in this way allows to introduce a *stabilizing factor*

$$S(\omega) = \frac{\sum \alpha_{amp}}{\sum \alpha_{damp}} \tag{IV-50}$$

Ibrahim et al. ([IV-29], [IV-30]) argued that if an acoustic eigenfrequencies ω_m of the combustor with $S(\omega_m) > 1$ exists, that eigenmode will be unstable.

The appealing feature of this method is that it should allow the combustor designer to investigate quickly and inexpensively a wide variety of potential design configurations and operating conditions. Validation studies carried out by Ibrahim et al. met moderate success because they used in their validation studies rather simplistic assumptions concerning the acoustic wave field in the combustor, i.e. the acoustic impedance at the location of heat release.

IV.7.3.2 Derivation of the acoustic energy budget from LES

A conceptually related approach has been proposed by Nicoud and Poinsot [IV-26] and Giauque et al. ([IV-31], [IV-32]). It is suggested to derive the acoustic energy budget from simulation data generated with Large Eddy Simulation (LES). Indeed, with computational fluid dynamics a complete closure of the energy budget should be possible, and all terms appearing in the budget may be analyzed in great detail.

It was important to note that the energy e_1 is not an appropriate measure of the fluctuation activity in a non-isentropic flow [IV-26]. Another quantity was used in the case of reacting flows to characterize the global amount of fluctuations properly and this energy included entropy fluctuations. A proper energy definition in reacting flows that includes not only velocity ($\bar{u}_1$) and pressure (p_1) perturbations, but also entropy (s_1) given by Chu [II-87]. It is not very well known in the combustion community but Poinsot and Nicoud ([II-86], [IV-26]) elaborated the **classical Chu formulation** and gave an **extended Chu's criterion**.

Using the equation for the sensible energy e_s (IV-27) and considering zero volume heat sources ($\dot{Q} = 0$), zero volume forces ($f_k = 0$), replacing $\sigma_{ij} = \tau_{ij} - p\delta_{ij}$, negligible viscous forces that is

no viscous stresses are retained in the volume ($\tau_{ij} = 0$; μ=0) and if all species have the same sensible enthalpy $\sum_{k=1}^{N} h_{s,k} Y_k V_{k,i} = h_s \sum_{k=1}^{N} Y_k V_{k,i} = 0$, yields:

$$\rho \frac{De_s}{Dt} = \dot{\omega}_T + \frac{\partial}{\partial x_i}\left(\lambda \frac{\partial T}{\partial x_i}\right) - p\frac{\partial u_i}{\partial x_i} \tag{IV-51}$$

To construct a *fluctuation energy* (FE) , the entropy contribution can now be defined by Gibbs equation:

$$de_s = Tds + \frac{p}{\rho^2} d\rho \tag{IV-52}$$

then

$$\rho \frac{De_s}{Dt} = \rho\left[\frac{\partial e_s}{\partial t} + u_i \frac{\partial e_s}{\partial x_i}\right] = \rho\left[\left(T\frac{\partial s}{\partial t} + \frac{p}{\rho^2}\frac{\partial \rho}{\partial t}\right) + u_i\left(T\frac{\partial s}{\partial x_i} + \frac{p}{\rho^2}\frac{\partial \rho}{\partial x_i}\right)\right]$$
$$= \rho T\frac{\partial s}{\partial t} + \frac{p}{\rho}\frac{\partial \rho}{\partial t} + \rho u_i T\frac{\partial s}{\partial x_i} + u_i \frac{p}{\rho}\frac{\partial \rho}{\partial x_i}$$

Using this last expression, using the continuity equation and the state equation ($\rho T = \frac{p}{R_g}$), yields:

$$\frac{Ds}{Dt} = \frac{r}{p}\left[\dot{\omega}_T + \nabla \cdot \left(\lambda \overline{\nabla} T\right)\right] \tag{IV-53}$$

Multiplying equation (IV-53) by $\frac{ps}{R_g c_p}$ and adding it to equation (IV-34) directly gives:

$$\rho \frac{D\left(\frac{\overline{u}^2}{2}\right)}{Dt} + \frac{1}{\rho c^2}\frac{D\left(\frac{p^2}{2}\right)}{Dt} + \frac{p}{R_g c_p}\frac{D\left(\frac{s^2}{2}\right)}{Dt} + \nabla \cdot \left(p\overline{u}\right) = \frac{(s+r)}{c_p}\left[\dot{\omega}_T + \nabla \cdot \left(\lambda \overline{\nabla} T\right)\right] \tag{IV-54}$$

This equation is exact and can be linearized around the mean state splitting the density (ρ), the velocity ($\overline{u}$), the pressure (p), the entropy (s), the heat release ($\dot{\omega}_T$) and the temperature (T) into a mean (index 0) and a fluctuating (index 1) component.
Approximating the total derivate of $\overline{u}^2$ by its partial derivate and neglecting higher-order terms, can be obtained:

$$\rho \frac{D\left(\frac{\bar{u}^2}{2}\right)}{Dt} \approx \rho_0 \frac{\partial\left(\frac{\bar{u}_1^2}{2}\right)}{\partial t}$$

Using the linearization of s (=s_0+s_1) and equation (IV-53), yields:

$$\frac{Ds}{Dt} = \frac{Ds_0}{Dt} + \frac{Ds_1}{Dt} = \frac{r}{p}\left[\dot{\omega}_T + \nabla \cdot \left(\lambda \overline{\nabla} T\right)\right]$$

where the total derivate of s_0 is

$$\frac{Ds_0}{Dt} = \bar{u}_1 \cdot \overline{\nabla} s_0$$

then it gives

$$\frac{Ds_1}{Dt} \approx \frac{R_g}{p}\left[\dot{\omega}_T^1 + \nabla \cdot \left(\lambda \overline{\nabla} T_1\right)\right] - \frac{Ds_0}{Dt} = \frac{R_g}{p}\left[\dot{\omega}_T^1 + \nabla \cdot \left(\lambda \overline{\nabla} T_1\right)\right] - \bar{u}_1 \cdot \overline{\nabla} s_0$$

This last equation shows that the acoustic modes are not isentropic when unsteady heat release ($\dot{\omega}_T^1$) and/or a mean entropy gradient ($\overline{\nabla} s_0$) are present.
With (s=s_0+s_1)

$$\frac{D\left(\frac{s^2}{2}\right)}{Dt} = \frac{D\left(\frac{s_1^2}{2}\right)}{Dt} + \frac{D(s_1 s_0)}{Dt} + \frac{D\left(\frac{s_0^2}{2}\right)}{Dt}$$

the following equation holds to third order

$$\frac{p}{R_g c_p} \frac{D\left(\frac{s^2}{2}\right)}{Dt} \approx \frac{p_0}{r c_p} \frac{\partial\left(\frac{s_1^2}{2}\right)}{\partial t} + \frac{1}{c_p}\left[\dot{\omega}_T^1 + \nabla \cdot \left(\lambda \overline{\nabla} T_1\right)\right] + \left(\frac{p_0}{r c_p} s_1\right) \bar{u}_1 \cdot \overline{\nabla} s_0$$

Finally, the linearized form of equation (IV-54) becomes:

$$\rho_0 \frac{\partial\left(\frac{\bar{u}_1^2}{2}\right)}{\partial t} + \frac{1}{\rho_0 c_0^2} \frac{\partial\left(\frac{p_1^2}{2}\right)}{\partial t} + \frac{p_0}{r c_p} \frac{\partial\left(\frac{s_1^2}{2}\right)}{\partial t} + \nabla \cdot \left(p_1 \bar{u}_1\right) = \frac{T_1}{T_0}\left[\dot{\omega}_T^1 + \nabla \cdot \left(\lambda \overline{\nabla} T_1\right)\right] - \left(\frac{p_0}{r c_p} s_1\right) \bar{u}_1 \cdot \overline{\nabla} s_0 \quad \text{(IV-55)}$$

and then

$$\frac{\partial e_{tot}}{\partial t} + \nabla \cdot \left(p_1 \bar{u}_1\right) = \frac{T_1}{T_0}\left[\dot{\omega}_T^1 + \nabla \cdot \left(\lambda \overline{\nabla} T_1\right)\right] - \left(\frac{p_0}{R_g c_p} s_1\right) \bar{u}_1 \cdot \overline{\nabla} s_0 \quad \text{(IV-56)}$$

where the **fluctuation energy** e_{tot} (**FE**)[5] now integrates velocity, pressure and entropy fluctuations:

$$e_{tot} = \rho_0 \frac{\overline{u}_1^2}{2} + \frac{1}{\rho_0 c_0^2} \frac{p_1^2}{2} + \frac{p_0}{R_g c_p} \frac{s_1^2}{2} = e_1 + \frac{p_0}{R_g c_p} \frac{s_1^2}{2} \tag{IV-57}$$

and now the source term r_1 is written:

$$r_1 = \frac{T_1}{T_0}\left[\dot{\omega}_T^1 + \nabla \cdot \left(\lambda \overline{\nabla} T_1\right)\right] - \left(\frac{p_0}{R_g c_p} s_1\right) \overline{u}_1 \cdot \overline{\nabla} s_0 \tag{IV-58}$$

It is notable that the diffusive terms can be written as follows:

$$T_1 \nabla \cdot \left(\lambda \overline{\nabla} T_1\right) = \lambda \nabla \cdot \left(T_1 \overline{\nabla} T_1\right) - \lambda \left(\overline{\nabla} T_1\right)^2$$

and under the zero Mach number assumption, the mean pressure field p_0 is constant so that

$$\overline{\nabla} s_0 = \frac{c_p}{T_0} \overline{\nabla} T_0$$

If we consider the case with the viscous forces ($\mu \neq 0$) and the viscous stresses ($\tau_{ij} \neq 0$) in the volume the complete **fluctuation acoustic equation** (**FEE**) is:

$$\frac{\partial e_{tot}}{\partial t} + \nabla \cdot \left(p_1 \overline{u}_1\right) = \frac{T_1}{T_0}\left[\dot{\omega}_T^1 + \nabla \cdot \left(\lambda \overline{\nabla} T_1\right)\right] - \left(\frac{p_0}{r c_p} s_1\right) \overline{u}_1 \cdot \overline{\nabla} s_0 + \overline{u}_1 \cdot \left(\overline{\nabla} \cdot \overline{\tau}_1\right) \tag{IV-59}$$

The equation (IV-56) generalizes the classic acoustic energy form (IV-35) to the case of entropy/acoustic fluctuations and degenerates naturally to it in isentropic flows (s_1=0).
At this point the fluctuation energy equation may be integrated over the whole volume V of the combustor and may be averaged time over a period of oscillation, as (IV-42), yields:

$$\frac{dE_1}{dt} + F_1 = R_1 \tag{IV-60}$$

The source term is obtained by setting viscosity coefficient λ to zero (λ=0):

$$R_1 = \frac{1}{\tau} \int_V \int_0^\tau r_1 dt\, dV = \frac{1}{\tau} \frac{1}{T_0} \int_V \int_0^\tau \left(T_1 \dot{\omega}_T^1 - \frac{p_0 T_0}{R_g c_p} s_1 \overline{u}_1 \cdot \overline{\nabla} s_0\right) dt\, dV$$

[5] Another expression ([II-86], [IV-26]) for e_{tot} is : $e_{tot} = \rho_0 \frac{\overline{u}_1^2}{2} + \frac{c_0^2}{\gamma \rho_0} \frac{\rho_1^2}{2} + \frac{\rho_0 c_v}{T_0} \frac{T_1^2}{2}$

The second term of R_1 expression was not present in Chu's article [II-87] and does not seem to have been discussed earlier than Poinsot and Nicoud ([II-86], [IV-26]). It describes how the overall fluctuation energy decrease when a positive fluctuation of entropy (s_1>0) is convected toward region with larger mean entropy ($\bar{u}_1 \cdot \bar{\nabla} s_0 > 0$), which is an expected result. A rough estimate of the order of magnitude of this term (without accounting for the phase shifts between the different terms) shows that the additional term related to the nonuniform mean entropy field is potentially larger than the classic Rayleigh term [IV-26]. Specific postprocessing of unsteady LES data is necessary to address this issue more precisely.
The instability criterion predicts that the combustion will be unstable if the source terms (R_1) due to combustion must be larger than the acoustic losses (F_1):

$$\boxed{\frac{1}{T_0}\int_V \int_0^\tau \left(T_1 \dot{\omega}_T^1 - \frac{p_0 T_0}{R_g c_p} s_1 \bar{u}_1 \cdot \bar{\nabla} s_0 \right) dt\, dV > \int_A \int_0^T p_1 \bar{u}_1\, dt\, dA} \qquad \text{(IV-61)}$$

IV.7.4 Considerations about criteria from energy equations

Two forms of energy have been defined: the first is the classic acoustic energy (AE) introduced by various authors, the second is the fluctuation energy (FE) presented by Chu [II-87].

Classic acoustic energy (AE)	$e_1 = \rho_0 \frac{\bar{u}_1^2}{2} + \frac{1}{\rho_0 c_0^2} \frac{p_1^2}{2}$
Fluctuation energy (FE)	$e_{tot} = \rho_0 \frac{\bar{u}_1^2}{2} + \frac{1}{\rho_0 c_0^2} \frac{p_1^2}{2} + \frac{p_0}{R_g c_p} \frac{s_1^2}{2}$

Table IV-1: Definitions of *classic acoustic energy* (AE) and *fluctuation energy* (FE).

The AE form uses only two variables (velocity and pressure) perturbations, while FE form uses the fluctuations of three variables (velocity, pressure and entropy).
The fact that entropy is present in this extended energy does not mean that the entropy mode of fluctuation has been added to the analysis [IV-26], because the zero Mach number was still used for the linearization process leading to the extended form of e_{tot}. This means that only acoustic fluctuations are oscillating over time because the entropy and vertical modes correspond to the null frequency.
The two different expressions of acoustic energy (Table IV-1) lead to two energy equations (Table IV-2) and to different instability criteria (Table IV-3) in the simplest case where thermal diffusivity (α) and viscosity (τ_{ij}) are both zero and mean entropy s_0 is constant.

Acoustic energy equation (AEE)	$\frac{\partial e_1}{\partial t} + \nabla \cdot (p_1 \bar{u}_1) = \frac{(\gamma - 1)}{\gamma\, p_0}\left[\dot{\omega}_T^1 + \nabla \cdot (\lambda \bar{\nabla} T_1)\right]$
Fluctuation energy equation (FEE)	$\frac{\partial e_{tot}}{\partial t} + \nabla \cdot (p_1 \bar{u}_1) = \frac{T_1}{T_0}\left[\dot{\omega}_T^1 + \nabla \cdot (\lambda \bar{\nabla} T_1)\right] - \left(\frac{p_0}{R_g c_p} s_1\right) \bar{u}_1 \cdot \bar{\nabla} s_0$

Table IV-2: Conservation equations for acoustic energy (AE) and fluctuation energy (FE).

The combustion instability occurs if the combustion source terms (R_1) overcome acoustic losses (F_1). Instability criteria are obtained by setting viscosity coefficient λ to zero (λ=0).

	Criteria for combustion instability	
Classical Rayleigh's criterion	$R_1 > 0$	$\int_V \int_0^\tau p_1 \dot{\omega}_T^1 \, dt\, dV > 0$
Extended Rayleigh's criterion	$R_1 > F_1$	$\frac{(\gamma - 1)}{\gamma\, p_0} \int_V \int_0^\tau p_1 \dot{\omega}_T^1 \, dt\, dV > \int_A \int_0^T p_1 \bar{u}_1 \, dt\, dA$
Classical Chu's criterion	$R_1 > F_1$	$\frac{1}{T_0} \int_V \int_0^\tau \left(T_1 \dot{\omega}_T^1\right) dt\, dV > \int_A \int_0^T p_1 \bar{u}_1 \, dt\, dA$
Extended Chu's criterion	$R_1 > F_1$	$\frac{1}{T_0} \int_V \int_0^\tau \left(T_1 \dot{\omega}_T^1 - \frac{p_0 T_0}{R_g c_p} s_1 \bar{u}_1 \cdot \bar{\nabla} s_0\right) dt\, dV > \int_A \int_0^T p_1 \bar{u}_1 \, dt\, dA$

Table IV-3: Summary criteria for combustion instability for zero viscosity coefficient (μ), zero thermal diffusivity (α) and constant mean entropy (s_0).

Interestingly, the **Rayleigh's criterion** predicts instability when pressure (p_1) and heat release ($\dot{\omega}_T^1$) fluctuations are in phase, while the **classical Chu's criterion** requires temperature (T_1) and heat release fluctuations ($\dot{\omega}_T^1$) to be in phase for the instability to grow.
The expression of integrated equation obtained by Chu suggests that the classic Rayleigh's criterion $\int_V \int_0^\tau p_1 \dot{\omega}_T^1 \, dt\, dV$ should be replaced by $\int_V \int_0^\tau T_1 \dot{\omega}_T^1 \, dt\, dV$ to characterize the stability of a combustor.
The Chu's criterion extends the classic Rayleigh's criterion to the case where the net energy flux at the boundaries can not be neglected and the entropy fluctuations are significant. It extended the analysis to the case where the entropy field is not constant over space, which is always the case when combustion occurs.
When acoustics and combustion get strongly coupled, oscillating regimes called combustion instabilities are observed. The mechanism leading to instability are numerous and many of them are still unknown so that is no reliable method to predict the occurrence and the characteristics of combustion instabilities without first firing the combustor.
The Rayleigh's criterion being derived in a linear framework, its application to *limit cycles* could also be misleading, then it is necessary to understand the mechanisms creating the instability and

not only their manifestation through Rayleigh-type criteria. This can be achieved experimentally by *studying combustion instabilities during their initial linear phase*.
An important approach is to use theoretical and numerical approaches of Chu type expressions to derive an exact solution of the problem, and not just a part of it like the Rayleigh's criterion approach.
Nicoud and Poinsot ([II-86] and [IV-26]) showed that *only FE form should be used in flames*, in contradiction to many current studies performed for combustion instabilities. This can be showed by pursing the simple case of a domain with zero fluxes on boundaries and no combustion source term. In this situation the energy should only decrease and this decrease should be caused by dissipation. For simplification, the thermal diffusivity (α) and molecular viscosity (μ) are assumed to be constant for this example, and the gradients of the mean entropy (s_0) and heat capacity ratio (γ) are neglected. A revelant question is then to determinate which of the two forms in the Table IV-1 is the most adequate. According to Chu's definition [II-87], a "good" fluctuation energy should be *"a positive quantity characterizing the mean level of fluctuations which, in the absence of heat transfer at boundaries and of work done by boundary or body forces and in the absence of heat and material sources, is a monotone non-increasing function of time"*, then the energy should only decrease in this situation and this decrease should be caused by dissipation.
For clarity, the thermal diffusivity (α) is assumed to be constant for this example, and the gradients of the mean entropy so are neglected ($\overline{\nabla} \cdot s_0 = 0$). Starting from the equations of Table IV-2, integrating over the whole domain and setting $\dot{\omega}_T^1$ and all boundary fluxes to zero ($\dot{\omega}_T^1 = 0$; $\nabla \cdot (\ ) = 0$) leads to the following equations:

$$\frac{\partial}{\partial t}\int_A e_1 \, dA = -\lambda \frac{\gamma - 1}{\gamma \, p_0} \int_A \nabla p_1 \nabla T_1 \, dA \tag{IV-62}$$

$$\frac{\partial}{\partial t}\int_A e_{tot} \, dA = -\lambda \frac{1}{T_0} \int_A \left(\nabla T_1\right)^2 dA \tag{IV-63}$$

since the following terms can be written:

$$p_1 \nabla \cdot \left(\lambda \overline{\nabla} T_1\right) = \lambda \nabla \cdot \left(p_1 \overline{\nabla} T_1\right) - \lambda \left(\overline{\nabla} p_1\right) \cdot \left(\overline{\nabla} T_1\right)$$
$$T_1 \nabla \cdot \left(\lambda \overline{\nabla} T_1\right) = \lambda \nabla \cdot \left(T_1 \overline{\nabla} T_1\right) - \lambda \left(\overline{\nabla} T_1\right)^2$$

If the flow is isentropic, pressure (p_1) and temperature (T_1) fluctuations are in phase and the right-hand side of equation (IV-62) is always negative so that the acoustic energy (AE) form e_1 is a proper estimate of energy. In all other cases (e.g. non-isentropic), however, the right-hand side of equation (IV-62) can take any sign, increasing or decreasing the energy and making the AE form e_1 a quantity of limited interest. On the other hand the term of extended Chu's equation (IV-63) integrated over the whole domain is truly dissipative term in all flows, even if they are non-isentropic.
Then a better understanding of the underlying physics can be obtained by using the fluctuation energy equation (FEE) rather than Rayleigh's criterion and the classic acoustic energy equation (AEE) to analyze the Large Eddy Simulation (LES) numerical results.

Postprocessing of LES fields of compressible reacting turbulent flows is needed to estimate the magnitude of the different terms of the criterion derived for the FE form, equation (IV-61). Specifically, such data would be necessary to study the behaviour of $T_1\dot{\omega}_T^1$ term with respect to its classic $p_1\dot{\omega}_T^1$ counterpart, as well as the magnitude of the term related to the mean entropy gradient.
Finally it is shown that the usual Rayleigh term is the source term (R_1) of this equation, but that another term (acoustic losses, F_1) plays a significant role in the budget of this equation. It also show that the AE form is insufficient to describe fluctuations in the flames where entropy waves play a role.

IV.7.5 Extended analysis for non-zero mean flow

Nicoud and Poinsot ([II-86] and [IV-26]) rederived the fluctuating energy equation of Chu and argued that **the Rayleigh's criterion is an incomplete description of the significant sources of fluctuating energy in combustion**. Entropy disturbances through the flame were argued to be a significant source of disturbance energy, but Nicoud and Poinsot's formulation was conceptually problematic because they assumed zero-mean flow quantities.
Dowling [II-134] showed that terms other than the Rayleigh's term existed for their differently defined acoustic energy equation, but she argued that these terms were small in practice.
Recently Giauque et al. [IV-31] showed that any equation stating disturbance energy conservation in combustion flows must start from equations of motion that at least include non-zero mean flow quantities and entropy variation. He considered a ducted premixed propane-air flame in a 2-D planar computational mesh resolved by a 50000 nodes mesh. Order of magnitude analysis suggests that the viscous stress, thermal diffusion and viscous dissipation terms are usually small in combustion. Some terms are 1000 times (or more) smaller than $\frac{dE_1}{dt}$ and do not contribute to the global budget. The numerical results of Giauque et al. suggest that the time evolution of the global fluctuating energy is mostly governed by the heat release ($\dot{\omega}_T^1$), heat flux $\nabla\cdot\left(\lambda\overline{\nabla}T_1\right)$ and entropy (s_1) source terms, the contribution arising from the mixture changes over space and time being the largest of the negligible terms.
Giauque et al. [IV-31] have identified additional and significant energy density, flux and source terms, thereby generalizing the recent results of Nicoud and Poinsot ([II-86], [IV-26]) to include non-zero mean flow quantities, large amplitude disturbances and varying specific heats. The associated stability criterion is therefore significantly different from the Rayleigh's criterion in several ways. The closure of the exact equation is performed on an oscillating 2-D laminar flame. Results show that in this case the general equation can be substantially simplified by considering only entropy, heat release and heat flux terms. The first one behaves as source term whereas the latter two dissipate the disturbance energy.
The most recent results [IV-32] confirm the importance of the entropy fluctuations and the non-linear terms. However, it is also pointed out that to account for these terms is analytically tedious and numerically challenging. It remains to be seen whether stability analysis for systems of practical interest can profit from these developments.

Stability criteria which are like the Rayleigh's criterion based on relative phases between fluctuations of velocity, pressure, fuel concentration, heat release rate, entropy, etc., have developed and used by Richards and Janus [II-30], Lawn et al. ([I-25], [I-26], [I-27], [I-28], [I-29], [IV-34]) and Polifke et al. ([IV-35], [IV-36]). Such criteria are certainly helpful for qualitative analysis of relevant feedback mechanisms, but one must be aware of their limitations. Phased-based criteria can be overly pessimist regarding the stability of a combustion system, because they cannot include the stabilizing effects of loss of acoustic energy.

References

[IV-1] Mühlbauer B., Ewert R., Kornow O., Noll B., Delfs J., Aigner M., "Simulation of combustion noise using CAA with stochastic sound sources from RANS", 14th AIAA/CEAS Aeroacoutics Conference, Vancouver, 2008.

[IV-2] Bui T.Ph., Schroder W., Meinke M., "Numerical analysis of the acoustic field of reacting flows via acoustic perturbation equations", Computers & Fluids, Vol. 37, pp. 1157–1169, 2008.

[IV-3] Mahan J.R., Program "COMMODE" (gas turbine COMbustor acoustic MODE predictor), Users' Manual prepared under contract to the General Electric Company, October 1980.

[IV-4] Mahan J.R. and Kasper J.M., "Influence of Heat Release Distribution on the Acoustic Response of Long Burners", ASME Paper No. 79-DET-31, Design Engineering Technical Conference, St . Louis, MO, 10-12 September 1979.

[IV-5] Mahan J.R., Jones J.D., Blevins L.R ., Cline J.G., "Mesure Indirecte du Spectre de Rendement Thermo-Acoustique d'un Brcleur Turbulent Long" (in French) La Recherche AGrospatiale, vol. 4, pp. 311-321, July-August 1983.

[IV-6] Mahan J.R. and Jones J.D., "Recovery of Acoustic Source Structure in a Long Turbulent Burner from Far-Field Sound Spectra", AIAA Paper 83-0763, AIAA 8th Aeroacoustics Conference, Atlanta, GA, 11-13 April 1983, (scheduled for publication in May 1984 AIAA Journal).

[IV-7] Zhu M., Bray K.N.C. and Dowling A., "Forced oscillations in combustors with spray atomizers", Journal of Engineering for Gas Turbines and Power, vol.124, Issue 1, pp.20-30, 2002.

[IV-8] Balachandran R., Ayoola B., Kaminski C., Dowling A., Mastorakos E., "Experimental investigation of the nonlinear response of turbulent premixed flames to imposed inlet velocity oscillations", Combustion and Flame, vol.143, Issue 1-2, pp.37-55, October 2005.

[IV-9] Nicoud F. and Poinsot T., "Thermoacoustic instabilities: Should the Rayleigh criterion be extended to include entropy changes?", Combustion and Flames, vol. 142, pp.153-159, 2005.

[IV-10] Ho C.M. and Huerre P., "Perturbed free shear layer", Annual Review of Fluid Mechanics, vol.16, pp.365-424, 1984.

[IV-11] Poinsot T., Angelberger C., Egolfopoulos F., Veynante D., "Large Eddy Simulations of combustion instabilities", 1st International Symposium on Turbulence and Shear Flow Phenomena, pp.1-6, Santa Barbara, USA,1999.

[IV-12] Baum J.D. and Levine J.N., "Numerical techniques for solving nonlinear instability problems in solid rocket motors", AIAA Journal, vol.20, pp. 955-961, 1982.

[IV-13] Kailasanath K., Garder J.H., Oran E.S., Boris J.P., "Numerical Simulations of unsteady reactive flows in a combustion chamber", Combustion and Flame, vol.86, pp.115-134, 1991.

[IV-14] Strahle W.C. and Muthukrishnan M., "Correlation of Combustor Rig Sound Power Data and Theoretical Basis of Results", AIAA Journal, vol. 18, Issue 3, pp. 269-274, March 1980.

[IV-15] Ho P.Y. And Doyle V.L., "Combustion Noise Prediction Update", AIAA Paper 79-0588, March 1979.

[IV-16] Rajaram R., "Frequency Scaling of Turbulent Premixed Flame Noise", AIAA-2005-2828, 11th AIAA/CEAS Aeroacoustics Conference (26th AIAA Aeroacoustics Conference), Monterey, California, 23-25 May 2005.

[IV-17] Belliard A., "Etude expérimentale de l'émission sonore des flammes turbulentes", PhD Dissertation, Universités d'Aix-Marseille, 1997.

[IV-18] Rajaram R. and Lieuwen T., "Parametric Studies of Acoustic Radiation from Turbulent Premixed Flames", Combustion Science and Technology, Vol. 175, Issue 12, pp. 2269-2298, 2003.

[IV-19] Wäsle J., Winkler A. and Sattelmayer T., "Influence of the Combustion Mode on Acoustic Spectra of Open Turbulent Swirl Flames", Twelfth International Conference on Sound and Vibration, 2005.

[IV-20] Clavin P., "Dynamics of Combustion Fronts in Premixed Gases: From Flames to Detonations", Twenty-Eighth International Symposium on Combustion, 2000.

[IV-21] Huff R.G., "Theoretical Prediction of the Acoustic Pressure Generated by Turbulence-Flame Front Interactions", Journal of Vibration, Acoustics, Stress, and Reliability in Design, Vol. 108, Issue 3, pp. 315-321, 1986.

[IV-22] Boineau P., "Modélisation et étude expérimentale des sources acoustiques entropiques en combustion turbulente", Phd thesis, Université de Poitiers, 1997.

[IV-23] Kotake S., "On combustion noise related to chemical reactions", Journal of Sound Vibration, vol. 42, pp. 399-410, 1975.

[IV-24] Landau L. and Lifchitz E., "Physique Theorique – Tome 6 : Mecanique des Fluides", Ed. Librairie du Globe-Editions MIR, 1984.

[IV-25] Kuo K. K., "Principles of Combustion", John Wiley, New York, 1986.

[IV-26] Nicoud F. and Poinsot T., "Thermoacoustic instabilities: Should the Rayleigh criterion be extended to include entropy changes?", Combustion and Flames, vol. 142, pp.153-159, 2005.

[IV-27] Culick, F.E.C., "Nonlinear behaviour of acoustic waves in combustion chambers, Parts I and II", Acta Astronautica vol.3, pp.714-757, 1976.

[IV-28] Samaniego J. M., Yip B., Poinsot T. and Candel S., "Low-frequency combustion instability mechanism in a side-dump combustor", Combustion and Flame, vol. 94, Issue 4, pp.363-381, 1993.

[IV-29] Ibrahim Z.M., Williams F.A., Buckley S.G. and Lee J.C.Y., "An acoustic energy approach to modelling combustion oscillations", Proceeding of 51th ASME International Gas Turbine & Aeroengine Congress & Exposition, ASME GT2006-90956, Barcelona, Spain, May 2006.

[IV-30] Ibrahim Z.M., Williams F.A., Buckley S.G. and Twardochleb C.Z., "A method for estimating the onset of acoustic instabilities in premixed gas-turbine combustion", Proceeding of 51th ASME International Gas Turbine & Aeroengine Congress & Exposition, ASME GT2007-27037, Montreal, Canada, 14-17 May 2007.

[IV-31] Giauque A., Poinsot T., Brear M. and Nicoud F., "Budget of disturbance energy in gaseous reacting flows", Proceedings of the Summer Program 2006, Center for Turbulence Research, NASA Ames/Stanford University, CA, USA, 2006.

[IV-32] Giauque A., Nicoud F. and Brear M., "Numerical assessment of stability criteria from disturbance energies in gaseous combustion", 13th AIAA/CEAS AeroAcoustics Conference, number AIAA-2007-3425, Rome, Italy, 21-23 May 2007.

[IV-33] Polifke W., "System modelling and stability analysis", Basics of Aero-Acoustics and Thermo-Acoustics, VKI LS 2007-09, Von Karman Institute, Brussels, BE, 3-7 December 2007

[IV-34] Savarianandam V.R. and Lawn C.J., "Thermoacoustic response of premixed turbulent flames in the weakly wrinkled regime", Proceedings of the Combustion Institute, vol. 31, Issue 1, pp.1419-1426, January 2007.

[IV-35] Polifke W., Paschereit C.O., Döbbeling K., "Constructive and destructive interference of acoustic and entropy waves in a premixed combustor with a choked exit", International Journal of Acoustics and Vibration, vol.6, Issue 3, pp.135-146, 2001.

[IV-36] Polifke W. and Lawn C.J., "On the Low Frequency Limit of Flame Transfer Functions", Combustion and Flame, vol.151, Issue 3, pp.437-451, 2007.

V. An application of instability control to Heavy Duty Gas Turbine: Siemens Vx4.3A

V.1 Siemens type Vx4.3A gas turbine

Siemens heavy duty gas turbines have been well known for their high power output combined with high efficiency and reliability for more than 30 years. Offering state of the art technology at all times, the requirements of the cooling and sealing air systems have increased with technological development over the years. In particular, the increase of turbine inlet temperature and reduced nitrous oxides emissions requirements demand a highly efficient cooling and sealing air system.
The new **Vx4.3A family** with an ISO turbine **inlet temperature of 1190 °C** work in the electric **power range of 70 to 270 MW**.
In 1995, Siemens started its first tests with the new gas-turbine family Vx4.3A in its test facility in Berlin. In contrast to the former gas-turbine family with silo-combustion chambers, annular combustion chambers were implemented to achieve an increased power density and efficiency and lower emission values. However, during the tests, combustion instabilities detrimental to a reliable operation of the gas turbines were observed. Already very early in the process of working out countermeasures against this phenomenon, it was decided that besides passive measures, such as operational modifications or an acoustic detuning by design modifications of the burner, also active measures for avoiding these instabilities should be developed and tested.
The *hybrid burner ring* (HBR) combustors of all Vx.yA engine are scaled according to the engine rotation speed and thus all have 24 geometrically scaled hybrid burners.
Fig. V-1, Tab. V-1, Tab. V-2 summarize the main performance data of the Vx4.3A series.
Fig. V-2 shows a longitudinal section through the upper half of this gas turbine. In contrast to former types of Siemens gas turbines that were fitted with silo combustion chambers, this family of gas turbines features ring combustion chambers. In total, this gas turbine comprises **24 Siemens hybrid burners** spread uniformly over the circumference of its annular combustion chamber (Fig. V-3). Any Siemens hybrid burner may be operated both on liquid and gaseous fuels.
At start-up and with gaseous fuel, the burner is operated in diffusion mode. When a specific turbine power is reached, there will be a switch-over from *pure diffusion* to so-called *mixed operation*. For this purpose, a combination of diffusion and premix flames is used. When the temperature within the combustion chamber is sufficiently high to stabilise a pure premix flame, operation is switched from this mixed mode to purely premixed operation. To stabilise the premixed flame, every Siemens hybrid burner features an additional small diffusion-based *pilot burner*. This is a diffusion burner delivering approximately 10% of the thermal power provided by the complete burner unit.
It was found that certain part load operating modes were subject to oscillations. In addition to high sound pressure levels at discrete frequencies, standing sound waves – typical of combustion instabilities – were measured; there are characterised by localised amplitude minima and maxima, also called nodes and antinodes.

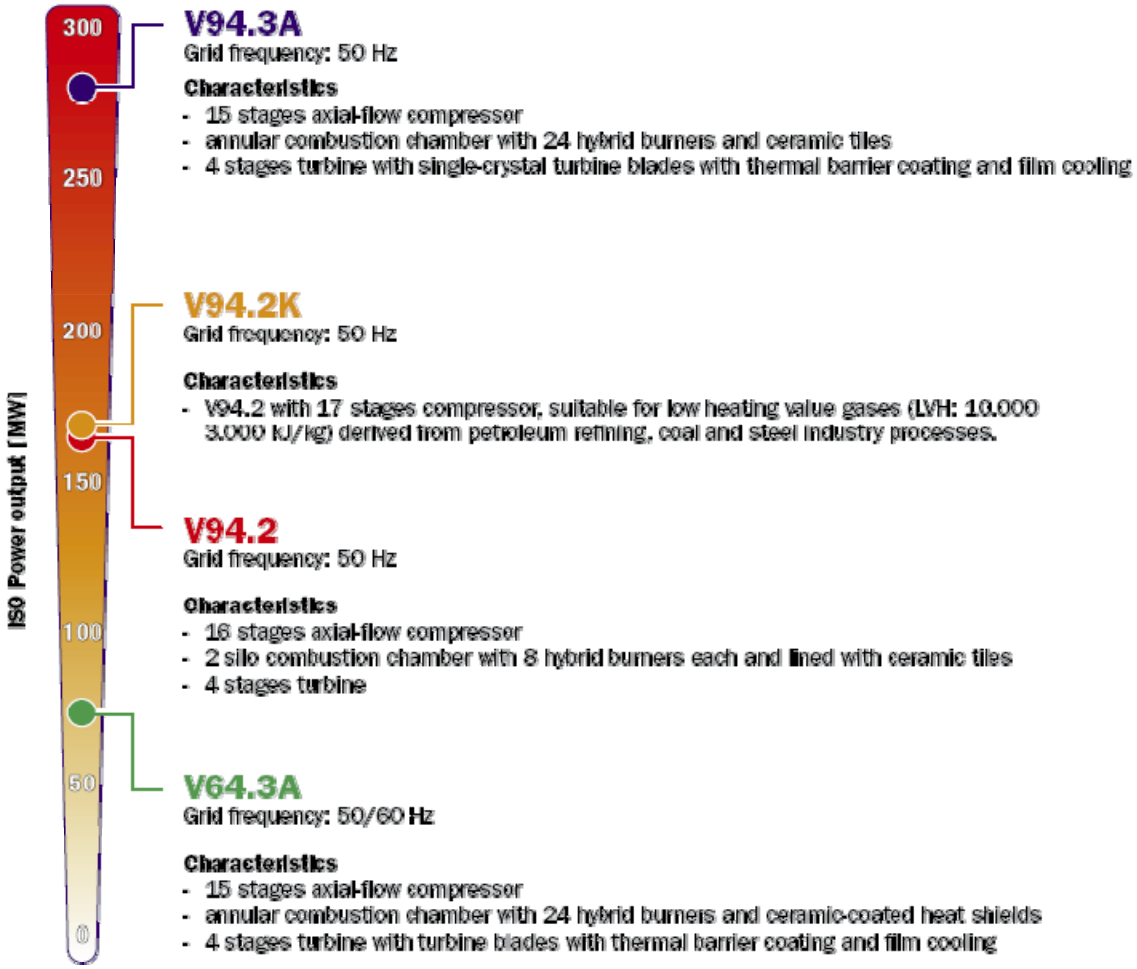

Fig. V-1: Features of Siemens-Ansaldo Turbo Gas.

Type	Electric power output [MWe]	Frequency [Hz]	Efficiency [%]
V94.3A	270	50	38
V84.3A	184	60	38
V64.3A	70	90	35

Tab. V-1: Performance Vx4.3A frames [I-24].

	50 Hz			
	V94.3A	**V94.3**	**V94.2**	**V64.3A**
Gross electric power output [MW]	266	222	159	67
Gross efficiency [%]	38.6	36.2	34.3	34.9
Gross heat rate [kJ/kWh]	9323	9945	10495	10305
Gross heat rate [Btu/kWh]	8836	9426	9947	9767
Pressure ratio	17.0	16.1	11.4	15.8

Tab. V-2: Siemens heavy duty gas turbine models [V-1].

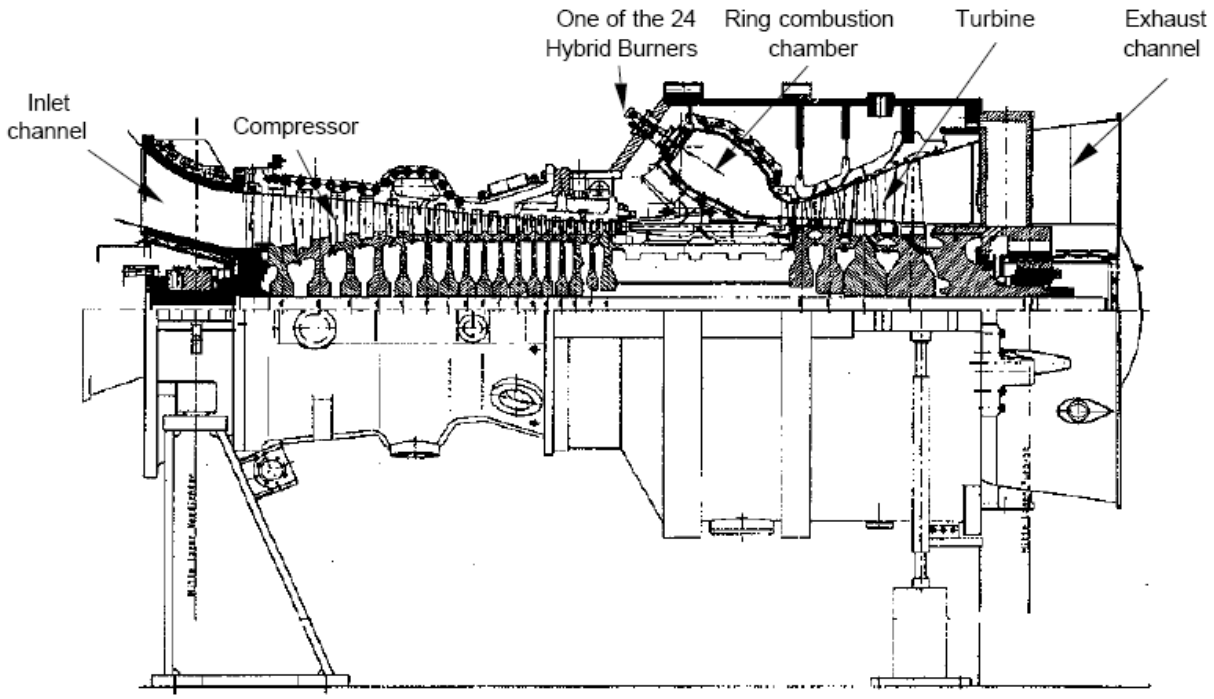

Fig. V-2: Half-section drawing of a Vx4.3A series gas turbine.

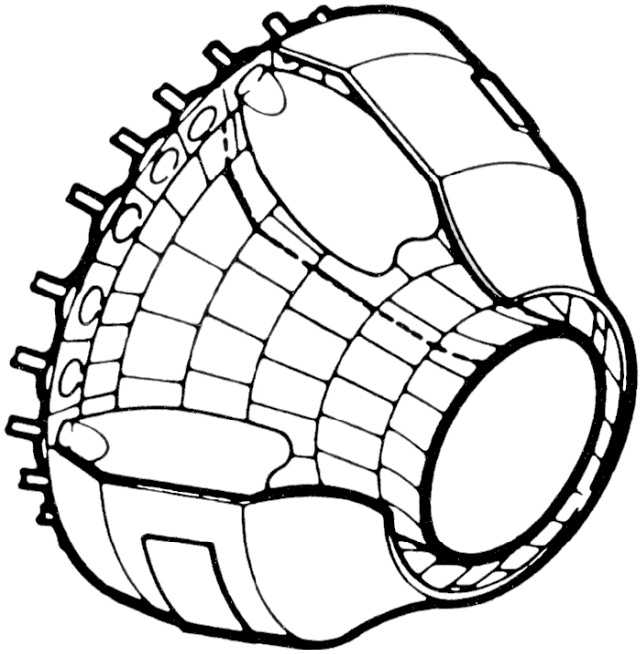

Fig. V-3: Three-dimensional drawing of the annular combustion chamber of Hybrid Burner Ring (HBR) Siemens Vx4.3A, with a total of 24 burners.

V.1.1 Combustion instabilities in Siemens type Vx4.3A gas turbine and ways of avoiding them

Basically, the possibilities available to prevent *self-excited combustion oscillations* can be subdivided into *passive* and *active* measures. For instance, increasing acoustical attenuation, acoustically detuning systems by design modifications, and operational modifications are considered passive measures. By contrast, active measures imply creating an external feedback loop using an actuator to influence combustion oscillations so as to damp them down.
The first industrial-size of an active control application was realised by Seume et al.([II-10], [III-29]) in 1997 in the test facility of Siemens on the **V84.3A** based on a land-based gas turbine delivering **160 MW** of electrical power. For this gas turbine, active control was achieved by means of anti-cyclical fuel injection, with *direct drive valves* (DDV) serving as actuators to modulate the pilot fuel. Six circumferentially mounted pressure transducers provided for the input signals of 6 independent feedback control loops, each featuring four valves. They were able to suppress the dominant frequencies at **217 Hz** and **433 Hz** by up to 86%.
This technique was then also extended to the largest type of this family of gas turbines, the **V94.3A** with an electric power output of **267 MW** ([II-34] § 19, [III-30], [III-31], [III-32], [V-2]). For the largest version of gas turbine type Vx4.3A, that is V94.3A, the eigenmode is excited at a frequency of approximating **170 Hz** (see Fig. V-4).
The equation $f = nc/(\pi d)$ provides a theoretical estimate for the characteristic acoustical frequencies of *azimuthal modes* of any annular combustion chamber. At an average combustion chamber diameter of d=3m and a speed of sound of c=844 m/s (assuming an average combustion

chamber temperature of 1500°C)[6], the resulting frequency for a V94.3A is **179 Hz** for the second harmonic (*n*=2), a value agreeing well with experimentally determined characteristic frequencies. To avoid or suppress these oscillations, various *passive* and *active control* were developed and successfully implemented.

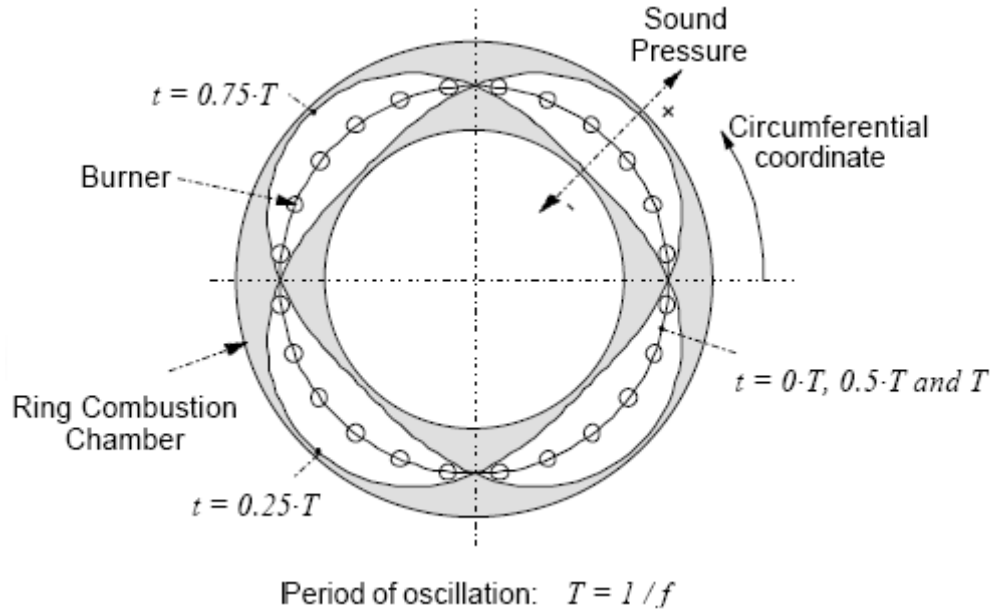

Fig. V-4: Excited azimuthal modes for the second harmonic with a frequency of 170 Hz in the V94.3A ([II-34] § 19, [III-32], [V-2]).

V.1.1.1 Passive control of Vx4.3A

Considering the fact that the generation of self-excited combustion instabilities depends on certain *time lags* (according Rayleigh criterion), selectively modifying those time lags is one possible means of suppressing combustion instabilities. The time lag most easily adapted is the **convective time lag or the time required to convey the fuel/air mixture into the combustion zone**. In order to make it possible a *cylindrical extension*, called a ***cylindrical burner outlet*** (CBO), was welded onto the burner nozzle (Fig. V-5). The length of this extension was selected so as **to prolong the convective time lag** by slightly more than on quarter of the period of self-excited oscillation.
One possible cause for fluctuations of the heat release rate of the flame and thus for combustion instabilities are periodically generated vortices (i.e. periodic vortex shedding), which can be provoked by flow disturbances in the shear layer. To prevent these flow instabilities, the cylindrical extensions attached to the burner nozzles were **inclined by 10°** in respect to the flow axis on two neighbouring burners. Owing to the angle of inclination characterising these extensions, they are designated ***asymmetric burner outlets*** (ABOs). ABOs cause an uneven shear

[6] They consider that the $\gamma * R_{gas}$ for CH_4/Air combustion is about 400 J/(kg K)

layer distribution around the burner nozzle, thus reducing the formation of coherent structures, and displace the combustion zone downstream of its former position, thus increasing the time lag. Then another passive measure taken is the use of **several burner types** characterised by differing flame frequency responses and installing burners belonging to the same type **asymmetrically**, with reference to potential azimuthal modes: if burners belonging to the same type are not precisely located, for example on the potential pressure antinodes of the azimuthal modes to be prevented, they will not be optimally excited to combustion oscillations by the prevailing acoustics. Then, to prevent the in-phase lock of all 24 burners promoting the excitation of any azimuthal mode, the burners were selected to have differential time lags, and were arranged asymmetrically within the annular combustion chamber.

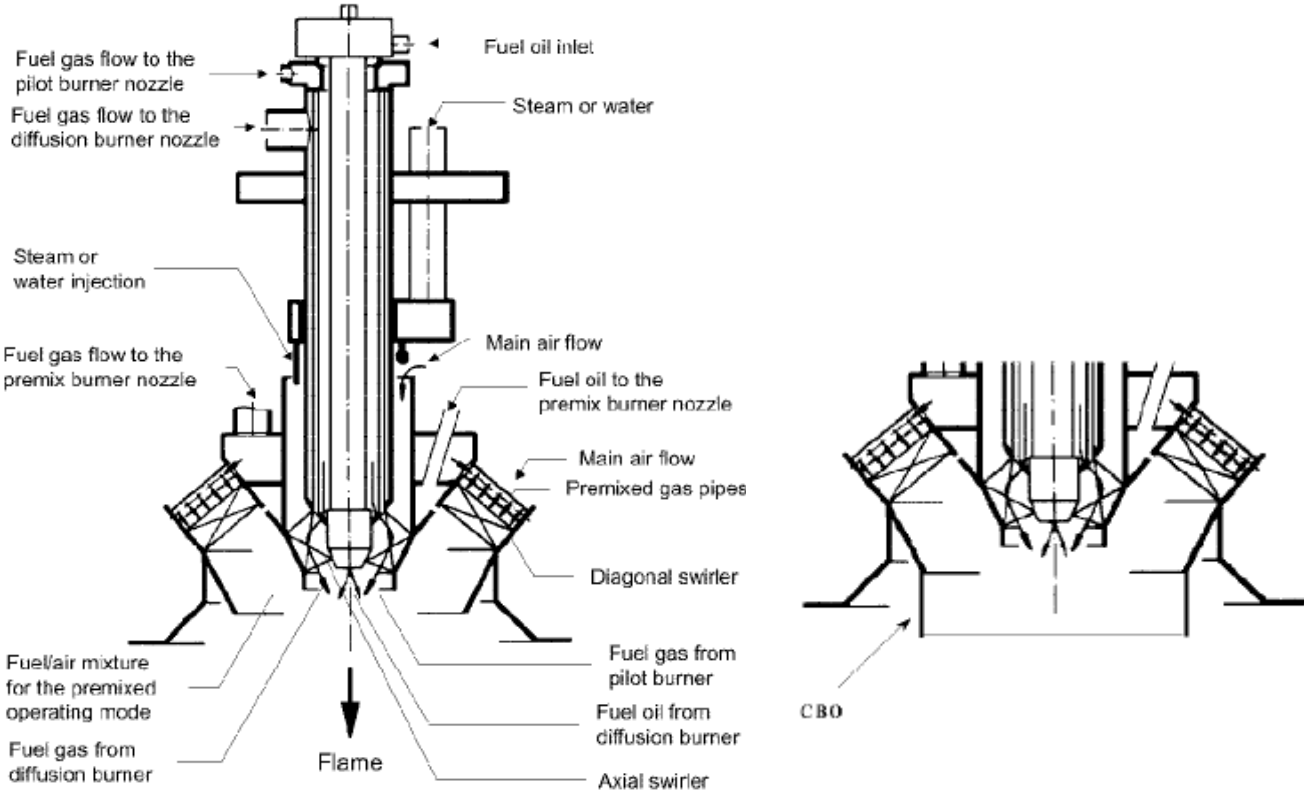

(a) (b)

Fig. V-5: The standard Siemens Hybrid Burner (a) and with schematic CBO extension (b), i.e. a cylindrical extension used to prolong the time lag required by the combustible mixture exiting the burner outlet to reach the combustion zone.

V.1.1.2 Active control of Vx4.3A

In addition to these passive control, a multi-channel *Active Instability Control* (AIC) system was implemented to achieve further damping.
In order to be able to damp combustion oscillations arising within this type of combustion chamber - appearing as azimuthal modes spreading along the circumference of the combustion chamber - every burner was fitted with a rapid ***Direct Drive Valve*** (DDV) ([II-34] § 19, [III-32], [V-2], [V-3], [V-4]): according to the frequency response of the used valve type the valves allow the control of *combustion oscillations with frequencies of up to 400 Hz*. This type of valve creates mass fuel flow modulations within the pilot gas supply of the burner which are anti-cyclical to the oscillations characterising the heat release rate within the flame, thus extinguishing them. Input signals for the feedback control system are obtained by measuring sound pressures with high temperature piezoelectric transducers within the combustion chamber indirectly at the burner flanges (Fig. V-6). In order to achieve optimum response, every single one of the 24 burners was fitted with its own actuator. Fuel supplies are normally particularly suitable for active control because, in industrial combustion systems, volume flow rates of fuel are often substantially lower than those of air: the fuel injection point **no more than 3-4% of additional fuel** will be required to control combustion oscillations.
Exploiting the symmetry characterising azimuthal modes, two actuators are driven by every feedback loop: a total of **12 control loops** were used, with each loop comprising **1 pressure sensor** and **2 valves as actuators** (Fig. V-7). In tests run on various type V94.3A gas turbines delivering up to 267 MW of electric power according to ISO, Active Instability Control (AIC) systems were used to damp successfully a great variety of combustion oscillations for several burner variants and operating points.
The results achieved by means of passive measures were improved even more by employing an active control. By using AIC in combination with the best arrangement of ABOs, it was possible to increase maximum turbine power by 3%, and in combination with the best CBO arrangement by 2%.
With the AIC off the frequency spectrum of sound pressure shows two dominant frequencies of prevailing combustion instability at 145 Hz and 290 Hz. AIC reduced the two dominant frequency peaks by 20 dB (2nd harmonic at 145 Hz) and 15 dB (3rd harmonic at 290 Hz).
The successful damping of combustion instabilities in various operating points of the gas turbine demonstrates the high flexibility of the employed active measures in dealing with this problem and allowing stable gas turbine operation over the entire range. The presented AIC system is currently being used with several V94.3A gas turbines.
This active control approach remains the first and only one which was actually applied in the field. **Over 50 engines** were equipped with this active instability control device.

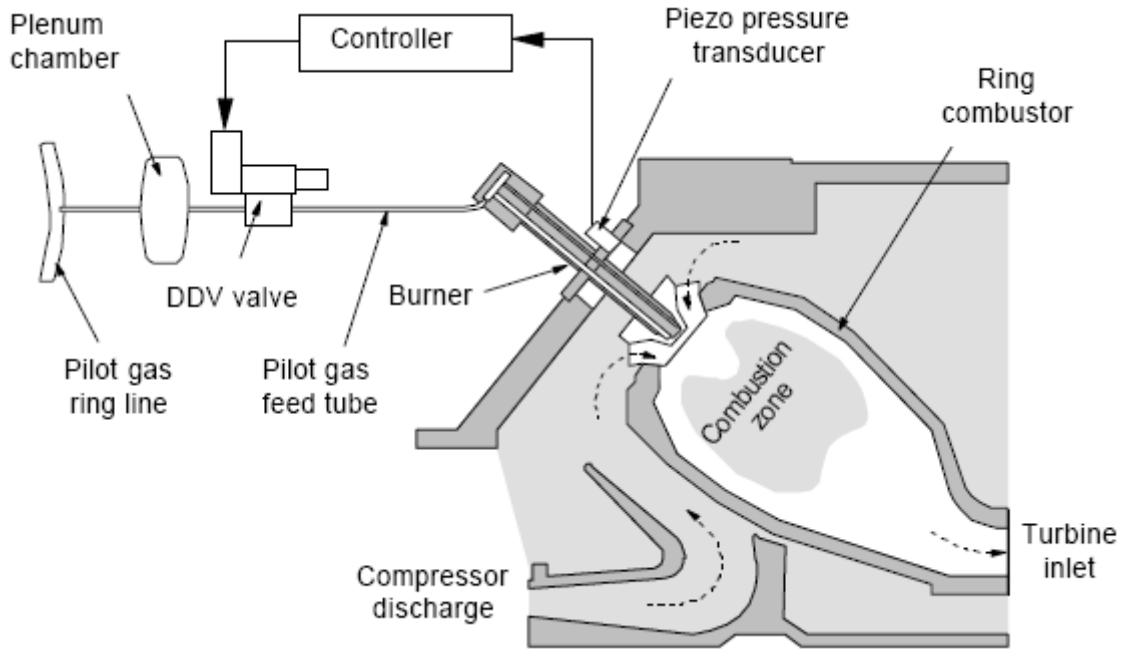

Fig. V-6: Schematic Active Instability Control (AIC) diagram of Siemens model Vx4.3A heavy duty gas turbine ([III-32], [V-2]).

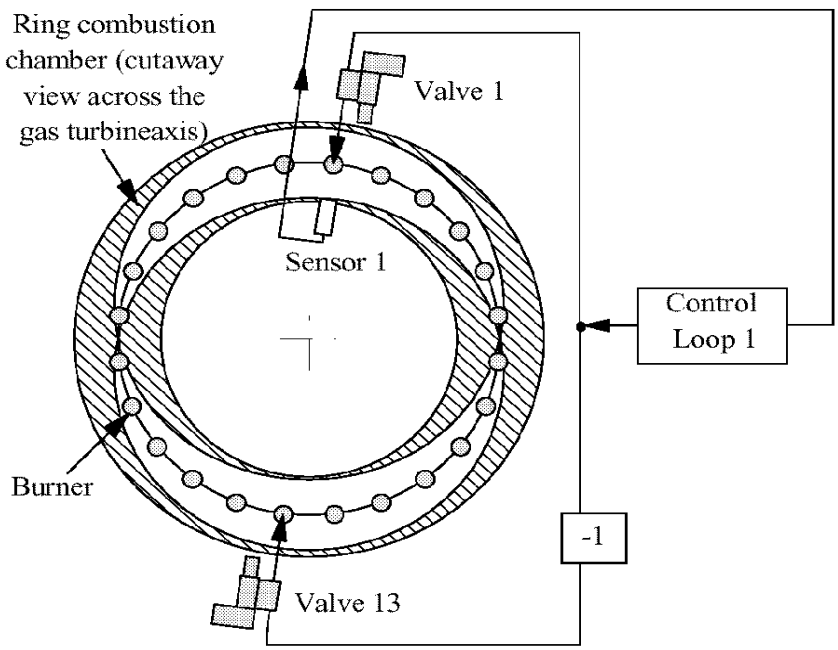

Fig. V-7: Use of the symmetry of azimuthal modes, e.g. for the first harmonic. One pressure sensor and one controller provide the input signals for two rapid Direct Drive Valves (DDV).

V.1.2 Burner systems for syngas application in Vx4.3A's annular combustion chamber

V.1.2.1 Integrated Gasification Combined Cycle technology and the employment of syngas

Integrated Gasification Combined Cycle (IGCC) is a strategically important technology. These integrated power systems offer the potential for reduced CO_2 emissions from power generation if combined with fuel gas decarbonisation [V-5]. IGCC also results in potentially improved efficiency compared to conventional pulverized coal. The fuel obtained from the gasification process is conventionally named syngas.
Syngas (*synthesis gas*) is a variable mixture of primarily *hydrogen* (H_2) and *carbon monoxide* (CO), that is commonly diluted with inerts such as nitrogen (N_2), steam (H_2O) or carbon dioxide (CO_2). Depending on the gasification process variables, and which solid is gasified (e.g. biomass, coal, tar), substantial changes in the resulting syngas *composition* occurs. These changes in the syngas composition can significantly alter the flame behaviour. Therefore, the composition of the fuel impacts the *turbine life* and *emissions*, and characterization of the flame behaviour at different fuel compositions is an important task. Furthermore, syngas combustion is prone to *flashback* due to high (laminar) flame speeds associated with its hydrogen content. Under atmospheric conditions the flame speed of a stoichiometric methane air mixture is about 40 cm/s whereas that of a hydrogen air flame is about 200 cm/s. Therefore, hydrogen flame propagates five times faster than a methane flame under atmospheric pressure. This mismatch between flame speeds leads to flame holding problems in a gas turbine engine environment.
To achieve a desired power output from syngas, *high volumetric fuel flow* rates are needed due to the lower heating value of the fuel per unit volume. This causes *mixing problems* inside the premixer due to high injection speeds of the fuel, and affects the combustion process downstream.
Another issue is the very lean burning of hydrogen-enriched mixture requires more combustion air. Resulting high volumetric flow rates then translate into higher axial speeds inside the premixer which lowers mixing time. This axial velocity also tries to push the flame away from its anchoring point (i.e. the center body) at the dump plane which poses significant problems with respect to flame holding and can yield to a complete *blow-off* (LBO). Gas turbine engines are operated near their lean blow-off limits due to emissions considerations. Hydrogen enrichment (i.e. $\%H_2$, percent of hydrogen volume fraction) considerably extends the lean blowout (LBO) limits of the methane fuel. Hydrogen enrichment extends the LBO limit quite extensively [V-6].
The combustion properties of syngases are mainly determined by their H_2 and CO contents and are generally characterized by very high (laminar) flame speeds, a wide range of flammability limits and low ignition delay times which all contribute to a high risk of flashback phenomena. H_2 distinguishes itself from CH_4 (the main constituent of natural gas) in that its flame speed is an order of magnitude higher. Beside the combustion characteristics also the physical properties of H_2 are different from the ones of natural gas; for example its density is an order of magnitude smaller.
One of the most important parameters to take into account, when talking about stable and safe gas turbine combustion, is the turbulent burning velocity. This fuel gas property plays an even more

important role in the combustor design for fuel gases with high hydrogen content such as syngas, as it assumes much higher values for hydrogen-rich gases than for natural gas.
Due to the peculiarity of this H_2-rich fuels, syngas combustion is mostly adopted and studied in diffusion flames and highly diluted (with N_2 or steam) combustion. Concerning premixed flames, despite of the increasing quantity of current research activity involving premixed syngas, a deficit exists in general for lean premixed combustion experiments at gas turbine relevant conditions (e.g. high inlet temperature, high pressure). The lack of data is very obvious specifically for turbulent flame speed at such conditions.

V.1.2.2 Syngas application in Siemens Vx4.3A

The problem of climate change has initiated big endeavours for efficiency increase as well as techniques for CO_2 capture. IGCC technology has a high efficiency potential and is open for effective pre-combustion CO_2 removal: processes for CO_2 separation from the pressurized fuel gas are state-of-the-art and lead to an only moderate efficiency decrease of typically 5 to 7 % points (product CO_2 at gaseous state).
Saving primary energy sources in combination with more stringent emissions limitations, especially with regard to CO_2, leverages advanced power plant technologies. IGCC is one technology which can meet these requirements while avoiding the use of high cost fuels such as natural gas. Via gasification IGCC is capable of operating on a wide range of fuels and offers the ability to produce a range of products including power, heat, hydrogen and other valuable chemicals. Future applications of IGCC can be configured to remove carbon components with minimal efficiency losses when compared to today's technologies. However, these new advanced IGCC concepts require additional component development in the areas of integration and gas turbine combustion in order to keep IGCC technology competitive and reliable. This induced Siemens to enter into several programs which emphasize on *syngas* and *hydrogen* rich gas combustion and the development of advanced IGCC concepts with and without CO_2 capture.
Enhancing efficiency and specific power output of future IGCC applications needs syngas burner technology which is applicable in high efficient gas turbines like **Siemens Vx4.3A** [V-1].
The application of the latest gas turbine technology in IGCC power plants is a vital next step in improving IGCC economics. This way, IGCC technology can profit from the enhanced efficiency resulting from higher turbine inlet temperature. Together with the higher unit power output this would lead to lower specific investment and improve IGCC's competitiveness to conventional steam power plants.
One of the main difference between the standard combustion system of the existing, low firing temperature gas turbines and the current more advanced engines is the design of the combustion chamber. The compact design results in low residence time and thus decreased NO_x formation. On the other side, for ensuring complete burnout of the different fuels (syngas, natural gas, fuel oil) combustor length has to be considered.
Modifications necessary for the integration into the advanced Vx4.3A as well as for NO_x emissions reduction and improved operational/fuel flexibility lead to a prototype design by Siemens (Fig. V-8). This phase was supported by computational fluid dynamics (CFD) simulations. The calculation model was adjusted especially to the specific combustion conditions of syngas. Thermo-acoustic aspects of syngas combustion, which are of high priority in terms of operational behaviour and availability, were the objectives. This was supported by small scale

generic thermoacoustic tests. Based on the design and simulation work, a prototype of the advanced combustor was tested in an adapted single burner test rig under atmospheric and pressurized conditions.

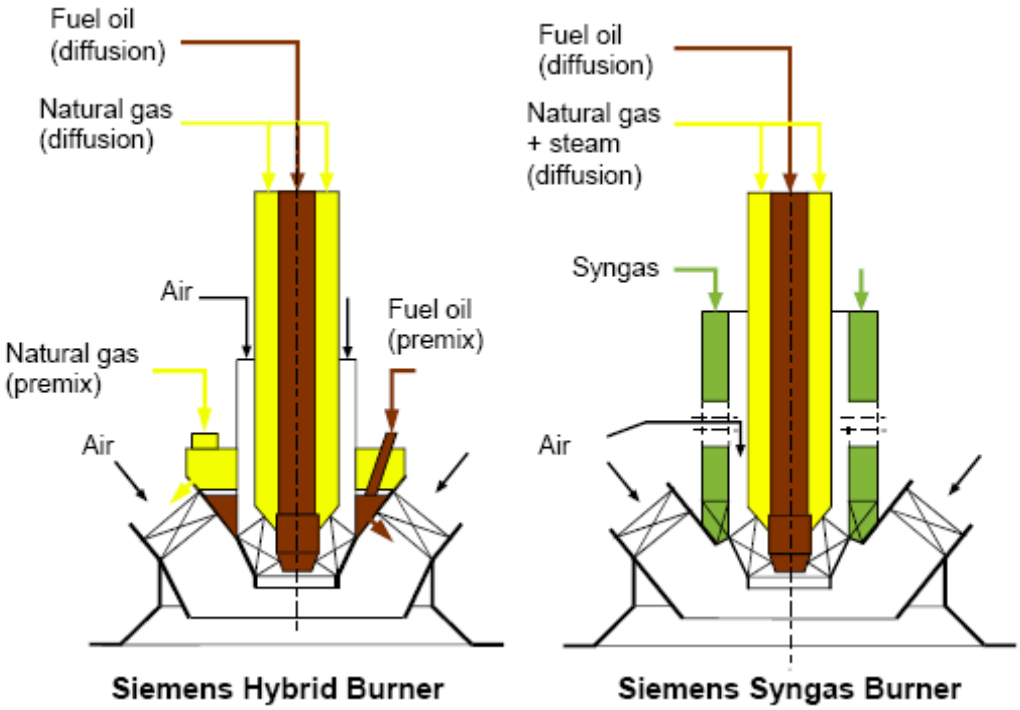

Fig. V-8: Scheme of Siemens V94 series hybrid burner.

References

[V-1] Hannemann F., Koestlin B., Zimmermann G., Morehead H., García Peña F., "Pushing Forward IGCC Technology at Siemens", 2003 Gasification Technologies Conference, San Francisco, California, October 12-15, 2003.

[V-2] Hermann J., Orthmann A., Hoffmann S., Berenbrink P., "Combination of Active Instability Control and Passive Measures to Prevent Combustion Instabilities in a 260MW Heavy Duty Gas Turbine", RTO AVT Symposium on "Active Control Technology for Enhanced Performance Operational Capabilities of Military Aircrqft, Land Vehicles and Sea Vehicles", Braunschweig, Germany, 8-11 May 2000.

[V-3] Hermann J., Gleis S., Vortmeyer D., "Active Instability Control (AIC) of Spray Combustors by Modulation of the Liquid Fuel Flow Rate", Combustion Science and Technology, Vol. 118, Issue 1-3, pp.1-25, 1996.

[V-4] Hantschk C., Hermann J., Vortmeyer D., "Active Instability Control with Direct Drive Servo Valves in Liquid-Fuelled Combustion Systems", 26th International Symposium on Combustion, Naples, 1996.

[V-5] Bozzolo M., Brandani M., Traverso A., Massardo A.F. "Thermoeconomic analysis of gas turbine plants with fuel decarbonization and carbon dioxide sequestration", Journal of Engineering for Gas Turbines and Power-Transactions of the Asme, Vol. 125, Issue 4, pp. 947-953, 2003.

[V-6] Tuncer O., Acharya S., Uhm J.H., "Dynamics, NOx and flashback characteristics of confined premixed hydrogen-enriched methane flames", International Journal of Hydrogen Energy, Vol. 34, pp. 496-506, 2009.

Part 2: A NEW DIAGNOSTIC METHODOLOGY FOR THERMOACOUSTIC INSTABLITIES DETECTION AND CONTROL

VI. Background concepts: conventional optical techniques and theoretical approach for thermal emission of flames

VI.1 Emission spectra of flames

When energy is supplied to a body in particular forms such as heat or electrical discharges, the body restores part of this energy in the form of electromagnetic radiation. Spectral analysis consists of sorting this radiation in function of its wavelength, this distribution being called an *emission spectrum*. The radiation can fall into the *visible* (VIS) domain or it can be comprised in the *infrared* (IR) and *ultraviolet* (UV) domains.
It is hardly possible to give a description of the spontaneous emission of flames because the radiation is not only sensitive to *temperature*, varying with *wavelength* and the *kind of gas mixture*, but also depends on many other factors which include the *gas/air* or *gas/oxygen mixture ratio*, the *gas purity*, the *burner type*, the *gas flow* (laminar or turbulent), the presence of *sprayed additives* and the height of observation in the flame. The appearance of a recorded flame spectrum is also affected by the *resolving power of the spectrometer*. When large slit widths are used the detailed structure of the spectrum is smeared out and molecular bands look more like continua (quasi-continua).
The emittance distribution in the infrared emission spectrum of a hot gas depends on the *temperature* and *pressure* of the gas, and on the *number of emitters* which radiate at each wavelength. When temperature gradients exist in a gas, it is often possible to consider the gas to consist of a series of regions, each of which is isothermal within the precision of measurement. *Temperature gradients* affect the exchange of radiant energy between different regions of a hot gas and, consequently, affect the observed spectrum. As a result, in principle, it is possible to obtain information about the temperature distribution in a hot gas from its emission and absorption spectra.
Experience shows that the energy distribution (or spectrum) the spontaneous emission from flames can be classified according to different shapes. Thus the following types of spectra can be distinguished:

1. ***Continuous spectra***, such as the ones radiated by the sun, in which the emitted energy is distributed in a continuous manner between all wavelengths within a certain domain, and which usually exhibits a maximum. This is the general case of radiation emitted by heated bodies in solid or liquid phase. Continuous spectra in combustion systems are generally observed in the sooty region of rich hydrocarbon flames. In some cases the continuous emission in flames may be due to processes such as recombination of ions, or associations of atoms and radicals.
2. ***Discontinuous spectra***, in which the energy is mainly confined around certain narrow wavelengths: these types of spectra are attributed to isolated atoms or molecules.

Spectra in the visible and ultra-violet regions are generally due to changes of electronic energy, i.e. to a transition from one configuration of electrons of the molecule to another configuration. This change determines the position of the band system as a whole. Accompanying changes in the vibrational energy of the atoms of the molecule determine the position of individual bands

within the band system. Accompanying changes of rotational energy of the molecule as a whole determine the fine structure of individual bands, i.e. the fine line structure of the band.
In the *reaction zone of flames*, corresponding to the inner cone of the Bunsen flame, many unstable radicals such as CH, C_2, HCO, NH, NH_2 etc. may be formed and these do give appreciable emission in the ***visible*** (370-700 nm) and near ***ultraviolet*** (190-370 nm).
The ***visible*** radiation (370-750 nm) comes mainly from the inner cone, while the ***near infrared*** (750-1400 nm) radiation comes from the main body of the gases, both interconal gases of potential core and burnt products.
In the ***near infrared*** (750-1400 nm) region of the spectrum H_2O, CO_2, CO, NO and OH have strong vibrational bands.
The flames usually studied are:

a) **Hydrogen flames**
   Compared with other flames the hydrogen flames have the characteristic of a weak background emission. The spectra always show the marked OH bands with band heads at 281 nm, 306 nm (strong) and 343 nm.

b) **Hydrocarbon flames**
   Much more complex are the spectra of hydrocarbon flames, which not only produce the bands and the continua observed in hydrogen flames, but also emit radiation of hydrocarbon radicals.

About the intensity of emission lines, the intensity relations of the lines in a spectrum are of greatest importance for practical spectroscopy. In fact a quantitative analysis of the spectra is based on the existence of a definite relationship between the concentration of atoms or molecules, to be determined, and the intensity of a specific radiation. Several phenomena have a play in the measured intensity.

VI.1.1 Origin of spectra

The assumption underlying the assignment of a temperature to a system is that the system is in a state of thermodynamic equilibrium. Such a state can be characterized by the fact that it satisfies a number of conditions with the use of a single value of the quantity T, which then represents the temperature of the system.
The emission of the *primary combustion zone* (main combustion zone) especially and, to some degree, of the flame region above it, cannot be described in terms of thermal equilibrium. Hence, for a quantitative interpretation of the flame emissions, not only the *concentrations* of the emitting molecules and the *flame temperature*, but also the various *formation and excitation mechanisms* have to be known. In spite of diverse comprehensive investigations, these mechanisms are not yet entirely clear.
Moreover the probability of quenching collisions between the superthermally excited species and the gas molecules as well as the possibility of self-absorption must be taken into account. An additional difficulty in dealing with the primary combustion zone arises from the very pronounced spatial variations of the gas composition.

Most of the investigations in this field were undertaken with the direct purpose of understanding the combustion reactions or the structure of the radiating molecule instead of explaining the background emission of flames.

a) *Formation of excited OH*:
Excited OH radical, OH*, can be formed in the primary combustion zone by the following chemiluminescent reaction:

$$CH + O_2 \rightarrow CO + OH\,*$$

Other possible reactions, also of importance for hydrogen flames, are:

$$O + H \rightarrow OH\,*$$
$$H + O_2 \rightarrow OH\,* + O$$

Here also intermediate excited states or complexes can occur. Furthermore, an OH radical can be raised from the ground state into the excited state when it is involved as a third partner in a recombination reaction between two other particles such as:

$$OH + (O)H + H \rightarrow OH\,* + H_2O$$

The *OH emission spectrum* is in the in the visible and ultra-violet regions (UV-VIS). The existence of the OH molecule in flames and in many other laboratory or natural sources, is proven through the ultraviolet bands with a widely open structure, the strongest of which lies at **λ=306.4 nm**. Due to the importance of OH in the kinetics of flames and related problems, the ultraviolet bands have extensively and thoroughly studied.

b) *Formation of excited CH and C_2*:
The formation of excited CH and C_2, CH* and C_2*, in flames has been debated for long time. Comparison of CH* emission from various flames leads to the conclusion that CH* is not formed by direct breakdown of acetylene but by a side reaction. The observation that CH* usually occurs higher in the reaction zone than C_2 suggests that it might be formed from C_2 by the reactions:

$$C_2 + OH \rightarrow CO + CH\,*$$
$$C_2H + O \rightarrow CO + CH\,*$$

The *CH emission spectrum* is in the in the visible and ultra-violet regions (UV-VIS). Three band systems ascribed to the CH molecule are emitted by the inner cone of the hydrocarbon flames; the strongest one is around **λ=431.5 nm**, another one is between **λ=362.8 nm** and **420.0 nm**, the last band is in the ultraviolet near **λ=315.0 nm**.

VI.1.2 Qualitative information on the heat release rate by flame spectral analysis

Flame spectral analysis has been extensively used ([II-37], [II-44], [II-45], [II-43], [II-64], [II-143], [III-20], [III-41], [VI-1], [VI-2], [VI-3], [VI-4]) to provide qualitative information on the *heat release rate*. Chemiluminescent emissions occur when excited radicals, such as OH*, CH*, and C_2*, formed within the flame front, return from an excited energy state to a lower energy state by emitting light at a characteristic wavelength.
The dependence of ultraviolet (UV) emissions on the combustion rate has been used by many investigators, particularly to obtain the time dependence of the heat release in unsteady combustion. Perhaps the first serious application was that of Hurle et al. [II-64] who measured C_2* and CH* emissions from a premixed ethylene/air flame and correlated them with acoustic pressure. Later, Büchner et al. [VI-5] and Keller and Saito [VI-6] both used OH* emission to deduce the heat release from pulse combustors, while Poinsot et al. [II-37] used C_2* emission to investigate combustion instabilities in a dump combustor. More recently, Pont et al. [VI-7] have recorded complete OH* images of a dump combustor flame on a CCD camera. Paschereit et al. [VI-8] have done the same on a swirl burner flame, phase-locking the camera to the pressure signal.
Usually it is thought that intensities of chemiluminescence from OH* and CH* and background intensity from CO_2* are **good indicators of *heat release rate***, whereas that from C_2* is not [II-143].
Early experiments in premixed flames suggested that the intensity of chemiluminescence from these radicals might be a good marker of *heat release* ([II-64], [III-41], [VI-1]). Subsequent studies used this hypothesis without additional evaluation of the influence of combustion parameters (i.e., equivalence ratio, pressure, temperature, and flame strain rate) on the chemistry of the excited radicals leading to chemiluminescence and its potential link to heat release ([II-37], [III-20], [VI-2], [VI-3], [VI-4]). Chemiluminescence from CO_2* has also been used to measure heat release in lean flames ([II-44], [II-45]), although higher uncertainties are expected in partially premixed flames, since the chemiluminescence from CO_2* is a continuum possibly contaminated by light emitted by other radicals.
Nonetheless, a recent attempt [II-43] to study numerically the chemistry of the radicals OH*, CH*, C_2*, and CO_2* suggested that their chemiluminescence does not follow well the heat release rate in unsteady premixed stoichiometric methane flames diluted with nitrogen. Instead, it was found that HCO radicals are more suitable to represent the *heat release rate*, since they are associated with the main reaction path of the fuel [II-43]. However, laser excitation of HCO radicals was found to be very difficult. That study was limited to unsteady flames with high curvature and did not present supporting experimental evidence to verify the chemical model used for calculating the chemiluminescence.
Therefore, additional work on the technique is required to evaluate the ability of chemiluminescence to monitor the heat release rate.

VI.2 Conventional optical techniques

Monitoring and controlling a flame's *heat release rate*, the *local equivalence ratio*, and the *degree of premixedness of the reacting mixture* are of great interest for industry, because of the dependence of pollutant emissions, combustion oscillations in gas turbines, and variability of automotive engine operation. It is, thus, important to have a reliable method to measure these parameters in combustion systems. For many years, sampling probes have been used to measure concentration of various species in flames, to estimate the fuel/air ratio. However, probes cannot identify the presence of reaction at the measurement location and cannot obtain time-dependent measurements; they disturb the flow and lead to large uncertainties, especially in regions with large concentration gradients. Therefore, *optical techniques* have been developed and are now briefly reviewed.
Turbulent combustion is complicated due to the fact that chemical kinetics and turbulent fluid flow mutually interact with each other. More insights into this mutual interplay can therefore be gained from simultaneous flow and scalar field measurements by optical techniques. It is important to remember that the development of optical spectroscopic techniques can be dated back to the beginning of the XX century.

VI.2.1 Optical techniques for concentration of chemical species

A thorough analysis of combustion environments cannot disregard the information on local concentrations of the molecular species taking part in the chemical reactions characterizing the combustion processes. Admittedly, the task is incredibly difficult because an ordinary event of combustion is made of tens (if not hundreds) of significant reactions running at the same time and involving many different molecular constituents. To track all of them is impossible. Nonetheless, there are a few species that are relatively easy to detect and, fortunately enough, are of great interest for their intimate relationship with the combustion as a whole. In particular, diatomics (molecules made of two atoms) can be measured under different circumstances because they possess not too complex schemes of energy levels. For instance, this is the case of nitrogen (N_2) and oxygen (O_2) molecules that have a primary importance in air-fed combustion, or we may also think of some of the most important polluting species, i.e. nitrogen and carbon monoxides (NO and CO). The situation becomes very problematic with more complex molecules. However, some triatomics (molecules made of three atoms) are still detectable, even though their optical response is complicated by the more intricate molecular photo-dynamics. The typical example is water (H_2O) that constitutes one of the major combustion products or we could name pollutants, such as nitrogen and carbon dioxides (NO_2 and CO_2). Other than di- and triatomics, there are just very few molecules that can be detected with a certain accuracy. Likely, the main hydrocarbon fuels, such as methane and ethane, or some interesting intermediate species (formaldehyde) can be spectrally identified with acceptable difficulty.
Despite the limited number of molecules that are technically detectable, the above-mentioned scenario is more than enough. Usually, one or two molecular species are observed for local concentration measurements (either spatially resolved through point-like acquisitions or imaged with field techniques). For instance, images of the distribution of hydroxil radical (OH) can be very rich in information. Rather often, this type of data is associated with other diagnostic means

capable of complementary data (e.g., temperature or velocity) so that the researchers can reach a comprehensive understanding of the processes they are looking at.
Premixed flame front can be characterized not only by a steep rise of temperature, but also by the presence of radical molecules, such as OH and CH, whose spatial distribution across the flame front is known and distinguished from that of non-premixed processes. The **radical CH** has a symmetric distribution and *is highly peaked in the proximity of the front inner layer*. The **radical OH** has, instead, a strong gradient in the thermal flame front but it decreases very slowly *in the region of combustion products*.
Several techniques are conceived to obtain measurements of chemical species. It is possible classifying these laser methods in reference to the characteristics of their signals. According to this criterion, we distinguish two groups [VI-9]:

1. One group is made of ***incoherent techniques***. The term "incoherent" refers to the fact that the molecules exposed to one (or more than one) laser beam react independently from each other and, for this reason, the final signal is proportional to the number of radiating molecules. Furthermore, the incoherence results in an optical response that is usually isotropic (i.e., the signal is dispersed over the whole solid angle) and, for this reason, the typical experimental set-up is prepared in a 90 degree geometry.
   The incoherence translates the independence of an excited molecule from the surrounding excited molecules. In other terms, each radiating molecule acts on its own and, caused by the random orientation of the molecules filling the interaction region, the scattering of the emitted light occurs in all directions.
   The most popular examples of incoherent techniques used in combustion science are **Laser Induced Fluorescence** (**LIF**), **Spontaneous Raman Scattering** (**SRS**, or SpRS), **Laser Induced Incandescence** (**LII**, that is particularly indicated for soot diagnostic) and, in some way, **Tunable Diode Laser Absorption Spectroscopy** (**TDLAS**).

2. The second group is made of ***coherent techniques***. Those laser methods emphasize the collective optical response of the excited molecules. The coherence is a collective phenomenon, in which molecules (or atoms) participate in coordination with each other. The coherence of the emitted macroscopic field is then the resultant cooperation of many microscopic fields, each one associated with the response of single molecules to the exiting laser fields. This fact leads to three important characteristics of the coherent techniques: they are *non-linear*, *fairly intense* and *show directional sensitivity* (*phase matching*). These aspects can be understood by considering that the macroscopic field stems from a vectorial sum of many microscopic fields. If these cooperate, the squared modulus of the resultant macroscopic field (note that this is the quantity measured by photo-sensitive detectors) depends non-linearly on the number of the microscopic sources, that is the number of molecules. The vectorial structure joined up with the coherent nature of the resultant field is also responsible for the directional properties. Finally, the constructive interference, typical of coherent phenomena, determines the increased strength of the signals found in coherent laser spectroscopies.
   Therefore the coherence manifests itself in a non-linear behaviour of the signal (this means that the emitted radiation is not proportional to the number of radiating molecules) and, additionally, the signal is not distributed over the whole solid angle, because it shows directional properties (*phase matching*). This is the reason why experimental set-ups for

coherent techniques require a line-of-sight optical access, and the direction of detection coincident with direction of propagation of the laser beams. The coherence is one of the fundamental properties of light beams.
The foregoing favourable characteristics are however tainted with critical disadvantages. The coherence is generated and controlled by more than one laser beam. Typically, three laser fields are needed for the purposes of the main popular combustion diagnostics (i.e. CARS). For this reason, it is commonly observed that coherent techniques are synonym of dielectric non-linearity (i.e., dependence on two or more electric fields). The feature is not without consequences. On the experimental side, the minimum requirement of two laser systems and the crucial sensitivity to the optical alignment render the measurements difficult. On the theoretical side, the data interpretation is very elaborate and much more sophisticated than the theoretical analysis of incoherent techniques.
The most common examples of coherent techniques used in combustion science for detection of chemical species are **Coherent Anti-Stokes Raman Scattering** (**CARS**) and **Degenerate Four Wave Mixing** (**DFWM**)

Among the optical laser-based techniques, which have become more and more important in recent years for temperature measurement applications, are [VI-10]:

a) **LIF** (*Laser Induced Fluorescence*).
The basic principal of the laser-induced fluorescence technique is that laser radiation is used to selectively excite an atomic or molecular species of interest to an upper-electronic state via a laser-absorption process. The excitation process is followed by the spontaneous emission of a photon when the excited atom or molecule decays back to a lower-energy level. The spontaneous emission is referred to as *fluorescence* or as *laser-induced fluorescence*, and its intensity can be related to the number density of the species of interest.
Then, LIF is a technique that is based on resonant excitation of small molecules. Laser induced fluorescence with excitation in the UV is frequently used for thermometry and the detection of minor combustion-related molecules such as OH, CH, NH, C_2, NO, CO, O_2, HCHO and others. Fluorescing organic molecules have found an interest as tracers that allow quantitatively observing fluid mixing processes as well as fuel concentration mapping.
One of the final remarks on LIF is about the possibility of two-dimensional imaging (**PLIF**, or Planar LIF). This version differs from traditional LIF in terms of laser excitation (a sheet of laser light is arranged by means of a proper optical system of lenses) and detection (usually made by means of an intensified CCD equipped with a specific interference filter). In effect, most of laser imaging as to detection of chemical species of combustion interest is based on two-dimensional fluorescence maps.
The fluorescence signal is directly proportional to the concentration of the absorbing species. It is important to note that quantitative fluorescence measurements are not always necessary and that useful information can often be obtained from qualitative measurements that provide a relative measure of the number density, or in some cases only indicate the location, of the species of interest.
A useful application of Laser-Induced Fluorescence in the study of combustion dynamics is in the characterization of fuel-air mixing. Measurement of fuel-air mixing is important

because both the temporal and spatial fuel distribution can have a significant effect on the stability characteristics of the combustor.

b) **SRS** (*Spontaneous Raman Scattering*, or **SpRS**).
Raman scattering is used to measure major species concentrations such as H_2, O_2, N_2, CO, H_2O, CO_2, and CH_4. Often it is applied simultaneously with Rayleigh scattering which is used to measure temperatures assuming the validity of ideal gas law.
Although SRS is very common in basic combustion research, where the extreme richness of the Raman processes is well recognized, industrial applications are problematic, however attempts on SRS detection in systems of industrial interest cannot be neglected.

c) **CARS** (*Coherent Anti-Stokes Raman Scattering*).
The CARS technique belongs to the class of nonlinear, coherent processes. The signals of coherent processes are generally strong and emitted in a laser-like beam, but the signal generation depends nonlinearly on the concentration of the probe molecules and is also intrinsically a nonlinear function of the exciting laser intensities. CARS therefore imposes stronger demands on the laser source such as stability, beam quality and mode structure, and, since two laser beams are involved, on alignment.
Three electric fields are necessary to produce the CARS response and, in turn, this implies that three laser beams are combined together to generate the fourth electric field, the anti-Stokes field, that gives rise to the CARS signal. Despite the difficulty of handling three interacting laser fields, the potential of CARS as an important approach for high-resolution molecular spectroscopy are clearly recognized.
Species of combustion interest, diatomics such as H_2, N_2, O_2, CO, NO, or the triatomics H_2O, CO_2 can be worked out by CARS. The CARS technique allows only point measurements. However, due to its high accuracy, CARS is often used to define a temperature standard for the investigation and validation of other thermometry methods.

d) **TDLAS** (*Tunable Diode Laser Absorption Spectroscopy*).
Actually, the first three techniques have been considered for sake of completeness, because they can hardly be applied to the case of interest on gas turbine plants. The only laser techniques that the comparative analysis has shown to be promising for the measurement of interest in gas turbines is TDLAS high resolution spectroscopy based on tunable diode lasers.
Tunable Diode Laser Absorption Spectroscopy (TDLAS) is a technique for measuring the concentration of certain species such as methane, water vapour and many more, in a gaseous mixture using tunable diode lasers and laser absorption spectrometry. The advantage of TDLAS over other techniques for concentration measurement is its ability to achieve very low detection limits. Apart from concentration, it is also possible to determine the *temperature*, *pressure*, *velocity* and *mass flux* of the gas under observation [VI-11].
This technique is recently becoming more and more popular for both *temperature* and *species concentration measurements* thanks to the diode laser advantages for field applications, such as compactness, high reliability, reduced maintenance, low cost. Very important for use in harsh or difficult to access industrial environment is also the diode laser suitability for coupling with optical fibers. TDL (*Tunable Diode Laser*) based

sensors have been developed for advanced aeropropulsion applications, but most of them are also applicable to land-based gas turbines. Typical temperature measurement range is 300 to 3000 K. Such sensors are at the moment recommended for use by the Research Community, but more development is underway to demonstrate the possibility of applying this technology also in real gas turbine combustors.
A method to detect frequency-resolved *temperature fluctuations* using a diode laser-based sensor was developed and applied to the scramjet test rig [VI-12].

Optical techniques need one or two optical access. Whereas for unconfined, atmospheric conditions an optical access entails non principal difficulty, pressurized conditions increase the effort dramatically. In any case an optical access to the interior of a nozzle is hindered by its rather small dimensions causing interfering reflections.

VI.2.2 Optical techniques for velocity measurements

A turbulent flow field is characterised by its mean and *rms*-values (root mean square = second statistical moment) of all three velocity components.
Any experiment of fluid dynamics faces the problem of measuring dynamical variables without perturbing them, and laser techniques can help us in that. Flow field measurements in turbulent combustion benefit from developments in fluid mechanics, then the most popular optical techniques used are:

a) **LDV** (*Laser Doppler Velocimetry*). LDV is a very famous non-intrusive method for the measurement of fluid velocities that could range from few millimetres per second up to supersonic flows. This laser technique allows only point measurements of the velocity. LDV measurements are free from calibration needs.

b) **PIV** (*Particle Image Velocimetry*). It is an imaging technique according to which the information about the velocity comes from a comparison between two successive images of the scattered light captured by a CCD camera that freezes the particles at the positions of the two subsequent (and known) instants of the laser pulses. Each image is then divided into sub-regions, usually called interrogation windows and a cross-correlation algorithm between two corresponding interrogation windows yields a map of vector displacement, each representing the average displacement of the particles contained in the interrogation windows. The knowledge of the pulse to pulse delay or, equivalently, the lag between the recorded images leads to the definition of a vector velocity map of a bi- or three dimensional fluid dynamic field.

c) **PTV** (*Particle Tracking Velocimetry*). It is a technique to measure velocity of particles. The name suggests that the particles are tracked according a lagrange-based approach, and not only recorded as an image.

d) **PDA** (*Phase Doppler anemometry*). Liquid fuels are often used and their injection into the combustion chamber through atomizers results in a spatial distribution of droplets (spray). It gives a simultaneous measurement of the velocity and size of the particles.

These techniques, however, cannot measure the fluid-dynamical state on the spatial scale of the molecular constituents of the fluid and, therefore, *seeding with solid particles* is the inescapable operative condition for the application of laser methods. Alternatively, if droplets are present (like in combustion of atomized liquid fuels or in seeding with oil droplets), these can function as laser light scatterers and the recourse to seeding with solid particles can be avoided.
Mie scattering is an elastic scattering process, that is, the wavelength of the scattered light is the same as the incident light, which occurs when the dimension of the object (i.e. seeding particles) from which the light is scattered is greater than the wavelength of the incident light.
In these three optical techniques Mie scattering off chemically inert particles (e.g. Al_2O_3, alumina; MgO, magnesium oxide; $ZrSiO_4$, zirconium silicate; TiO_2, titanium dioxide) are seeded into the flow upstream the nozzle that is monitored. The melting point of the seeding material must be well above the adiabatic flame temperature to access post-flame regions. On the one hand the particle size needs to be sufficiently small to minimize slip relative to the continuous phase. On the other hand the particle response time should allow tracking velocity fluctuations of several kHz with slip of less than 1%. In practise, an upper limit of mean seed particle diameter is at the order of 1-2 μm. However, Mie scattering intensity decreases in a non-linear manner with decreasing particles sizes. With common instruments the signal-to-noise might be too low for particles smaller than 0.5 μm. However, as Mie scattering intensity decreases in a non-linear manner with decreasing particle diameter, particles too small will result in poor signal-to-noise.
Flames burning very close to extinction are very sensitive to external disturbances. Particle seeding required for Velocimetry can cause significant shift of the extinction limits. Thus seeding densities must be reduced and this entails poor spatial resolution for PIV.

VI.2.3 Optical techniques for temperatures

Temperature is a particularly important variable in industrial combustion applications because it directly or indirectly affects a number of other important variables. The product temperature is often a critical parameter in most processes. While there is usually a minimum temperature that must be reached for adequate processing, there may also be a maximum temperature above which product quality is reduced. Higher than necessary product temperatures not only increase fuel costs, but they may also increase cooling costs after the product exits the combustion process.
Thermometric measurements are of primary importance in the analysis and the control of combustion processes. As a matter of fact, the chemical routes, established by specific chemical reactions, depend very much on the temperature at which they take place. For this reason, the temperature is one of the most important parameters that influence dramatically the whole combustion efficiency as well as heat release and formation of the pollutants. It is then not surprising that many laser measurements, designed for diagnostic purposes, face the problem of how to obtain an experimental evaluation of the high temperatures developed during the combustion. Various techniques can offer a solution to the problem. The most known are **Rayleigh**, **LIF**, **SRS**, **CARS** and **TDLAS**. These thermometries are subject to calibration.
Laser-based techniques imply the use of sophisticated technology which is hardly suitable for industrial applications. The main disadvantages of conventional techniques lie in their poor spatial resolution and in the fact that they provide an average measurement over the entire gas path length investigated. Although it is in general better than intrusive probe-techniques

(thermocouple, hot-wire anemometer, etc.) smallest length scales of highly turbulent combustion processes often cannot be resolved.
Conventional optical spectroscopic techniques for temperature measurements can be distinguished into two main categories:

2. The first category are techniques based on **thermal irradiance measurements** (derived from the ***Planck distribution law*** and the ***Kirchhoff radiation law***).
   Most measuring methods are based on the comparison between the radiation emitted by hot gases and by an ideal blackbody. All of them assume that gas reflectivity is negligible even if, for gases containing high concentrations of solid particles, this condition is not always satisfied. In addition, such methods are not generally suited for reacting gas mixtures. From the practical point of view, since an attenuation or absorption measurement of light emitted by an IR source turns out to be always necessary, two opposed optical ports of significant diameters are required.
   In order to obtain the true thermodynamic gas temperature it is necessary to know the gas emissivity in the spectral range used for described measurements.
3. The second category are techniques based on **intensity distribution** (dependent on the ***Boltzmann distribution function***).

CARS is nowadays considered to be the most mature coherent technique for temperature measurements in hostile environments. However, accurate thermometry is accomplished after very complex spectral analysis that requires very heavy computational work.
CARS thermometry is widespread. The reason of this success is due to several factors. The signal is collimated and therefore is exceptionally strong in comparison with other accurate laser-based thermometric diagnostics (LIF and SRS). Limitation to temperature ranges, such as in LIF thermometry from radicals, does not matter here for CARS. Besides, there is sufficient knowledge of some of the main Raman species produced in flames, furnaces or other combustion systems. Indeed, in analogy with SRS thermometry, the typical CARS molecule is nitrogen that is well studied and is ubiquitous in air-fed combustion environments. For other applications where nitrogen is not one of the main constituents, there are other suitable molecules (hydrogen, oxygen, carbon and nitrogen oxides, water vapour) whose CARS spectrum is well-established and can be used for thermometric purposes. Another factor that promotes CARS thermometry is its versatility in view of the fact that different experimental strategies are available.
Tunable Diode Laser Absorption Spectroscopy (**TDLAS**) involves measuring the attenuation of a beam from a diode laser as it passes through a gaseous region to measure temperature and/or species concentrations. The laser wavelength is scanned over a small range that encompasses at least one absorption line of the molecule of interest. Transmitted light intensities are measured using a photodetector and the signals are analyzed to obtain the desired parameters. The beam from a diode laser is typically highly divergent, and thus needs to be collimated using a lens or parabolic mirror so that it can traverse a path long enough for the given application. As it transits the measurement zone, the beam gets absorbed by the molecules of interest, and the remaining intensity is measured by the detector. Since molecular absorption is typically a function of wavelength, the laser wavelength is scanned while acquiring the data, producing a transmission spectrum.
Several existing instruments, including suction pyrometers, IR spectrometers, and acoustic pyrometers are already in regular use for combustion gas temperature measurement. However, convectional sensors are often subject to errors due to disturbances caused by the presence of the probe and slow response time. *Tunable Diode Laser* (TDL) absorption spectroscopy seeks to

overcome limitations sometimes associated with these traditional instruments. This technique is of particular interest for industrial combustion applications since it provides the following features:

- capability to measure temperatures in excess of 1650 °C,
- nonintrusive and *in situ*,
- optional capability to simultaneously measure concentrations of species such as H_2O, CO, CO_2 and O_2,
- fast response time,
- well-defined measurement zone geometry.

Recent TDL temperature sensor installations in combustion environments have revealed difficulties that require innovative solutions. Challenges are related to the robustness of the sensor hardware, interferences from harsh environments, and spectroscopic uncertainties. The full potential of TDL-based sensor systems for industrial combustion monitoring has not yet been realized, and it is only a matter of time before diode laser sensors enable new levels of efficiency through active control of industrial processes such as power generation.

VI.2.4 Combined laser techniques for simultaneous measurements

Promising applications concern turbulent combustion, where the diagnostic of the interaction between the chaotic fluid-dynamic field and thermo-chemical reactions of combustion is of primary importance.
Premixed combustion is of increasing technological relevance due to lower NO_x emissions at lean equivalence ratios. A proper design of future low NO_x combustors depends on more reliable numerical simulations of turbulent premixed combustion processes. Although a variety of models such as the *Bray-Moss-Libby* (BML) model, the thickened flame model, the *Linear-Eddy Model* (LEM), or the G-equation approach have been applied in a RANS (*Reynolds averaged Navier-Stokes*) or LES (*Large Eddy Simulation*) context during the last two decades, there is still an ongoing scientific debate how to model turbulent premixed flames. To check the validity of single unclosed terms in the transport equations or to validate integral models determining entire turbulent flames, there is a need for experimentally well investigated target flames.
Whereas much progress has been attained already for non-premixed flames, much less comprehensive experimental data suitable for model validation of turbulent premixed target flames exist. Transient phenomena (e.g. flame extinction, humming or combustion roar), founded on the complex interaction between turbulent mixing and chemical reactions, are little understood. The possibility of measurements of different combustion parameters taken at the same time is a general and intriguing perspective, which could be accomplished by a suitable coupling of two or more techniques. Different combined techniques for simultaneous measurements can be made:

1. **Simultaneous LDV and OH-PLIF measurement**
   The transient OH-contour deduced from single-shot PLIF-images was used to determinate the radial displacement Δr of the actual velocity measurement from the turbulent flame front allowing designation of conditional velocities.

2. **Simultaneous PIV and OH-PLIF measurement**
   A simultaneous application of PIV and a visualization of the reaction zone by PLIF is preferable because the two-dimensional nature of PIV provides estimates of vorticity and dilatation. Transient locations of the reaction zones can be identified by radical distribution such as OH or CH measurable by PLIF and serve to deduce local flow field properties conditioned by the reaction zone.

VI.2.4.1 PIV study of acoustic-flame interaction

An experimental technique suitable for studying fluid dynamic-acoustics interaction is the *Particle Image Velocimetry* (PIV). Although PIV requires seeding of the flow, PIV is known as a non-intrusive technique since it has been well-verified through applications, such as the measurement of turbulent flows. However, the presence of a sound field in the fluid under investigation arise some issues that may make this concept questionable [VI-13]. First, to capture acoustic motions, images must be recorded rapidly enough to track fast tracer particles: due to difficulties associated with this issue, the literature on this topic is quite sparse ([VI-13], [VI-14], [VI-15]). Second, the interaction between sound field and tracer particles in a PIV measurement is mutual and may have a strong intrusive participation ([VI-13], [VI-16] § 8.10). In fact, when a fluid contains inhomogeneities such as suspended particles or regions of turbulence, a sound beam looses its acoustic energy faster than in homogeneous media. The excess attenuation in suspensions arises from absorption (the conversion of acoustic energy into thermal energy) and scattering (the reradiation of incident acoustic energy out of the incident beam). Hence, the presence of tracer particles in a fluid can cause attenuation of the propagation of sound in that fluid. At the same time, it must be observed that the effect of sound field on the tracer particles was found to be negligible for low to moderate acoustic frequencies and sound intensities [VI-13]. Despite the difficulties in tracking the tracer particles, periodic vortex shedding induced by an external acoustic field has been observed by several authors at orifices and at the open end of tubes ([VI-17], [VI-18]) without jets. Furthermore, the shear layer instability and the response of a bluff-body flame to fluid-dynamic oscillations have been recently analyzed by means of PIV ([II-113], [II-114]).
While PIV technique can be used to gain information on the fluid-dynamic field, LIF (Laser Induced Fluorescence) can be used to investigate changes in the flame front topology and combustion.

VI.2.4.2 PLIF study of acoustic-flame interaction and flame front

Planar LIF imaging (PLIF) is one of the most widely used non-invasive techniques to measure species concentration distribution in two-dimension. A great difficulty in PLIF is converting the measured LIF signal into absolute concentrations. Nevertheless, semi-quantitative LIF has been used advantageously in several applications [VI-19] to understand qualitatively the flow and the species concentration field, especially in combustion environments. PLIF based on the excited radical OH* is very powerful and attractive since OH gradients are generally found to correlate well with the position of the local flame front ([VI-20], [VI-21], [VI-22], [VI-23], [VI-24], [VI-25], [VI-26], [VI-27], [VI-28], [VI-29], [VI-30]). Furthermore, information about the heat

release in flames can be estimated from conventional chemiluminescence measurements of naturally excited OH*, CH*, C_2* or CO_2* [VI-31]. Clark [VI-32] correlated OH*, CH*, C_2* and CO_2* chemiluminescence to flow rate, fuel type, and equivalence ratio as early as in 1958. More recently, the dynamic behaviour of flames was studied using measurements of OH* chemiluminescence as an indicator of chemical reaction rate [VI-33]. OH* chemiluminescence was shown to be an accurate indicator of chemical heat release rate in both steady ([II-51], [VI-34]) and unsteady conditions [VI-35].

VI.2.4.3 Simultaneous PIV and PLIF measurement

As a matter of fact optical techniques result quite powerful in combustion studies. Fundamental studies about acoustics-flame interaction are commonly focused on simple configurations, such as laminar flames acoustically perturbed by means of loudspeakers, and performed using PIV or PLIF techniques separately. For example, Khanna [VI-36] measured the response of a laminar flat-flame and a turbulent swirl-stabilized flame to velocity fluctuations produced by a loudspeaker using OH* chemiluminescence as an indicator of heat release rate. Recently parallel use of PIV and PLIF was shown to be attractive to understand acoustics-flame interaction ([VI-28], [VI-36], [VI-37], [VI-38], [VI-39], [VI-40], [VI-41], [VI-42], [VI-43], [VI-44]). The use of PIV and PLIF can reveal the effects produced by forced acoustic waves onto combustion.

VI.3 Image-based techniques for the monitoring of flames: CCD cameras

Industrial flames are an outstanding example of complex reacting flows. They involve many physical and chemical magnitudes (velocity, temperature, radiation, chemical species, reaction rates, etc.), usually displaying large spatial and temporal variations. An enormous amount of information is, therefore, necessary to describe a flame in detail. Scientists have developed many diagnostic methods which have contributed significantly to the progress of the combustion science. However, their use is still mostly restricted to research studies, with scarce applications for the supervision of practical flames. In general, most industrial combustors use convectional instrumentation, whose capabilities for flame monitoring are notably poor; in many cases, only input flow rates and flue gas composition are measured. There is an obvious need for new monitoring techniques, suitable for industrial use and, preferably, capable of providing direct information on the properties of the flame, which is the core of a combustion process. New developments in this field might open new possibilities for the supervision of the process and, ultimately, would greatly facilitate the development of advanced combustion controls.
In this context, *vision-based techniques* are emerging as a viable alternative for the monitoring of practical combustion equipment. These methods are based on the capture of radiation spontaneously emitted by a flame (as opposed to laser-based techniques, requiring external illumination) and offer some important advantages:

- they are nonintrusive,
- flame images can be recorded with rugged, relatively cheap sensors,
- they provide direct information on the flame
- include a large amount of data in the form of 2D-maps.

This, together with the fast progress in sensor technology, probably explains the growing interest in the use of **CCD** (***Charge Coupled Device***) **cameras** for the monitoring of industrial flames. A significant shortcoming is, however, the difficulty of converting flame images into meaningful results.
A wide range of imaging methods is currently available. Active techniques (i.e., requiring external illumination, usually a laser) are used in research studies to determine the spatial distribution of species concentrations, temperature or velocities.
Practical reasons still prevent, however, their use for the monitoring of industrial flames: lack of ruggedness, high cost, difficult optical access, and so on. Much more feasible is the use of passive techniques (i.e., recording of radiation naturally emitted by the flame) and is the approach usually selected for the monitoring of practical flames.
The radiation spontaneously emitted in flames includes different contributions. ***Hot solid particles*** produce a *continuous spectrum*, in according with Plank's law. The radiation emitted by ***gaseous species***, on the contrary, occurs at *discrete wavelengths* and is due to different effects.
The chemiluminescence flame images can provide a most valuable insight into the characteristics of the combustion process. It should be noted that those data are rarely meaningful by themselves and their physical interpretation or their use for monitoring or optimization purposes require the participation of experienced researchers or operators as well as some prior knowledge on the values (e.g., peak temperatures) or patterns associated to different combustion regimes and/or to optimal operation.
In recent years there has been a growing interest in the development of image-based techniques for the monitoring of practical flames. On the one hand, this is motivated by the need for advanced diagnostic and optimization methods for combustion applications, which might entail important benefits in terms of efficiency, pollutant reduction, reliability, and flexibility of combustion equipment. On the other hand, the continuous increase in the performance-to-cost ratio of sensors and data-processing devices enables the development of powerful, yet affordable vision-based monitoring systems, suitable for industrial environments. Flame images contain a large amount of information that might be used to characterize a particular combustion state. However, the main difficulty in this field is thought to be the conversion of visual data into practical information or in the form of physical combustion parameters.
Widely different approaches can be found in the literature. Some authors work with **band-filtered radiation** (infrared, chemiluminescence bands) whereas others capture **broad-band light** (usually, in the visible range). Then, the images collected are post-processed to calculate a few selected magnitudes. These can have a direct physical meaning (e.g., temperature) or constitute a set of representative parameters related to the geometry, luminosity, or colour of the flame. Temporal or spatial averaging can be a serious drawback for monitoring methods based on physical parameters (e.g., derived by pyrometry or chemiluminescence).

VI.4 Recent optical sensors

Optical sensor assemblies provide a great advantage for gas turbine engine measurements and analysis as there is non sensitivity to electro magnetic interference and have the potential for multiple measurements from a single sensor installation. Optical sensors are in general non susceptible to chemical reaction and are ideal for high temperature environments.

Most development tools today use optical sensors in fans and compressors to minimize the spot size and maximize the measurement resolution. Optical sensors using ***Fabry-Perot Interferometer*** (FPI) and ***Fiber Bragg Gratings*** (FBG) technology is becoming an increasingly mature approach to provide temperature and pressure measurements for aero propulsion and power generation engine product development. These sensors, based on the combination of sapphire and silicon micromachining and optical sensing technologies, are sufficiently robust to provide the capability of directly measuring on-engine parameters such as pressure and temperature.
Fabry-Perot cavity-based sensors have been widely used for their versatility; for example they have been used to sense both pressure and temperature transducers. This kind of sensor detects changes in optical path length induced by either a change in the refractive index or a change in physical length of the cavity.
An advantage of optical probes is that they are capable of providing a higher degree of spatial resolution. A disadvantage of optical probes is that they require frequent cleaning of the probe tip as they are susceptible to flow contaminants. Improving the reliability, uncertainly, and flexibility of the sensor and data system is a key objective. The sensor size need to be small to enable the technology to be more widely applied in all engine classes and sizes.
Optical sensors are ongoing area of technology development with their ability to operate at elevated temperatures.

VI.5 Applicability of infrared emission and absorption spectra to determination of hot gas temperature profiles

The fundamental relation used in techniques based on irradiance measurements for infrared emission (IR) is the *Plank radiation law*, according to which an ideal blackbody (i.e. a body which is completely opache and non-reflecting in all directions at all wavelengths) in equilibrium at absolute temperature T [K] radiates (over 2π solid angle) the *blackbody spectral irradiance* $I_B(\lambda,T)$, that is measured in [$Wm^{-3} = J\ m^{-3}s^{-1}$] given by:

$$I_B(\lambda,T) = \frac{1}{\lambda^5}\ \frac{C_1}{\exp\left(\frac{C_2}{\lambda T}\right)-1} \qquad \text{(VI-1)}$$

where:

$\lambda = \frac{c}{f}$ = the wavelength [m]

$C_1 = 2hc^2 = 3.74\cdot 10^{-16}\ [\,J\,m^2\,s^{-1}\,]$

$C_2 = \frac{hc}{k_B} = 1.44\cdot 10^{-2}\ [m\,K\,]$

h =Plank constant [J s] = $6.626\cdot 10^{-34}$ [J s] = $4.135\cdot 10^{-15}$ [eV s]
c = speed of light [m s^{-1}]
k_B = Boltzmann constant [J K^{-1}] = $1.380\cdot 10^{-23}$ [J K^{-1}] = $8.617\cdot 10^{-5}$ [eV K^{-1}]
T = absolute temperature of the blackbody [K]

The *grey body spectral irradiance* (or *spectral line irradiance*) $I(\lambda,T)$ is defined by the product of *blackbody spectral irradiance* $I_B(\lambda,T)$ (over 2π solid angle) and the *grey body absorption* $a(\lambda,T)$:

$$I(\lambda,T) = I_B(\lambda,T)\ a(\lambda,T) \tag{VI-2}$$

The measuring techniques work in a selected bandwidth $\Delta\lambda = \lambda_2 - \lambda_1$, then under the hypothesis that the combustion gas is strongly absorbing in the selected bandwidth Δλ and therefore can be considered as a blackbody, the only dependence on temperature is given by the blackbody irradiance. As consequence, the gas temperature can be determined from an irradiance measurement.

$$I(T) = \int_{\lambda 1}^{\lambda 2} I\ (\lambda,T)\ d\lambda \tag{VI-3}$$

By collecting through an optical access on the combustion chamber the radiation emitted by the hot gases it is possible to get a signal which is proportional to the temperature behaviour.
Since the *measured radiation signal* M_I also depends on geometrical (f_{geom}) and optical parameters ($f_{optical}$) that can be hardly evaluated, it turns out that it is very difficult to directly get the measurement of the absolute temperature.

$$M_I(\lambda,T) = f_{geom} \cdot f_{optical} \cdot I(\lambda,T) \tag{VI-4}$$

Under the hypothesis that operation at such wavelengths is characterized by the same values of *absorption* $a(\lambda,T)$ and *spectral bandwidth* $\Delta\lambda = \lambda_2 - \lambda_1$, from the ratio ($M_{I\ 1}/M_{I2}$) of two measured signals $M_{I1}(\lambda,T)$ and $M_{I2}(\lambda,T)$ one can directly achieve the temperature value, according to the relation:

$$T = C_2 \frac{\lambda_2 - \lambda_1}{\lambda_2\ \lambda_1 \left[5 \ln \frac{\lambda_2}{\lambda_1} - \ln \frac{M_{I\ 1}}{M_{I\ 2}} \right]} \tag{VI-5}$$

The principle of operation described above is based on the ideal hypothesis that the hot gas is a unique "body" with uniform temperature. The consideration about the real case of non-uniform temperature distribution will be analyzed in the next paragraph.

VI.6 Theoretical approach of the radiation absorption/emission process

Temperature profile variations produce characteristic measurable changes in the emission and absorption spectra of a sample. In order to understand to which gas temperature the measured optical signal is related in the real case of *non-uniform temperature distribution*, a model of IR radiation absorption/emission process has been developed ([VI-45], [VI-46]).

VI.6.1 Homogeneous system and monochromatic radiation

To obtain a working equation relating the radiant energy and the temperature profile in a hot gas to spectroscopically observable quantities, we have to start from the well known differential equation for emission and absorption of a perfectly monochromatic radiation. In a hot gas in local thermodynamic equilibrium (homogeneous system, then gas temperature and concentration are constant along the optical path), the spectral irradiance by a one-dimensional beam of monochromatic radiation (λ_i) varies according to equation ([VI-45], [VI-46]):

$$dI(\lambda_i, x) = a(\lambda_i, x)\left[I_B(\lambda_i, T_x) - I(\lambda_i, x)\right] dx \qquad \text{(VI-6)}$$

where:

$I(\lambda_i, x)$ = irradiance at wavelength λ_i at position x,

$I_B(\lambda_i, T_x)$ = *Plank blackbody* irradiance at wavelength λ and temperature T_x at position x,

$a(\lambda_i, x)$ = the *absorption coefficient* at wavelength λ at position x,

In equation (VI-6) the radiant energy travels in the direction of increasing x. The left hand side of the equation represents the variation of the irradiance on going from a point x to a point x+dx. The first term of the right hand side is the increase in irradiance due to the *emittance* of the hot gas, as given by the *Kirchoff's law*, while the second term is the decrease in irradiance due to absorption along the path *dx*, as given by the *Beer-Lambert's law* (see Attachment E). Scattering is assumed to be negligible.
Equation (VI-6) is a first order linear equation that can be easily integrated to give:

$$I(\lambda_i, L)\left\{\exp\left[-\int a(\lambda_i, x)\,dx\right]\right\} = \int I_B(\lambda_i, T_x)\,\exp\left[-\int a(\lambda_i, x)\,dx\right] a(\lambda_i, x)\,dx + C \qquad \text{(VI-7)}$$

where *C* is a constant of integration.

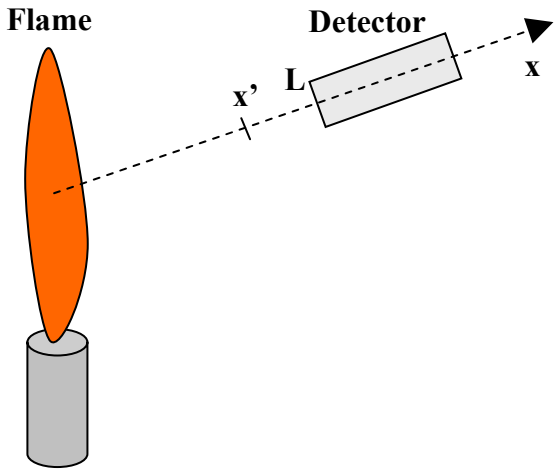

Fig. VI-1: Sketch for the emittance of the hot gas.

Integrating equation (VI-6) with the boundary condition $I(\lambda,0)=0$, then C=0, which means that the gas specimen is the only source of radiation. By assuming a gas path of length L and evaluating it at the boundary (x') nearest the detector, the spectral irradiance impinging onto the detector is ([VI-45], [VI-46]):

$$I(\lambda_i,L)\cdot\left\{\exp\left[-\int_L^0 a(\lambda_i,x')\,dx'\right]\right\}=\int_L^0 I_B(\lambda_i,T_x)\cdot\exp\left[-\int_L^x a(\lambda_i,x')\,dx'\right]a(\lambda_i,x)\,dx \qquad \text{(VI-8)}$$

$$I(\lambda_i,L)=\left\{\exp\left[\int_L^0 a(\lambda_i,x')\,dx'\right]\right\}\cdot\int_L^0 a(\lambda_i,x)\cdot I_B(\lambda_i,T_x)\cdot\exp\left[-\int_L^x a(\lambda_i,x')\,dx'\right]dx \qquad \text{(VI-9)}$$

The right hand side of equation (VI-9) cannot be integrated in closed form for the general case. However, in the case temperature and pressure can be considered uniform ($T=T_x$=cost, p=cost), the absorption coefficient (*a*) and the *Plank function* (I_B) are independent of *x* and it reduce to:

$$\begin{aligned}
I(\lambda,L)&=\left\{\exp\left[\int_L^0 a(\lambda_i)\,dx'\right]\right\}\cdot\int_L^0 a(\lambda_i)\,I_B(\lambda_i,T)\cdot\exp\left[-\int_L^x a(\lambda_i)\,dx'\right]dx=\\
&=\left\{\exp\left[-a(\lambda_i)\,L\right]\right\}\cdot\int_0^L a(\lambda_i)\,I_B(\lambda_i,T)\cdot\exp\left[-a(\lambda_i)\,(x-L)\right]dx=\\
&=I_B(\lambda_i,T)\left\{\exp\left[-a(\lambda_i)\,L\right]\right\}\cdot\int_0^L a(\lambda_i)\cdot\exp\left[-a(\lambda_i)\,(x-L)\right]dx=\\
&=I_B(\lambda_i,T)\left\{\exp\left[-a(\lambda_i)\,L\right]\right\}\cdot\left\{-\left[1-\exp\left(a(\lambda_i)\,L\right)\right]\right\}=\\
&=I_B(\lambda_i,T)\left\{1-\exp\left[-a(\lambda_i)\,L\right]\right\}=I_B(\lambda_i,T)\left[1-\tau(\lambda_i)\right]
\end{aligned} \qquad \text{(VI-10)}$$

where $\tau(\lambda_i) = \exp[-a(\lambda_i)L]$ is the *transmittance* of the hot gases, in according with *Beer-Lambert's law*. The quantity between square brackets is the gas absorptivity α_λ or, according to the Kirchhoff's law, the emissivity ε_λ. Therefore equation (VI-10) can be rewritten as:

$$I(\lambda, L) = I_B(\lambda_i, T)\,[1-\tau(\lambda_i)] = I_B(\lambda_i, T)\,\alpha_\lambda = I_B(\lambda_i, T)\,\varepsilon_\lambda \qquad \text{(VI-11)}$$

Equation (VI-11) clearly shows that in the case of very large gas path length (L>>0), where it is possible to consider the *transmittance* $\tau_\lambda \approx 0$ (and therefore, for *Kirchhoff's law*, $\varepsilon_\lambda \approx 1$) a measurement of the monochromatic irradiance does provide an estimation of the blackbody irradiance and consequently the measurement of the hot gas temperature (this is the basis of the **optical pyrometric technique**).

VI.6.2 Non-homogeneous system and monochromatic radiation

If *gas temperature and concentration are not constant along the optical path* (i.e. the path crossed by the optical radiation), equation (VI-9) has to be numerically integrated. For this purpose the optical path can be divided into N zones, each with *approximately uniform temperature*. The solution of equation (VI-9) can then be expressed as a sum of solutions of the form of equation (VI-10). Thus, by serially numbering these zones from 1 to N, with zone 1 nearest to the detector, the irradiance at the detector is ([VI-45], [VI-46]):

$$\begin{aligned} I(\lambda_j) &= \sum_{i=1}^{N} I_B(\lambda_j, T_i)\,\left\{1-\exp\left[-a_i(\lambda_j)\Delta l_i\right]\right\}\exp\left[-\int_{x=l_{i+1}}^{L} a_x(\lambda_j)\,dx\right] = \\ &= \sum_{i=1}^{N} I_B(\lambda_j, T_i)\,\left\{1-\exp\left[-a_i(\lambda_j)\Delta l_i\right]\right\}\exp\left[-\sum_{j=i+1}^{N} a_j \Delta l_j\right] = \\ &= \sum_{i=1}^{N} I_B(\lambda_j, T_i)\left[1-\tau_i(\lambda_j)\right]\prod_{j=i+1}^{N}\tau_j(\lambda_j) = \sum_{i=1}^{N} I_B(\lambda_j, T_i)\left[\overline{\tau_{i+1}}(\lambda_j) - \overline{\tau_i}(\lambda_j)\right] \end{aligned} \qquad \text{(VI-12)}$$

where:
Δl_i = the thickness of the *i-th* zone
l_i = the value of x at the border between zones *i* and *(i+1)*
l_i+1 = the abscissa of the *(i+1)-th* zone
$\overline{\tau_i}(\lambda_j) = \prod_{h=i}^{N}\tau_h(\lambda_j)$ = the transmittance of the gas section between the *i-th* zone and the *N-th* zone.
T_i = the temperature of zone *i*
$\overline{\tau_{N+1}}(\lambda_j)$ = the *transmittance* of the optical path between the gas layer and the detector, and it is usually assumed equal to 1.
The *Plank function* is considered negligible for everything in the optical path except the sample.
One can readily see that equation (VI-10) is just the special case of equation (VI-12) in which N=1 and the path between sample and detector is nonabsorbing.

VI.6.3 Non-homogeneous system and wide-band radiation

In real systems the measured radiant energy is never truly *monochromatic* or *unidirectional*. As consequence, measurements have to be carried out by integrating the impinging radiation over the bandwidth of the collecting filter ($\Delta\lambda' = \lambda' - \lambda_0$). It is convenient in this case to define $g(\lambda_0, \lambda')$ as the *optical system monochromatic transmittance* at wavelength λ' when the optical system is centered at wavelength λ_0. The function $g(\lambda_0, \lambda')$ contains wavelength independent constituents such as numerical aperture and mechanical slit-width $\Delta\lambda'$ as well as wavelength-dependent factors like lens and window transmittances, mirror reflectances, and dispersion. If the detection system bandwidth is narrow enough, the blackbody irradiance (I_B) can be considered constant over the band so that, if we carry out a measurement on a blackbody-like emitting source, we will obtain:

$$I_{Bm}(\lambda_0, T) = I_B(\lambda_0, T) \int_{\Delta\lambda'} g(\lambda_0, \lambda')\, d\lambda' \qquad \text{(VI-13)}$$

where $I_{Bm}(\lambda_0, T)$ is the *blackbody irradiance at temperature T and wavelength* λ_0 measured by means of a wide-band collecting filter. As a consequence, by calibrating the system by means of a blackbody-like source at different temperatures, it is possible to obtain the optical *transfer function* of the system necessary to correctly interpret the measurements.
It is important to note that, since the blackbody emittance is effectively constant over the values of $\Delta\lambda'$ corresponding to practical slit-widths, $I_{Bm}(\lambda_0, T)$ can be separated into two factors, of which one is independent of temperature and the other is independent of slit function.
Since, in general, variations of both the absorption coefficient $a(\lambda_i)$ and the *transmittance* $\tau(\lambda_i)$ within the instrument spectral bandwidth cannot be ignored, an integration over the wavelengths becomes mandatory.
For a *homogeneous system*, using equation (VI-10), we obtain:

$$I_m(\lambda_0) = \int_{\Delta\lambda'} I(\lambda')\, g(\lambda_0, \lambda')\, d\lambda' = I_B(\lambda_0, T) \int_{\Delta\lambda'} \left[1 - \tau(\lambda')\right] g(\lambda_0, \lambda')\, d\lambda' \qquad \text{(VI-14)}$$

That, according to the Lagrange mean value theorem, can be written as:

$$I_m(\lambda_0) = I_{Bm}(\lambda_0, T)\left[1 - \tau(\lambda_C)\right] = I_{Bm}(\lambda_0, T)\left[1 - \overline{\tau_{\Delta\lambda'}}\right] = I_{Bm}(\lambda_0, T)\ \overline{\varepsilon_{\Delta\lambda'}} \qquad \text{(VI-15)}$$

where:
λ_C = a properly chosen wavelength within the spectral range $\Delta\lambda'$
$\tau(\lambda_C) = \overline{\tau_{\Delta\lambda'}}$ is the average transmittance of the gas in the spectral range $\Delta\lambda'$ of the measuring filter.
This equation has the form of *Kirchhoff's law*.

In the monochromatic case the average *transmittance* τ is a function of different experimental parameters like the gas temperature and pressure as well as the optical path.

For a non-homogeneous system the equation describing the **wide-band infrared irradiance** is more complex. In fact, in this case equation (VI-12) has to be integrated over the measuring system spectral range (e.g., see Fig. VI-2); we obtain:

$$I_m(\lambda_0) = \sum_{i=1}^{N} I_B(\lambda_0, T_i) \int_{\Delta\lambda'} \left\{ \left[1-\tau(\lambda')\right] \prod_{j=i+1}^{N} \tau_j(\lambda') \right\} g(\lambda_0, \lambda')\, d\lambda' \qquad \text{(VI-16)}$$

By repeating the procedure utilized before, it becomes:

$$I_m(\lambda_0) \approx \sum_{i=1}^{N} I_{Bm}(\lambda_0, T)\left[1-\tau_i(\lambda_i)\right] \prod_{j=i+1}^{N} \tau_j(\lambda_j) \qquad \text{(VI-17)}$$

The solution of this equation requires some a priori knowledge of *transmittances* of the molecular species comprising the hot-gas specimen, particularly how they vary with temperature. This knowledge may take the form of empirical data, theoretical formulas, or a combination of these.
It has to be emphasized that the wavelengths λ_i depend on the selected gas layer, on its temperature as well as on its thickness.

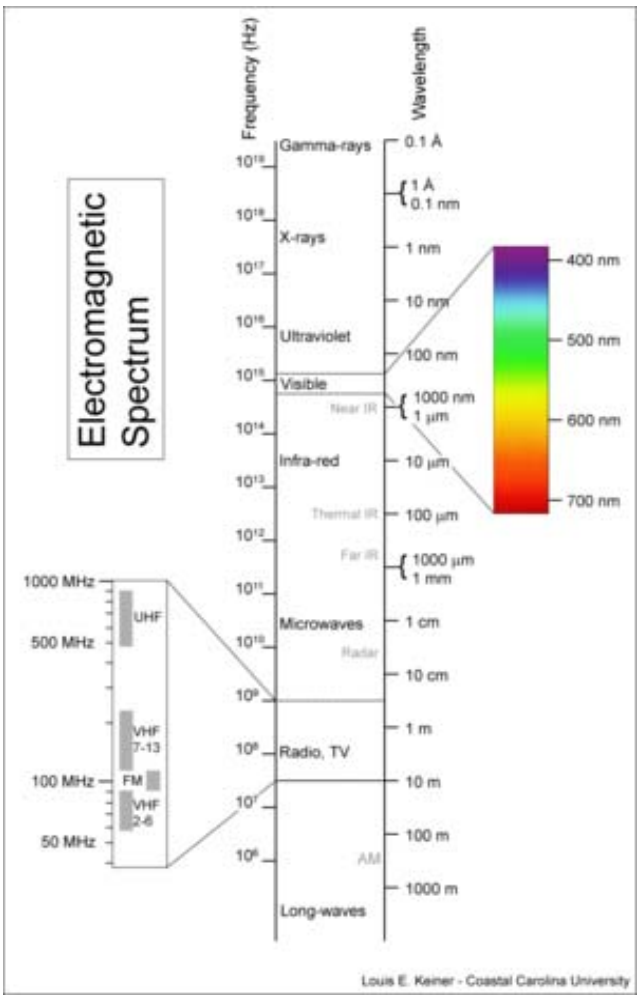

Fig. VI-2: Generic electromagnetic spectrum.

References

[VI-1] John R.R., Summerfield M., "Effect of turbulence on radiation intensity from propane-air flames", Jet Propulsion, Vol.27, pp.169–178, 1957.

[VI-2] Yip B. and Samaniego J.M., "Direct C2 Radical Imaging in Combustion Instabilities", Combustion Science and Technology, Vol.84, pp.81-89, 1992.

[VI-3] Keller J.O., Hongo I., "Pulse combustion: the mechanisms of NOx production. Combust Flame", Combustion and Flame, Vol.80, pp.219–237, 1990.

[VI-4] Yoshida A., Narisawa M., Tsuji H., Hirose T., "Chemiluminescence emission of C2, CH and OH radicals from opposed jet burner flames", JSME international journal, Series B, Japan Society of Mechanical Engineers (JSME), Tokyo, Japon, Vol. 38, pp.222–229, 1995.

[VI-5] Büchner H., Hirsch C., Leuckel W., "Experimental Investigations on the Dynamics of Pulsated Premixed Axial Jet Flames", Combustion Science and Technology, Vol. 94, Issue 1, pp. 219–228, 1993.

[VI-6] Keller J.O., Saito K., "Measurements of the Combusting Flow in a Pulse Combustor", Combustion Science and Technology, Vol. 53, Issue 2, pp. 137–163, 1987.

[VI-7] Pont G., Willis J.W., Karagozian A.R., Smith O.I., "Effects of External Acoustic Excitation on Waste Surrogate Destruction in an Resonant Incinerator", 26th Symposium (International) on Combustion, Proceedings of the Combustion Institute, Pittsburgh, Vol. 26, pp. 2463-2470, 1996.

[VI-8] Paschereit C.O., Gutmark E., Weisenstein W., "Control of Thermoacoustic Instabilities and Emissions in an Industrial Type Gas-Turbine Combustor", 27th International Symposium on Combustion, Proceeding of the Combustion Institute, Vol. 27, pp. 1817-1824, August 2-7, 1998.

[VI-9] Marrocco M. and Troiani G., "Industrial Combustion Testing", Chapter 12: Laser Measurements, 2009.

[VI-10] Dreizler A., "Experiments in turbulent combustion", VKI Lecture Series 2009-07, Turbulent Combustion, Von Karman Institute for Fluid Dynamics, May 25-29 2009.

[VI-11] Werle P., Slemr F., Maurer K., Kormann R., Mucke R., Janker B., "Near- and mid-infrared laser-optical sensors for gas analysis", Optics and Lasers in Engineering, Vol. 37, pp.101-114, 2002.

[VI-12] Rieker G.B., Jeffries J.B., Hanson R.K., Mathur T., Gruber M.R., Carter C.D., "Diode laser-based detection of combustor instabilities with application to a scramjet engine", Proceedings of the Combustion Institute, Vol.32, pp.831–838, 2009.

[VI-13] Tonddast-Navaei A., "Acoustic particle image velocimetry: development and applications", PhD thesis, The Open University, United Kingdom, UK, 2005.

[VI-14] Campbell M., Cosgrove J., Greated C., Jack S., Rockliff D., "Review of LDA and PIV applied to the measurement of sound and acoustic streaming", Optics and Laser Technology, vol. 32, issue 7, pp. 629–639, 2000.

[VI-15] Tonddast-Navaei A. and Sharp D., "The use of particle image velocimetry in the measurement of sound fields", Proceeding of the International Symposium on Musical Acoustics, Perugia, Italy, pp.379-382, 2001.

[VI-16] Kinsler L., Frey A., Coppens A., Sanders J., "Fundamentals of Acoustics", 4th edition, New York, 2000.

[VI-17] Skulina D., "PIV applied to the measurement of the acoustic particle velocity at the side hole of a duct", PhD thesis, University of Edinburgh, Scotland, 2005.

[VI-18] Skulina D., "A study of non-linear acoustic flows at the open end of a tube using Particle Image Velocimetry", The Journal of Acoustical Society of America vol.120, issue 5, p.3363, 2006.

[VI-19] Schulz C. and Sick V. "Tracer-LIF diagnostics: quantitative measurement of fuel concentration, temperature and fuel/air ratio in practical combustion systems", Progress in Energy and Combustion Science, vol. 31, pp.75-1212005.

[VI-20] Kaminski C., Hult J., Alden M., "High repetition rate planar laser induced fluorescence of OH in a turbulent non-premixed flame", Applied Physics B: Laser and Optics, vol. 68, issue 4, 1999.

[VI-21] Kaminski C., Hult J., Alden M., Lindenmaier S., Dreizler A., Mass U., Baum M., "Spark ignition of turbulent methane/air mixtures revealed by time-resolved planar laser induced fluorescence and direct numerical simulations", Proceedings of the Combustion Institute, vol 28, pp 399–405, 2000.

[VI-22] Dreizler A., Lindenmaier S., Maas U., Hult J., Aldin M., Kaminski C., "Characterisation of a spark ignition system by Planar-Laser-Induced fluorescence of oh at high repetition rates and comparisons with chemical kinetics calculations", Applied Physics B: Laser and Optics, vol.70, issue 2, pp. 287-294, 2000.

[VI-23] Donbar J., Driscoll J., Carter C., "Reaction zone structure in turbulent nonpremixed jet flames from CH-OH PLIF images", Combustion and Flame, vol.122, issue 1-2, pp.1–19, 2000.

[VI-24] Abu-Gharbieh R., Hamarneh G., Gustavsson T., Kaminski F., "Flame front tracking by laser induced fluorescence spectroscopy and advanced image analysis", Optics Express, vol. 8, issue 5, pp.278–287, 2001.

[VI-25] Haq M., Sheppard C., Woolley R., Greenhalgh D., Lockett R., "Wrinkling and curvature of laminar and turbulent premixed flames", Combustion and Flame, vol.131, pp.1-15, 2002.

[VI-26] Lee J.G. and Santavicca D.A., "Experimental diagnostics for the study of combustion instabilities in lean premixed combustors", AIAA Journal of Propulsion and Power, vol.19, issue 5, pp.735–750, 2003.

[VI-27] Gashi S., Hult J., Jenkins K., Chakraborty N., Cant S., Kaminski C., "Curvature and wrinkling of premixed flame kernels-comparisons of OH, PLIF and DNS data", Proceedings of the Combustion Institute, vol. 30, pp. 809–817, 2005.

[VI-28] Tanahashi M., Murakami S., Choi G., Fukuchi Y., Miyauchi T., "Simultaneous CH-OH PLIF and Stereo-scopic PIV measurements of turbulent premixed flames", Proceedings of the Combustion Institute, vol. 30, pp. 1665–1672, 2005.

[VI-29] Tanahashi M., Taka S., Hirayama T., Miyauchi T., "Simultaneous CH DPPLIF/OH PLIF and stereoscopic PIV in turbulent premixed flames", 21st ICDERS (International Colloquium on the Dynamics of Explosions and Reactive Systems), Poitiers, France, 2007.

[VI-30] Hult J., Gashi S., Chakraborty N., Klein M., Jenkins K., Cant S., Kaminski C., "Measurement of flame surface density for turbulent premixed flames using PLIF and DNS", Proceedings of the Combustion Institute, vol. 31, pp. 1319–1326, 2007.

[VI-31] Balachandran R., Ayoola B., Kaminski C., Dowling A., Mastorakos E., "Experimental investigation of the nonlinear response of turbulent premixed flames to imposed inlet velocity oscillations", Combustion and Flame, vol. 143, issue 1-2, pp. 37–55, 2005.

[VI-32] Clark T., "Studies of OH, CO, CH and C2 radiation from laminar and turbulent propane-air and ethylene-air flames", Technical report, NACA Technical Note 4266, 1958.

[VI-33] Paschereit C. and Polifke W., "Investigation of the thermo-acoustic characteristics of lean premixed gas turbine burner", ASME International Gas Turbine and Aeroengine Congress and Exposition, International Gas Turbine Institute (IGTI), ASME Turbo Expo98, paper 98-GT-582, Stockholm, Sweden, 1998.

[VI-34] Haber L., Vandsburger U., Saunders W., Khanna V., "An examination of the relationship between chemiluminescent light emissions and heat release rate under non-adiabatic conditions", ASME International Gas Turbine Institute (IGTI), ASME Turbo Expo98, paper 2000-GT-0121, Munich, pp. 1–8, 2000.

[VI-35] Haber L. and Vandsburger U., "Combustion and heat transfer dynamics in a premixed laminar flat-flame burner", Aerospace Sciences Meeting, 2004.

[VI-36] Khanna V., "Dynamic analysis of burner stabilized flames part 1: laminar premixed flames", International Symposium on American Flame Research Committee (AFRC), 2000.

[VI-37] Frank H., Kalt P., Bilger R., "Measurements of conditional velocities in turbulent premixed flames by simultaneous OH PLIF and PIV", Combustion and Flame, vol. 116, pp. 220–232, 1999.

[VI-38] Hult J., Josefsson G., Aldin M., Kaminski C., "Flame front tracking and simultaneous flow field visualisation in turbulent combustion", Proceedings of the 10th international Symposium on Applications of Laser Techniques to Fluid Mechanics, Lisbon, Portugal, paper No. 26-2, 2000.

[VI-39] Hult J., Harvey A., Kaminski C., "Combined high repetition-rate OH PLIF and stereoscopic PIV for studies of turbulence/chemistry interactions", Optical Society of America (OSA), 9th Topical Meeting on Laser Applications to Chemical and Environmental Analysis, Annapolis, Maryland, USA, 2004.

[VI-40] Kothnur P., Tsurikov M., Clemens N., Donbar J., Carter C., "Planar imaging of CH, OH, and velocity in turbulent non- premixed jet flames", Proceedings of the Combustion Institute, vol. 29, pp. 1921–1927, 2002.

[VI-41] Harvey A., Hult J., Kaminski C., Stonestreet P., "Simultaneous stereo PIV and PLIF measurements on the tecflam standard flame", Conference on Laser Applications to Chemical and Environmental Analysis, Boulder, USA, 2002.

[VI-42] Abu-Gharbieh R., Harmaneh G., Gustavsson T., Kaminski C., "Level set curvematching and particle image velocimetry for resolving chemistry and turbulence interactions in propagating flames", Journal of Mathematical Imaging and Vision, vol. 19, pp.199–218, 2003.

[VI-43] Tanahashi M., Kato S., Choi G., Miyauchi T., "Measurements of turbulent premixed flames by simultaneous CH-OH PLIF and stereoscopic PIV", Proceedings of Thermal Engineering, Tokyo, Japan, pp 311–312, 2004.

[VI-44] Boxx I., Stöhr M., Carter C., Meier W., "Temporally resolved planar measurements of transient phenomena in a partially pre-mixed swirl flame in a gas turbine model combustor", Combustion and Flame, Vol.157, Issue 8, pp. 1510-1525, 2010.

[VI-45] Tourin R.H. and Krakow B., "Applicability of Infrared Emission and absorption spectra to determination of hot gas temperature profiles", Applied Optics, Vol. 4, Issue 2, pp. 237-242, February 1965.

[VI-46] Gianinoni I., "Non-intrusive IR sensor for real time direct measurement of turbine inlet temperature", VKI Lecture Series 2009-06, High temperature pressure sensors for gas turbine applications, Von Karman Institute for Fluid Dynamics, May 11-14 2009.

VII. A novel approach: the ODC technique

VII.1 Motivations and objectives

A wide explanation about the importance and the need of studying thermo-acoustic instabilities was given in Part 1 of this PhD thesis, then now we summarize it in the first part of this paragraph.
The need to reduce the consumption of hydrocarbon fossil fuel energies and greenhouse gas emissions are worldwide imperatives that drive the Gas Turbine industry to continue to improve performance. Greater thermodynamic cycle efficiency cannot occur without engines operating at higher temperatures.
Higher cycle temperatures and pressure brings new challenges to the instrumentation community for better measurement methods and development of new approaches and innovation in test technology.
As the requirements for reducing emissions become more stringent, the combustor designs move towards a "lean" burning solution where the fuel/air mixture contains more air to allow for complete combustion of the fuel while forming less pollutants. However, such combustor designs are more susceptible to instability due to thermo-acoustic driven pressure oscillations. *Active control* of such oscillations can allow for more efficient, lower emissions combustor designs. Then, in recent years, there has been considerable research into combustion instability suppression.
Effective suppression of the high frequency combustion instabilities is a critical enabling technology for lean-burning low emission combustors and requires *sensors* and *algorithms* able to detect and interpret the instability.
Today new sensors and measurement techniques are needed to provide for high temperature hot section analyses and characterization and that data used to improved CFD and engine modelling tools.
New sensor and measurement technology provide one of the greatest opportunities to optimize the engine component efficiencies and allow higher operating temperatures. Simplicity in application and durability in operation are two important goals for any new sensor or measurement system.
High temperature sensors are routinely used in-service for the measurement of combustion instabilities in industrial gas turbine where the use of very lean fuel/air mixtures, which are required to achieve economical operation, can be accompanied by combustion instabilities which must be minimized to avoid structural damage.
Aim of this PhD thesis is to give a *novel approach* to study combustion instabilities using a new sensor sampling the radiant energy of flames. Attention is closed to radiant energy since it is intrinsically linked to combustion, thus containing information about chemical scales, and since it contains also information about turbulent scales.
The *novel proposed approach* shows that the usefulness of measurements of radiant energy emission from flames can be enhanced by focusing on a spatially limited region, by means of the *auto-correlation* and *cross-correlation* of signals from two points. Radiant energy is not sampled

pointlike, but in a wide region of reacting zone, in order to monitor eventual growing of instability precursors in different parts of flame.
Concluding aims of this PhD thesis are:

- Give a more practical, robust and simpler new diagnostic technique for industrial applications: ODC (*Optical Diagnostics of Combustion*; ENEA's patent).
- Investigate the use of flame Radiant Energy signal: due to its relation with both Turbulence and Chemical Kinetics (never before explored at such details), it may reveal the state of a flame and the eventual instability precursor events.
- Experimental proof that real-time information of combustion instabilities and mean velocity component can be performed by analyzing Radiant Energy captured by means photo-diodes (*ODC*).
- Experimental analysis of turbulent premixed combustion by means of ODC and application of it to a wide number of experimental and industrial burners, either premixed or not, fed with different fuels.

A collection of radiative emissions by several flames is analyzed in this chapter that is an extract of [I-12]. Such flames have been obtained in a number of burners, either premixed or not, fed with different fuels, while radiative emission is collected by means of a photo-diode according to the novel approach of ODC technique. The sampled signal is able to carry a large amount of information about chemistry of flames and its interaction with turbulence. All of the spectra computed show a decaying trend towards high frequencies with a slope of -5/3, that is known to be the inertial scaling of kinetic energy for homogeneous, isotropic, non-reacting turbulent flows. Aim of this chapter is to propose a *physical model to justify the radiant energy scaling law coming from this simple instrument*. To this purpose radiative emission of the flame has been splitted into two contributions, and its dynamics analyzed. The first contribution is the *chemiluminescence effect*, while the other is to be accounted for *thermal emission of a gray/black body*, ruled by Planck radiative equation. The time fluctuation of radiative emission is proposed to be linked to a thin reacting surface fluctuating in time and space under the constraint of turbulent fluid dynamic field. The thin reacting surface should be considered as the local flame front in premixed combustion, and as the local stoichiometric mixture fraction in nonpremixed case. Taking into account such emission mechanisms, a physical interpretation of the -5/3 slope is proposed.

VII.2 ODC: new diagnostic technique in ENEA

The **ENEA** headquartered in Rome, Italy (www.enea.it) is the ***Italian National Agency for New Technologies, Energy and Sustainable Economic Development***. ENEA has labs located in multiple locations in Italy and conducts a wide range of industrial combustion ranging in may application areas with particular emphasis on the environment, climate change and sustainability. In particular it provides online diagnostic systems and control expertice, related to a new technology.
ENEA has well established know-how in combustion:

- advanced nonintrusive diagnostics, with high spatial and temporal resolution, to identify and characterize combustion instabilities (flame blow-off, humming) and their precursors;

- integration of diagnostics within control loops;
- measurement campains with experimental equipment on laboratory scale, pilot and industrial plants.

Flame chemiluminescence is an electromagnetic radiation directly connected to combustion. The intensity of light emission is proportional to the production rate of some molecules; this implies that chemiluminescence can be used to measure reaction rates and heat release rate. Radiant energy emitted by flames of burners can be sampled by means of a photo-diode and a *new diagnostic technique* named **ODC** (***Optical Diagnostics of Combustion***) was developed and patented in **ENEA** ([VII-1], [VII-2]).
ODC is made by a *photodiode* that work in the range of 300-1100 nm (Fig. VII-1b), by a long monomodal (20 m) *quartz fiber* remoting the acquisition system, an by optical probe (Fig. VII-1a) with a *monomodal sapphire head* (d=1 mm) and an *alumina protection* (D= 7 mm). The *sapphire head* can work at high temperature (1800°C), then ODC techniques allows to monitoring directly the combustion process inside the combustion chamber, and it is able to analyse the thermo-acoustic flame instability in industrial applications.
The features of optical fibers, i.e. low intrusivity, robustness to mechanical vibrations, harsh environments and high temperatures, make ODC suitable to detect the stable or unstable state of a flame, and to be used as sensor for Active Control of combustion in Gas-Turbines.

(a)

(b)

Fig. VII-1: Component parts of ODC technique: monomodal sapphire head with alumina protection (a) and photodiode connection with optical fiber (b).

Radiative emission can be collected by means of a photo-diode, whose sampled signal is able to carry a large amount of information about chemistry of flames and its interaction with turbulence.
ODC methodology is based on radiant energy analysis emitted during combustion processes and lets to characterize at *high frequency* and in *real time* the dynamics of instability conditions, average flow speed, chemical species and temperature. This technique was also integrated in control loops aimed to widen the stable operating range of combustors [VII-3].
The sampled brightness spectrum contains information related to chemistry, because radiant energy is sampled at very high frequency, i.e., 5 MHz.

VII.3 Introduction about total radiation emitted by flames

Total radiation emitted by flames consist of two type of sources. The first is *chemiluminescence*, while the other is *thermal emission* associated to the Planck function ([III-60], [VII-4]).
Flame *chemiluminescence* is an electromagnetic radiation directly connected to combustion. It is due to electronically excited molecules produced by oxidation reactions emitting light when relaxing to lower energy states. In hydrocarbon flames the primary sources of chemiluminescence are electronically excited OH* (emitting near 308 nm in the ultraviolet (UV) region), CH* (emitting around 430 nm in the visible region, blue), C_2* (emitting around 519 nm in the visible region, green) and CO_2 (emitting continuously with a peak around 10600 nm). In lean hydrocarbon flames, OH* radical is responsible for most of the emission, followed by CH*, while C_2* emission is little. Rich flames instead, are characterized by stronger emission bands of CH* and C_2* ([VII-5], [VII-6], [VII-7]).
The intensity of light emission is proportional to the production rate of some molecules; this implies that chemiluminescence can be used to measure reaction rates [VII-8] and heat release rate ([II-143], [II-144], [VI-6], [VII-9], [VII-10], [VII-11], [VII-12]). Chemiluminescence intensity ratio OH*/CH* has also been used to measure equivalence ratio in partially premixed flames [II-143] and it has been observed that chemiluminescence intensities C_2*/CH* may provide indication of strain rate in perfectly premixed flames with known equivalence ratio [II-143]. Furthermore, OH* has also been measured by means of PITLIF (PIcosecond Time-resolved Laser-Induced Fluorescence) and used as tracer of turbulent scales [VII-13]; the capability of this tracing has been confirmed by LES simulations.
On the other hand, the *thermal contribution* to the total radiation has been used to estimate temperature, soot volume fraction, and gas species concentrations ([VII-14], [VII-15]).
Flame radiation has also been exploited as a tool to investigate flame extinction. In fact, both pre-mixed and nonpremixed flames close to lean blow-off (LBO) are characterized by large scale pulsations ([VII-16], [VII-17]) and lack of OH* radical for a significant amount of time ([VII-18], [VII-19]). The transition from stable combustion to LBO happens through a transient regime in which the flame experiences *localized extinctions and reignitions*; *large scale pulsations produce noise*, *changes in radiative emissions* ([II-150], [VII-20], [VII-21]), and *cyclic thermal loads*, that can be dangerous for the combustor walls and for the turbine blades located downstream of the combustor. These phenomena can be assumed as precursors for LBO; the number of precursor events in a given time window, and the duration of the event (usually defined as time spent outside of a threshold), increase as the LBO equivalence ratio limit is approached [VII-19]. Furthermore, frequency analysis shows that energy content increases dramatically near the LBO limit, both in radiative ([II-150], [VII-19], [VII-20]) and acoustic ([II-150], [VII-20], [VII-22]) forms.
It follows that flame radiative emission contains information related to both *chemistry* and *turbulence*, and it can be successfully used for monitoring flame stability and to detect flame blowout. This suggests to give a closer look at flame radiative energy and its relation with chemistry and turbulence.
In fact, analysis of flame radiation carried out in this work reveals that time spectra gives also evidence of a wide range of frequencies characterized by a clear scaling. What is quite surprising is that these findings have been obtained by using data coming from different experiments: different burners, fed with different fuels, either premixed or not; and what is more curious is that

this scaling, whose **exponent is -5/3**, is the same of turbulent kinetic energy in the inertial range of a homogeneous and isotropic non-reacting flow.
In this work an attempt to justify the characteristic scaling of time fluctuation of radiative emission, is proposed. In particular, radiant energy dynamics is reduced to the *dynamics of flame front* (for premixed flames) or of *stoichiometric mixture fraction surface* (for nonpremixed flames). Both these quantities fluctuate in time and space under the constrains of the turbulent fluid dynamic field. The physical model adopted is able to justify either the scaling of *time spectra* and the fact that such a scaling is *insensitive to probe orientation and type of combustion, premixed or not*.

VII.4 Optical apparatus and burners

In this chapter, data coming from different experimental works have been exploited to give a physical interpretation of radiative emission scaling by the spectral analysis. In particular:

1. **Burner A**: it has a rectangular cross-section and anchors a CH_4/Air premixed flame, whose nominal power is 3 kW, by means of a prismatic (triangular cross-section) bluff-body [VII-23]; the Reynolds number based on the wider side of the inlet channel was 12755 and the equivalence ratio was 0.8 .
2. **Burner B**: this is a 300 kW nonpremixed burner, burning H_2/O_2 at stoichiometric conditions; hydrogen is injected through a circular array of jets, and oxygen coflows; the flame is anchored by means of a recirculation zone due to the chamber geometry (MICOS plant in ENEA Casaccia Research Center, Italy). The single hydrogen jet Reynolds number is ~ 1000.
3. **Burner C**: it is fed with the same mixture as Burner A, resulting in a nominal power of 2 kW, operating in premixed conditions. It has an axisymmetric configuration with a conical bluff-body. Two cases are considered: in the "stable" one the flame was stably anchored, the Reynolds number based on the equivalent diameter of the burner exit section was 10400 and the equivalence ratio was 1.04; in the "unstable" case the flame was close to extinction, the Reynolds number was 8700 and the equivalence ratio was 1.44.

Radiant energy emitted by flames of burners A, B, and C was sampled by means of a photo-diode (Blue/UV Enhanced Silicon model 10530D) whose characteristics are reported in Fig. VII-2. The photo-diode was provided with lens for collimation. The angle of view of the instrument was ~ 18 deg (left panel of Fig. VII-2). Signals were collected for one second at 50 kHz thus using the whole bandwidth of the instrument (right panel in Fig. VII-2).

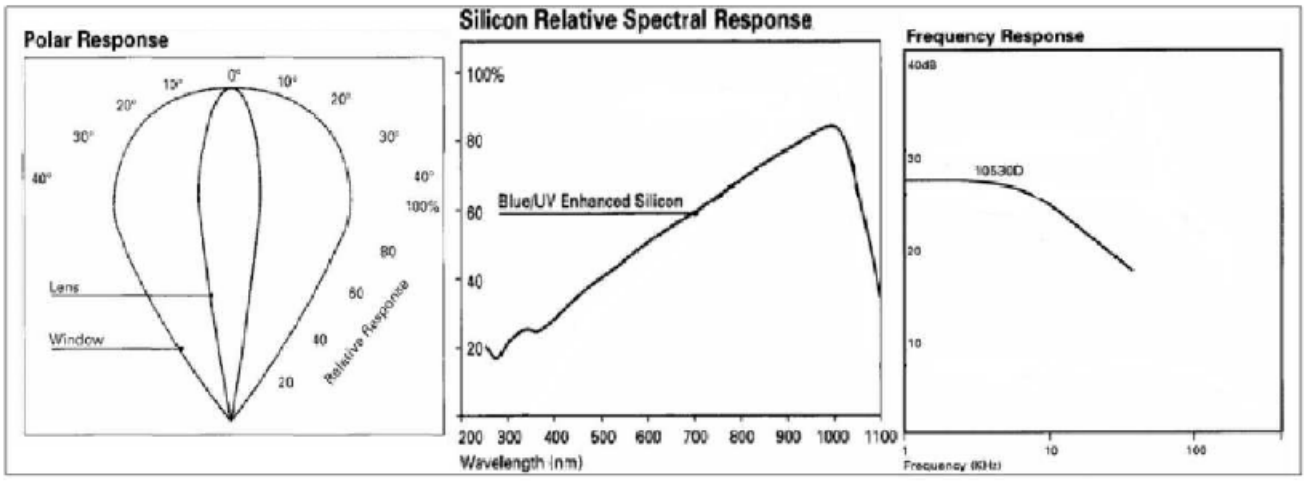

Fig. VII-2: Characteristics of the photo-diode used in the experiments.

VII.5 Spectral analysis of radiative emission by ODC technique

Radiation emitted by flames in burners A, B, and C was analyzed in time spectral domain with no optical filtering and experimental evidences are reported in the following. According to Fig. VII-2 (central panel), the sampled emissions refer to the continuous range [300-1100 nm] of wavelengths.

In particular, Fig. VII-3a (left panel) refers to burner A fed with a CH_4/Air mixture. The photo-diode point of view was normal to the burner axis and observed a ~ 4 cm diameter circular area towards a region where the flame behaves in a jet-like manner (120mm downstream of the bluff-body) [VII-23]. This spectrum results from the average of 60 spectra, each one associated to a time window of 1 s and sampled at 50 kHz. Inspection of this figure shows that radiative energy decays "inertially" following the power law $f^{-5/3}$, within a wide range of frequencies (more than one decade).

Furthermore, Fig. VII-3a reports a comparison between the radiative emission spectrum coming from burner A and a velocity spectrum obtained by means of Laser Doppler Anemometry (LDA) at the center of the region seen by the photo-diode [VII-23]. What is quite striking is that both the spectra exhibit a clear range of $f^{-5/3}$ scaling and that the same main frequency (10Hz) is measured by both techniques.

Fig. VII-3b (right panel) refers instead to a different burner (burner B) fed with H_2 and O_2 in a stoichiometric ratio. Here the only accessible viewpoint into the chamber was at the exit. The photo-diode point of view was coaxial with the burner and located at a distance of 1m from the inlet, pointing towards the burner itself. Also in this case the $f^{-5/3}$ scaling emerged in the radiative emission spectrum.

Fig. VII-4 refers to a third burner (burner C) with the photo-diode located as for case A. It was fed with a CH_4/Air mixture and it was operating at two different conditions. The "stable" condition was associated to a stable non-pulsating anchoring of the flame, while the "unstable" condition, close to extinction, was reached by decreasing the air mass flow rate. Both conditions exhibit the $f^{-5/3}$ scaling in the same frequency range.

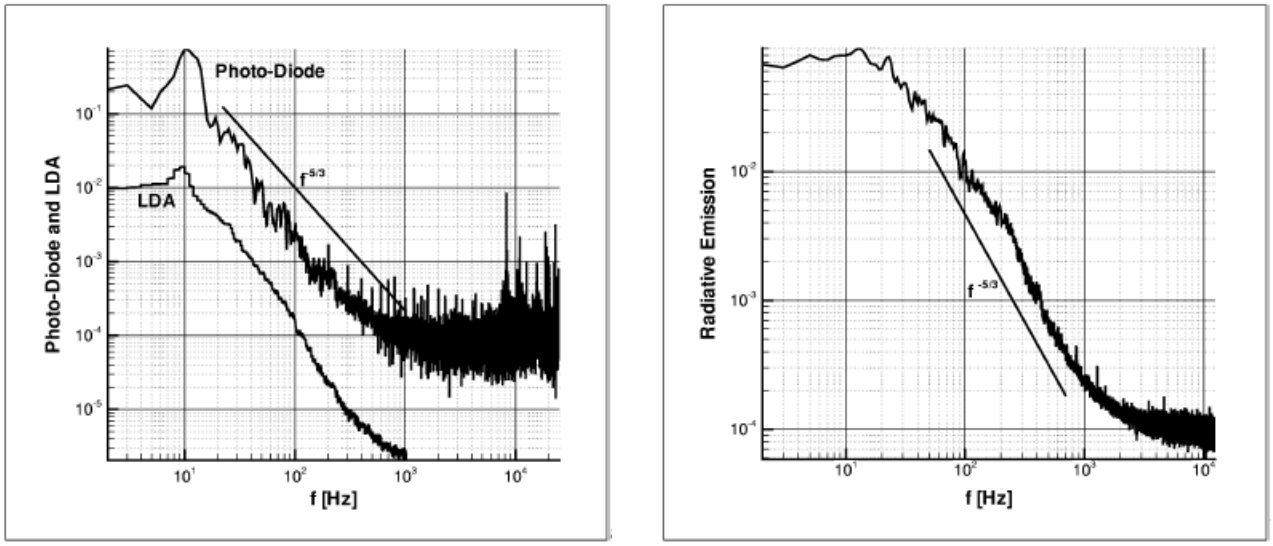

(a) **(b)**

Fig. VII-3: Flame radiative emission spectra obtained by means of a photo-diode (ODC). Figure ***a*** refers to a CH_4/Air premixed bluff-body flame (burner A) [VII-23] and it also shows axial velocity fluctuation spectrum obtained by means of LDA at the center point of the sampling area of the diode (LDA velocity spectrum must be considered reliable up to 100Hz, since particle data-rate was 1 kHz). Figure *b* refers to a H_2/O_2 stoichiometric nonpremixed flame (burner B). All spectra reveal a $f^{-5/3}$ energy decay.

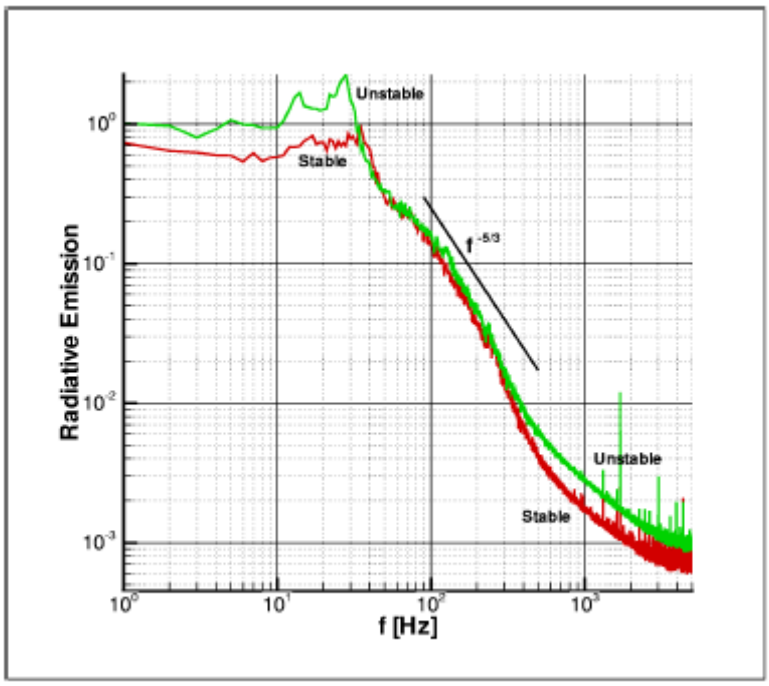

Fig. VII-4: Flame radiative emission spectra, obtained by means of a photo-diode, for a CH_4/Air premixed bluff-body flame (burner C) operating in two modes: in the "stable" case the flame was stably anchored and did not oscillate, whilst in the "unstable" case it was close to extinction and exhibited large oscillations.

Aforementioned radiative emission spectra were collected by the photo-diode with no optical filtering devices applied. Fig. VII-5, instead, reports several spectra associated to burner C and obtained by using different low-pass optical filters whose characteristic cut-off frequencies are reported in the legend of the same figure. All the spectra reported show the same scaling even if the amplitudes decrease when the upper limit (larger wavelengths) of the optical filter is decreased. Such a decrease could be associated to the fact that flame radiative emission is higher at large wavelengths, close to infrared region, and to the lower sensitivity of the photo-diode at shorter wavelengths (see Fig. VII-2).
As a summary, it can be said that the analysis of data coming from three different burners characterized by different *fuel composition*, type (premixed and nonpremixed), geometry and *probe point of view*, gives the same result: the presence of *a clear scaling well approximated by a power law whose exponent is -5/3*. Even sampling data by varying optical filtering width and position of the sensor, results have always displayed the same scaling law. As further support similar scaling can be educed also from spectra obtained by LIF OH* concentration measurements [VII-13]. Such an exponent -5/3 is known to have a profound meaning in different aspects of fluid dynamics. Nonreactive turbulent flows under the hypothesis of high Reynolds numbers, isotropy and homogeneity, undergo to Kolmogorov scaling law for turbulent kinetic energy spectrum, E(f) ~$f^{-5/3}$. Passive scalar (such as temperature) statistical fluctuations exhibit a spectral behaviour well approximated by a power law like T (f) ~ $f^{-5/3}$. Even active scalars under the hypothesis of high Reynolds and Peclet numbers follow a similar -5/3 trend [VII-24].
This present case deserves a special attention. In fact, combustion processes can be treated neither as isothermal turbulence nor as an active scalar. Actually active scalars interact with the velocity field but continuity equation in the form of $\nabla \cdot \bar{u} = 0$ still holds. This is not true for a flame where thermal expansions are great. Next sections will be devoted to the analysis of physical meaning of radiative emission and a plausible explanation of such scaling law will be attempted.

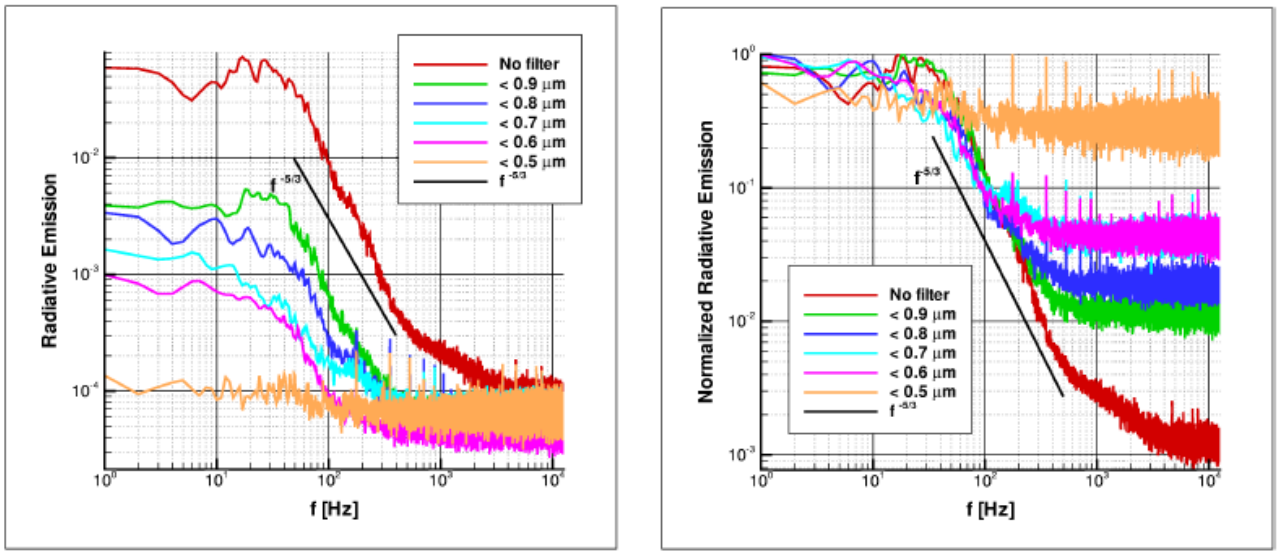

(a) **(b)**

Fig. VII-5: Optically filtered radiative emission spectra (in figure b normalized by their peak values) for a CH_4/Air premixed bluff-body flame (burner C, "stable" mode), obtained by means of a photo-diode.

VII.6 Physical Interpretation of Radiative Emission Scaling

Radiant energy sampled by the photo-diode is *integrated over the wavelength range* [λ_1, λ_2], *spatially filtered over a control volume* defined by its view angle, sketched in Fig. VII-6 (filtered quantities will be hereafter referred to as $\overline{...}$). In order to give a physical interpretation of the sampled signal we have to take into account the non-resolved physical mechanisms affecting filtered radiant energy. Being this control volume large enough (e.g., ~12 cm^2 for burners A and C) to constantly embrace a portion of the flame brush, where the flame does not experience any localized extinctions, it is likely to find four different volumes, respectively associated to cold reactants (V_R), to a thin reacting region (V_f), to hot products (V_P) and to the "surrounding space" (V_S). This thin reacting volume (V_f) must be considered as the local flame front in premixed combustion, and as the local stoichiometric mixture fraction front in nonpremixed case.
It is observed that the cold reactant volume V_R does not contribute to radiant energy emission due to its low temperature. Concerning the volume V_S associated to the medium (air, in all the cases examined) between the radiation source (the flame) and the observer (the photo-diode), it can be reasonably assumed that it has no effect on the dynamics of the sampled signal. In fact, in presence of a flame, two zones at different temperatures can be identified, one is the flame itself, and the other is the surrounding space. Temperatures in the flame are sufficiently high to emit even in the visible range, whilst in the outer space temperatures are so low to emit only in the *infrared range*, [750 –1000000 nm = 0.75 – 1000 μm], not detected by the photo-diode (see Fig. VII-2 central panel). Moreover, the absorption coefficient of the surrounding space (atmosphere) can be considered negligible in the photo-diode wavelength sensitivity range, [300−1100 nm = 0.3−1.1 μm] [VII-25]. This implies that the surrounding space can be thought transparent with respect to all the wavelengths up to the near infrared, thus not altering the dynamics of flame radiant energy sampled by the photo-diode: the sampled electromagnetic emission signal in the range of the photo-diode wavelengths is generated only close to the flame.
Founding on previous observations, the two volumes V_R and V_S will not be taken into account in the following analysis. Consequently, the control volume will consist of V_P and V_f , with $V_P >> V_f$. From the photo-diode point of view, volumes are reduced to overlapped emitting surfaces, hence, A_P and S_f for hot products and reacting zone, respectively. The thin *reacting surface* S_f is at temperature T_f and can be characterized by its *surface density* Σ. Recalling that $V_P >> V_f$, the hot product volume can be assumed at temperature T_P less than T_f and close to $\overline{T}$, that is the temperature spatially filtered over the photo-diode control volume, V; this leads to $T_P \cong \overline{T}$.
Within a constant burning rate, V_P , T_f and $\overline{T}$ can be considered constant in time, according to burner geometry, reactant flow rate and equivalence ratio. With this conceptual and physical model, the spatially filtered radiant energy can be expressed as:

$$\overline{I(t)} = \overline{\int_{\lambda 1}^{\lambda 2} A_e \, I(t,\lambda) \, d\lambda} \qquad \text{(VII-1)}$$

where A_e is the total emitting nonresolved surface, given by the sum of the *reacting surface* $S_f = \int \Sigma \, d\nu$ and the hot products emitting region A_P , and $I(t, \lambda)$ is the specific radiant energy per unit area and wavelength.

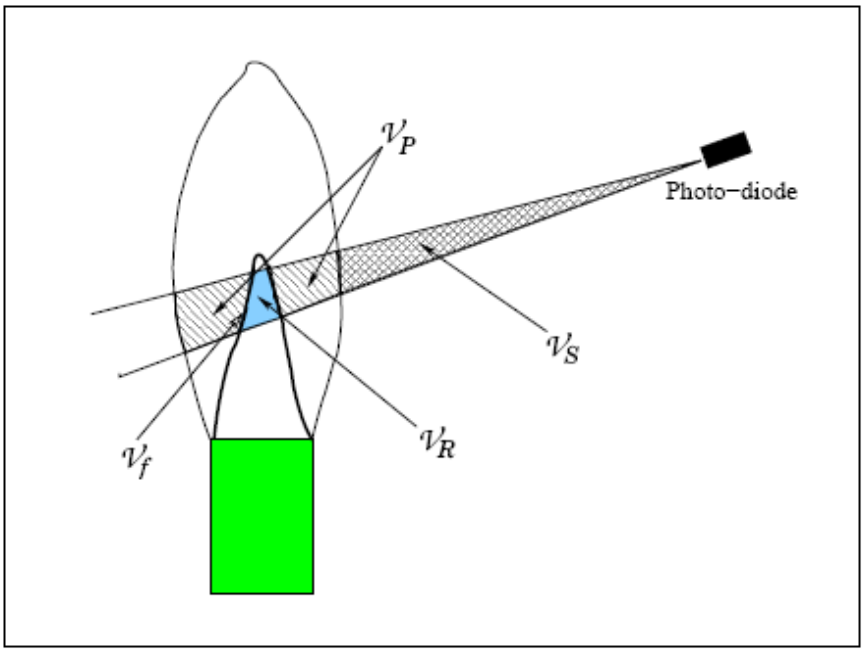

Fig. VII-6: Sketch of the control volume sampled by the photo-diode. The thin reacting volume V_f is evidenced by the thick line. V_P is the emitting *volume of hot products*, V_R is the *cold, non-emitting volume of reactants*, and V_S is the *transparent surrounding space*.

Light emitted by flames can be produced by two mechanisms: one is **chemiluminescence emission**, I_{ch}, associated to excited radical species within the thin *reacting region of the flame* S_f, and the other is the **thermal emission**, I_{th}, associated to the *Planck function* ([III-60], [VII-4]) and to the whole emitting surface $A_P + S_f$. Flame chemiluminescence is the natural UV-visible emission produced by excited radical species – CH* and OH* as an example, created by chemical reactions – when relaxing to their ground state. This mechanism is for example responsible for the blue light of H_2/O_2 flames. Such emitting species have no time to be neither advected nor diffused in the surrounding flow while they are in their excited state, since light emission lifetime is very short, of the order of 10^{-8} s ([III-60], p. 17). Chemical creation time of radicals is very short too, of the order of 10^{-4} s. Hence, according to Fig. VII-7 both chemiluminescence and chemistry time scales are well separated from turbulent fluctuations of the flow. On the other hand, flames can emit electromagnetic radiations accordingly to their temperature [VII-4]. This type of emission is the continuum contribution observed in typical spectral emission of flames [VII-26].
Thus,

$$\begin{aligned}\overline{I(t)} &= \overline{\int_{\lambda 1}^{\lambda 2} \left[S_f\, I_{ch} + A_p I_{th}\big|_{Ap} + S_f I_{th}\big|_{Sf} \right] d\lambda} = \\ &= \overline{\int_{\lambda 1}^{\lambda 2} S_f\, I_{ch}\, d\lambda} + \overline{\int_{\lambda 1}^{\lambda 2} \left(A_p I_{th} + S_f I_{th} \right) d\lambda} = \overline{\Psi_{ch}} + \overline{\Psi_{th}}\end{aligned} \qquad \text{(VII-2)}$$

Considering that *chemiluminescence emission* (I_{ch}) for individual radicals (subscript *rad*) is proportional to the product $i_{rad}\,\gamma^*_{rad}Y_{rad}$, where *i* is the *specific chemiluminescence emission*, *Y* is the *mass fraction* and γ* its *excited fraction*, it follows that

$$\overline{I(t)} \approx \underbrace{\overline{\int_{\lambda 1}^{\lambda 2} S_f(t) \sum_{rad=1}^{Nrad} i_{rad}\,\gamma^*_{rad}(T_f)Y_{rad}(t)\,d\lambda}}_{\overline{\Psi ch}} + \underbrace{\overline{\int_{\lambda 1}^{\lambda 2} \left[A_p\, I_{th}(\overline{T},\lambda) + S_f(t)\, I_{th}(T_f,\lambda)\right] d\lambda}}_{\overline{\Psi th}} \qquad \text{(VII-3)}$$

having explicited the functional dependences on temperature, wavelength and time of involved quantities. Finally, the spatially filtered radiant energy sampled by the photo-diode is given by

$$\overline{I(t)} \approx \overline{S_f(t) \sum_{rad=1}^{Nrad} i_{rad}\,\gamma^*_{rad}(T_f)\,Y_{rad}(t)\,\delta(\lambda-\lambda_{rad})} + \overline{\Psi_{th}} \qquad \text{(VII-4)}$$

where the peaked shape of radical spectral emission has been evidenced by replacing the integral over wavelengths with the Dirac delta function $\delta(\lambda-\lambda_{rad})$.

Some time-dependences expressed in equation (VII-4) can be neglected:

- Within a statistical constant burning rate assumption, since Y_{rad}(t) fluctuates at high frequency according to radical lifetime (see Fig. VII-7), it can be considered a constantly present tracer advected by the flow. Moreover, γ^*_{rad} depends on temperature T_f, that is constant, and i_{rad} depends only on the nature of molecule considered.
- It is also observed that the integral over wavelengths of the first addendum (related to A_P) in $\overline{\Psi_{th}}$ can be considered nearly constant in time, since $\overline{T}$ and A_P have been assumed constant. This means that the contribution to thermal emission due to the hot product region A_P can be considered as a slowly varying background radiation.

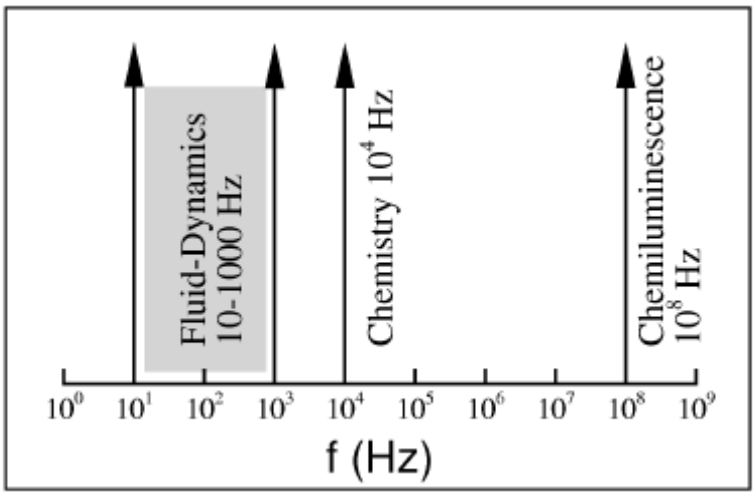

Fig. VII-7: Ranges of frequencies characterizing turbulent flames.

Thus, the time dependency of $\overline{I}$ is only given by the fluctuation of the thin flame front S_f, and thus of its surface density Σ. Having stated that time fluctuations of radiation are only due to Σ-fluctuations it is not feasible to discern between *chemiluminescence* ($\overline{\Psi_{ch}}$) and *thermal emissions* ($\overline{\Psi_{th}}$) once the photo-diode performed its wavelength integration.
Consequently, with a *wide separation between the frequency range of turbulence and of chemiluminescence*, and under the assumption of a *statistical steady burning rate* (i.e., constant reactants flow rate, hence, constant creation of emitting radicals, constant maximum temperature T_f and constant spatially filtered temperature $\overline{T}$), the dynamics of radiant emission from equation (VII-4) can be expressed as

$$\frac{D\overline{I}}{Dt} \approx \overline{\left[\sum_{rad=1}^{Nrad} i_{rad}\, \gamma^*_{rad}(T_f)\, Y_{rad}(t)\, \delta(\lambda - \lambda_{rad}) + \int_{\lambda 1}^{\lambda 2} I_{th}(T_f, \lambda)\, d\lambda \right] \frac{DS_f}{Dt}} \qquad \text{(VII-5)}$$

It is remarked that, since thermal emission due to hot product region A_P has been assumed nearly constant in time, its dynamical contribution is nil.
It is finally observed that ***radiant energy dynamics is reduced to the dynamics of*** $S_f = \int \Sigma\, dv$ ***and thus of flame surface density Σ***. *Being Σ advected by fluid dynamics, it is expected to undergo to the multi-scale nature of turbulence and its energy cascade evidenced by the -5/3 slope of the radiant energy power spectrum*. Actually, the dependency of radiation on wavelengths has been checked by using low-pass optical filters, thus limiting the upper integration bound of the photo-diode. Results of this analysis are reported in Fig. VII-5, where it can be observed a persistency of the -5/3 slope, even if the lower photodiode sensitivity towards UV region reduces the signal amplitude. Furthermore, the dynamics of radiant energy in terms of fluctuations of Σ is able to justify the ***indifference to the probe point of view***, since Σ time and space fluctuations are not direction dependent.

VII.7 Conclusions

This work has reported the experimental evidence that time spectra of turbulent flame radiative emissions have an inertial-like behaviour in a wide range of frequencies. Such a characteristic has been evidenced widely in a number of burners.
The main assumption is *that electromagnetic emission in the range of wavelengths* [0.3 - 1.1 μm] *is generated only close to the flame*, where temperatures are high enough, while the outer (and colder) space can be treated as a transparent, non-interacting medium. The emitted flame radiation has been considered as the superimposition of two effects. The first is the *chemiluminescence due to radicals located on a reacting surface*, i.e., the flame front or the stoichiometric contour for premixed and nonpremixed flames, respectively, and the second is the *thermal emission of hot products*. Under the assumption of a statistical steady burning rate and a wide separation between the time scales of turbulence and of chemistry/chemiluminescence, the time dependency of sampled electromagnetic emission signal is only given by the fluctuation of the thin reacting surface S_f. Expressing S_f in terms of its surface density Σ, that is advected by

fluid dynamics, it is expected to undergo to the multi-scale nature of turbulence and its energy cascade evidenced by the -5/3 slope of the radiant energy power spectrum.
The adopted physical model, confirming the experimental results, is able to justify either the scaling of time spectra and the fact that *such a scaling is insensitive to probe orientation and type of combustion, premixed or not*. Proof of such a model could come from the analysis of temporal fluctuations of Σ. This could be performed by using data from numerical simulations, since experimental recording of dynamics of Σ is still unfeasible.

References

[VII-1] Bruschi R., Stringola C., Casasanta V., Giacomazzi E., Coratella D., and Caruggi M. "Sistema di rivelazione e diagnosi di stato di combustione e relativo procedimento, applicabile in particolare a combustori", Italian Patent RM2004A000157, 29 March 2004.

[VII-2] Bruschi R., Grottadaurea M., Giacomazzi E., Giulietti E., Stringola C., Casasanta V., and Giammartini S., "Metodo e relativo dispositivo per la misura della velocità assiale dei gas combusti", Italian Patent RM2006A000159, 22 March 2006.

[VII-3] Bruschi R., Daniele S., Giacomazzi E., Giammartini S., Giulietti E., Manfredi F., Stringola C.; "Optical Unsteady Characterization of Turbulent Combustion: Application in an Active Control System", 41st AIAA/ASME/SAE/ASEE Joint Propulsion Conference & Exhibit.; number AIAA 2005-4328; Tucson (Arizona, USA), 10-13 July 2005.

[VII-4] Planck M., "The Theory of Heat Radiation", 2nd edition, Dover, New York, 1959.

[VII-5] Dandy D.S. and Vosen S.R., "Numerical and experimental studies of hydroxyl radical chemiluminescence in methane-air flame", Combustion Science and Technology, vol.82, Issue 1-6, pp.131–150, 1992.

[VII-6] Roby R.J., Reaney J.E., Johnsson E.L., "Detection of temperature and equivalence ratio in turbulent premixed flames using chemiluminescence", American Society of Mechanical Engineers (ASME International Joint Power Generation Conference), Fuel and Combustion Technologies Division (Publication) FACT, vol.22, pp.593-600, Baltimore, MD, 23-26 August, 1998.

[VII-7] Morrell R., Seitzman J., Wilensky M., Lee J., Lubarsky E., Zinn B., "Interpretation of optical flame emissions for sensors in liquid-fueled combustors", 39th Aerospace Sciences Meeting and Exhibit, AIAA paper 2001-1787, Reno, Nevada, 2001.

[VII-8] Gaydon A.G. and Wolfhard H.G., "Flames: Their Structure, Radiation, and Temperature", Chapman and Hall, London, 4th edition, 1979.

[VII-9] Mehta G., Ramachandra M.K., Strahle W.C., "Correlations between light emission, acoustic emission and ion density in premixed turbulent flames", Eighteenth Symposium (International) on Combustion, The Combustion Institute, Pittsburg, pp.1051-1059, 1981.

[VII-10] Roby R., Hamer A., Johnsson E., Tilstra S., Burt T., "Improved method for flame detection in combustion turbines", Journal of Engineering for Gas Turbines and Power, vol.117, Issue 2, pp.332–340, 1995.

[VII-11] Lawn C., "Distributions of instantaneous heat release by the cross-correlation of chemiluminescent emissions", Combustion and Flame, vol.123, Issue 1-2, pp.227-240, October 2000.

[VII-12] Ghosh A., Young G., Yu K., "Characterization of oscillatory heat release in unstable combustion", 41st AIAA/ASME/SAE/ASEE Joint Propulsion Conference and Exhibit, AIAA, AIAA paper 2005-4325, Tucson, Arizona, 2005.

[VII-13] Renfro H., Chaturvedy A., King G., Laurendau N.M., Kempf A., Dreizler A., Janicka J., "Comparison of OH time-series measurements and large-eddy simulations in hydrogen jet flames", Combustion and Flame, vol.139, Issue 1-2, pp.142–151, 2004.

[VII-14] Hilton M., Lettington A., Mills I., "Quantitative analysis of remote gas temperatures and concentrations from their infrared emission spectra", Measurement Science and Technology, vol.6, Issue 9, pp.1236-1241, September 1995.

[VII-15] Lim J., Sivathanu Y., Ji J., Gore J., "Estimating scalars from spectral radiation measurements in a homogeneous hot gas layer", Combustion and Flame, vol.137, Issue 1-2, pp.222–229, April 2004.

[VII-16] Nicholson H. and Field J., "Some experimental techniques for the investigation of mechanism of flame stabilization in the wakes of bluff bodies", Third Symposium (International) on Combustion, The Combustion Institute, Pittsburg, 1951.

[VII-17] Chao Y., Chang Y., Wu C., Cheng T., "An experimental investigation of the blowout process of a jet flame", 28th Symposium (International) on Combustion, The Combustion Institute, pp. 335–341, Pittsburg, Edinburgh, UK, July-August 2000.

[VII-18] Hedman P., Fletcher T., Flores D., Graham S., Haslam J., Murray R., Timothy G. "Observation of flame behavior in a laboratory-scale premixed natural gas/air gas turbine. combustor from planar laser induced fluorescence measurements of OH, Laser Doppler Anemometer velocity measurements, and coherent anti-stokes roman spectrometer temperature measurements", Journal of Engineering for Gas Turbines and Power-Transactions of the ASME vol.127, Issue 4, pp.724–739, 2005.

[VII-19] Muruganandam T., Nair S., Neumeier Y., Lieuwen T., Seitzman J., "Optical and acoustic sensing of lean blowout precursors", 38th AIAA/ASME/SAE/ASEE Joint

Propulsion Conference and Exhibit, AIAA paper 2002-3732, Indianapolis, Indiana, 2002.

[VII-20] Bruschi R., Giacomazzi E., Stringola C., Casasanta V., Manfredi F., Caruggi M., "Diagnostics of flow dynamics bringing to the onset of thermo-acoustic instabilities in gas-turbine combustors", 14th IFRF Members' Conference, IFRF, Noordwijkerhout, The Netherlands, 2004.

[VII-21] Muruganandam T. and Seitzman J., "Characterization of extinction events near blowout in swirl-dump combustors", 41st AIAA/ASME/SAE/ASEE Joint Propulsion Conference and Exhibit, AIAA paper 2005-4331, Tucson, Arizona, 2005.

[VII-22] Nair S., Muruganandam T., Hughes R., Wu L., Seitzman J., Lieuwen T., "Acoustic characterization of a piloted premixed flame under near blowout conditions", 38th AIAA/ASME/SAE/ASEE Joint Propulsion Conference and Exhibit, AIAA paper 2002-4011, indianapolis, Indiana, 2002.

[VII-23] Giacomazzi E., Giammartini S., Picchia F., Giulietti E., "Experimental and numerical tools for unsteady flows", XXVIII Event of the Italian Section of the Combustion Institute, paper number 006, Naples, Italy, 4-7 July, 2005.

[VII-24] Monin A.S., Yaglom A.M., "Statistical Fluid Mechanics: Mechanics of Turbulence", Volume 1, John L. Lumley, 1975.

[VII-25] Wallace J.M. and Hobbs P.V., "Atmospheric science: an introductory survey", 1st edition Academic Press, New York, p. 332, 1977.

[VII-26] Mavrodineau R. and Boiteux H., "Flame Spectroscopy", John Wiley and Sons, New York, 1965.

VIII. Results in industrial burners, Discussion and Conclusions

VIII.1 Introduction

This chapter focuses on thermo-acoustic instabilities in turbulent reactive flows. The coupling between fluctuations of the heat release rate and pressure oscillations drives this type of combustion instability. Self excited oscillations need a feedback mechanism to induce growing amplitude oscillations of pressure. Usually (but not always) this feedback is determined by the acoustics of the system: pressure waves generally due to the feeding system make the incoming fuel flow rate fluctuate; in turns this drives a further oscillation of the heat release rate, and this induces a new pressure wave.
A technique for determining the instantaneous *heat release* from a localized region of a flame and correlating it with the fluctuating pressure is described. The technique ODC is based on radiant emission sampled by a photodiode.
A novel feature of the approach is the use of the *rms* fluctuations in signal rather than the mean level as the indicator of mean turbulent heat release. Results of applying this novel technique to a premixed swirling flame under conditions of low acoustic self-excitation are presented.
The purpose of this chapter is to show that the usefulness of measurements of radiant energy emission from flames can be enhanced by focusing on a spatially limited region, by means of the *auto-correlation* and *cross-correlation* of signals from two points. This technique is explored in the context of investigating the acoustic excitation of flames.
Radiant energy signals will be received from a particular region as the flamelets are convected across the field of view. The signals will thus have a similar spectrum to that of the turbulent velocity components, and the instantaneous intensity is assumed to be proportional to the heat release rate per unit volume.
A technique based on the ultraviolet at 307 nm by the chemiluminescence of the OH* radical, which is closely associated with the combustion reactions in gaseous hydrocarbon flames, was investigated by Lawn in 2000 ([VII-11], [VIII-1]). The UV radiation at 307 nm from a turbulent flame is assumed to be a measure of the instantaneous rate of heat release from within the collection volume. Any spectral component of the signal is approximately proportional to the heat release fluctuation associated with that particular frequency band. Determination of the convection velocity of the turbulent flame between two lines-of-sight is possible using two photodiode having an optic filter centered on 307 nm, and this provides a measure of the average velocity in the flame. Displacements of not much more than 1 mm were sufficient to give rise to this phase difference, and the coherence between the two signals remained high (above 0.6) for displacements of up to 3 mm. Then, information about the local characteristics of a flame can be obtained by examining the product of the emissions along two different directions. The variation of the phase with axial displacement is a measure of the mean axial convection velocity ([VII-11], [VIII-1]). The volume from which correlated signals might be expected is related to the ***integral length scale*** of the flame surface fluctuations.

VIII.2 Experimental set-up and first ODC applications

The strategy proposed to characterize the unsteadiness of a turbulent flame and to detect its stable or unstable state is based on a new diagnostic methodology optical system called **ODC** (***Optical Diagnostics of Combustion***) ([I-12], [VII-1], [VII-2], [VII-23]) that uses photo-diodes as sensor and optical fibers. Furthermore, two pressure transducer are used for validation and to look for correlation with heat release in one of different burners examined (Fig. VIII-10).
In this chapter, data coming from previous experimental works have been exploited [VIII-2]. In particular:

- **Burner A: 250kW Premixed Liquid Oil/Air Burner**
  This burner, sketched in Fig. VIII-1A, is the LRPM (Liquid Rapid PreMixer) facility in Savona Combustion Laboratory (DIMSET/SCL, Italy). This facility is equipped with an air compressor and an air preheater.
  The mixer length is 1.5m, the combustion chamber length is 0.3m, and the chimney length is 1.2m. Air and liquid oil are uniformly mixed by means of the Rapid Premixer swirler. Ignition does not require any pilot flame. This facility was equipped with a photo-diode (ODC system) and a pressure transducer. Both the pressure transducer and the ODC were located in front of the flame, as shown in Fig. VIII-1A.

- **Burner B: 300kW Nonpremixed H_2/O_2 Burner**
  This 300kW burner, sketched in Fig. VIII-1B, is mounted on the MICOS plant in ENEA Casaccia Research Center (Rome, Italy). It is a nonpremixed burner feeded with H_2/O_2 at stoichiometric conditions; hydrogen is injected through a circular array of jets, and oxygen coflows; the flame is anchored by means of a recirculation zone due to the chamber geometry.

- **Burner C: 500kW Premixed CH_4/Air Burner**
  This premixed, CH_4/Air, burner, sketched in Fig. VIII-1C, is located in ANSALDO Ricerche center in Gioia del Colle (Italy). Mixing is achieved by means of a swirler.

Radiant energy is not sampled pointlike, but in a wide region of reacting zone, in order to monitor eventual growing of instability precursors in different parts of flame [VIII-2]. By means of optical devices like photo-diodes, signal can be sampled at very high frequency, thus providing an excellent statistics. Moreover, it is easy to implement efficient and fast diagnostic algorithm suitable for real-time control [VII-3]. Attention is closed to radiant energy since it is intrinsically linked to combustion, thus containing information about chemical scales, and since it contains also information about turbulent scales. In fact, it has been shown that chemical scales are captured because radiant energy is sampled at high frequency (at least 25 kHz), and turbulent scales are captured because radiant energy dynamics is proportional to temperature dynamics that behaves as turbulent passive or active scalar [I-12].

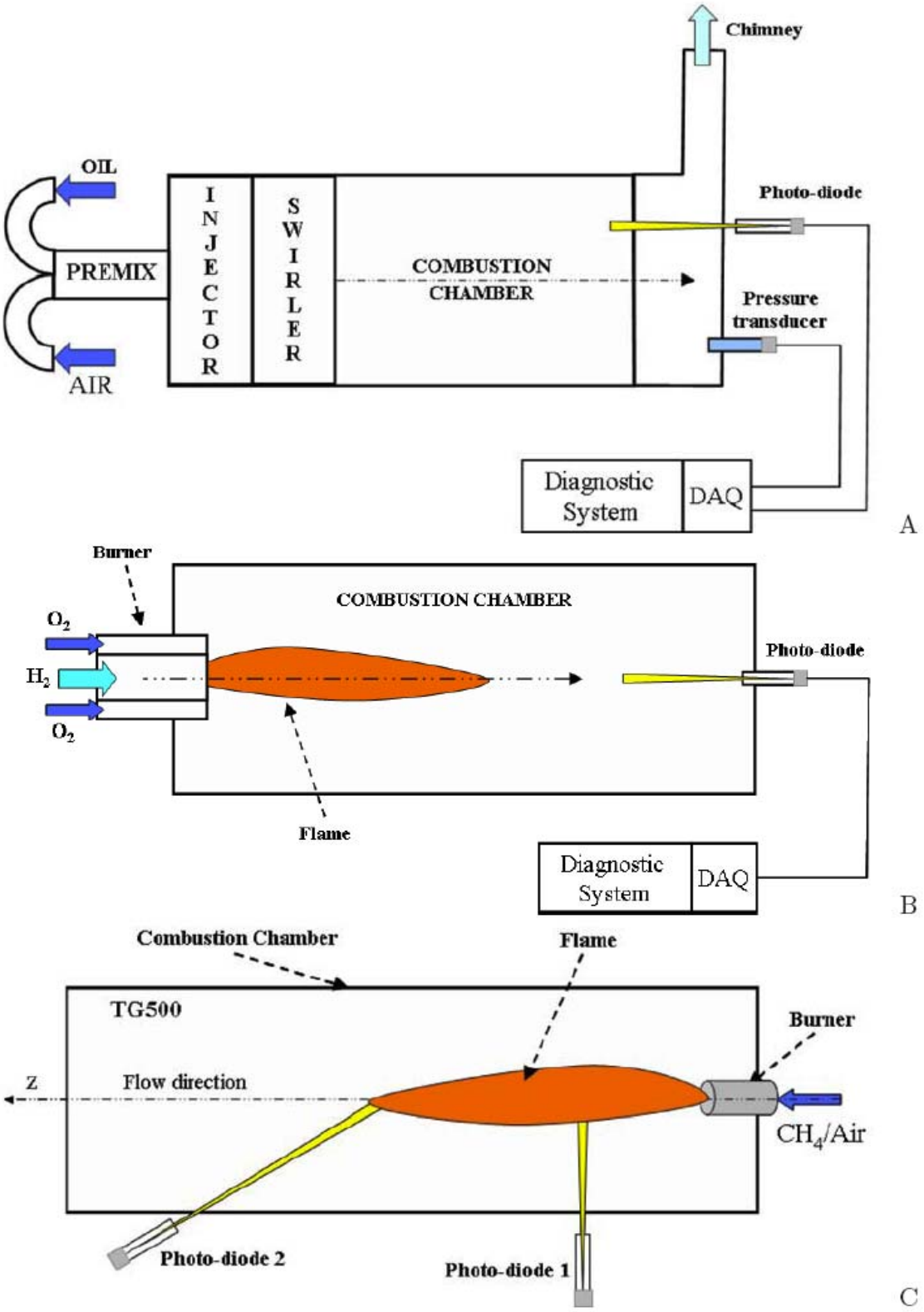

Fig. VIII-1: Sketch of the burners examined in this work. Burner A is the 250kW Liquid Rapid Premixed burner in Savona combustion laboratory; burner B is the 300kW MICOS burner in ENEA Casaccia Research center in Rome; burner C is the 500kW ANSALDO Ricerche burner in Gioia del Colle. [VIII-2]

In a nutshell, ODC system uses radiant energy as a nonintrusive and natural seeding to describe turbulent combustion dynamics. This means that combustion instabilities, both fluid-dynamic and thermo-acoustic, extinctions and reignitions, and pulsations can be detected. In particular, this work shows that the nonzero auto-correlation function of radiant energy signal identifies the onset of thermo-acoustic instabilities.
Furthermore, being the radiant energy dynamics proportional to temperature dynamics, ODC also reveals time evolution of the average (in space) temperature inside the combustion chamber; measurements show that temperature increases rapidly before (a few seconds) the onset of thermo-acoustic instability.

VIII.2.1 250kW Premixed Liquid Oil/Air Savona Burner

This burner, when feeded by means of 288 g/s of air and 0.168 g/s of liquid oil, is in a stable mode. Increasing fuel mass flow rate up to 0.232 g/s, the operating mode switches to unstable; the type of instability is not fluid-dynamic, but thermo-acoustic. Air is preheated at 1073 K. The operating mode transition from stability to "humming" is analyzed by using a pressure transducer and ODC with not collimated photodiode.
Fig. VIII-2 shows the time evolution of radiant energy (black line) and pressure (red line) raw signals in a 30 s time window. The radiant energy signal increases slowly as the fuel mass flow rate is increased, meaning an increase of the averaged temperature inside the burner. Seven time windows, each of 0.5 s and marked in the same figure from A to G, are here examined as representative of different operating conditions of the burner: they range from stability (A) to situations showing precursors of instability without (B) and with (C) temperature increase (drift), up to the quick onset of instability (D), then to "humming" (E) and then, through a quick exit from this regime (F), back to stability (G). These conditions are reached by firstly increasing and then decreasing the fuel mass flow rate.

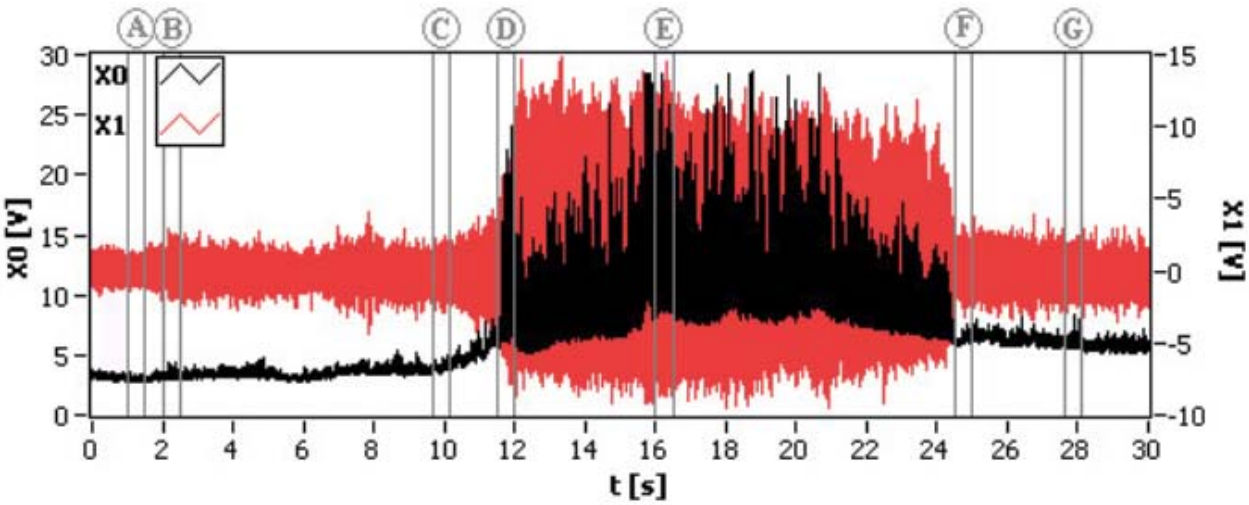

Fig. VIII-2: Characterization of transition from stable to unstable mode in the 250kW premixed liquid oil/air burner located in Savona Combustion Laboratory (Savona, Italy). The red line refers to pressure signal, while the black one to radiant energy. [VIII-2]

Fig. VIII-3 shows some information associated to the intervals marked in Fig. VIII-2. In particular, the first column from left (index 1) reports ***cross-correlation*** between pressure and radiant energy signals; the central column (index 2) reports ***auto-correlation*** for both signals (it was calculated without subtracting the average value of the signal in the time window considered, and normalized by its variance); the third column (index 3) reports semi-log plots of ***frequency spectra***.

Looking at Fig. VIII-3, it can be observed that when the burner is in the *stable operating mode* (A), pressure and radiant energy are not correlated (plot A1), nor auto-correlated (plot A2). Furthermore, this condition does not show any dominant frequencies, apart from some peaks with amplitude negligible with respect to those present in the other time windows (plot A3): 15, 39, 52 and 66Hz for *radiant energy* and 17, 54, 74, 80Hz for *pressure*. It is stressed that pressure peaks are at frequencies slightly higher than radiant energy.

While increasing fuel mass flow rate, some *precursors of instability* appear, thus increasing correlation and auto-correlation of both signals (plots B1 and B2). When this condition is reached the system shows a dominant frequency at ~ 80 Hz (plot B3). It is interesting to note that this dominant frequency was in fact already present in the pressure field of the stable regime (plot A3); increasing fuel mass flow rate forced radiant energy field to synchronize with pressure field, since pressure field is expected to modulate inlet flow rates and consequently heat release.

Unstable situations like the previous one have short life-time and the system quickly tends to dampen these fluctuations. Continuing to increase fuel mass flow rate more energy is released inside the system; then temperature increases (as the radiant energy drift of Fig. VIII-2 from C to D confirms), and the precursor events become more frequent. The dominant frequency evidenced in plot B3 (i.e., ~ 80 Hz) tends to become steady, being present (plot C3) also when cross-correlation between pressure and radiant energy is negligible (plot C1). “Calm” situations like this may arise during transition to “humming”. In plot C3 radiation shows a richer frequency spectrum than pressure, especially at frequencies lower than the dominant 80Hz, with a peak at 32 Hz, even though amplitudes of both signals are lower than in plot B3. Pressure is not auto-correlated (plot C2), while the auto-correlation of radiant energy is not negligible, thus providing information about the unstable state of the system. It is noted that radiant energy auto-correlation in plot C2 seems not to show a “burst mode” as in plot B2, but this is due to the specific expression used to calculate it in all this work: not removing the local average of signal in the 0.5 s time window used to calculate the auto-correlation normalized by means of variance enhances the effect of signal drift between C and D. This fact also explains the zero cross-correlation between pressure and radiant energy (plot C1).

In correspondence of the steep radiant energy gradient (D) there is the onset of instability, i.e, the transition to a fully established unstable condition (“humming”): cross-correlation and auto-correlation grow (plots D1, D2, E1, E2); characteristic frequencies are shifted (112 and 136Hz in plot D3) according to the increase in temperature of the medium (that increases the sound speed, i.e., propagation velocity of acoustic wave), and then “selected” up to the establishment of a single frequency (112 Hz in plot E3). It is observed that if the wavelength of the standing acoustic wave is assumed constant during the transition from B to E, it follows that the ratio between the dominant frequencies, i.e., 112/80 = 1.4, is equal to the ratio between the sound speeds; thus, the ratio between temperatures inside the chamber is TE/TB = 1.96, that might be considered in agreement with the increase of the radiation amplitude in Fig. VIII-2.

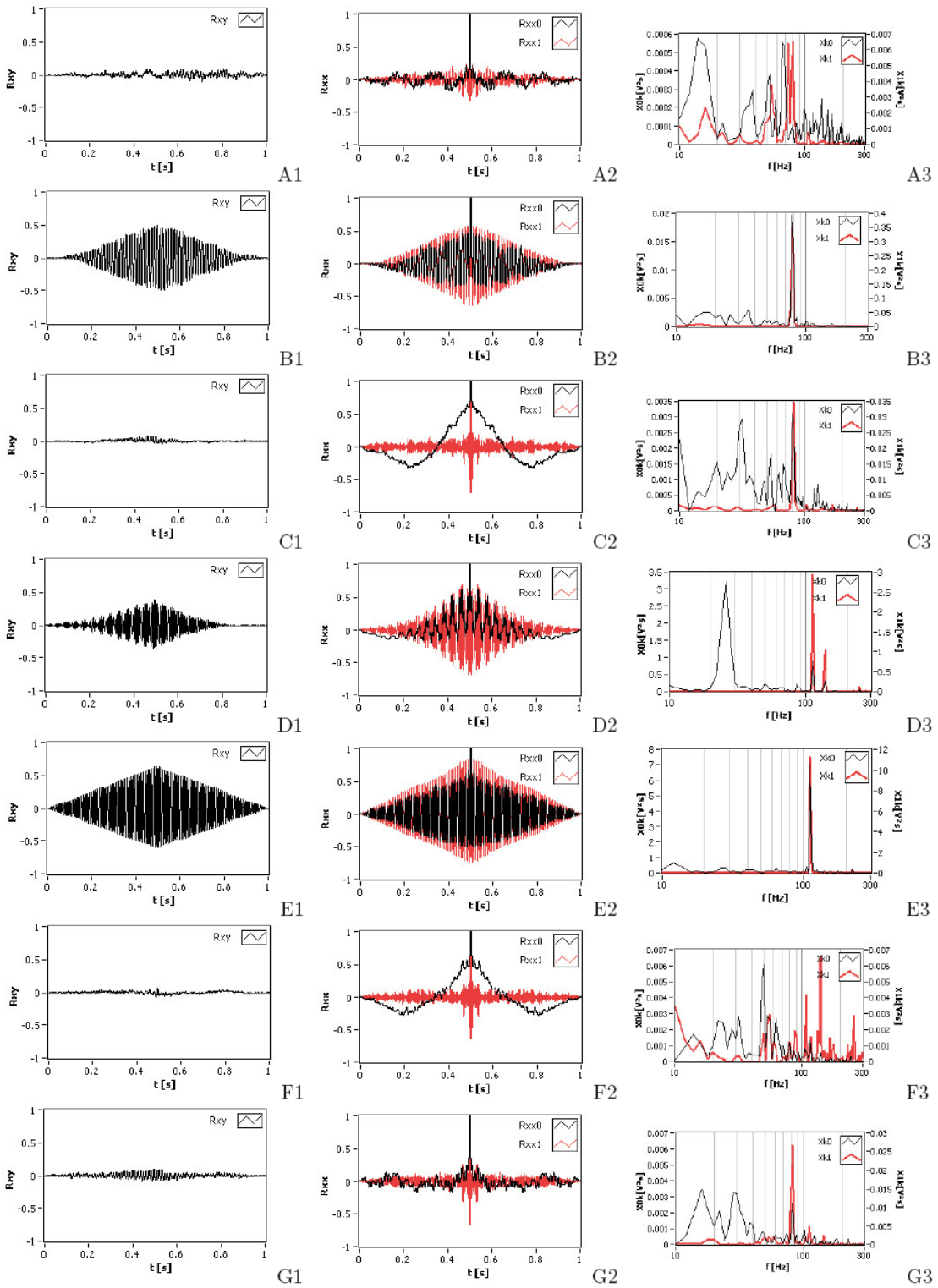

Fig. VIII-3: Characterization of transition from stable to unstable mode in the Liquid Rapid Premixed burner of Savona combustion laboratory. The letters from A to G refer to time intervals in Fig. VIII-2. The first column from left (index 1) reports cross-correlation between pressure and radiant energy signals; the central column (index 2) reports autocorrelation for both signals; the third column (index 3) reports frequency spectra. In the last two type of graphics the red line refers to pressure signal, while the black one to radiant energy. [VIII-2]

When fuel mass flow rate is decreased down to its initial value the system tends to exit from the unstable regime (F) in a way similar to its entrance (C). Pressure and radiation are not correlated anylonger exhibiting rich frequency spectra of low amplitudes (plot F3); in particular, pressure spectrum spreads over a wide range of frequencies, while radiation is confined to frequencies lower than the ~ 80 Hz dominant in condition B. It is interesting to note that the acoustic frequencies 108 and 140 Hz, approximatively already present in plot D3, appear again.
Finally, the system slowly turns back to its stable initial configuration (G). Averaged temperature level inside the combustor stays still high (in the time 30 s window analyzed), likely due to walls, now hotter than before "humming". This means that transition to the stable mode is slow and that the system may turn back to "humming" easier than before, i.e., by a less increase of the fuel mass flow rate.
As concluding remark, it is stressed that precursor events tend to grow many seconds prior the fully establishment of instability, as in case B (see plot B2 and E2); in particular, they are detected ~ **14 s earlier by the photo-diode**. This feature is strategic for active control applications.

VIII.2.2 300kW Nonpremixed H2/O2 MICOS Burner

This burner, when feeded by means of 1.5Nm3/h of O_2 and 3.5Nm^3/h of H_2, is in a stable stoichiometric condition. Increasing O_2 mass flow rate up to 6 Nm^3/h, the operating mode becomes unstable, and combustion produces a lot of noise. The transition from stability to "humming" is analyzed by using the ODC in a 150 s time window.
Fig. VIII-4 shows the time evolution of radiant energy. Five time windows, each of 0.5 s and marked in the same figure from A to E, are considered as representative of different operating conditions of the burner: they range from stability (A) to instability (B and C) and then, through a quick exit from this regime (D), back to stability (E).
Fig. VIII-6 shows some information associated to the intervals marked in Fig. 5. In particular, the first column (index 1) reports normalized auto-correlation and the second one (index 2) reports semi-log plots of frequency spectra.
Looking at Fig. VIII-6, it can be observed that when the burner is in the stable operating mode (A) radiant energy is weakly correlated (plot A1). Furthermore, this condition shows a dominant frequency (~ 70Hz).
While increasing oxygen mass flow rate, mixture becomes poor and tends to show unstable characteristics. These are identified by looking at auto-correlation that increases (plot B2); furthermore, the system shows two dominant frequencies at ~ 60 and 250Hz. The latter frequency was not present in the radiation field of the stable regime (plot A2), and does not change from B2 to C2. In C the lower frequency is decreased in amplitude. Looking at Fig. VIII-4, it is observed that the radiant energy increases from B to C, but the amplitude of spectrum is greater in B (plot B2) than in C (plot C2); also the number of peaks in autocorrelation is greater in plot B1 than in plot C1. This means that the system can turn back to stable condition also when heat release (radiant energy) increases, because changes of sound speed may strongly alter the synchronization between heat release and pressure waves.
Turning back to the initial oxygen mass flow rate, the heat release decreases. The auto-correlation of radiant energy decreases too (plot D1 and E1) and does not show a "burst mode" as in plots B1

and C1. It is stressed that the case D is located where there is a steep gradient of radiant energy; therefore, as in plots C2 and F2 of Fig. VIII-3, plot D1 shows the effect of temperature drift. The frequency spectra (plots D2 and E2) turn back similar to that in plot B2.

VIII.2.3 500kW Premixed CH4/Air TG500 Burner

This burner is analyzed in a 80 s time window, as shown in Fig. VIII-5. Looking at plots A1 and A2 of Fig. VIII-7, it is observed that weak instabilities are experienced also at initial nominal conditions. By changing mass flow rates these instabilities are enhanced up to the establishment of a dominant frequency of ~ 50Hz in plot B2 that shifts up to ~ 60 Hz in plot D2. It is noted that in this case, when heat release is maximum, the system goes out from "humming" state (see plot E2), even though plot E1 shows a nonnegligible autocorrelation due to the temperature drift of the system.

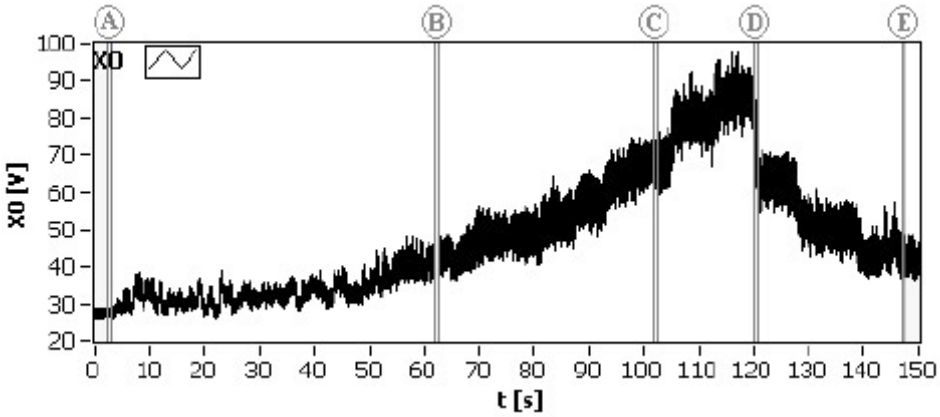

Fig. VIII-4: Characterization of transition from stable to unstable mode in the 300kW nonpremixed H2/O2 MICOS burner located in ENEA Casaccia research center (Rome, Italy). [VIII-2]

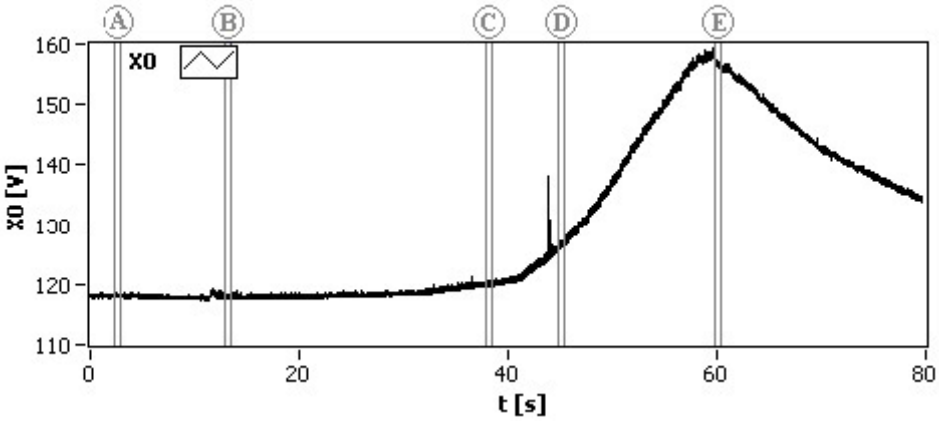

Fig. VIII-5: Characterization of transition from stable to unstable mode in the 500kW premixed CH4/Air TG500 burner located in ANSALDO research center (Gioia del Colle, Bari, Italy).[VIII-2]

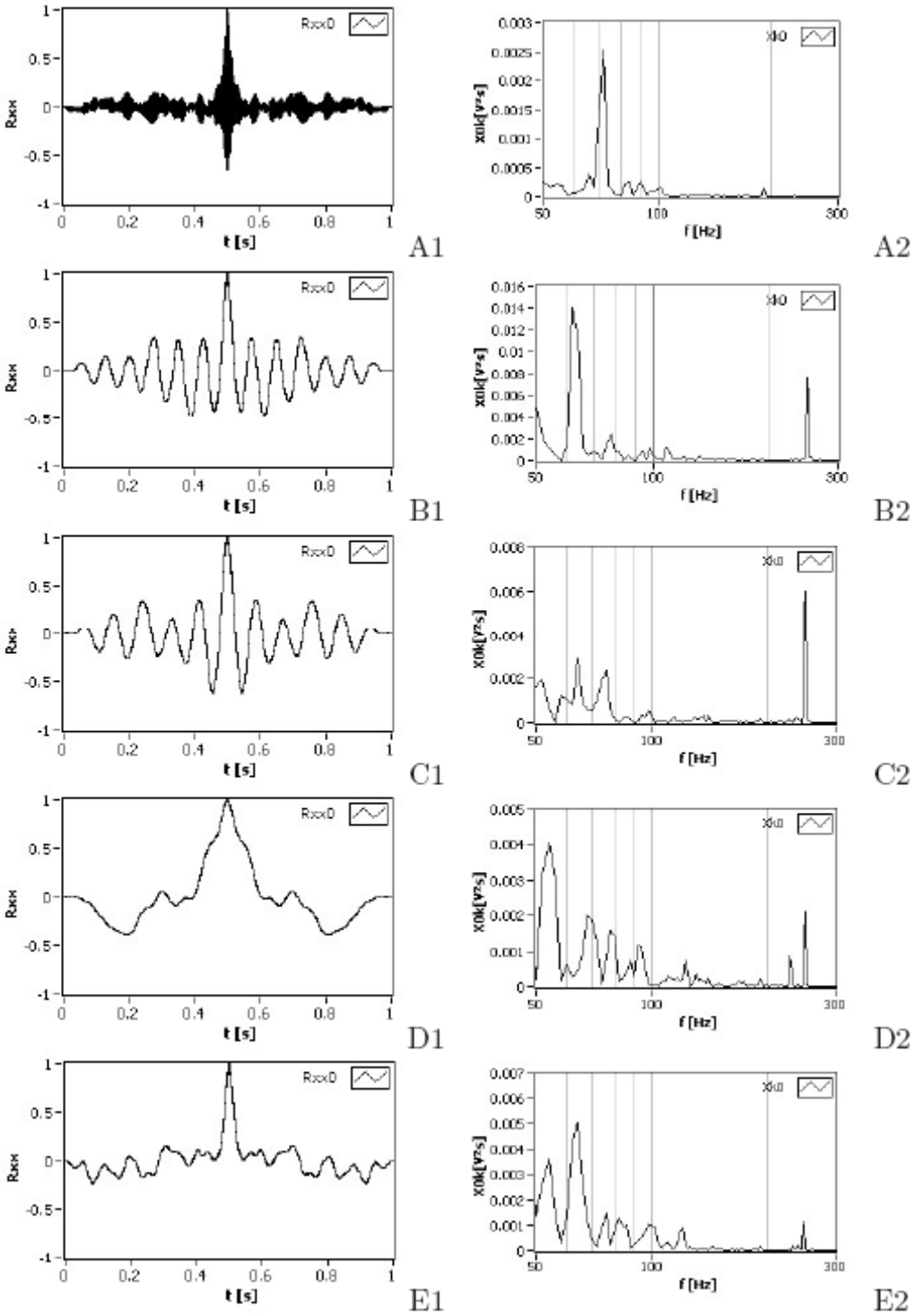

Fig. VIII-6: Characterization of transition from stable to unstable mode in the MICOS burner. The letters from A to E refer to time intervals in Fig. VIII-4. The first column from left (index 1) reports auto-correlation of radiant energy signal; the second column (index 2) reports its frequency spectra. [VIII-2]

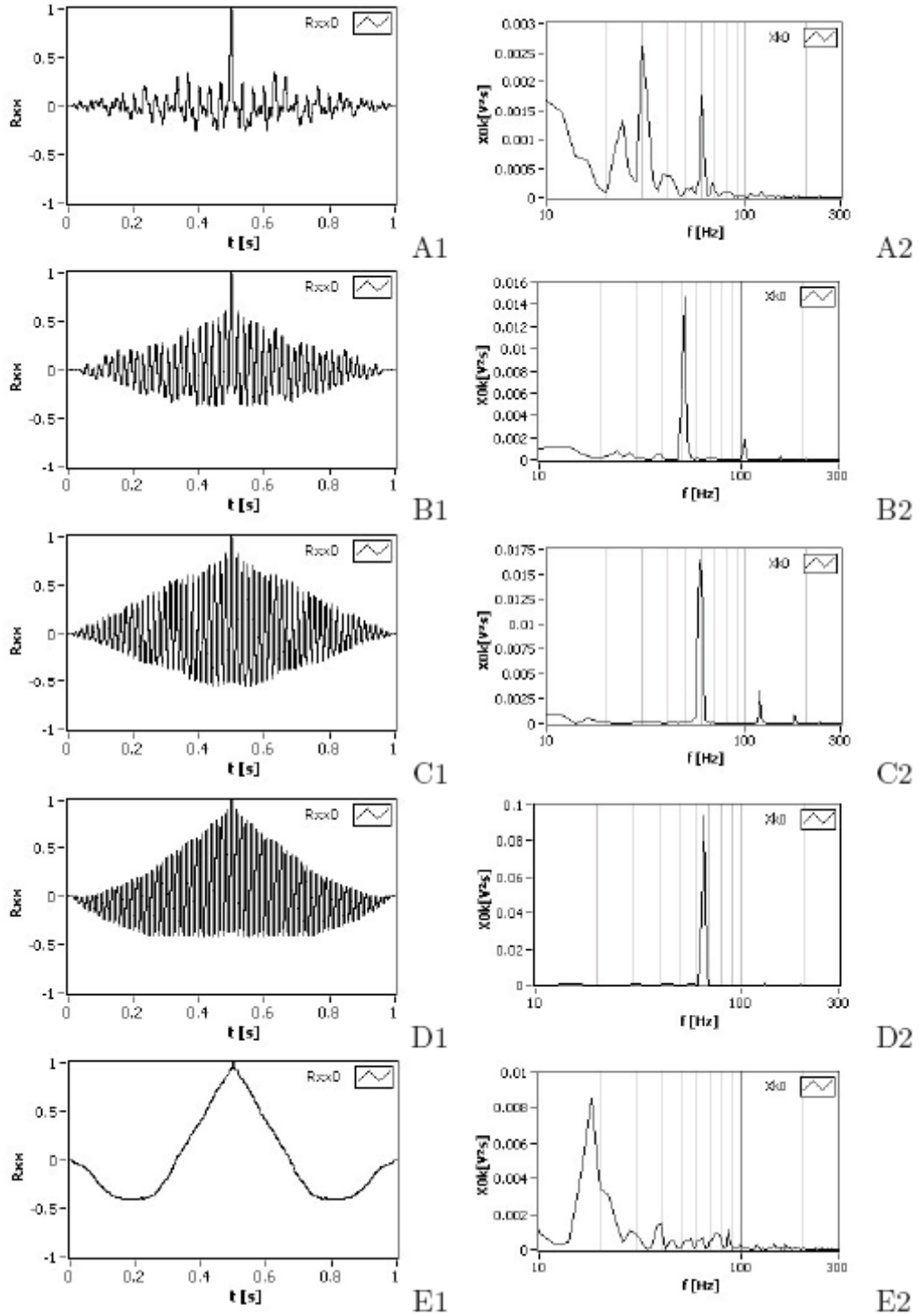

Fig. VIII-7: Characterization by means of radiant energy of transition from stable to unstable mode in the TG500 burner. The letters from A to E refer to time intervals in Fig. VIII-5. The first column from left (index 1) reports auto-correlation of radiant energy signal; the second column (index 2) reports its frequency spectra.. [VIII-2]

VIII.3 1MW Premixed CH4/Air COMET-HP Burner

VIII.3.1 Burner V64.3A

For the present study a single model burner which mimics a typical design of a heavy duty gas turbine burner is used: Siemens-Ansaldo V64.3A ([I-24], [VIII-3]).
The burner is equipped with three different injection lines, respectively called *"pilot"*, *"diffusion"* and *"premix"*. The fuel injection directions respect to the air flow is axial for the "pilot"; at about 30° for the "diffusion"; orthogonal for the "premix". The "diffusion" line is employed to keep the flame stable during the burner start-up, whilst in the full power operation only the premix and the pilot lines are used. The "pilot" gas nozzle stabilizes the premixed flame. The air is injected into the combustion chamber through two coaxial convergent ducts. Most of the air goes through the external one, where also the "premix" fuel is injected, and where some blades are located to induce a swirling motion in the flow. A little fraction of air (around 10%) goes through the inner duct, where both the "diffusion" and "pilot" injections are located.
Then, the V64.3A burner is fired by natural gas (i.e., methane) and can be operated with either non-premixed (i.e., diffusion) or premixed mode gas injection.
A sketch of the burner is shown in Fig. VIII-8. The air passage consists of two concentric annular air swirlers. The inner one is equipped with nozzles for pilot gas and non-premixed gas injection. In case of non-premixed operation, the natural gas is injected through the non-premixing nozzles. In premixed mode the premixing gas nozzles and optionally to a minor part the pilot nozzles are used. In both modes, the air is fed through the axial as well as the diagonal swirling passages with the same flow split. The swirler has 18 blades (one each 20°), oriented to 69°. Each blade has 10 holes of 1 mm diameter. The swirl number is S~0.4-0.6 .
The exit diameter D is 119 mm and the outlet velocity of the burner is 5-6 m/s.
The engine is started, accelerated and loaded in diffusion mode up to a certain flame temperature (or turbine outlet temperature respectively) which is needed to stabilize a premixed flame. After the transition to full premix mode (with a small pilot flame) the further loading up to base load.
In the gas turbine the burner is usually operated in premixed mode with pilot gas injection for better flame stability. Under test rig conditions, pilot gas injection was used.

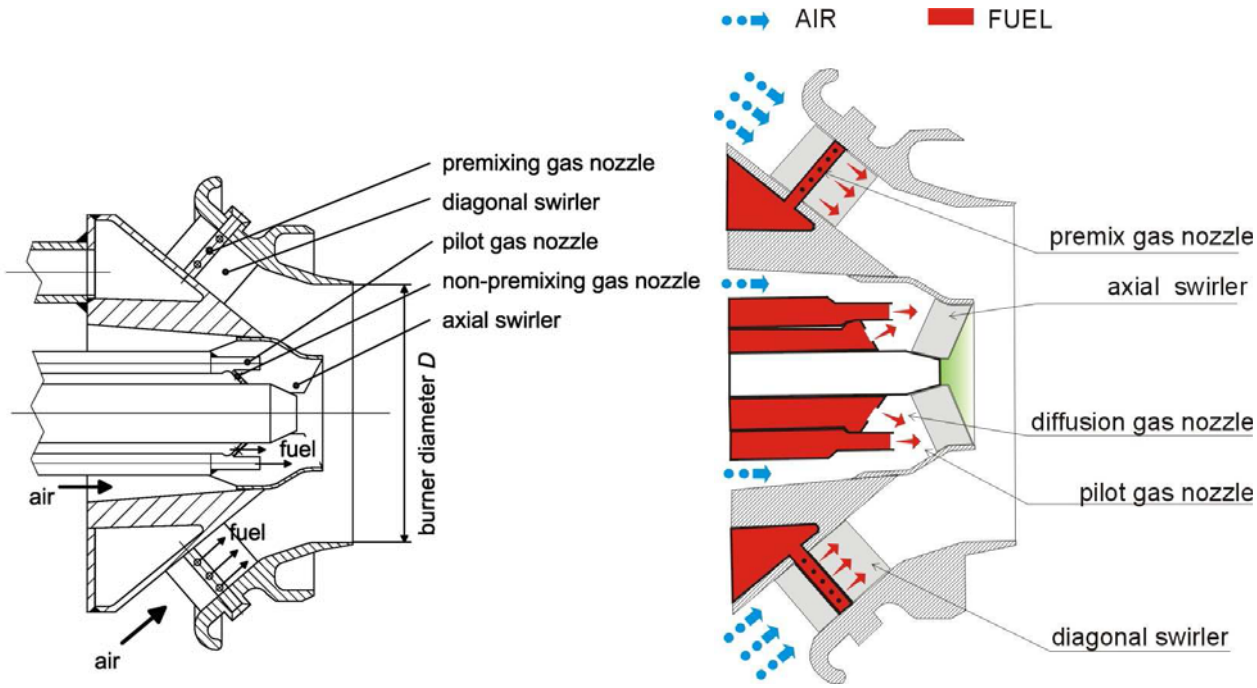

Fig. VIII-8: Schematic layout of the Siemens-Ansaldo V64.3A burner.

VIII.3.2 Test Rig

The burner is implemented into a single burner test rig operating at atmospheric pressure.
COMET-HP (***COMbustion Experimental Tests in High Pressure conditions***) is a combustion test chamber in ENEA Casaccia Research center in Rome (Fig. VIII-9), and it is an experimental facility to study combustion processes in turbogas (TG). It was made to study thermo-acoustic instability in the last generation of premixed TG and to develop new nonintrusive diagnostic systems and control methodologies. This test facility can work with a burner in full-scale for maximum power of 1 MWt and maximum pressure of 7 bar. The oxidizer used in this facility is atmospheric air that is preheated at the maximum of 450°C (usually it is preheated at 250°C in our experiments). The experimental set-up has three line-of-sight optical access for the laser techniques. They are placed at 90° each in correspondence of the flame region.
Fig. VIII-10 shows a sketch of the test rig. The combustion chamber has a circular cross-section with diameter of 300 mm, that is about 2.5 D, where D is the diameter of the burner outlet. The overall length of the combustor is about 3.74 m. The combustion chamber has refractory walls.
The test rig was equipped with two pressure transducers and two ODC, i.e. two collimated photodiodes.

(a)

(b)

(c)

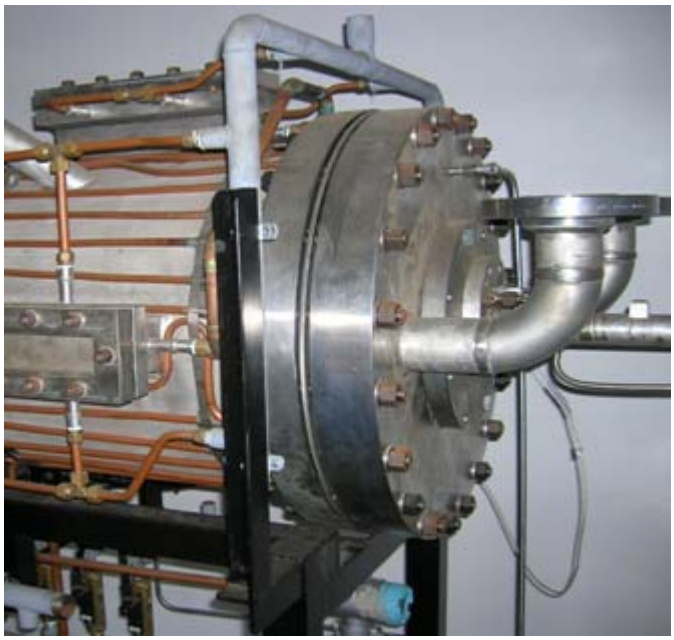

Fig. VIII-9: Images of COMET-HP installation in ENEA Casaccia Research center in Rome.

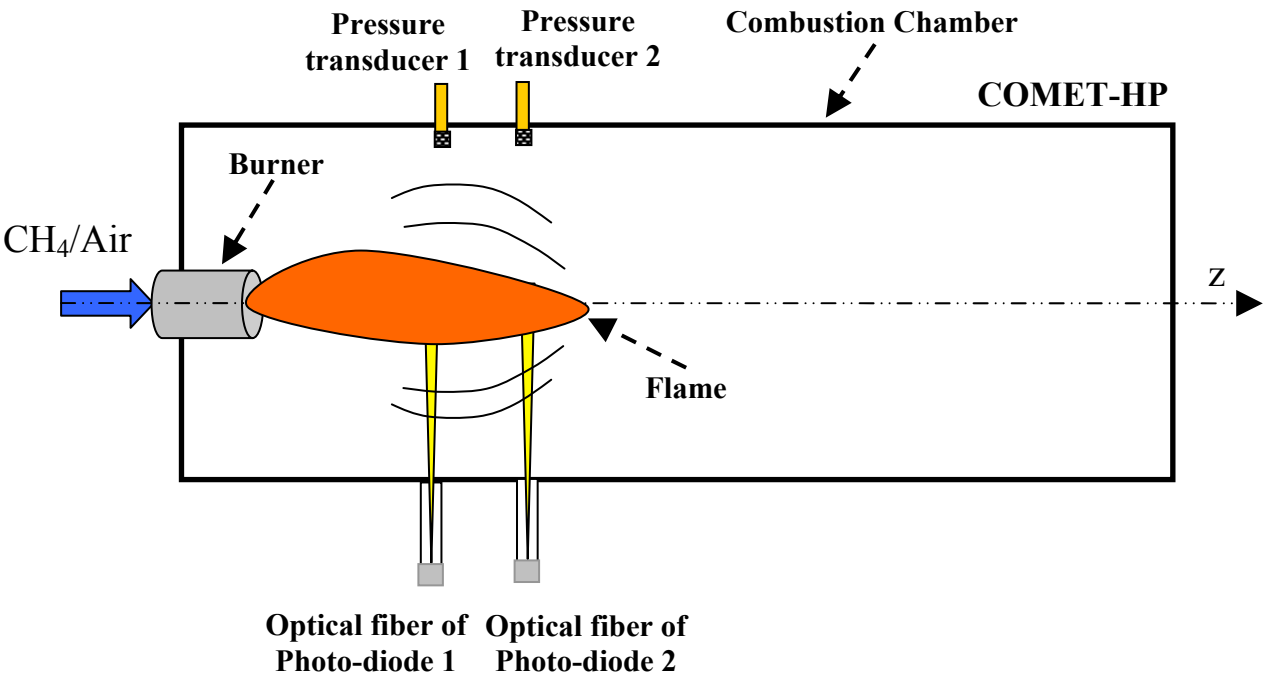

Fig. VIII-10: Sketch of the COMET-HP burner examined in this work. It is 1 MW burner in ENEA Casaccia Research center in Rome. It is possible to observe the positions of two collimated photodiodes and two pressure transducers in our experimental set-up.

VIII.3.3 Operating conditions

In premixed mode, three different operating points where combustion oscillations are present were investigated:

- First, a **stable condition** at Φ_{global}=0.58 and Φ_{premix}=0.56 . The OASPL is 133 dB.
- Second, **a weakly unstable flow** at Φ_{global}=0.36 and Φ_{premix}=0.34 . The OASPL is 140 dB.
- Third, a **strongly unstable flow** at Φ_{global}=0.27 and Φ_{premix}=0.25 . In this condition the combustion oscillations became quite loud and the OASPL is 155 dB.

It is important to define that

$$\Phi_{global} = \frac{\left(\frac{F}{A}\right)}{\left(\frac{F}{A}\right)_{St}} = \frac{\left(\frac{\text{Primary fuel} + \text{Pilot fuel}}{\text{total air}}\right)}{\left(\frac{F}{A}\right)_{St}} \qquad \Phi_{premix} = \frac{\left(\frac{\text{Primary fuel}}{0.9 \cdot \text{total air}}\right)}{\left(\frac{F}{A}\right)_{St}}$$

where total air is the sum of primary and secondary air of service pipe.
These conditions are reached by increasing the air mass flow rate, then going towards lean mixture.
In all cases the air was preheated to 523 K.
The optical and pressure signals are sampled at *fs*=5 MHz (DAQ sampling frequency), with signal averaging of 100 samples, time windows of 2 s and acquiring the signals for 1 minute.

VIII.3.4 Flame chemiluminescence spectrum of V64.3A burner

An interesting work of ENEL [VIII-3] verify the scalability to industrial scale of optical techniques based on chemiluminescence of excited radicals such as OH^*, CH^* or C_2^*.

a) UV and visible range

The relative intensity of the emission band changes depending on the fuel injection mode (premixed or diffusion); the intensity of OH^* signal remains the same in both fuel injection ways, while the intensity of CH^* and C_2^* becomes lower for the premixed one. The ratio between the peaks and the background intensity becomes lower because of an increment of background emission. In the 600-900 nm range the light emission intensity increases and some new feeble peaks appear: the light intensity is very high and the imperceptible peaks, presumably due to the emission from water molecules [III-41], stand out from the background.

b) Red and very near IR range

The growing of the spectral signal in the 600 nm to 900 nm range would be linked to the black-body emission from incandescent sections of the combustor.
This is confirmed by the flame image taken inside the combustor through the image channel of camera.

The black-body emission becomes significant over 500 nm and the total spectrum acquired is the sum of two contributions: flame emission and black-body emission [III-41].

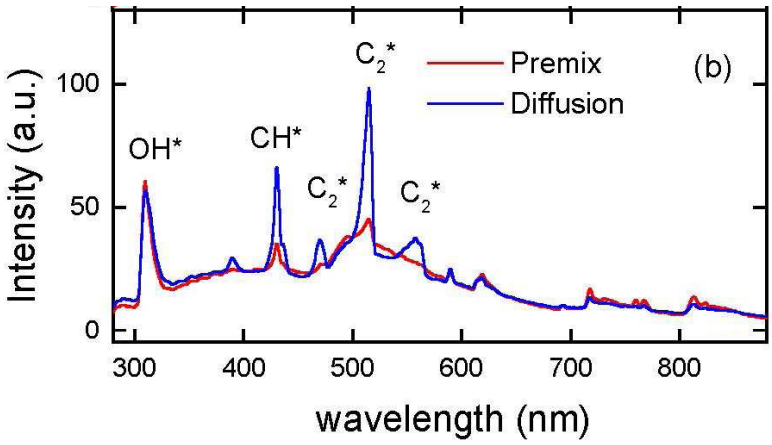

Fig. VIII-11: Flame spectrum of Siemens-Ansaldo V64.3A burner [VIII-3].

The NO_x emissions are better correlated to the optical emission than to the equivalent ratio [III-41]. In fact NO_x formation takes place in the non homogenous part of the combustion; while the equivalence ratio is an average value and it doesn't take combustion fluctuations into account. On the contrary, the OH^* chemiluminescence is due to all the internal mechanisms of the combustion. This might be the reason for the relatively good correlation between the OH^* chemiluminescence intensity and the NO_x emission.

VIII.3.5 Experimental unsteady characterization and results

Looking at the Fig. VIII-13a, Fig. VIII-14a and Fig. VIII-15a it can be observed that autocorrelation coefficients of both acoustic and radiant energy signals increase when moving towards instability, i.e., a leaner combustion. The acoustic signal has more information than the optical one, since the amplitude of radiant energy fluctuation is low with respect to the mean, hence resulting into a low dynamic information, and it suggests to use some filters. Besides, comparing the present results with those obtained without collimation in the Savona burner (Fig. VIII-3) it can be concluded that the angle of view of the ODC probe has to be wider to monitor combustion instability, i.e., the portion of the flame to be monitored has to be as wider as possible. Furthermore, the more convenient location of ODC to more likely capture the flame should be the front view position.
Looking at cross-correlations of signals of the same type (Fig. VIII-13b, Fig. VIII-14b and Fig. VIII-15b), i.e., pressure-pressure and ODC-ODC at different positions, the same conclusions may be drawn.
The cross-correlation coefficient of pressure signals in all the cases considered have the first peak to τ=0.0055 s. Since the distance between the two pressure transducers is 3 cm, the predicted mean velocity inside the combustion chamber is 5.45 m/s, that perfectly agrees with the expected

value. It gives an important information about the *pseudo-sound velocity*[7]. The cross-correlation coefficient of pressure signals is not able to reveal the acoustic velocity since of the resolution of it.
Finally, the ODC signal in this configuration is unable to diagnostic the operating state of the combustor since it is too collimated and it can't capture the global dynamics. Hence, the frequency analysis is performed only for the acoustic signals.
The geometry of V64.3A burner is very complicated, then frequency spectra (Fig. VIII-13c, Fig. VIII-14c and Fig. VIII-15c) reveal some peaks presents at all the three regimes examined (Fig. VIII-12), although with different amplitudes:

1) At the first condition in **stable mode** the pressure spectra shows dominant frequencies (Fig. VIII-13c): in particular **7**, 18, **25**, **75**, 141, 213, **~350**, 512, **758**, **5754**, **11481** Hz.
2) At the second condition in **weakly unstable mode** the pressure spectra show dominant frequencies (Fig. VIII-14c): in particular **7**, 22, **26**, **75**, 144, **~185**, **~360**, 543, 653, **758**, **5754**, 8912, **11481** Hz.
3) At the third condition in **strongly unstable mode** the pressure spectra show dominant frequencies (Fig. VIII-15c): in particular **6**, 22, **37**, **~70**, 109, **~185**, **~370**, 562, **~758**, **5754**, 8511, **11481** Hz, and others peaks.

The experimental data show that the combustion noise is broadband, in particular:

- It is important to note that in the most unstable condition the system shows a frequency of **~185 Hz**, named f_{LR} (***longitudinal resonant frequency***). This is associated to the fundamental longitudinal acoustic frequency of the combustor. In fact, the length of the combustor from the reaction zone up to a first restriction is L = 3.74 m. The resulting sound speed is $a = \lambda\, f_{LR} = L\, f_{LR}$ = 690 m/s. Considering that the $\gamma * R_{gas}$ for CH_4/Air combustion is about 390 J/(kg K), the associated and predicted average temperature is $\overline{T_C} = 1220\text{K} = \bar{c}^2/(\gamma\, R_{gas})$, that is plausible and in agreement with the local temperature measurement 1800 K in the reaction zone.

- The frequency of **5754 Hz** named f_{TRR} (***transverse radial resonant frequency***) is associated to the fundamental transverse acoustic frequency of the combustor. In fact, the radius of the combustor is r=0.15 m. The resulting sound speed is $\bar{c} = \lambda\, f_{TRR} = r\, f_{TRR} \cong$ 860 m/s. Considering that the $\gamma * R_{gas}$ for CH_4/Air combustion is about 390 J/(kg K), the associated and predicted average temperature in the reactive zone near the pressure transducers is $\overline{T_R} \cong 1890\text{K} = \bar{c}^2/(\gamma\, R_{gas})$, that is plausible and in agreement with the local temperature measurement 1880 K in the reaction zone where is present a pilot diffusive flame.

- The frequency of **758 Hz** named f_{TAR} (***transverse azimuthal resonant frequency***) is associated to the fundamental azimuthal acoustic frequency of the combustor. The equation

[7] The pressure pulsation that are not a solution of pressure wave equations and that are produced by non-stationary vortex motion of the medium as an incompressible are called *"pseudo-sound"*. In addition to the direct noise radiation, the surface-pressure fluctuations and vorticity waves, i.e. hydrodynamic pressure fluctuations (*pseudo-sound*), are of importance because they tend to excite structural vibration and low-frequency noise.

$f = n\bar{c}/(\pi d)$ provides a theoretical estimate for the characteristic acoustical frequencies of *azimuthal modes* of any annular combustion chamber. At an average combustion chamber diameter of d=0.3m and a speed of sound of $\bar{c}$=690 m/s (assuming an average combustion chamber temperature of 1220 K), the resulting frequency for the combustion chamber is **732 Hz** for the first harmonic (n=1), a value in agreement with experimentally determined characteristic frequency.

- The frequency of **~70 Hz** named f_{HR1} (***first Helmholtz resonant frequency***) is associated to the "bulk" frequency of the combustion chamber for the neck of *premixed burner*. The equation $f_{HR} = \frac{\bar{c}}{2\pi}\sqrt{\frac{S_{neck}}{l_{eff}\,V}}$ provides a good theoretical estimate of this type of resonance. V is the volume of the combustion chamber (i.e., cavity) that have an average diameter of 0.3 m and a length of about 3.74 m. The diameter of the premixed mixture opening (or neck) is 0.119 m, and his length l is about 0.1 m. At an average combustion chamber temperature of 1220 K, f_{HR} corresponds to an average speed of sound of $\bar{c}$=690 m/s.

- The frequency of **~30 Hz** named f_{HR2} (***second Helmholtz resonant frequency***) is associated to the "bulk" frequency of the combustion chamber for the neck of *pilot burner*. The diameter of the pilot flame opening is 0.05 m, and his length l is about 0.1 m.

- There is a low frequency peak of **~7 Hz** that could be due to mechanical frequency, e.g. the valve regulation of the mass flow rate.

- While the amplitude of ~22Hz and 758 Hz grow going towards the unstable state, the amplitude of ~75 and 5754 Hz decreases.

- The frequency of **11481 Hz** can be associated to the fuel flow injection in the 12 blades of the swirl that has 10 holes each (d_{holes}=1 mm) where the $u_f \cong$22.5 m/s, with St=0.24 . The characteristic length considered in the Strouhal number is the radius of holes (r_h~0.5 mm).

- The spectra reveal frequency peak of **~350-360 Hz** that could be associated to the *precession motion* of the *central recirculation zone* that is likely to occur in this swirled flow. This precession mode has a characteristic *St* number.
  The effect of confinement and partial premixing for weak equivalence ratios, Φ=0.1–0.3, show the value of Strouhal number being reduced by up to a factor of 3 compared to the isothermal state: in particular if the swirl number is S~0.7 the value of Strouhal number drops dramatically from that of the isothermal state, 1.2 to ~0.5 [I-30].
  The Strouhal number ($St = \frac{f\,D_b}{u_b}$=0.5) is derived from the burner flow rate and is based on the burner exhaust area. D_b is the exhaust diameter of swirl burner (in our case D_b=119 mm), i.e. the diameter of the burner, u_b is the average bulk burner exit axial velocity.
  In our case, $Q_{air}\cong$1800 kg/h then $u_b\cong$80 m/s [ρ_{air}(T=250°C)=0.6 kg/m^3], and the resulting frequency of PVC is about 350 Hz.

Separate work on unconfined swirling flames shows that even when the vortex core precession is suppressed the resulting swirling flames are unstable and tend to wobble in response to minor perturbations in the flow, most importantly close to the burner exit.
The PVC can be completely suppressed by combustion with premixed flames [I-30].

The V64.3A burner has a pilot gas nozzle to stabilize the premixed flame, and the sound field from non-premixed flames is less well characterized than that radiated by premixed flames. Theoretical analysis of nonpremixed flames is more difficult because the rate of heat release is less easily modelled in this case, and this quantity also can not be extracted from direct measurements of free radical emission.

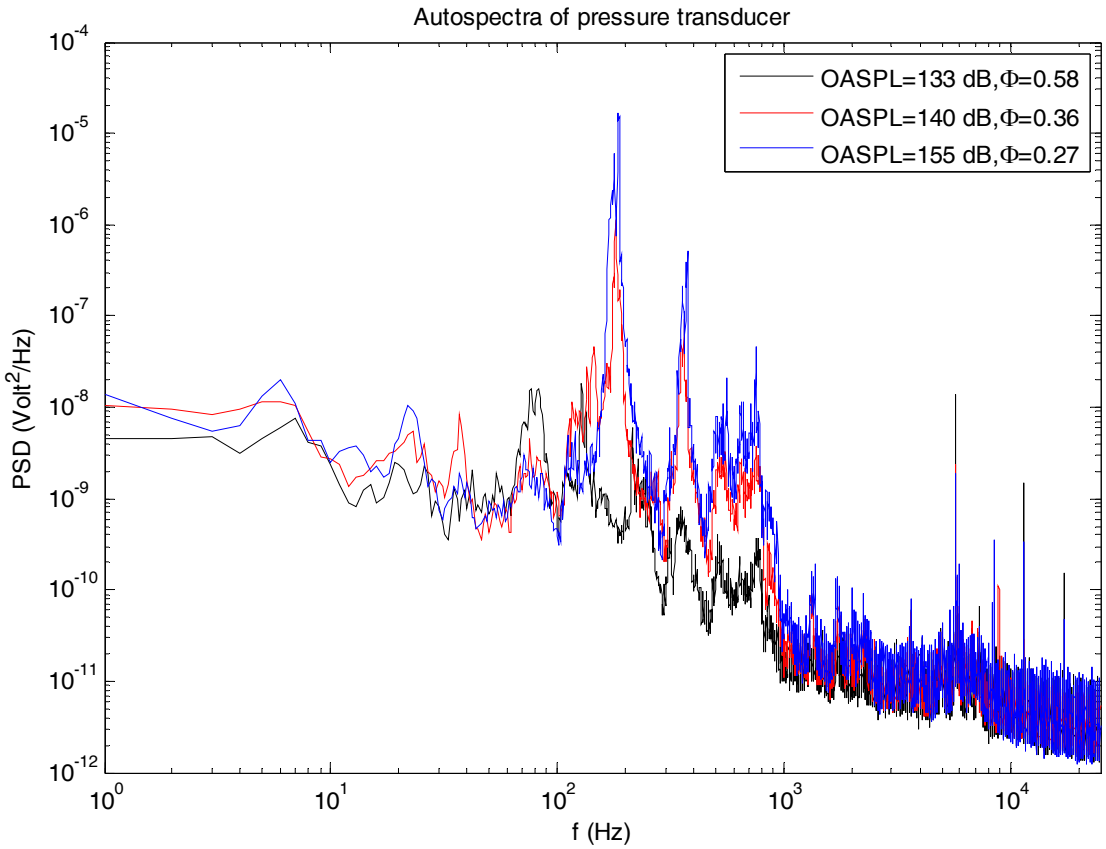

Fig. VIII-12: Comparison of autospectra of pressure transducer of characterization of transition from stable (Φ_{global}=0.58) to unstable mode (Φ_{global}=0.27) in the COMET-HP burner of ENEA.

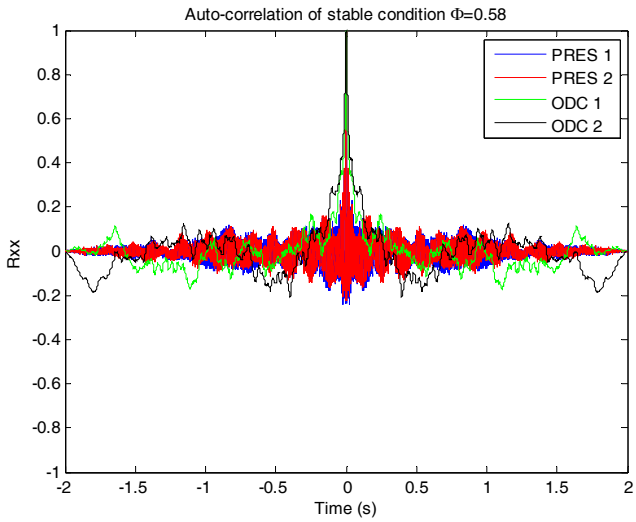

(a)

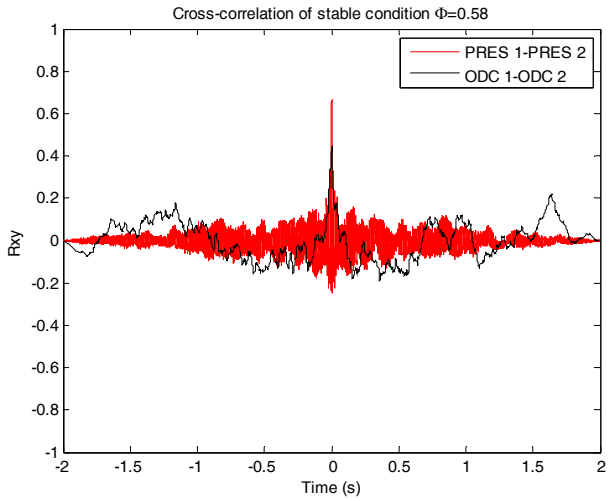

(b)

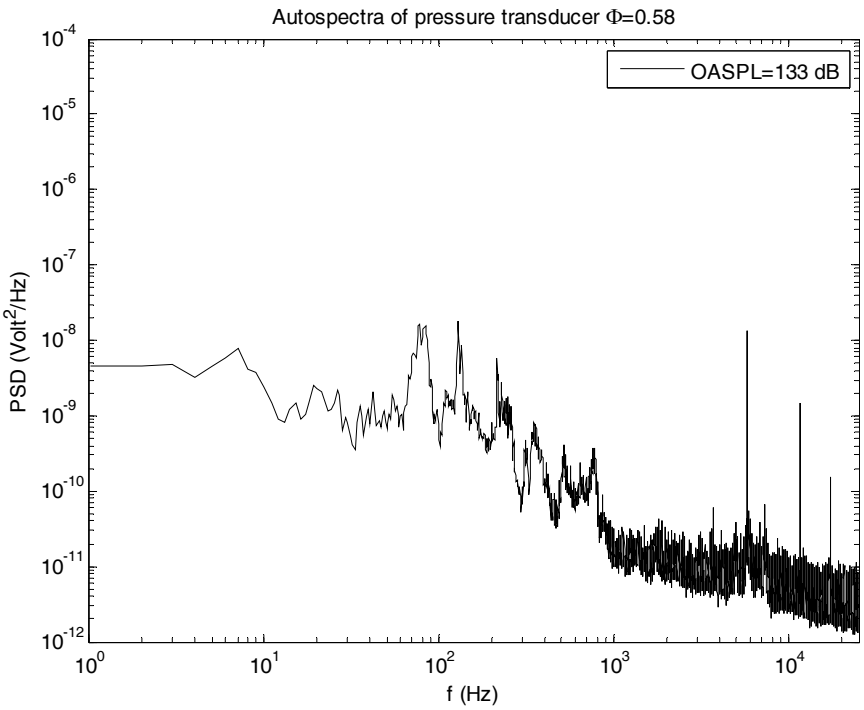

(c)

Fig. VIII-13: Characterization of stable condition Φ_{global}=0.58 in the COMET-HP burner of ENEA. It reports autocorrelation (a) of all probes, and cross-correlation (b) between two pressure transducers and ODC signals. It reports frequency autospectra of pressure transducer (c). In the first two type of graphics the red line refers to pressure signal, while the black one to radiant energy.

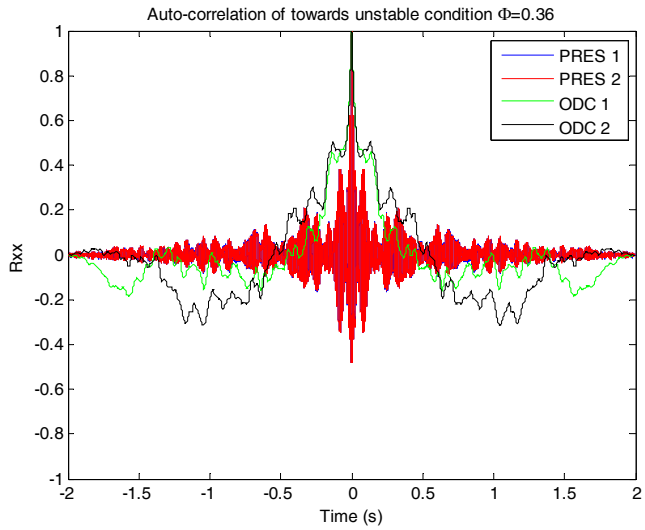

(a)

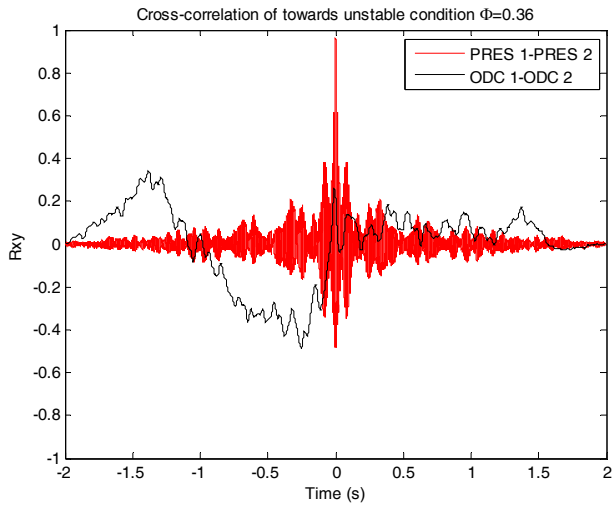

(b)

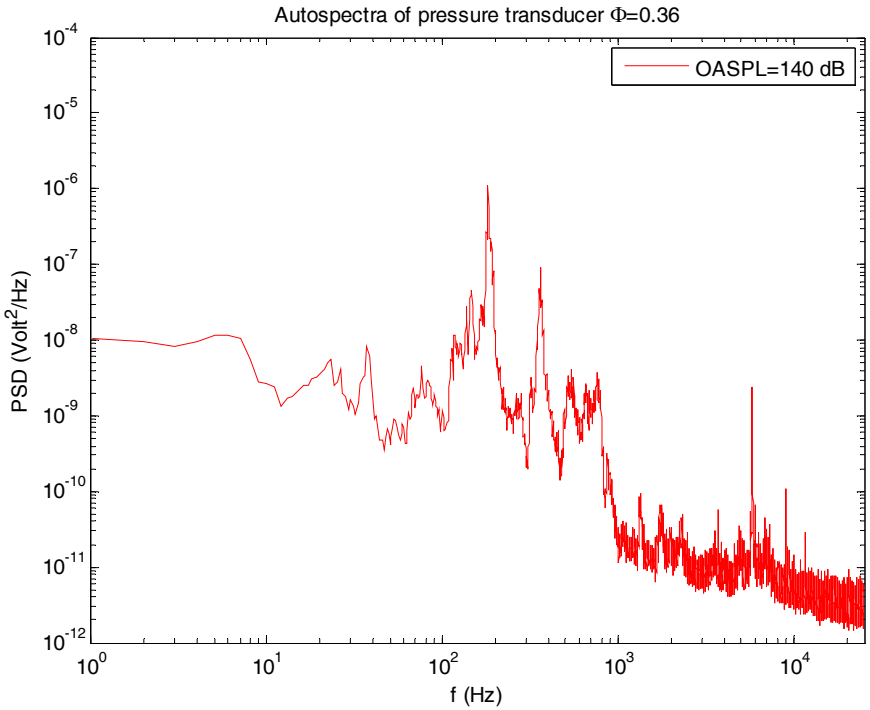

(c)

Fig. VIII-14: Characterization of unstable condition Φ_{global}=0.36 in the COMET-HP burner of ENEA. It reports autocorrelation (a) of all probes, and cross-correlation (b) between two pressure transducers and ODC signals. It reports frequency autospectra of pressure transducer (c). In the first two type of graphics the red line refers to pressure signal, while the black one to radiant energy.

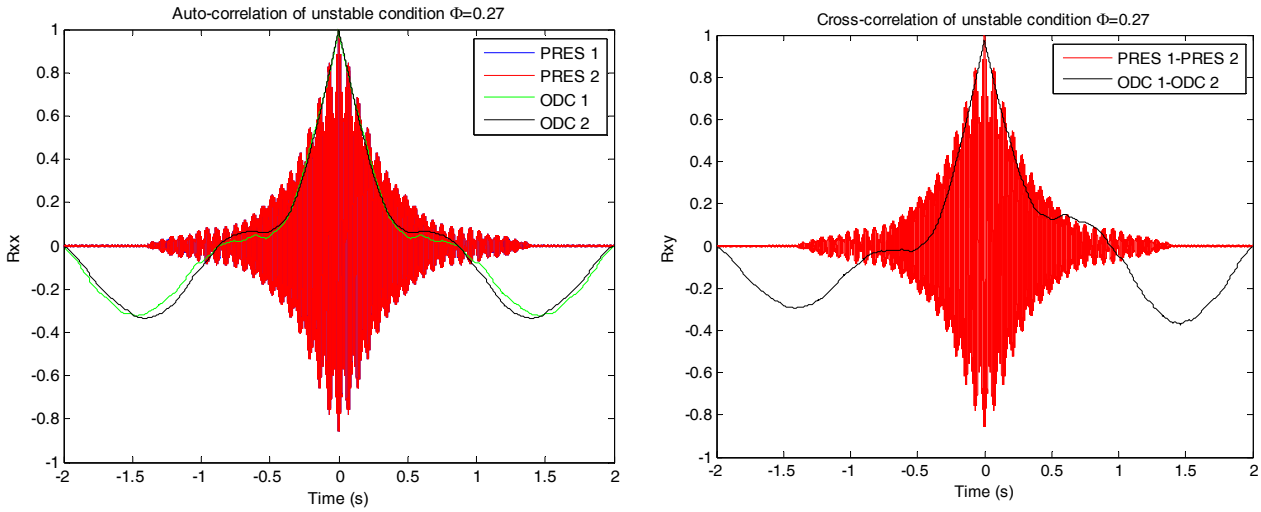

(a) (b)

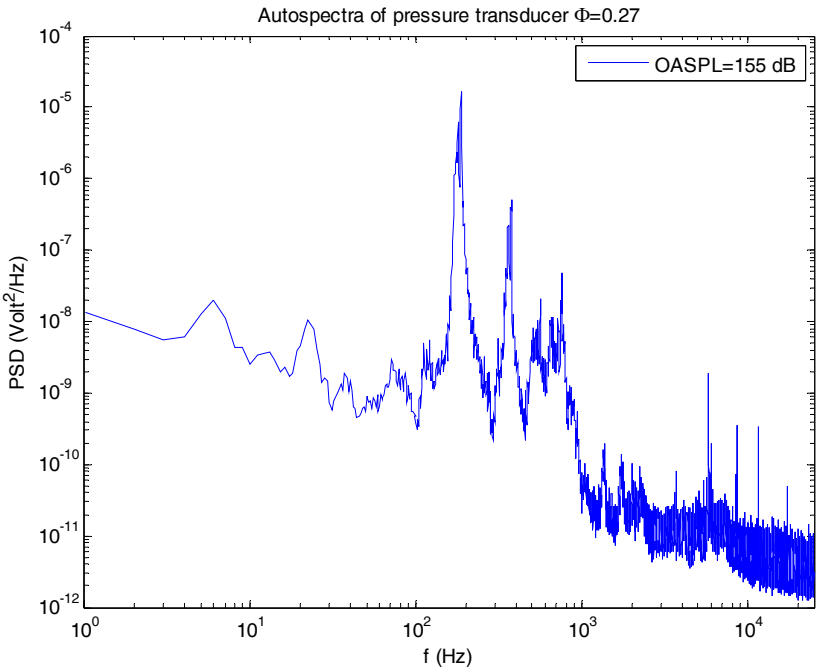

(c)

Fig. VIII-15: Characterization of unstable condition Φ_{global}=0.27 in the COMET-HP burner of ENEA. It reports autocorrelation (a) of all probes, and cross-correlation (b) between two pressure transducers and ODC signals. It reports frequency autospectra of pressure transducer (c). In the first two type of graphics the red line refers to pressure signal, while the black one to radiant energy.

VIII.4 Application to Control Systems

Combustors based on some form of premixing to reduce pollutant emissions generally exhibit instabilities produced via a fluid-dynamic and/or thermo-acoustic way. Transition from stable to unstable combustion, and in particular to blowout, happens through a transient regime in which flame experiences large scale pulsations that produce localized extinctions and reignitions, noise and changes in radiant emissions. Thus, acoustic and optical sensors are suitable for instability monitoring and control. Unstable events may become critical and bring about dangerous situations. Devices for diagnostics and monitoring are therefore needed to early detect some precursor events. Once identified the "right" precursors and the physical quantity (usually of acoustic or optical nature) to sample to detect them, signal tresholding and frequency analysis can be implemented as strategies in an active control system to avoid the establishment of unstable regimes.

Usually, combustion instabilities are studied on ***pressure signal*** base. However, this strategy has some problems. In fact, acoustic energy is too much affected by external parameters (location of transducers, vibration of the structure), and acoustics of the system can hidden some effects of combustion dynamics in spectra of pressure; furthermore, thermal energy, i.e., heat release, produces pressure fluctuations that interact with combustion chamber acoustics, which is not steady because depends on temperature (this is critical when the burner is unstable).

Optical sensors seem to be a better choice. It has been shown [VII-19] that the most limiting constraint on the detector time response is set by the duration of the precursor events, such as extinctions and reignitions; typically such events have a duration above 1 ms but in particular situations this time may decrease due to preheating effects or strong thermo-fluid-dynamic interactions (vortex stretching). Thus the sensors need a frequency response ranging from 10 kHz to 1 MHz. Optical sensors suitable for these applications are
photo-diodes and photomultipliers. Besides high frequency response, that permits real time control, a sensor should be also robust enough to operate in a combustor or, much better, if non-intrusive. Work done shows that photo-diodes meet these requirements.

Photo-diodes working up to 10MHz are available at low cost (~ 50−100 Eur). They are passive elements, i.e., they require low voltages (10−30V for the one used in this article); they are small, require small space and have a low weight (~0.05 kg).

Photomultipliers usually work at much higher frequency than photo-diodes, but cost more (~ 10 times). They are active sensors, i.e., require higher voltages provided by a high voltage supply; they are bigger than photo-diodes, require more space (usually have also optics) and weigh more (~ 0.5 kg only for the sensor). They have a high signal to noise ratio, higher than photo-diodes, but they are strongly influenced by mechanical vibrations that increase noise.

Furthermore, these optical sensors can be coupled to optical fibers (that must withstand high temperatures) to keep the sensor far from a harsh environment. However, if focusing on small volumes is needed, Cassegrain optics is required [II-143], but this complicates the set-up.

From the previous characteristics of photo-diodes and photomultipliers, it is concluded that photomultipliers are very sensitive instruments but due to their structural characteristics are unpractical for aero- and space- systems, where there are size and weight constrains and vibrations.

To identify the precursor events via radiant energy sampling, a threshold method can be used. This strategy is based on a relative measurement (e.g., with respect to a mean signal measured

over a short time window prior to the event) and therefore it is less affected by engine aging, detector deterioration (such as partial coating of the diode or of the fiber end in the combustor due to soot deposition), and slow variations in engine settings. An identification strategy based on a threshold method working on lower statistical moments (such as mean) provides also good time response. It is important to note that since the acoustic pressure has a zero mean value, the relative measure cannot be based on means but needs higher statistical moments, such as rms or kurtosis ([VII-19], [VII-22]). This is a negative point for using pressure transducers in control system, requiring longer analysis.
Aiming to control by means of optical sensors, the field of view and the location of the optical port are also important. Since precursors can correspond to localized extinctions of the flame in regions of critical stability, the optical port should be located close to the injectors not directly looking at them, but at a wide area downstream in the combustor. Though not directly discussed in this work, the photo-diode sensing has already been used in an active control system to prevent flame blowout [VII-3].

VIII.5 Conclusions

A new optical instrument based on photo-diodes, called ODC, has been applied for thermoacoustic instability analysis. ODC provides information at very low cost and in real time about turbulent and chemical scales. It has been shown that the sampled flame radiant energy signal can be used for early detection of thermo-acoustic instabilities, i.e., before reaching the critical state of the system, or in other words, before self-excited oscillations are established inside the combustor. Coupling acoustics and radiant energy analysis showed that ODC system alone is able to detect thermo-acoustic instability: the onset happens when the **auto-correlation of the radiant energy** signal grows. Precursor events of instability are detected many seconds before its fully developed state; this suggests to use ODC as controller in Active Control systems in Gas Turbine to avoid dangerous unstable state.

References

[VIII-1] Lawn C.J., “The Acoustic Self-Excitation of a Bluff-Body Stabilised, Premixed Flame”, Combustion Science and Technology, Vol.154, Issue 1, pp.57–74, 2000.

[VIII-2] Bruschi R., Giacomazzi E., Giulietti E., Pagliaroli T., Stringola C., Nobili M.; “Optical Investigastion of Thermo-Acoustic instabilities in turbulent flames”, 13th AIAA/CEAS Aeroacoustics Conference (28th AIAA Aeroacoustics Conference); Roma (Italy), 21-23 May 2007.

[VIII-3] Cipriano A., Gasperetti S., Mariotti G., Paganini E., “Analysis of the spectral properties of premixed and diffusion natural gas flames at different scales”, Proceedings of the European Combustion Meeting (ECM), 2003.

Acknowledgments

During this work I have had support from a large number of people, for which I would like to thank them.

First of all I would like to thank my supervisor Prof. Roberto Camussi for the good co-operation and his constant friendship. I wish to thank him particularly for the support in the last months, when I had to finish it.

I would like to thank Romano Bruschi for his creative ideas, critical thinking, and incredible effort have served as an excellent model for me throughout the research process. His ideas and tremendous support had a major influence on this thesis.

I wish to thank my dear colleague and friend Eugenio Giacomazzi for his encouragement during the whole thesis, and for useful discussions about chemiluminescence, radiative emission physics and turbulent reacting flows dynamics.

It was a pleasure for me to work with all the wonderful people in our labs in ENEA. I have been fortunate to work with outstanding colleagues in ENEA group, in particular thanks to Stefano Giammartini, Caterino Stringola, Mirko Nobili, Stefano Cassani, Leandro Pagliari, Federico Manfredi, Riccardo Scipinotti, Michele Marrocco and Guido Troiani, for their patience, their vital support and for their crucial help in laboratory experiences and useful discussions.

The research project has been made possible by the financial support from ENEA and ENSYEN. Thanks to ENEA for the availability of its facilities.

I have been fortunate to come across many funny and good friends, without whom life would be bleak. Thanks to my dear friends Alessandro Di Marco and Tiziano Pagliaroli of "Roma TRE" University for their continuous support and friendship. The help of Tiziano in post-processing data was very useful during the whole thesis.

I would like to thank my mum, my dad and my brother for everything they have ever done and for making me a nice family.

Finally, the last but not the least, thanks to God for everything forever: *"then we will praise You forever"* (Psalm 79,13).

ATTACHMENT A: Lighthill's theory

A.1 Introduction

Aeroacoustics is a branch of acoustics that studies noise generation via either turbulent fluid motion or aerodynamic forces interacting with surfaces. Noise generation can also be associated with periodically varying flows. Although no complete scientific theory of the generation of noise by aerodynamic flows has been established, most practical aeroacoustic analysis relies upon the so-called **Acoustic analogy**, whereby the governing equations of motion of the fluid are coerced into a form reminiscent of the wave equation of "classical" (i.e. linear) acoustics.
Acoustic analogies are applied mostly in numerical aeroacoustics to reduce aeroacoustic sound sources to simple emitter types. They are therefore often also referred to as **aeroacoustic analogies**.
In general, aeroacoustic analogies are derived from the compressible Navier-Stokes equations. The compressible Navier-Stokes equations are rearranged into various forms of the inhomogeneous acoustic wave equation. Within these equations, source terms describe the acoustic sources. They consist of pressure and speed fluctuation as well as stress tensor and force terms.
Approximations are introduced to make the source terms independent of the acoustic variables. In this way, linearized equations are derive which describe the propagation of the acoustic waves in a homogeneous, resting medium. The latter is excited by the acoustic source terms, which are determined from the turbulent fluctuations.
In the aeroacoustic field we have three principal analogy:

a) The **Lighthill analogy** ([A-1], [A-2]) in 1952 considers a free flow, as for example with an engine jet. The nonstationary fluctuations of the stream are represented by a distribution of quadrupole sources in the same volume.
b) The **Curle analogy** [A-3] is a formal solution of the Lighthill analogy, which takes hard surfaces into consideration.
c) The **Ffowcs Williams-Hawkings analogy** [A-4] is valid for aeroacoustic sources in relative motion with respect to a hard surface, as is the case in many technical applications for example in the automotive industry or in air travel. The calculation involves quadrupole, dipole and monopole terms.

A.2 Lighthill's equation

The most common and a widely-used of the acoustic analogies is **Lighthill's aeroacoustic analogy**. It was proposed by James Lighthill in the 1950s ([A-1], [A-2]) when noise generation associated with the jet engine was beginning to be placed under scientific scrutiny.
Lighthill's theory of aerodynamic noise is based on the exact equations of fluid flow. Lighthill showed that the energy radiated outward as sound from an unsteady fluid flow is such a small fraction of the flow kinetic energy.
Lighthill (1952) rearranged the Navier-Stokes equations, which govern the flow of a compressible viscous fluid, into an inhomogeneous wave equation, thereby making an analogy between fluid mechanics and acoustics.

The exact flow equations for a perfect gas relate to the conservation of *mass*, *momentum* and *energy* can be written, respectively, as:

$$\frac{\partial \rho}{\partial t} + \nabla \cdot \rho \bar{v} = \rho m \tag{A-1}$$

$$\frac{\partial}{\partial t} \rho \bar{v} + \nabla \cdot \left(\rho \bar{v} \bar{v} - \bar{\tau} \right) + \nabla p = \rho g k + \rho F \tag{A-2}$$

$$\frac{\partial}{\partial t} \rho h_s + \nabla \cdot \left(\rho v h_s - q - \tau \cdot v \right) - \frac{\partial p}{\partial t} = \rho E + \rho F \cdot v \tag{A-3}$$

where the density ρ and velocity v of the fluid depend on space and time.

It is important to remember that $\nabla \tau = \frac{\partial \tau_{ij}}{\partial x_i}$ where τ_{ij} is the Stokes stress tensor. This stress tensor is written

$$\tau_{ij} = -p\delta_{ij} - \frac{2}{3}\mu\varepsilon_{kk}\delta_{ij} + 2\mu\varepsilon_{ij}$$

where p is the fluid pressure and $\varepsilon_{ij} = \frac{1}{2}\left(\frac{\partial u_i}{\partial x_j} + \frac{\partial u_j}{\partial x_i} \right)$ are the fluid rates of strain.

Neglecting the gravitational term ($\rho g k$) and source terms (ρm, ρF), we can write the conservation of mass equation (A-1) and the conservation of momentum equation (A-2) in non-conservative form, in the following way:

$$\frac{\partial \rho}{\partial t} + \nabla \cdot \rho \bar{v} = 0 \tag{A-4}$$

$$\rho \frac{\partial \bar{v}}{\partial t} + \rho \left(\bar{v} \cdot \nabla \right) \bar{v} = -\nabla p + \nabla \cdot \bar{\tau} \tag{A-5}$$

Now, multiplying the conservation of mass equation by v and adding it to the conservation of momentum equation gives

$$\frac{\partial}{\partial t}\left(\rho \bar{v} \right) + \nabla \cdot \left(\rho \bar{v} \times \bar{v} \right) = -\nabla p + \nabla \cdot \bar{\tau} \tag{A-6}$$

Note that $\times$ is a tensor product, then $\left(\rho v \times v \right)$ is a tensor. Differentiating the conservation of mass equation with respect to time, taking the divergence $\left(\nabla \cdot \right)$ of the conservation of momentum equation and subtracting the latter from the former, we arrive at

$$\frac{\partial^2 \rho}{\partial t^2} - \nabla^2 p + \nabla \cdot \nabla \cdot \bar{\tau} = \nabla \cdot \nabla \cdot \left(\rho \bar{v} \times \bar{v} \right) \tag{A-7}$$

Subtracting $c_0^2\nabla^2\rho$, where c_0 is the speed of sound in the medium in its equilibrium state, from both sides of the last equation (A-7) and rearranging it results in

$$\frac{\partial^2\rho}{\partial t^2} - c_0^2\nabla^2\rho = \nabla\cdot\left[\nabla\cdot\left(\rho\bar{v}\times\bar{v}\right) + \nabla\ p - \nabla\cdot\bar{\tau} - c_0^2\nabla\ \rho\right] \tag{A-8}$$

which is equivalent to

$$\frac{\partial^2\rho}{\partial t^2} - c_0^2\nabla^2\rho = \left(\nabla\times\nabla\right):\left[\left(\rho\bar{v}\times\bar{v}\right) - \tau + \left(p - c_0^2\rho\right)\bar{I}\ \right] \tag{A-9}$$

where $\bar{I}$ is the identity tensor, and : denotes the (double) tensor contraction operator.
The above equation is the celebrated **Lighthill equation of aeroacoustics**. It is a wave equation with a source term on the right-hand side, i.e. an inhomogeneous wave equation. The argument of the "double-divergence operator" on the right-hand side of last equation, i.e., is the so-called **Lighthill turbulence stress tensor** for the acoustic field, and it is commonly denoted by T.

$$T = \left(\rho\bar{v}\times\bar{v}\right) - \tau + \left(p - c_0^2\rho\right)\bar{I}$$

Using Einstein notation, Lighthill's equation can be written as

$$\frac{\partial^2\rho}{\partial t^2} - c_0^2\nabla^2\rho = \frac{\partial^2 T_{ij}}{\partial x_i\partial x_j} \tag{A-10}$$

where, the exact expression for T_{ij} in viscous compressible flow is

$$T_{ij} = \rho v_i v_j - \tau_{ij} + \left(p - c_0^2\rho\right)\delta_{ij}$$

where the velocity components v_i and v_j are evaluated in the flow at emission points y, and the pressure p and the density ρ are the local instantaneous pressure and density of the fluid.
The left side of Lighthill's equation (A-10) describe the propagation of acoustic disturbances through the ambient medium at the speed of sound c_0. The right side is then interpreted as a forcing function or source term.
The left hand side of equation (A-10) has the form of a linear wave equation and the right hand side of this inhomogeneous wave equation can be considered as a source term presuming no viscous terms and small Mach numbers. While the turbulent reacting flow acts as a source, the acoustic waves propagate in a uniform acoustic medium. The transfer of information from the sources to the external medium is achieved through the Lighthill stress tensor T_{ij}. In a turbulent reacting flow, the viscous stress τ_{ij} in T_{ij} is very small in comparison to the other terms and can be neglected. The velocity correlation term $\rho v_i v_j$ (Reynolds-stress term) and $(p - c_0^2\rho)$ represent the sources caused by the turbulent flow and by the unsteady heat release.
An order of magnitude analysis of the Lighthill's tensor showed [A-5] that the ratio of both terms scales to Ma^2, which indicates further, that for turbulent reacting flows at low Mach numbers $Ma^2 << 1$, the dominant term will be the last one on the right hand side of equation (A-10).

The T_{ij} is the **Lighthill's stress tensor**, and the tensor $\rho v_i v_j$ is called the **Reynolds stress tensor** that expresses the intensity of the turbulence in the source region. The term τ_{ij} is just the viscous part of Stokes stress tensor and the term $\left(p - c_0^2\rho\right)$ expresses the differential between the actual pressure fluctuation (p) and those which would be caused by purely isentropic density fluctuations in the ambient fluid medium which has been characterized by c_0.
The exact expression for T_{ij} is the Lighthill acoustic analogy instantaneous applied stress tensor, and δ_{ij} is the *Kronecker* delta, i.e. $\delta_{ij}=0$ when $i \neq j$ and $\delta_{ij}=1$ when $i=j$. Each of the acoustic source terms, i.e. terms in T_{ij}, may play a significant role in the generation of noise depending upon flow conditions considered.
In Lighthill's acoustic analogy the unsteady fluid flow is replaced by a volume distribution of equivalent acoustic sources throughout the entire flow field. In this analogy the sources are embedded in a uniform medium at rest, in which the sources may move but not the fluid.
The essence of the Lighthill theory of aeroacoustic noise is the formulation of an **acoustic analogy**, in which the complicated process of sound generation by *turbulence is modelled in terms of an acoustically equivalent set of acoustic sources embedded in an otherwise uniform medium at rest*.
In practice, it is customary to neglect the effects viscosity of the fluid, i.e. one takes $\sigma = 0$, because it is generally accepted that the effects of the latter on noise generation, in most situations, are orders of magnitude smaller than those due to the other terms. Lighthill (1952) provides an in-depth discussion of this matter.
In aeroacoustic studies, both theoretical and computational efforts are made to solve for the acoustic source terms in Lighthill's equation in order to make statements regarding the relevant aerodynamic noise generation mechanisms present.
The following term

$$A(x,t) = \frac{\partial^2 T_{ij}}{\partial x_i \partial x_j}$$

is the **source term**, with i=1,2,3.

In the inhomogeneous wave equation (A-10) the source terms that involve $\frac{\partial}{\partial t}$, $\frac{\partial}{\partial x_i}$, $\frac{\partial^2}{\partial x_i \partial x_j}$ and $\frac{\partial^3}{\partial x_i \partial x_j \partial x_k}$ are labelled, respectively, monopole, dipole, quadrupole and octopole. For the source distribution function A(x,t) given in equation (A-10) the source is quadrupole.
In the case of hot jets, Michalke and Michel gave in 1979 [A-6] an expression for the source term of Lighthill's equation that takes the form

$$\frac{1}{c_0^2}\frac{\partial^2 \rho}{\partial t^2} - \nabla^2 \rho = \underbrace{\rho_0 \frac{\partial^2}{\partial x_i \partial x_j}\left[\left(1 + \frac{p'}{\rho_0 c_0^2}\right) v_i v_j\right]}_{quadrupole} - \underbrace{\frac{\partial}{\partial x_i}\left[p' \frac{\partial}{\partial x_i}\left(\frac{\rho_0}{\rho}\right)\right]}_{dipole}$$

$$- \underbrace{\frac{\partial^2}{\partial x_i^2}\left[\left(1 - \frac{\rho_0}{\rho}\right) p'\right]}_{quadrupole} + higher\ order \qquad \text{(A-11)}$$

where $p = p_0 + p'$ and $\rho = \rho_0 + \rho'$.
The knowledge of the behaviour of the stress tensor T_{ij} in the source region is crucial to the analytical modelling of acoustic radiation.
The pressure and density in the far-field ambient undisturbed fluid are p_0 and ρ_0, and since these quantities are constant so that

$$\frac{\partial \rho_0}{\partial t} = 0 \qquad \frac{\partial^2 \rho_0}{\partial x_i \partial xj} = 0 \qquad \text{for pressure;}$$

$$\frac{\partial p_0}{\partial t} = 0 \qquad \frac{\partial^2 p_0}{\partial x_i \partial xj} = 0 \qquad \text{for density.}$$

Thus we can write the wave equation for the instantaneous density fluctuation (in the absence of mass-injection)

$$\frac{\partial^2(\rho-\rho_0)}{\partial t^2} - c_0^2\nabla^2(\rho-\rho_0) = \frac{\partial^2}{\partial x_i \partial x_j}\left\{\rho v_i v_j - \tau_{ij} + \left[(p-p_0) - c_0^2(\rho-\rho_0)\right]\delta_{ij}\right\}$$

For inviscid and isentropic fluid motions the T_{ij} reduces to the $\rho v_i v_j$ which is just the nonlinear residue of the combination of the momentum and continuity equations.
Often the magnitudes of the turbulent Reynolds stresses ($\rho v_i v_j$) dominate the viscous stresses (T_{ij}) in turbulent motion so the latter may be neglected.

$$A(x,t) = \frac{\partial^2 T_{ij}}{\partial x_i \partial x_j} = \frac{\partial^2(\rho u_i u_j)}{\partial x_i \partial x_j}$$

In this case the wave equation in the absence of mass injection is now finally to the more simplified form

$$\frac{\partial^2(\rho-\rho_0)}{\partial t^2} - c_0^2\nabla^2(\rho-\rho_0) = \frac{\partial^2(\rho u_i u_j)}{\partial x_i \partial x_j}$$

which shows that *the acoustic field is driven by the region of fluctuating Reynolds stresses*. *Outside the region of Reynolds stress fluctuations, the velocity fluctuations are acoustic*. Thus, outside the region of turbulent fluid motion, Lighthill's equation reduces to the wave equation of linear acoustics theory.

A.3 Consideration about the exact solution of Lighthill's equation

It is very important to realize that **Lighthill's equation is exact** in the sense that no approximations of any kind have been made in its derivation.
Lighthill's equation is exact and has the following solution for an unbounded flow:

$$\rho(x,t) = \frac{1}{4\pi c_0^2}\iiint \frac{A(y,\tau)}{|x-y|}dy \qquad \text{(A-12)}$$

where ρ is the density fluctuation, relative to the ambient density ρ_0 received by an observer in the point Q(x,t) in the far field due to disturbance of source strength A(y,τ) per unit volume generated in the flow field at the point P(y,τ), $\tau = t - \frac{|x-y|}{c_0}$ is the retarded time, and $\frac{|x-y|}{c_0}$ is the time for sound to travel from the flow disturbance at P(y) to the field point Q(x) at the ambient speed of sound c_0. Then we can see that in the Lighthill acoustic analogy the acoustic source distribution A(y,τ) replaces the actual fluid flow and, moreover, the sources may move, but the fluid in which they are embedded may not. In the Lighthill's acoustic analogy *the equivalent sources may move but the fluid may not*.
According to Lighthill's acoustic analogy, all acoustic sources within a flow volume radiate to far field regardless of their position with respect to the flow boundaries.
If we consider the sources moving at a uniform velocity U, we can define $M = \frac{U}{c_0}$, the so-called acoustic Mach number. Then we introduce a system of moving coordinates
$\eta = y - c_0 M \tau$
and the solution to equation (A-10) in moving coordinates is then

$$\rho(x,t) = \frac{1}{4\pi c_0^2} \iiint \frac{A(\eta,\tau)}{\left| \, |x-y| - M(x-y) \, \right|} d\eta \qquad \text{(A-13)}$$

where τ is the retarded time.
This exact solution to the fluid flow equations represents one of the major advances in the solution of unsteady fluid flow problems and is one of the most significant advances in the study of acoustics following the pioneering work of Lord Rayleigh.
An immediate deduction from Lighthill's theory is that at low Mach numbers the **acoustic power P_a radiated from a jet** is given by

$$P_a = \frac{K \rho_j^2 A_j U_j^8}{\rho_0 c_0^5} \qquad \text{(A-14)}$$

where K is a constant of the order of 10^{-5}, ρ_j is the value of the density, A_j is the cross-sectional area and U_j is the velocity at the jet exit.
This is one of the more important results derived directly from the Lighthill acoustic analogy. It shows that **the sound power per unit volume of the flow is proportional to the eight power of the flow velocity**.
Lighthill's theory of aerodynamic noise has shown that for a jet at ambient temperature and low Mach number, the far-field noise intensity varies with M_j^8. However many experimental studies on jet noise have shown a dependence of noise intensity on M_j^6 at low Mach numbers.
Since the kinetic energy flux is proportional to $P_j = \rho_j A_j U_j^3$, we can see that

$$\frac{P_a}{P_j} = K \frac{\rho_j}{\rho_0} \left(\frac{U_j}{c_0} \right)^5$$

then the total acoustic power is a small fraction of the flow kinetic energy flux.
Although Lighthill's theory provides the essential framework for a full understanding of the noise generation in turbulent jets and the overall characteristics of its propagation to the far field, it is difficult to apply when acoustic interaction occurs with the flow field. This interaction involves consideration of the actual flow field and results in changes in the directivity and amplitude of the radiated sound field and its dependence on the flow speed relative to that of external medium.

A.4 Related model equations and approximation

In their classical text on fluid mechanics, Landau and Lifshitz (1987) [A-7] derive an aeroacoustic equation analogous to Lighthill's (i.e., an equation for sound generated by "turbulent" fluid motion) but for the incompressible flow of an inviscid fluid. The inhomogeneous wave equation that they obtain is for the pressure p rather than for the density ρ of the fluid. Furthermore, unlike Lighthill's equation, Landau and Lifshitz's equation **is not exact; but it is an approximation.**
If one is to allow for approximations to be made, a simpler way (without necessarily assuming the fluid is incompressible) to obtain an approximation to Lighthill's equation is to assume that

$$p - p_0 = c_0^2(\rho - \rho_0)$$

where ρ_0 and p_0 are the (characteristic) density and pressure of the fluid in its equilibrium state: $p = p_0 + p'$ and $\rho = \rho_0 + \rho'$. If $\rho << \rho_0$ and $p << p_0$, then the assumed relation follows directly from the *linear theory* of sound waves, in fact, the approximate relation between p and ρ that we assumed is just a *linear* approximation to the generic barotropic equation of state of the fluid. Using a linear relation to simplify a nonlinear wave equation it is a very common practice in nonlinear acoustics. Then, upon substitution the assumed relation between pressure and density into equation (A-10) we obtain the equation

$$\frac{1}{c_0^2}\frac{\partial^2\rho}{\partial t^2} - \nabla^2\rho = \frac{\partial^2\tilde{T}_{ij}}{\partial x_i \partial x_j} \tag{A-15}$$

where $\tilde{T}_{ij} = \rho v_i v_j$
For the case when the fluid is indeed incompressible, i.e. $\rho = \rho_0$ everywhere, then we obtain exactly the equation given in Landau and Lifshitz (1987)

$$\frac{1}{c_0^2}\frac{\partial^2\rho}{\partial t^2} - \nabla^2\rho = \rho_0 \frac{\partial^2\hat{T}_{ij}}{\partial x_i \partial x_j} \tag{A-16}$$

where $\hat{T}_{ij} = v_i v_j$. A similar approximation was suggested by Lighthill (1952) [A-2].

A.5 Noise in Jet engine: turbojet and turbofan

The *jet propulsion* is the method of propulsion in which an object is propelled in one direction by a jet, or stream of gases, moving in the other. This follows from Isaac Newton's third law of motion: *"To every action, there is an equal and opposite reaction"*. The most widespread application of the jet principle is in the jet (gas turbine) engine, the most common kind of aircraft engine.
The *jet engine* is a kind of gas turbine. Air, after passing through a forward-facing intake, is compressed by a compressor, or fan, and fed into a combustion chamber. Fuel (usually kerosene) is sprayed in and ignited. The hot gas produced expands rapidly rearwards, spinning a turbine that drives the compressor before being finally ejected from a rearward-facing tail pipe, or nozzle, at very high speed. Reaction to the jet of gases streaming backwards produces a propulsive thrust forwards, which acts on the aircraft through its engine-mountings, not from any pushing of the hot gas stream against the static air.
Two forms of jet engine are possible:

1. In the **turbojet** (Fig. A-1: a), air passing into the air intake is compressed by the compressor and fed into the combustion chamber where fuel burns. The hot gases formed are expelled at high speed from the rear of the engine, driving the engine forwards and turning a turbine which drives the compressor.
   In a turbojet, air enters the inlet, is compressed to several atmospheres in the compressor, and enters the combustor where it is mixed with fuel and ignited. The high temperature, high pressure gases resulting from the combustion process then pass through the burner nozzles and drive the turbine stages (and thus the compressor), finally exiting as a high velocity, high temperature jet through the exhaust nozzle. Turbulent mixing of this exit jet with the atmosphere is the main mechanism for jet noise, which is the dominant source of noise for turbojet engines and low bypass turbofans during takeoff and sideline conditions.
2. In the **turbofan** (Fig. A-1: b), some air flows around the combustion chamber and mixes with the exhaust gases. This arrangement is more efficient and quieter than the turbojet.
   The turbofan engine is similar to the turbojet except that it includes a large diameter initial compressor section or fan. The partially compressed air leaving the fan stage is divided into two streams, one entering the compressor section as in the turbojet, and the other bypassing the engine core and exiting at increased pressure and velocity through the fan exhaust. This fan discharge may be exhausted into the outside air through a fan jet nozzle shortly after it leaves the fan, or it may be carried aft by an annular fan discharge duct that surrounds the basic engine for most or all of its length, either non-mixed or mixed with the core exhaust.

(a)

(b)

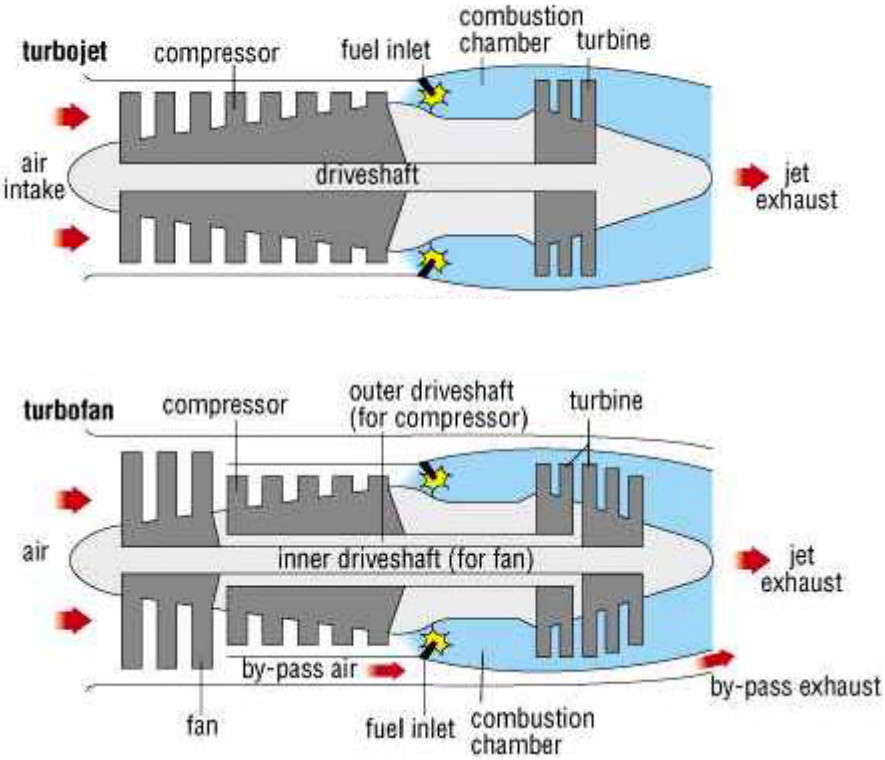

Fig. A-1: Two forms of jet engine: a turbojet (a) and a turbofan (b).

The *turbojet* is the simplest form of gas turbine, used in aircraft well into the supersonic speed range.
The *turbofan* is best suited to high subsonic speeds. It is fitted with an extra compressor or fan in front, and some of the airflow bypasses the core engine, and mixes with the jet exhaust stream, to give it lower temperature and velocity. This results in greater economy, efficiency and quietness compared with the turbojet.
The jet noise benefits of a turbofan arise from the fact that turbofan jet exhaust velocities are lower than those of a turbojet. This behaviour is analytically described by the famous U^8 law of jet noise obtained by Lighthill, which states that the total sound power emitted by a jet is approximately proportional to the jet velocity to the eighth power.
The causes of velocity reduction of a turbofan are two:

1. there is a reduction in jet temperature resulting from the mixing of the cooler, bypass fan exhaust with the core flow;
2. additional energy is extracted from the engine exhaust gases as they pass through the extra turbine stages required to drive the fan.

References of attachment A

[A-1] Lighthill M. J., "On sound generated aerodynamically. I. General theory", Proceeding of the Royal Society of London, series A, vol. 211, pp.564-587, London, 1952.

[A-2] Lighthill M. J., "On sound generated aerodynamically. II. Turbulence as a source of sound", Proceeding of the Royal Society of London, series A, vol. 222, pp. 1-32, London, 1954.

[A-3] Curle, N., "The Influence of solid boundaries upon aerodynamic sound", Proceeding of the Royal Society of London, series A, vol. 231, Issue 1187, pp. 505-514, London 1955.

[A-4] Ffowcs Williams, J. E. and Hawkings, D. L., "Sound Generation by Turbulence and Surfaces in Arbitrary Motion", Philosophical Transactions of the Royal Society of London, vol. 264, Issue 1151, pp. 321-342, London, 1969.

[A-5] Cabana M., Fortune V., Jordan P., "A look insight the Lighthill source term", 12th AIAA/CEAS Aeroacoustics Conference, AIAA-2006-2484, Cambridge, MA, USA, 2006.

[A-6] Michalke A. and Michel U., "Prediction of Jet Noise in Flight from static tests", Journal of Sound and Vibration, vol.67, Issue 3, pp.347-367, 1979.

[A-7] Landau L.D. and Lifshitz E.M., "Fluid Mechanics" 2nd rev. Ed., Course of Theoretical Physics, vol. 6, Pergamon Press, Butterworth-Heinemann, Oxford, 1987.

ATTACHMENT B: Random signals and spectral analysis

A system is vibrating if it is shaking or trembling or moving backwards and forwards in some way. If this motion is unpredictable then the system is said to be in *random vibration* [B-1].
The subject of random signals, e.g. random vibrations, is concerned with finding out how the statistical (or average) characteristics of the motion of a randomly excited system depend on the statistics of the excitation and the dynamic properties of the vibrating system, e.g. mass or damping.
The displacement *x(t)* from an arbitrary datum can be plotted as a function of the time *t* (e.g. see Fig. B-1). Since motion is random, the precise value of x at any chosen time $t=t_0$ can not be precisely predicted. The best we can do is to find the chance, or *probability*, that *x* at t_0 will lie within certain limits.

B.1 Probability density function

A *random signal* cannot be described by an explicit mathematical relation. Rather, the value of the signal at a particular time may be expressed only in terms of some describable probability of occurrence, then there is a continuum of "frequencies" that may be used to characterize the function.
When we say that *x(t)* is random, we mean that the values of x(t) can not be precisely predicted *in advance*. Fig. B-1 shows a sample time history for a random process with the times for which $x \leq x(t) \leq x+dx$ identified by the shaded strips. During the time interval *T*, *x(t)* lies in the band of values *x* to *x+dx* for a total time of $(dt_1+dt_2+dt_3+dt_4+...)$. We can therefore say that, if T is long enough, the probability density function *p(x)* is given by

$$p(x)dx = \text{fraction of the total elapsed time for which x(t) lies in the x to (x + dx) band} =$$
$$= \frac{(dt_1 + dt_2 + dt_3 + dt_4 + ...)}{T} = \frac{\sum dt}{T} \qquad \text{(B-1)}$$

For equation (B-1) to be mathematically correct, the time interval *T* must be infinite, which means that the sample time history must go on for ever and must not change its character with time.
When x(t) is a *random function* of *t*, we can not use equation (B-1) to calculate a mathematical expression for p(x). Alternatively an instrument called a ***probability analyser*** will do the same thing much more quickly by sampling the time history and the sample record at a series of closely spaced intervals. In this case, the probability function is given by:

$$p(x)dx = \text{fraction of total number of samples which lie in the x to (x + dx) band} =$$
$$= \frac{dn}{N} \qquad \text{(B-2)}$$

where *N* are sample values and *dn* are the values that lie in the band *x* to *x+dx*.

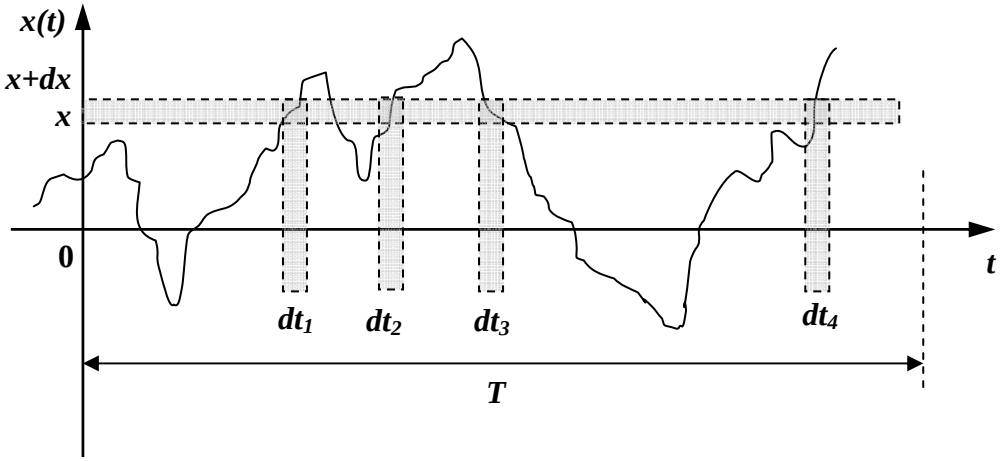

Fig. B-1: Calculation of the *probability density function p(x)* for a random process.

The *first-order probability density function p(x)* specifies the probability *p(x)dx* that a random variable lies in the range of values *x* to *x+dx*.
The *second-order probability density function p(x,y)* is defined in the same way but extends the number of random variables from one to two, in this case *x* and *y*. The probability that the *x* random variable lies in the range *x* to *x+dx* and that the *y* random variable lies in the range *y* to *y+dy* is given by *p(x,y)dxdy*.

B.2 Probability distribution function

In addition to using the *probability density function p(x)* to describe the distribution of values of a random variable, the closely related *probability distribution function P(x)* is also often referred to and is usually computed by a *probability analyser*. *P(x)* is defined by the equation:

$$P(x) = \int_{-\infty}^{x} p(x)\,dx \qquad \Rightarrow \qquad \frac{dP(x)}{dx} = p(x) \tag{B-3}$$

and may therefore be interpreted as the shaded area under the probability density curve shown in Fig. B-2.

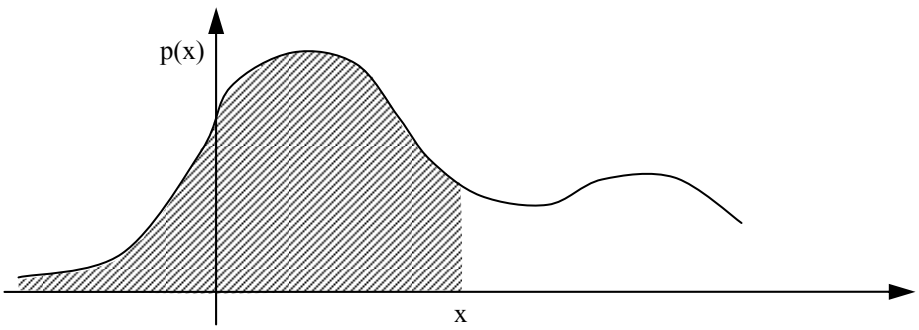

Fig. B-2: The shaded area gives the value of *probability distribution function P(x)*.

The value of P(x) lies between zero and unity since $P(x=\infty)=\int_{-\infty}^{\infty} p(x)\,dx = 1$, and gives the probability that a sample value of the random variable is *less than x*.

B.3 Calculation of averages

Assuming that the probability density function *p(x)* is available for a random process, it can be used to calculate certain statistics of the random process *x(t)*.

B.3.1 Mean value (first statistic moment)

The ***mean value*** of the time history of *x* over the interval *T*, which is usually denoted by *E[x]* where the *E* stands for *"statistical expectation of x"*, is defined by

$$\begin{aligned} E[x(t)]\cdot T &= \text{Total area under the x(t) curve during the interval T} \\ &\quad \text{(areas below the zero line subtracting from the total area)} = \\ &= \int_0^T x(t)dt \end{aligned} \tag{B-4}$$

and hence,

$$E[x(t)] = \int_0^T x(t)\frac{dt}{T} \tag{B-5}$$

that using equation (B-1), the summation over time can be converted to a summation over *x*:

$$\boxed{m = E[x(t)] = \overline{x(t)} = \int_{-\infty}^{\infty} x\,p(x)\,dx} \tag{B-6}$$

It is important to note that *E*[*x(t)*] may be calculated whenever the *probability density p(x)* is known.

B.3.2 Mean square value (second statistic moment)

The ***mean square value*** of x, E[x^2], is defined as the average value of x^2 which is given by

$$\boxed{E[x^2] = \overline{x^2(t)} = \int_0^T x^2(t)\frac{dt}{T} = \int_{-\infty}^{\infty} x^2\,p(x)\,dx} \tag{B-7}$$

B.3.3 Central moment: standard deviation, variance, skewness and kurtosis

The ***standard deviation*** of x, usually denoted by σ, and the ***variance*** σ^2, are defined by the equation

$$\sigma^2 = E[(x - E[x])^2] = E[(x - m)^2] \tag{B-8}$$

That is to say the *variance* is the mean of the square of the deviation of x from its mean level E[x].
Equation (B-8) may be simplified by multiplying out the terms which are squared to give

$$\begin{aligned}\sigma^2 &= E[x^2 - 2xE[x] + (E[x])^2] = \\ &= E[x^2] - 2E[x]E[x] + (E[x])^2\end{aligned} \tag{B-9}$$

since the average of a sum of terms is the same as the sum of the averages of each term separately, and the average of a constant is of course just the constant. Collecting terms, (B-9) gives

$$\sigma^2 = E[x^2] - (E[x])^2 = E[x^2] - m^2 \tag{B-10}$$

or

$$(\text{variance}) = (\text{standard deviation})^2 = \left\{\text{Mean square} - (\text{Mean})^2\right\} \tag{B-11}$$

Then the **variance** σ^2=E[(x–E[x])^2] is the ***second central moment***.
The ***third normalized central moment*** E[(x–E[x])^3]/ σ^3 is a measure of the lopsidedness of the distribution; any symmetric distribution will have a third central moment, if defined, of zero. The normalized third central moment is called the **skewness**. A distribution that is skewed to the left (the tail of the distribution is heavier on the right) will have a negative skewness. A distribution that is skewed to the right (the tail of the distribution is heavier on the left), will have a positive skewness.
The ***fourth normalized central moment*** ({E[(x–E[x])^4] / σ^4 }–3) is called **kurtosis** (or **flatness**) and it is a measure of whether the distribution is tall and skinny or short and squat, compared to the normal distribution of the same variance. Since it is the expectation of a fourth power, the fourth central moment, where defined, is always non-negative; and except for a point distribution, it is always strictly positive. The *kurtosis* is defined to be the normalized fourth central moment minus 3.
A distribution with positive excess kurtosis is called *leptokurtic*, or *leptokurtotic*. *"Lepto-"* means "slender". In terms of shape, a leptokurtic distribution has a more acute peak around the mean (that is, a lower probability than a normally distributed variable of values near the mean) and fatter tails (that is, a higher probability than a normally distributed variable of extreme values).
A distribution with negative excess kurtosis is called *platykurtic*, or *platykurtotic*. *"Platy-"* means "broad". In terms of shape, a platykurtic distribution has a lower, wider peak around the mean (that is, a higher probability than a normally distributed variable of values near the mean) and thinner tails (if viewed as the height of the probability density—that is, a lower probability than a normally distributed variable of extreme values).

B.3.4 Random process and ensemble averaging

The random process consists of a (theoretically) infinite number of a sample functions each of which can be thought of as resulting from a separate experiment. Instead of being measured along a single sample, *ensemble averages* are measured across the ensemble.
The random process is said to be ***stationary*** if the probability distributions obtained for the ensemble do not depend on absolute time. Of course the term *"stationary"* refers to the probability distributions and not to the samples themselves. This implies that all the averages are independent of absolute time and, specifically, that the mean, mean square, variance and standard deviation are independent of time altogether. Since all engineering random process must have a beginning and ending, they cannot be truly stationary, but for practical purposes it is very often adequate to assume that a process is stationary for the majority of its lifetime, or that it can be divided into several separate periods each of which is approximately stationary.
The term ***weakly stationary*** is sometimes used to describe processes in which only the first- and second-order probability distributions, i.e. *mean value* E[x] and *mean square value* $E[x^2]$, are invariant with time.
A ***strictly stationary*** process is one for which all probability distributions of the ensemble are invariant with time.
A stationary process is called an ***ergodic process*** if, in addition to all the ensemble averages being stationary with respect to a change of the time scale, the averages taken along any single sample are the same as the ensemble averages. In practical terms, each sample function is then completely representative of the ensemble that constitutes the random process. Notice that if a process is *ergodic* it must also be *stationary*.

B.4 Correlation

Two variables *x(t)* and *y(t)* like in Fig. B-3 are accordingly said *correlated*.
If we wish to express an approximate functional relationship between *x(t)* and *y(t)* in the form of a straight line, one way of doing this is to *minimize the square of the deviation* (Δ) of the actual values of y from their values predicted by the straight line approximation, then the quantity $\Delta = y - m \cdot x$.

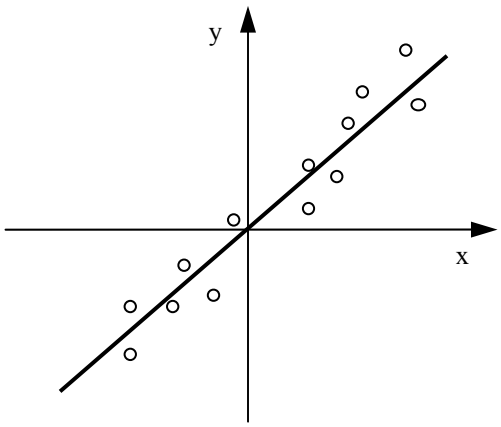

Fig. B-3: Correlation between two random variables x and y.

The equation for the *line of regression of y on x* is

$$\frac{y-m_y}{\sigma_y}=\left\{\frac{E[(x-m_x)(y-m_y)]}{\sigma_x\,\sigma_y}\right\}\frac{x-m_x}{\sigma_x} \tag{B-12}$$

where m_x and m_y are the mean values of x and y respectively (i.e., E[x] and E[y]). The parameter

$$\rho_{xy}=\frac{E[(x-m_x)(y-m_y)]}{\sigma_x\,\sigma_y}=\frac{\mathrm{cov}(x,y)}{\sigma_x\,\sigma_y} \tag{B-13}$$

is called ***correlation coefficient*** or ***normalized Covariance***.
If $\rho_{xy}=\pm 1$ there is perfect correlation, but if $\rho_{xy}=0$ there is no correlation (see Fig. B-4).
Two harmonic functions of time will be correlated if they move in phase or anti-phase, and uncorrelated if they are in quadrature to each other.

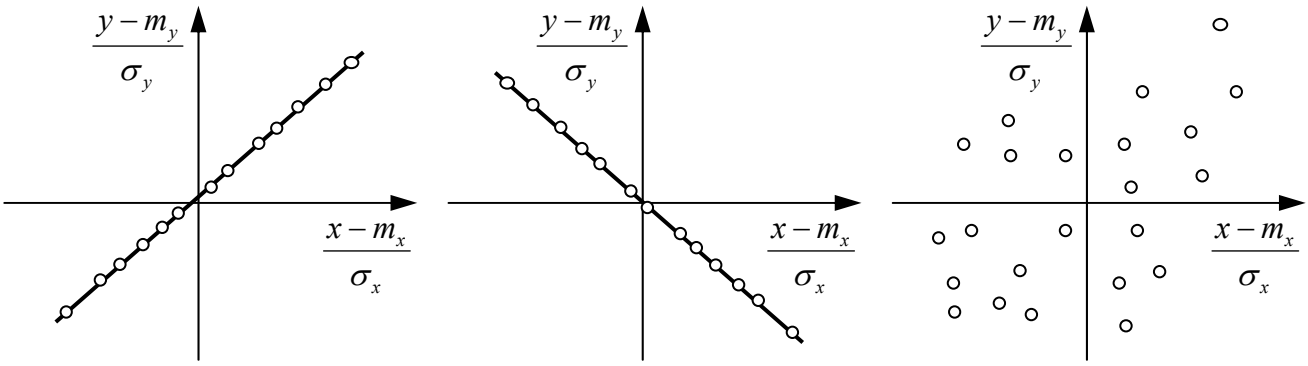

(a) $\rho_{xy}=+1$ (b) $\rho_{xy}=-1$ (c) $\rho_{xy}=0$

Fig. B-4: Regression lines for different values of the correlation coefficient ρ_{xy}.

B.4.1 Auto-correlation

The autocorrelation for a random process x(t) is defined as the average value of the product $x(t)x(t+\tau)$. The process is sampled at time t and then again at time $t+\tau$.
Provided that the process is stationary, the value of E[x(t)x(t+τ)] will be independent of absolute time t and will depend only on the *time separation* τ so that we may put

$$E\,[x(t)\,x(t+\tau)]=f(\tau)=R_x(\tau) \tag{B-14}$$

where $R_x(\tau)$ is the ***autocorrelation function*** for x(t).
If the process is *ergodic* any one sample function is completely representative of the process as a whole. We can average along a single sample function by thinking of the measuring time t_0 as a random variable uniformly distributed along the time axis. Since x(t) is periodic we need only consider a single full cycle of the time history, and the range of values of t_0 need only extend from 0 to T. All values within this range [0,T] are equally likely, and therefore the probability distribution $p(t_0)$ for t_0 is as shown in Fig. B-5.

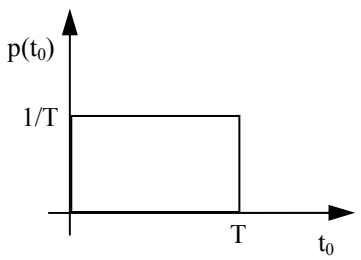

Fig. B-5: Probability distribution for values equally likely.

$$R_x(\tau) = E\,[x(t_0)\,x(t_0+\tau)] = \int_{-\infty}^{\infty} x(t_0)\,x(t_0+\tau)\,p(t_0)\,dt_0 = \\ = \int_0^T x(t_0)\,x(t_0+\tau)\frac{1}{T}dt_0 = \int_0^{2\pi} x(t_0)\,x(t_0+\tau)\frac{1}{2\pi}d\theta \tag{B-15}$$

where $p(t_0)$ is the probability density function for the random time of sampling t_0, and T is the time period ($T = \frac{2\pi}{\omega}$).

We can deduce at once some of the properties of $R_x(\tau)$:

- If $x(t)$ is ***stationary***, the *mean* (m) and the *standard deviation* (σ) will be independent of t, so that

$$E\,[x(t)] = E\,[x(t+\tau)] = m \tag{B-16}$$

and

$$\sigma_{x(t)} = \sigma_{x(t+\tau)} = \sigma \tag{B-17}$$

- The ***cross-correlation coefficient*** (***normalized Covariance***, ***nondimensional Covariance***, then the nondimensional definition of auto-correlation)[1] for two random variables $x(t)$ and $x(t+\tau)$, defined by (B-13), is therefore given by, in stationary case,

$$\rho_{xy} = \rho = \frac{\mathrm{cov}(x,y)}{\sigma_x\,\sigma_y} = \frac{E[(x-m_x)(y-m_y)]}{\sigma_x\,\sigma_y} = \frac{E\left[\{x(t)-m\}\{x(t+\tau)-m\}\right]}{\sigma^2} = \\ = \frac{E\left[x(t)x(t+\tau)\right] - mE\left[x(t+\tau)\right] - mE\left[x(t)\right] + m^2}{\sigma^2} = \frac{R_x(\tau)-m^2}{\sigma^2} = R_x^* \tag{B-18}$$

then

$$R_x(\tau) = \rho\sigma^2 + m^2 \tag{B-19}$$

and since the limiting values of ρ are ± 1, it follows that

$$-\sigma^2 + m^2 \le R_x(\tau) \le \sigma^2 + m^2 \tag{B-20}$$

[1] I know there is a lot of disagreement on the difference between *covariance* and *correlation*, or whether there is a difference, but it seems to be the consensus that ***Correlation coefficient*** does involve dividing by the sigmas, while ***Covariance*** does not divide by the sigmas.

$R_x(\tau)$ is a maximum for values of *t* for which *x(t)* and *x(t+τ)* are in *phase* and a minimum for values of *t* for which they are in *antiphase*.

- When the time interval τ separating the two measuring points is zero, then

$$R_x(\tau = 0) = E[x(t)^2] = E[x^2] \tag{B-21}$$

and is just equal to the ***mean square value*** for the process.

B.4.2 Cross-correlation and covariance

The ***cross-correlation function*** between two different stationary random functions of time x(t) and y(t) is defined as:

$$\begin{aligned} R_{xy}(\tau) = E\,[x(t)\,y(t+\tau)] &= \int_{-\infty}^{\infty} x(t)\,y(t+\tau)\,p(t)\,dt = \\ &= \int_0^T x(t)\,y(t+\tau)\frac{1}{T}dt = \int_0^{2\pi} x(t)\,y(t+\tau)\frac{1}{2\pi}d\theta \end{aligned} \tag{B-22}$$

The ***covariance*** of two different random variables x(t) and y(t) is defined as:

$$\mathrm{cov}(x,y) = E\,\{[x(t)-E(x)]\,[y(t)-E(y)]\,\} = E[(x-m_x)(y-m_y)] \tag{B-23}$$

It's not the sigmas that distinguish *cross-correlation* function from *covariance* (i.e., the covariance does not divide by the sigmas), it's **the subtraction of the means**. The difference is usually blurred because in many important cases the mean is zero.
We can deduce at once some of the properties of $R_{xy}(\tau)$:

- Because the process are stationary, it follows that:

$$R_{xy}(\tau) = R_{yx}(-\tau) \tag{B-24}$$

- The utility of the cross-correlation is greatly enhanced when it is used with the *cross-correlation coefficient* (*normalized covariance*, or *nondimensional covariance*):

$$\rho_{xy} = \frac{\mathrm{cov}(x,y)}{\sigma_x\,\sigma_y} = \frac{R_{xy}(\tau) - m_x m_y}{\sigma_x \sigma_y} = R^*_{xy} \tag{B-25}$$

where $m_x = E\,[x(t)]$ and $m_y = E\,[y(t)]$

- From (B-18) and (B-19), each cross-correlation function can be expressed in terms of the corresponding *normalized Covariance* (or *cross-correlation coefficient*) ρ_{xy}, to give:

$$R_{xy}(\tau) = \sigma_x \sigma_y\,\rho_{xy}(\tau) + m_x m_y \tag{B-26}$$

and since the limiting values of the ρ_{xy}'s are ±1 for perfect in-phase or anti-phase correlation, the limiting values of the cross-correlation functions must be

$$-\sigma_x \sigma_y + m_x m_y \le R_{xy}(\tau) \le \sigma_x \sigma_y + m_x m_y \tag{B-27}$$

We expect that:

- there will be no correlation between x and y when the time separation τ_0 is very large, therefore $R_{xy}(\tau_0) \to m_x m_y$.
- the maximum vales will be $R_{xy}(\tau_0) = \sigma_x \sigma_y + m_x m_y$

B.5 Fourier analysis

Most engineers are familiar with the idea of frequency analysis by which a periodic function can be broken down into its harmonic components and readily accept that a periodic function may be synthesized by adding together its harmonic components.

B.5.1 Fourier series

If *x(t)* is a periodic function of time *t*, with period *T*, then we can always express *x(t)* as an infinite trigonometric series (a *Fourier series*) of the form

$$\begin{aligned} x(t) &= a_0 + a_1 \cos\frac{2\pi t}{T} + a_2 \cos\frac{4\pi t}{T} + \ldots \\ &+ b_1 \sin\frac{2\pi t}{T} + b_2 \sin\frac{4\pi t}{T} + \ldots = a_0 + \sum_{k=1}^{\infty}\left(a_k \cos\frac{2\pi k t}{T} + b_k \sin\frac{2\pi k t}{T}\right) \end{aligned} \tag{B-28}$$

where a_0 and the a_k and b_k are constant Fourier coefficients given by

$$\begin{aligned} a_0 &= \frac{1}{T}\int_{-T/2}^{T/2} x(t)dt \\ a_k &= \frac{2}{T}\int_{-T/2}^{T/2} x(t)\cos\frac{2\pi k t}{T}dt = \frac{2}{T}\int_{-T/2}^{T/2} x(t)\cos\omega_k t\, dt \\ b_k &= \frac{2}{T}\int_{-T/2}^{T/2} x(t)\sin\frac{2\pi k t}{T}dt = \frac{2}{T}\int_{-T/2}^{T/2} x(t)\sin\omega_k t\, dt \end{aligned} \tag{B-29}$$

where k≥1, $\omega_k = \frac{2\pi k}{T} = k\Delta\omega$ is the frequency of the *k*-th harmonic, and $\Delta\omega = \frac{2\pi}{T}$ is the spacing between adjacent harmonics. When the period T becomes large, the frequency spacing $\Delta\omega$ becomes small.

Wavenumber is property of a wave proportional to the reciprocal of the wavelength. It can be defined as the number of wavelengths per unit distance, that is, 1/λ where λ is the wavelength[2]: $k_w = \frac{1}{\lambda}$.

[2] Alternatively as 2π/λ, sometimes termed the *angular wavenumber* or *circular wavenumber* or - most often - simply wavenumber.

B.5.2 Fourier integral

A *Fourier integral* may be regarded as the formal limit of a *Fourier series* as the period tends to infinity. The reason for introducing this concept is because Fourier integrals indicate the frequency composition of an aperiodic function.
Substituting (B-29) into (B-28), for a_0=0, and considering that when the period T→∞, Δω→dω and the Σ becomes an integral with the limits ω=0 to ω=∞, in this case

$$x(t) = 2\int_0^\infty A(\omega)\cos\omega t\, d\omega + 2\int_0^\infty B(\omega)\sin\omega t\, d\omega = \int_{-\infty}^\infty A(\omega)\cos\omega t\, d\omega + \int_{-\infty}^\infty B(\omega)\sin\omega t\, d\omega \qquad \text{(B-30)}$$

where we had put

$$\begin{aligned} A(\omega) &= \frac{1}{2\pi}\int_{-\infty}^\infty x(t)\cos\omega t\, dt \\ B(\omega) &= \frac{1}{2\pi}\int_{-\infty}^\infty x(t)\sin\omega t\, dt \end{aligned} \qquad \text{(B-31)}$$

Note that the integrals for *x(t)* now run from -∞ to +∞ instead of from 0 to +∞ and the factor 2 disappears. The idea of a "negative" frequency has been introduced but this is purely a mathematical artifice to simplify the equation.
Note that the physical dimensions of the Fourier transform components $A(\omega)$ and $B(\omega)$ (which are those of x/ω) are different from those of the Fourier series coefficients a_k and b_k (which are those of x).
For engineering applications, the important condition for *Classical Fourier analysis theory* is usually expressed in the form

$$\int_{-\infty}^\infty |x(t)|\, dt < \infty \qquad \text{(B-32)}$$

It means that *classical theory* applies only to functions which decay to zero when $|t| \to \infty$. This condition may be removed when impulse functions are introduced in the *generalized theory of Fourier analysis*.

B.5.3 Complex form of the Fourier transform

It has become customary in random theory to write (B-30) and (B-31) in complex form, making use of the result that

$$e^{+i\theta} = \cos\theta + i\sin\theta \quad \Rightarrow \quad e^{-i\theta} = \cos\theta - i\sin\theta \qquad \text{(B-33)}$$

Defining *X(ω)*, the complex Fourier transform of x(t), as

$$X(\omega) = A(\omega) - iB(\omega) \qquad \text{(B-34)}$$

and using equations (B-31), it gives

$$X(\omega) = \frac{1}{2\pi}\int_{-\infty}^\infty x(t)(\cos\omega t - i\sin\omega t)\, dt = \frac{1}{2\pi}\int_{-\infty}^\infty x(t)\, e^{-i\omega t}\, dt \qquad \text{(B-35)}$$

Since $A(\omega)$ is an even function (while $B(\omega)$ is an odd function), and $sin(\omega t)$ is an odd function of ω (while $cos(\omega t)$ is an even function), $A(\omega)sin(\omega t)$ and $B(\omega)cos(\omega t)$ are odd function and so

$$\int_{-\infty}^{\infty} A(\omega)\sin\omega t\ d\omega = 0 \qquad \text{and} \qquad \int_{-\infty}^{\infty} B(\omega)\cos\omega t\ d\omega = 0 \tag{B-36}$$

We can therefore write the (B-30) in the following form

$$\begin{aligned} x(t) &= \int_{-\infty}^{\infty} A(\omega)\cos\omega t\, d\omega + \int_{-\infty}^{\infty} B(\omega)\sin\omega t\, d\omega = \\ &= \int_{-\infty}^{\infty} A(\omega)\cos\omega t\, d\omega + i\left[\int_{-\infty}^{\infty} A(\omega)\sin\omega t\, d\omega\right] + \int_{-\infty}^{\infty} B(\omega)\sin\omega t\, d\omega - i\left[\int_{-\infty}^{\infty} B(\omega)\cos\omega t\, d\omega\right] = \\ &= \int_{-\infty}^{\infty} \{A(\omega) - iB(\omega)\}\ \{\cos\omega t + i\sin\omega t\}d\omega = \int_{-\infty}^{\infty} X(\omega)e^{+i\omega t}\ d\omega \end{aligned} \tag{B-37}$$

Summarising, we have that $X(\omega)$ is the complex Fourier transform of $x(t)$ and we can write

$$\boxed{X(\omega) = \frac{1}{2\pi}\int_{-\infty}^{\infty} x(t)e^{-i\omega t}\ dt} \tag{B-38}$$

$$\boxed{x(t) = \int_{-\infty}^{\infty} X(\omega)e^{+i\omega t}\ d\omega} \tag{B-39}$$

which may be regained from X(ω) by the *inverse Fourier integral equation*.
Authors differ over the position of the factor 1/2π which appears in these equations. Some include the 1/2π in the *inverse transform equation* (B-39), while others include a factor $1/\sqrt{2\pi}$ in both (B-38) and (B-39). However the definition of X(ω) given here is the one popularly used in random theory.

B.6 Power Spectral Density (PSD)

The autocorrelation function gives information about the frequencies present in a random process indirectly. The Fourier transform of $R_x(\tau)$ and its inverse, are given by

$$\boxed{S_x(\omega) = \frac{1}{2\pi}\int_{-\infty}^{\infty} R_x(\tau)e^{-i\omega\tau}\ d\tau = \Im\{R_x(\tau)\}} \tag{B-40}$$

$$\boxed{R_x(\tau) = \int_{-\infty}^{\infty} S_x(\omega)e^{+i\omega\tau}\ d\omega = \Im^{-1}\{S_x(\omega)\}} \tag{B-41}$$

where $S_x(\omega)$ is called the ***spectral density*** (or *auto-spectral density*, or *Power Spectral Density*, *PSD*) of the *x(t)* process and it is a function of angular frequency ω, the symbol $\Im\{\}$ denotes the Fourier transform and $\Im^{-1}\{\}$ the inverse transform.
The most important property of $S_x(\omega)$ becomes apparent when we put τ=0 in (B-41). In this case, using (B-21):

$$R_x(\tau = 0) = \int_{-\infty}^{\infty} S_x(\omega)\, d\omega = E[x^2] \tag{B-42}$$

The ***mean square value*** $E[x^2]=\sigma^2$ of a stationary random process *x(t)* is therefore given by the area under a graph of spectral density $S_x(\omega)$ against ω, Fig. B-6.

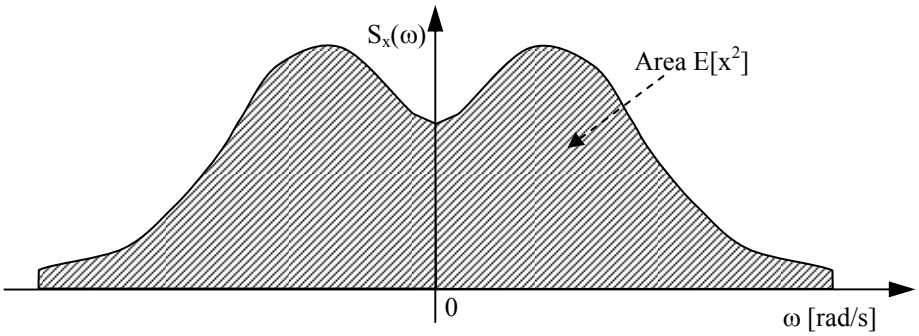

Fig. B-6: The area under a spectral density curve is equal to $E[x^2]$.

$S_x(\omega)$ is never negative, therefore the mean square spectral density of a stationary process x(t) is a real, even and non-negative function of ω, of the form illustrated in Fig. B-6.
A more complete name for $S_x(\omega)$ is the ***mean square spectral density***.
The *practical form* of the mean square $E[x^2]$ is

$$E[x^2] = R_x(\tau = 0) = \int_0^\infty W_x(f)\,df \qquad \text{(B-43)}$$

where *f* is the frequency in Hz and $W_x(f)$ is the ***equivalent one-sided spectral density function***, shown in Fig. B-7b. The frequency band ω to (ω+dω) rad/s in Fig. B-7a corresponds to ω/2π to (ω+dω)/2π Hz in Fig. B-7b, so that for equal contributions to the mean square in this frequency band, the shaded areas in both (a) and (b) must be the same. Hence, the single-sided spectrum $W_x(f)$ is related to the double-sided spectrum $S_x(\omega)$ by the following formula:

$$2S_x(\omega)\,d\omega = W_x(f)\frac{d\omega}{2\pi} \quad \Rightarrow \quad W_x(f) = 4\pi\, S_x(\omega) \qquad \text{(B-44)}$$

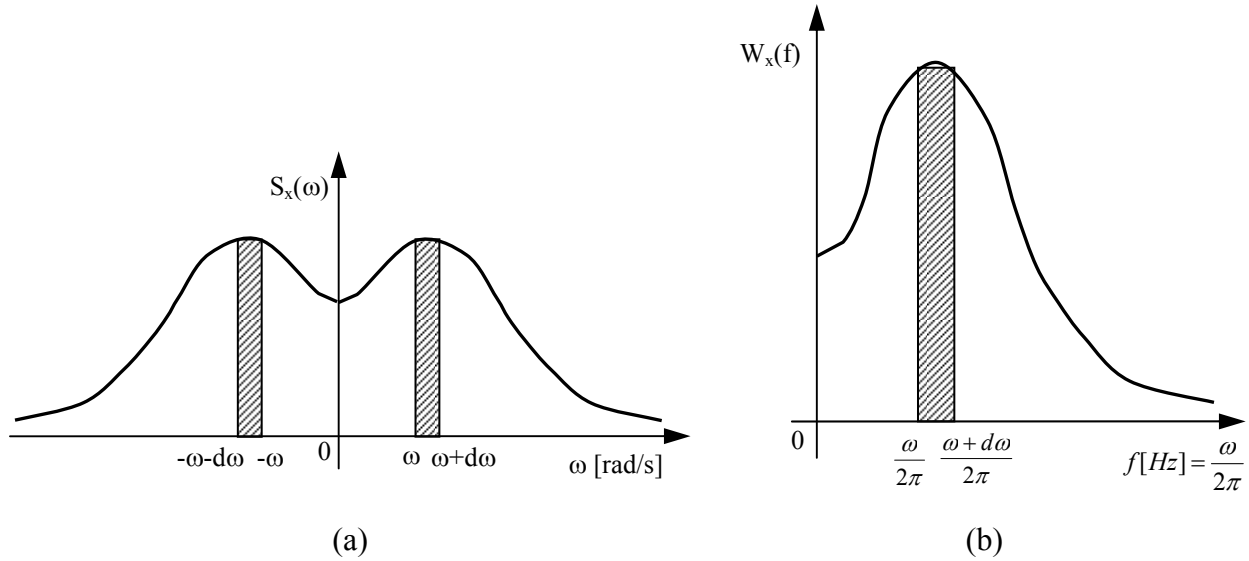

Fig. B-7: Illustrating the relationship between alternative spectral density parameters: double sided spectrum (a), and one-sided spectrum (b).

The *units* of the double-sided spectrum $S_x(\omega)$ are accordingly those of [x^2/*(unit of angular frequency)*], while that of one-sided spectrum $W_x(f)$ are [x^2/*(unit of frequency)*].

B.6.1 Narrow-band and broad-band processes

A process whose spectral density has the form shown in Fig. B-8b is called a ***narrow band*** process because its spectral density occupies only a narrow band of frequency. The autocorrelation function has the form shown in Fig. B-8c where the predominant frequency of $R_x(\tau)$ against τ is the average value $\omega_0 = (\omega_1 + \omega_2)/2$. Correlation is a maximum when τ=0.

A ***broad band*** process is one whose spectral density covers a broad band of frequencies and the time history is then made up of the superposition of the whole band of frequencies as shown in Fig. B-9b. In the limit when the frequency band extends from ω_1=0 to ω_2=∞, the spectrum is called *white*. From (B-42) the mean square value of a *white noise* process must be infinite, so white noise is only a theoretical concept, but in practical terms a spectrum is called white if *it is broad band noise whose bandwidth extends well past all the frequencies of interest*. The original analogy of ***"white noise"*** was with "white" light (whose spectrum is approximately constant over the range of visible frequencies) but the term "noise" is derived from the study of electrical noise. A *broad band* random process is now often described loosely as *"noise"*.

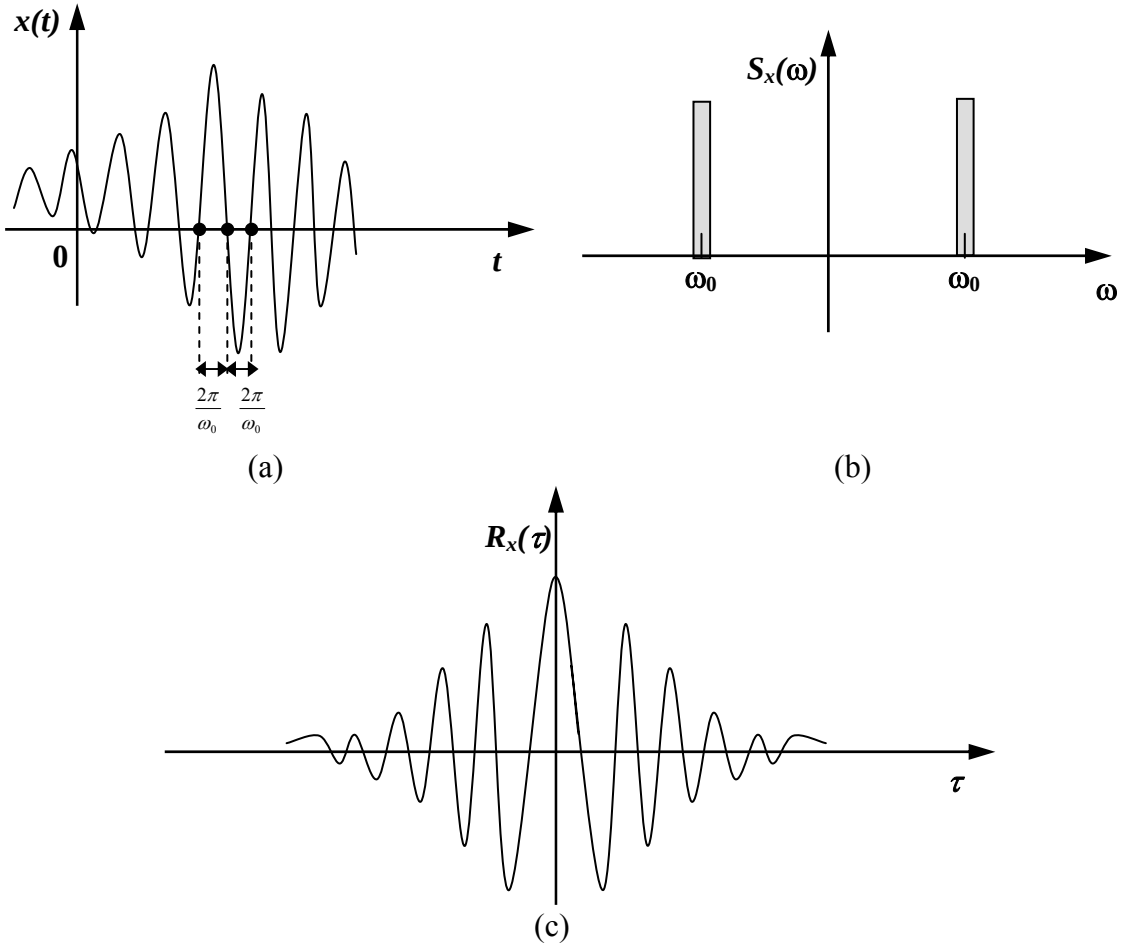

Fig. B-8: Time history (a), spectral density (b) and autocorrelation function (c) of a ***narrow band*** random process.

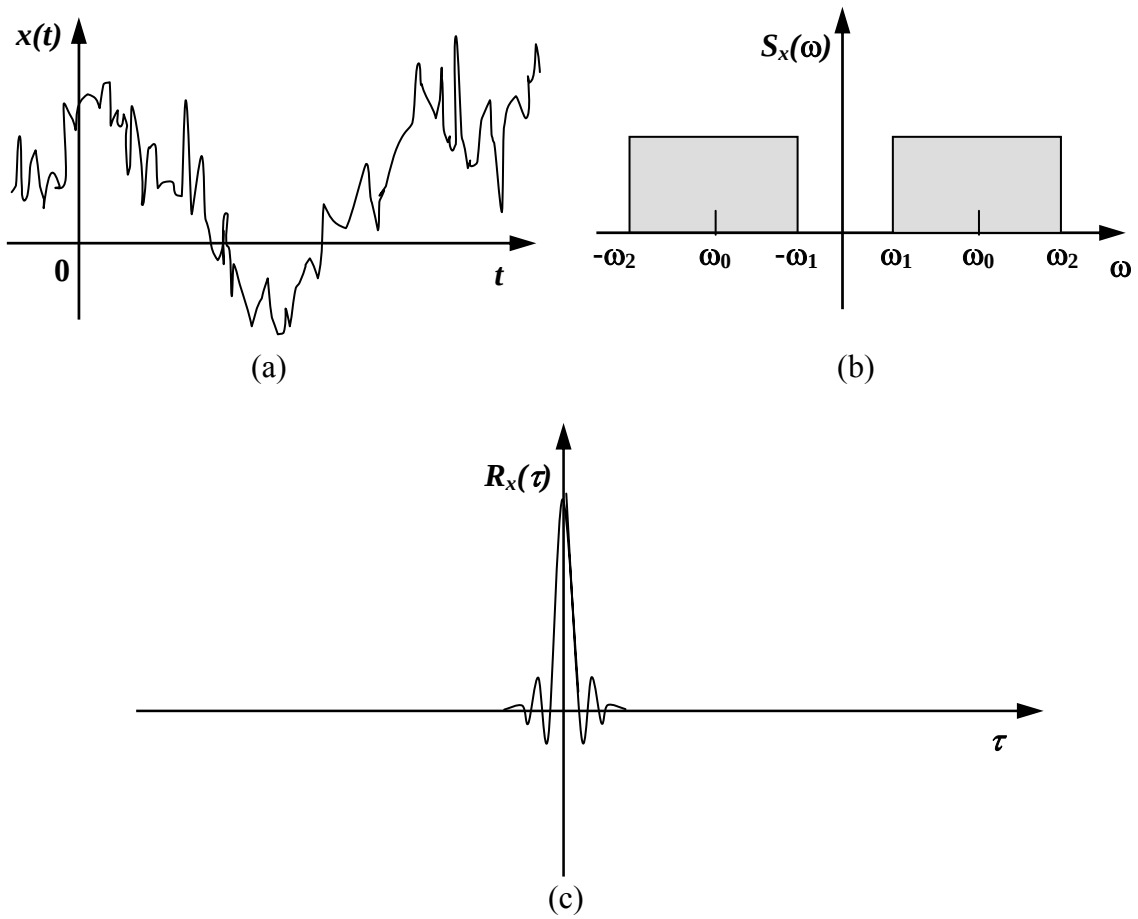

Fig. B-9: Time history (a), spectral density (b) and autocorrelation function (c) of a ***broad band*** random process (e.g., ***white noise***).

The behaviour of ***white noise*** may be represented mathematically by using Dirac's delta function $\delta(\tau)$, which is impulse function. The delta function $\delta(\tau)$ is defined so that it is zero everywhere except at $\tau=0$, when it is infinite in such a way that

$$\int_{-\infty}^{\infty} \delta(\tau)\, d\tau = 1 \tag{B-45}$$

More generally, $\delta(\tau-T)$ is zero everywhere except at $\tau=T$, and has the property that

$$\int_{-\infty}^{\infty} \delta(\tau - T)\, f(\tau) d\tau = f(\tau = T) \tag{B-46}$$

where $f(\tau)$ is any arbitrary continuous function of τ.

B.6.2 Cross-spectral density (CSD)

We have seen how the *spectral density* of random process is defined as the Fourier transform of its *autocorrelation function*. In the same way, the ***cross-spectral density*** (CSD) of a pair of random processes is defined as the Fourier transform of the corresponding ***cross-correlation function*** for the two processes. Therefore if $R_{xy}(\tau)$ is the cross-correlation function, we have

$$\boxed{S_{xy}(\omega) = \frac{1}{2\pi}\int_{-\infty}^{\infty} R_{xy}(\tau)e^{-i\omega\tau}\, d\tau} = \left|S_{xy}(\omega)\right| e^{-i\varphi_{xy}(\omega)} \tag{B-47}$$

$$\boxed{R_{xy}(\tau) = \int_{-\infty}^{\infty} S_{xy}(\omega)e^{+i\omega\tau}\, d\omega} \tag{B-48}$$

Since the *cross-correlation* are related by (B-24), and defining $S_{xy}(\omega)$, the complex Fourier transform of $R_{xy}(\tau)$, as (B-34), we can deduce some of the properties of $S_{xy}(\omega)$:

- If A(ω) and B(ω) are real function of ω,

$$S_{xy}(\omega) = A(\omega) - iB(\omega) \tag{B-49}$$

$$S_{yx}(\omega) = A(\omega) + iB(\omega) \tag{B-50}$$

  hence $S_{xy}(\omega)$ are the same except that the sign of their imaginary parts is reversed. $S_{xy}(\omega)$ is therefore the complex conjugate of $S_{yx}(\omega)$, which is usually written

$$S_{yx}(\omega) = S_{xy}^{*}(\omega) \tag{B-51}$$

  The cross-spectrum contains the same information as the cross-correlation but in a more convenient form. The cross-spectrum has a real part A(ω) and an imaginary part B(ω) or, alternatively, it can be expressed as a *magnitude* (or *amplitude*) and a *phase*:
  - the *magnitude* at a given frequency represents the degree to which two signals have common harmonic content at that frequency;

    $$\left|S_{xy}(\omega)\right| = \left[A^2(\omega) + B^2(\omega)\right]^{\frac{1}{2}}$$

  - the *phase* is the true phase angle between the two signals at that frequency. The phase spectrum measures the phase shift between the data sets at each frequency.

    $$\varphi_{xy}(\omega) = tg^{-1}\frac{B(\omega)}{A(\omega)}$$

  Sometimes the complete frequency spectrum is graphed in 2 parts, *"amplitude"* versus *frequency* (which is the *spectral density*) and *"phase"* versus *frequency* (which contains the rest of the information from the frequency spectrum). The variable function x(t) cannot be recovered from the "amplitude" of spectral density part alone because the "temporal information" is lost.
- The same result of (B-44) also applies for the magnitude of cross-spectral density function:

$$W_{xy}(f) = 4\pi S_{xy}(\omega) \tag{B-52}$$

The *units* of the double-sided cross-spectrum $S_{xy}(\omega)$ are accordingly those of [*x·y/(unit of angular frequency)*] and that of double-sided spectrum $W_{xy}(f)$ are [*x·y/(unit of frequency)*].

B.6.3 Coherence function

If we want to get a good idea of the similarity of two signals in different frequency bands, we can use a different function called the ***coherence function*** (also known as a ***cross-power spectral density function***, or CPSD).
A function related to *cross-correlation* is the *coherence function*, defined in terms of power spectral densities and the cross-spectral density by

$$C_{xy} = \frac{\left| S_{xy}(\omega) \right|^2}{S_x(\omega)\, S_y(\omega)} \tag{B-53}$$

The *correlation coefficient* is in time domain and it is calculated from covariance and standard deviation coefficients. The *coherence function* is in frequency domain and it is calculated from cross and auto spectrum functions.
This is considerably more complicated than calculating the *correlation coefficient*, but in some cases, the two produce related results.
The utility of the *cross-correlation* is greatly enhanced when it is used with the *coherence.* It is a real function between zero and one which gives a measure of correlation between two time series x(t) and y(t) at each frequency.
The higher the coherence at a given frequency, the greater the probability either that one signal is causing the other or that the two signals are caused by the same agent. At any frequency for which the coherence is low, either the signals are relatively independent of each other, or the signal-to-noise ratio on one or both channels is low.

References of attachment B

[B-1] Newland D.E., “An Introduction to Random vibrations, spectral and wavelet analysis”, Third edition, Person Education Limited, 1993.

ATTACHMENT C: Acoustic signals analysis

This chapter presents a analytical treatment of the acoustic signals. Measuring and analyzing acoustic signals are increasingly important in modern society.
The failure modes produced by acoustic noise excitation are similar to those associated with other types of vibratory structural fatigue. These include failures due to excessive displacement, in which one deflecting component makes contact with another, as well as fractured structural members and loose fasteners. Broken solder joints and cracked circuit boards and wave guides can also occur.
Electronic components whose function depends on the motion of structural parts, such as relays and pressure switches, are particularly susceptible.
Large flat panels are most susceptible to damage by acoustic energy as they can undergo large displacements while oscillating at low frequency.

C.1 Acoustic auto-correlations and auto-spectra

A function of considerable importance in the analysis of signals is *Auto-correlation*. As formalized in [C-1], given the pressure signal $p(z_i,t)$, the temporal auto-correlation function is computed as follows:

$$R_{pp}(z_i,\tau) = E\left[\, p(z_i,t)\, p(z_i,t+\tau)\right] = \lim_{T\to\infty}\frac{1}{T}\int_0^T p(z_i,t)\, p(z_i,t+\tau)\, dt \qquad \text{(C-1)}$$

where E […] denotes the *expected value* (i.e. ensemble averaged value) of the quantity in square brackets, z_i is the *position of a transducer* and τ is the *delay time*. The τ may be set to vary continuously. It is to be noted that the *auto-correlation* function for τ =0 is the *mean square value* of p ($\overline{p^2}$), in fact if the ***average*** of random function is defined as a limit

$$E[p(t)] = \overline{p(t)} = \lim_{T\to\infty}\frac{1}{T}\int_0^T p(z_i,t)\, dt$$

then similarly the ***mean square value*** is

$$E[p^2(t)] = \overline{p^2(t)} = \lim_{T\to\infty}\frac{1}{T}\int_0^T p^2(z_i,t)\, dt = E\left[\, p^2(z_i,t)\,\right] = R_{pp}(z_i,\tau=0)$$

The *Auto-Spectra* or *Power Spectral Density* (*PSD*) can be obtained from the Fourier transform of the *auto-correlation* function:

$$S_{pp}(z_i,\omega) = PSD_p(z_i,\omega) = \Im\{R_{pp}(z_i,\tau)\} = \int_{-\infty}^{+\infty} R_{pp}(z_i,\tau)\, e^{-j\omega\tau}\, d\tau \qquad \text{(C-2)}$$

where the symbol $\Im\{\,\}$ denotes the Fourier transform and $\Im^{-1}\{\,\}$ the inverse transform.
Thus, an alternative to equation (C-1) is the following inverse formula which can be used for the auto-correlation computation:

$$R_{pp}(z_i,\tau) = \Im^{-1}\{S_{pp}(z_i,\omega)\} = \frac{1}{2\pi}\int_{-\infty}^{+\infty} S_{pp}(z_i,\omega)\, e^{j\omega\tau}\, d\omega \qquad \text{(C-3)}$$

The *nondimensional* definition of the auto-correlation is given by the *auto-correlation coefficient*, which follows:

$$R^*_{pp}(z_i,\tau) = \frac{R_{pp}(z_i,\tau)}{\sigma_p^2(z_i)} \tag{C-4}$$

where σ_p is the pressure standard deviation, i.e. the integral of auto-spectral density.
It is expressed as a number between minus one and one.

C.1.1 The r.m.s. pressure coefficient

The r.m.s. pressure coefficient Cp_{rms} is

$$Cp_{rms} = \frac{\sigma_p(z_i)}{q} = \frac{\sigma_p(z_i)}{\frac{1}{2}\rho_0 U^2}$$

where q is the fluid dynamic pressure.

C.2 Acoustic cross-correlations and cross-spectra

Cross-correlations and *cross-spectra* represent fundamental quantities which are needed input for estimating the structural response and the acoustic transmission from the external field of fluctuating pressure. Their knowledge allows for the *forcing* functions to be correctly computed in the evaluation of the structural dynamics, and e.g. the flow induced vibrations of a launcher panel surfaces [C-2].
The *Cross-correlation* gives a direct measure of the time delay between incidences of an event common to two signals. It is therefore useful for measuring the time required for a pressure signal to propagate from one transducer to another. A typical application would be to determine whether a disturbance is acoustic or nonacoustic. If the signal travels between the two transducers at the mean sound speed, it is acoustic, but if it travels at the mean convective velocity, it is nonacoustic (e.g. pseudo-sound). It could be a structural vibrations if it travels with a very short time delay.
Let us denote with $p(z_i^a,t)$ and $p'(z_i^b,t+\tau)$ the pressure signals obtained from two pressure transducers (a and b) located at z_i^a and z_i^b respectively and measured simultaneously. The formal definition of the cross-correlation between the two signals, follows [C-1]:

$$R_{pp'}(z_i^a,z_i^b,\tau) = E\left[p(z_i^a,t)p'(z_i^b,t+\tau)\right] = \lim_{T\to\infty}\frac{1}{T}\int_0^T p(z_i^a,t)p'(z_i^b,t+\tau)\,dt \tag{C-5}$$

Using the Fourier transform it is possible to define the *Cross-spectrum Density* (CSD) and to obtain the inverse formula equivalent to equation (C-2):

$$S_{pp'}(z_i^a,z_i^b,\omega) = \Im\{R_{pp'}(z_i^a,z_i^b,\tau)\} = \int_{-\infty}^{+\infty} R_{pp'}(z_i^a,z_i^b,\tau)\,e^{-j\omega\tau}d\tau \tag{C-6}$$

$$R_{pp'}(z_i^a, z_i^b, \tau) = \Im^{-1}\{S_{pp'}(z_i^a, z_i^b, \omega)\} = \frac{1}{2\pi}\int_{-\infty}^{+\infty} S_{pp'}(z_i^a, z_i^b, \omega)\, e^{j\omega\tau} d\omega \qquad \text{(C-7)}$$

The *Cross-spectrum* between two signals is the Fourier transform of their *Cross-correlation*.
As for the auto-correlation, a *cross-correlation coefficient* (or *normalized covariance*) can be defined as follows, that change between -1 and 1:

$$R^*_{pp'}(z_i^a, z_i^b, \tau) = \frac{R_{pp'}(z_i^a, z_i^b, \tau)}{\sigma_p \sigma_{p'}} \qquad \text{(C-8)}$$

$$\lim_{\tau \to 0} R^*_{pp'}(z_i^a, z_i^b, \tau) = R^*_{pp'}(z_i^a, z_i^b, 0) = 1$$

The cross-spectrum is very useful for studying wave propagation and for identifying the presence of standing waves.
The importance of equations (C-6) and (C-8) lies that the *cross-spectrum density* and the *normalized covariance* of turbulence are (in theory) physically identifiable and measurable quantities, while the instantaneous source distribution is not necessarily a practical physical quantity to work with because it is a random variable of time and space. The utility of the spectral representation is found in the fact that it is often the *acoustic intensities of specific frequencies*, rather than the *overall intensity*, that is of importance in many applications.

C.3 Convection velocity

As pointed out in [C-1], the cross correlation function globally characterizes the propagation of the pressure perturbation close to a wall. If the perturbation propagates with a velocity $U_c(z_i)$, the so called *convection velocity*, a delay time (τ_0) should be experimental observed in the cross-correlation between two pressure transducers sufficiently close to each other. Specifically, if the cross-correlation exhibits a maximum at the instant τ_0, the convection velocity can be determined as follows:

$$U_C(z_i) = \frac{\xi}{\tau_0(z_i)} \qquad \text{(C-9)}$$

where $\xi = z_i' - z_i$ is the (streamwise) separation between two pressure transducers. An example of a typical result is given in Fig. C-1. The delay time can be clearly calculated and, from equation (C-9), also the convection velocity can be easily computed.

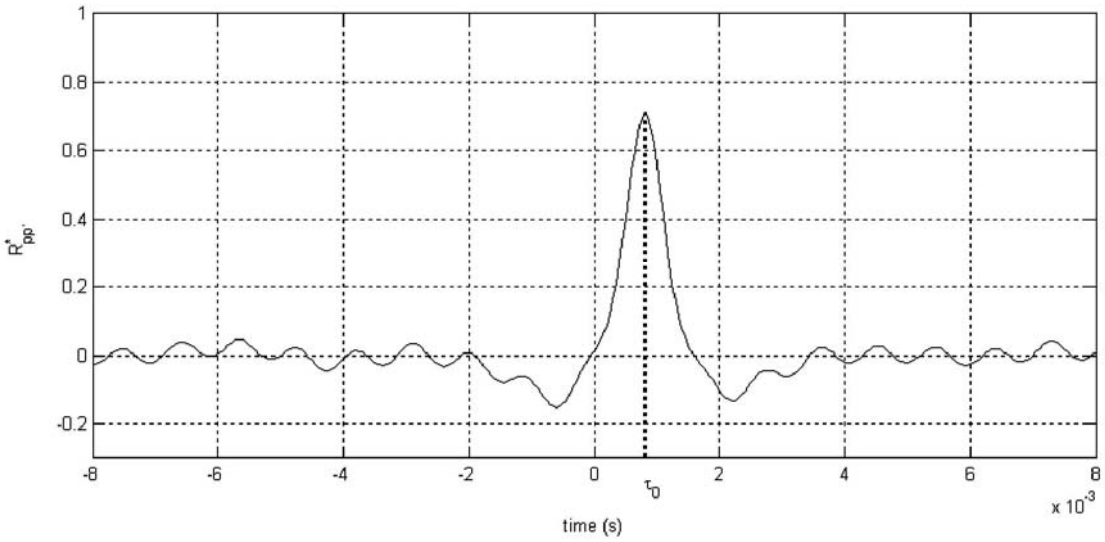

Fig. C-1: Example of cross-correlation obtained between two wall pressure signals in a TBL. The delay time τ_0 can be clearly estimated.

C.4 The concept of decibel

The decibel (dB) is a logarithmic unit of measurement that expresses the magnitude of a physical quantity (usually power or intensity) relative to a specified or implied reference level. Its logarithmic nature allows very large or very small ratios to be represented by a convenient number, in a similar manner to scientific notation. Since it expresses a ratio of two (same unit) quantities, it is a dimensionless unit.

$$A = 10\log_{10}\frac{p_A}{p_0}$$
$$B = 10\log_{10}\frac{p_B}{p_0} \qquad \text{(C-10)}$$
$$\frac{A}{B} = 10\log_{10}\frac{p_A}{p_B}$$

0 decibels represents the softest sound we can hear, the threshold of hearing. An increase of 3 dB corresponds to an approximate doubling of power (in exact terms, the factor is $10^{3/10}$, or 1.9953, about 2). An increase of 10 dB (A=10B) represents a little more than a 3-fold increase (about 3.16) in the air pressure change created by the sound wave. A 20 dB (A=20B) increase is more than a 3 times 3 increase in sound pressure (about 10 times greater). And a 30 dB (A=30B) increase is an increase in sound pressure of more than 3 times 3 times 3 (3.16 raised to the third power or 3.16 cubed). In other words, a 40 decibel sound creates sound pressure levels that are more than 30 times as great as a 10 decibel sound. The threshold of pain for the average human ear is 120 decibels.

$$p_A = p_B \quad \rightarrow \quad \text{dB}=0 \tag{C-11}$$

$$\frac{A}{B} = 3 \quad \rightarrow \quad 3dB = 10\log_{10}\frac{p_A}{p_B} \quad \rightarrow \quad \left(\frac{p_A}{p_B}\right)^{10} = 10^3 \quad \rightarrow \quad \left(\frac{p_A}{p_B}\right) = 10^{\frac{3}{10}} \tag{C-12}$$

$$\frac{A}{B} = 10 \quad \rightarrow \quad 10dB = 10\log_{10}\frac{p_A}{p_B} \quad \rightarrow \quad \left(\frac{p_A}{p_B}\right)^{10} = 10^{10} \quad \rightarrow \quad \left(\frac{p_A}{p_B}\right) = 10 \tag{C-13}$$

Sometimes scientists collect sound level data using measurements that take other factors into account. There are special scales that include *weighting factors*. Weighting refers to the range of frequencies that the sound level meter is measuring:

- **"A"-weighting** primarily measures frequencies in the range which corresponds to the range of greatest sensitivity for the human ear.
- **"C"-weighting** means that the meter will measure sound levels uniformly over the frequency range from 32-10,000 Hz, giving an indication of the overall sound level.

Noises above 85 dB can hurt our ears by damaging the sensitive hair cells of the inner ear.

C.4.1 Sound Power level

Transmission of sound is generally considered on a power basis, then the sound power level is defined as:

$$L_S(z_i) = 10\log_{10}\left[\frac{\mathrm{P}}{\mathrm{P}_{ref}}\right]$$

where P is the sound power transmitted across a specified surface and P_{ref} is a reference quantity conventionally taken as 10^{-12} W.

C.4.2 Sound Intensity level

The sound intensity level may be found from

$$L_S(z_i) = 10\log_{10}\left[\frac{\mathrm{I}}{\mathrm{I}_{ref}}\right]$$

where $I_{ref}=10^{-12}$ W/m and the acoustic intensity is related to the mean-square pressure by

$$I(z_i) = \frac{\sigma_p(z_i)}{\rho_0 c_0}$$

C.5 Sound Pressure Level distribution and OASPL

The most important quantity giving an idea of the overall pressure intensity is the *Overall Sound Pressure Level* (OA*SPL*) that analyses the signal of *random pressure* in all frequencies with statistical approach. In the case of *not random signals* where the fluctuating pressure standard deviation corresponds to the max value of amplitude or for a range of acoustic frequencies, the name of *Sound Pressure Level* (SPL) is used.
The OASPL, according to [C-2], is defined as follows:

$$SPL(z_i) = 20\log_{10}\left[\frac{\sigma_p(z_i)}{p_{ref}}\right] = 20\log_{10}\left[\frac{\sqrt{\int_{-\infty}^{\infty} S_{pp}(\omega)\,d\omega}}{p_{ref}}\right] \qquad \text{(C-14)}$$

where $\sigma_p(z_i)$ is the fluctuating pressure standard deviation of the pressure time series obtained from a pressure transducer located at a point of coordinate z_i. , and S_{pp} is the *auto-spectral density*. The standard deviation is therefore obtained from time averaging while p_{ref} is the reference pressure ($p_{ref} = 20\ \mu Pa = 2\cdot10^{-5}\ Pa$ in the air, $p_{ref} = 2\ \mu Pa$ for sounds in liquids and $p_{ref} = 1\ \mu Pa$ for underwater acoustics).
It is important to note that the *pressure standard deviation* (σ_p) is the square of the variance (σ_p^2) that is the integral of the *auto-spectral density*.
When sounds are independently generated by two or more incoherent sources, their sound powers add. The combined SPL of *n* different sources is

$$SPL = 10\ \log_{10}\sum_{i=1}^{n} 10^{\frac{SPL_i}{10}}$$

The last equation can be used to combine or separate the SPLs of various sources and the background.

C.6 Spectra in terms of 1/n-octaves

Spectral analysis is the process of breaking down a signal into its components at various frequencies, and in the context of acoustics there are two very different ways of doing this, depending on whether the result is desired on a linear frequency scale with constant resolution (in Hz) or on a logarithmic frequency scale with constant percentage resolution.
The human ear has a frequency range of three decades (20 Hz–20 kHz) which can only be expressed on a logarithmic frequency scale with constant percentage bandwidth, i.e., where the bandwidth of a filter at any frequency is a fixed percentage of its center frequency.
The human ear tends to interpret equal intervals on a logarithmic frequency scale as equal steps (e.g., ***octaves*** with a frequency ratio of 2 between the highest and lowest frequencies covered by the band, or ***1/3-octaves*** with a ratio of $2^{1/3}$). For estimating spectra in terms of 1/*n*-octaves, it is most efficient to pass the signal through a series of filters with constant percentage bandwidth and measure the power transmitted by each filter. The filters can be either analogue or digital, but there is an increasing tendency to use the latter, since, as explained below, by efficient "timesharing" it is

possible to use a very limited number of actual filter units to filter in parallel over any number of octaves, simply by processing data streams with different sampling frequencies varying in octave (2:1) steps.
The decibel pressure levels in acoustic noise spectra are not generally provided at each and every frequency. Instead, they are often specified over bands of width Δf, which span 1/3 of a frequency octave. Table C-2 is an example of such a 1/3 octave band specification. An octave is the interval between one frequency (f_1) and another (f_2) with half or double it (Table C-1).

In the case of **octave band**:

$$f_C = \sqrt{f_1 f_2} = \sqrt{2 f_1^2} = f_1\sqrt{2}$$
$$f_2 = f_C\sqrt{2}$$
$$\frac{f_2 - f_1}{f_C} = \frac{1}{\sqrt{2}} = 0.70$$

where f_C is the *center frequency*.

Center frequency of octave, f_C [Hz]
31.5
63.0
125.0
250.0
500.0
1000.0
2000.0
4000.0
8000.0
16000.0

Table C-1: Octave band specification

In the case of **1/3 octave band** we have that

$$f_1 = f_{C1}\sqrt[6]{2}$$
$$f_C = f_1\sqrt[6]{2} = f_{C1}\sqrt[3]{2}$$
$$f_2 = f_C\sqrt[6]{2} = f_1\sqrt[3]{2}$$
$$f_{C2} = f_2\sqrt[6]{2} = f_C\sqrt[3]{2}$$
$$f_C = \sqrt{f_{C1} f_{C2}}$$
$$\frac{f_2 - f_1}{f_C} = \frac{f_1\left(\sqrt[3]{2} - 1\right)}{f_1\sqrt[6]{2}} \cong 0.23$$

An example is: f_{C1}=800 Hz; f_1=896 Hz; f_C=1000 Hz; f_2=1120 Hz; f_{C2}=1250 Hz.

Center frequency of 1/3 octave, f_C [Hz]
20.0
31.5
40.0
50.0
63.0
80.0
100.0
125.0
160.0
200.0
250.0
315.0
400.0
500.0
630.0
800.0
1000.0
1250.0
1600.0
2000.0
2500.0
3150.0
4000.0
5000.0
6300.0
8000.0
10000.0
12500.0
16000.0
20000.0

Table C-2: 1/3 Octave band specification

1/*n*th-octave spectra are sometimes calculated from FFT spectra where the upper decade of three separate FFT spectra is converted into constant percentage bandwidth and assembled into a single spectrum over three decades. The original FFT spectra are assumed to have constant PSD in each line, so the spectrum can be considered as a bar graph. The lower and upper cutoff frequencies of each 1/*n*th-octave filter are calculated, and the PSD in the corresponding lines (and parts of lines) of the FFT spectrum is integrated to give the total power in the 1/*n*th-octave filter. The problem with this approach is that the filter characteristic of the synthesized filter changes abruptly at the junctions between decades, since the slope changes by a factor of 10.

C.6.1 Filters and frequency weighting

Filters and *frequency weightings* are used to give emphasis or de-emphasis to parts of a signal based on its frequency content.
The frequency range for filters is often separated in one or more **passbands** and one and more **stopbands**. The *stopband* consists of the band of those frequencies where we want the filter to remove the signal energy (high attenuation); the *passband* consists of the band of those frequencies where we want a low attenuation. An example is an *octave-band filter* where the passband is one octave wide. The filter will have low attenuation at frequencies within the octave band and high attenuation for signals outside the band.
The term *"frequency weighting"* is used when we want a more gradual emphasis/de-emphasis. An example is the A-weighting used in sound level meters introduced to mimic the variation in the sensitivity for the human auditory organ to sound with different frequencies.
The human response to a continuous sound depends on the frequency. Traditionally, sound in the frequency range 20 Hz–20 kHz is regarded as audible. However, in reality there is a gradual change between audible and non-audible sound. A tone with a high or a low frequency outside this range may be audible if it has a sufficient strength, and a tone with a frequency inside this range may be inaudible if the strength is too low.
A network with a frequency-dependent gain may be used to mimic the frequency response of the human auditory organ. The most common network is the A-weighting. Historically, there were three common weightings for sound level measurements: A, B and C, to mimic the auditory response at low, medium and high sound levels. Today, we have better methods for describing the auditory response, and only A- and C-weightings are in general use. The "**A"-weighting** is mainly applied for general sound level measurement and to access the risk for hearing impairment due to loud noise. **"C"-weighting** is mainly used to access the risk of hearing impairment due to short time/high amplitude or peak values in the sound. Since the C-weighting is relatively flat within the normal audible frequency range, it is often used for indicating the non-weighted response. Recently, the **"Z"-network** has been introduced for this purpose.

C.7 Fluctuating pressures and vibration of structures

Acoustic noise results from the propagation of sound pressure waves through air or other media. During the launch of a rocket, such noise is generated by the release of high velocity engine exhaust gases, by the resonant motion of internal engine components, and by the aerodynamic flow field associated with high speed vehicle movement through the atmosphere. This environment places severe stress on flight hardware and has been shown to severely impact subsystem reliability.
The fluctuating pressures associated with acoustic energy during launch can cause vibration of structural components over a broad frequency band, ranging from about 20 Hz to 10,000 Hz and above. Such high frequency vibration can lead to rapid structural fatigue.
To quantify the acoustic environment during launch, launch vehicles are often instrumented with internal microphones, which measure noise levels within the rocket fairing. This data is telemetered to the ground for processing and ultimately plotted in the form of a sound pressure level versus frequency spectrum. Since the acoustic forcing function is stochastic, depending on many atmospheric and other variables, data from a number of such flights are generally gathered.

The rationale for acoustic noise testing is straightforward, as acoustic energy is the primary source of vibration input to a space launch vehicle. During the initial phases of a rocket launch, high velocity gases are ejected from motor nozzles and reflected from the ground, creating turbulence in the surrounding air and inducing a vibratory response of the rocket structure. During the subsequent ascent phase of a launch, as the vehicle accelerates through the atmosphere to high velocity, aerodynamic turbulence induces pressure fluctuations which again cause structural vibration. These pressure fluctuations increase in severity as the vehicle approaches and passes through the speed of sound, due to the development and instability of local shock waves. The high-level acoustic noise environment continues during supersonic flight, generally until the maximum dynamic pressure condition is reached.

Acoustic energy is transmitted to the mission payload in two ways:

1. First, fluctuating pressures within the payload fairing impinge directly on exposed spacecraft surfaces, inducing vibration in high gain antennae, solar panels and other components having a large ratio of area-to-mass.
2. Secondarily, the fluctuating external pressure field causes an oscillatory response of the rocket structure, which is ultimately transmitted through the spacecraft attachment ring in the form of random vibration. From the spacecraft perspective, this random input is generally lowest at the launch vehicle attachment plane, and increases upward along the payload axis.

At the integrated spacecraft level, then, acoustic noise is a primary source of vibration excitation.

References of attachment C

[C-1] Bendat J. S. and Piersol A. G., “Random Data: Analysis & Measurement Procedures”, Wiley-Interscience; 2nd edition, 1986.

[C-2] Blake W. K., “Mechanics of flow induced sound and vibrations”, Applied Mathematics and Mechanics, vol. 17, Academic Press Inc., Orlando (FL), 1986.

ATTACHMENT D: Thermodynamic equations

D.1 Introduction

Turbulent combustion is a multi-scale problem where complexity lies in the interaction between fluid dynamics and chemistry. The main aim of this chapter is to provide a theoretical understanding of some of the scale physics in turbulent reacting flows.
Combustion and turbulence interact in several ways. Looking at the turbulent kinetic energy spectrum reveals some of these mechanisms. It is known that in nonreactive homogeneous isotropic turbulence, kinetic energy flows preferentially from large to small structures, with a scaling exponent −5/3. Each scale, with an associated wavenumber, interacts only with scales associated to adjacent wavenumbers.
High frequency heat release (order of 10^4 Hz) typical of turbulent flames drives local (spatial) dilatation. Thus the classic shape of the cold (unreactive) turbulent spectrum may be significantly altered. In particular, at high wavenumbers it does not follow the k^{-7} scaling law typical of the unreactive dissipative range and some peaks may appear. Consequently, a reverse energy cascade is expected to occur and to increase with respect to non-reactive flows.
It is physically true and widely accepted to assume combustion as a small scale phenomenon. *Nondimensional Navier-Stokes equations* not only show the changing of physics with scale, but also that the particular way turbulent combustion takes place at small scale depends on compressibility and changes with the local Mach number.
The heat release and its dilatational effects induce pressure waves that affect vorticity production or destruction via the baroclinic effect. Besides, dilatational effects change locally the reaction rate and may promote combustion.

D.2 The transport equations

Gaseous combustion is governed by a set of transport equations expressing the **conservation of mass**, **momentum**, **energy**, and **species mass fraction** and by a **thermodynamic equation of state** describing the gas behaviour.
For a mixture of N_s ideal gases (multicomponent reacting systems) in local thermodynamic equilibrium and chemical nonequilibrium, the corresponding conservation equations (extended Navier-Stokes equations) are:

a) Transport equation of **mass**
b) Transport equation of **momentum**
c) Transport equation of **total energy** (internal + mechanical)
d) Transport equation of **species mass fraction**
e) Thermodynamic **Equation of State**

In the index notation of governing equations for a multi-species, reacting gaseous mixture, summation rule is henceforth implied over repeated indices (Einstein's rule of summation).

D.2.1 Transport equation of mass

$$\frac{\partial \rho}{\partial t} + \nabla \cdot \left(\rho \bar{u} \right) = 0 \tag{D-1}$$

then, in other form, it is possible to write:

$$\frac{D\rho}{Dt} + \rho \nabla \cdot \bar{u} = 0 \tag{D-2}$$

or

$$\frac{\partial \rho}{\partial t} + \frac{\partial \rho u_i}{\partial x_i} = 0 \tag{D-3}$$

The total mass conservation equation is unchanged compared to non reacting flows (combustion does not generate mass).

D.2.2 Transport equation of momentum

The equation of momentum is the same in reacting and non reacting flows:

$$\frac{\partial \rho \bar{u}}{\partial t} + \nabla \cdot \left(\rho \bar{u}\, \bar{u} \right) = \nabla \cdot \bar{\sigma} + \rho \sum_{i=1}^{N_S} Y_i \bar{f}_i \tag{D-4}$$

where N_S is the number of chemical species.
The basic assumption is that we are dealing with continuous, isotropic, and homogeneous media. We shall consider the special case of a Newtonian fluid, that is, a fluid exhibiting a linear relationship between viscous stress tensor ($\bar{\tau}$) and strain rate tensor of deformation ($\bar{E}$), resulting in the Navier-Stokes equation.
The momentum equation in indicial notation is:

$$\frac{\partial \left(\rho u_k \right)}{\partial t} + \frac{\partial \left(\rho u_k u_j \right)}{\partial x_j} = \frac{\partial \sigma_{kj}}{\partial x_j} + \rho \sum_{i=1}^{N_S} Y_i \bar{f}_{i,k} \tag{D-5}$$

where σ_{ij} is the stress tensor and $f_{i,k}$ is the force per unit mass (volume force) acting on the i-th chemical species in direction k.
A Newtonian fluid is assumed, which is characterized by the following constitutive linear relation between the stress tensor $\bar{\sigma}$ and the strain rate tensor $\bar{E}$:

$$\sigma_{ij} = -p\delta_{ij} + \tau_{ij} = -p\delta_{ij} + \left\{ \lambda \frac{\partial u_i}{\partial x_i}\delta_{ij} + 2\mu \left[\frac{1}{2}\left(\frac{\partial u_i}{\partial x_j} + \frac{\partial u_j}{\partial x_i} \right) \right] \right\} \tag{D-6}$$

then

$$\bar{\sigma} = \left(-p + \lambda \nabla \cdot \bar{u}\right) \bar{I} + 2\mu \bar{E} = -p\bar{I} + \bar{\tau}$$

where $\bar{\tau}$ is the viscous part of stress tensor, λ and μ are the two viscosity coefficient (Lamè modules).
The difference between the bulk viscosity (μ_B) and the dynamic viscosity (μ, the first viscosity coefficient) is named the second viscosity (λ):

$$\lambda = \mu_B - \frac{2}{3}\mu$$

The usual practice is to employ the hypothesis made by Stokes in 1845 [D-1], that is $\mu_B = 0$, in combustion processes also. The bulk viscosity takes into account nonequilibrium effects between the translational and rotational degrees of freedom of molecules; it becomes important when rotational energy adjustment times (~10 collisions) are longer than translational adjustment times (~1 collision), thus for both "rapid" compressions, such as across shock waves, or expansions, as in supersonic expansion from holes in vacuo.
Then the stress tensor τ_{ij} may be written:

$$\tau_{xx} = \frac{2\mu}{3}\left(2\frac{\partial u}{\partial x} - \frac{\partial v}{\partial y} - \frac{\partial w}{\partial z}\right) \qquad \tau_{xy} = \mu\left(\frac{\partial u}{\partial y} + \frac{\partial v}{\partial x}\right)$$

$$\tau_{yy} = \frac{2\mu}{3}\left(2\frac{\partial v}{\partial y} - \frac{\partial u}{\partial x} - \frac{\partial w}{\partial z}\right) \qquad \tau_{xz} = \mu\left(\frac{\partial u}{\partial z} + \frac{\partial w}{\partial x}\right)$$

$$\tau_{zz} = \frac{2\mu}{3}\left(2\frac{\partial w}{\partial z} - \frac{\partial u}{\partial x} - \frac{\partial v}{\partial y}\right) \qquad \tau_{yz} = \mu\left(\frac{\partial v}{\partial z} + \frac{\partial w}{\partial y}\right)$$

In CFD codes for multi-species flows the molecular viscosity is often assumed to be independent of the gas composition and close to that of air (this introduces errors that are less important than those related to the thermodynamic properties) so that the classical Sutherland law can be used:

$$\mu = c_1 \frac{T^{\frac{3}{2}}}{T + c_2} \frac{T_0 + c_2}{T_0^{\frac{3}{2}}} \tag{D-7}$$

where c_1 and c_2 must be determined so as to fit the real viscosity of the mixture. For air at T_0=273K, c_1=1.71e^{-5} kg/s·m and c_2=110.4 K [D-2].
A second law is sometimes preferred, called *Power law*:

$$\mu = c_1 \left(\frac{T}{T_0} \right)^b \tag{D-8}$$

with b typically ranging between 0.5 and 1.0 (e.g. b=0.76 for air).
Substituting the constitutive equation (D-6) in the momentum equation (D-5), we will obtain the **Navier-Stokes equation** in indicial form:

$$\rho \left[\frac{\partial u_i}{\partial t} + u_j \frac{\partial u_i}{\partial x_j} \right] = \frac{\partial}{\partial x_j} \left\{ -p\delta_{ij} + \lambda \frac{\partial u_k}{\partial x_k} \delta_{ij} + 2\mu \left[\frac{1}{2} \left(\frac{\partial u_i}{\partial x_j} + \frac{\partial u_j}{\partial x_i} \right) \right] \right\} + \rho \sum_{i=1}^{N_S} Y_i \bar{f}_i \tag{D-9}$$

Even though the equation (D-5) does not include explicit reaction terms, the flow is modified by combustion: the dynamic viscosity (μ) strongly changes because temperature varies in a ratio from 1:8 or 1:10. Density also changes in the same ratio and dilation through the flame front increases all speeds by the same ratio. As consequence, the local Reynolds number varies much more than in a non reacting flow: even though the momentum equations are the same with and without combustion, the flow behaviour is very different. A typical example is found in jets: turbulent non reacting jets may become laminar once they are ignited.

D.2.3 Transport equation of total energy (internal + mechanical)

If e_t is the energy stored per unit mass defined as: $e_t = e + \frac{u_i u_i}{2}$

it is possible to write

$$\frac{\partial \rho e_t}{\partial t} + \nabla \cdot \left(\rho \bar{u} e_t \right) = -\nabla \cdot \bar{q} + \dot{Q} + \nabla \cdot \left(\bar{\sigma} \bar{u} \right) + \rho \sum_{i=1}^{N_S} Y_i \bar{f}_i \cdot \left(\bar{u} + \bar{V}_i \right) \tag{D-10}$$

The law of conservation of energy for a fluid contained within a volume element in indicial notation is:

$$\rho \left[\frac{\partial e_t}{\partial t} + u_i \frac{\partial e_t}{\partial x_i} \right] = -\frac{\partial q_i}{\partial x_i} + \dot{Q} + \frac{\partial \sigma_{ij} u_i}{\partial x_i} + \rho \sum_{i=1}^{N_S} Y_i f_{i,k} \left(u_k + V_{i,k} \right)$$

where:

– on the left side
  - The first term ($\rho \frac{\partial e_t}{\partial t}$) is the rate of accumulation of internal and kinetic energy.
  - The second term ($\rho u_i \frac{\partial e_t}{\partial x_i}$) is the net rate of influx of internal and kinetic energy by convection.

– on the right side

- The first term ($-\frac{\partial q_i}{\partial x_i}$) is the net rate of heat addition due to the heat flux q; which contains the conduction heat, the energy flux caused by interdiffusion processes and the Dufour effect (heat flux produced by concentration gradients).

  The energy flux q_i includes a heat diffusion term expressed by Fourier's Law ($-\lambda\frac{\partial T}{\partial x_i}$) and a second term associated with the diffusion of species with different enthalpies which is specific of multi-species gas ($\rho\sum_{i=1}^{N_S} h_i Y_i V_{i,k}$).

$$q_i = -\lambda\frac{\partial T}{\partial x_i} + \rho\sum_{i=1}^{N_S} h_i\, Y_i\, V_{i,k}$$

- The second ($\dot{Q}$) is the rate of heat added by heat source (due for example to an electric spark, a laser or radiative flux), not to be confused with the heat released by combustion.
- The last two terms are the net rate of work done on system by surroundings, in particular the term $\rho\sum_{i=1}^{N_S} Y_i f_{i,k}\left(u_k + V_{i,k}\right)$ is the power produced by volume forces f_k.

D.2.4 Transport equation of species mass fraction

$$\frac{\partial \rho Y_i}{\partial t} + \nabla\cdot\left(\rho\bar{u}Y_i\right) = -\nabla\cdot\bar{J}_i + \dot{\omega}_i \qquad \text{(D-11)}$$

or, in other form, it is possible to write:

$$\frac{\partial \rho Y_i}{\partial t} + \frac{\partial}{\partial x_k}\left[\rho\left(u_k + V_{i,k}\right)Y_i\right] = \dot{\omega}_i \qquad \text{for i =1, … , } N_S \qquad \text{(D-12)}$$

where J_i ($= \rho V_{i,k} Y_i = -\rho D_i \nabla Y_i$, where D_i is the effective diffusion coefficient of species i into the gas mixture and it is a function of the thermal diffusivity α) is the chemical species diffusive mass flux and $\dot{\omega}_i$ is the reaction rate of chemical species i, that is production destruction rate of species i. $V_{i,k}$ is the k-component of the diffusion velocity V_i of species i, and $\dot{\omega}_i$ is the reaction rate of species i.

In a general multicomponent system there are N_s equations of this kind (or N_s–1 if the equation for the mixture is used). The addition of these equations gives the equation of continuity for the mixture.

It is possible to define the ***heat release per unit volume*** due to combustion:

$$\dot{\omega}_T = -\sum_{i=1}^{N_S}\Delta h^0_{f,i}\dot{\omega}_i$$

where $h^0_{f,i}$ is the chemical formation enthalpies.

D.2.5 Thermodynamic Equation of State

$$p = \rho \sum_{i=1}^{N_s} \frac{Y_i}{W_i} R_u T \tag{D-13}$$

These equations must be coupled with the constitutive equations which describe the molecular transport properties of the flow.
It is important to note that the N_s species transport equations (D-11) and the mass conservation equation (D-1) are linearly dependent and one of them is redundant. Furthermore, to be consistent with mass conservation, the diffusion fluxes ($J_i = \rho Y_i \overline{V}_i$) and chemical source terms must satisfy, by the definition:

$$\sum_{i=1}^{N_S} \overline{J}_i = 0 \qquad \Rightarrow \qquad \sum_{i=1}^{N_S} Y_i V_{i,k} = 0 \tag{D-14}$$

$$\sum_{i=1}^{N_S} \dot{\omega}_i = 0 \tag{D-15}$$

In particular, the constraint on the summation of chemical source terms ($\dot{\omega}_i$) derives from mass conservation for each of the N_r chemical reactions of a chemical mechanism. With the tensor notation this chemical reactions mechanism can be written as

$$\sum_{i=1}^{N_s} \nu'_{ij} A_i \leftrightarrow \sum_{i=1}^{N_s} \nu''_{ij} A_i \qquad \text{with} \qquad i = 1, \dots, N_S \qquad \text{and} \qquad j = 1, \dots, N_r \tag{D-16}$$

where ν'_{ij} and ν''_{ij} are the stoichiometric coefficients of species i on the left (′) and right side (″) of the j−th chemical reaction, and A_i is the generic chemical species. Since mass is given by the product of number of moles (ν_{ij}) times molecular weight (W_i), mass concentration for each j−th reaction is written as

$$m'_j = m''_j \qquad \Rightarrow \qquad \sum_{i=1}^{N_S} \nu'_{ij} W_i = \sum_{i=1}^{N_S} \nu''_{ij} W_i \quad \Rightarrow \quad \sum_{i=1}^{N_S} \left(\nu''_{ij} - \nu'_{ij}\right) W_i = 0 \qquad \text{with } j = 1, \dots, N_r$$

The net source/sink term of the i-th chemical species is

$$\dot{\omega}_i = \sum_{j=1}^{N_r} \dot{\omega}_{ij} = W_i \sum_{j=1}^{N_r} \left(\nu''_{ij} - \nu'_{ij}\right) \dot{\omega}_{R\,j} \qquad \text{with} \quad i = 1, \dots, N_S$$

where $\dot{\omega}_{R\,j} = \dfrac{\left(\nu''_{ij} - \nu'_{ij}\right) W_i}{\dot{\omega}_i}$ is the *reaction rate* associated to the j-th reaction, that is the rate of progress of reaction j. Summering the last equation over the number of chemical species N_s

$$\sum_{i=1}^{N_{Ss}} \dot{\omega}_i = \sum_{i=1}^{N_S} {}_{ij} W_i \sum_{j=1}^{N_r} \left(\nu''_{ij} - \nu'_{ij} \right) \dot{\omega}_{R\,j} = \sum_{j=1}^{N_r} \dot{\omega}_{R\,j} \sum_{i=1}^{N_S} W_i \left(\nu''_{ij} - \nu'_{ij} \right) = 0$$

This results shows that total mass is conserved.
The $\dot{\omega}_i$ in each species continuity equation is determined by the phenomenological chemical kinetic expression:

$$\dot{\omega}_i = W_i \sum_{j=1}^{N_r} \left(\nu''_{ij} - \nu'_{ij} \right) B_k T^{\alpha_k} \exp - \frac{E_{a\,k}}{R_u T} \prod_{j=1}^{N_s} \left(\frac{X_j p}{R_u T} \right)^{\nu'_{j,k}}$$

where $\dot{\omega}_{R\,j}$ being usually modelled using the empirical Arrhenius law.

D.3 Solution of a multicomponent-species system

If the diffusion velocities can be substituted by Fick's Law in the species and energy equations, then in a system with N_S chemical species there are N_S+6 unknowns.
The N_S+6 equations to be solved are:

- 1 overall mass continuity
- 3 momentum equations
- 1 energy equation
- N_S – 1 species equations
- 1 equation of state
- 1 equation relating all Y_i

If the diffusion velocities must be solved from the diffusion equation for a multicomponent system, there will be 5N_S+6 unknowns. Further there are 4N_S equations:

- 3N_S diffusion equations
- N_S equations relating X_i to Y_i

D.4 Some chemistry definitions

Some useful relationships among mass fraction Y_i, mole fractions X_i, molar concentrations, $[X_i]$, species molecular weights W_i, and mixture molecular weight W_{mix}, are reported.

- Mixture molecular weight (mean molecular weight)

$$W_{mix} = \frac{1}{\sum_{i=1}^{N_s} \frac{Y_i}{W_i}} = \sum_{i=1}^{N_s} X_i W_i = \frac{\sum_{i=1}^{N_s} [X_i] W_i}{\sum_{i=1}^{N_s} [X_i]}$$

- Mole or volume fractions / mass fractions

$$X_i = Y_i \frac{W_{mix}}{W_i}$$

$$Y_i = X_i \frac{W_i}{W_{mix}}$$

- Mass fraction / molar concentrations

$$[X_i] = \frac{p W_{mix} Y_i}{RTW_i} = \frac{\rho Y_i}{W_i}$$

$$Y_i = \frac{[X_i] W_i}{\sum_{j=1}^{N_s} [X_j] W_j}$$

- Mole fractions / molar concentration

$$[X_i] = \frac{p X_i}{RT} = \frac{\rho X_i}{W_{mix}}$$

$$X_i = \frac{[X_i]}{\sum_{j=1}^{N_s} [X_j]}$$

D.5 Some thermodynamics definitions

In a multi-species continuum, enthalpy, $H(Y_i, T)$, and internal energy, $E(Y_i, T)$, are the sum of two contributions: one is the potential energy of the Coulomb atomic molecular force field (expressed in terms of formation energies), and the other is the kinetic energy of molecules (sensible internal energy) associated to all their degrees of freedom (translational, rotational, vibrational and electronic)[D-3], as expressed by all terms forming the specific heat.

D.5.1 Enthalpy

The specific enthalpy $H(Y_i,T)$ is defined as

$$H(Y_i,T)=\sum_{i=1}^{N_S} Y_i H_i(T)=\sum_{i=1}^{N_S} Y_i\left[h_{f,i}^0(T_0)+h_{S,i}(T)\right]=\sum_{i=1}^{N_S} Y_i\, h_{f,i}^0(T_0)+h_S(Y_i,T) \qquad \text{(D-17)}$$

where Y_i is the mass fraction of the N_s chemical species *i*, $h_{f,i}^0(T_r)$ and $h_{S,i}(T)$ are respectively the formation enthalpy at the reference temperature T_0 and the sensible enthalpy of species *i*.
The sensible enthalpy is defined thermodynamically, and for an ideal gas

$$dh_S = c_p dT \qquad \text{(D-18)}$$

and therefore

$$h_S(Y_i,T)=\int_{T_0}^{T} c_p(Y_i,T)\,dT$$

$$h_{S,i}(Y_i,T)=\frac{h_{S,i}(Y_i,T_i)-h_{S,i}(Y_i,T_0)}{W_i}$$

where T_0 is a reference temperature, usually assumed as 298.15 K (=25°C), and $c_p(Y_i,T)$ is the specific heat at constant pressure, given by

$$c_P(Y_i,T)=\sum_{i=1}^{N_S} Y_i c_{P,i}(T)$$

It depends on the local gas composition (Y_i).
At the reference temperature the sensible quantities are nil.

D.5.2 Entropy

The entropies (s_i) for each species can be evaluated by:

$$s(Y_i,T)=\frac{s_i(T_i)-s_i(T_0)}{W_i} \qquad \text{(D-19)}$$

D.5.3 Internal Energy

The specific internal energy is defined as

$$E(Y_i,T)=\sum_{i=1}^{N_S} Y_i E_i(T)=\sum_{i=1}^{N_S} Y_i\left[e^0_{f,i}(T_0)+e_{S,i}(T)\right]=\sum_{i=1}^{N_S} Y_i\, e^0_{f,i}(T_0)+e_S(Y_i,T) \qquad \text{(D-20)}$$

where $e^0_{f,i}(T_0)$ and $e_{S,i}(T)$ are respectively the formation internal energy at the reference temperature T_0 and the sensible internal energy of species *i*.
Just as the sensible enthalpy, also the sensible internal energy is defined thermodynamically as (for an ideal gas)

$$de_S = c_v dT \qquad \text{(D-21)}$$

and therefore

$$e_S(Y_i,T)=\int_{T_0}^{T} c_v(Y_i,T)\,dT+\frac{R}{W}T_0$$

where $c_v(Y_i,T)$ is the specific heat at constant volume, given by

$$c_v(Y_i,T)=\sum_{i=1}^{N_S} Y_i c_{v,i}(T)$$

It depends on the local gas composition (Y_i).
At the reference temperature the sensible quantities are nil.
The relationship between h_s and e_s is obtained by subtracting equation (D-18) from (D-21),

$$dh_S = de_S+\left(c_p-c_v\right)dT = de_S + R_g dT \qquad \text{(D-22)}$$

since $R_g = c_p - c_v$.

D.5.4 Sound velocity

Under the assumptions of no heat release and no viscous terms, the flow remains isentropic ($s=s_0$) if it is homogeneous and isentropic at the initial time t=0. The energy equation may then replaced by the isentropic relation that provides a direct relation between pressure and density perturbations:

$$s_0 = c_v \ln\left(\frac{p}{\rho^\gamma}\right) \qquad \text{or} \qquad p=\rho^\gamma e^{\frac{s_0}{c_v}} \qquad \text{(D-23)}$$

where $\gamma = \frac{c_P}{c_V}$

Linearizing equation (D-23), yields:

$$p_1 = c_0^2 \rho_1 \tag{D-24}$$

where

$$c_0^2 = \left(\frac{\partial p}{\partial \rho} \right)_{S=S_0} \tag{D-25}$$

where c_0 is the sound speed. For a perfect gas, the sound speed is obtained using equation (D-23):

$$c_0 = \sqrt{\gamma \frac{p_0}{\rho_0}} = \sqrt{\gamma \frac{R_u}{W} T_0} \qquad \Rightarrow \qquad \frac{1}{\gamma} = \frac{p_0}{\rho c_0^2} \tag{D-26}$$

where R_u=8.3143 J/mol·K.

References of attachment D

[D-1] Stokes, G.G., "On the theories of internal friction of fluid in motion, and of the equilibrium and motion of elastic solids", Transactions of the Cambridge Philosophical Society, vol.8, pp. 287-305, 1845.

[D-2] White F., "Fluid Mechanics", McGraw-Hill, 4th edition, 1999.

[D-3] Anderson D. A., "Computational Fluid Mechanics and Heat Transfer", pp. 415-419, New York, 1984.

ATTACHMENT E: Laws for Thermal Radiation

E.1 The importance of emissivity for physical processes

All matter emits radiant energy, also referred to as ***thermal radiation***, simply as a consequence of its temperature. The mechanism of emission is related to energy released by the constant motion of the constituent atoms or molecules of which the matter is composed. In similar fashion radiant energy emitted by the surroundings is partially absorbed by a material and converted into heat.
In thermal radiation there is an ideal entity called a ***blackbody*** (a term introduced by Kirchhoff) that **absorbs all radiant energy incident on it and emits the maximum possible amount of radiant energy at any given temperature**. This is an ideal concept since there is no real material that can completely absorb all radiation incidence on it. All real materials reflect part of the incident radiation on them and emit less radiant energy than a blackbody at the same temperature.
Emissivity can be calculated for a specularly reflecting (mirror-like) material surface by applying *Maxwell's equations* and it depends on the electrical and optical properties of the material. The emissivity of a metal is determined largely by the behaviour of the free electrons within the material whilst for a dielectric it is largely due to the bound electrons.
At high temperatures or in evacuated environments thermal radiation is the main mode of heat transfer.
Total emissivity governs the amount of thermal radiation lost or gained by an object and can therefore either cool or heat it, respectively. The reliable prediction of energy gains and losses to and from such structures as buildings, greenhouses, radomes, space vehicles and industrial process plant has become an important part of energy conservation and control.
Finally, emissivity is required for radiation thermometry, i.e. **to deduce the temperature of objects from a measurement of their thermal radiation and use of *Planck's radiation law***.

E.2 Physical laws for thermal radiation

E.2.1 Radiant heat transfer

When radiant thermal energy passes a medium, any object within the path can *absorb*, *reflect* and *transmit* the incident thermal radiation. Use *absorptivity* a, *reflectivity* ρ, and *transmissivity* τ to represent the fractions of the incident thermal radiation that a body absorbs, reflects and transmits, respectively, giving (according the *conservation of energy*):

$$a + \rho + \tau = 1 \qquad \text{(E-1)}$$

where:

a = *absorptivity* (or ***absorption coefficient***, or *absorptivity coefficient*, or *molar absorptivity*)
ρ = *reflectivity*,
τ = *transmissivity*

In general, the three factors in equation are functions of the temperature, the electromagnetic wave length and the surface properties of the incident body. Simplifications are usually made for fire engineering calculations. An extreme case is that all the incident thermal radiation is absorbed by the body, i.e. a=1: such an ideal body is called a ***blackbody***. Greybody has a<1.
In particular, the *absorptivity coefficient* (a) is a function of environment of the measured species and other important factor:

$a = a$ (λ, sw, solv, [pH], temp, μ_Θ, B, etc.)

where:

λ = wavelength
sw = slit-width in use ($\Delta\lambda$')
solv = solvent or Mixture or Matrix.
T = temperature
pH = equivalent proton concentration
μ_Θ = physical and chemical reaction state.
B = magnetic field.

The ***absorption coefficient*** a (or ***absorptivity coefficient***) is one of many ways to describe the absorption of electromagnetic waves. It can be expressed in terms of the imaginary part of the refractive index, Γ, and the wavelength of the light (in free space), λ_0, according to

$$a = \frac{4\pi\Gamma}{\lambda_0} \tag{E-2}$$

E.2.2 Planck radiation law

The fundamental relation used in techniques based on irradiance measurements is the *Plank radiation law*, according to which an ideal blackbody (i.e. a body which is completely opache and non-reflecting in all directions at all wavelengths) in equilibrium at absolute temperature T [K] radiates (over 2π solid angle) the *blackbody spectral irradiance* $I_B(\lambda,T)$, that is measured in [Wm^{-3} = $J\ m^{-3}s^{-1}$] given by:

$$I_B(\lambda,T) = \frac{1}{\lambda^5}\ \frac{C_1}{\exp\left(\frac{C_2}{\lambda T}\right)-1} \tag{E-3}$$

where:

$\lambda = \frac{c}{f}$ = the wavelength [m]

$C_1 = 2\,h_P\,c_{light}{}^2 = 3.74\cdot10^{-16}\,[\,J\,m^2\,s^{-1}\,]$

$C_2 = \frac{h_P\,c_{ligt}}{k_B} = 1.44\cdot10^{-2}\,[\,m\,K\,]$

h_P = Plank constant [J s] = $6.626\cdot10^{-34}$ [J s] = $4.135\cdot10^{-15}$ [eV s]

c_{light} = speed of light [m s^{-1}]
k_B = Boltzmann constant [J K^{-1}] = 1.380 ·10^{-23} [J K^{-1}] = 8.617 ·10^{-5} [eV K^{-1}]
T = absolute temperature of the blackbody [K]

It is the basis for all thermal radiation measurements. All of the other important relationships can be derived from this equation.

E.2.3 Stefan-Boltzmann equation

The blackbody thermal radiation is of fundamental importance to radiant heat transfer. It has many special proprieties, but the most important one being that it is a perfect emitter. This means that no other body can emit more thermal radiation per unit surface area than blackbody at the same temperature. The total amount of thermal radiation (E_{rad_b}) emitted by a blackbody surface is a function of its temperature only and is given by the Stefan-Boltzmann law:

$$E_{rad\_b} = \sigma T^4 \qquad \text{(E-4)}$$

where:
σ = Stefan-Boltzmann constant [W m^{-2} K^{-4}] = 5.67 ·10^{-8} [W m^{-2} K^{-4}]

It determines the radiation emitted over all wavelengths at a particular temperature T (see Fig. E-1). This equation can be derived by integrating the Planck equation over all wavelengths.
The fact that the temperature is raised to the fourth power means that even a small change in temperature translates into a large change in radiated energy.

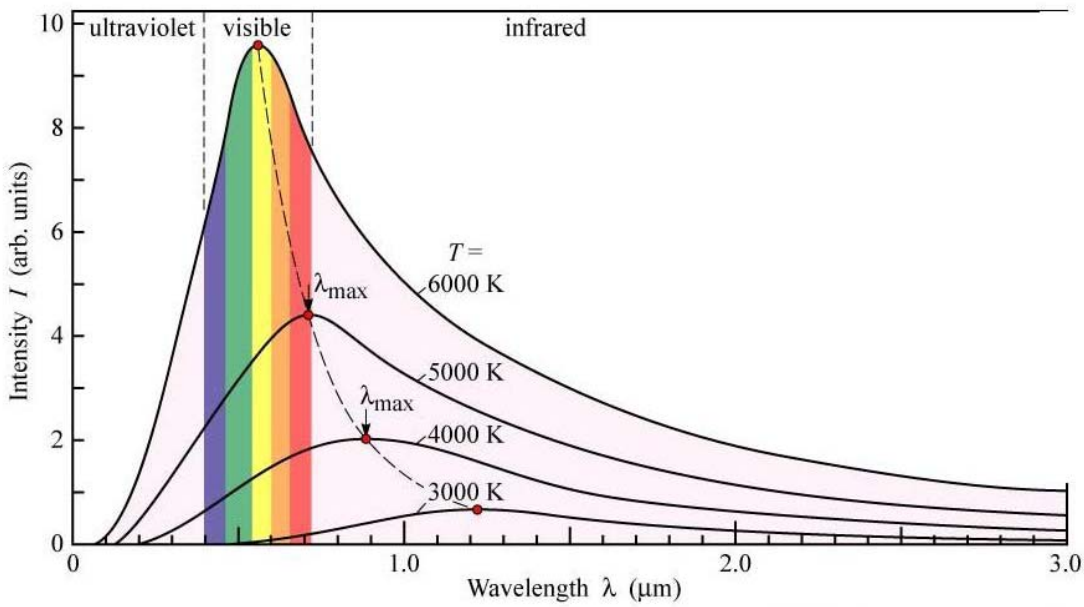

Fig. E-1: Black body radiation according to Planck's Law.

No real material emits and absorbs radiation according to laws of blackbody. In general, an additional term is necessary to define the radiant energy of an emitting surface. This is the ***emissivity*** ε. This term is defined as the ratio of the total energy emitted by a surface to that of a blackbody surface at the same temperature. Thus, the total radiant energy emitted by a general surface is:

$$E = \varepsilon E_{rad\_b} = \varepsilon \sigma T^4 \qquad \text{(E-5)}$$

Greybody radiation is adopted in fire engineering calculations.
The terms ***emittance*** (*M*) and ***emissivity*** (ε_λ) are often used interchangeably. There is, however, a technical distinction. *Emissivity* refers to the properties of a material; *emittance* to the properties of a particular object. Thermal *emissivity* (ε_λ) is a spectrum-dependent ability of a material to release absorbed heat, although the terms are related. *Emittance* (*M*) is given in units of watts per square meter (W/m^2), and *emissivity*, e, is a scale factor, between 0 and 1, used along with temperature, to calculate *emittance* for a given material. *Emissivity* is only one component in determining *emittance*. Other factors, including shape of the object, oxidation and surface finish must be taken into account.
The apparent emittance of a material also depends on the temperature at which it is determined, and the wavelength at which the measurement is taken. Surface condition affects the value of an object's emittance, with lower values for polished surfaces, and higher values for rough or matte surfaces. In addition, as materials oxidize, emittance tends to increase, and the surface condition dependence decreases.
The values for the *emissivities* of almost all substances are known and published in reference literature. However, the *emissivity* determined under laboratory conditions seldom agrees with actual *emittance* of an object under real operating conditions. For this reason, one is likely to use published emissivity data when the values are high.
Spectral emissivity is the ratio of emittance at a specific wavelength or very narrow band to that of a blackbody at same temperature.

E.2.4 Wien's displacement equation

The blackbody spectral radiance is characterised by a maximum (see Fig. E-1) and the wavelength of this maximum, λ_{max}, depends on temperature. λ_{max} may be obtained by differentiating the spectral radiance with respect to λ and setting the result equal to zero:

$$\lambda_{\max} \cdot T = \text{constant} = 2.897 \cdot 10^{-3} \, [m\,K] \qquad \text{(E-6)}$$

E.2.5 Kirchhoff's law of radiation

"The absorptivity of a body equals its emissivity" ($\varepsilon = a$): this is known as *Kirchhoff's law*.
A body that is a good emitter (or radiator) is also a good absorber, in fact the radiant energy per unit time per unit area emitted by the blackbody in thermal equilibrium equals the radiant energy per unit time per unit area absorbed by it. A black body is both a perfect absorber and a perfect emitter.
In simple mathematical terms, Kirchhoff's law can take on several formulations, which stem from the equivalence between the coefficients of emission (ε) and absorption (*a*) at thermal equilibrium. A number of consequences follow:

- The ***total emissivity*** equals the ***total absorptivity***, $\varepsilon = \alpha$ in a blackbody in thermal equilibrium.
- The ***spectral emissivity*** (ε_λ) equals the ***spectral absorptivity*** (α_λ) in a blackbody in thermal equilibrium: $\varepsilon_\lambda = \alpha_\lambda = 1 - \tau(\lambda_i)$
- The most general expression of Kirchhoff's law for opaque bodies is a statement of ***Stewart's law***, $\varepsilon = 1 - \rho$, namely, where ρ corresponds to the coefficient of reflection.

Kirchhoff's Law of thermal emission was formulated in 1859. It is at the same time the simplest and least understood law in physics. Kirchhoff's law states that given thermal equilibrium with an enclosure, the radiation inside will be always black, or normal, in a manner which is independent of the nature of the walls, or the objects they contain. This is known as the concept of universality. That is, that the radiation within an enclosure can always be described by a universal function dependent only on temperature and frequency. This universal function was first given to us by Max Planck, in 1900. Kirchhoff's law stands at the heart of all of modern astrophysics. It is the basis for setting the temperature of the stars, for the gaseous model of the Sun, and for believing that we now know the temperature of the entire universe.
Tragically, Kirchhoff's belief that radiation within an enclosure was independent of the nature of the walls is not correct! Kirchhoff arrived at universality because he did not properly address reflection within cavities. As a result, the proper law of thermal emission was brought to us by Balfour Stewart, in 1858. Like Kirchhoff's law, Stewart's law properly equates the emissivity and absorptivity of an object at thermal equilibrium, but it does not lead to universality. Stewart's law states that the radiation is determined not only by temperature and frequency, but also by the nature of the walls themselves.

E.2.6 Beer–Lambert–Bouguer law for absorption

Many compounds absorb ultraviolet (UV: 190 nm-370 nm) or visible (VIS: 370 nm-700 nm) light. The diagram below shows a beam of radiation of radiant intensity (or power) I_0, directed at a sample solution. Absorption takes place and the beam of radiation leaving the sample has radiant intensity (or power) I.

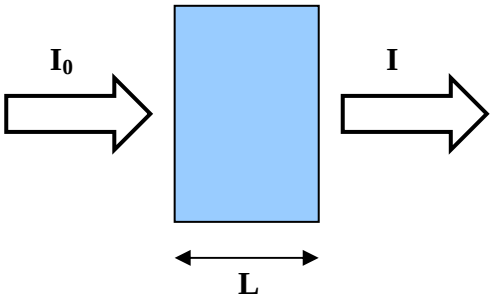

Fig. E-2: Absorption of a beam radiation of intensity I_0 that become a beam radiation of intensity I.

In optics, the ***Beer–Lambert law***, also known as ***Beer's law*** or the ***Lambert–Beer law*** or the ***Beer–Lambert–Bouguer law*** (in fact, most of the permutations of these three names appear somewhere in literature) is an empirical relationship that relates the absorption of light to the properties of the material through which the light is traveling.
The law states that there is a logarithmic dependence between the *transmission* (or ***transmissivity***), τ, of light through a substance and the product of the ***absorption coefficient*** of the substance, a (synonyms are: *absorptivity*, ***absorptivity coefficient***, *absorption* or *absorption coefficient*) and the distance the light travels through the material (i.e. the path length of the sample, that is, the path length of the cuvette in which the sample is contained), L.

$$\tau = \frac{I}{I_0} = \exp(-a\,L) \tag{E-7}$$

where I_0 and I are the intensity (or power) of the incident light and that after the material, respectively.
Historically, the Lambert law states that absorption is proportional to the light path length, whereas the Beer law states that absorption is proportional to the concentration of absorbing species in the material.
The transmission (or transmissivity) is expressed in terms of an ***absorbance*** which is a nondimensional number and it is usually defined for gases as:

$$A = -\ln(\tau) = -\ln\left(\frac{I}{I_0}\right) = a\,L \tag{E-8}$$

The reason why usually we prefer to express the law with this equation is because *absorbance* A is directly proportional to the other parameters, as long as the law is obeyed.
There are at least five conditions that need to be fulfilled in order for *Lambert–Beer*'s law to be valid. These are:

1. The absorbers must act independently of each other;
2. The absorbing medium must be homogeneously distributed in the interaction volume and must not scatter the radiation;
3. The incident radiation must consist of parallel rays, each traversing the same length in the absorbing medium;
4. The incident radiation should preferably be monochromatic, or have at least a width that is more narrow than the absorbing transition; and
5. The incident flux must not influence the atoms or molecules; it should only act as a non-invasive probe of the species under study. In particular, this implies that the light should not cause optical saturation or optical pumping, since such effects will deplete the lower level and possibly give rise to stimulated emission.

If any of these conditions is not fulfilled, there will be deviations from Beer's law.
The *Lambert–Beer law* tends to break down at very high concentrations, especially if the material is highly scattering. If the light is especially intense, nonlinear optical processes can also cause variances.